



Synthesis of α -Cationic Phosphines and Their Applications as Ligands

Synthese von α -Kationischer Phosphine und deren Anwendung als Liganden

DISSERTATION

zur Erlangung des akademischen Grades eines
Doktors der Naturwissenschaften
(Dr. rer. nat.)

Fakultät für Chemie und Chemische Biologie
der TU Dortmund vorgelegt von
Lianghu Gu

2016

Eidesstattliche Erklärung:

Hiermit versichere ich, dass ich die eingereichte Dissertation nur unter Mitwirkung der an gegebner Stelle erwähnten Personen verfasst und keine anderen als die angegebenen Quellen und Hilfsmittel benutzt, sowie Zitate kenntlich gemacht habe.

Datum: _____

(Unterschrift)

1. Berichterstatter: Prof. Dr. Alois Fürstner
2. Berichterstatter: Prof. Dr. Klaus Jurkschat

Die vorliegende Arbeit entstand auf Anregung und unter Anleitung von Prof. Dr. Manuel Alcarazo am Max-Planck-Institut für Kohlenforschung in Mülheim an der Ruhr in der Zeit vom September 2012 bis November 2015. Teile dieser Arbeit wurden in den folgenden Artikeln veröffentlicht: L. Gu, G. Gopakumar, P. Gualco, W. Thiel, M. Alcarazo, *Chem Eur. J.* **2014**, *20*, 8575-8578; J. Carreras, G. Gopakumar, L. Gu, A. Gimeno, P. Linowski, J. Petuškova, W. Thiel Alcarazo, *M. J. Am. Chem. Soc.*, **2014**, *136*, 3319-3319; E. Haldón, Á. Kozma, H. Tinnermann, L. Gu, R. Goddard, M. Alcarazo, *Dalton Trans.* **2016**, *45*, 1872-1876.

to my lovely family

Danksagung

Mein herzlichster Dank gilt Prof. Dr. Manuel Alcarazo für die Aufnahme in seinen Arbeitskreis und die Vergabe des interessanten Promotionsthemas.

Herrn Prof. Dr. Alois Fürstner, MPI für Kohlenforschung, und Herrn Prof. Dr. Klaus Jurkschat, TU Dortmund, danke ich für die freundliche Übernahme des Referats und Koreferats.

Weiterhin möchte ich der Max-Planck-Gesellschaft und im Besonderen dem Max-Planck-Institut für Kohlenforschung für die Bereitstellung meines Arbeitsplatzes und die finanzielle Unterstützung danken.

Ich möchte mich bei dem Stipendium CSC und bei der Georg-August-Universität Göttingen für die finanzielle Unterstützung bedanken.

Mein herzlichster Dank gilt Prof. Manuel Alcarazo für seine große Hilfe, die mich sowohl auf fachlicher und persönlicher Ebene stark zu entwickeln erlaubte. Ich bin ihm zutiefst dankbar für all die Motivation und kompetente Beratung, die er mir zur Verfügung gestellt hat.

Allen Mitgliedern der Arbeitsgruppen Fürstner und Alcarazo danke ich für die gute Zusammenarbeit, das angenehme Arbeitsklima und die schönen Stunden innerhalb und außerhalb des Laboralltags. Ich danke herzlich Sigrid Holle, Gerlinde Mehler, Pascal Ortsack, Christian Wille, Helga Krause, Günter Seidel, Karin Radkowski und Saskia Schulthoff für die ständige Hilfsbereitschaft im Labor. Für die große Hilfe bei organisatorischen Angelegenheiten danke ich recht herzlich Frau Lickfeld.

Mein Dank geht an die Mitarbeiter aller analytischen Abteilungen für die zuverlässige und schnelle Durchführung und Auswertung zahlreicher Analysen. Besonders bedanke ich mich bei Frau Phillips, Herrn Kochius, Herrn Dr. Farès und Frau Wirtz aus der NMR-Abteilung, bei Herrn Kampen, Frau Blumenthal und Herrn Klein aus der MS-Abteilung, bei Herrn Deege, Frau Kestermann und Frau Hinrichs aus der HPLC-Abteilung, und Herrn Dr. Goddard, Herrn Prof. Lehmann, Herrn Rust, Herrn Dr. Mondal, Frau Dreier und Frau Dreher aus der Kristallographie-Abteilung.

Mein Dank geht an die Mitarbeiter der theoretischen Abteilung für die gute Berechnung und hilfreichen Informationen zur Aufklärung der Mechanismen. Besonders bedanke ich mich bei Dr. Gopinadhanpillai Gopakumar, Dr. Larry Wolf, Dr. Yiying Zheng und Prof. Walter Thiel. Mein Dank geht an Dr. Eckhard Bill und Herrn Frank Reikowski, MPI für chemische Energieconversion, für die EPR-Messungen und für die Simulation. Mein Dank geht an Herrn Christian Wille, Herrn Hendrik Tinnermann und Herrn Leo Nicholls, aus der Arbeitsgruppe Alcarazo für die Cyclovoltammetrie-Messungen.

Mein Dank geht an Dr. Pauline Gualco für die Synthese der Verbindungen **61**, **66**, **75**, **78** und **81** und die Untersuchungen an N-gebundenen mehrkationigen Phosphinen. Mein Dank geht an Dr. Estela Haldón für die Hilfe bei der Synthese der Verbindungen **138a**, **138b**, **139a** und **139b**. Mein Dank geht an Dr. Jonathan Dube für die Hilfe bei der Synthese der Verbindungen **146**.

Für das gründliche Korrekturlesen danke ich Prof. Manuel Alcarazo, Leo Nicholls, Dr. Jonathan Dube, Frau Lauren Dube und Dr. Yin Zhang herzlich.

Ich möchte an alle Freunde besonders danken für die gemeinsam verbrachte Zeit in Mülheim.

Mein ganz besonderer Dank geht meinen Ehefrau Fang Fang für ihre Unterstützung! Ich möchte ihr diese Arbeit widmen!

Abbreviations

Å	Angstrom
Ac	Acetyl
acac	Acetylacetonone
Ad	Adamantyl
Ar ^F	Pentafluorophenyl
atm	atmosphere
BIAN	1,2-Bis(imino)acenaphthene
[BMIM][BF ₄]	1-Butyl-3-methylimidazolium tetrafluoroborate
Bu	Butyl
cod	1,5-Cyclooctadiene
Cy	Cyclohexyl
DAB	1,4-Diazabutadiene
dba	Dibenzylideneacetone
DBN	1,5-Diazabicyclo(4.3.0)non-5-ene
DBU	1,8-Diazabicycloundec-7-ene
dec.	Decomposition
DCE	1,2-Dichloroethane
DIBAL	Diisobutylaluminium hydride
dipp	2,6-Diisopropylphenyl
DMAP	4-Dimethylaminopyridine
DMF	Dimethylformamide
DFT	Density functional theory
δ	Chemical shift (NMR)
Et	Ethyl
Equiv.	Equivalent
EtOAc	Ethyl acetate
eV	Electronvolt
GC-MS	Gas chromatography – mass spectrometry
h	Hour
Hal	Halogen
Hex	Hexyl
HOMO	Highest occupied molecular orbital

HPLC	High-performance liquid chromatography
HRMS	High-resolution mass spectrometry
Hz	Hertz
IR	Infrared
J	Coupling constant
KHMDS	Potassium hexamethyldisilazane
L	Generalized ligand
L_nM	Generalized metal fragment with n ligands
LDA	Lithium diisopropylamide
LUMO	Lowest unoccupied molecular orbital
m	Meta
M	Generalized metal
Me	Methyl
MeO	Methoxy
Mes	Mesityl
min	Minutes
MS	Mass spectrometry
Ms	Methanesulfonate
MTBE	Methyl <i>tert</i> -butyl ether
n	Normal
NHC	<i>N</i> -Heterocyclic carbenes
NMM	<i>N</i> -Methylmorpholine
NMR	Nuclear magnetic resonance
$\tilde{\nu}$	Frequency
<i>o</i>	Ortho
<i>p</i>	Para
Ph	Phenyl
PPTS	Pyridinium <i>p</i> -toluenesulfonate
Pr	Propyl
Py	Pyridine
r.t.	Room temperature
<i>t</i>	Tertiary
Tf	Triflate
THF	Tetrahydrofuran

THT	Tetrahydrothiophene
TLC	Thin layer chromatography
TMEDA	<i>N,N,N',N'</i> -Tetramethylethylenediamine
TMS	Trimethylsilyl
Ts	Tosyl
vs	Versus
X	Generalized 1e anionic ligand

SYNTHESIS OF α -CATIONIC PHOSPHINES AND THEIR APPLICATIONS AS LIGANDS . 1

1	INTRODUCTION	17
1.1	Phosphines in Organometallic Chemistry and Catalysis.....	17
1.2	Introduction of Charge (Cationic Phosphines)	17
1.3	α -Cationic Phosphines.....	19
1.3.1	Definition and Scope	19
1.3.2	Synthetic Approaches to Monocationic Phosphines.....	20
1.3.2.1	Imidazolium-Substituted Cationic Phosphines	20
1.3.2.2	Cyclopropenium-Substituted Cationic Phosphines.	22
1.3.2.3	Pyridinium-Substituted Cationic Phosphines.	23
1.3.2.4	Nitrogen-Substituted Cationic Phosphines.....	24
1.3.3	Synthetic Approaches to Polycationic Phosphines.	24
1.3.4	Electronic Properties of α -Cationic Phosphines.....	27
1.3.5	Applications of Cationic Phosphine Ligands.....	31
1.4	Summary I.....	36
2	BIS- AND TRISPYRAZOYLBORATE/METHANE-STABILIZED P(III)-CENTERED CATIONS	37
2.1	Introduction	37
2.2	Results and Discussion	38
2.2.1	Synthesis of bis- and trispyrazolylborate-Stabilized P-centered Cations.....	38
2.3	Electronic Properties	43
2.4	Attempts of Coordination	44
2.5	Summary II.....	44
3	DICATIONIC CHELATING PHOSPHINES: SYNTHESIS, STRUCTURE AND REACTIVITY	45
3.1	Introduction	45
3.2	Synthesis.....	46
3.2.1	Synthesis of Chelating Dicationic Ligands	46

3.2.2	Synthesis of Monodentate Dications	50
3.3	Electronic Properties of the phosphines	51
3.4	Coordination Study	55
3.5	Reductive Elimination of Bis(pentafluorophenyl)palladium Complexes	59
3.5.1	Synthesis of the Biaryl palladium Complexes	59
3.5.2	Experimental Investigation of the Effect of Cationic Ligands in Reductive Elimination Processes	61
3.5.3	Theoretical Investigation of Cationic Ligands in Reductive Elimination.....	62
3.5.4	Reactivity of Dication 92 towards Pd(0) and Ni (0)	65
3.6	Application in Catalysis	67
3.6.1	Theoretical Investigation of Chelating Dicationic Ligands in Catalysis.....	69
3.7	Summary III.....	70
4	ISOLATION AND COORDINATION CHEMISTRY OF CAACS SUBSTITUTED α- RADICAL PHOSPHINES.....	71
4.1	Introduction	71
4.2	α-Radical Phosphines based on CAACs	73
4.2.1	Synthesis of Cationic Phosphines	73
4.2.2	Electronic Properties of Cationic Phosphines	76
4.2.3	Coordination of the Cationic Ligands.	78
4.3	α-Radical Phosphines	80
4.3.1	Synthesis of the Radical Phosphines	80
4.3.2	Coordination of α -Radical Phosphines towards Au(I)	83
4.3.3	Coordination of α -Radical Phosphines towards Other Metal Salts.....	87
4.4	Synthesis of Cationic Phosphine Oxide and the Radical thereof	88
4.5	Theoretical Analysis of Properties of α-Radical Phosphines	91
4.6	Summary IV.....	95
5	EXPERIMENTAL PART	96
5.1	General Experimental Conditions.....	96
5.1.1	Working Techniques	96
5.1.2	Analytical Methods	97

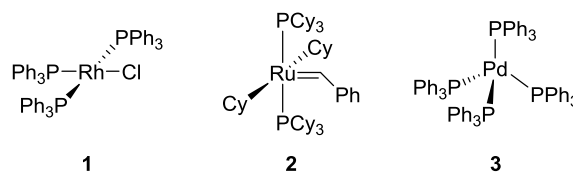
5.1.3	Starting Materials as well as in Working Group-made Chemicals	98
5.2	Synthesis.....	99
6	APPENDIX.....	140
6.1	NMR Spectra of Representative Compounds	140
6.2	X-ray Structures.....	255
6.2.1	Crystal Data and Structure Refinement of Compound 63	255
6.2.2	Crystal Data and Structure Refinement of Compound 65	256
6.2.3	Crystal Data and Structure Refinement of Compound 67	257
6.2.4	Crystal Data and Structure Refinement of Compound 76	258
6.2.5	Crystal Data and Structure Refinement of Compound 79	259
6.2.6	Crystal Data and Structure Refinement of Compound 91	260
6.2.7	Crystal Data and Structure Refinement of Compound 92b	261
6.2.8	Crystal Data and Structure Refinement of Compound 101a	262
6.2.9	Crystal Data and Structure Refinement of Compound 103	263
6.2.10	Crystal Data and Structure Refinement of Compound 107a	264
6.2.11	Crystal Data and Structure Refinement of Compound 108	265
6.2.12	Crystal Data and Structure Refinement of Compound 109a	266
6.2.13	Crystal Data and Structure Refinement of Compound 109c	267
6.2.14	Crystal Data and Structure Refinement of Compound 109d	268
6.2.15	Crystal Data and Structure Refinement of Compound 109f	269
6.2.16	Crystal Data and Structure Refinement of Compound 110	270
6.2.17	Crystal Data and Structure Refinement of Compound 112b	271
6.2.18	Crystal Data and Structure Refinement of Compound 112f	272
6.2.19	Crystal Data and Structure Refinement of Compound 112g	273
6.2.20	Crystal Data and Structure Refinement of Compound 112h	274
6.2.21	Crystal Data and Structure Refinement of Compound 113	275
6.2.22	Crystal Data and Structure Refinement of Compound 114	276
6.2.23	Crystal Data and Structure Refinement of Compound 138a	277
6.2.24	Crystal Data and Structure Refinement of Compound 138b	278
6.2.25	Crystal Data and Structure Refinement of Compound 138c	279
6.2.26	Crystal Data and Structure Refinement of Compound 139a	280
6.2.27	Crystal Data and Structure Refinement of Compound 139b	281
6.2.28	Crystal Data and Structure Refinement of Compound 139c	282
6.2.29	Crystal Data and Structure Refinement of Compound 140a	283
6.2.30	Crystal Data and Structure Refinement of Compound 140c	284
6.2.31	Crystal Data and Structure Refinement of Compound 141	285

6.2.32	Crystal Data and Structure Refinement of Compound 142	286
6.2.33	Crystal Data and Structure Refinement of Compound 143	287
6.2.34	Crystal Data and Structure Refinement of Compound 144	288
6.2.35	Crystal Data and Structure Refinement of Compound 145	289
6.2.36	Crystal Data and Structure Refinement of Compound 146	290
6.2.37	Crystal Data and Structure Refinement of Compound 147	291
7	BIBLIOGRAPHY	292

1 Introduction

1.1 Phosphines in Organometallic Chemistry and Catalysis

Phosphines are the most widely used ligands in organometallic chemistry; hundreds of mono-, di-, or tridentate phosphines with various backbones and coordinating abilities have been devised and prepared for specific applications in homogeneous catalysis.^[1-2] Perhaps the most popular phosphine ligand used is triphenylphosphine, a shelf-stable solid that undergoes oxidation in air relatively slowly. Moreover, phosphines are able to coordinate metals in multiple oxidation states^[3] and, unlike most metal amine complexes, metal phosphine complexes tend to be lipophilic, displaying good solubility in organic solvents. These two features make metal phosphine complexes really useful in homogeneous catalysis. Prominent examples of metal phosphine complexes include Wilkinson's catalyst ($\text{Rh}(\text{PPh}_3)_3\text{Cl}$), Grubbs' catalyst, and tetrakis(triphenylphosphine)palladium(0) (Scheme 1).

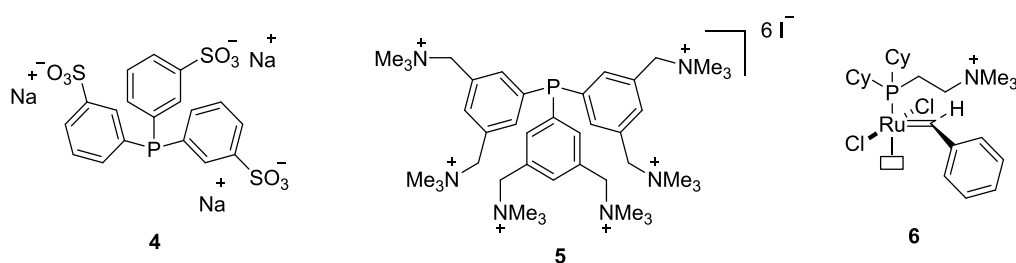


Scheme 1. Examples of phosphine metal complexes with application in catalysis.

1.2 Introduction of Charge (Cationic Phosphines)

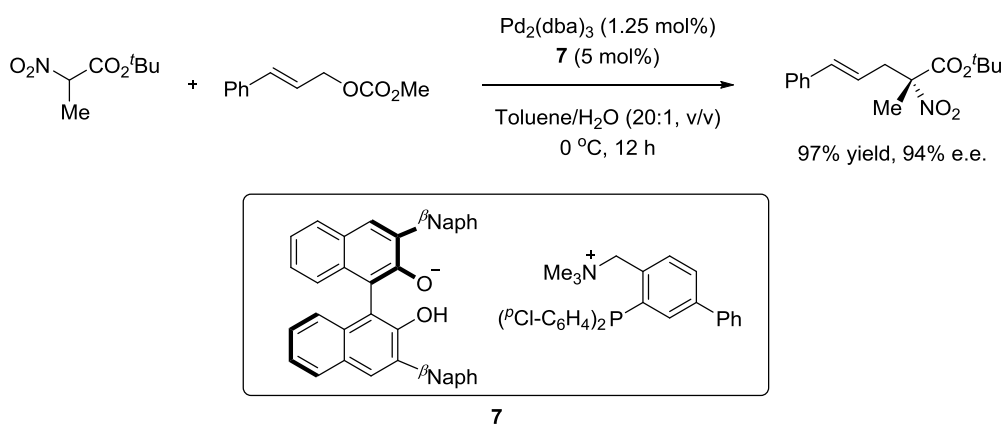
Homogeneous catalysts offer a number of important advantages over their heterogeneous counterparts. For example, all catalytic sites are accessible because the catalyst is usually a dissolved metal complex. Furthermore, it is often easier to tune the chemoselectivity, regioselectivity, and/or enantioselectivity by modification of the ancillary ligands.^[4] Despite of these advantages, heterogeneous catalytic systems are preferred in industry due to one major disadvantage of homogeneous ones: the difficulty to separate the reaction products from the catalysts and solvents. Distillation, which would be the most efficient process to conduct this separation, often requires elevated temperatures, at which most homogeneous catalysts decompose. Other conventional separation processes, for example, chromatography or extraction lead to catalyst loss and are typically time-consuming and expensive, since the use and recycling of big amounts of solvents are required.^[5-6]

In order to deal with this kind of problems, chemists have devoted efforts to modify the substituent on the ligands, thus providing catalysts with appropriate physical properties that allow their easy separation from the reaction mixture. One of these strategies consists of the attachment of polar groups or charges to the ligands, aiming to increase the solubility of the resulting catalyst in polar solvents.^[7-8] Several industrial processes already benefit from this strategy; an illustrative example is the Ruhrchemie/Rhône-Poulenc process for the Rh-catalyzed hydroformylation of propene by the use of the highly water-soluble trisulfonated phosphine **4**. After the reaction is completed, the effective separation and recovery of noble metal containing catalysts can be achieved by a simple phase separation. Subsequently, the recovered catalyst can be directly used for the next cycle.^[9]



Scheme 2. Examples of ionic phosphines with application in catalysis.

Another interesting application regarding charged phosphines is the *in situ* analysis of reaction intermediates and catalytic species by electrospray ionization mass spectrometry.^[10] ESI-MS was developed in the late 1980s by Fenn and co-workers^[11] and exploded in popularity in the 1990s due to its ability to analyze thermally fragile or highly polar (bio)molecules.^[12] The fundamental ability of this technique to transfer ions from solution to the gas phase with little or no fragmentation enables the direct study of complex mixtures. In combination with the standard advantages of mass spectrometry, the use of cationic ancillary ligands has led to the rise of the employment of ESI-MS in the investigation of catalytic mechanisms.^[13-19] For example, a cationic version of Grubbs' first-generation catalyst **6** has been imaginatively exploited by Chen and co-workers, who used it to explore the reactivity of an olefin metathesis catalyst in the gas phase using ESI-MS (Scheme 2).^[20-22] Finally, Ooi and his coworkers recently developed an achiral cationic ammonium-phosphine hybrid ligand which was paired with a chiral binaphtholate anion. This ion-paired chiral ligand **7** is able to impart a remarkable stereocontrolling ability and catalyzes a highly enantioselective allylic alkylation of α -nitrocarboxylates (Scheme 3).^[23]



Scheme 3. Ion-paired chiral ligands applied in asymmetric catalysis.

The above examples demonstrate that remote cationic (or ionic) functional groups have dramatic influences on the physical properties of phosphine ligands, which results in interesting applications. It is worth to remind that this kind of modification normally does not significantly alter the coordination properties of the phosphorus center provided that a long distance between the positive charge and the phosphorus atoms exist.

1.3 α -Cationic Phosphines

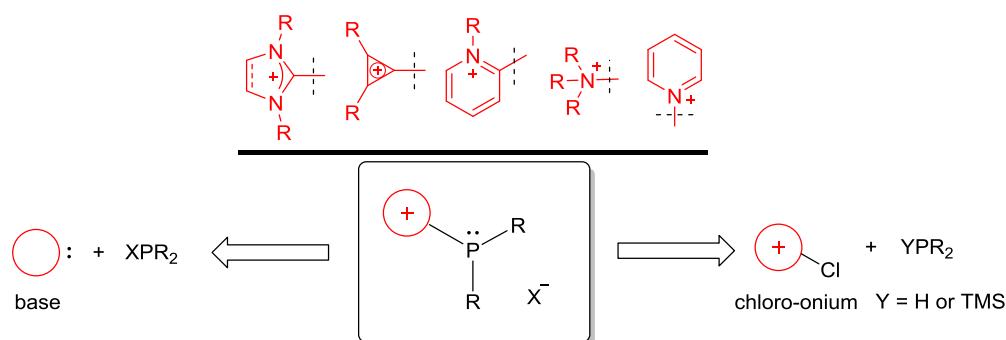
The well-established ligand toolbox, containing different types of phosphines ranging from electron-rich to electron-poor ones, provides a very powerful manifold to tune the primary reactivity of a metal catalyst. When a catalytic cycle demands very strong donation to the metal, trialkylphosphines are one of the most appropriate ancillary ligands; on the other hand, if moderate π -acceptor properties are necessary, phosphites are the ligands of choice.^[24] However, in some cases the catalytic process demands auxiliary ligands with even stronger π -acceptor properties than phosphites. Then, only few polyhalogenated phosphines, such PF_3 , PCl_3 or $\text{P}(\text{CF}_3)_3$, are available. However, due to their difficult handling (flammable and toxic gases) and their moisture and oxygen sensitivity, their coordination chemistry is basically unexplored.^[25-26] It is in these situations that more stable and easy to use π -acceptor phosphines are required. The synthesis of ligands of this type by attachment of a positively charged group directly to the P-atom is one of the objectives of this thesis.^[27]

1.3.1 Definition and Scope

By definition, all α -cationic phosphines contain positive charged groups that are directly attached to the phosphorus atom. Due to their cationic nature and close position of the positive charge to phosphorus, ligands containing such moieties display not only different

solubility in organic solvents but also very different coordination properties. It can be anticipated that the presence of positive charges will simultaneously decrease the σ -donor and increase the π -acceptor abilities of the phosphines; therefore, dramatically influencing the electronic properties of the metal fragment to which they are attached.^[24, 27]

Most α -cationic phosphines known to date have been prepared by reaction of chlorophosphines with an appropriate amount of a Lewis base. This process is normally promoted by halide sequestering reagents and can be seen as a formal abstraction of the halide to generate a transient phosphonium cation, which is then immediately trapped by the base. A complementary synthetic pathway involves the nucleophilic attack of secondary phosphines or TMS-substituted ones to chloro-onium salts. Both strategies satisfactorily afford α -cationic phosphines by either use of carbon based nucleophiles (carbenes) or nitrogen based ones (amines) as shown in Scheme 4.^[24]



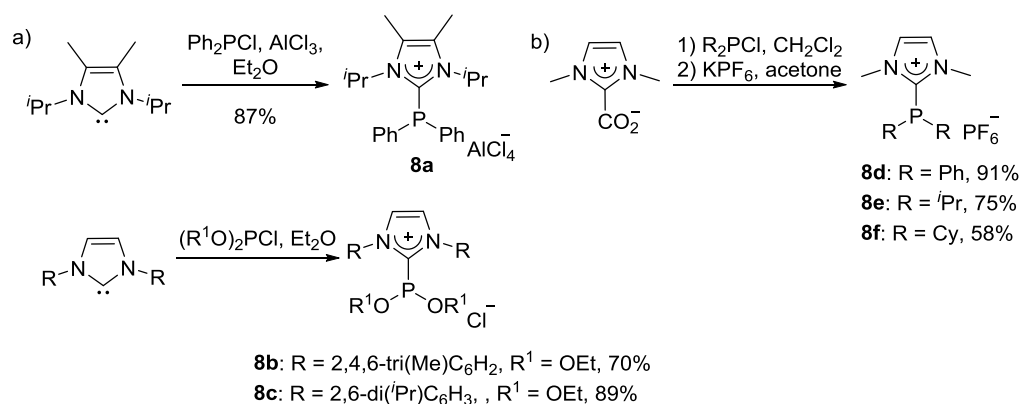
Scheme 4. Synthetic pathways to α -cationic phosphines with different substituents.

1.3.2 Synthetic Approaches to Monocationic Phosphines

1.3.2.1 Imidazolium-Substituted Cationic Phosphines

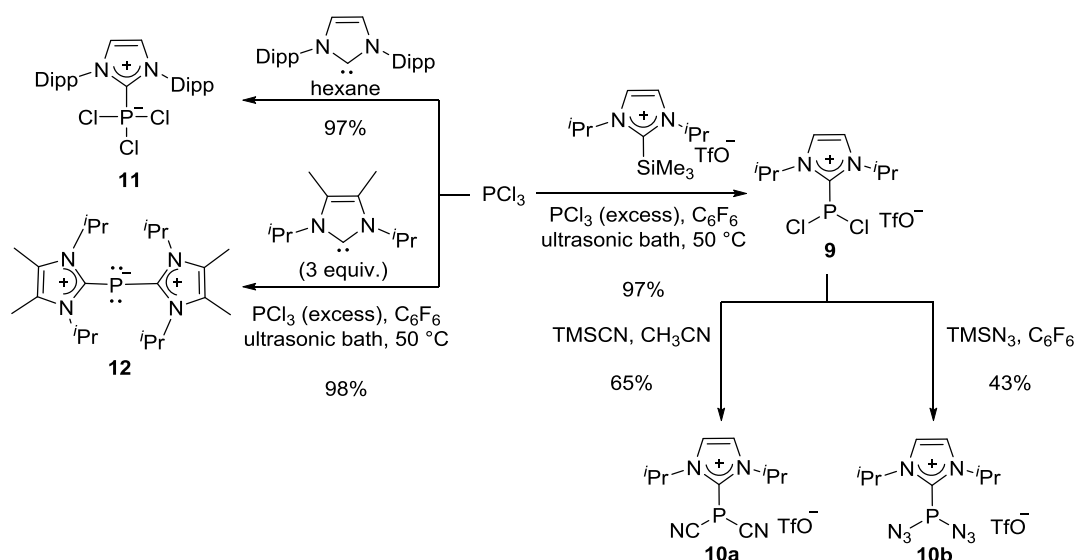
The majority of α -cationic phosphines known are imidazophosphines, which were first briefly mentioned by Zoller in 1988,^[28] and completely characterized by Kuhn *et al.* ten years later.^[29] He described the preparation of imidazophosphine **8a** in good yield by reaction of the corresponding carbene, imidazol-2-ylidene, with Ph_2PCl . Following this procedure, Chauvin *et al.* synthesized the imidazophosphines **8b** and **8c** bearing additional electron-withdrawing substituents, such as alkoxy groups (Scheme 5a).^[30] To avoid the use of free carbenes, which are sensitive to oxygen and moisture, Andrieu *et al.* described a new synthetic method consisting on the reaction of imidazolium-2-carboxylates with chlorophosphines. Under the reaction conditions applied, the free carbene, obtained by release of CO_2 , reacted with R_2PCl to afford the desired compounds. Using this method, they could prepare a library of imidazolium phosphines **8d-8f** (Scheme 5b).^[31] In the case of **8e**, the molecular structure was

analyzed by X-ray diffraction analysis. This showed that the lone pair of electrons on the phosphorus atom is not delocalized along the imidazolium fragment and thus, remains available for metal coordination.^[31]



Scheme 5. Alternative routes to imidazolium-substituted cationic phosphines.

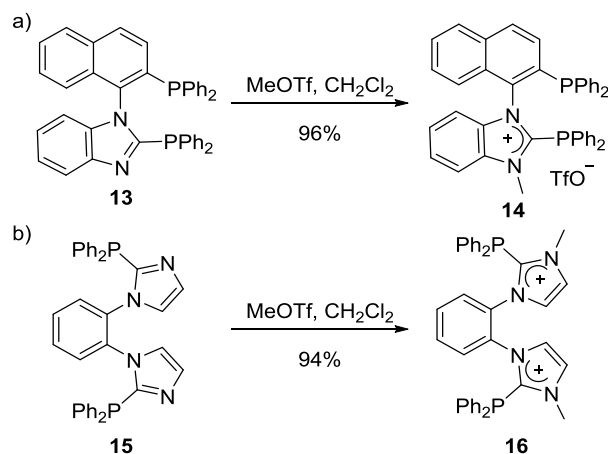
Weigand *et al.* recently reported an alternative synthesis of cationic phosphines using silyl protected carbenes $[\text{NHC-SiMe}_3][\text{TfO}]$ instead of free ones (Scheme 6). Subsequent substitution of the Cl moieties on phosphorus provides access to cationic cyano- and azido-substituted derivatives **10a** and **10b**.^[32] Interestingly, if free NHCs instead of $[\text{NHC-SiMe}_3][\text{TfO}]$ are used for the same reaction, either adducts of the type NHC-PCl_3 **11**^[33] or products coming from the reduction of the central phosphorus such as cation **12**^[34] were obtained.



Scheme 6. Alternative routes to imidazolium-substituted cationic phosphines.

Finally, a completely different method to prepare cationic imidazolium phosphines consists on the selective *N*-alkylation of neutral imidazophosphine precursors.^[35] This strategy was

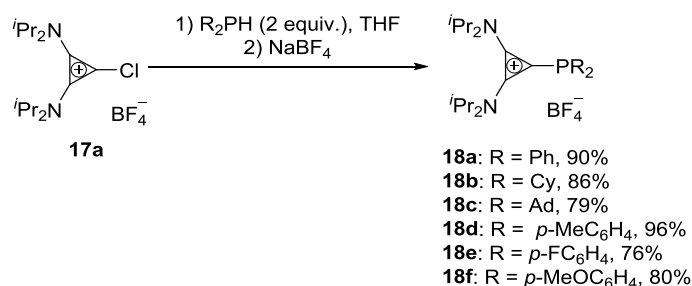
recently applied for the preparation of phosphine-imidazophosphines **14** (Scheme 7a)^[36-37] and bis(imidazophosphine) **16**, through a double methylation strategy (Scheme 7b).^[38] With the correct selection of the methylating reagent, in this case MeOTf, this synthetic route could be used to alkylate the N-atom even if the phosphine moiety is already present on the ligand structure.^[39]



Scheme 7. Alternative routes to imidazolium-substituted cationic phosphines.

1.3.2.2 Cyclopropenium-Substituted Cationic Phosphines.

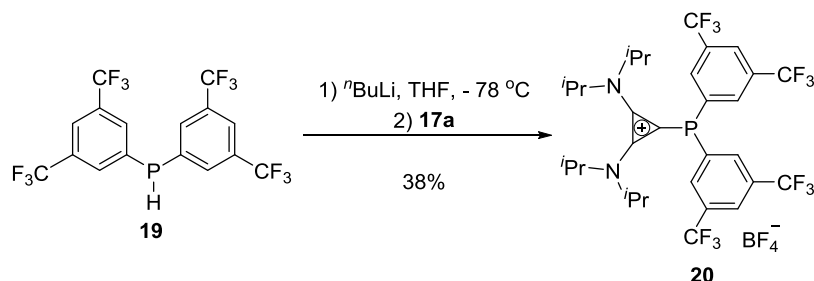
The preparation of cyclopropenylidene stabilized cationic phosphines **18a-g** was achieved in good to excellent yields by condensation of the readily available chlorocyclopropenium salt **17a** with a range of secondary phosphines and subsequent anion exchange, if necessary.^[40] This synthetic strategy allowed the preparation of the desired salts on a multigram scale as white, air-stable solids. It has been observed that these compounds exhibit attributes similar to classical phosphites (Scheme 8).^[41]



Scheme 8. Synthesis of cyclopropenium-substituted cationic phosphines **18a-f**.

The π -acceptor properties of this type of cationic phosphines can be further increased by introduction of additional electron withdrawing groups in their structure. For example, ligand **20**, containing two very electron-withdrawing 3,5-bis-(trifluoromethyl)phenyl substituents was much stronger π -acceptor character (Scheme 9). However, none of the synthetic

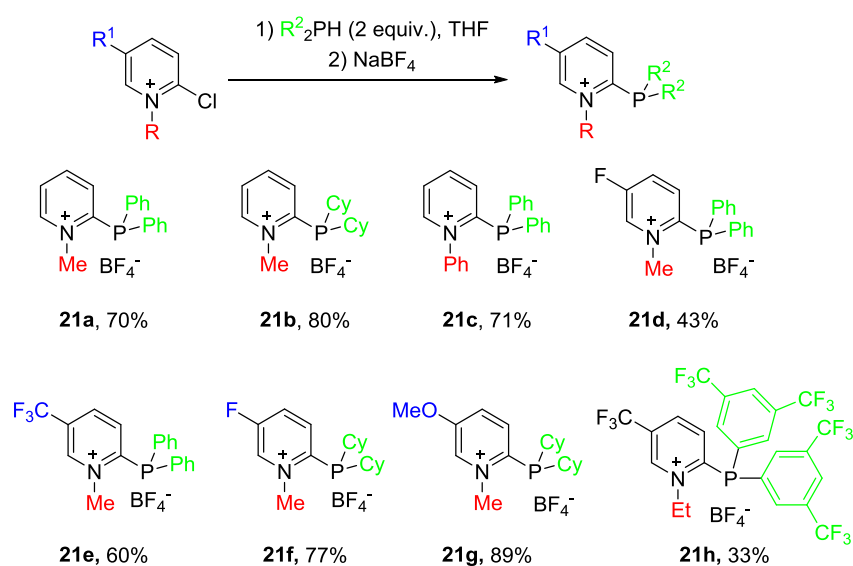
procedures described above worked in this particular case due to the low nucleophilicity of bis(trifluoromethyl)phenyl phosphine. Hence, the secondary phosphine had to be first treated with $n\text{BuLi}$ to form a phosphide, which was reacted with **17a to afford the desired ligand **20** albeit in moderate yield.^[42]**



Scheme 9. Alternative routes to cyclopropenylylidene-stabilized cation **20**.

1.3.2.3 Pyridinium-Substituted Cationic Phosphines.

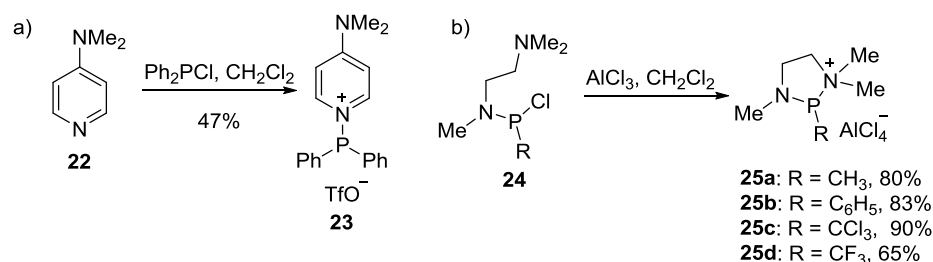
In addition, our group has also reported the preparation of N-alkyl/aryl pyridiniophosphines **21a-h** by condensation of 2-chloropyridinium salts with a range of secondary phosphines. Pyridinium substituted phosphines **21a-h** are envisioned as potentially very useful family of strong π -acceptor ligands owing to their much lower lying LUMO than those of cyclopropenium and imidazolium containing phosphines.^[24] Moreover, an increased solubility in organic solvents as well as very strong π -acceptor properties could be accessible by carefully selection of the two R groups at phosphorus or by introduction of substituents on the pyridinium ring (Scheme 10).^[43] Compared with polycationic phosphines, which show low tendency to form metal complexes, these monocationic ligands are able to coordinate a range of metals, due to the decreased Coulombic repulsive interaction.



Scheme 10. Synthesis of pyridinium-substituted phosphines.

1.3.2.4 Nitrogen-Substituted Cationic Phosphines.

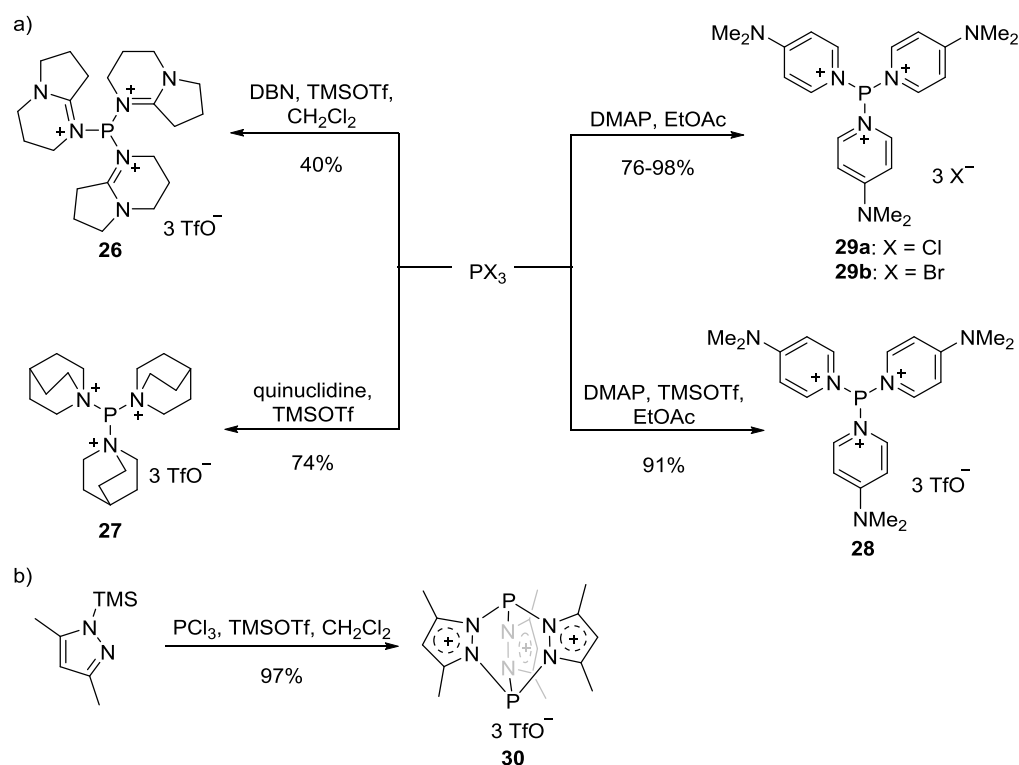
Pyridines, guanidines and amines have also been used to effect halide displacement from halophosphines. An example is the synthesis of **23** from Ph_2PCl and DMAP complex **23** (Scheme 11a).^[44] Another representative one for this reactivity is the intramolecular halide displacement by a tertiary amine **24** with the aid of AlCl_3 to produce a series of cationic phosphines **25a-d** (Scheme 11b).^[45]



Scheme 11. Halide displacement from halophosphines by amines to form cationic phosphines.

1.3.3 Synthetic Approaches to Polycationic Phosphines.

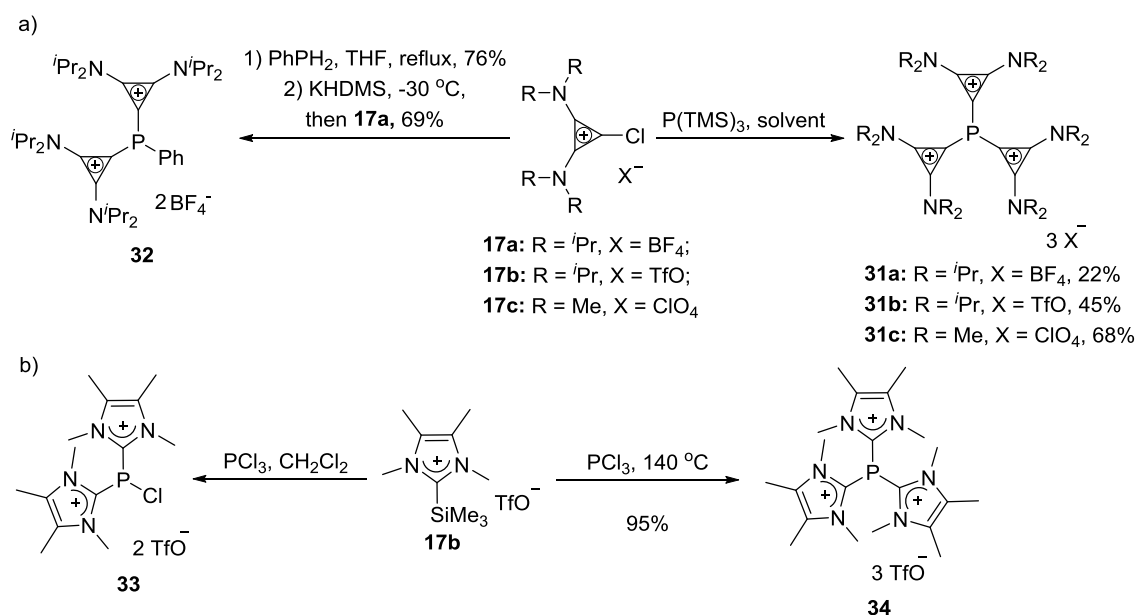
Monocationic phosphines are relatively common and can be prepared via the reaction of strong N-, P-, or C-based Lewis bases with dialkyl- or diaryl-chlorophosphines.^[31, 46-49] Dicationic, and specifically tricationic phosphines of the general formula $[\text{L}_3\text{P}]^{3+}$ are much more scarce.^[48] In 1991, Weiss *et al.* reported the syntheses of di- and tri-cations **26**, **27** and **28** by reaction of PCl_3 with DMAP or DBN.^[50] Similar reactions for the synthesis of **29** were subsequently reported by Bertrand and coworkers in 1994 (Scheme 12a).^[51] It should be pointed out that only spectroscopic evidence has been reported for these compounds. Later in 2010, Lammertsma and coworkers reported a trication **30** by reaction of PCl_3 and 3,5-dimethyl-1-trimethylsilylpyrazole in the presence of TMSOTf (Scheme 12b). In this compound the positive charges are evenly distributed over two phosphorus centers. Although **30** was extremely moisture-sensitive, it appeared to be indefinitely stable at ambient temperature in a dry inert atmosphere and have also been characterized in the solid state.^[52]



Scheme 12. Halide displacement from chlorophosphines by amines to form cationic phosphines.

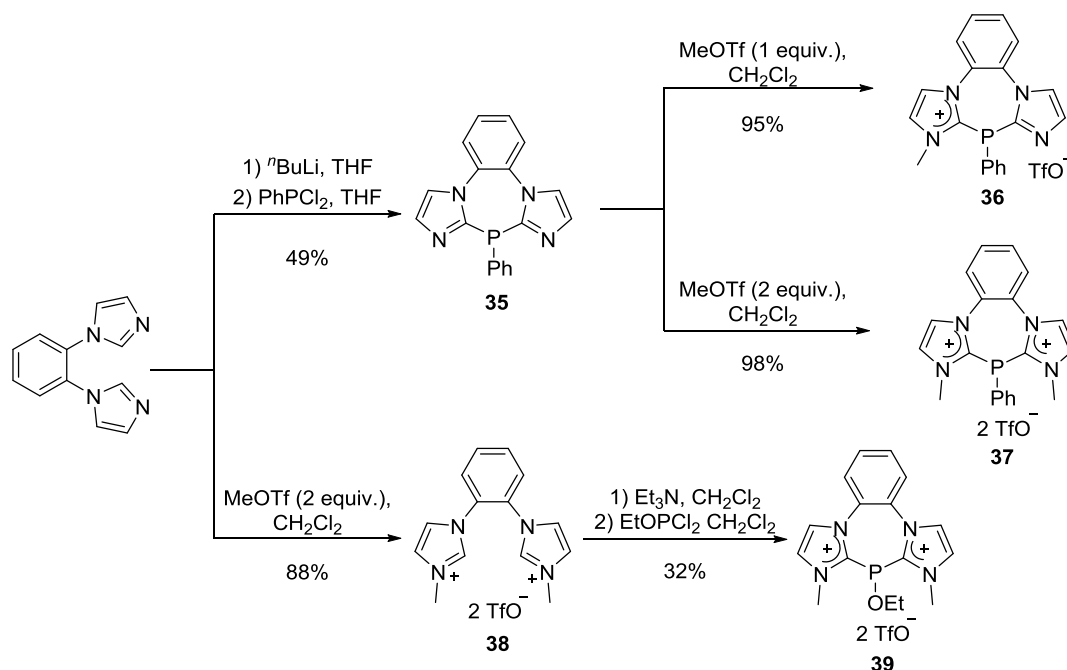
In 2011, our group described for the first time the isolation and structural characterization of the elusive $[(\text{carbene})_3\text{P}]^{3+}$ species **31** (carbene = cyclopropenylydene) by use of an alternative synthetic approach, based on the use of an unprecedented “reverse electron demand” onio-substituent transfer strategy. Instead of using silylated bases and PCl_3 as starting materials, the alternative conceivable reaction partners, silyl-substituted phosphines and chlorocyclopropenium salts were used in this transformation. 1-Chlorocyclopropenium cations were the key precursors for this synthesis instead of the more common chloroimidazolium salts mainly due to the following beneficial factors: (a) an enhanced tendency to undergo nucleophilic attack at the chlorinated carbon;^[53] (b) the smaller steric hindrance derived from a carbene embedded in a three membered ring that facilitates the coordination of several of these ligands to the same central atom;^[54-57] (c) the stronger σ -donor and weaker π -acceptor properties of cyclopropenylenes as compared with NHCs. Note that the net donation from the carbene ligand must compensate for the continuous increase of formal positive charge on the phosphorus atom in order to allow the consecutive nucleophilic substitution process to take place.^[40, 58-59] Thus, by gentle heating of a mixture of 1-chloro-2,3-bis(dialkylamino)cyclopropenium salts with $\text{P}(\text{SiMe}_3)_3$, the desired P(III)-centered trications **31** were isolated as white or light orange solids in moderate to good yields (Scheme 13a). Dication **32** could also be prepared by a two-step sequence. First, condensation of the readily available chlorocyclopropenium tetrafluoroborate **17a** with PhPH_2 in refluxing

THF afforded monocationic salt in 76% yield. Deprotonation of this salt with KHDMS at $-30\text{ }^{\circ}\text{C}$ and *in situ* trapping of the phosphalkene intermediate with a second equivalent of **17a**, finally yielded **32** as an air and water stable white solid. Consistent with the X-ray data, density functional calculations indicate that these compounds, despite their high positive charge, still feature a nonbonding electron pair on the P-atom (HOMO) and a very low-lying LUMO, depicting them as poor σ -donors and excellent π -acceptors.^[60] In 2015, Weigand *et al.* reported the synthesis of dication **33** and trication **34** by a similar strategy. In contrast to **31**, trication **34** is not able to coordinate metal fragments (Scheme 13b).^[61]



Scheme 13. Synthesis of [L₃P]³⁺ cations.

Finally, it worth to mention that the preparation of bisimidazolium salts **37** has been reported by Chauvin group using a double methylation of **35** with MeOTf.^[62-63] Alternatively, the addition of two equivalents of MeOTf to 1,2-di(*N*-imidazolyl)benzene afforded the dicationic salt **38** in 88% yield. Subsequent addition of one equivalent of dichloro(ethyl)phosphite in the presence of Et₃N (2 equiv.) afforded diamidiniophosphinite **39** in 32% yield, which is expected to be a really electron poor ligand (Scheme 14).^[30]



Scheme 14. Alternative routes to imidazolium-substituted polycationic phosphines.

1.3.4 Electronic Properties of α -Cationic Phosphines

In phosphines the non-shared electron pair at phosphorus accounts for their σ -donor ability, while the $\sigma^*(\text{P-C})$ orbitals are responsible for the π -acceptor properties. A formal increment of the electronegativity of one of the R groups on phosphorus is expected to lower the energy of all the molecular orbitals of the resulting phosphine. As a consequence, the resulting phosphine must behave as a poorer σ -donor, but also as a better π -acceptor ligand (Figure 1a). Regarding α -cationic ligands, the positive charges directly connected to the phosphorus atom can be considered as very strong electron withdrawing substituent and for this reason, decreased σ -donation and increased π -accepting properties on the resulting phosphines are expected (Figure 1b). Moreover, most positively charged substituents are aromatic rings containing empty low lying π^* orbitals, which are able to overlap with those of the phosphine that have adequate symmetry as is the case of the P electron pair. This also withdraws electron density from the phosphorus.^[24]

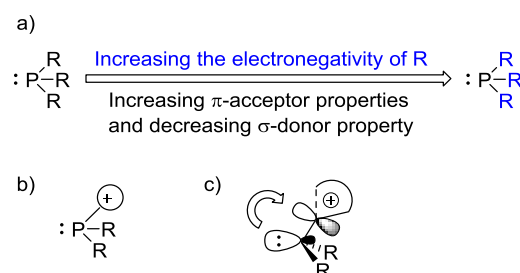


Figure 1. Molecular structure diagram for the explanation of electronic properties of α -cationic ligands.

The electronic properties of phosphine ligands were evaluated by Tolman by measuring the carbonyl stretching frequency $\tilde{\nu}(\text{CO})$ of the nickel complexes $[\text{Ni}(\text{CO})_3\text{L}]$ (L= monodentate phosphine ligand).^[64-65] This frequency depends on the combination of σ -donating and π -accepting character of L with respect to the metal center. Electron density donated by L to the metal enhances back donation from the metal center into the LUMO orbital of the CO ligand, which is the antibonding π^* (CO) orbital, leading to a decrease of $\tilde{\nu}(\text{CO})$. Strong donation from the phosphine thus corresponds to a lower carbonyl stretching frequency. Compared with Ph_3P and $(\text{PhO})_3\text{P}$, the complexes containing cationic ligands **8d-f** result in $\tilde{\nu}(\text{CO})$ similar to those of phosphites (Table 1).^[31]

Table 1: Carbonyl stretching frequencies in $\text{RhCl}(\text{CO})(\text{L})_2$ complexes in the solid state.

Entry	Ligand	R	$\nu(\text{CO})^{[a]}$ $\text{LNi}(\text{CO})_3$
1	8d	Ph	2082
2	8e	<i>i</i> Pr	2075
3	8f	Cy	2078
4	Ph_3P		2069
5	$\text{P}(\text{O}^i\text{Pr})_3$		2076
6	$\text{P}(\text{OPh})_3$		2085

[a] Values in cm^{-1}

To avoid the use of highly toxic $\text{Ni}(\text{CO})_4$, a range of other metal complexes, for example *trans*- $[\text{RhCl}(\text{CO})\text{L}_2]$, have also been investigated as model to evaluate donor properties of ancillary ligands (Table 2). In general, analogous trends are observed,^[66] however, we have detected some contradictions.

Firstly, the donor ability of the cyclopropenium substituted phosphines slightly surpasses that of Ph_3P (entries 2-6 and 16) when compared on this scale. Moreover, introduction of two $-\text{CF}_3$ group on the ligand structure should weaken its donor properties; however, **20** seems to be better donor than $(\text{MeO})_3\text{P}$ according to the recorded $\tilde{\nu}(\text{CO})$ data (entries 7 and 17).

Additional not matching results have also been found in the pyridinium family of ligands, when the donor properties were evaluated by analysis of the CO stretching frequencies in *trans*- $[\text{RhCl}(\text{CO})\text{L}_2]$ complexes (Table 2, entries 9-14). For example, ligand **21h** that bears five CF_3 groups should be weaker electron donor than **21e** that shares the same skeleton but carries only one $-\text{CF}_3$ substituent (Table 2, entries 11 and 14). According to the CO stretching frequencies (**21e**: 2004 cm^{-1} vs **21h**: 2001 cm^{-1}), the trends seem to be the opposite.^[43]

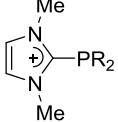
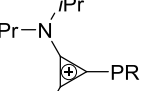
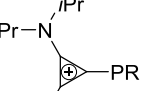
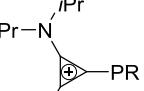
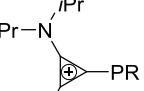
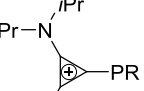
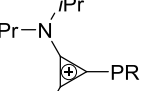
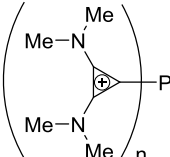
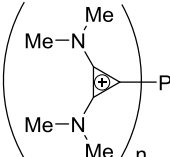
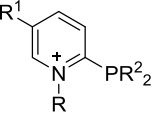
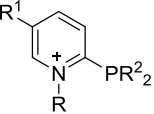
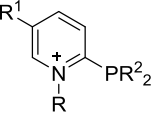
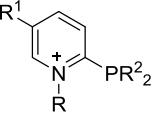
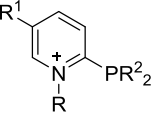
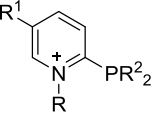
An explanation for this incongruence may come from the structure of the Rh complexes. For $\tilde{\nu}(\text{CO})$ analysis, the *cis*-located CO ligand may not be only sensitive to electronic effects, but also reflect geometrical distortions around the metal center owing to steric hindrance or through-space interactions between the CO and the other ligands. These distortions influence the overlap of the related CO orbitals and therefore, they decrease the wave number measured by IR spectroscopy. In fact, some structural distortions from the ideal square planar structure could be observed in the solid state of related rhodium carbonyl complexes.^[67-69]

An alternative experimental technique to rank the donor properties of phosphines is the determination of their oxidation potentials $E_p(\text{ox})$ by cyclic voltammetry.^[70-72] Electron-rich phosphines are easier to oxidize than electron-deficient ones and, as a consequence, the former should exhibit lower oxidation potentials than the latter if the orbital containing the electron pair is of similar shape, which is normally the case. This classification, although used to a lesser extent than the Tolman scale, has several intrinsic advantages; namely, it does not require the preparation of any metal-carbonyl complex to carry out the measurements and therefore it is also formally independent of steric factors.^[24]

Hence, the oxidation potential $E_p(\text{ox})$ of all these compounds were determined by cyclic voltammetry.^[73-74] These data follow the expected tendency and suggest that ligands **18a**, **18f** and **18g** were donor abilities similar to that of $(\text{MeO})_3\text{P}$, while **20**, **31** and **32** are even weaker donors than phosphites. This new ranking is in complete agreement with experiments on the catalytic activity of Au or Pt complexes bearing these ligands.

In addition, a quite complete Tolman stereoelectronic map has recently been reported by our group,^[24] combining experimental TEPs together with calculated ones employing Gusev's method for both cationic and neutral phosphines (Figure 2).^[75] It demonstrates that the overall donor ability of cationic phosphines **8a**, **18** and **32** are similar or slightly weaker than those depicted by typical phosphites. Therefore, they might be used as interesting phosphite surrogates in catalytic transformations. Even more interesting is the TEP estimated for **31** (2111 cm^{-1}). This value reveals that **31** can be ranked as weaker donors than any phosphite ligand; only the highly reactive PF_3 and $\text{P}(\text{CF}_3)_3$ were similar electronic properties. However, in sharp contrast to these polyfluorinated phosphines, **31** is easy to handle, air-stable solid. It is of note that the predicted donor endowment of bisimidazolium-substituted phosphines **39** is characterized by a calculated TEP of 2115 cm^{-1} and, hence, it is expected to be the weakest donor along the complete series. Unfortunately, no metal complex bearing this ancillary ligand has been prepared to date.^[24, 30] The lack of electron density at the phosphorus atom probably inhibits its coordination chemistry.

Table 2: Carbonyl stretching frequencies in RhCl(CO)L₂ complexes in the solid state and electrochemical redox potential of the ligands. The values of commonly used phosphorus ligands are also included for comparison.

Entry	Ligand	R	ν (CO) ^[a] RhCl(CO)L ₂	$E_{p_{ox}}$ ^[b]	
1	8d		Ph	2003	-
2	18a		Ph	1971	1.207
3	18b		Cy	1968	- ^[c]
4	18d		<i>p</i> -(Me)C ₆ H ₄	1969	- ^[c]
5	18e		<i>p</i> -(F)C ₆ H ₄	1976	1.246
6	18f		<i>p</i> -(MeO)C ₆ H ₄	1969	1.040
7	20		3,5-di(CF ₃)C ₆ H ₄	1991	1.548
8	31		<i>n</i> = 3	-	2.062
9	32		<i>n</i> = 2	-	1.541
10	21a		R = Me, R ¹ = H, R ² = Ph;	1996	1.398
11	21d		R = Me, R ¹ = F, R ² = Ph;	1994	1.355
12	21e		R = Me, R ¹ = CF ₃ , R ² = Ph;	2004	1.436
13	21f		R = Me, R ¹ = F, R ² = Cy;	1982	1.297
14	21g		R = Me, R ¹ = OMe, R ² = Cy;	1974	1.267
15	21h		R = Et, R ₁ = CF ₃ , R ₂ = 3,5-(CF ₃) ₂ (C ₆ H ₃)	2001	1.578
16		Ph ₃ P		1979	0.687
17		(MeO) ₃ P		2011	1.287
18		Cy ₃ P		1943	0.542
19		^t Bu ₃ P		-	0.534
20		[<i>p</i> -(MeO)Ph] ₃ P		-	0.520
21		[<i>p</i> -(F)Ph] ₃ P		1943	0.502

[a] Values in cm⁻¹. [b] Oxidation peak potentials reported in V. Calibrated versus Cp^{*}₂Fe/Cp^{*}₂Fe⁺ ($E_{1/2}$ = 0.24 V), Bu₄NPF₆ (0.1 M) in CH₂Cl₂. [c] Not determined.

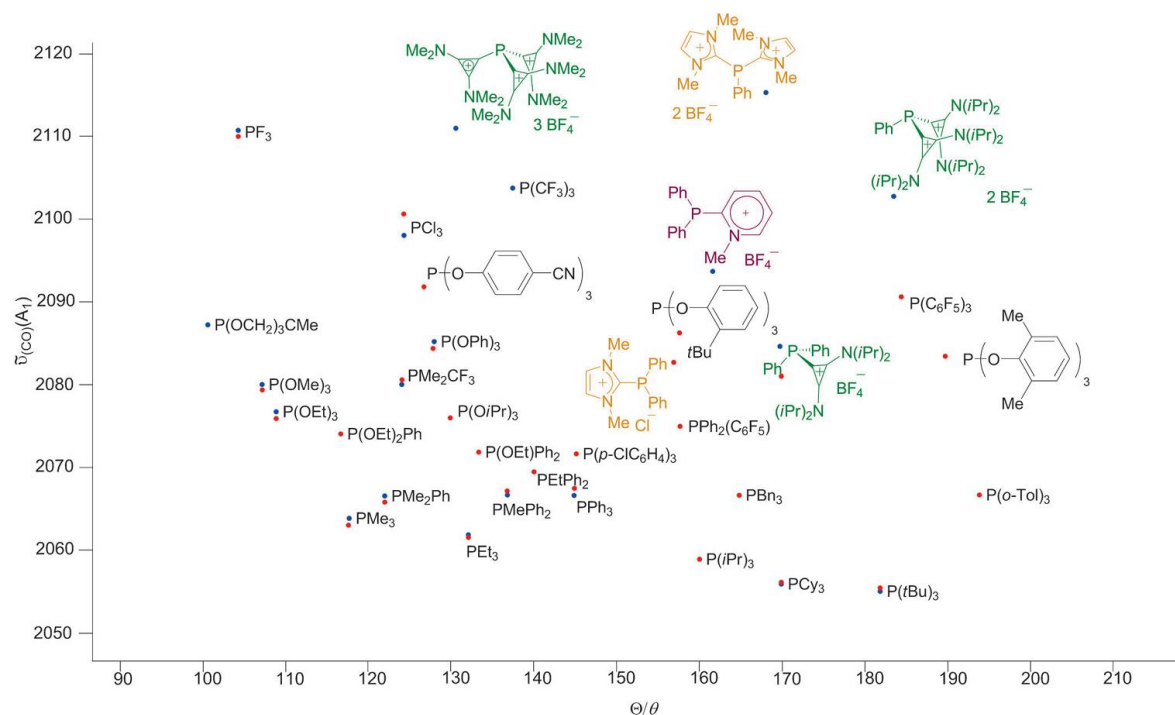
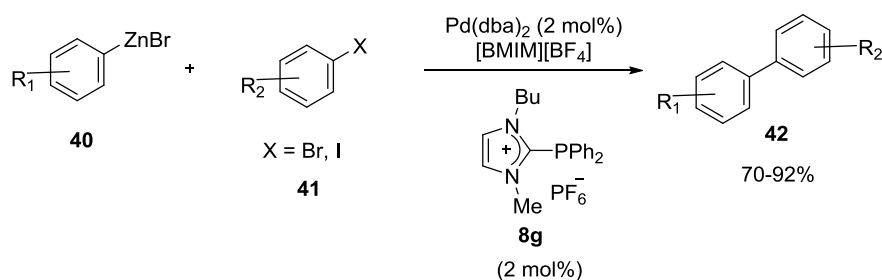


Figure 2. Tolman stereoelectronic map for neutral and cationic phosphines.

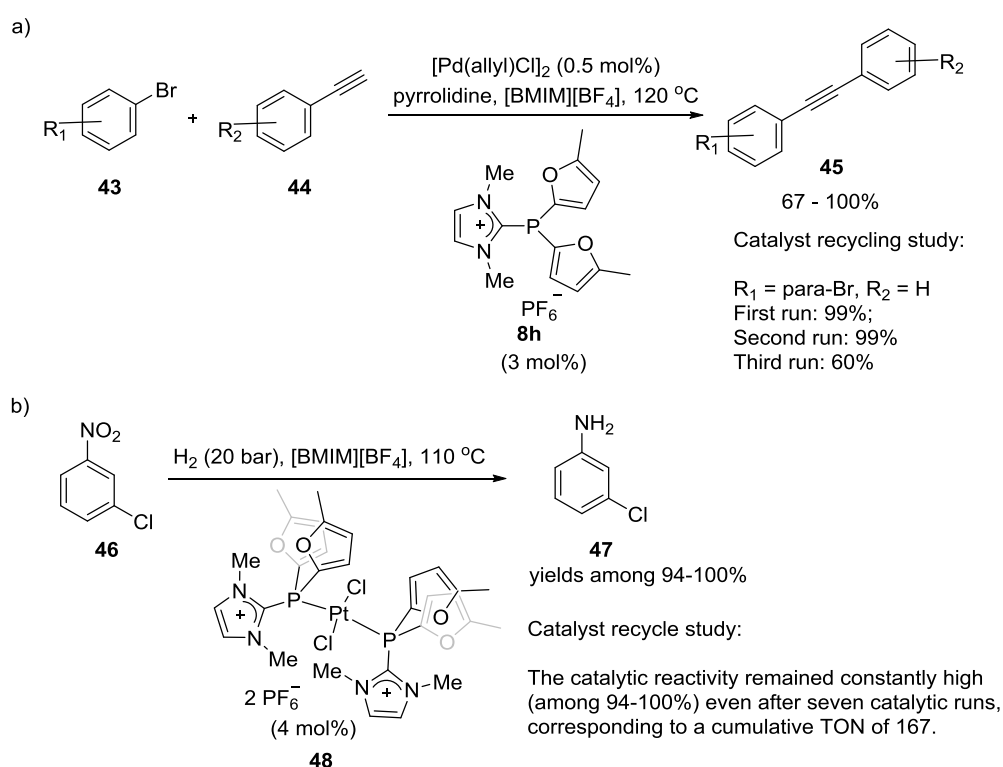
1.3.5 Applications of Cationic Phosphine Ligands.

Pioneering research in the area of α -cationic phosphines was focused on the synthesis of phosphite mimics with high solubility in ionic liquids. The derived catalysts could benefit from the recycling opportunities provided by these ligands. For example, Knochel *et al.* reported that in the presence of the cationic phosphine **8g**, the use of an ionic liquid/toluene biphasic solvent system allows for fast palladium catalyzed cross coupling reaction between organozinc reagents and aryl iodides (Scheme 15). The work-up of these reactions is remarkably simple, since the ionic liquid phase containing the palladium catalyst is separated by decantation from the toluene phase. Attempts to reuse the palladium catalytic system show that after the third cycle, a significant decrease in yield is observed (20% lower yield and triple reaction time).^[76]



Scheme 15. The application of cationic ligands in Negishi coupling.

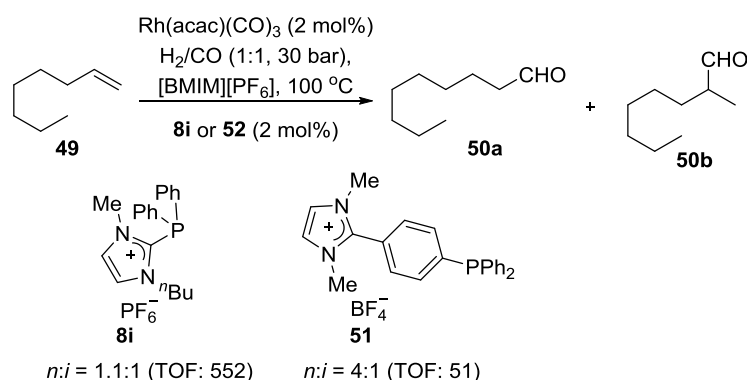
Andrew and coworkers have investigated the catalytic activity of a related ligand **8h**, which also exhibited very strong π -accepting character, in two transformations, both in an ionic liquid phase (Scheme 16a and 16b). In the first of these two reactions, it was observed that the increase of the π -acceptor character in ligand **8h** was beneficial for the alkylation reaction of aryl bromides with phenylacetylene. The catalytic activity decreased after catalyst recycling due to the sensitivity of ligands to protonation in the ionic phase. Moreover, the accumulation of a large excess of acidic pyrrolidinium bromide might promote the C-P bond cleavage through the protonation of the carbenic 1,3-dimethylimidazol-2-ylidene moiety of the ligand at the relatively high temperatures employed. Multiple recycling of the catalyst in non-acidic media could be achieved for the platinum-catalyzed hydrogenation reaction of *m*-chloronitrobenzene to the corresponding aniline. The selectivity of the reaction is also improved by decreasing the undesirable formation of dehalogenation products. The system was recycled six times without noticeable metal leaching in the organic phase, and no loss of activity.^[77]



Scheme 16. The application of cationic ligands in alkylation and hydrogenation.

Another transformation where imidazolium phosphines have found application is the hydroformylation of alkenes (Scheme 17). Stelzer and coworkers have reported the synthesis of two cationic ligands **8i** and **51**, both of which have been tested in the hydroformylation of 1-octene in the ionic liquid $[BMIM][PF_6]$. In these experiments, the active catalyst was

prepared *in situ* by mixing $\text{Rh}(\text{CO})_2(\text{acac})$ with two equivalents of the ligand in the ionic liquid $[\text{BMIM}][\text{PF}_6]$. The reaction was carried out at $100\text{ }^\circ\text{C}$ and 30 bar synthesis gas pressure ($\text{CO}:\text{H}_2 = 1:1$) for 1 h. The biphasic hydroformylation of 1-octene under these conditions showed significantly higher turnover frequency (TOF) values with ligand **8i** (TOF 552, linear/branched ratio = 1.1), in which the positive charge is near to the P-atom. Thus, these data demonstrated that the increased π -acceptor character of α -cationic phosphines make the catalyst superior in this transformation^[78] In addition, it should be noted that in both cases no significant leaching of the Rh catalyst into the almost colorless organic layer was observed.^[79]

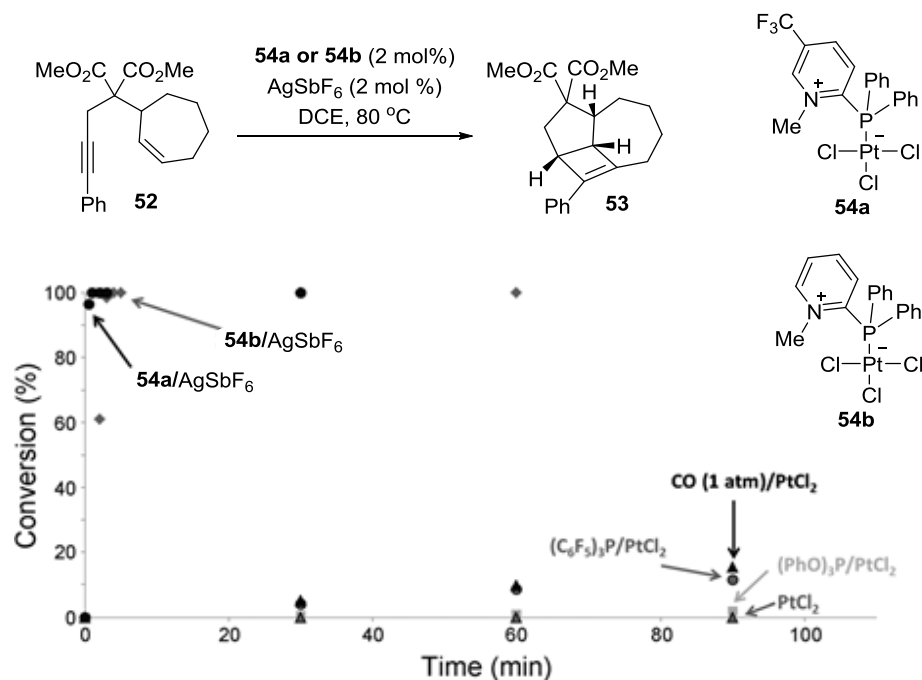


Scheme 17. The application of cationic ligands in hydroformylation.

As already shown in Table 2, most cationic ligands are more electron-poor than neutral phosphines and many even surpass phosphites in this regard. Even more intriguing than just preparing phosphite surrogates is to utilize their strong π -accepting properties as ancillary ligands in transition-metal catalysis. These phosphines withdraw electron density from the metals they coordinate to and, consequently, they are expected to improve catalytic processes whenever high π -acidity at the metal center is required, such as in π -acid catalysis promoted by Pt(II) and Au(I) complexes.

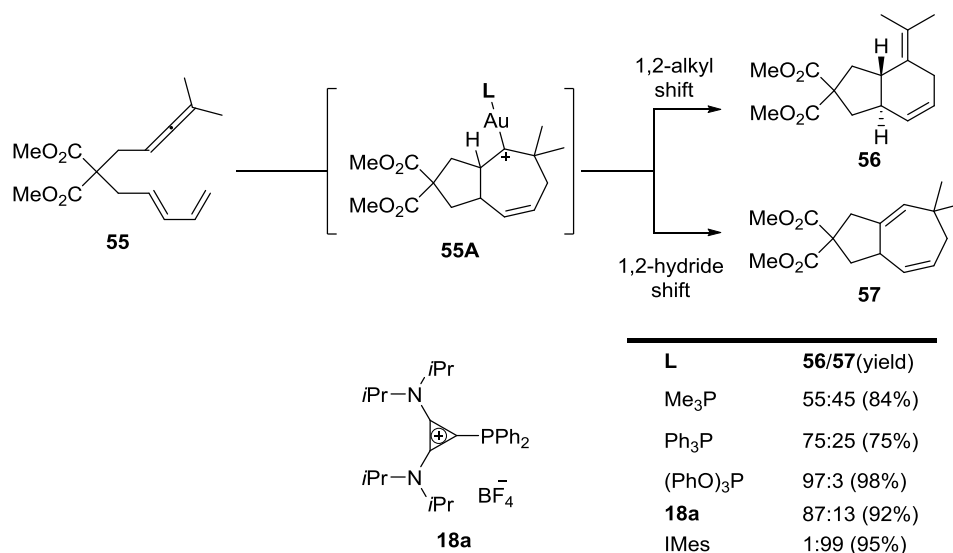
As mentioned before, N-alkyl/aryl pyridiophosphines are also quite weak σ -donor and quite strong π -acceptor ligands due to the very low lying π^* orbitals in the pyridinium cation. These attributes confer a substantially enhanced π -acidity to the derived Pt(II) and Au(I) complexes which, as a result, also show improved ability to activate alkynes towards nucleophilic attack, when compared to other monocationic ligands. This superior performance has been demonstrated for several mechanistically diverse Pt(II) and Au(I) catalyzed transformations such as the hydroarylation of propargyl aryl ether to chromene and the cycloisomerization of enynes to cyclobutenes (Scheme 18). In particular, the study of this reaction allows a direct comparison between pyridiophosphines and commercially available π -acceptor ligands. As can be seen in Scheme 18, CO (1 atm), which is the paradigmatic π -acceptor ligands,

performed better in terms of reactivity than any the other ligands tested: $(\text{PhO})_3\text{P}$ and $(\text{C}_6\text{F}_5)_3\text{P}$. However, catalysts **54a** and **54b** were much more efficient and cyclobutene **53** could be obtained in excellent yields after only few minutes.^[43]



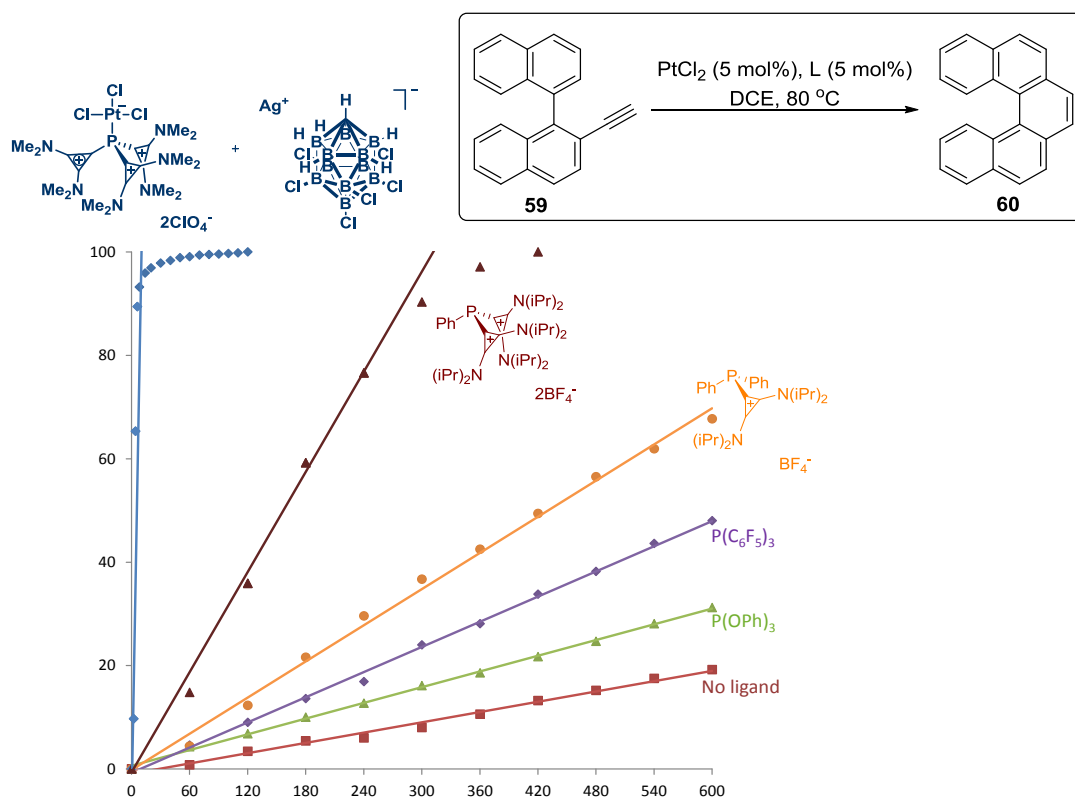
Scheme 18. Ligand effect on the Pt-catalyzed cycloisomerization of enyne to cyclobutene

Apart from the reaction above, the cyclization of **55**, which is known to be extremely dependent on the global electron density at the gold atom,^[80-81] provides an additional measurement for donor properties of the ligands. π -Acidic ligands **L** can enhance the carbocationic nature of intermediate **55A**, thus promoting ring contraction by a 1,2-alkyl shift to afford **56**. In contrast, the formation of **57** through the 1,2-hydride migration process is favored by strongly σ -donating ligands at the gold center that increase the carbene character of **55A**. As illustrated in Scheme 19 the selectivity obtained using cationic ligands with cyclopropenium group is comparable to that of phosphines.^[41]



Scheme 19. Comparison of the selectivity of different ligands in the gold-catalyzed cyclization of allene diene.

Polycationic phosphines have also proven to be excellent π -acceptor ligands in catalysis. A catalyst intensively studied in our group is complex **[31]**[PtCl₃]. The three positive charges of this ligand dramatically enhance the ability of Pt to activate π -systems toward nucleophilic attack. As a consequence, a remarkable acceleration of hydroarylation reaction was observed when compared with other classical π -acceptor ligands such as P(OPh)₃ or P(C₆F₅)₃ (Scheme 20).^[82] Although the Pt-catalyst derived from the trication **31** is more reactive than those derived from phosphites or fluorophenylphosphines, this catalyst still has some limitations: (a) only Pt(II) has been successfully coordinated to ligand **31**, which severely limits its range of application; (b) stereochemical properties of **31** are difficult to modulate and (c) the low solubility of **31** in organic solvents demands the use of non-coordinating apolar anion.



Scheme 20. Cyclization of 2-Ethynyl-1,1'-binaphthalene into pentahelicene as model reaction.

1.4 Summary I

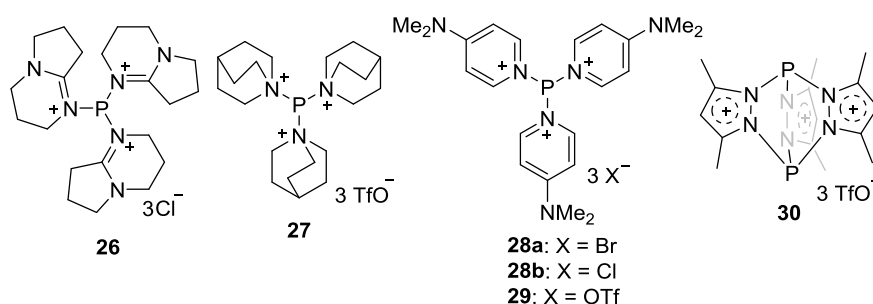
α -Cationic ligands originally received attention because of their intrinsic advantages regarding catalyst recycling. However, our group has demonstrated that the strong π -acceptor character induced at the P-atom by the positive charge can also be beneficial in catalytic cycles where the rate determining step is accelerated by increasing the Lewis acidity at the metal center. Further development for this type of ligands are expected in two directions. First, the synthesis of even more electron-poor cationic ligands is interesting because it may help to develop new reactions that do not proceed with traditional catalysts. In addition, the coordination chemistry of polycationic ligands should be further studied, since ligands with two or three positively charged substituents at α -position only coordinate Au(I) and Pt(II) so far. Once the coordination was expanded to a diverse metal scope, an entire inventory of new reactions might be developed.

2 Bis- and Trispyrazoylborate/methane-Stabilized P(III)-Centered Cations

2.1 Introduction

As mentioned before, our group have prepared a series of α -cationic phosphines that have C-based substituents at P-atom. These ligands are stable towards oxygen and moisture. Moreover, they show superior performance in π -acid catalysis due to their excellent π -acceptor character induced by the positive charges.^[24, 27, 36, 41, 82-83]

To further improve the π -acceptor character of these phosphines, α -cationic phosphines containing N-based substituents might be appropriate options because N is more electron negative than C. Specifically, regarding P-based trications stabilized by N-bases, the precedents reported in the literature are **26-29**, which were obtained by reaction of PCl_3 with DMAP, DBN or guanidine; however, their connectivity was only evidenced by spectroscopy.^[50-51] Only recently, a solid structure of trication **30**, in which the three positive charges are equally distributed on two phosphorus centers, has been reported by Lammertsma and coworkers. Unfortunately, this compound is highly sensitive towards moisture and air, and therefore its coordination chemistry remains unexplored.^[52]



Scheme 21. Representative polycationic phosphines.

In this regard, we envisioned that the replacement of monodentate ligands by chelating ones or even scorpionates should be beneficial to mitigate their inherent instability and obtaining more amenable P-centered polycations. Moreover, the introduction of a remote negative charge on the ligand architecture might additionally increase the stability of the resulting complexes through attractive Coulombic interaction between the anionic ligand and the positively charged phosphorus atom.^[84] This rationale makes bis-/trispyrazoylmethane and

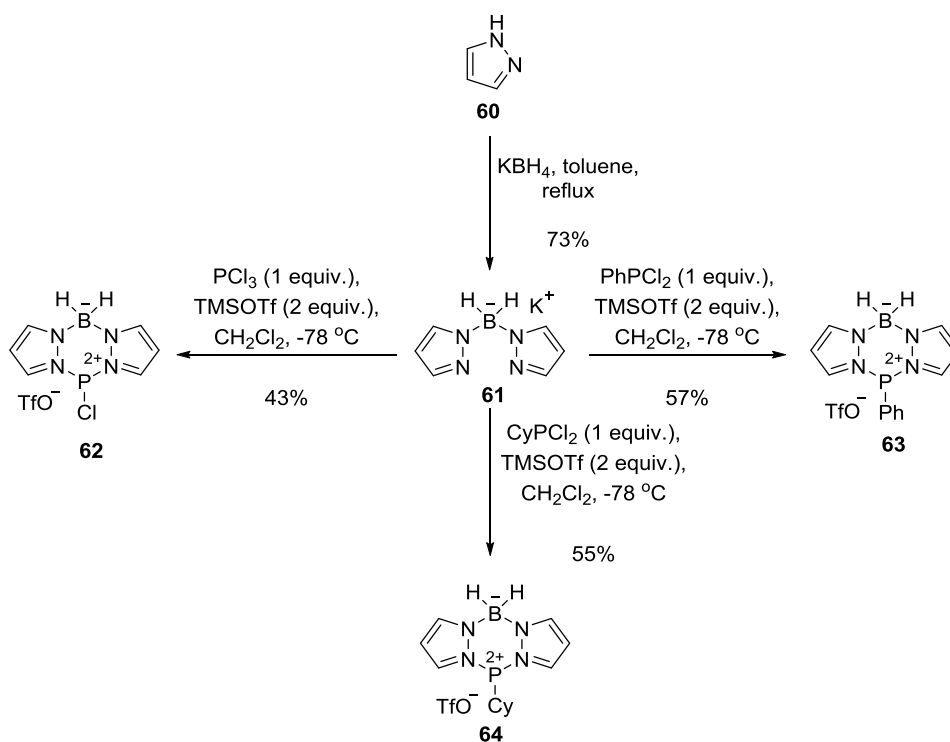
bis-/trispyrazoylborate ligands ideal candidates to attempt the synthesis of more robust P-centered polycations and study their coordination properties.

2.2 Results and Discussion

2.2.1 Synthesis of bis- and trispyrazoylborate-Stabilized P-centered Cations

To test this hypothesis, we embarked on the preparation of the desired cationic phosphanes using pyrazolyl borate ligands.^[50-51] Our starting material, potassium bispyrazoyl borate **61** was prepared from the condensation of pyrazol (4 equiv.) and NaBH₄ (1 equiv.) in toluene.^[85] Suspensions of potassium bispyrazoyl borate **61** in CH₂Cl₂ were then treated with three different chlorinated phosphines (PCl₃, PhPCl₂, and CyPCl₂) in the presence of TMSOTf (2 equiv.) to afford white to yellow precipitates that could be easily separated from the reaction mixtures in all cases. Their ³¹P-NMR spectra showed signals at $\delta = 86.2, 87.1, \text{ and } 102.8$ ppm, respectively, which are consistent with the desired coordination of **61** to the P center and formation of **62-64** (Scheme 22). Subsequently, the expected connectivity could be unambiguously confirmed by X-ray diffraction of a single crystal of **62** (Figure 3).

Remarkable features of **62** are the P1-N1 and P1-N2 bond distances [1.7474(11) Å and 1.7500(11) Å, respectively] that are only slightly longer than those found in trispyrazoylphosphine [1.714(4) Å], despite their dative nature.^[86] Likewise the degree of pyramidalization at phosphorus (71.7%) is notable which clearly indicates retention of a nonbonding electron pair on this atom.^[87] Also interesting is the P1-O1 distance (3.139 Å), which is shorter than the sum of the van der Waals radii, as well as the nearly linear arrangement observed for O1, P1, and N4 (171.8°). These two structural parameters indicate donation of electron density from the triflate anion to a $\sigma^*(\text{P1-N4})$ orbital of the cation which is indicative of some Lewis acid character at the phosphorus atom.



Scheme 22. Synthesis of **62-64**.

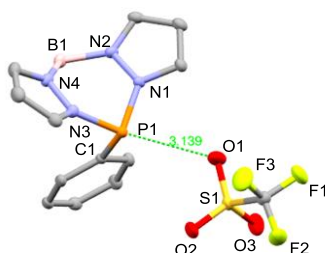
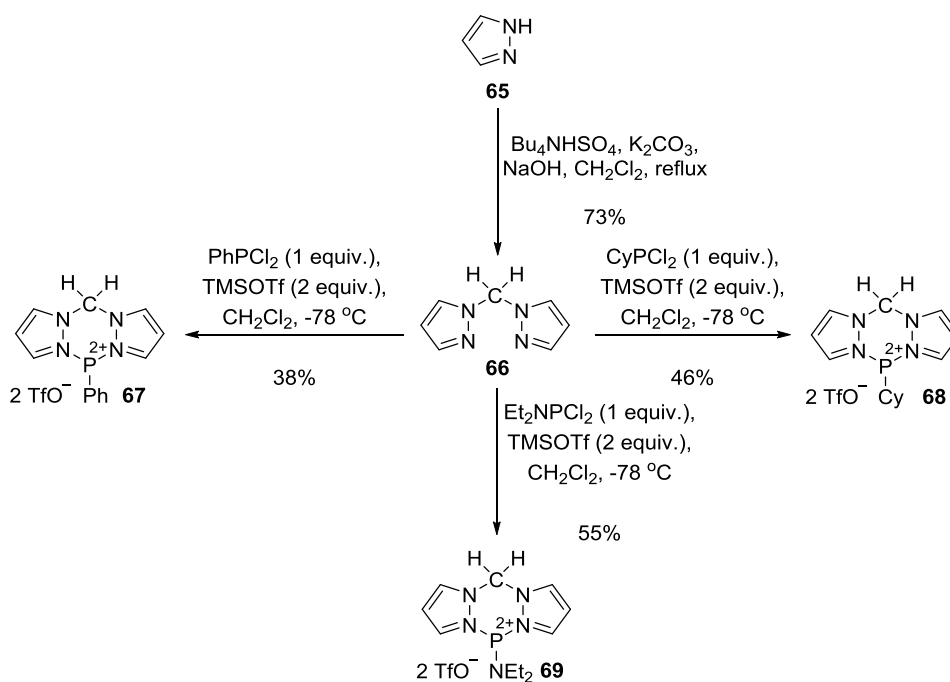


Figure 3. Molecular structure of **63** in the solid state (hydrogen atoms and solvent molecules removed for clarity; ellipsoids set at 50% probability)

Once the preparation of compounds **62-64** was achieved, we evaluated the synthesis of dicationic species by employing the neutral bispyrazolylmethane ligand **66**, which was prepared from pyrazole and CH_2Cl_2 in the presence of $n\text{Bu}_4\text{NHSO}_4$ and K_2CO_3 .^[88] Treatment of a CH_2Cl_2 solution of PhPCl_2 , CyPCl_2 , or $(\text{Et}_2\text{N})\text{PCl}_2$ with an equimolar amount of **66** and two equivalents of TMSOTf induced the slow precipitation of white solids **67-68**, which were found to be analytically pure. Their ^{31}P NMR spectra displayed resonances at $\delta = 85.8$, 110.1, and 107.8 ppm, respectively, which support the coordination of **66** to the P-center (Scheme 23 and Figure 4).

Quite intriguing are the structural features observed in the molecular structure of **69** (Figure 5). In this compound both P1-N1 and P1-N2 bond lengths [1.8376(12) and 1.8328(13) Å] are clearly elongated compared with those in **67** [1.7581(13) and 1.7692(13) Å]. On the other hand, the P1-N5 distance [1.6264(13) Å] is shorter than expected for a typical covalent

P-N bond. Moreover, the nitrogen atom shows a planar trigonal environment (sum of angles = 360°) and the C1-N5-C1 plane bisects the N1-P1-N3 angle.



Scheme 23. Synthesis of **67-69**.

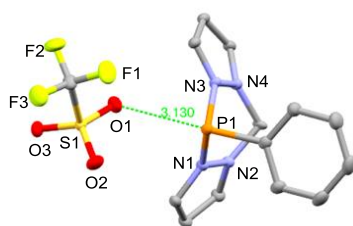


Figure 4. Molecular structure of **67** in the solid state (hydrogen atoms, solvent molecules and one triflate anion removed for clarity; ellipsoids set at 50% probability).

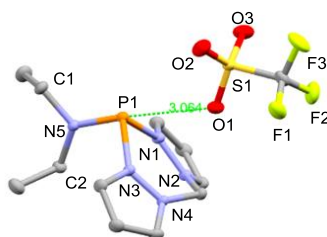
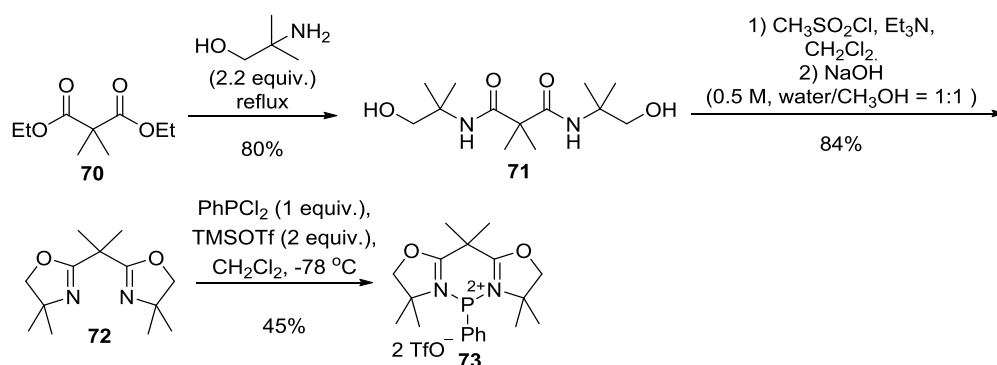


Figure 5. Molecular structure of **69** in the solid state (hydrogen atoms, solvent molecules and one triflate anion removed for clarity; ellipsoids set at 50% probability).

The isolation of **67-69** suggests that similar compounds may be prepared in a related manner employing other neutral bidentate ligands instead of pyrazolylmethanes. Particularly interesting is the possible use of bisoxazolidines^[89] (BOX ligands) since they might offer a fast and highly modular route for the preparation of chiral enantiopure P-centered dication.

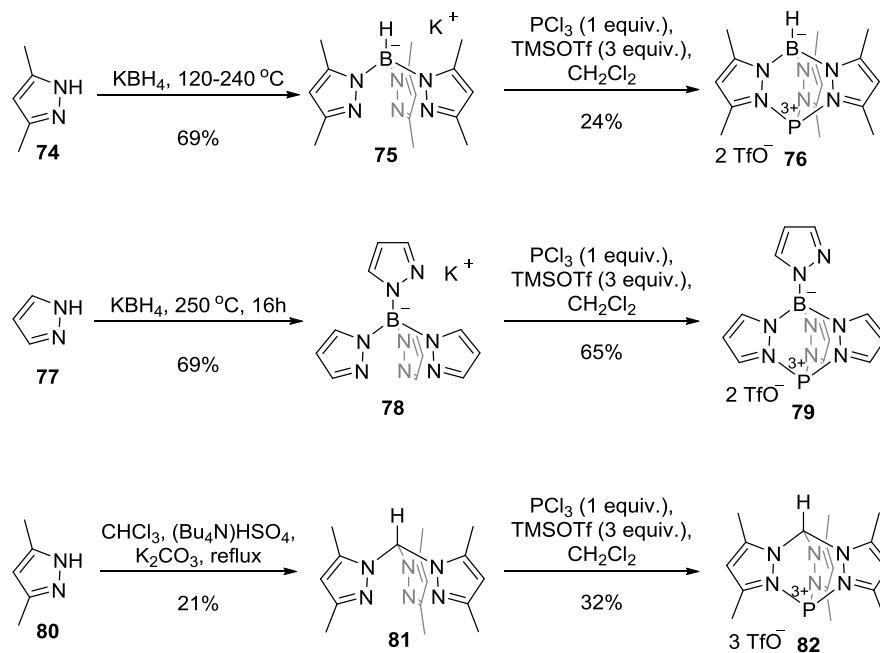
We were pleased to see that bisoxazolidine **72** indeed reacted with PhPCl_2 , under the conditions already developed for bispyrazoyl methane ligands, affording the desired complex **73** as a crystalline material in moderate yield. Although the limited data quality impeded satisfactory structure refinement, X-ray diffraction of a crystal **73** was good enough to confirm the structure of **73** (Scheme 24).



Scheme 24. Synthesis of **73**.

Finally, we also attempted the isolation of formal P^{3+} cations stabilized by scorpionate ligands. To this end, we chose tris(3,5-dimethylpyrazoyl)borate **75**^[90], tetra(pyrazoyl)borate **78**^[91], and tris(3,5-dimethylpyrazoyl)methane **81**^[92] as ancillary ligands, and treated them with PCl_3 and three equivalents of TMSOTf. The white solids that precipitated from the reaction mixture were crystallized from $\text{CH}_3\text{CN}/\text{Et}_2\text{O}$, affording compounds **76**, **79** and **82** in an analytically pure form. The ^1H NMR spectra of **76** and **82** showed only two singlets in the aliphatic region, indicative of C_3 symmetry of the newly formed complexes. Moreover, ^{31}P NMR resonances at 7.3 (**76**), -2.4 (**79**), and -9.9 (**82**) ppm also support a tridentate coordination of the pyrazoyl ligands to the central phosphorus atom in these compounds (Scheme 25). Single crystals suitable for X-ray diffraction analysis could be obtained for **76** and **79** confirming the proposed connectivities (Figure 6 and 7). It was observed that the P-N distances in **76** and **79** are practically identical to those observed for **63** and **67**. However, the geometry of the trispyrazoyl ligand produces a higher degree of pyramidalization at the phosphorus center that reaches 85.7% in **76** and 92.4% in **79**.^[87] In addition, each P atom is closely surrounded by three triflate anions in the unit cell. The P1-O1 distance in **79** is, as expected, the shortest among the complete series of compounds under study (2.734 Å), while the much longer P1-O1 contact in **76** (3.192 Å) must be attributed to the steric hindrance derived from the additional methyl groups on the pyrazol rings. The positive charges at P-atom efficiently stabilize the three $\sigma^*(\text{P}-\text{N})$ orbitals and thus, confer Lewis acid character to

the phosphorus atom. This explains the observed short distances between the central P-atom and the triflate anion in these compounds.



Scheme 25. Synthesis of **76**, **79** and **82**.

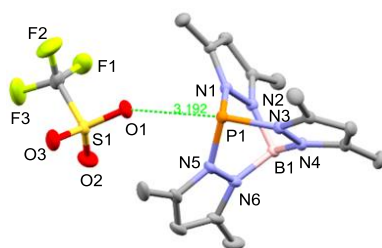


Figure 6. Molecular structure of **76** in the solid state (hydrogen atoms, solvent molecules and one triflate anion removed for clarity; ellipsoids set at 50% probability).

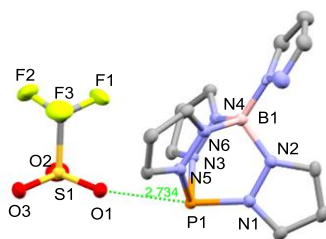


Figure 7. Molecular structure of **79** in the solid state (hydrogen atoms, solvent molecules and one triflate anion removed for clarity; ellipsoids set at 50% probability).

2.3 Electronic Properties

To better understand the electronic structure and bonding of these compounds, DFT calculations were performed at the BP86/6-311++G** level. The Wiberg bond index (W_i) on cation **63** was found to be 0.94 for the P1-C1 bond, but only 0.73 for both P1-N1 and P1-N3 bonds, which is in line with their dative nature. The computed charge at phosphorus was +1.23e (natural population analysis), which explained the low energy of the lone pair at phosphorus (HOMO-6; $E = -11.46$ eV) and of the antibonding $\sigma^*(\text{P-N})$ orbital (LUMO+1; $E = -5.99$ eV) that confers Lewis acidity at the phosphorus center (Figure 8).



Figure 8. Lone pair (HOMO-6, left) and low lying $\sigma^*(\text{P-N})$ orbital (LUMO+1, right) of **63**.

DFT calculations were again very useful to explain the structural features found in **69**. Figure 9 shows the shape of the HOMO in this cation. The P1-N5 bond exhibits significant π -bonding character due to the overlap between the σ^* (P-N) orbital (LUMO+1) and the electron lone pair on N5 (Figure 9). As a result, electron density is transferred from nitrogen to phosphorus and a partial double bond is established between these two atoms. Consequently, the P1-N5 W_i value increases to 1.13. On the other hand, the partial population of the antibonding orbital of 2e symmetry weakens the P-N bonds between phosphorus and pyrazol (W_i value of only 0.57) and lengthens them considerably (Figure 9).

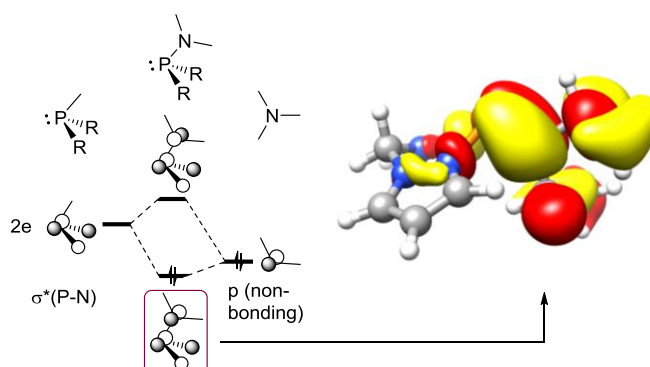


Figure 9. Fragment analysis of the HOMO of **69**.

2.4 Attempts of Coordination

The polycationic species were shown to display Lewis acid properties. Presumably for this reason, all attempts to use them as ligands resulted in either no reaction or decomposition. Moreover, despite their stability in argon for days at room temperature, once exposed to air, they decomposed immediately, demonstrating strongly hygroscopic properties.

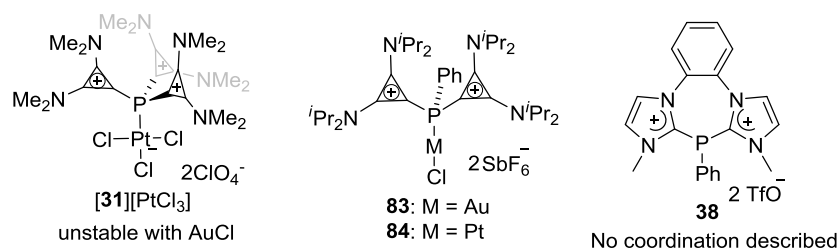
2.5 Summary II

In summary, making use of an –onium substituent transfer strategy, we have been able to isolate and structurally characterize several P-centered polycations stabilized by bis- and tris-(pyrazoyl)borate or methane ligands. In all of these compounds, the phosphorus center adopts a pyramidal environment, which is indicative of the presence of a lone pair mainly located on this atom. However, the high positive charge at phosphorus lowers the energy of this orbital to a level that makes it unavailable for donation. The same positive charge also stabilizes quite efficiently the $\sigma^*(\text{P-N})$ orbitals, thus conferring Lewis acid character to the phosphorus atom. This Lewis acidity is evident from the short contacts observed between the triflate anions and the phosphorus centers.

3 Dicationic Chelating Phosphines: Synthesis, Structure and Reactivity

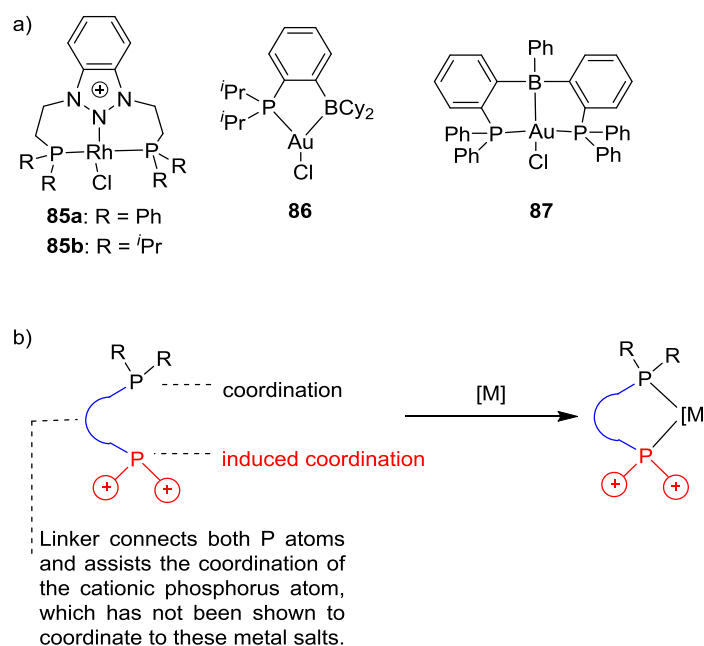
3.1 Introduction

α -Cationic phosphines have attracted increased attention during the past years due to the superior performance of the catalysts containing these ligands.^[24, 27, 93-94] However, the strongest cationic π -acceptor phosphines that can be prepared following this strategy, namely di- and tricationic ones, show little affinity to form coordination complexes and, until now, they have only been able to bind metal fragments that efficiently engage in back donation such as Au(I) and Pt(II). Our attempts, and that of others, to expand the coordination to other metal sources unfortunately failed.^[30, 60, 83]



Scheme 26. Coordination chemistry of polycationic ligands.

In an attempt to circumvent the intrinsic shortage of polycationic ligands and gain access to a broader repertoire of potential metal catalysts bearing these ligands, the introduction of an additional donating group was envisioned as an anchor to bring the cationic moiety into the vicinity of the metal and thus, induce its coordination. This strategy has been used previously to coordinate Lewis acidic centers such as boranes to metals (Scheme 27a).^[95-96] Another example of the use of this strategy is the coordination of N-heterocyclic nitrenium ions **85**^[97] after the introduction of chelating phosphorus atoms on their architecture (Scheme 27a), even though it is known that boranes or nitrenium cations by itself are not able to coordinate these metals. More intriguingly, some of these complexes display superior performance in catalysis due to the strong π -acceptor properties of the ligands they bear. In this regard, we reasoned that it might be possible to use a similar strategy to facilitate the coordination of the dicationic ligands to metals. Hence, we decide to prepare dicationic chelating phosphines bearing a latent $-PPh_2$ moiety, such as the ones described in Scheme 27b.

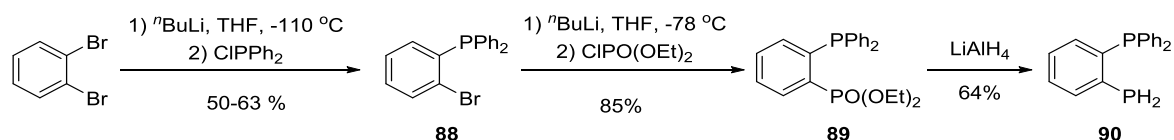


Scheme 27. Representative examples for induced coordination and the simplified structure of chelating polycationic ligands.

3.2 Synthesis

3.2.1 Synthesis of Chelating Dicationic Ligands

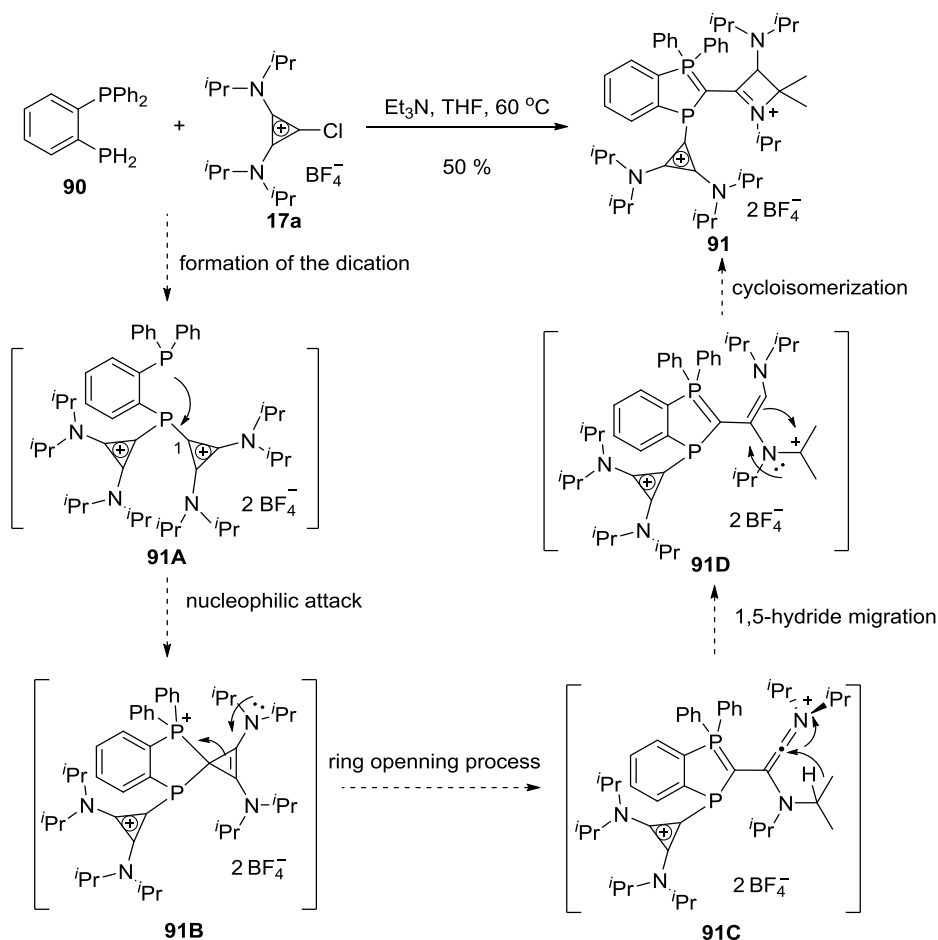
To put our idea into practice, we first prepared phosphine **90** from dibromobenzene in three steps according to a modified literature procedure (Scheme 28).^[98-99] First, monolithiation of dibromobenzene with ^{*n*}BuLi in dry THF at -110 °C followed by addition of Ph₂P-Cl afforded the corresponding monophosphinated product **88**. A subsequent second lithiation with ^{*n*}BuLi in dry THF at -78 °C followed by reaction with ClPO(OEt)₂ gave phosphonate **89** which was finally reduced with LiAlH₄ to diphosphine **90** in 64% yield.



Scheme 28. Synthesis of primary phosphine **90**.

Unfortunately, reaction of primary phosphine **90** with **17a** in the presence of Et₃N (2 equiv.) at 60 °C afforded an unexpected cyclic compound **91**, whose structure was confirmed by single X-ray diffraction analysis (Figure 10). Once the connectivity of **91** was elucidated, we concluded that probably the desired salt **91A** was formed as an intermediate, but an attack of the electron lone pair from the -PPh₂ moiety to C-1 of one cyclopropenium center, led to the formation of spirocyclic compound **91B**, which ring opens to afford intermediate **91C**.

Subsequent 1,5-hydride migration afforded intermediate **91D**, which cyclisomerized to **91** (Scheme 29).



Scheme 29. Proposed mechanism for the formation of **91**.

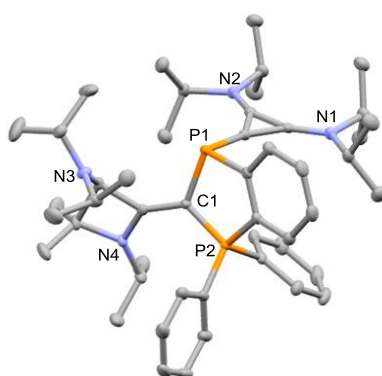
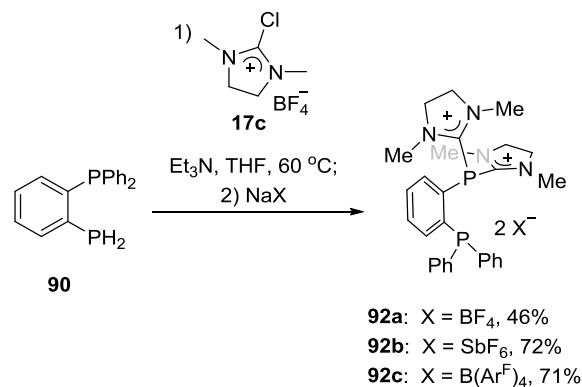


Figure 10. Molecular structure of compound **91** in the solid state. Thermal ellipsoids at 50% probability; hydrogen atoms, tetrafluoroborate counter anions and solvent molecules have been omitted for clarity.

Because the formation of the undesired compound **91** requires the attack of the electron pair from the P(neutral) atom to the 3-membered cyclopropenium ring, other cationic groups less prone to suffer from this attack were also tested. Thus, dimethyldihydroimidazolium groups

were selected as more appropriate substituents due to the less strained nature of these cycles. In fact, treatment of 2-chloro-3,5-dihydroimidazolium with primary diphosphine **90** in the presence of base easily provided the desired dication **92a**. Anion exchange gave access to dication **92b-c**, containing SbF_6^- and $\text{B}(\text{Ar}^{\text{F}})_4^-$ counter anions. The structure of dication **92b** was unambiguously confirmed by single X-ray diffraction analysis (Scheme 30 and Figure 11).



Scheme 30. The synthesis of dihydroimidazolium substituted dication **92**.

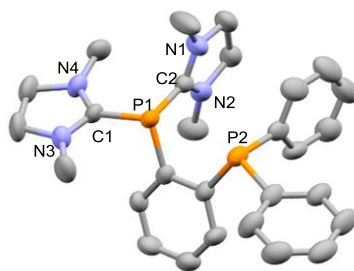


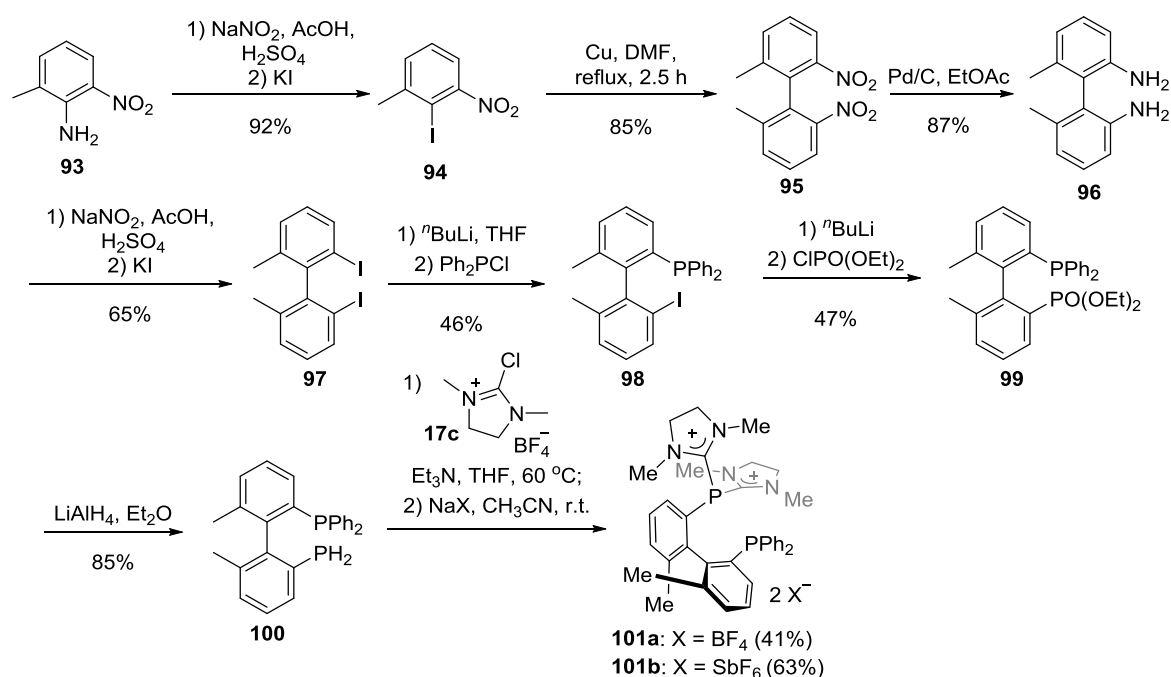
Figure 11. Molecular structure of compound **92b** in the solid state. Thermal ellipsoids at 50% probability; hydrogen atoms, hexafluoroantimonate counter anions and solvent molecules have been omitted for clarity.

As a structure modification of the basic architecture of dication **92**, our first goal was to replace the phenyl backbone by a biphenyl one that functions as a linker between the two phosphorus atoms. This was desirable for two reasons: (a) the increased distance and flexibility between the two phosphorus atoms may result in completely different reactivity, and (b) the species derived from a rotationally hindered biphenyl system could later be prepared in enantiopure form once the synthesis is optimized.

The route depicted in Scheme 31 was designed for the synthesis of dication **101**. Dianiline **96** was prepared in three steps according to a known literature procedure, consisting Sandmeyer reaction, Ullmann coupling,^[100] and the reduction of both nitro groups.^[100] Then **96** was subjected to Sandmeyer reaction conditions to afford the biaryl diiodide **97**, which was lithiated with $n\text{BuLi}$ in dry THF at -78°C followed by reaction with Ph_2PCl to afford the corresponding monophosphinated product **98**. Subsequent lithiation with $n\text{BuLi}$ in dry THF at -78°C ,

followed by reaction with $\text{ClPO}(\text{OEt})_2$ afforded phosphonate **99**, which was finally reduced by LiAlH_4 to deliver the desired diphosphine **100** in 85% yield. Treatment of this compound with 2-chloro-3,5-dihydroimidazolium **17c** in the presence of base easily provided the desired dication **101a**. Anion exchange allowed the access to dication **101b**, containing SbF_6^- counter anion.

The ^{31}P NMR spectra of both dications, **92** and **101**, consists of two doublets ($\delta_{\text{P}} = -8.5, -43.8$ ppm; $J_{\text{P-P}} = 212$ Hz for **92**, and $\delta_{\text{P}} = -14.7, -44.1$ ppm; $J_{\text{P-P}} = 86.7$ Hz for **101**), which can be attributed to the $-\text{PPh}_2$ and $[-\text{P}(\text{H}_2\text{Im})_2]^{2+}$ moieties, respectively. Single crystals suitable for X-ray structure determination were obtained (depicted in Figures 11 and 12). All C-P bond lengths from **92** and **101** are in accord with typical single bonds,^[101] but interestingly, the P1-P2 distance in **92** (3.076 Å) is shorter than in its neutral analogue 1,2-bis(diphenylphosphino)benzene (3.165 Å).^[102] This shortening might indicate a reduction of the repulsive interaction between the electron lone pairs on the two phosphorus atoms.



Scheme 31. The synthesis of dication **101a-b**.

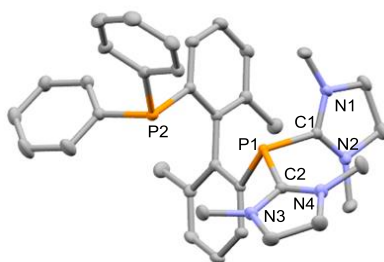
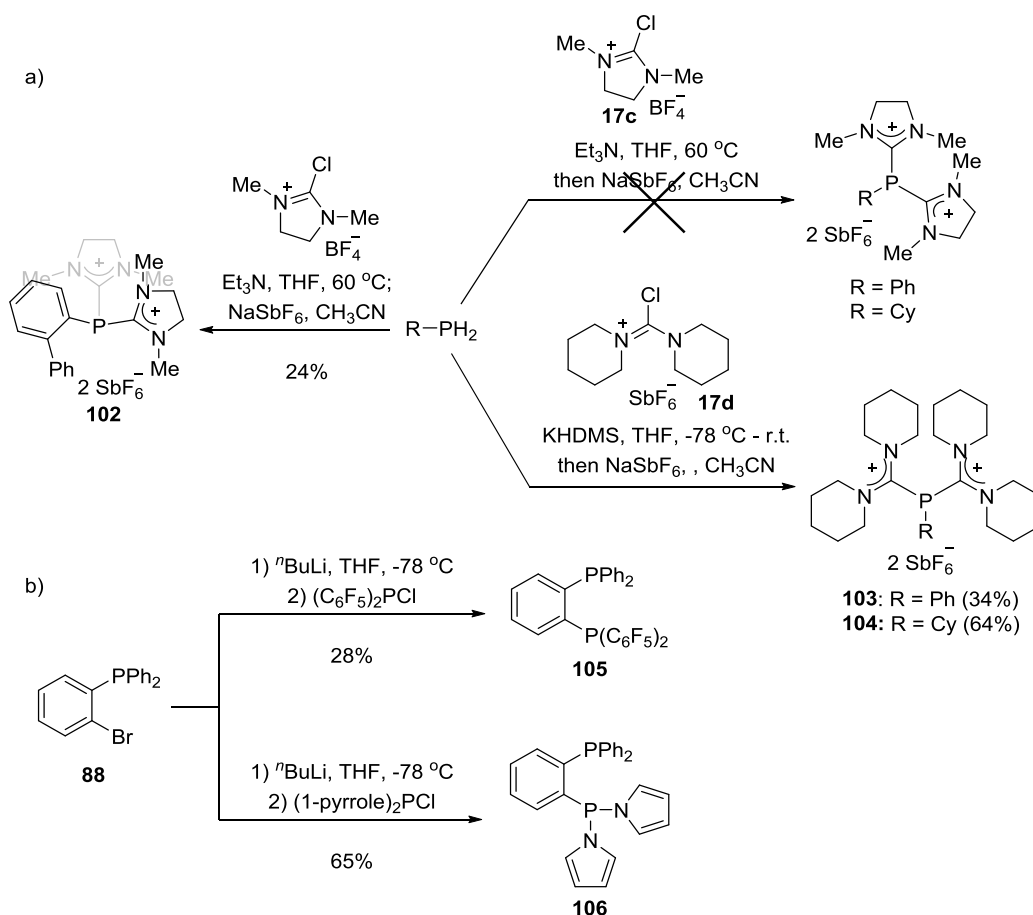


Figure 12. Molecular structure of compound **101a** in the solid state. Thermal ellipsoids at 50% probability; hydrogen atoms, tetrafluoroborate counter anions and solvent molecules have been omitted for clarity.

3.2.2 Synthesis of Monodentate Dications

In order to compare the coordination properties of chelating and monodentate dications, compounds **102-104** were also prepared following a similar sequence. Initially, PhPH₂ and CyPH₂ were reacted with chlorodihydroimidazolium salts; however, after many trials, these reactions failed to produce the desired dications in a clean manner. Once the chloroimidazolium **17c** was replaced by chloroamidinium **17d**, the desired dications **103** and **104** were obtained in moderate yield. Thus, it was estimated that the failed condensation between chlorodihydroimidazolium and either PhPH₂ or CyPH₂ might be caused by the insolubility of the monocationic intermediate that is necessarily formed after the first condensation. Hence, 2-biphenylphosphine, which contains a more lipophilic substituent and thus, depicts increased solubility in organic solvents, was chosen as the starting material. To our delight, after this modification dication **102** could be isolated as a white solid, albeit in low yield (Scheme 32a). In addition, chelating diphosphine **105** and **106**, prepared for comparison reasons, were synthesized by lithiation of **88** followed by reaction of (C₆F₅)₂PCl^[103] and (1-pyrrole)₂PCl^[104] respectively (Scheme 32b).



Scheme 32. The synthetic route of monodentate dication and bidentate phosphines.

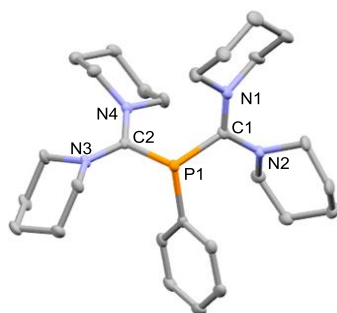


Figure 13. Molecular structure of compound **103** in the solid state. Thermal ellipsoids at 50% probability; hydrogen atoms and hexafluoroantimonate counter anions have been omitted for clarity.

3.3 Electronic Properties of the phosphines

At this point the donor abilities of the newly prepared ligands were estimated by comparative analysis of their cyclic voltammograms.^[69, 73-74] Ligand **92** and **101** showed oxidation peaks at 1.050 and 0.974 V respectively, which can be assigned to the oxidation of the –PPh₂ groups. Comparison with reference compounds reveals that the –PPh₂ lone pair in **92** and **101** is less available than that in PPh₃ (Table 3, Entry 3), probably as result of the strong electron

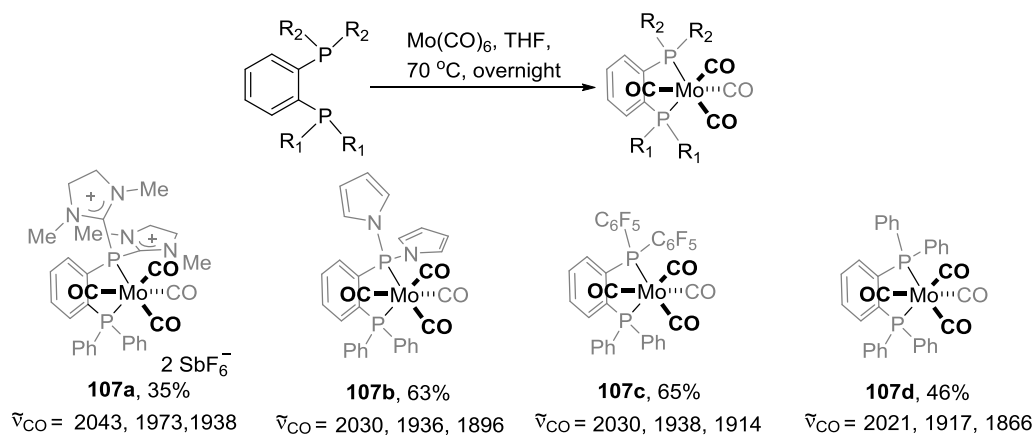
withdrawing effect that the dicationic group exerts on the neutral phosphine moiety. This influence is markedly stronger in **92** due to the closer proximity of the two phosphorus atoms imposed by the *o*-phenylene linker. Accordingly, the reduction potentials of **92** and **101** (-1.528 V and -1.504 V respectively), that can be ascribed to the electrophilic character of the $[-P(H_2Im)_2]^{2+}$ fragments, are slightly lower than that of **102** (Table 3, Entry 5) denoting, as expected, a marginal loss of their strong acceptor properties when compared with their monodentate analogue.

Table 3: Electrochemical redox potentials of ligands **92** and **101**. The values for commonly used phosphorus-based ligands and reference compounds are included for comparison.

Entry	Ligand	Ep(ox) ^[a]	Ep(red) ^[a]
1	92	1.050	-1.528
2	101	0.974	-1.504
3	PPh ₃	0.687	_[b]
4	P(OMe) ₃	1.297	_[b]
5	102	_[c]	-1.457
6	103	1.812	-1.350
7	104	1.855	-1.319
8	105	0.870	_[b]

[a] Oxidation/reduction peaks potential reported in V and calibrated versus Cp^{*}₂Fe/Cp^{*}₂Fe⁺, Bu₄NPF₆ (0.1 M) in CH₂Cl₂; [b] No reduction signal observed from 0 to -2.5 V; [c] no signal detected from 0 to 2V;

To further investigate the electronic properties of these ligands, a series of Mo-derivatives **107a-d**^[105] were synthesized by reaction with Mo(CO)₆ in THF (Scheme 33). The donor endowment of **92** was compared with that of other chelating phosphines of similar structure by analysis of the CO stretching frequencies in the corresponding $[LMo(CO)_4]^{n+}$ (n = 0 or 2) derivatives. These data suggest that the dihydroimidazolium substituents impart stronger acceptor properties to the phosphorus atom than 1-pyrrole or -C₆F₅ units. Thus, **92** and **101** can be defined as bidentate ligands which possess a neutral σ -donating group together with an exceptionally good π -acceptor functionality. The structure of the dicationic complex **107a** was confirmed by single X-ray diffraction analysis, as shown in Figure 14.



Scheme 33. Evaluation of the donor ability of **92** by IR spectroscopy

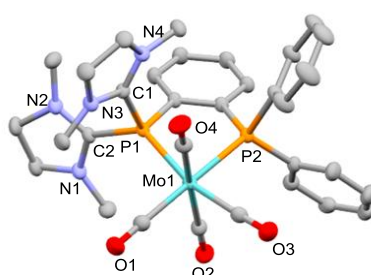
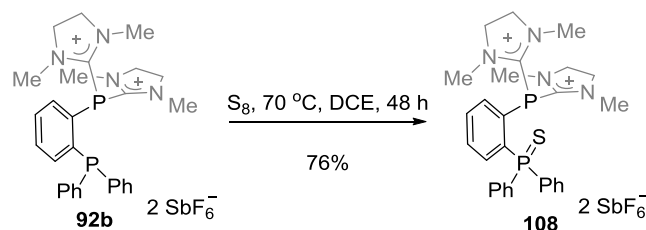


Figure 14. Molecular structure of compound **107a** in the solid state. Thermal ellipsoids at 50% probability; hydrogen atoms, hexafluoroantimonate counter anions and solvent molecules have been omitted for clarity.

Finally, an additional probe of the Lewis acidity of the $[-\text{P}(\text{H}_2\text{Im})_2]^{+2}$ moiety could be obtained from the X-ray structure of compound **108**, which was itself prepared by selective oxidation of the $-\text{PPh}_2$ group in **92** with elemental sulfur (Scheme 34 and Figure 15). This compound features a S1-P1 distance of only 3.200 Å, which is significantly shorter than that of a neutral analogue.^[106] This value also reveals an attractive P1-S1 interaction in **108** that is attributed to donation from sulfur to one of the low lying $\sigma^*(\text{P1-C1})$ orbital.



Scheme 34. Selective oxidation of the phosphorus atom on dication **92b**.

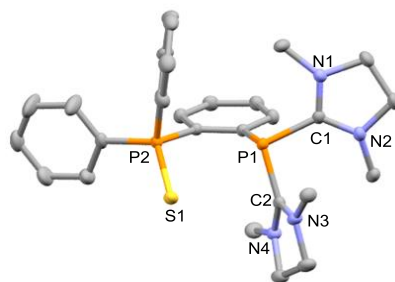


Figure 15. Molecular structure of compound **108** in the solid state. Thermal ellipsoids at 50% probability; hydrogen atoms and hexafluoroantimonate counter anions have been omitted for clarity.

To better understand the electronic properties of dication **92**, its electronic structure was evaluated theoretically at the M06-L/TZVP level. The optimized structure compares well with that obtained from X-ray analysis (Figure 16). The inspection of the frontier orbitals sheds light on the multifaceted properties of **92**. The HOMO is localized largely on the neutral phosphorus atom, while the significant localization of the LUMO and LUMO+1 orbitals on the positively charged fragment suggests suitable symmetry for π -acidic character upon metal coordination. Also noteworthy is the observation that the HOMO-LUMO gap for ligand **92** is 1.0 eV lower than that of the analogous neutral ligand of 1,2-bis(diphenylphosphino)benzene. This suggests the possibility of a P-P bonding interaction.

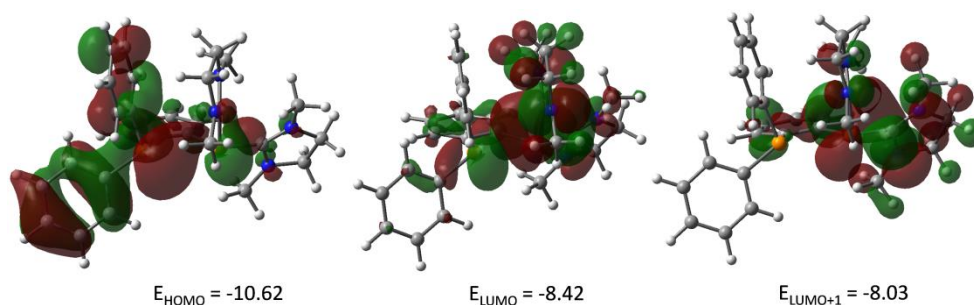
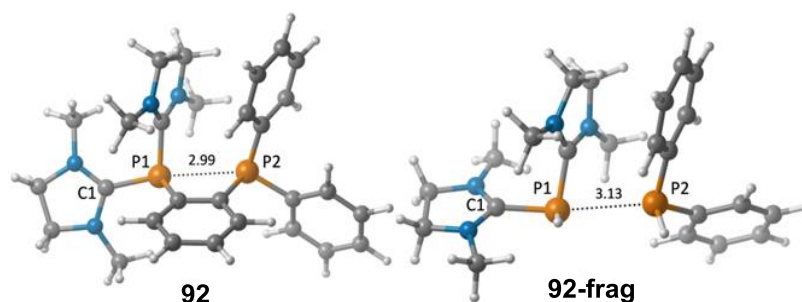


Figure 16. Molecular orbitals of **92** and their orbital energies computed at the M06-L/TZVP level.

An AIM and bond order analysis in fact supports the presence of a bonding interaction. The electron density and its corresponding Laplacian reveal a closed shell, dative interaction between the P-P atoms. To assess whether the interaction is attributed purely to the proximity induced by the bridging ligand backbone, the phenyl backbone was replaced by two hydrogen atoms to determine the approximate bond strength (Figure 17). A constraint free optimization of the fragments resulted in **92-frag** where the P-P distance increased only slightly to 3.13 Å from 2.99 Å in **92**. The M06-L/TZVP bonding energy is determined to be -31.3 kcal/mol. The physical nature of the interaction was evaluated through energy decomposition at the BP86/TZ2P//M06-L/TZVP level. While dispersion interactions (ΔE_{disp}) are expected to make

up a large percentage of the total favorable interaction due to a π -stacking component in this case, the most prominent favorable interaction component is attributed to orbital interactions (ΔE_{orb} ; 40%). Moreover, this bonding interaction may effectively account for the slightly reduced oxidation and reduction potentials for **92** in comparison to its monodentate analogue (Table 3, entries 1 and 5) through mixing of the lone pair orbital on the neutral phosphorus with the antibonding orbitals on the dicationic phosphorus.



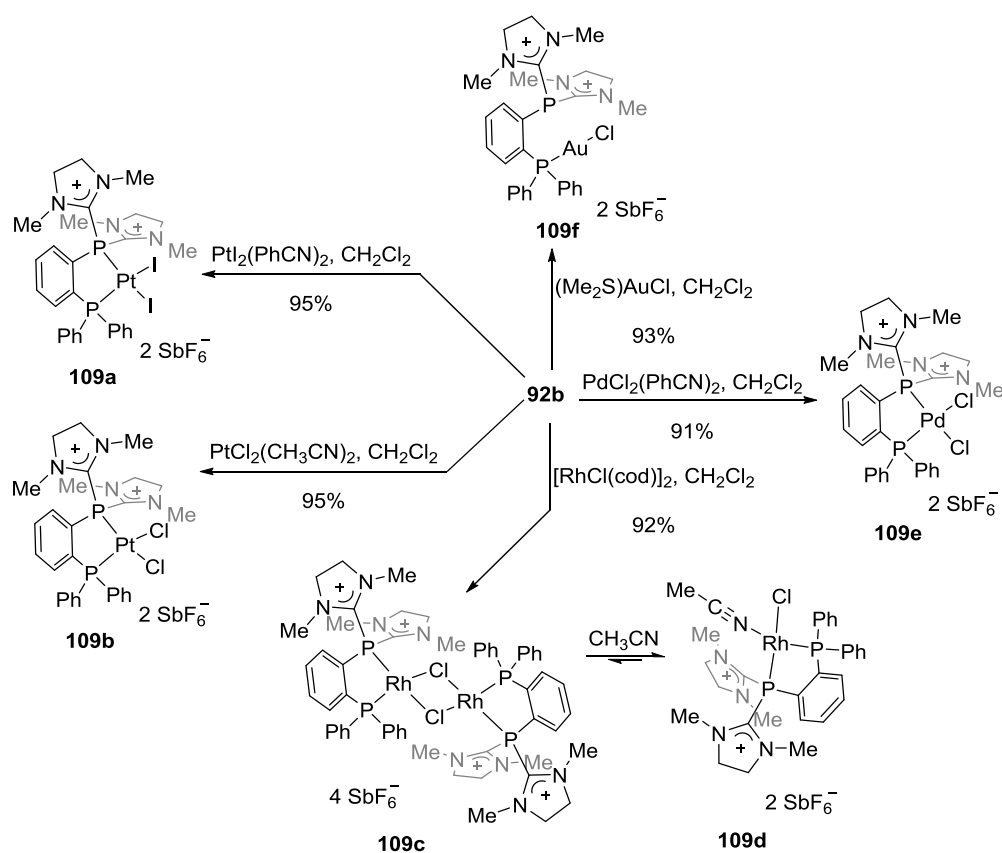
	92	92-frag	92-frag	
$\rho_b(\text{P1-P2})$	0.033	0.024	ΔE_{Pauli}	34.2
$\nabla^2 \rho_b(\text{P1-P2})$	0.036	0.030	ΔE_{elstat}	-26.4
BO	0.124	0.155	ΔE_{orb}	-29.6
$n_{\text{P1}} \rightarrow \sigma^*_{\text{P1-C1}}$	6.7	8.6	ΔE_{disp}	-18.0
			ΔE_{int}	-39.8
			ΔE_{dist}	3.5
			ΔE	-36.3

Figure 17. Theoretical investigation of the interaction of the two phosphorus atom on **92**. Geometries, AIM parameters ρ_b and $\nabla^2 \rho_b$, Wiberg bond index, NBO perturbation energies (kcal/mol), and ETS energy decomposition analysis for **92** and the **92-frag** computed at the BP86-D3/TZ2P//M06-L/TZVP level.

3.4 Coordination Study

Encouraged by this analysis we decided to evaluate the ability of **92** to function as a chelating ligand for different metals. To our delight, when **92b** was allowed to react with $\text{PtI}_2(\text{PhCN})_2$, a yellow solid **109a** was obtained. The ^{31}P -NMR spectrum of this product showed downfield shifts ($\delta_P = 39.2, 5.4$ ppm, $J_{P-P} = 4.6$ Hz) compared to the original chemical shift of the free ligand **92b** ($\delta_P = -12.3, -47.6$ ppm, $J_{P-P} = 212.4$ Hz), as well as the appearance of characteristic ^{195}Pt satellites ($J_{P(\text{neutral})-\text{Pt}} = 2856.1$ Hz, $J_{P(\text{cationic})-\text{Pt}} = 3457.9$ Hz) which indicated the coordination of both phosphorus centers to platinum. Subsequently, this connectivity was unambiguously confirmed by X-ray diffraction analysis (Figure 18). In **109a** the geometry about the Pt center is slightly distorted square planar and the P1(cationic)-Pt1 bond distance [2.2058(10) Å] is shorter than the P2(neutral)-Pt1 bond [(2.2559(10) Å], a clear

consequence of the strong π -acceptor character of the $[-P(\text{Im})_2]^{2+}$ group. Reactions with $\text{PtCl}_2(\text{CH}_3\text{CN})_2$ and $\text{PdCl}_2(\text{CH}_3\text{CN})_2$ were equally successful, affording isostructural complexes **109b** and **109e** respectively. The reactivity of **92b** towards Rh(I) centers was also analyzed. Salt **92b** readily displaced cyclooctadiene in $[\text{RhCl}(\text{cod})]_2$ to generate a binuclear tetracation **109c** in which both $[-P(\text{H}_2\text{Im})_2]^{2+}$ groups adopted a distal orientation (Figure 19). Again in this structure the shorter P1(cationic)-Rh1 bond length [2.1319(13) Å], compared to the P2(neutral)-Rh1 one [2.1924(13) Å], indicates strong π -acceptor properties at the cationic phosphine. In compound **109c**, the columbic repulsion between the fragments facilitates its dissociation and thus, after the addition of a few drops of acetonitrile to solutions of **109c**, an equilibrium was established and the monomeric **109d** was the predominant species, as depicted in Scheme 35. As expected from a coordinately saturated metal fragment, in complex **109f** the Au atom coordinates with **92b** only through the R-PPh₂ moiety. However, it is worth mentioning that the P1(cationic)-Au1 distance in this compound (3.365 Å), which is just below the sum of the Van der Waals radii of both elements, suggests a weak Au \rightarrow P(cationic) interaction. In addition, an aurophilic interaction was also observed in the solid state of **109f** (3.147 Å) (Figure 21).



Scheme 35. The coordination study of dication **92b**.

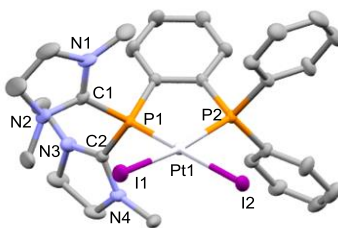


Figure 18. Molecular structure of compound **109a** in the solid state. Thermal ellipsoids at 50% probability; hydrogen atoms, hexafluoroantimonate counter anions and solvent molecules have been omitted for clarity.

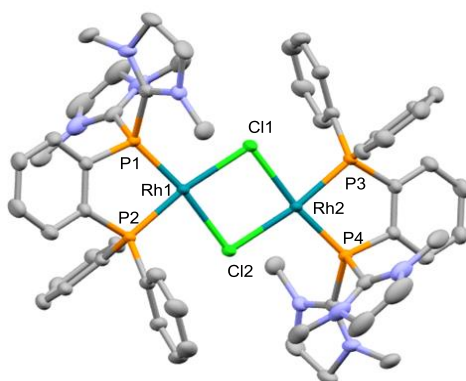


Figure 19. Molecular structure of compound **109c** in the solid state. Thermal ellipsoids at 50% probability; hydrogen atoms, hexafluoroantimonate counter anions and solvent molecules have been omitted for clarity.

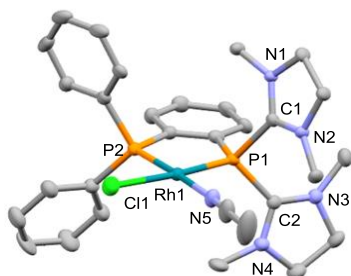


Figure 20. Molecular structure of compound **109d** in the solid state. Thermal ellipsoids at 50% probability; hydrogen atoms, hexafluoroantimonate counter anions and solvent molecules have been omitted for clarity.

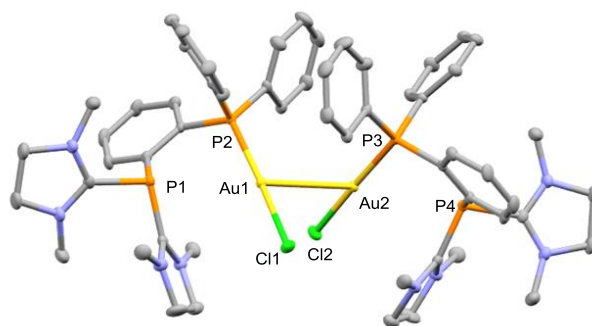
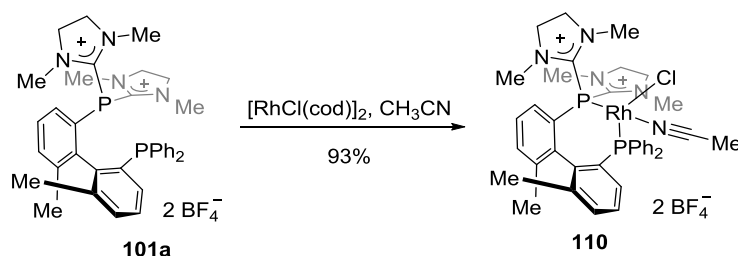


Figure 21. Molecular structure of compound **109f** in the solid state. Thermal ellipsoids at 50% probability; hydrogen atoms and hexafluoroantimonate counter anions have been omitted for clarity.

Dicationic bisphosphine **101a** was also allowed to react with $[\text{RhCl}(\text{cod})]_2$ affording an orange solid **110** (Scheme 36). The ^{31}P -NMR spectrum showed downfield shifts ($\delta_{\text{P}} = 38.1, 9.9$ ppm, $J_{\text{P-P}} = 50.4$ Hz) compared to the original resonances of **101** ($\delta_{\text{P}} = -15.0, -44.4$ ppm, $J_{\text{P-P}} = 87.0$ Hz), along with the appearance of characteristic P-Rh coupling constants ($J_{\text{P}(\text{neutral})-\text{Rh}} = 154$ Hz, $J_{\text{P}(\text{cationic})-\text{Rh}} = 216$ Hz) that indicate the coordination of both P centers to Rh. Subsequently, this connectivity was unambiguously confirmed by X-ray diffraction analysis (Figure 22). In product **110** the geometry about the Rh center is slightly distorted square planar and the cationic P1(cationic)-Rh1 bond distance [2.1608(8) Å] is shorter than the P2(neutral)-Rh1 one [2.2358(8) Å], again as consequence of the strong π -acceptor character of the $[-\text{P}(\text{Im})_2]^{2+}$ group. The bigger coupling constant and the shorter bond length for the cationic P-atom demonstrate its strong interaction with the Rh center.



Scheme 36. The coordination study of dication **101a**.

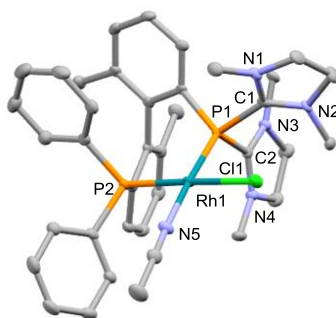


Figure 22. Molecular structure of compound **110** in the solid state. Thermal ellipsoids at 50% probability; hydrogen atoms and hexafluoroantimonate counter anions have been omitted for clarity.

Interestingly, mixing monodentate dication **102** with different metal precursor in CD_2Cl_2 did not produce any metal complex as could be demonstrated by analysis of ^{31}P NMR of the reaction mixtures. Compared with the free ligands, no modification was observed. This result strongly confirms that the coordination of **102** to various metal salts is only possible due to the incorporation of a chelating phosphorus atom (Figure 23).

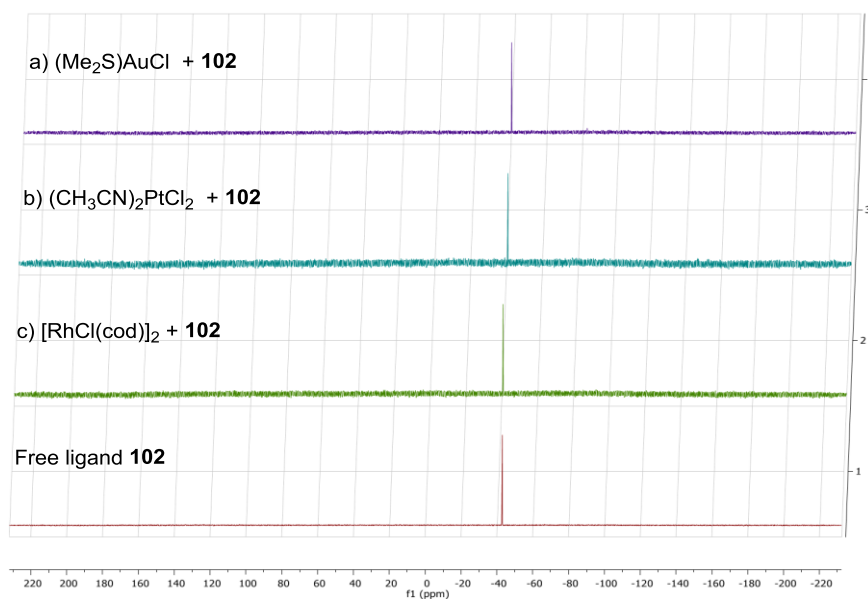


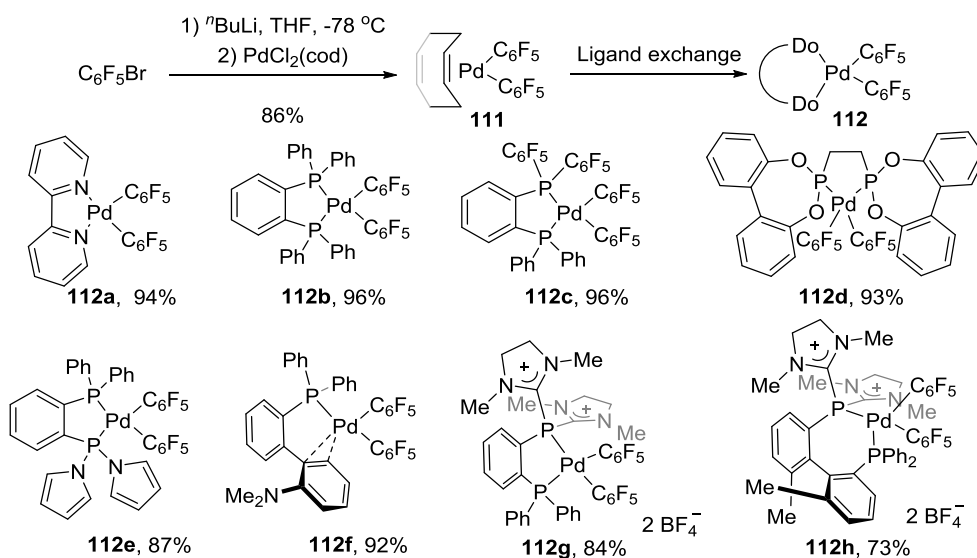
Figure 23. ^{31}P NMR Spectra of the reaction of compound **102** with different metal salts. Ligand **102** (5.0 mg, 0.006 mmol) in CD_2Cl_2 (0.6 ml) and the corresponding metal salts were added to an NMR tube and the sample stirred for 5 h. After that, the magnetic stirrer was removed and ^{31}P NMR spectra were recorded.

3.5 Reductive Elimination of Bis(pentafluorophenyl)palladium Complexes

3.5.1 Synthesis of the Biarylplatinum Complexes

Reductive elimination is an elementary reaction step present in many catalytic cycles. During this process, the oxidation state from the metal is reduced by two units, making the metal more electron-rich. For this reason, strong π -acceptor ligands usually facilitate this step, since the additional charge on the metal can be easily delocalized along the ligand. This makes our ligands potentially quite interesting in transformations where the rate-determining step is reductive elimination.^[107-108]

In order to test this working hypothesis, relevant biarylplatinum complexes **112a-h** were prepared, all of them bearing $-\text{C}_6\text{F}_5$ substituents.^[109] Polyfluorinated aryls were chosen, because the reductive elimination of these very electron-poor moieties is known to be especially difficult. In fact, the reaction is known to proceed only under extremely harsh conditions (concentrated HNO_3).^[109]



Scheme 37. Synthesis of biarylpalladium complexes.

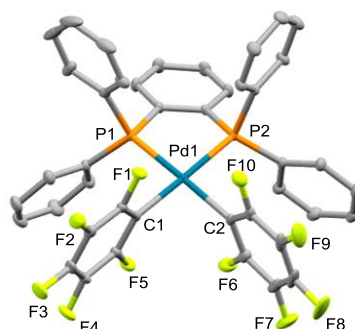


Figure 24. Molecular structure of compound **112b** in the solid state. Thermal ellipsoids at 50% probability; hydrogen atoms have been omitted for clarity.

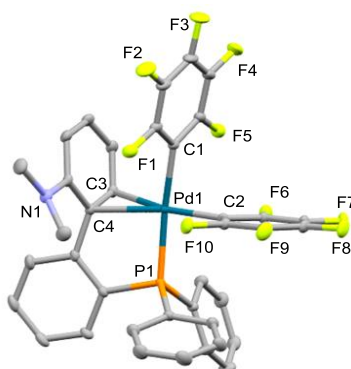


Figure 25. Molecular structure of compound **112f** in the solid state. Thermal ellipsoids at 50% probability; hydrogen atoms have been omitted for clarity.

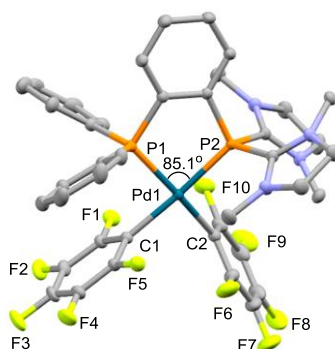


Figure 26. Molecular structure of compound **112g** in the solid state. Thermal ellipsoids at 50% probability; hydrogen atoms, tetrafluoroborate counter anions and solvent molecules have been omitted for clarity.

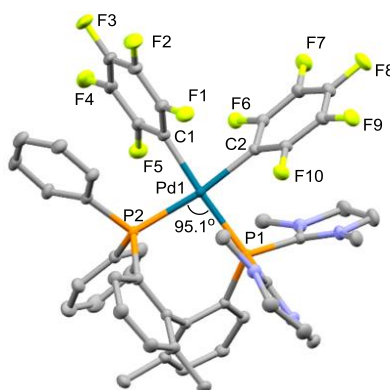


Figure 27. Molecular structure of compound **112h** in the solid state. Thermal ellipsoids at 50% probability; hydrogen atoms, tetrafluoroborate counter anions and solvent molecules have been omitted for clarity.

3.5.2 Experimental Investigation of the Effect of Cationic Ligands in Reductive Elimination Processes

Compounds **112a-e** were completely ineffective for this process, and no trace of the desired perfluorobiphenyl was detected under our working conditions (CD_3CN at 70°C). Gratifyingly, the reductive elimination of $\text{C}_6\text{F}_5\text{-C}_6\text{F}_5$ from **112g** proceeded smoothly and a remarkable conversion of 72% was achieved in 15 hours (Figure 28).

This preliminary evidence on the beneficial effect of dicationic ligand **92a** encouraged us to test the complex **112h** in this same transformation (Figure 28). It is well known in palladium catalysis that the employment of ancillary ligands with large bite angles also facilitates reductive elimination steps, because they better stabilize the linear zero valent complex resulting from the elimination and efficiently delocalize the excess electron density on the metal after this step.^[110-111] The kinetic profile for **112h** was illustrated in Figure 28. Acetone was used as solvent due to the instability of **112h** in acetonitrile. The reactivity clearly surpasses that of **112g**, and gave rise to the quantitative formation of perfluorobiphenyl in only six hours, thus confirming our predictions. It should be mentioned that complex **112f**

also provided reasonable conversion under the same conditions and the rate of the reaction is even superior to the one of **112g**. This reductive elimination surely takes place through a tricoordinated palladium species. Therefore, a new question arose. Do **112h** and **112g** eliminate directly through four coordinated palladium species, or is a coordination site liberated (by decooordination of the $[-P(\text{Im})_2]^{2+}$ moiety) before the actual reductive elimination takes place? Calculations were performed to answer this question.

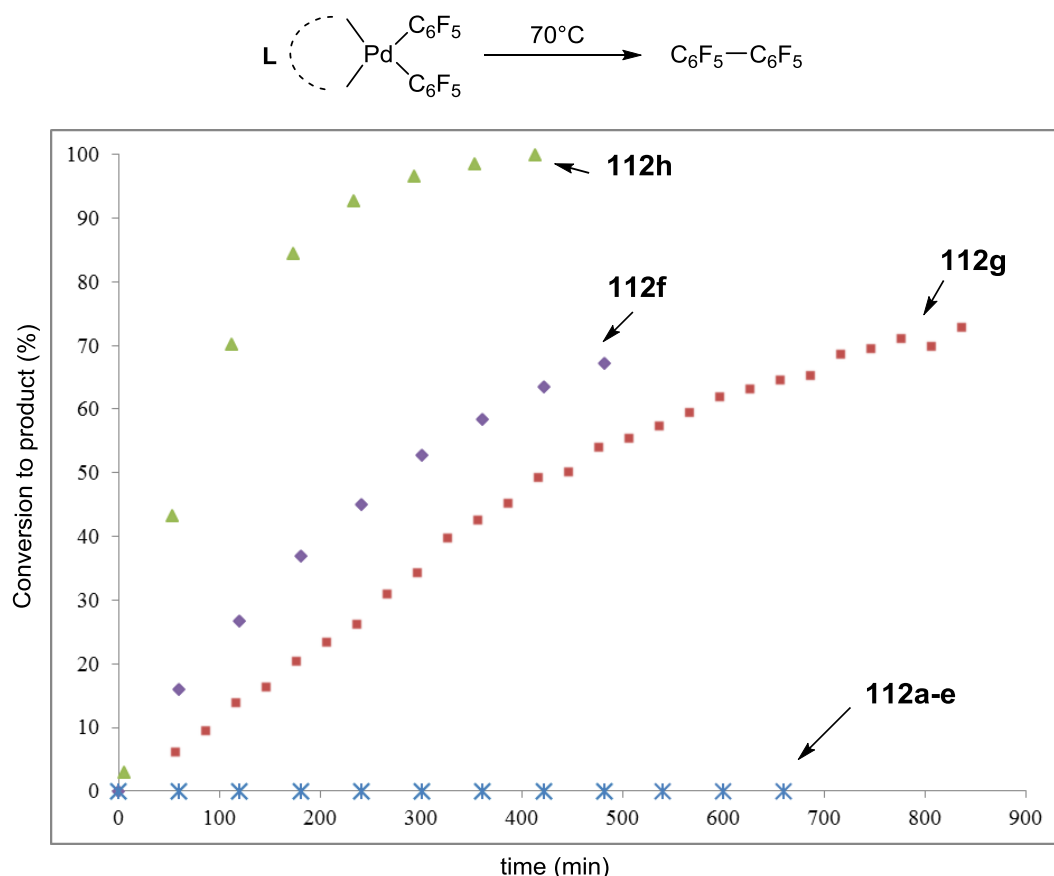


Figure 28: The reductive elimination of the related biarylpalladium complexes. [a] Ligand effect on the reductive elimination of $\text{C}_6\text{F}_5\text{---C}_6\text{F}_5$ from Pd(II) complexes **112a-h**. Reactions were carried out in acetonitrile at 70°C . Due to its instability in acetonitrile, acetone was used as the solvent in the case of **112h** and DCE was used as the solvent in the case of **112f**. Conversions were determined by ^{19}F NMR.

3.5.3 Theoretical Investigation of Cationic Ligands in Reductive Elimination

The energy profiles for the reductive elimination of **112g**, **112h**, and **112b** were explored at the M06-L(SMD- CH_3CN)/def2-TZVP//BP86-D3/def2-TZVP level of DFT (Figure 29). The direct reductive elimination from **112g** is predicted to occur with a relatively facile barrier of $22.9 \text{ kcal mol}^{-1}$ and is overall exergonic by $8.8 \text{ kcal mol}^{-1}$. The possibility for hemilability in ligand **92** during or before the reductive elimination of **112g** is dismissed on account of monodentate structure **112g-1** being $3.4 \text{ kcal mol}^{-1}$ higher in energy than the transition state

for the bidentate coordination mode in **112g-TS**. In contrast, the analogous neutral complex **112b** experiences a reductive elimination barrier that is $9.3 \text{ kcal mol}^{-1}$ higher in energy than that for **112g**. In addition, the reaction is endergonic by $11.3 \text{ kcal mol}^{-1}$. The difference in reaction free energies suggests that ligand **92** binds more strongly to Pd(0) than Pd(II) while 1,2-bis(diphenylphosphino)benzene forms a much stronger complex **112b** with Pd(II) than Pd(0). Lastly, the reaction barrier for ligand **101** is predicted to be 1.3 kcal/mol lower than that for **112g**. Hence, the increase in activity observed with **112h** can be readily rationalized based on the increased bite angle which diminishes the C-Pd-C angle and consequently, less distortion is required to reach the product resulting in a lower overall barrier.

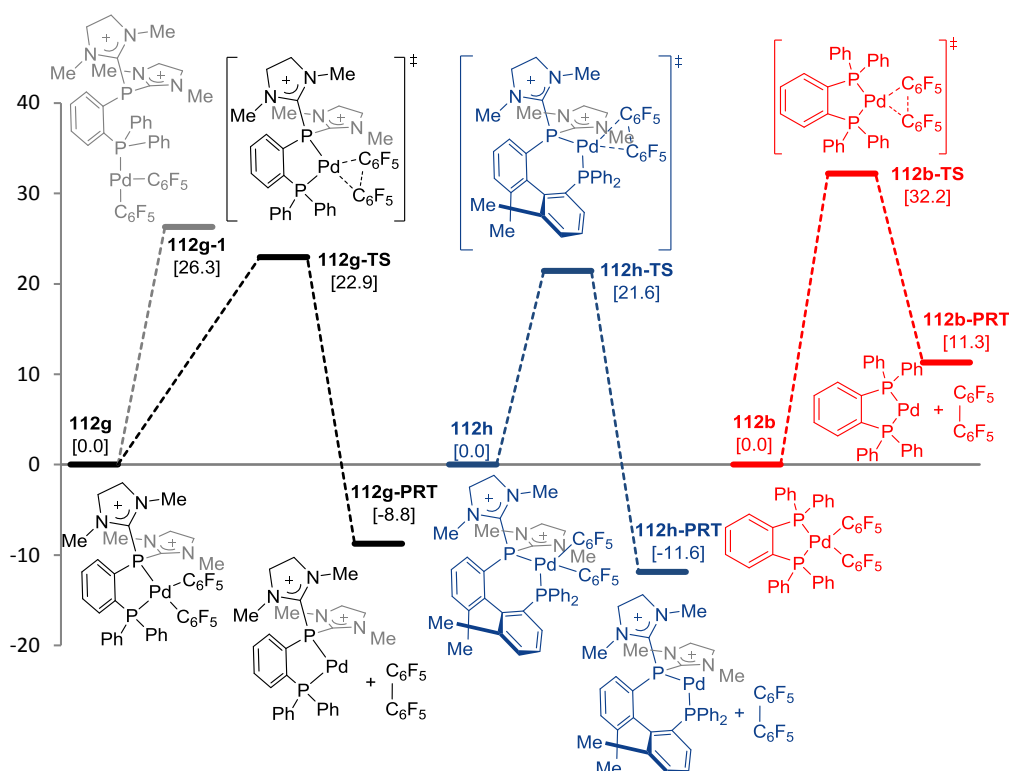


Figure 29. Gibbs Free Energy profile for the reductive elimination of complexes **112g** (black), **112h** (blue) and **112b** (red) determined at the M06-L(SMD_{CH₃CN})/def2-TZVP//BP86-D3/def2-TZVP level of DFT.

The details of the L-Pd binding energy were deconstructed with the aid of energy decomposition from the Pd(II) complex to the reductive elimination product. While the change in the repulsion terms ($\Delta\Delta E_{\text{Pauli}}$ and $\Delta\Delta E_{\text{dist}}$) is greater in **112g-TS**, it exhibits far greater compensation interaction terms than **112b-TS**. The orbital term is the strongest of the interaction terms favoring **112g-TS** and indicates that the decreasing orbital interactions for reaching the TS is significantly less than that for **112b-TS**. Moreover the change in charge transfer ($\Delta\Delta q$) from the ligand to the Pd(C₆F₅)₂ fragment on going from the reactant complex

to the transition state of reductive elimination is less for **112g** than for **112b** which may contribute to the reduced energy barrier for **112g**.

Table 4. Energy decomposition analysis and NBO charge transfer ($\text{Pd}(\text{C}_6\text{F}_5)_2 \rightarrow \text{L}$). $E_a = \Delta\Delta E_{\text{int}} + \Delta\Delta E_{\text{dist}}$

	$\Delta\Delta E_{\text{Pauli}}$	$\Delta\Delta E_{\text{elec}}$	$\Delta\Delta E_{\text{orb}}$	$\Delta\Delta E_{\text{disp}}$	$\Delta\Delta E_{\text{int}}$	$\Delta\Delta E_{\text{dist}}$	E_a	$\Delta\Delta q$
112g	0.0	0.0	0.0	0.0	0.0	0.0	0.0	0.0
112g-TS	-22.95	4.30	22.88	4.94	9.17	10.84	20.01	-0.35
112g-PRT	30.20	-63.48	17.00	25.13	8.85	-13.98	-5.13	-0.76
112b	0.0	0.0	0.0	0.0	0.0	0.0	0.0	0.0
112b-TS	-38.19	16.98	41.73	8.86	29.38	0.96	30.34	-0.41
112b-PRT	24.46	-41.57	29.50	23.26	35.65	-18.27	17.38	-0.83

Charge transfer from the ligand inhibits $\text{Pd}(\text{II}) \rightarrow \text{Pd}(0)$ reduction. The principle orbital interaction governing this conversion is that between the ligand HOMO and the Pd complex LUMO and thus, the preference can be probed through this interaction. The orbital energies and corresponding orbital overlaps between the ligand and $\text{Pd}(\text{C}_6\text{F}_5)_2$ fragments for the reactant complexes **112b** and **112g** as well as their transition states of reductive elimination **112b-TS** and **112g-TS** are shown in Table 4. The large fragment orbital energy difference for **112g** ($\Delta E = 4.94$ eV) as compared with **112b** ($\Delta E = -0.89$ eV) implies a much stronger interaction in the latter. Moreover the HOMO in ligand **112g** is more localized on the neutral phosphorus atom whereas in **112b** the HOMO is equally distributed on both phosphorus atoms. This distribution difference is reflected in a more enhanced orbital overlap for the equally distributed neutral ligand in **112b**. Upon conversion to the transition state a much greater distortion in the $\text{Pd}(\text{C}_6\text{F}_5)_2$ fragment for **112b** than that for **112g** is required. This demand is expressed in diminished Ar-Ar bond distance resulting in an increased energy for the corresponding LUMO. Furthermore the overlap is diminished by 26% upon conversion to the TS for **112b** whereas the overlap is only diminished by 10% in **112g**. The greater decrease in the overlap combined with the increased orbital energy difference in **112b** \rightarrow **112b-TS** signifies the greater need for reduced charge transfer from the ligand as the change in oxidation state favors charge removal from the $\text{Pd}(\text{C}_6\text{F}_5)_2$ as the Ar-Ar bond forms (Figure 30).

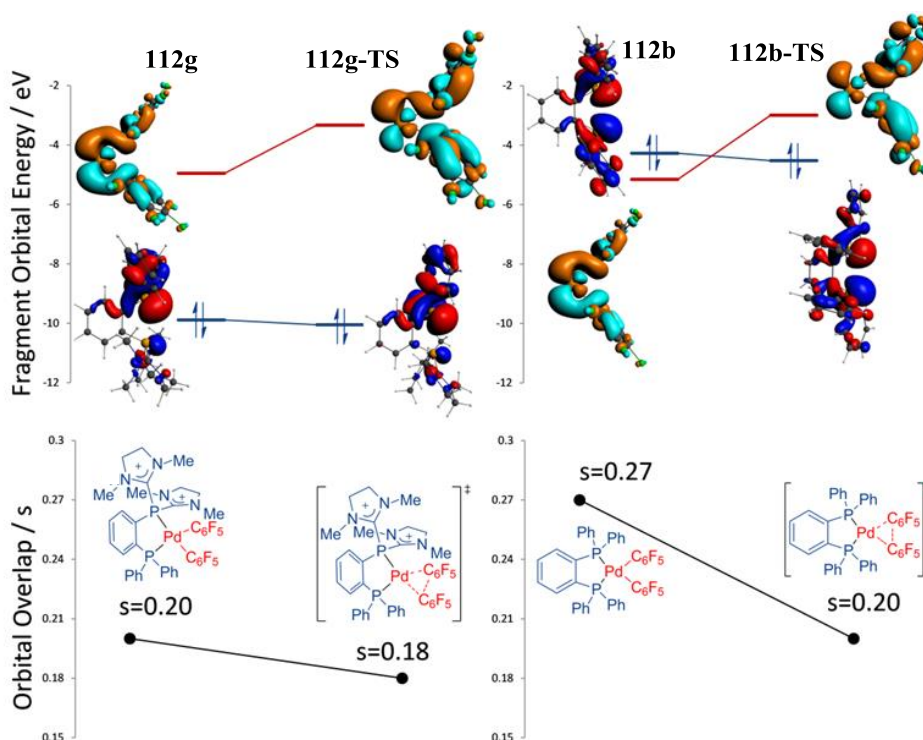


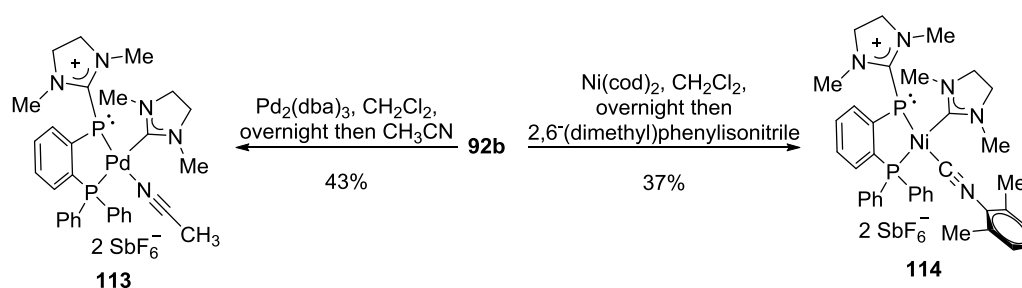
Figure 30. Frontier fragment orbitals for **112g**, **112g-TS**, **112b**, and **112b-TS** with their orbital energies and orbital overlaps, s , computed at the BP86/TZ2P//BP86/def2-TZVP level.

By virtue of the positive charge in ligand **92**, a bimodal adjustment to the ligand is imparted as compared to the neutral analogue for the ligand in complex **112b**. The energy of the HOMO relating to the lone pair orbitals on the phosphorus atoms is significantly lowered by ~ 5.6 eV as compared with the neutral analogue, resulting in a significantly weaker bonding interaction. The second effect is the localization of the HOMO on the neutral phosphorus atom. This asymmetry in a chelating ligand results in diminishing overlap with transition metal d orbitals translating to a weaker bond as compared with a chelating ligand with a suitably symmetric HOMO distribution as in **112b**.

3.5.4 Reactivity of Dication **92** towards Pd(0) and Ni(0)

Encouraged by these results, we decided to study the coordination of **92** towards Pd(0) and Ni(0) complexes, since metal complexes are formed after reductive elimination of the biaryl moiety from compound **112g-h**. Hence, treatment of **92b** with an equivalent amount of $\text{Pd}_2(\text{dba})_3$ in CH_2Cl_2 resulted in the precipitation of a yellow solid **113**, depicting two singlets in its ^{31}P NMR spectrum, one at $\delta_{\text{P}} = 49.4$ ppm, which surely corresponds to the R-PPh_2 fragment, and a quite indicative signal at $\delta_{\text{P}} = 15.9$ ppm, which could not be directly attributed to the original $[-\text{P}(\text{H}_2\text{Im})_2]^{2+}$ group (Scheme 38). Moreover, in contrast to the complex formed before, the ^1H NMR spectrum of **113** indicated unequivalency of its four methyl groups.

Fortunately, after several attempts, crystallization from acetonitrile afforded single crystals of this product and its connectivity could be determined (Figure 31). In product **113** an oxidative addition of Pd(0) into one of the C-P(H₂Im) bonds has taken place, providing a phosphinidene complex where the Pd(II) atom additionally coordinates an acetonitrile molecule. Identical reactivity was observed on reaction of **92b** with Ni(cod)₂, although in this case the exchange of acetonitrile by 2,6-(dimethyl)phenylisocyanide was necessary to obtain a crystalline material **114** (Figure 32). It is worth mentioning that the cationic P(H₂Im)-fragments in **113** and **114** still bear a non-shared electron pair at phosphorus that might still be used for coordination of a second metal center.



Scheme 38. The coordination study of dication **92b** with Pd(0) and Ni(0).

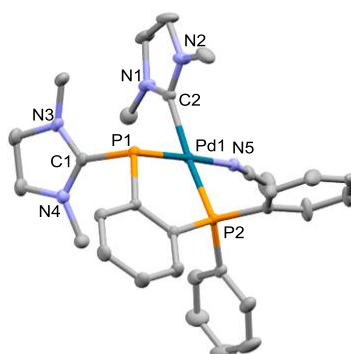


Figure 31. Molecular structure of compound **113** in the solid state. Thermal ellipsoids at 50% probability; hydrogen atoms and hexafluoroantimonate counter anions have been omitted for clarity.

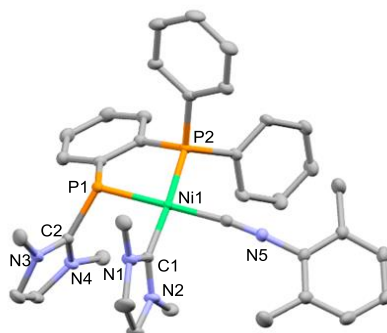


Figure 32. Molecular structure of compound **114** in the solid state. Thermal ellipsoids at 50% probability; hydrogen atoms and hexafluoroantimonate counter anions have been omitted for clarity.

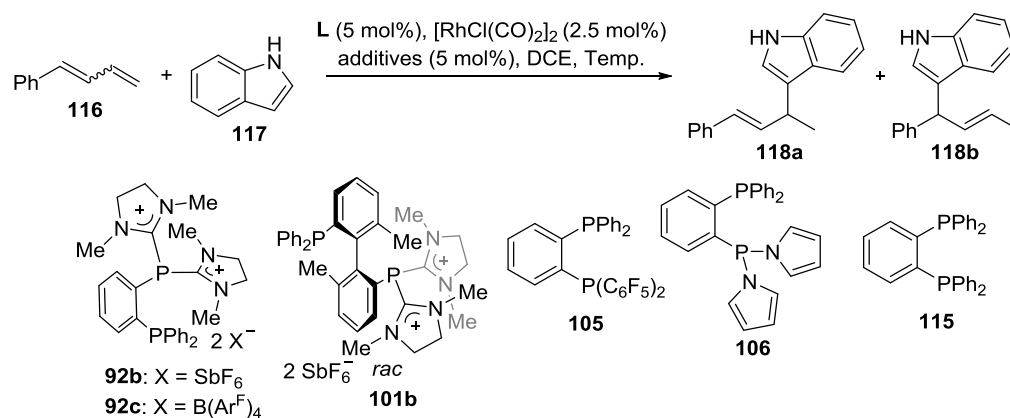
3.6 Application in Catalysis

The catalytic hydroalkylation of alkenes is a valuable, atom-economical methodology for the formation of C–C bonds from readily available starting materials.^[112] Pioneering studies have led to the development of intermolecular processes that employ styrenes,^[113] inactivated alkenes,^[114-115] allenes,^[116-117] and alkynes^[118-119] as effective substrates that can react with appropriate C-based nucleophiles.^[120] The hydroalkylation of diene substrates is synthetically useful; such reactions convert readily available unsaturated hydrocarbons into versatile allyl-containing building blocks, in which the double bond can be functionalized in a later reaction. Normally, the process of hydroarylation requires the activation of the alkenes by π -acidic metal centers. This renders them electrophilic and therefore, susceptible to addition by arene nucleophiles.^[121]

In the coordination study of **92** with Rh, it was observed that an equilibrium was established between **109c** and its monomeric **109d**, which has a vacant coordinate site available for further coordination. Considering the strong π -acceptor properties of **92**, we reasoned that **109d** might be suitable catalyst for the type of processes mentioned above. Hence, the intermolecular hydroarylation of 1,3-dienes with electron-rich aromatics was chosen as model to test the reactivity of our catalyst. We began our investigations by treatment of phenylbutadiene with **92b** (5 mol %), $[\text{RhCl}(\text{CO})_2]_2$ (2.5 mol %) in the presence of indole as nucleophiles. $\text{KB}(\text{Ar}^{\text{F}})_4$ (Potassium tetrakis(pentafluorophenyl)borate, 10 mol %) was added as anion exchange reagent to increase the solubility of **109d** in DCE. Under these conditions, 94% conversion of **116** into **118** was observed. The regioselectivity was also very good (96:4 γ : α), probably due to the hindrance originated by the -Ph group that precluded the nucleophilic attack at the γ position of phenylbutadiene (Table 5). Further control experiments proved that neither $\text{KB}(\text{Ar}^{\text{F}})_4$ nor $[\text{RhCl}(\text{CO})_2]_2$ could catalyze this reaction. In order to determine if $\text{KB}(\text{Ar}^{\text{F}})_4$ was responsible for the increased catalyst reactivity, the cationic ligand **92c** was synthesized. Hydroarylation of **116** in the presence of $[\text{RhCl}(\text{CO})_2]_2$ and **92c** (5 mol %) also afforded the desired compound in 91% conversion and a 92:8 γ / α ratio. This reaction demonstrated that the K^+ from $\text{KB}(\text{Ar}^{\text{F}})_4$ did not influence the catalytic activity. When ligands **101b**, **105**, **106** or **115** were used instead of **92b** under identical conditions, the desired product was formed in less than 5% conversion. These initial observations demonstrated the ability of ligand **92** as a π -acceptor ligand to increase the acidity of the Rh atom, thus facilitating the catalytic transformation. Of note, the use of 4-methyl-2,6-di-*t*Bu-pyridine (5 mol%) as a Brønsted acid scavenger did not inhibit the reaction as depicted in entry 13, while

a strong Brønsted acid like TfOH led to decomposition of the diene, resulting in a complicated mixture (entry 7).

Table 5: Optimization of Rh(I)-catalyzed hydroarylation of phenyldiene with indole.



Entry	Ligand	Additives	$[\text{RhCl}(\text{CO})_2]_2$ (%)	Temp. (°C)	Conv. (ratio) (%) ^[a]
1	92b	$\text{KB}(\text{Ar}^F)_4$	2.5	70 °C	94 (96:4) (86) ^[b]
2	-	KSbF_6	2.5	70 °C	0
3	-	$\text{KB}(\text{Ar}^F)_4$	-	70 °C	0
4	92c	-	2.5	70 °C	91 (92:8)
5	101b	-	2.5	70 °C	0
6	101b	$\text{KB}(\text{Ar}^F)_4$	2.5	70 °C	<5
7	-	TfOH	-	70 °C	decomp. ^[c]
8	92b	$\text{KB}(\text{Ar}^F)_4$	2.5	50 °C	0
9	115	$\text{KB}(\text{Ar}^F)_4$	2.5	70 °C	0
10	105	$\text{KB}(\text{Ar}^F)_4$	2.5	70 °C	0
11	106	$\text{KB}(\text{Ar}^F)_4$	2.5	70 °C	0
12	105	-	2.5	70 °C	0
13	92b	$\text{KB}(\text{Ar}^F)_4$ / 4-methyl-2,6-di- ^t Bu-pyridine ^[d]	2.5	70 °C	87 (94:6)

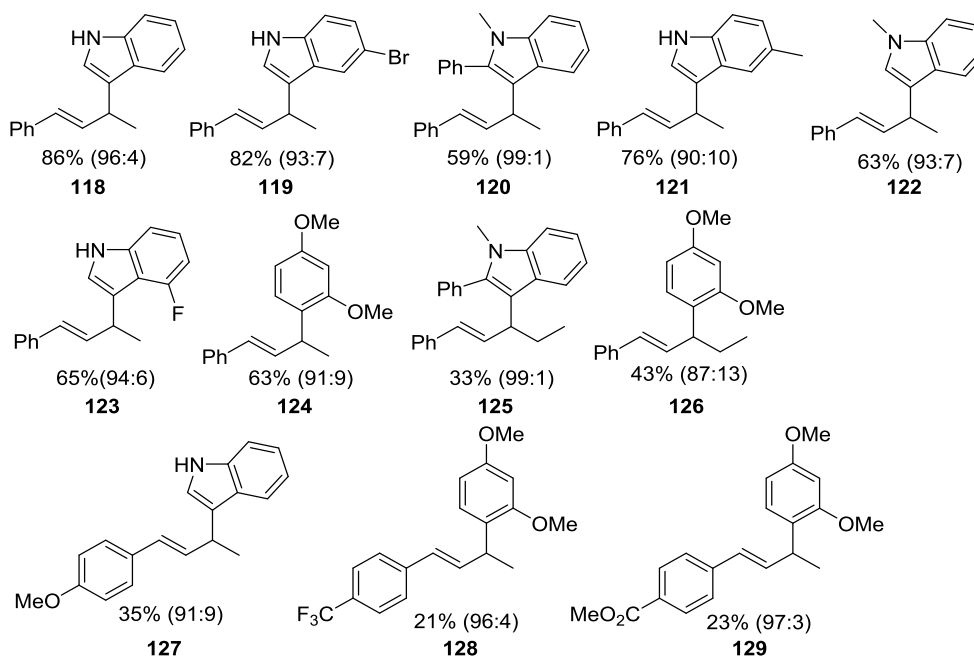
[a] Conversion to the products and the ratio of **118a** and **118b**; values determined by analysis of ^1H NMR spectra of unpurified mixtures with CH_2Br_2 as an internal standard; [b] Isolated yield; [c] The diene decomposed; [d] 4-methyl-2,6-di-^tBu-pyridine (5 mol%) was added to the reaction.

Next, a range of electron-rich arenes was investigated. As shown in Table 6, phenyl-substituted 1,3-diene underwent site-selective hydroarylation with a series of indoles at 70 °C to afford **118-124** in moderate to excellent yields with good to excellent selectivity. More

intriguingly, 1,3-dimethoxybenzene also participates in the reaction, delivering **124** in 63% yield (91:9 γ : α).

In addition, we could expand the scope of the Rh(I)-catalyzed protocol to more challenging site-selective additions using internal dienes as substrates, but at expense of the yield. Thus, 1-aryl-4-alkyl-substituted dienes underwent catalytic hydro-heteroarylation with *N*-methyl-2-phenylindole and 1,3-dimethoxybenzene to deliver functionalized products **125** and **126** in 33% and 43% yields respectively, with a significant increase in regioselectivity (99:1 γ : α) in the case of the more hindered *N*-methyl-2-phenylindole. Electron-deficient dienes could be also used for this transformation,^[122] although the yields were low in all cases. The selectivity of the addition was 96:4 γ : α and 97:3 γ : α for **128** and **129** respectively.

Table 6: Substrate scope of Rh(I)-catalyzed hydroarylation of diene with electron-rich aromatic compounds.



[a] Diene (0.2 mmol), aromatics (0.2 mmol), **92b** (5 mol%), $[\text{RhCl}(\text{CO})_2]_2$ (2.5 mol%), $\text{KB}(\text{Ar}^{\text{F}})_4$ (10 mol%) in DCE (1.0 ml) was heated for 18 h at 70 °C; [b] Isolated yield; [c] the ratio of products were determined by analysis of ^1H NMR spectra of unpurified mixtures or GCMS.

3.6.1 Theoretical Investigation of Chelating Dicationic Ligands in Catalysis

The origin of activation for ligand **92** was theoretically evaluated by comparing the reactant complex **INT2** to the complex with the analogous neutral ligand (Figure 33). Presumably, the lowest unoccupied orbital on the diene would be the relevant orbital to interact with the nucleophile in the addition step. In the neutral complex, this orbital is the LUMO and in **INT2**, the orbital is the LUMO+3 (the LUMO, LUMO+1, and LUMO+2 orbitals are localized elsewhere but are all similar in energy). The LUMO+3 on **INT2** is significantly lower than

the LUMO on the neutral complex by ~ 5 eV. Furthermore, the computed NBO charge transfer upon complexation reveals a net transfer of 0.02 e from the metal to the diene while complexation in **INT2** results in a net transfer of 0.21 e from the diene to the Rh complex. The significantly lower LUMO of the diene and resulting positive charge accumulation readily accounts for the enhanced reactivity using ligand **92** relative to neutral chelating ligands.

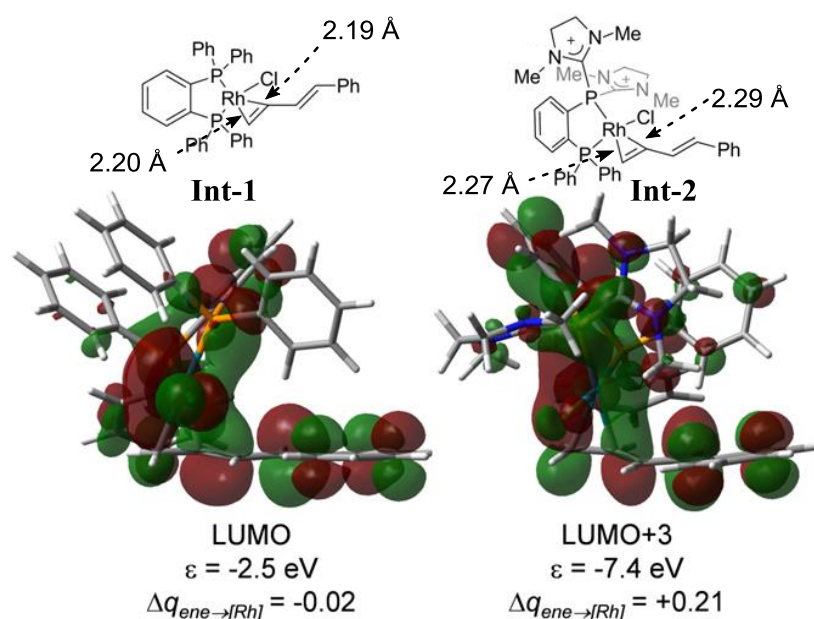


Figure 33. The relevant unoccupied orbitals are shown for **INT1** and a neutral analogue. The NBO charge transfer is also shown.

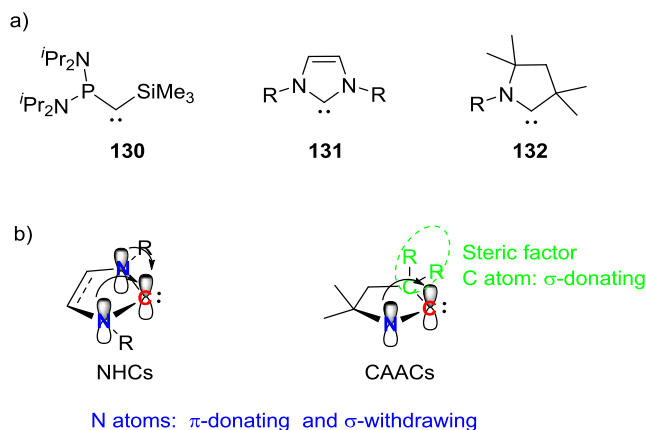
3.7 Summary III

In summary, we outlined herein the preparation of new bidentate dicationic phosphines and their coordination chemistry towards different metals. Moreover, we showcased for the first time the utility of cationic ligands to promote difficult reductive elimination processes under mild condition, such as the formation of polyfluorinated biaryls from Pd(II) centers. Finally, the unique properties of these ligands in catalysis has been proven in the hydrosilylation of phenyl diene with indoles and electron rich arenes.

4 Isolation and Coordination Chemistry of CAACs substituted α -Radical Phosphines

4.1 Introduction

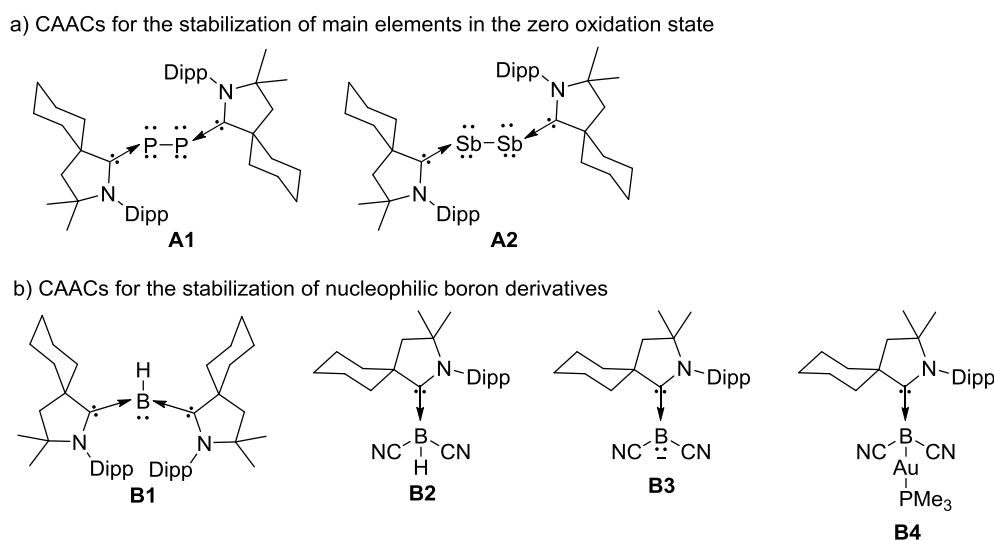
Carbenes are compounds that feature a divalent carbon atom with only six electrons in its valence shell. In the singlet state, they possess a lone pair of electrons and a vacant orbital and therefore exhibit Lewis acidic and Lewis basic properties, which explains their high reactivity.^[123] Following the preparation by Bertrand group in 1988 of the first representative [bis-(diisopropylamino)phosphino](trimethylsilyl)carbene **130**,^[124] a variety of stable carbenes were prepared and are now available, the most popular being the cyclic diaminocarbenes **131** also known as NHCs.^[125-126] Following the pioneering work by Herrmann, NHCs have been recognized as excellent ancillary ligands for transition metal-based catalysts and also as organic catalysts in their own right.^[127-129] In the last decade, Bertrand *et al.* have developed a new type of carbene **132**, namely the cyclic (alkyl)(amino)carbenes (CAACs), which have attracted more and more attention due to their unusual reactivity in main group chemistry derived from special electronic and steric properties.^[123, 130]



Scheme 39. Representative carbenes that have been developed recently.

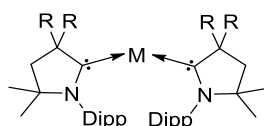
In CAACs one of the electronegative and π -donor amino substituents of diaminocarbenes is formally replaced by a σ -donating but not π -donating alkyl group. As a consequence, CAACs are more nucleophilic (σ -donating) but also more electrophilic (π -accepting) than diaminocarbenes. Additionally, the presence of a quaternary carbon in the position α to the carbene center provides steric environments that differentiate CAACs dramatically from all other carbenes (Scheme 39b). These peculiar stereoelectronic properties of CAACs allow for

the stabilization of unusual diamagnetic and paramagnetic main group based species.^[123, 130] For examples, Bertrand and coworkers described the preparation of room temperature stable diphosphorus^[131] and diantimony^[132] derivatives in which the central heteroatom is in the zero oxidation state (Scheme 40a). Nucleophilic boron compounds have also been synthesized using CAACs (Scheme 40b).^[133-134]



Scheme 40. Structurally characterized CAACs stabilized main group compounds.

CAACs are also excellent ligands for transition metal complexes. Their most recent application consists in their use for the stabilization of paramagnetic complexes, in which the metal is in a formal zero or even lower oxidation state. Indeed, bis(CAAC)M complexes have been isolated in which the central metal is gold^[135-136], platinum^[137], palladium^[138], copper^[139], cobalt^[140-141], iron^[140], nickel^[142], manganese^[141, 143], and zinc^[144]. These results demonstrate that CAACs are excellent π -acceptor ligands, a necessary property for the stabilization of zero-valent mononuclear metal complexes (Scheme 41).

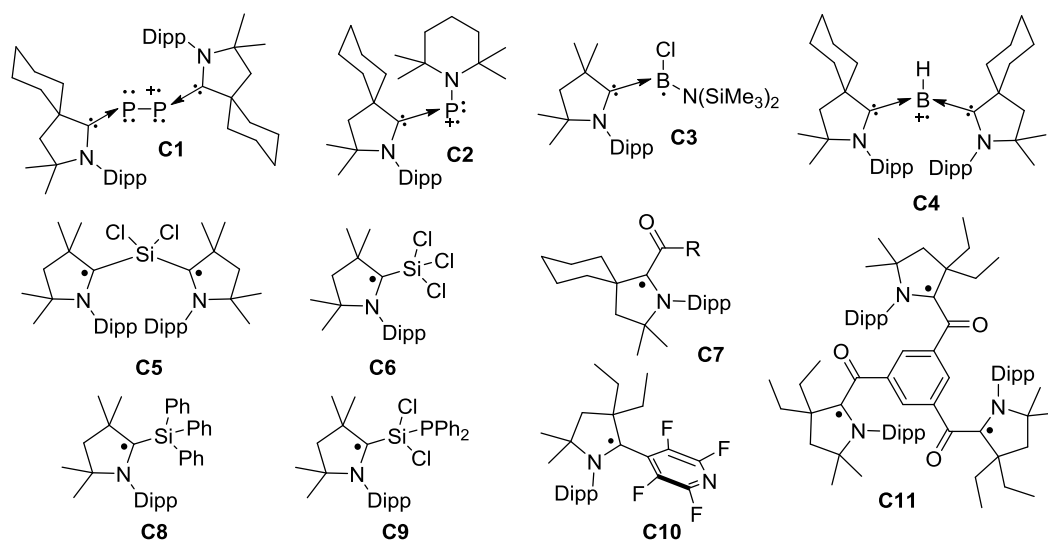


M: Au, Pt, Pd, Cu, Co, Fe, Ni, Mn, Zn

Scheme 41. Structurally characterized CAACs stabilized metal complexes with zero oxidation state.

Because CAACs possess a singlet spin ground state and a smaller energy gap between the HOMO and the lowest unoccupied molecular orbital (LUMO) than NHCs.^[145] The isolation of CAACs stabilized radicals is also possible. The better π -accepting properties of CAACs are able to enhance the delocalization of the single electron to their π system, resulting in the decreased energetic state of the SOMO. Moreover, the presence of a quaternary center

adjacent to the carbene makes CAACs sterically demanding. This avoids radical dimerization. As a consequence, CAACs have proved to be excellent ligands for the stabilization of phosphorus-,^[146-147] boron-,^[133, 148] silicon-^[149-152] and even carbon-centered neutral or cationic radicals^[153-155] (Scheme 42).



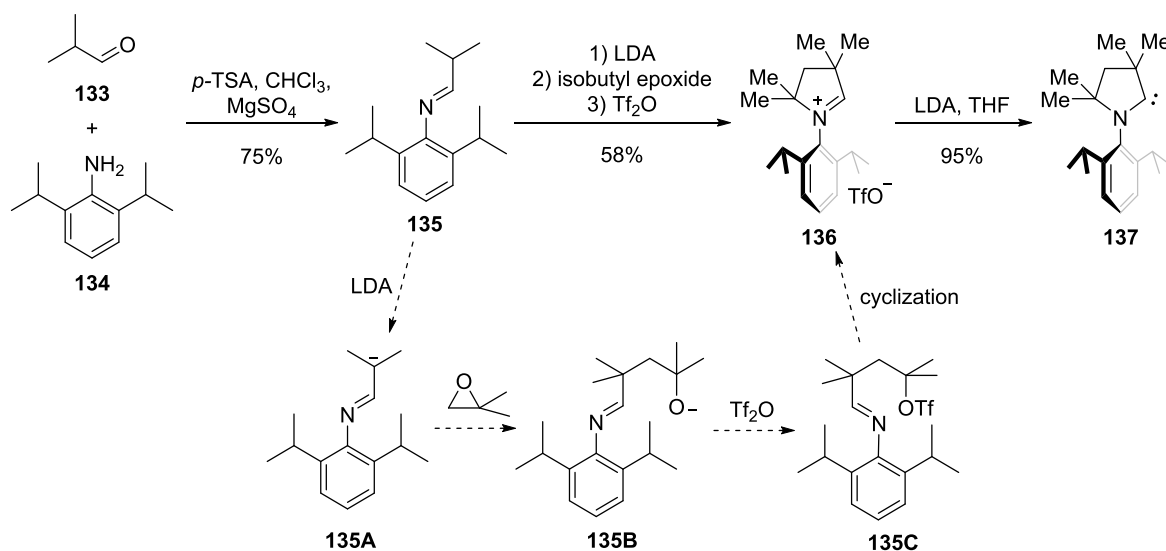
Scheme 42. Structurally characterized CAACs stabilized radicals.

4.2 α -Radical Phosphines based on CAACs

The major task of my research was to synthesize α -cationic ligands with stronger π -accepting character via reaction of diverse carbenes with chlorophosphine and to explore the isolation of the derived radicals.^[123]

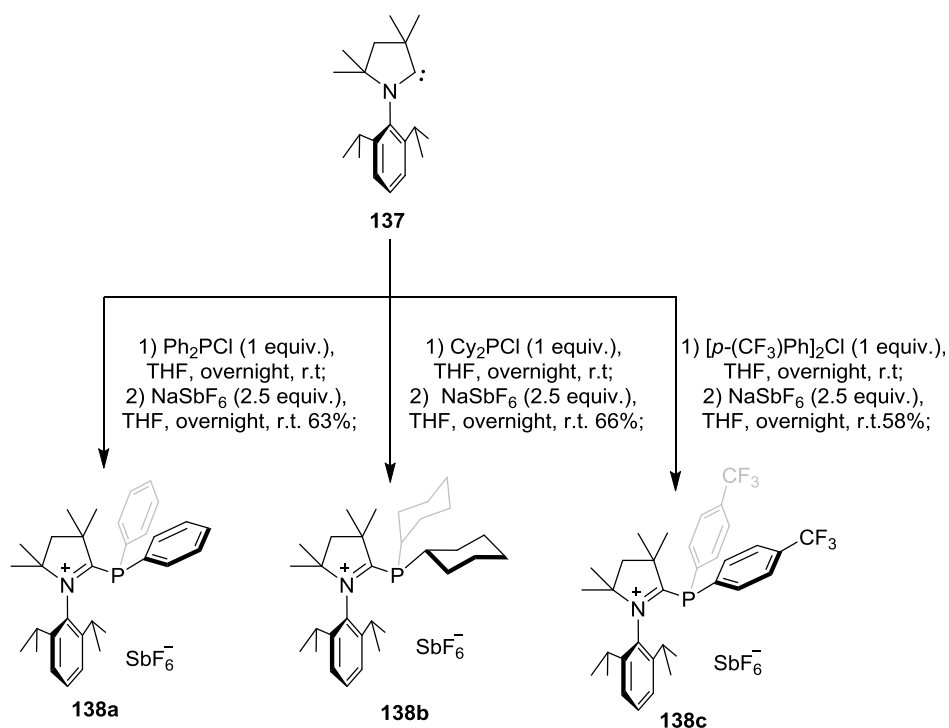
4.2.1 Synthesis of Cationic Phosphines

CAAC **137** was obtained via the same method reported by the Bertrand group.^[130] Imine **135**, formed by condensation of isobutylaldehyde with 2,6-diisopropylaniline, was lithiated with LDA followed by reaction with isobutyl epoxide and addition of Tf_2O to afford imine **136** in one pot. This compound was deprotonated by LDA to afford carbene **137** (Scheme 43).



Scheme 43. Synthesis of **137**.

Then, CAAC **137** in THF was treated with Ph_2PCl , Cy_2PCl and $[\text{p}-(\text{F})\text{Ph}]_2\text{PCl}$ to generate yellow precipitates, which were separated from the reaction mixture by simple filtration. After anion exchange and recrystallization, CAAC-stabilized phosphines **138a**, **138b** and **138c** were obtained in moderate to good yields (58-66%), proving the generality of our strategy (Scheme 44).^[156]



Scheme 44. Synthesis of CAAC stabilized cationic ligand **138a-c**.

The formation of cations **138a-c** was first indicated by the appearance of a signal in the ^{31}P NMR resonance ($\delta = 0.0, 21.6, -4.3$ ppm). These values were comparable to the ones reported

for imidazolium or cyclopropenium substituted compounds. Moreover, the molecular structures of **138a-c** were unambiguously characterized by X-ray crystallography (Figure 34-36). Two structural parameters are crucial for the understanding of the electron environment around the phosphorus atom in **138a-c**. The P1-C1(carbene) bond lengths [**138a**: 1.864(3) Å, **138b**: 1.8846(11) Å, **138c**: 1.8529(15) Å] are similar to those observed in neutral aromatic phosphines, but are significantly longer than typical P=C double bonds.^[157] On the other hand, the N1-C1(carbene) bond lengths [**138a**: 1.305(3) Å, **138b**: 1.3057(14) Å, **138c**: 1.3067(19) Å] are comparable to the C=N bond observed from imines (1.279 Å in DBN). In addition, the degrees of pyramidalization at phosphorus (**138a**: 56.5%, **138b**: 55.3%, **138c**: 53.3%) are comparable to those observed for neutral aromatic phosphines (56.7% for PPh₃).^[87] These two parameters reveal marginal back-donation from the phosphorus to the CAAC rings and suggest retention of a nonbonding electron pair on this atom. The pyramidalization in **138c** is smaller than in **138a** and **138b**, probably because the -CF₃ group on the phenyl ring lowers the energy of the π -system of the phenyl group, increasing delocalization of the P electron pair into this ring. This also suggests indirectly that the P1-C1(carbene) bond in **138c** contains more single bond character than **138a** and **138b**.

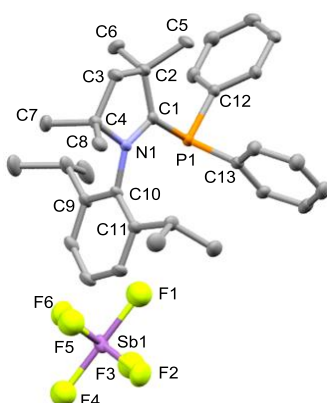


Figure 34. Molecular structure of compound **138a** in the solid state. Thermal ellipsoids at 50% probability; hydrogen atoms and solvent molecules have been omitted for clarity.

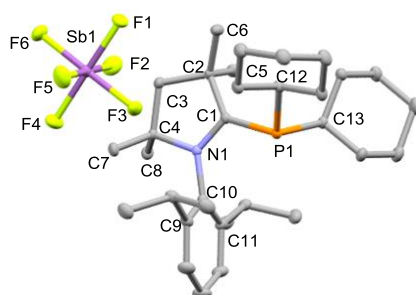


Figure 35. Molecular structure of compound **138b** in the solid state. Thermal ellipsoids at 50% probability; hydrogen atoms have been omitted for clarity.

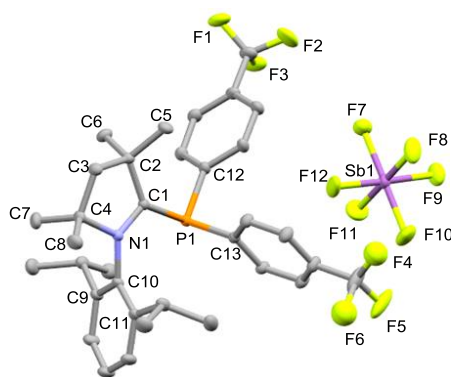


Figure 36. Molecular structure of compound **138c** in the solid state. Thermal ellipsoids at 50% probability; hydrogen atoms have been omitted for clarity.

4.2.2 Electronic Properties of Cationic Phosphines

The donor abilities of phosphines **138a-c** were evaluated by cyclic voltammetry. Phosphines **138a-c** display higher oxidation potential than phosphites and even most monocationic phosphines, which suggests their stronger π -acceptor properties. Among them, **138c** containing $-\text{CF}_3$ groups on the phenyl ring shows the highest oxidation potential and therefore, should represent the strongest π -acceptor properties. In addition, it was observed that the one electron reduction is quasi-reversible at $E_{1/2}$ (**138a**: -1.347 V, **138b**: -1.436 V, **138c**: -1.187 V) against the $\text{Cp}^*_2\text{Fe}/\text{Cp}^*_2\text{Fe}^+$, as shown in Table 7 and Figures 37-39, which indicates the formation of stable radical that might be isolated and characterized.

Table 7: Electrochemical redox potentials of ligands **138a-c**. The values for commonly used phosphorus-based ligands and reference compounds are included for comparison.

Entry	Ligand	$E_{\text{p(ox)}}^{\text{[a]}}$	$E_{\text{p(red)}}^{\text{[a]}}$
1	138a	1.536	-1.347
2	138b	1.494	-1.436
3	138c	1.791	-1.187
4	PPh_3	0.687	.[b]
5	P(OMe)_3	1.297	.[b]

[a] Oxidation/reduction peaks potential reported in V and calibrated versus $\text{Cp}^*_2\text{Fe}/\text{Cp}^*_2\text{Fe}^+$, Bu_4NPF_6 (0.1 M) in CH_2Cl_2 ; [b] No reduction signal observed from 0 to -2.5 V; [c] no signal detected from 0 to 2V.

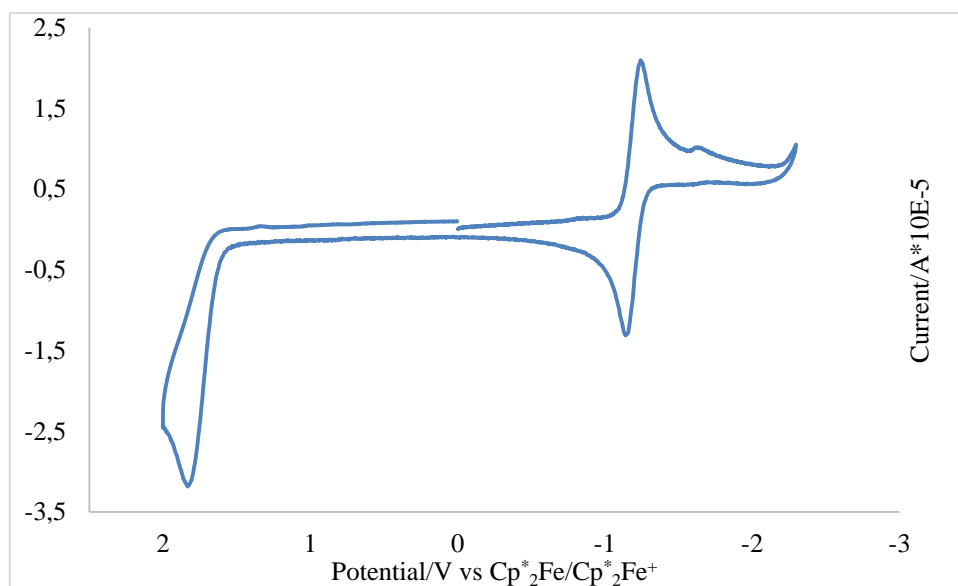


Figure 37. Cyclic voltammograms of **138a** reported in V and calibrated versus Cp*₂Fe/Cp*₂Fe⁺, Bu₄NPF₆ (0.1 M) in CH₂Cl₂.

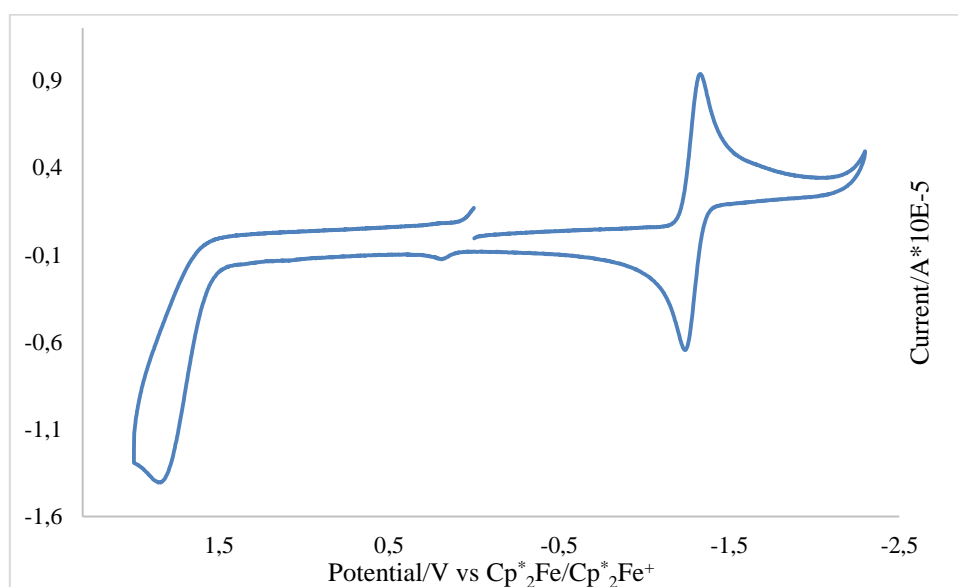


Figure 38. Cyclic voltammograms of **138b** reported in V and calibrated versus Cp*₂Fe/Cp*₂Fe⁺, Bu₄NPF₆ (0.1 M) in CH₂Cl₂.

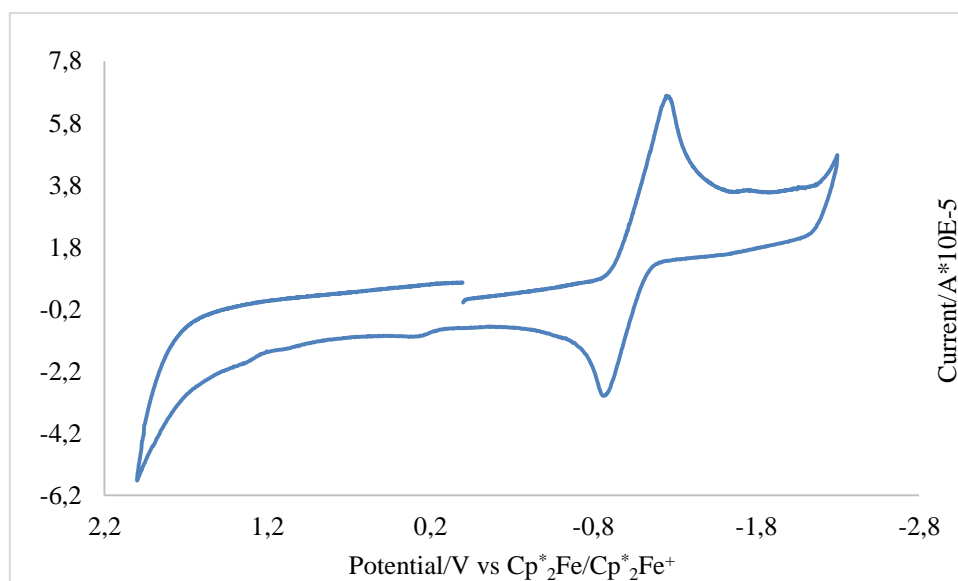
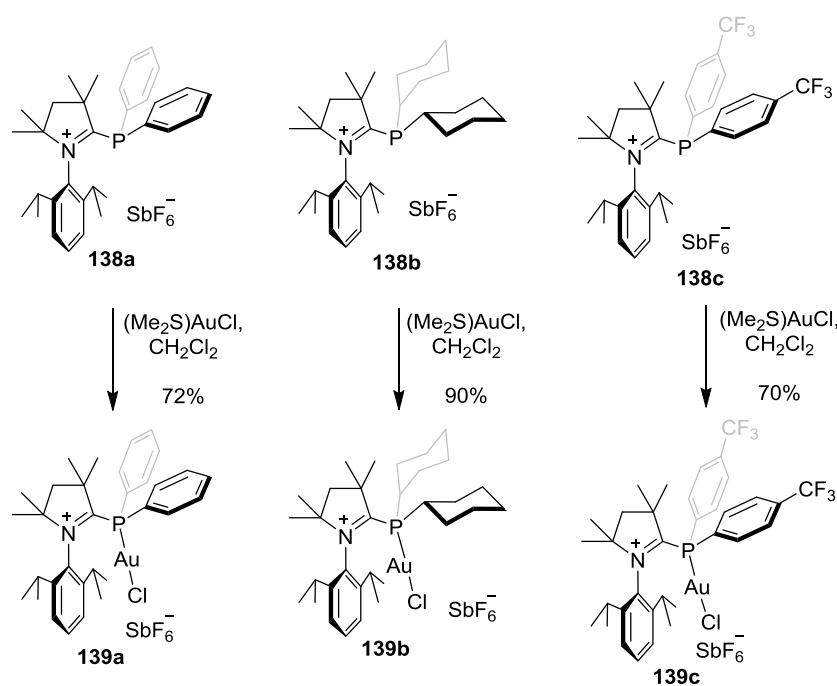


Figure 39. Cyclic voltammograms of **138c** reported in V and calibrated versus $\text{Cp}^*_2\text{Fe}/\text{Cp}^*_2\text{Fe}^+$, ${}^n\text{Bu}_4\text{NPF}_6$ (0.1 M) in CH_2Cl_2 .

4.2.3 Coordination of the Cationic Ligands.

Based on the analysis of the donor ability of **138a-c**, it is expected that the electron lone pairs on the phosphorus atoms are still available for coordination to metal salts. Thus ligands **138a-c** were reacted with $(\text{Me}_2\text{S})\text{AuCl}$ to afford **139a-c** as shown in Scheme 45. Importantly, the coordination of phosphorus to the gold center in each complex was confirmed by the displacement of the original ${}^{31}\text{P}$ NMR signal, and ultimately by X-ray diffraction (Figure 40-42).



Scheme 45. Synthesis of **139a-c**.

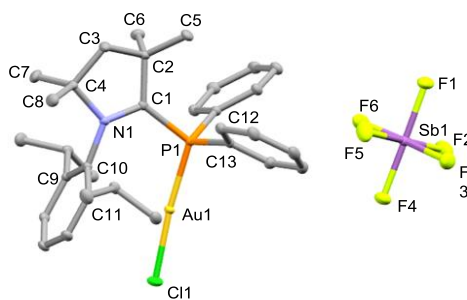


Figure 40. Molecular structure of compound **139a** in the solid state. Thermal ellipsoids at 50% probability; hydrogen atoms have been omitted for clarity.

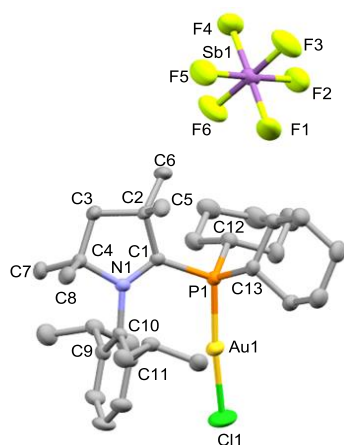


Figure 41. Molecular structure of compound **139b** in the solid state. Thermal ellipsoids at 50% probability; hydrogen atoms have been omitted for clarity.

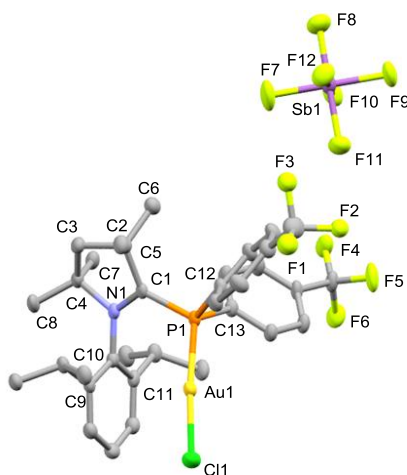
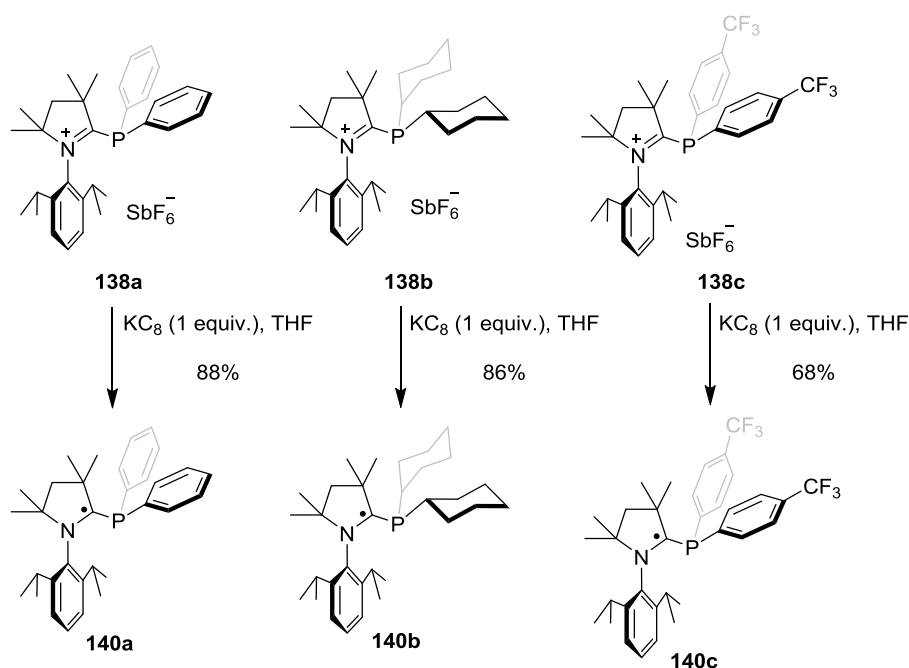


Figure 42. Molecular structure of compound **139c** in the solid state. Thermal ellipsoids at 50% probability; hydrogen atoms have been omitted for clarity.

4.3 α -Radical Phosphines

4.3.1 Synthesis of the Radical Phosphines

Encouraged by the distinctive cyclic voltammetry observed for these compounds, we decided to ascertain whether stoichiometric one electron reduction of these cations to the corresponding radicals could be carried out. To this end, **138a** was treated with Mg(0) powder^[155] or Li(0) sand in THF at room temperature; however, no significant change was observed by the ³¹P NMR analysis and only starting material was recovered. This suggested that the reductants used were not strong enough to transfer electrons to the cationic phosphorus ligands.



Scheme 46. Synthesis of radical **140a-c**.

When one of the strongest reductants KC_8 (potassium graphite) was used for the same purpose, the reaction mixture turned deep red, indicating the possibility of radical formation, since the majority of radicals are quite colorful (Scheme 46). To further prove this hypothesis, a small amount of the deep red solution was taken out from the Schleck and exposed to air, losing its color within a few seconds. To confirm the existence of radicals, the solid obtained after evaporation of the solvent from the reaction mixture was dissolved in toluene and analyzed by EPR. The X-band EPR spectrum of **140a** in toluene displays a multiplet ($g = 2.0056$) due to a large hyperfine coupling constant with the phosphorus nucleus [$a(^{31}\text{P}) = 18.00 \text{ G}$] and a small hyperfine coupling constant with the nitrogen nucleus [$a(^{14}\text{N}) = 6.00 \text{ G}$] (Figure 43). This spectrum was well-simulated with that of a carbon-centered radical that

shows coupling with phosphorus and nitrogen atoms. Thus, this experiment unambiguously supported the radical nature of **140a**. In a similar manner, radicals **140b** and **140c** were also synthesized from **138b** and **138c** in excellent yields respectively. Their EPR spectra are shown in Figure 44 and 45.

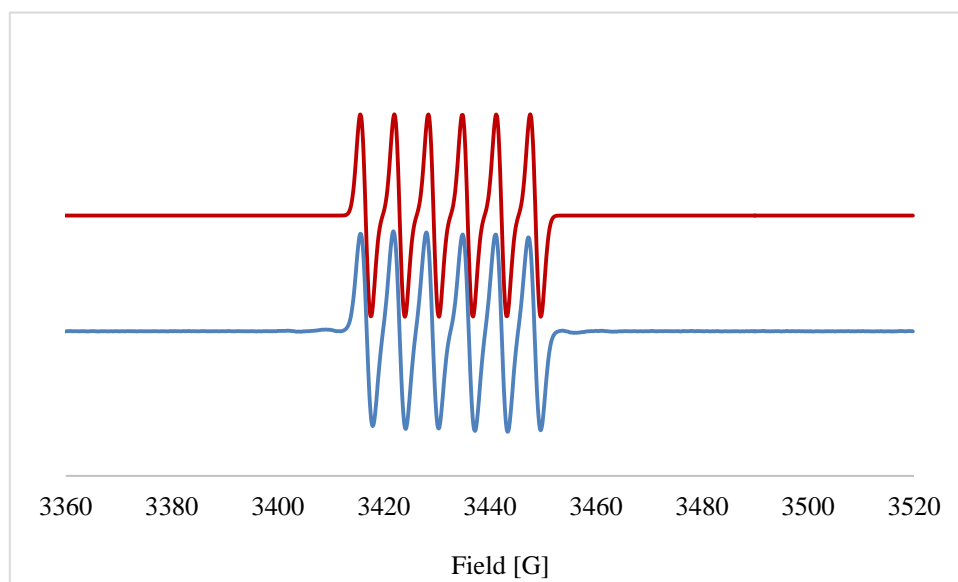


Figure 43. X-band EPR spectrum of **140a** in toluene [observed spectrum in blue, simulated spectrum in red; $g = 2.0056$, $a(^{31}\text{P}) = 18.00$ G, $a(^{14}\text{N}) = 6.00$ G].

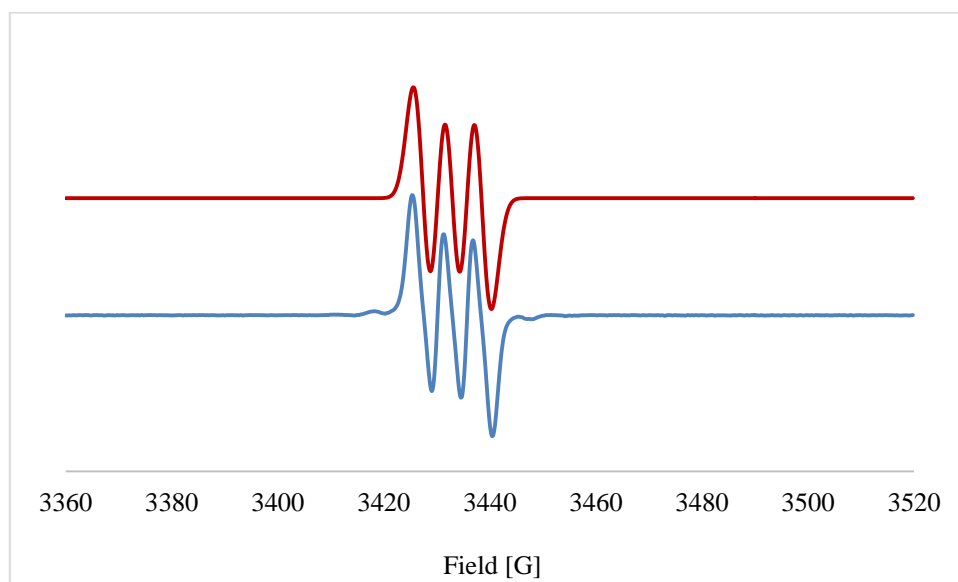


Figure 44. X-band EPR spectrum of **140b** in toluene [observed spectrum in blue, simulated spectrum in red; $g = 2.0055$, $a(^{31}\text{P}) = 1.04$ G, $a(^{14}\text{N}) = 5.17$ G].

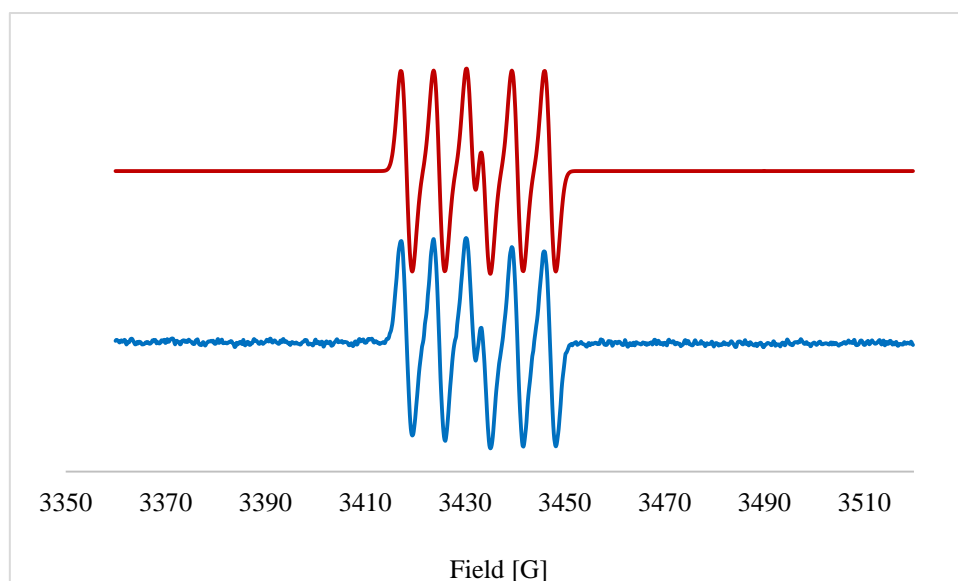


Figure 45. X-band EPR spectrum of **140c** in toluene [observed spectrum in blue, simulated spectrum in red; $g = 2.0056$, $a(^{31}\text{P}) = 14.69$ G, $a(^{14}\text{N}) = 6.12$ G].

Finally, the connectivity of **140a** and **140c** was unambiguously confirmed by single X-ray diffraction analysis after obtaining crystals by cooling solutions of **161a** and **161c** in pentane (Figure 46 and 47). The first evidence for the formation of the radicals from cationic phosphines was the absence of SbF_6^- counter anions that was present in the starting material. Due to the single electron reduction, the $\text{N}1=\text{C}1(\text{carbene})$ double bonds [**133a**: 1.305(3) Å, **138c**: 1.3067(19) Å] on cationic phosphines reduce their bond order as reflected in the elongation of the bond lengths [**140a**: 1.3979(17) Å, **140c**: 1.394(3) Å]. On the other hand, the $\text{P}1-\text{C}1(\text{carbene})$ bonds on radicals [**140a**: 1.7881(14) Å, **140c**: 1.785(2) Å] were shorter than those in their cationic precursors [**133a**: 1.864(3) Å, **138c**: 1.8529(15) Å], showing partial delocalization of the single electron into the σ^* orbitals of $\text{P}-\text{C}(\text{Ph})$.^[158] In addition, the degree of pyramidalization at phosphorus (**140a**: 53.6%, **140c**: 53.8%) was slightly smaller than that observed for neutral aromatic phosphines (56.76 for PPh_3). This parameter revealed that back-donation from the phosphorus to the CAAC rings must be marginal and suggest retention of a nonbonding electron pair on this atom.

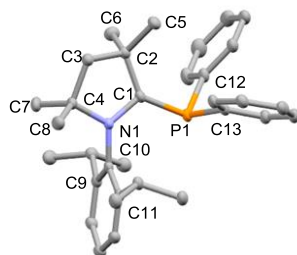


Figure 46. Molecular structure of radical **140a** in the solid state. Thermal ellipsoids at 50% probability; hydrogen atoms have been omitted for clarity.

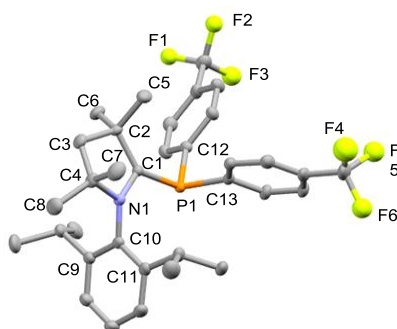
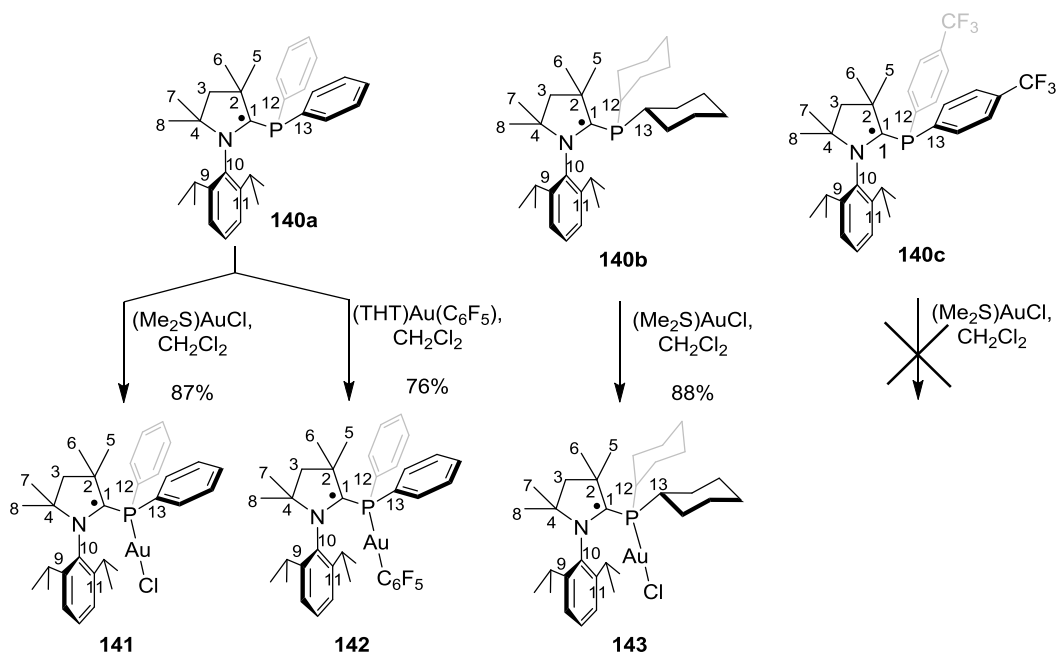


Figure 47. Molecular structure of radical **140c** in the solid state. Thermal ellipsoids at 50% probability; hydrogen atoms have been omitted for clarity.

4.3.2 Coordination of α -Radical Phosphines towards Au(I)

The electron lone pairs on the phosphorus atoms of **140a-c** were still available for the coordination to metal salts. To the best of our knowledge, there is no successful example of α -radical phosphines ever investigated in coordination chemistry, probably due to its highly reactive properties. Hence, our next goal was to study radicals **140a-c** in coordination chemistry.

Initially, **140a** smoothly reacted with $(\text{Me}_2\text{S})\text{AuCl}$ in THF affording the radical complex **141**, which was insoluble in pentane, giving the first indication of the successful coordination. In a similar manner, **142** and **143** were synthesized from **140a** and **140b** respectively in excellent yields. However, mixing **140c** and $(\text{Me}_2\text{S})\text{AuCl}$ in THF led to a complicated mixture, in which black precipitates, probably Au(0) were formed in the reaction mixture. During this process, the radical phosphine was probably oxidized to the cationic phosphine (Scheme 47).



Scheme 47. Synthesis of **141-143**.

Subsequently, to additionally confirm the existence of radicals, each of the solids **141-143** was dissolved in toluene and evaluated by EPR analysis. The X-band EPR spectrum of product **141** in toluene (Figure 48) displays a multiplet ($g = 2.0053$) due to a small hyperfine coupling constant with the phosphorus nucleus [$a(^{31}\text{P}) = 7.70 \text{ G}$] and a large hyperfine coupling constant with the nitrogen nucleus ($a(^{14}\text{N}) = 13.83 \text{ G}$). The resulting spectrum could be well-simulated and matched that of a carbon-centered radical involving phosphorus and nitrogen atoms. In a similar manner, radicals **142** and **143** in toluene were also analyzed by EPR spectra as shown in Figures 49-50 and their spectra were well-simulated with that of a carbon-centered radical that shows coupling with phosphorus and nitrogen atoms.

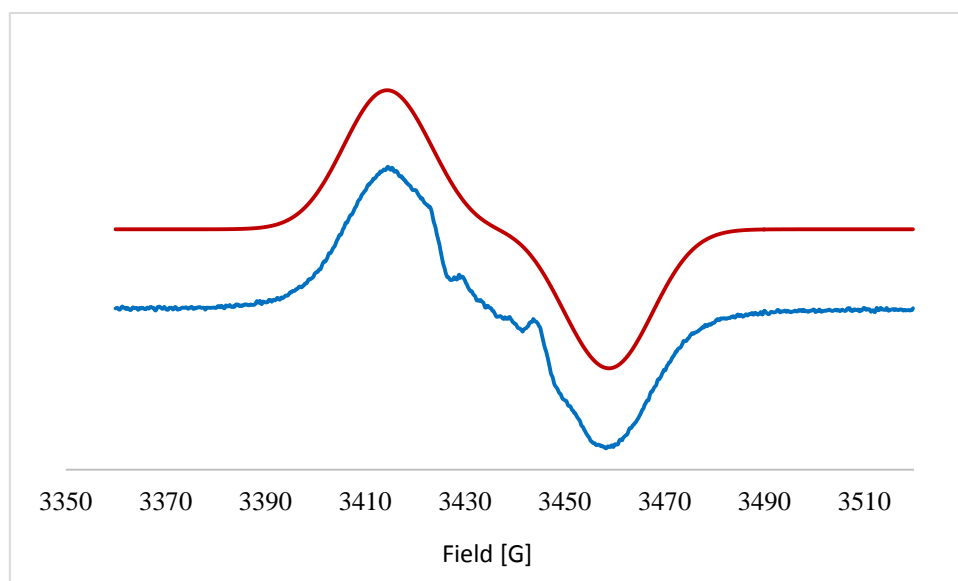


Figure 48. X-band EPR spectrum of **141** in toluene [observed spectrum in blue, simulated spectrum in red; $g = 2.0053$, $a(^{31}\text{P}) = 7.70$ G, $a(^{14}\text{N}) = 13.83$ G].

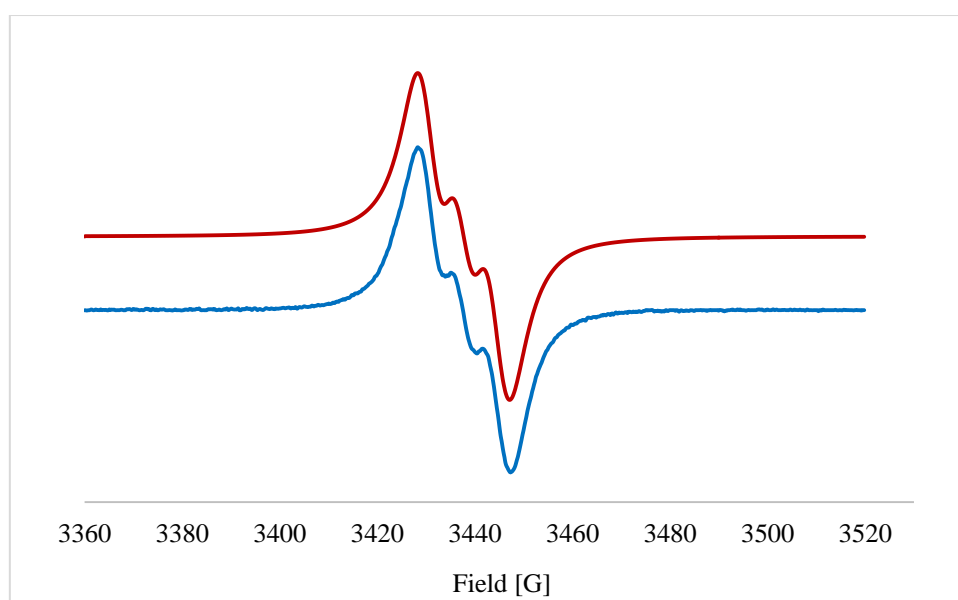


Figure 49. X-band EPR spectrum of **142** in toluene [observed spectrum in blue, simulated spectrum in red; $g = 2.0046$, $a(^{31}\text{P}) = 2.05$ G, $a(^{14}\text{N}) = 6.16$ G].

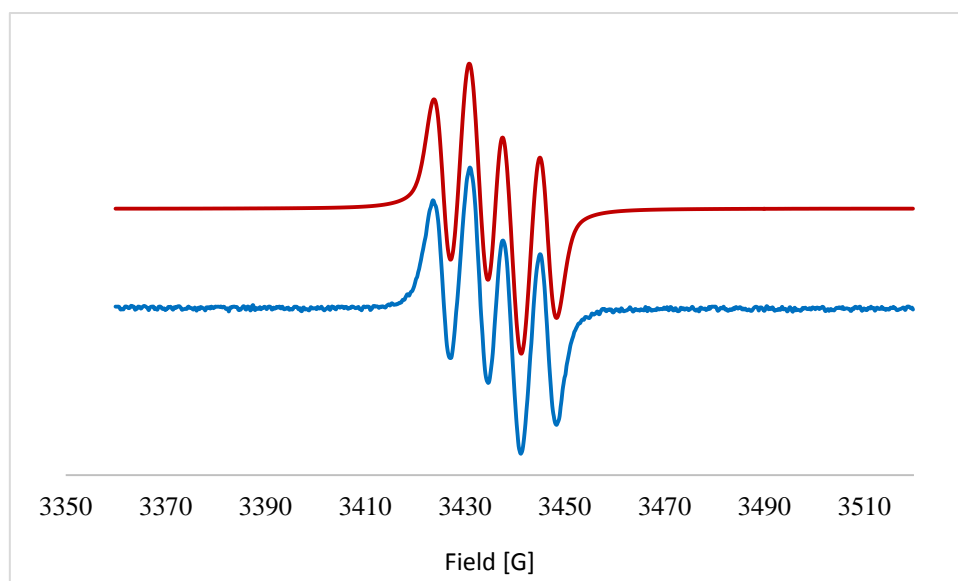


Figure 50. X-band EPR spectrum of **143** in toluene [observed spectrum in blue, simulated spectrum in red; $g = 2.0056$, $a(^{31}\text{P}) = 7.75$ G, $a(^{14}\text{N}) = 5.90$ G].

Finally, radicals **141-143** derived from **140a** and **140b** were unambiguously confirmed by single X-ray diffraction analysis (Figure 51-53). The absence of counter anions proved the presence of neutral radical Au complexes. Like in the free ligands, the P1-C1(carbene) bond lengths [**141**: 1.7825(13) Å, **142**: 1.7985(9) Å, **143**: 1.7715(13) Å] were shorter in comparison to their cationic species [**139a**: 1.873(2) Å, **139b**: 1.883(4) Å], showing the delocalization of the single electron into σ^* orbitals of the P-C(Ph) bonds. Conversely, the N1-C1(carbene) bond lengths [**141**: 1.3955(16) Å, **142**: 1.4018(12) Å, **143**: 1.3904(16) Å] were elongated in comparison to their cationic species [**139a**: 1.300(3) Å, **139b**: 1.301(5) Å], since the N1=C1(carbene) double bond reduce the bond order after the single electron reduction. The Au1-P1 bond lengths [**141**: 2.2377(4) Å, **142**: 2.2473(4) Å, **143**: 2.2840(5) Å] were similar to those of their cationic species [**139a**: 2.2221(6) Å, **139b**: 2.2269(10) Å].

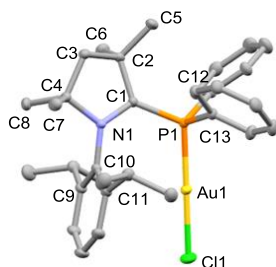


Figure 51. Molecular structure of compound **141** in the solid state. Thermal ellipsoids at 50% probability; hydrogen atoms have been omitted for clarity.

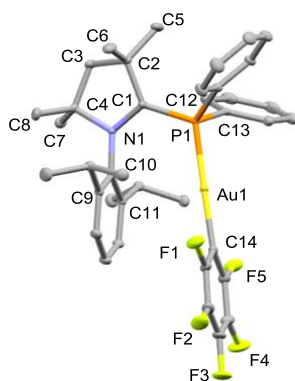


Figure 52. Molecular structure of compound **142** in the solid state. Thermal ellipsoids at 50% probability; hydrogen atoms have been omitted for clarity.

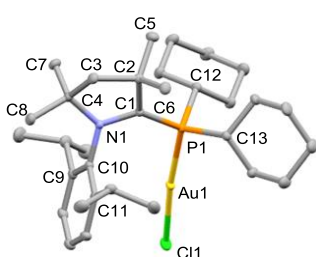
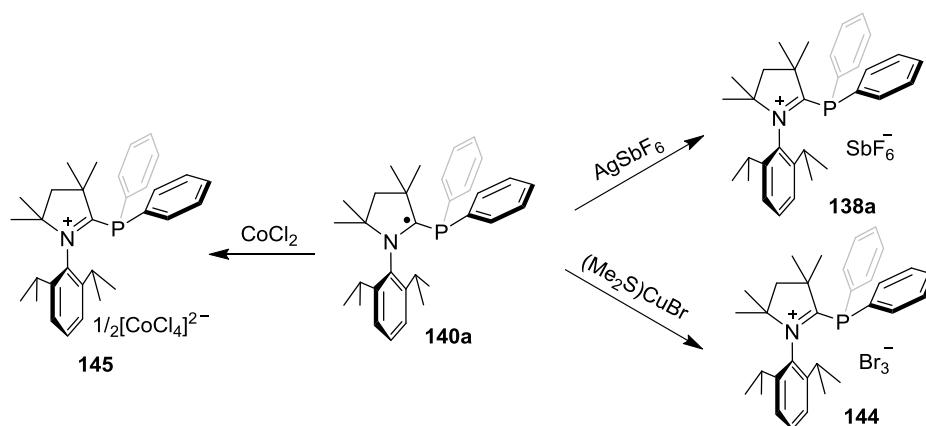


Figure 53. Molecular structure of compound **143** in the solid state. Thermal ellipsoids at 50% probability; hydrogen atoms and solvent molecules have been omitted for clarity.

4.3.3 Coordination of α -Radical Phosphines towards Other Metal Salts

In order to further explore the coordination chemistry of the radical ligands, **140a** was chosen as model ligand. Initially, AgSbF_6 and $(\text{Me}_2\text{S})\text{CuBr}$ were reacted with **140a**, affording cationic phosphines **138a** and **144**, in which the metal salts were reduced by single electron transfer. Similarly, mixing of **140a** with CoCl_2 afforded the cationic compound **145**, with $[\text{CoCl}_4]^{2-}$ as the counter anion (Scheme 48).



Scheme 48. Attempts to coordinate **140a** to other metal salts.

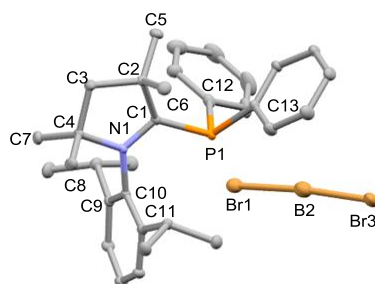


Figure 54. Molecular structure of the decomposed product **144** in the solid state. Thermal ellipsoids at 50% probability; hydrogen atoms have been omitted for clarity.

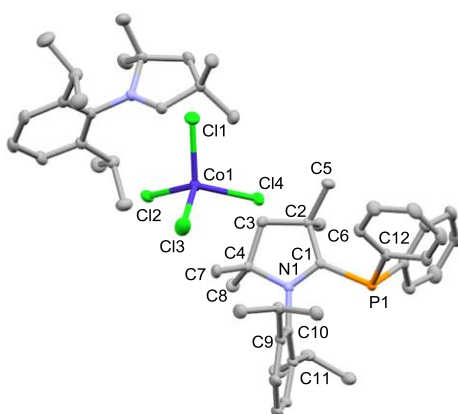
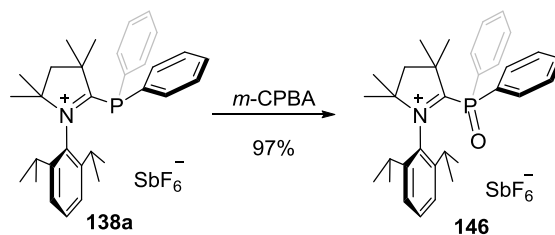


Figure 55. Molecular structure of the decomposed product **145** in the solid state. Thermal ellipsoids at 50% probability; hydrogen atoms and solvent molecules have been omitted for clarity.

4.4 Synthesis of Cationic Phosphine Oxide and the Radical thereof

Phosphine oxides feature tetrahedral phosphorus centers, in which the P-O bond is short and polar. Phosphine oxides are useful ligands in various reactions, such as Kumada–Corriu cross-couplings^[159] and Suzuki–Miyaura Reactions^[160]. In addition, it is quite popular to use phosphine oxides as hemilabile pre-ligands in catalysis.^[161-162] Therefore, it would be interesting to know whether we could obtain the cationic phosphine oxides by the oxidation of cationic phosphine **138a**. Thus, we subjected compound **138a** to oxidation using *m*-CPBA in CH₂Cl₂ at room temperature. The oxidation proceeded in quantitative yield affording a white solid **146**, which was unambiguously confirmed by X-ray diffraction analysis to be the desired oxide (Scheme 49 and Figure 56). Subsequently, compound **146** was investigated by cyclic voltammetry, depicting a quasi-reversible redox potential, which indicated the possibility of isolating the corresponding radical (Figure 57).



Scheme 49. Synthesis of cationic phosphine oxide **146**.

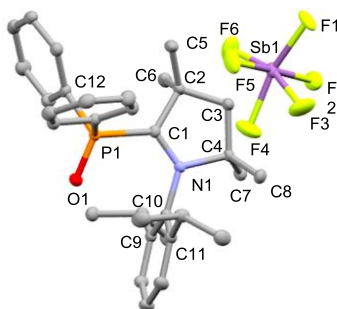


Figure 56. Molecular structure of **146** in the solid state. Thermal ellipsoids at 50% probability; hydrogen atoms have been omitted for clarity

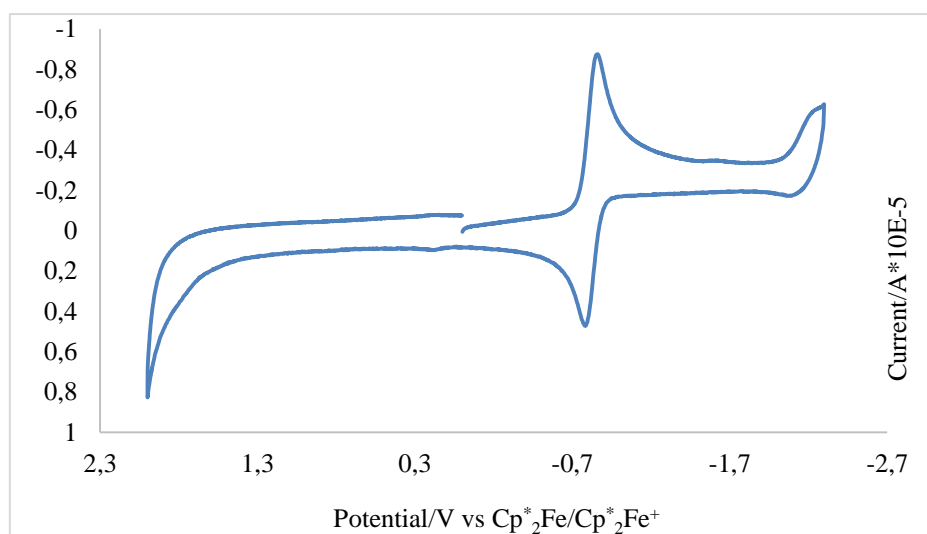
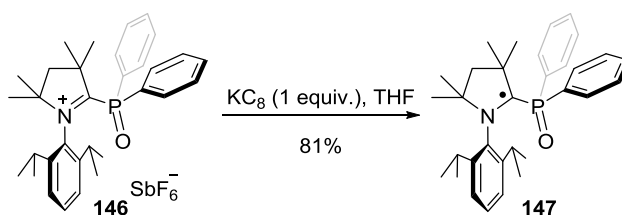


Figure 57. Cyclic voltammograms of **146** reported in V and calibrated versus $\text{Cp}^*{}_{2}\text{Fe}/\text{Cp}^*{}_{2}\text{Fe}^+$, ${}^n\text{Bu}_4\text{NPF}_6$ (0.1 M) in CH_2Cl_2 .

The oxide **146** was subjected to the same reaction conditions as before, using KC_8 . This produced a new red solid **147** (Scheme 50). The confirmation about the radical nature of **147** came from EPR and X-ray analysis (Figures 58 and 59). The X-band EPR spectrum of **147** in toluene displayed a multiplet ($g = 2.0057$) due to a small hyperfine coupling constant with the phosphorus nucleus [$a(^{31}\text{P}) = 6.14$ G] and a large hyperfine coupling constant with the nitrogen nucleus ($a(^{14}\text{N}) = 16.96$ G) (Figure 59). The resultant spectrum was well-simulated

with that of a carbon-centered radical involving phosphorus and nitrogen atoms. Thus, the EPR data unambiguously supported the presence of a radical **147**. Finally, red crystals of **147** suitable for X-ray crystallography studies were obtained from pentane in the freezer and its structure in the solid state was confirmed by X-ray diffraction. The most obvious evidence for the radical is the absence of counter anions that are present in the starting material. Like in the ligands, the P1-C1(carbene) bond length [**147**: 1.7878(7) Å] was shorter in comparison to their cationic species [**146**: 1.8819(16) Å], showing the delocalization of the single electron into σ^* orbital of P-C(Ph) bond. Conversely, the N1-C1(carbene) bond length [**147**: 1.3940(9) Å] was elongated in comparison to their cationic species [**146**: 1.299(2) Å], since the N1=C1(carbene) double bonds on cationic phosphine oxide again reduces its bond order.



Scheme 50. Synthesis of radical **147**.

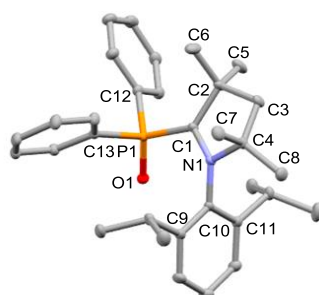


Figure 58. Molecular structure of the decomposed product **147** in the solid state. Thermal ellipsoids at 50% probability; hydrogen atoms have been omitted for clarity.

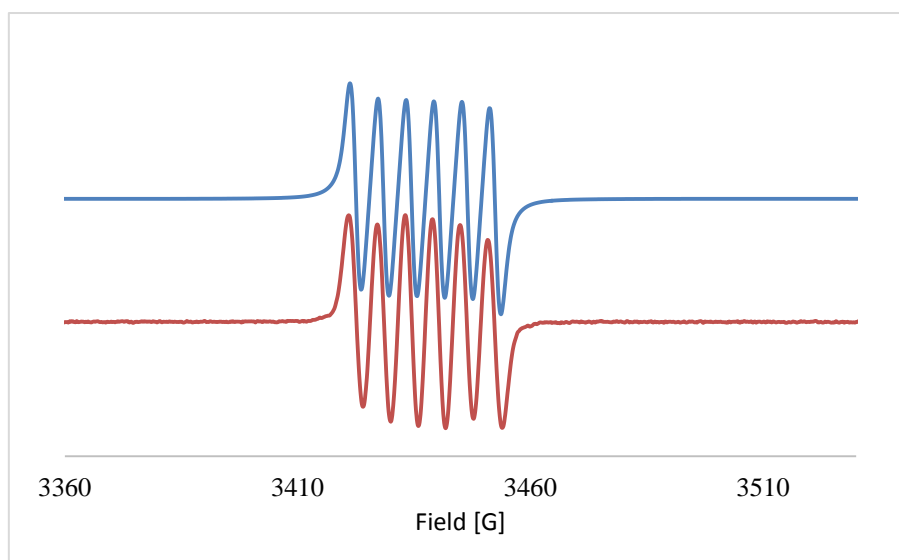


Figure 59. X-band EPR spectrum of **147** in toluene [observed spectrum in blue, simulated spectrum in red; $g = 2.0057$, $a(^{31}\text{P}) = 6.14$ G, $a(^{14}\text{N}) = 16.96$ G].

4.5 Theoretical Analysis of Properties of α -Radical Phosphines

The coordination between **AuCl** and radical phosphine **140a** was evaluated as an example using charge decomposition analysis (CDA) and extended charge decomposition analysis (ECDA). The result displayed in Figure 60 reveals that the HOMO/SOMO of complex **140a-AuCl** is mainly contributed by the HOFO of **140a**. The LUFO of **AuCl** with d_{z^2} of Au and the HOFO-1 of **140a** with lone pair on P atom contribute to the HOMO-5 of **140a-AuCl**, which involves the Au-P bond formation. Hence, the closer energy difference for LUFO of **MCl** (**M** = Au, Cu, Ag) and HOFO-1 of ligands is more favorable for **M-P** bond formation of the complex.

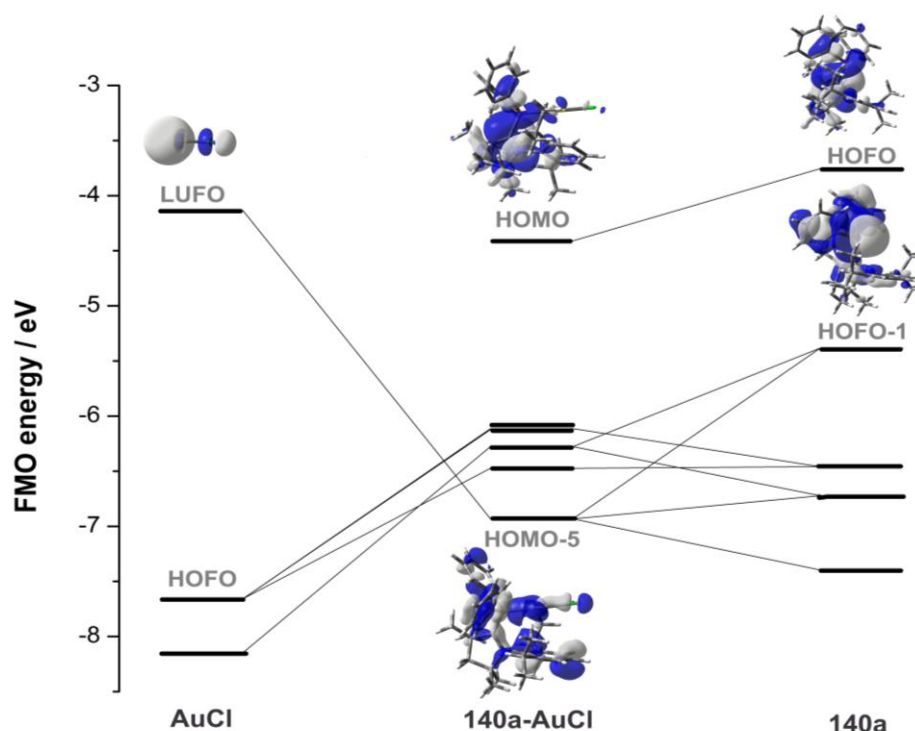
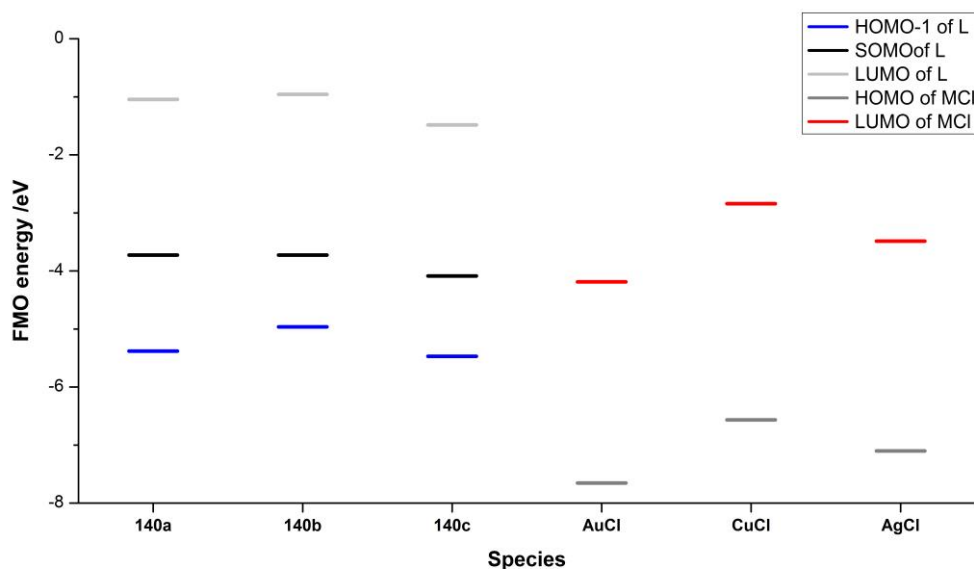


Figure 60. Orbital correlation diagram for **140a-AuCl** of the interaction between fragments **AuCl** and **140a**. A plot of important molecular orbitals of **140a-AuCl** and its related fragments are also presented. LUMO: lowest unoccupied molecular orbital; HOMO: highest occupied molecular orbital; LUFO: lowest unoccupied fragment orbital; HOFO: highest occupied fragment orbital; SOMO: single occupied molecular orbital.

The important frontier orbital energies (in eV) for all radical phosphines **140a-c** and metal salts **MCl** (**M** = Au, Cu, Ag) were computed at the UB3LYP-D3/def2-TZVP level as shown in Table 8. The LUMO energies of CuCl ($E_{\text{LUMO}} = -3.30$ eV) and AgCl ($E_{\text{LUMO}} = -3.63$ eV) are much higher than that of AuCl ($E_{\text{LUMO}} = -4.21$ eV). Thus, the reaction of metal salt CuCl and AgCl with radical phosphine ligands may be less stable than the ones of AuCl. This is also consistent with the complex forming energies ($E_{\text{L-MCl}}$) shown in Table 8 that the $E_{\text{L-MCl}}$ values for CuCl and AgCl related complexes are more than 10 kcal/mol less than the ones for **140a-AuCl**. The energy of HOMO-1 for **140b** ($E_{\text{HOMO-1}} = -5.06$ eV) and **140c** ($E_{\text{HOMO-1}} = -5.59$ eV) is, respectively, slightly higher and lower than that of **140a** ($E_{\text{HOMO-1}} = -5.48$ eV). Comparatively, complex **140b-AuCl** might be more stable than **140a-AuCl**, while the complex **140c-AuCl** might be less stable.

Table 8. The SOMO/HOMO and LUMO energies (in eV) for all the species at the UB3LYP-D3/def2-TZVP level. SOMO-1 and SOMO represent occupied and unoccupied SOMO respectively.

Entry	Species	$E_{\text{SOMO-1}}^1$	E_{SOMO^2}	$E_{\text{LUMO+1}}$	$E_{\text{L-MCl}}$
1	140a	-3.83	-1.19	-0.80	
2	140b	-3.81	-1.09	-0.27	
3	140c	-4.24	-1.68	-1.62	
4	140a -AuCl	-4.52	-1.84	-1.32	-73.2
5	140b -AuCl	-4.49	-0.18	-0.38	-77.9
6	140c -AuCl	-4.89	-2.24	-2.06	-70.6
7	140a -CuCl	-4.40	-1.76	-1.25	-58.8
8	140b -CuCl	-4.38	-1.68	-0.47	-63.2
9	140c -CuCl	-4.75	-2.22	-2.00	-56.4
10	140a -AgCl	-4.49	-1.85	-1.33	-52.7
11	140b -AgCl	-4.47	-1.77	-0.44	-57.3
12	140c -AgCl	-4.86	-2.26	-2.09	-50.1
		$E_{\text{HOMO-1}}$	E_{HOMO}	E_{LUMO}	
13	AuCl	-7.81	-7.81	-4.21	
14	CuCl	-7.20	-7.20	-3.30	
15	AgCl	-7.33	-7.33	-3.63	



¹The HOMO-1 and HOMO orbitals for MCl (M = Au, Cu, and Ag) are degenerated. ²The HOMO orbital for the ligands and coordinated species is a SOMO orbital due to the stable radical.

In the case of the free ligands, the Mulliken spin density is mostly concentrated at the C1 (ca. 65%) and N (ca. 25%) atoms, and also some small distribution on the P atom. Similar results could be perceived by visualizing the SOMO. There is also some small distribution of spin density on C13 (Scheme 47) for **140a** and **140c**. This is consistent with the DFT calculated larger hyperfine coupling constant of C13 for both ligands in comparison with **140b**. Consequently, the spin densities on P for both ligands are slightly higher. The ³¹P atom still exhibit detectable hyperfine coupling in the EPR spectrum despite rather small spin densities

on it (<5%). The computed hyperfine coupling constants for ^{14}N and ^{31}P agree well with the ones from the simulated EPR, while the overestimation of ^{31}P on **140b** might be caused by the negative spin density (Table 10). Computationally, the α -spin density is positive, and the β -spin density is negative. When the computed absolute β -spin density value is bigger than the α -spin density, the total spin density is negative. In this case the discrepancy may be related to the use of an unrestricted approach, which is known to generally overestimate the difference between α -spin and β -spin populations.^[163-164] After the ligand binds to AuCl, the spin density distributed on Au is very small. This is also consistent with the experimental EPR simulation results that indicate no coupling for Au. Hence, both spin density and hyperfine coupling constant results are similar with the ones observed for ligands.

Table 9. The Mulliken spin densities and SOMO-1 plot of all the ligands and AuCl coordinated species at the UB3LYP-D3/def2-TZVP level.

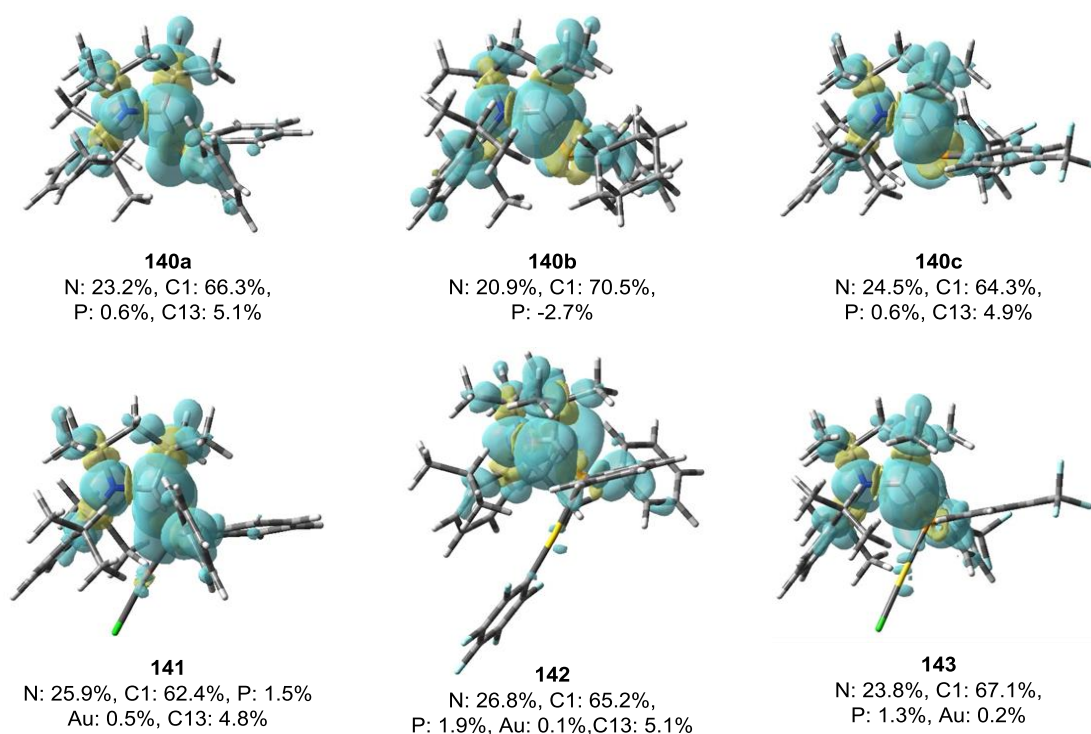


Table 10. Calculated hyperfine coupling constants (A in 10^{-4} cm^{-1}) of all species at the UB3LYP-D3/def2-TZVP level of theory. A_{iso} values greater than 2.0 are only reported. Experimental data was reported in red color.

Atom	140a	140b	140c	141	142	143
P	13.06	5.14	10.95	2.67	2.29	6.38
P(exp)	18.00	1.04	14.69	7.70	2.05	7.75
N	4.34	3.58	4.50	4.51	10.71	4.62
N(exp)	6.00	5.17	6.12	13.83	6.16	5.90
C ₁	18.24	20.68	17.27	17.38	44.68	19.78
C ₂	-6.27	-6.23	-6.06	-5.83	-8.58	-6.14
C ₃	2.24	2.62	2.19	2.65	2.61	/
C ₄	-2.81	-2.62	-2.86	/	-4.27	-2.78
C ₅	4.69	12.05	2.37	3.68	4.35	9.80
C ₆	12.90	10.23	4.36	11.86	13.61	10.62
C ₇	5.12	3.02	3.19	4.53	5.42	3.51
C ₈	3.09	/	5.11	3.72	4.16	/
C ₉	/	/	/	-2.91	-4.16	/
C ₁₀	3.12	4.79	5.60	3.25	6.59	4.87
C ₁₁	5.59	2.90	3.19	6.46	4.29	2.33
C ₁₂	2.11	6.32	2.53	2.10	3.91	4.52
C ₁₃	15.05	6.10	15.52	11.11	18.83	4.24

4.6 Summary IV

We have successfully isolated and characterized a series of CAAC derived cationic phosphines. Their cyclovoltammetry showed a quasi-reversible redox potential, which indicated that stable radicals were formed after one electron reduction. As a result, a series of α -radical phosphines have been synthesized and fully characterized. More intriguingly, these radical phosphines could coordinate to Au(I) and form a range of stable gold complexes that are unprecedented. In addition, we were also able to synthesize the radical phosphorus oxide. All of the synthesized radicals have been characterized by EPR and most have been crystallized. These novel compounds could be named as α -radical phosphine ligands, which might be useful in catalysis.

5 Experimental Part

5.1 General Experimental Conditions

5.1.1 Working Techniques

All moisture- and oxidation-sensitive reactions were performed in carefully dried glassware under argon atmosphere. The saturated aqueous solutions of sodium chloride, sodium bicarbonate, sodium carbonate and ammonium chloride, were saturated over sediment, unless indicated otherwise.

Solvents and reagents

All solvents were purified by distillation before use by following standard procedures. Dry solvents were obtained by distillation over the appropriate drying agent (*vide infra*) and then kept under argon atmosphere: diethyl ether, tetrahydrofuran, toluene, benzene, pentane and ⁿhexane (sodium, benzophenone as indicator); *N,N'*-dimethylformamide (Desmodur[®], dibutyltin dilaurate); CH₂Cl₂, acetone, acetonitrile, Et₃N (calcium hydride); fluorobenzene (phosphorus pentoxide), methanol and ethanol (magnesium). 1,2-Dichloro-ethane was purchased from Sigma-Aldrich and used as received. Other commercial reagents were obtained from various sources and used without further purification.

Inert gas atmosphere

Air and moisture-sensitive reactions were conducted under argon atmosphere. Argon was obtained from *Air Liquide* with higher than 99.5% purity.

Chromatographic methods

Reactions were mostly monitored by **thin layer chromatography** (TLC) using silica gel pre-coated polyester sheets (40 × 80 mm, Polygram[®] SIL G/UV254 from Macherey-Nagel). The spots were visualized with UV-light ($\lambda = 254$ nm) and/or by staining with phosphomolybdic acid or potassium permanganate stains.

Flash column chromatography was performed using silica gel 60 (Merck, 60 Å, 230-400 mesh 0.040-0.063 mm) and separations were conducted at slightly elevated pressure in a glass column.

5.1.2 Analytical Methods

Nuclear magnetic resonance spectroscopy (NMR)

Spectra were recorded on Bruker DPX 300 (^1H : 300 MHz, ^{13}C : 75 MHz, ^{31}P : 121 MHz), Bruker AV 400 (^1H : 400 MHz, ^{13}C : 100 MHz, ^{31}P : 161 MHz), and Bruker AV 500 (^1H : 500 MHz, ^{13}C : 125 MHz, ^{31}P : 202 MHz) spectrometers at room temperature (298 K). Chemical shifts (δ) are given in parts per million (ppm) relative to tetramethylsilane (^1H and ^{13}C , internal standard) and H_3PO_4 (^{31}P , external standard) and coupling constants (J) in Hertz (Hz). The corresponding solvent signals were used as a references: CDCl_3 : δC 77.0 ppm, δH 7.26 ppm; CD_2Cl_2 : δC 54.0 ppm, δH 5.32 ppm; CD_3CN : δC 1.32 ppm, δC 118.26 ppm δH 1.94 ppm; [D8]-toluene δC 20.4 ppm, δC 125.5 ppm, δC 128.3 ppm, δC 129.2 ppm, δC 137.9 ppm, δH 2.08 ppm, δH 6.97 ppm, δH 7.01 ppm and δH 7.09 ppm. The ^1H NMR multiplicities are assigned as follows: singlet (s), doublet (d), triplet (t), quartet (q), quintet (quin), sextet (sext), septet (sept), multiplet (m), broad (br.). The signals have been assigned using 1D and 2D experiments.

Infrared spectroscopy

IR spectra were recorded using ATR (attenuated total reflection) on a Spectrum One (Perkin-Elmer) spectrometer at room temperature. The characteristic absorption bands are given in wavenumbers [cm^{-1}].

Analytical gas chromatography

GC-MS couplings were performed on an *Agilent Technology* GC 6890 Series and MSD 5973 (carrier gas: helium) with HP6890 Series Injector, employing an MN Optima[®] 5 column (30 m \times 0.25 mm \times 0.25 mm). The mass spectra were recorded with an *Agilent Technology* 5973 Network MSD spectrometer. Quantitative evaluation of the integration was based on the substance peaks without considering response factors, unless stated otherwise.

Mass spectrometry (MS)

Mass spectra were measured on a Finnigan MAT 8200 (70 eV) or MAT 8400 (70 eV) spectrometer by electron ionization, chemical ionization, or fast atom/ion bombardment techniques. High resolution masses were determined on a Bruker APEX III FT-MS spectrometer (7 T magnet). All masses are given in atomic units per elementary charge (m/z) and reported in percentage relative to the basic peak. The mechanistic studies (cf. Chapter 4.5.2) were performed by ESI-MS with a Finnigan Ultra Mass TSQ 7000.

X-ray crystal structure analysis

The crystal structures were measured in the X-ray department of the Max Planck Institute for Coal Research in Mülheim an der Ruhr, led by Dr. C. W. Lehmann. The measurements were made using a Bruker-AXS Kappa CCD diffractometer.

Electron paramagnetic resonance (EPR)

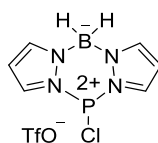
X-band EPR spectra were recorded on a Bruker ELEXSYS E500 spectrometer equipped with a Bruker dual-mode cavity (ER4116DM) and a Bruker high-sensitivity microwave bridge Super-X (ER-049X) with integrated microwave frequency counter. The magnetic field controller was externally calibrated with a Bruker NMR field probe (ER035M). The liquid samples were measured in 2mm quartz tubes and the spectra were simulated with the program ESIM/ISO (available from E. Bill by mail to ebill@gwdg.de).

5.1.3 Starting Materials as well as in Working Group-made Chemicals

Commercially available chemicals were used without further purification unless otherwise stated. Working group's internal chemicals: 2-phenylphosphine.

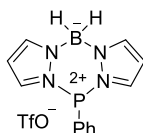
5.2 Synthesis

Compound 62



PCl_3 (0.16 ml, 1.8 mmol) and TMSOTf (0.65 ml, 3.6 mmol) were added at -78°C to a solution of $\text{K}[\text{BH}_2(\text{Pz})_2]$ (0.334 g, 1.8 mmol) in CH_2Cl_2 (5 ml). The mixture was allowed to warm up to r.t. overnight. Then the solvent was filtered off and the yellow solid washed with CH_2Cl_2 (2 x 5 ml). The crude product thus obtained was extracted with CH_3CN (2 x 5 ml) at 0°C and the combined solvents removed *in vacuo* to afford **62** as a white solid (157.1 mg, 24 %). m.p.: 95°C (dec.). ^1H NMR (CD_3CN , 300 MHz): $\delta = 8.60$ (d, $J = 2.1$ Hz, 2H), 8.42 (s, 2H), 6.86 (m, 2H), 4.08 – 3.53 ppm (br s, 2H). ^{13}C NMR (CD_3CN , 100 MHz): $\delta = 146.9$, 143.2 (d, $J_{\text{C-P}} = 30.8$ Hz), 122.2 (q, $J_{\text{C-F}} = 320.2$ Hz), 111.1 ppm (d, $J_{\text{C-P}} = 6.0$ Hz). ^{31}P NMR (CD_3CN , 121 MHz): $\delta = 85.7$ ppm. ^{11}B NMR (CD_3CN , 128 MHz): $\delta = 8.1$ ppm. ^{19}F NMR (CD_3CN , 282 MHz): $\delta = -79.3$ ppm. IR $\tilde{\nu} = 442, 516, 575, 633, 779, 913, 1024, 1060, 1084, 1162, 1225, 1419, 2456, 3112, 3139$ cm^{-1} . Elemental analysis for $\text{C}_7\text{H}_8\text{BClF}_3\text{N}_4\text{O}_3\text{PS}$ (362.46): *calcd.* for C 23.20%, H 2.22%, N 15.46%, *found:* C 23.14%, H 2.56%, N 16.12%.

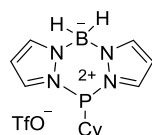
Compound 63



PhPCl_2 (1.5 ml, 10.7 mmol) and TMSOTf (1.9 ml, 10.7 mmol) were added at -78°C to a suspension of $\text{K}[\text{H}_2\text{B}(\text{Pz})_2]$ (2.0 g, 10.7 mmol) in CH_2Cl_2 (10 ml) and the mixture was allowed to warm up to r.t. overnight. Then the solvent was filtered off and the white solid left washed with CH_2Cl_2 (2 x 5 ml). The crude product was then extracted with CH_3CN (2 x 5 ml) at 0°C and the combined solvent removed *in vacuo* to afford **63** as a white solid (2.5 g, 57%). Colourless crystals suitable for X-ray crystallography were obtained from a $\text{CH}_3\text{CN}/\text{Et}_2\text{O}$ at -30°C . m.p.: 101°C (dec.). ^1H NMR (CD_3CN , 400 MHz): $\delta = 8.62$ (dd, $J = 3.3$ Hz, $J_{\text{H-P}} = 3.9$ Hz, 2H), 8.29 (s, 2H), 7.57 (m, 1H), 7.48 (m, 2H), 7.09 (m, 2H), 6.88 (dd, $J = 2.4$ Hz, $J_{\text{H-P}} = 5.1$ Hz, 2H), 3.25 ppm (br, $J_{\text{H-B}} = 138$ Hz). ^{13}C NMR (CD_3CN , 100 MHz): $\delta = 145.8, 144.0$ (d, $J_{\text{C-P}} = 26.7$ Hz), 133.3, 131.6 (d, $J_{\text{C-P}} = 17.4$ Hz), 130.7 (d, $J_{\text{C-P}} = 19.4$ Hz), 130.3 (d, $J_{\text{C-P}} = 5.6$ Hz), 122.2 (q, $J_{\text{C-F}} = 319.7$ Hz), 110.7 ppm (d, $J_{\text{C-P}} = 5.2$ Hz). ^{31}P NMR (CD_3CN , 162 MHz): $\delta = 87.1$ ppm. ^{11}B NMR (CD_3CN , 128 MHz): $\delta = -7.1$ ppm (t, $J_{\text{B-H}} = 105$ Hz). ^{19}F

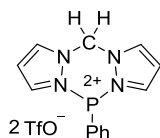
NMR (CD₃CN, 282 MHz): $\delta = -79.3$ ppm. IR $\tilde{\nu} = 416, 443, 465, 517, 633, 690, 746, 780, 950, 983, 1027, 1061, 1092, 1139, 1252, 1388, 1419, 2461, 3020, 3138$ cm⁻¹. Elemental analysis for C₁₃H₁₃BF₃N₄O₃PS (404.05) *calcd.* for: C 38.64%, H 3.24%, N 13.86%, *found*: C 37.78%, H 2.89%, N 13.65%.

Compound 64



CyPCl₂ (0.21 ml, 1.3 mmol) and TMSOTf (0.24 ml, 1.300 mmol) were added at -78°C to a suspension of K[H₂B(Pz)₂] (250.0 mg, 1.301 mmol) in CH₂Cl₂ (5 ml) and the mixture was allowed to warm up to r.t. overnight. Then the solvent was filtered off and the white solid obtained washed with CH₂Cl₂ (2 x 5 ml). Then the crude product was extracted with CH₃CN (2 x 5 ml) at 0 °C and the organic solvent removed *in vacuo* to afford **64** as a white solid (302.1 mg, 55%). mp: 113 °C (dec), ¹H NMR (CD₃CN, 400 MHz): $\delta = 8.42$ (dd, $J = 3.3$ Hz, $J_{H-P} = 3.3$ Hz, 2H), 8.3702 (s, 2H), 6.32 (dd, $J = 2.7$ Hz, $J_{H-P} = 4.6$ Hz, 2H), 4.01 (br, $J_{H-B} = 128$ Hz), 3.16 (m, 2H), 1.79 (m, 3H), 1.35 (m, 7H) ppm, ¹³C NMR (CD₃CN, 100 MHz): $\delta = 145.5, 143.7$ (d, $J_{C-P} = 25.3$ Hz), 122.1 (q, $J_{C-F} = 320.9$ Hz), 110.6 (d, $J_{C-P} = 5.4$ Hz), 39.5 (d, $J_{C-P} = 20.5$ Hz), 25.9, 25.8, 25.7, 25.6, 25.5 ppm. ³¹P NMR (CD₃CN, 162 MHz): $\delta = 102.8$ ppm. ¹¹B NMR (CD₃CN, 128 MHz): $\delta = -8.1$ ppm. ¹⁹F NMR (CD₃CN, 282 MHz): $\delta = -79.3$ ppm. IR $\tilde{\nu} = 635, 697, 792, 875, 1027, 1073, 1137, 1222, 1263, 1414, 2425, 2490, 2859, 2928, 3105, 3137$ cm⁻¹. Elemental analysis for C₁₃H₁₉BF₃N₄O₃PS (410.16): *calcd.* for C 38.07%, H 4.67%, N 13.66%, *found*: C 38.03%, H 4.23%, N 13.12%.

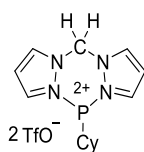
Compound 67



PhPCl₂ (1.8 ml, 13.5 mmol) and TMSOTf (4.9 ml, 27.0 mmol) were added at -78°C to a solution of [H₂C(Pz)₂] (2.0 g, 13.500 mmol) in CH₂Cl₂ (10 ml) and the mixture allowed to warm up to r.t. overnight. Then the solvent was filtered off and the white solid thus obtained washed with CH₂Cl₂ (2 x 5 ml). The crude product was dissolved in CH₃CN (5 ml), precipitated with Et₂O (15 ml) and dried *in vacuo* to afford **67** as a white solid (2.83 g, 38%). Colourless crystals suitable for X-ray crystallography were obtained from a CH₃CN/Et₂O at -30°C. m.p.: 86 °C (dec.). ¹H NMR (CD₃CN, 400 MHz): $\delta = 8.98$ (dd, $J = 2.5$ Hz, $J_{H-P} = 2.5$

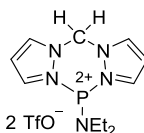
Hz, 2H), 8.75 (s, 2H), 7.70 (m, 1H), 7.60 (m, 2H), 7.39 (m, 2H), 7.29 (d, $J = 14.9$ Hz, 1H), 7.10 (m, 2H), 5.87 (d, $J = 14.9$ Hz, 1H) ppm. ^{13}C NMR (CD_3CN , 100 MHz): $\delta = 147.9$ (d, $J_{\text{C-P}} = 19.4$ Hz), 145.1, 134.7, 131.9 (d, $J_{\text{C-P}} = 18.7$ Hz), 131.0 (d, $J_{\text{C-P}} = 5.5$ Hz), 128.3 (d, $J_{\text{C-P}} = 24.3$ Hz), 121.9 (q, $J_{\text{C-F}} = 320.3$ Hz), 111.7 (d, $J_{\text{C-P}} = 2.2$ Hz), 63.3 ppm. ^{31}P NMR (CD_3CN , 162 MHz): $\delta = 85.8$ ppm. ^{19}F NMR (CD_3CN , 282 MHz): $\delta = -79.3$ ppm. IR $\tilde{\nu} = 675, 838, 894, 1029, 1162, 1220, 1241, 1377, 1563, 1580, 2827, 3136$ cm^{-1} . Elemental analysis for $\text{C}_{15}\text{H}_{13}\text{F}_6\text{N}_4\text{O}_6\text{PS}_2$ (554.38): *calcd.* for C 32.50%, H 2.36%, N 10.11%, *found:* C 32.11%, H 2.76%, N 10.60%.

Compound **68**



CyPCl_2 (0.26 ml, 1.7 mmol) and TMSOTf (0.61 ml, 3.4 mmol) were added to a suspension of $[\text{H}_2\text{C}(\text{Pz})_2]$ (250.0 mg, 1.7 mmol) in CH_2Cl_2 (5 ml) at -78°C and the mixture allowed to warm up to r.t. overnight. The solvent was then evaporated *in vacuo* and the resulting solid dissolved in CH_3CN (2 ml). Then Et_2O (10 ml) was added to precipitate the product **68** as a white solid (433.3 mg, 46%). m.p.: 93°C (dec.). ^1H NMR (CD_3CN , 400 MHz): $\delta = 8.80$ (s, 2H), 8.76 (s, 2H), 7.56 (s, 1H), 7.05 (s, 2H), 6.84 (s, 1H), 2.97 (m, 1H), 1.94 (m, 2H), 1.85 (m, 1H), 1.54 (m, 4H), 1.34 ppm (m, 3H). ^{13}C NMR (CD_3CN , 100 MHz): $\delta = 147.3$ (d, $J_{\text{C-P}} = 20.9$ Hz), 144.9 (d, $J_{\text{C-P}} = 2.8$ Hz), 121.9 (q, $J_{\text{C-F}} = 320.4$ Hz), 112.1 (d, $J_{\text{C-P}} = 5.4$ Hz), 63.4, 40.5 (d, $J_{\text{C-P}} = 26.9$ Hz), 25.6, 25.5, 25.4, 25.3, 25.2 ppm. ^{31}P NMR (CD_3CN , 162 MHz): $\delta = 110.1$ ppm. ^{19}F NMR (CD_3CN , 282 MHz): $\delta = -79.3$ ppm. IR $\tilde{\nu} = 573, 609, 759, 1023, 1159, 1246, 1567, 2744, 2853, 3039, 3121$ cm^{-1} . Elemental analysis for $\text{C}_{15}\text{H}_{19}\text{F}_6\text{N}_4\text{O}_6\text{PS}_2$ (560.42): *calcd.* for C 32.15%, H 3.24%, N 10.00%, *found:* C 31.18%, H 3.34%, N 9.68%.

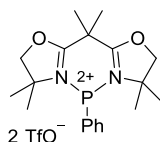
Compound **69**



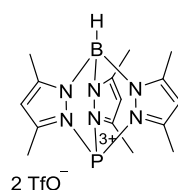
$(\text{Et}_2\text{N})\text{PCl}_2$ (0.29 ml, 2.0 mmol) and TMSOTf (0.73 ml, 4.0 mmol) were added to a solution of $[\text{H}_2\text{C}(\text{Pz})_2]$ (296.0 mg, 2.0 mmol) in CH_2Cl_2 (4 ml) at -78°C and the mixture was allowed to warm up to r.t. overnight. The solvent was then filtered off and the white solid thus obtained washed with CH_2Cl_2 (2 x 5 ml). Crude **69** was then dissolved in CH_3CN and

precipitated with Et₂O (362.1 mg, 33%). Colourless crystals suitable for X-ray crystallography were obtained from CH₃CN/Et₂O at – 30°C. m.p.: 103 °C (dec.). ¹H NMR (CD₃CN, 400 MHz): δ = 8.69 (s, 2H), 8.61 (s, 2H), 7.27 (d, *J* = 11.36 Hz, 1H), 7.08 (t, *J* = 2.88 Hz, 1H), 7.08 (d, 11.36 Hz, 1H), 3.38 (m, 4H), 1.23 ppm (t, *J* = 7.1 Hz, 6H). ¹³C NMR (CD₃CN, 75 MHz): δ = 143.7 (d, *J*_{C-P} = 9.0 Hz), 142.1, 111.7, 63.2, 43.9, 43.7, 13.8, 13.7 ppm. ³¹P NMR (CD₃CN, 162 MHz): δ = 107.8 ppm. ¹⁹F NMR (CD₃CN, 282 MHz): δ = – 79.3 ppm. IR $\tilde{\nu}$ = 515, 574, 632, 759, 1023, 1100, 1158, 1347, 1391, 1445, 1522, 1567, 2854, 2997, 3120 cm⁻¹. Elemental analysis for C₁₃H₁₈F₆N₅O₆PS₂ (549.40): *calcd.* for C 28.42%, H 3.40%, N 12.75%, *found*: C 28.23%, H 3.28%, N 12.75%.

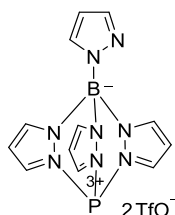
Compound 73



PhPCl₂ (0.75 ml, 5.4 mmol) and TMSOTf (2.0 ml, 10.8 mmol) were added at – 78°C to a suspension of bisoxazoline **72** (1.28 g, 5.4 mmol) in CH₂Cl₂ (20 ml) and the mixture allowed to warm up to r.t. overnight. Filtration of the solvent afforded a white solid that was subsequently washed with CH₂Cl₂ (2 x 10 ml). Crude **73** was then dissolved in CH₃CN at 0°C and precipitated with Et₂O to afford the desired product as a white solid (1.55 g, 45%). m.p.: 65.2– 67.8 °C. ¹H NMR (CD₃CN, 300 MHz): δ = 8.11 – 8.05 (m, 2H), 7.94 – 7.90 (m, 1H), 7.80 – 7.74 (m, 2H), 5.08 – 5.04 (m, 4H), 2.19 (s, 3H), 2.04 (s, 3H), 1.85 (s, 6H), 1.08 (s, 6H) ppm. ¹³C NMR (CD₃CN, 75 MHz): δ = 175.7 (d, *J*_{C-P} = 6.9 Hz), 138.1, 135.9 (d, *J*_{C-P} = 33.9 Hz), 131.7 (d, *J*_{C-P} = 11.1 Hz), 129.3 (d, *J*_{C-P} = 29.2 Hz), 86.3, 75.6 (d, 12.9), 41.9 (d, *J* = 1.1 Hz), 29.6, 26.5 (d, *J* = 2.1 Hz), 25.6 (d, *J* = 10.0 Hz), 22.7 ppm (d, *J* = 1.9 Hz). ³¹P NMR (CD₃CN, 162 MHz): δ = 88.8 ppm. ¹⁹F NMR (CD₃CN, 282 MHz): δ = – 79.17 ppm. IR $\tilde{\nu}$ = 435, 493, 516, 573, 634, 693, 739, 934, 1026, 1149, 1245, 1329, 1382, 1495, 1599, 1656, 2941 cm⁻¹. Elemental analysis for C₂₁H₂₇F₆N₂O₈PS₂ (644.54): *calcd.* for C 39.13%, H 4.22%, N 4.35%, *found*: C 38.33%, H 4.22%, N 4.35%.

Compound **76**

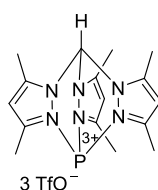
PCl_3 (0.56 ml, 6.4 mmol) and TMSOTf (2.3 ml, 12.8 mmol) were added at -78°C to a suspension of $\text{K}[\text{HB}(3,5\text{-Me}_2\text{Pz})_3]$ (2.05 g, 6.1 mmol) in CH_2Cl_2 (10 ml) and the mixture was allowed to warm up to r.t. overnight. Filtration of the solid afforded a white solid that was subsequently washed with CH_2Cl_2 (2 x 5 ml). The crude product was extracted with CH_3CN (2 x 10 ml) and the solvent evaporated *in vacuo* to afford **76** as a white solid (1.134 g, 24%). Colourless crystals suitable for X-ray crystallography were obtained from $\text{CH}_3\text{CN}/\text{Et}_2\text{O}$ solution at -30°C . m.p.: 118°C (dec), ^1H NMR (CD_3CN , 300 MHz): $\delta = 6.44$ (d, $J_{\text{H-P}} = 4.4$, Hz, 3H), 4.79 (br, $J_{\text{H-B}} = 162$ Hz), 2.70 (s, 9H), 2.57 ppm (s, 9H). ^{13}C NMR (CD_3CN , 101 MHz): $\delta = 158.3$, 156.2 (d, $J_{\text{C-P}} = 19.3$ Hz), 122.0 (d, $J_{\text{C-F}} = 320.7$ Hz), 111.2 (q, $J_{\text{C-P}} = 2.2$ Hz), 13.1 (d, $J_{\text{C-P}} = 8.8$ Hz), 12.8 ppm. ^{31}P NMR (CD_3CN , 121 MHz): $\delta = 7.3$ ppm. ^{11}B NMR (CD_3CN , 128 MHz): $\delta = -9.9$ (d, $J_{\text{B-H}} = 129$ Hz) ppm. ^{19}F NMR (CD_3CN , 282 MHz): $\delta = -79.3$ ppm. IR $\tilde{\nu} = 516, 573, 605, 633, 691, 756, 789, 906, 1023, 1099, 1160, 1223, 1435, 1522, 2700, 3040, 3142\text{ cm}^{-1}$. Elemental analysis for $\text{C}_{17}\text{H}_{22}\text{BF}_6\text{N}_6\text{O}_6\text{PS}_2$ (626.29): *calcd.* for C 32.60%, H 3.54%, N 13.42%, *found*: C 32.11%, H 3.52%, N 12.95%.

Compound **79**

PCl_3 (0.16 ml, 1.8 mmol) and TMSOTf (0.65 ml, 3.6 mmol) were added at -78°C to a solution of $\text{K}[\text{B}(\text{Pz})_4]$ (572 mg, 1.8 mmol) in CH_2Cl_2 (5 ml) and the mixture was allowed to warm up to r.t. overnight. After filtration of the supernatant the white solid obtained washed with CH_2Cl_2 (2 x 5 ml) and extracted with CH_3CN (2 x 10 ml). Evaporation of the solvent *in vacuo* afforded the desired product **79** as a white solid (588 mg, 43%). Colourless crystals suitable for X-ray crystallography were obtained from a $\text{CH}_3\text{CN}/\text{Et}_2\text{O}$ solution at 5°C . m.p.: 122°C (dec.). ^1H NMR (CD_3CN , 300 MHz): $\delta = 8.86$ (s, 3H), 8.61 (s, 3H), 8.28 (s, 1H), 8.08 (s, 1H), 6.85 (d, $J_{\text{H-P}} = 2.6$, 3H), 6.82 (s, 1H). ^{13}C NMR (CD_3CN , 75 MHz): $\delta = 146.5$ (d, $J_{\text{C-P}} = 19.3$ Hz), 145.5, 136.3, 121.8 (q, $J_{\text{C-F}} = 320.2$ Hz), 110.8, 110.7 (d, $J_{\text{C-P}} = 3.2$ Hz) ppm.

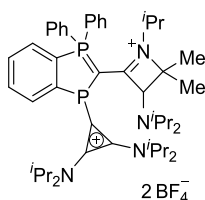
^{31}P NMR (CD_3CN , 121 MHz): $\delta = -0.4$ ppm. ^{11}B NMR (CD_3CN , 128 MHz): $\delta = -1.3$ ppm. ^{19}F NMR (CD_3CN , 282 MHz): $\delta = -79.3$ ppm. IR $\tilde{\nu} = 567, 594, 766, 864, 1065, 1109, 1157, 1243, 1392, 1157, 2659, 3133$ cm^{-1} . Elemental analysis for $\text{C}_{14}\text{H}_{12}\text{BF}_6\text{N}_8\text{O}_6\text{PS}_2$ (608.20): *calcd.* for C 27.65%, H 1.99%, N 18.42%, *found:* C 27.96%, H 1.67%, N 18.14%.

Compound **82**



PCl_3 (0.23 ml, 2.6 mmol) and TMSOTf (1.4 ml, 7.9 mmol) were added to a solution of $[\text{HC}(3,5\text{-Me}_2\text{Pz})_3]$ (790 mg, 2.6 mmol) in CH_2Cl_2 (5 ml) at -78°C and the mixture was allowed to warm up to r.t. overnight. Filtration of the solvents afforded a white solid that washed with CH_2Cl_2 (2 x 5 ml). Crude **82** was then dissolved in CH_3CN (5 ml) and precipitated with Et_2O (15 ml) to afford a white solid (608 mg, 29%). m.p.: 102°C (dec.). ^1H NMR (CD_3CN , 400 MHz): $\delta = 9.60$ (s, 1H), 6.75 (d, $J_{\text{H-P}} = 4.8$ Hz, 3H), 2.89 (s, 9H), 2.88 ppm (s, 9H). ^{13}C NMR (CD_3CN , 101 MHz): $\delta = 161.6$ (d, $J_{\text{C-P}} = 15.2$ Hz), 158.5, 121.8 (q, $J_{\text{C-F}} = 320.2$ Hz), 112.6, 70.8 (d, $J_{\text{C-P}} = 3.6$ Hz), 15.1 (d, $J_{\text{C-P}} = 5.4$ Hz), 13.6 ppm. ^{31}P NMR (CD_3CN , 121 MHz): $\delta = -9.9$ ppm. ^{19}F NMR (CD_3CN , 282 MHz): $\delta = -79.2$ ppm. IR $\tilde{\nu} = 447, 515, 573, 631, 707, 760, 844, 944, 1022, 1078, 1160, 1207, 1417, 1584, 2709, 2940, 3135$ cm^{-1} . Elemental analysis for $\text{C}_{19}\text{H}_{22}\text{F}_9\text{N}_6\text{O}_9\text{PS}_3$ (776.56): *calcd.* for C 29.39%, H 2.86%, N 10.82%, *found:* C 29.52%, H 3.02%, N 10.50%.

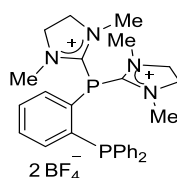
Compound **91**



To a solution of [2-(diphenylphosphino)phenyl]phosphine (200.0 mg, 0.340 mmol) in THF (10 ml) was added with chlorocyclopropenium salt (243.7 mg, 0.680 mmol) and Et_3N (0.1 ml, 0.710 mmol). The resulting mixture was stirred at 60°C overnight. After cooling to r.t., the solvent was removed *in vacuo*, the left was dissolved in CH_2Cl_2 and the resulting solution washed three times with sat. NaBF_4 . Once dried over Na_2SO_4 , the organic phase was concentrated and the left was crystallized from $\text{CH}_2\text{Cl}_2/\text{Et}_2\text{O}$ to afford compound **91** as a

white solid (146.0 mg, 46%). Colourless crystals suitable for X-ray crystallography were obtained from $\text{CH}_2\text{Cl}_2/\text{Et}_2\text{O}$ at r.t. ^1H NMR (CD_2Cl_2 , 500 MHz): $\delta = 8.19 - 8.16$ (m, 1H), 7.92 – 7.80(m, 1H), 7.71 – 7.67 (m, 2H), 7.42 – 7.38 (m, 2H), 4.47 (d, $J = 2.70$ Hz, 1H), 3.86 (br, 1H), 3.67 – 7.62 (m, 1H), 3.35 – 7.32 (m, 1H), 2.84 – 2.81 (m, 1H), 1.48 – 0.90 (m, 48H), 0.50 ppm (d, $J = 6.80$ Hz, 3H). ^{13}C NMR (CD_3CN , 125 MHz): $\delta = 178.5$ (dd, $J = 90.6$ Hz, $J = 1.7$ Hz), 143.5 (d, $J = 22.5$ Hz), 137.2 (d, $J = 5.6$ Hz), 136.3 (d, $J = 5.2$ Hz), 136.2 (dd, $J = 20.2$ Hz, $J = 3.0$ Hz), 135.5 (dd, $J = 20.6$ Hz, $J = 2.9$ Hz), 134.3 (d, $J = 11.4$ Hz), 133.3 (d, $J = 11.3$ Hz), 133.2 (d, $J = 11.4$ Hz), 132.9 (dd, $J = 65.4$ Hz, $J = 8.9$ Hz), 132.3 (d, $J = 14.0$ Hz), 131.4 (d, $J = 12.5$ Hz), 131.0 (d, $J = 13.0$ Hz), 121.4 (d, $J = 84.2$ Hz), 120.1 (d, $J = 80.9$ Hz), 107.6 (d, $J = 91.9$ Hz), 81.2, 69.5 (dd, $J = 8.7$ Hz, $J = 4.2$ Hz), 52.1, 50.0, 46.8 (dd, $J = 81.2$ Hz, $J = 22.0$ Hz), 44.1, 27.0, 26.0, 25.1, 24.4 (d, $J = 8.5$ Hz), 23.5 (d, $J = 6.0$ Hz), 22.92, 22.86, 21.4, 20.1 ppm. ^{31}P NMR (CD_3CN , 121 MHz): $\delta = 31.9$ (d, $J = 24.8$ Hz), -16.2 ppm (d, $J = 24.8$ Hz). ^{11}B NMR (CD_3CN , 96 MHz): $\delta = -1.1$ ppm. ^{19}F NMR (CD_3CN , 282 MHz): $\delta = -152.5$ ppm. HRMS *calcd.* for $\text{C}_{48}\text{H}_{70}\text{N}_4\text{BF}_4\text{P}_2^+$: 851.510320, *found* 851.509943. IR $\tilde{\nu} = 491, 528, 585, 646, 690, 724, 911, 1050, 1099, 1149, 1205, 1249, 1353, 1376, 1440, 1462, 1543, 1568, 1856, 2129, 2262, 2880, 2938, 2974$ cm^{-1} .

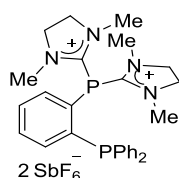
Compound **92a**



2-Chloro-1,3-dimethylimidazolium tetrafluoroborate (150.0 mg, 0.680 mmol) and Et_3N (0.100 ml, 0.710 mmol) were added to a solution of [2-(diphenylphosphino)phenyl]phosphine (100.0 mg, 0.340 mmol) in THF (5 ml) and the resulting mixture stirred at 60°C overnight. After cooling to r.t., the solvent was filtered and the left washed with CHCl_3 to afford a white solid. This solid was stirred with NaBF_4 (149.6 mg, 1.360 mmol) in CH_3CN (5 ml) overnight. Subsequently the solvent was removed *in vacuo* and the resulting white solid extracted with CH_2Cl_2 (3×20 ml). The combined organic phase thus obtained was evaporated *in vacuo* to afford **92a** as a white solid (146.3 mg, 65%). ^1H NMR (CD_3CN , 400 MHz): $\delta = 7.76 - 7.68$ (m, 3H), 7.53 – 7.45 (m, 6H), 7.42 – 7.38 (m, 1H), 7.34 – 7.30 (m, 4H), 3.84 – 3.80 (m, 8H), 2.98 ppm (s, 12H). ^{13}C NMR (CD_3CN , 100 MHz): $\delta = 164.4$ (dd, $J = 47.5$ Hz, $J = 18.0$ Hz), 144.3 (dd, $J = 35.6$ Hz, $J = 5.1$ Hz), 137.1 (d, $J = 7.8$ Hz), 136.6 (d, $J = 8.2$ Hz), 135.2 (d, $J = 1.4$ Hz), 134.5, 134.3, 134.0 (dd, $J = 6.0$ Hz, $J = 1.0$ Hz), 133.2, 131.3, 130.4, (d, $J = 7.3$ Hz), 127.3 (dd, $J = 39.5$ Hz, $J = 3.1$ Hz), 53.4, 36.8 ppm (d, $J = 8.7$ Hz). ^{31}P NMR (CD_3CN , 121

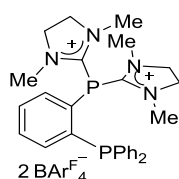
MHz): $\delta = -12.3$ (d, $J_{P-P} = 211.6$ Hz), -47.6 ppm (d, $J_{P-P} = 212.6$ Hz). ^{11}B NMR (CD_3CN , 96 MHz): $\delta = -1.2$ ppm. ^{19}F NMR (CD_3CN , 282 MHz): $\delta = -151.8$ ppm. HRMS *calcd.* for $\text{C}_{28}\text{H}_{34}\text{N}_4\text{BF}_4\text{P}_2^+$: 575.228360, *found* 575.228243. IR $\tilde{\nu} = 425, 457, 522, 653, 699, 741, 762, 936, 998, 1094, 1111, 1300, 1337, 1418, 1434, 1445, 1523, 1579, 3105$ cm^{-1} .

Compound **92b**



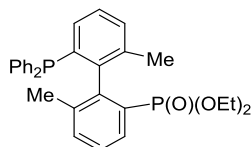
2-Chloro-1,3-dimethylimidazolium tetrafluoroborate (150.0 mg, 0.680 mmol) and Et_3N (0.100 ml, 0.710 mmol) were added to a solution of [2-(diphenylphosphino)phenyl]phosphine (100.0 mg, 0.340 mmol) in THF (5 ml) and the resulting mixture stirred at 60°C overnight. After cooling to r.t., the solvent was filtered and the left washed with CHCl_3 to afford a white solid. This solid was stirred with NaSbF_6 (352.0 mg, 1.360 mmol) in CH_3CN (5 ml) overnight. Subsequently the solvent was removed *in vacuo* and the resulting white solid extracted with CH_2Cl_2 (3×10 ml). The combined organic phase thus obtained was evaporated *in vacuo* to afford **92b** as a white solid (234.9 mg, 72%). Colourless crystals suitable for X-ray crystallography were obtained from $\text{CH}_2\text{Cl}_2/\text{Et}_2\text{O}$ at -20°C . ^1H NMR (CD_3CN , 400 MHz): $\delta = 7.76 - 7.68$ (m, 3H), $7.53 - 7.45$ (m, 6H), $7.42 - 7.38$ (m, 1H), $7.34 - 7.30$ (m, 4H), $3.84 - 3.80$ (m, 8H), 2.98 ppm (s, 12H). ^{13}C NMR (CD_3CN , 100 MHz): $\delta = 164.4$ (dd, $J = 47.5$ Hz, $J = 18.1$ Hz), 144.3 (dd, $J = 30.0$ Hz, $J = 4.9$ Hz), 137.1 (d, $J = 7.2$ Hz), 136.6 (d, $J = 8.4$ Hz), 135.0, 134.4 (d, $J = 18.6$ Hz), 134.0 (dd, $J = 6.0$ Hz, $J = 1.0$ Hz), 133.2, 131.3, 130.4, (d, $J = 7.3$ Hz), 127.3 (dd, $J = 40.6$ Hz, $J = 4.2$ Hz), 53.4, 36.8 ppm (d, $J = 8.7$ Hz). ^{31}P NMR (CD_3CN , 121 MHz): $\delta = -10.7$ (d, $J_{P-P} = 212.4$ Hz), -46.1 ppm (d, $J_{P-P} = 212.4$ Hz). ^{19}F NMR (CD_3CN , 376 MHz): $\delta = -124.0$ ppm (sextet, $J_{F-Sb(I=5/2)} = 1933$ Hz, octet, $J_{F-Sb(I=7/2)} = 1049$ Hz). HRMS *calcd.* for $\text{C}_{28}\text{H}_{34}\text{N}_4\text{SbF}_6\text{P}_2^+$: 723.119040, *found* 723.119040. IR $\tilde{\nu} = 422, 456, 518, 653, 699, 745, 767, 934, 998, 1090, 1107, 1300, 1335, 1412, 1434, 1445, 1521, 1576, 3103$ cm^{-1} .

Compound **92c**



92b (96.0 mg, 0.100 mmol) and $\text{KB}(\text{Ar}^{\text{F}})_4$ (143.6 mg, 0.2 mmol) in CH_2Cl_2 (2 ml) stirred for 10 min at r.t. After filtration, the filtrate was evaporated *in vacuo* to afford the desired compound **92c** as a white solid (183.0 mg, 99%). ^1H NMR (CD_2Cl_2 , 400 MHz): $\delta = 7.82 - 7.77$ (m, 1H), 7.64 – 7.59 (m, 1H), 7.57 – 7.51 (m, 3H), 7.50 – 7.45 (m, 4H), 7.36 – 7.31 (m, 1H), 7.28 – 7.22 (m, 4H), 3.87 – 3.80 (m, 8H), 3.04 ppm (s, 12H). ^{13}C NMR (CD_2Cl_2 , 125 Mz): $\delta = 164.1$ (dd, $J = 54.8$ Hz, $J = 23.9$ Hz), 149.4 (br), 147.6 (br), 144.3 (dd, $J = 35.7$ Hz, $J = 1.8$ Hz), 139.7 (m), 137.7 (m), 135.8 (d, $J = 1.8$ Hz), 135.7 (m), 133.9 (d, $J = 9.2$ Hz), 133.6, 133.5, 133.4, 131.6, 131.5, 130.2 (d, $J = 8.0$ Hz), 125.1 (dd, $J = 42.6$ Hz, $J = 7.0$ Hz), 52.8, 36.5 ppm (d, $J = 8.7$ Hz). ^{31}P NMR (CD_2Cl_2 , 162 MHz): $\delta = -9.8$ (d, $J_{\text{P-P}} = 213.8$ Hz), -49.1 ppm (d, $J_{\text{P-P}} = 213.8$ Hz). ^{19}F NMR (CD_2Cl_2 , 282 MHz): $\delta = -133$ (m), -163.2 (t, $J_{\text{F-F}} = 20.2$ Hz), -167.3 ppm (t, $J_{\text{F-F}} = 18.1$ Hz). ^{11}B NMR (CD_2Cl_2 , 96 MHz): $\delta = -16.7$ ppm. HRMS *calcd.* for $\text{C}_{28}\text{H}_{34}\text{N}_4\text{P}_2^+$: 244.112390, *found* 244.112387. IR $\tilde{\nu} = 489, 501, 573, 610, 661, 683, 713, 756, 774, 930, 954, 976, 1084, 1274, 1297, 1374, 1413, 1460, 1513, 1577, 1643$ cm^{-1} .

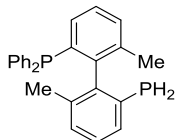
Compound **99**



$n\text{BuLi}$ (1.6 M in hexanes, 2.92 ml, 4.672 mmol) was added dropwise to *Rac*-**98** (2.3 g, 4.672 mmol) in THF (25 ml) at -78 °C and the mixture stirred for 1 h at -78 °C. Then $\text{ClP}(\text{O})(\text{OEt})_2$ (0.680 ml, 4.672 mmol) in THF (5 ml) was added dropwise and the mixture was allowed to warm to r.t. overnight. After that all volatiles were removed *in vacuo* and the crude phosphate was purified by column chromatography (SiO_2 , hexane:EtOAc = 3:1) to afford the *rac*-phosphate **99** (1.1 g, 47%). ^1H NMR (CDCl_3 , 400 MHz): $\delta = 7.90$ (dd, $J = 15.2$ Hz, $J = 7.12$ Hz, 1H), 7.38 – 7.34 (m, 1H), 7.32 – 7.18 (m, 14H), 3.99 – 3.12 (m, 4H), 1.97 (s, 3H), 1.27 (s, 3H), 1.15 ppm (q, $J = 5.8$ Hz, 6H). ^{13}C NMR (CDCl_3 , 100 MHz): $\delta = 145.5$ (dd, $J = 33.5$ Hz, $J = 4.1$ Hz), 143.4 (d, $J = 8.2$ Hz), 143.3 (d, $J = 9.0$ Hz), 139.7 (d, $J = 13.9$ Hz), 138.4 (dd, $J = 15.3$ Hz, $J = 2.3$ Hz), 138.0 (d, $J = 11.4$ Hz), 137.0 (d, $J = 6.5$ Hz), 136.9 (d, $J = 13.4$ Hz), 135.4 (d, $J = 22.7$ Hz), 133.9 (d, $J = 2.9$ Hz), 133.0 (d, $J = 17.1$ Hz), 131.7 (d, $J = 1.8$ Hz), 131.1 (d, $J = 9.2$ Hz), 130.5, 129.0, 128.4 (d, $J = 7.7$ Hz), 128.0 (d, $J = 4.9$ Hz), 127.5 (d, $J = 10.4$ Hz), 127.3 (d, $J = 15.6$ Hz), 127.1 (d, $J = 2.8$ Hz), 61.8 (t, $J = 5.4$ Hz), 20.5 (d, $J = 2.7$ Hz), 19.4, 16.4 ppm (dd, $J = 11.7$ Hz, $J = 6.0$ Hz). ^{31}P NMR (CDCl_3 , 121 MHz): $\delta = 17.7, -16.2$ ppm. HRMS *calcd.* for $\text{C}_{30}\text{H}_{32}\text{O}_3\text{P}_2\text{Na}^+$: 525.171490, *found*

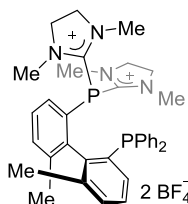
525.171893. IR $\tilde{\nu}$ = 426, 445, 485, 514, 539, 574, 591, 696, 751, 787, 878, 953, 998, 1051, 1090, 1156, 1192, 1254, 1367, 1391, 1433, 1444, 1479, 1584, 2864, 2902, 2977, 3051 cm^{-1} .

Compound **100**



To LiAlH_4 (135.9 mg, 3.582 mmol) in Et_2O (5 ml) at -78°C was added the previously prepared *rac*-phosphate **99** (600.0 mg, 1.194 mmol) in Et_2O (5 ml) over the course of ca. 0.5 h. This gray suspension stirred at -78°C for an additional 15 min, allowed to warm to r.t. overnight. After this time, the reaction mixture was cooled to 0°C . Deoxygenated water was carefully added and stirred until gas evolution ceased. The organic layer was then transferred into a schlenk and the solid was extracted with Et_2O (2×15 ml). Subsequently, the combined organic phases were dried with Na_2SO_4 , filtered through Celite and the solvent removed *in vacuo* to afford **100** as a white solid (404.1 mg, 85%). ^1H NMR (CDCl_3 , 400 MHz): δ = 7.43 (t, J = 6.8 Hz, 1H), 7.27 – 7.15 (m, 13H), 7.12 – 7.10 (m, 1H), 7.10 – 7.03 (m, 1H), 3.72 (dd, J = 31.6 Hz, J = 12.0 Hz, 1H), 3.21 (dd, J = 31.6 Hz, J = 12.0 Hz, 1H), 1.93 (s, 3H), 1.48 ppm (s, 3H). ^{13}C NMR (CDCl_3 , 400 MHz): δ = 146.4 (dd, J = 31.4 Hz, J = 3.7 Hz), 144.1 (dd, J = 16.2 Hz, J = 7.0 Hz), 137.9 (d, J = 12.3 Hz), 137.5 (d, J = 9.8 Hz), 137.2 (t, J = 3.0 Hz), 136.7 (d, J = 12.3 Hz), 136.4 (d, J = 6.3 Hz), 134.6 (d, J = 21.1 Hz), 133.6 (d, J = 19.2 Hz), 132.5 (d, J = 9.8 Hz), 132.2 (d, J = 2.0 Hz), 131.1, 130.0, 129.9 (d, J = 2.9 Hz), 128.8, 128.4 (d, J = 4.1 Hz), 128.36 (d, J = 2.7 Hz), 128.30, 127.9, 127.6 (d, J = 4.7 Hz), 20.1, 19.8 ppm. ^{31}P NMR (CDCl_3 , 121 MHz): δ = -15.0 (d, $J_{\text{P-P}}$ = 20.1 Hz), -125.6 ppm (d, $J_{\text{P-P}}$ = 20.1 Hz). HRMS *calcd.* for $\text{C}_{26}\text{H}_{25}\text{P}_2^+$: 399.142680, *found* 399.142604, IR $\tilde{\nu}$ = 438, 490, 506, 537, 553, 573, 743, 768, 787, 827, 914, 998, 1026, 1067, 1094, 1147, 1206, 1261, 1306, 1379, 1400, 1434, 1475, 1566, 1584, 2294, 2851, 2913, 3001, 3048 cm^{-1} .

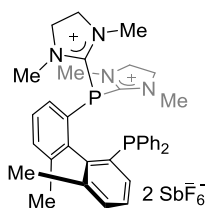
Compound **101a**



2-Chloro-1,3-dimethylimidazolium tetrafluoroborate (110.0 mg, 0.502 mmol) and Et_3N (0.070 ml, 0.527 mmol) were added to a solution of **100** (100.0 mg, 0.251 mmol) in THF (5

ml). The resulting mixture was stirred at 60 °C overnight. After cooling to r.t., the solvent was filtered and the left washed with CHCl₃, affording a white solid. This solid was stirred with NaBF₄ (220.0 mg, 2.008 mmol) in CH₃CN (5 ml) overnight. Subsequently the solvent was removed *in vacuo* and the resulting white solid extracted with CH₂Cl₂. The combined organic phase thus obtained was evaporated *in vacuo* to afford **101a** as a white solid (78.9 mg, 41%). Colourless crystals suitable for X-ray crystallography were obtained from CH₃COCH₃/Et₂O at r.t. ¹H NMR (CD₃CN, 400 MHz): δ = 7.71 – 7.70 (m, 1H), 7.56 – 7.50 (m, 2H), 7.47 – 7.26 (m, 10H), 7.16 – 7.09 (m, 3H), 4.07 (d, *J* = 2.4 Hz, 4H), 3.95 – 3.90 (m, 2H), 3.83 – 3.79 (m, 2H), 3.13 (s, 6H), 2.78 (s, *J* = 0.6 Hz, 6H), 1.81 (s, 3H), 1.20 ppm (m, 3H). ¹³C NMR (CD₃CN, 100 MHz): δ = 166.1 (dd, *J* = 47.6 Hz, *J* = 0.8 Hz), 163.2 (dd, *J* = 53.2 Hz, *J* = 4.9 Hz), 145.7 (dd, *J* = 34.8 Hz, *J* = 5.7 Hz), 142.2 (dd, *J* = 8.2 Hz, *J* = 1.9 Hz), 141.5 (d, *J* = 7.2 Hz), 141.2 (d, *J* = 7.0 Hz), 140.0 (dd, *J* = 6.2 Hz, *J* = 1.4 Hz), 139.7 (dd, *J* = 34.8 Hz, *J* = 5.7 Hz), 137.1 (d, *J* = 8.9 Hz), 136.3 (d, *J* = 22.4 Hz), 135.9, 134.6, 133.8 (dd, *J* = 8.0 Hz, *J* = 3.9 Hz), 133.6 (d, *J* = 1.8 Hz), 133.4 (d, *J* = 3.4 Hz), 133.3 (d, *J* = 2.8 Hz), 132.8, 131.2, 131.1 (d, *J* = 0.9 Hz), 130.3 (d, *J* = 2.4 Hz), 129.9 (d, *J* = 5.9 Hz), 129.8 (d, *J* = 8.6 Hz), 54.5, 52.6, 38.0 (dd, *J* = 11.2 Hz, *J* = 3.5 Hz), 37.2 (d, *J* = 10.8 Hz), 19.5 (d, *J* = 2.3 Hz), 18.9 ppm (d, *J* = 3.2 Hz). ³¹P NMR (CD₃CN, 121 MHz): δ = – 14.6 (d, *J*_{P-P} = 87.0 Hz), – 44.3 ppm (d, *J*_{P-P} = 87.0 Hz). ¹¹B NMR (CD₃CN, 96 MHz): δ = – 1.2 ppm. ¹⁹F NMR (CD₃CN, 282 MHz): δ = – 151.8 ppm. HRMS *calcd.* for C₃₆H₄₂N₄BF₄P₂⁺: 679.290520, *found* 679.290843. IR $\tilde{\nu}$ = 438, 461, 480, 493, 506, 531, 576, 633, 646, 698, 746, 754, 767, 787, 931, 1024, 1047, 1223, 1297, 1332, 1363, 1411, 1435, 1447, 1526, 1579, 1709, 2923, 3504 cm⁻¹.

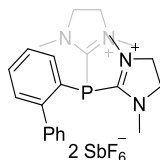
Compound **101b**



2-Chloro-1,3-dimethylimidazolidinium tetrafluoroborate (110.0 mg, 0.502 mmol) and Et₃N (0.070 ml, 0.527 mmol) were added to a solution of **100** (100.0 mg, 0.251 mmol) in THF (5 ml). The resulting mixture was stirred at 60 °C overnight. After cooling to r.t., the solvent was filtered and the left washed with CHCl₃, affording a white solid. This solid was stirred with NaSbF₆ (517.5 mg, 2.000 mmol) in CH₃CN (5 ml) overnight. Subsequently the solvent was removed *in vacuo* and the resulting white solid extracted with CH₂Cl₂. The combined organic phase thus obtained was evaporated *in vacuo* to afford **101b** as a white solid (162.9 mg, 61%).

^1H NMR (CD_3CN , 400 MHz): $\delta = 7.78 - 7.72$ (m, 1H), $7.58 - 7.52$ (m, 2H), $7.49 - 7.26$ (m, 10H), $7.18 - 7.12$ (m, 3H), 4.10 (s, 4H), $3.98 - 3.92$ (m, 2H), $3.85 - 3.80$ (m, 2H), 3.15 (s, 6H), 2.79 (s, $J = 0.6$ Hz, 6H), 1.81 (s, 3H), 1.21 ppm (m, 3H). ^{13}C NMR (CD_3CN , 100 MHz): $\delta = 165.7$ (d, $J = 47.9$ Hz), 163.0 (dd, $J = 53.2$ Hz, $J = 4.9$ Hz), 145.5 (dd, $J = 34.8$ Hz, $J = 5.7$ Hz), 141.8 (d, $J = 8.1$ Hz), 141.3 (d, $J = 6.8$ Hz), 141.0 (d, $J = 7.0$ Hz), 139.8 (d, $J = 6.2$ Hz), 139.5 (dd, $J = 7.8$ Hz, $J = 1.7$ Hz), 136.9 (d, $J = 8.9$ Hz), 136.1 (d, $J = 22.4$ Hz), 135.6 , 134.4 , 133.6 (dd, $J = 8.4$ Hz, $J = 4.0$ Hz), 133.3 (d, $J = 17.7$ Hz), 133.1 , 132.5 , 131.0 , 130.9 , 130.1 (d, $J = 2.4$ Hz), 129.8 (d, $J = 5.9$ Hz), 129.6 (d, $J = 8.6$ Hz), 54.3 , 52.4 , 37.8 (dd, $J = 11.2$ Hz, $J = 3.5$ Hz), 37.0 (d, $J = 10.8$ Hz), 19.2 (d, $J = 1.8$ Hz), 18.7 ppm (d, $J = 3.0$ Hz). ^{31}P NMR (CD_3CN , 121 MHz): $\delta = -15.0$ (d, $J_{\text{P-P}} = 85.1$ Hz), -44.4 ppm (d, $J_{\text{P-P}} = 87.0$ Hz). ^{19}F NMR (CD_3CN , 282 MHz): $\delta = -122.4$ ppm (sextet, $J_{\text{F-Sb}(I=5/2)} = 1945$ Hz, octet, $J_{\text{F-Sb}(I=7/2)} = 1071$ Hz). HRMS *calcd.* for $\text{C}_{32}\text{H}_{41}\text{ONP}^+$: 486.292280. HRMS *calcd.* for $\text{C}_{36}\text{H}_{42}\text{N}_4\text{SbF}_6\text{P}_2^+$: 827.182162, *found* 827.1829. IR $\tilde{\nu} = 438, 461, 480, 493, 506, 531, 576, 633, 646, 698, 746, 754, 767, 787, 931, 1024, 1047, 1223, 1297, 1332, 1363, 1411, 1435, 1447, 1526, 1579, 1709, 2923, 3504$ cm^{-1} .

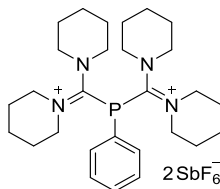
Compound **102**



2-Chloro-1,3-dimethylimidazolidinium tetrafluoroborate (132.6 mg, 0.602 mmol) and Et_3N (0.088 ml, 0.632 mmol) were added to a solution of Diphenyl(2-phosphinophenyl)phosphine (56.0 mg, 0.340 mmol) in THF (5 ml) and the resulting mixture stirred at 60°C overnight. After cooling to r.t., the solvent filtered off to afford a white powder, which was dissolved in CH_2Cl_2 and washed with sat. NaSbF_6 twice. Evaporation of the organic phase afforded the desired product **102** as a white solid, which could be purified by recrystallization in $\text{CH}_3\text{CN}/\text{Et}_2\text{O}$ (60.9 mg, 24%). ^1H NMR (CD_3CN , 400 MHz): $\delta = 7.84 - 7.79$ (m, 1H), $7.66 - 7.57$ (m, 6H), $7.43 - 7.41$ (m, 2H), $3.96 - 3.82$ (m, 8H), 2.88 ppm (s, 12H). ^{13}C NMR (CD_3CN , 100 MHz): $\delta = 164.1$ (d, $J = 47.1$ Hz), 150.1 (d, $J = 34.1$ Hz), 139.7 (d, $J = 8.0$ Hz), 135.7 , 135.0 , 133.0 (d, $J = 6.0$ Hz), 130.8 (d, $J = 1.4$ Hz), 130.5 (d, $J = 13.8$ Hz), 130.3 (d, $J = 4.0$ Hz), 128.9 (d, $J = 24.1$ Hz), 128.6 , 53.4 , 36.9 ppm (d, $J = 9.0$ Hz). ^{31}P NMR (CD_3CN , 121 MHz): $\delta = -43.1$ ppm. ^{19}F NMR (CD_3CN , 282 MHz): $\delta = -122.4$ ppm (sextet, $J_{\text{F-Sb}(I=5/2)} = 1945$ Hz, octet, $J_{\text{F-Sb}(I=7/2)} = 1071$ Hz). HRMS *calcd.* for $\text{C}_{22}\text{H}_{29}\text{N}_4\text{F}_6\text{PSb}^+$: 615.106410, *found*

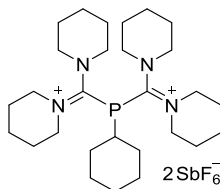
615.106603. IR $\tilde{\nu}$ = 435, 455, 468, 554, 653, 707, 761, 779, 935, 1206, 1301, 1337, 1413, 1447, 1526, 1583 cm^{-1} .

Compound 103



At $-78\text{ }^{\circ}\text{C}$, PhPH_2 (50.0 mg, 0.454 mmol) in THF (5 ml) was cannulated to chlorodipiperidinocarbenium hexafluoroantimonate (410.1 mg, 0.908 mmol) and KHDMS (181.2 mg, 0.908 mmol) in one schlenk and the resulting mixture was warmed to r.t. overnight. The solvent was removed *in vacuo* and the left was stirred with NaSbF_6 (352.0 mg, 1.360 mmol) in CH_3CN (5 ml) overnight. Subsequently the solvent was removed *in vacuo* and the resulting white solid extracted with CH_2Cl_2 . The combined organic phase thus obtained was evaporated *in vacuo* and the resulting solid washed with Et_2O and a small amount of CH_2Cl_2 to afford the desired compound **103** as a white solid (155.5 mg, 41%). Colourless crystals suitable for X-ray crystallography were obtained from $\text{CH}_2\text{Cl}_2/\text{Et}_2\text{O}$ at r.t. ^1H NMR (CD_3CN , 400 MHz): δ = 7.91 – 7.36 (m, 5H), 4.22 – 3.21 (m, 16H), 1.82 – 1.37 ppm (m, 24H). ^{13}C NMR (CD_3CN , 100 MHz): δ = 173.9 (d, J = 25.0 Hz), 137.5 (d, J = 23.6 Hz), 134.8, 132.1 (d, J = 10.3 Hz), 122.8, 56.0, 26.3, 23.3 ppm. ^{31}P NMR (CD_3CN , 121 MHz): δ = -15.3 ppm. ^{19}F NMR (CD_3CN , 282 MHz): δ = -124.0 ppm (sextet, $J_{\text{F-Sb}(I=5/2)}$ = 1933 Hz, octet, $J_{\text{F-Sb}(I=7/2)}$ = 1049 Hz). HRMS *calcd.* for $\text{C}_{28}\text{H}_{45}\text{N}_4\text{SbF}_6\text{P}_1^+$: 703.231110, *found* 703.231803. IR $\tilde{\nu}$ = 460, 496, 586, 654, 752, 859, 1013, 1132, 1255, 1290, 1362, 1441, 1538, 1557, 2864, 2945 cm^{-1} .

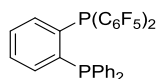
Compound 104



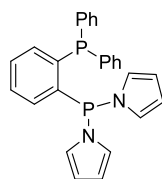
At $-78\text{ }^{\circ}\text{C}$, cyclohexylphosphine (50.0 mg, 0.430 mmol) in THF (5 ml) was cannulated to chlorodipiperidinocarbenium hexafluoroantimonate (388.7 mg, 0.861 mmol) and KHDMS (171.8 mg, 0.861 mmol) in one schlenk and the resulting mixture was warmed to r.t. overnight. The solvent was removed *in vacuo* and the left was stirred with NaSbF_6 (352.0 mg, 1.360 mmol) in CH_3CN (5 ml) overnight. Subsequently the solvent was removed *in vacuo* and

the resulting white solid extracted with CH_2Cl_2 (3×10 ml). The combined organic phase thus obtained was evaporated *in vacuo* and the resulting solid washed with Et_2O and a small amount of CH_2Cl_2 to afford the desired compound **104** as a white solid (297 mg, 73%). ^1H NMR (CD_3CN , 400 MHz): $\delta = 3.68$ (m, 16H), 3.32 – 3.13 (m, 1H), 1.92 – 1.84 (m, 4H), 1.84 – 1.26 ppm (m, 30H). ^{13}C NMR (CD_3CN , 100 MHz): $\delta = 174.5$ (d, $J = 34.7$ Hz), 55.9 (d, $J = 5.1$ Hz), 38.88 (d, $J = 23.2$ Hz), 32.83 (d, $J = 17.8$ Hz), 27.1 (d, $J = 15.9$ Hz), 26.5, 25.7 (d, $J = 2.1$ Hz), 23.3 ppm. ^{31}P NMR (CD_3CN , 121 MHz): $\delta = -3.7$ ppm. ^{19}F NMR (CD_3CN , 282 MHz): $\delta = -124.0$ ppm (sextet, $J_{\text{F-Sb}(I=5/2)} = 1933$ Hz, octet, $J_{\text{F-Sb}(I=7/2)} = 1049$ Hz), HRMS *calcd.* for $\text{C}_{28}\text{H}_{51}\text{N}_4\text{SbF}_6\text{P}_1^+$: 709.278630, *found* 709.278753. IR $\tilde{\nu} = 483, 578, 653, 780, 860, 1012, 1130, 1255, 1354, 1445, 1533, 2862, 2943$ cm^{-1} .

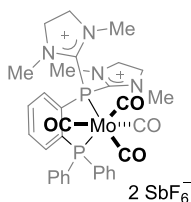
Compound **105**



$n\text{BuLi}$ (1.6 M in hexanes, 0.340 ml, 0.590 mmol) was added dropwise to (2-Bromophenyl)diphenylphosphine (200.0 mg, 0.586 mmol) in THF (5 ml) at -78 °C and the mixture stirred for 1 h at -78 °C. $(\text{C}_6\text{F}_5)_2\text{PCl}$ (238.0 mg, 0.590 mmol) in THF (2 ml) was added dropwise. The reaction was then allowed to warm to r.t. overnight and after that all volatiles were removed *in vacuo*. The crude was purified by column chromatography (SiO_2 , hexane: toluene = 5: 1) to afford the desired diphosphine **105** as a white solid (103.5 mg, 28%). ^1H NMR (C_6D_6 , 400 MHz): $\delta = 7.32 - 7.30$ (m, 1H), 7.18 – 7.13 (m, 1H), 7.05 – 7.02 (m, 5H), 6.95 – 6.88 ppm (m, 7H). ^{13}C NMR (C_6D_6 , 100 MHz): $\delta = 149.5$ (m), 146.9 (m), 142.6 (dm, $J_{\text{C-F}} = 258.5$ Hz), 138.3 (dd, $J = 34.0$ Hz, $J = 11.4$ Hz), 138.2 (d, $J = 34.3$ Hz, $J = 11.4$ Hz), 137.7 (q, $J_{\text{C-F}} = 252.8$ Hz), 135.9 (q, $J = 5.0$ Hz), 133.7, 133.5, 132.7 (d, $J = 8.9$ Hz), 130.4, 129.8, 129.0, 128.8 ppm (d, $J = 7.0$ Hz). ^{31}P NMR (C_6D_6 , 121 MHz): $\delta = -16.6$ (dt, $J_{\text{P-F}} = 184.5$ Hz, $J_{\text{P-P}} = 5.1$ Hz), -56.4 ppm (dq, $J_{\text{P-F}} = 184.5$ Hz, $J_{\text{P-P}} = 30.2$ Hz). ^{19}F NMR (C_6D_6 , 282 MHz): $\delta = -129.2$ (m), -149.8 (m), -160.5 ppm (m). HRMS *calcd.* for $\text{C}_{30}\text{H}_{14}\text{F}_{10}\text{P}_2$: 626.040937, *found* 626.041114. IR $\tilde{\nu} = 407, 439, 478, 494, 511, 521, 586, 631, 675, 745, 800, 840, 972, 1026, 1082, 1260, 1284, 1306, 1378, 1434, 1440, 1514, 1585, 1641, 2859, 2963, 3055$ cm^{-1} .

Compound **106**

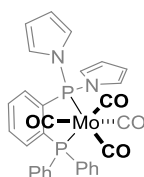
n BuLi (1.6 M in hexanes, 0.689 ml, 1.102 mmol) was added dropwise to (2-Bromophenyl)diphenylphosphine (376.0 mg, 1.102 mmol) in THF (5 ml) at -78 °C. The mixture stirred for 1 h at -78 °C and (pyrrolyl) $_2$ PCl (218.9 mg, 1.102 mmol) in THF (2 ml) was added dropwise. The reaction was then allowed to warm to r.t. overnight and after that all volatiles were removed *in vacuo*. The crude was purified by column chromatography (SiO $_2$, hexane:toluene = 3:1) to afford the desired diphosphine **106** as a white solid (304.2 mg, 65%). ^1H NMR (C $_6$ D $_6$, 300 MHz): δ = 7.29 – 7.26 (m, 1H), 7.21 – 7.19 (m, 3H), 7.00 – 7.97 (m, 7H), 6.92 – 6.88 (m, 2H), 6.81 – 6.78 (m, 1H), 6.76 – 6.74 (m, 4H), 6.23 ppm (t, J = 2.1Hz, 4H). ^{13}C NMR (C $_6$ D $_6$, 100 Mz): δ = 144.6 (dd, $J_{\text{C-P}}$ = 32.3, $J_{\text{C-P}}$ = 12.6 Hz), 141.9 (dd, $J_{\text{C-P}}$ = 28.3, $J_{\text{C-P}}$ = 14.2 Hz), 136.5 (dd, $J_{\text{C-P}}$ = 10.3, $J_{\text{C-P}}$ = 4.6 Hz), 135.5 (d, $J_{\text{C-P}}$ = 3.2 Hz), 133.8 (d, $J_{\text{C-P}}$ = 19.6 Hz), 130.6 (dd, $J_{\text{C-P}}$ = 10.3, 5.3 Hz), 130.5 (d, $J_{\text{C-P}}$ = 73.1 Hz), 128.8, 128.7 (d, $J_{\text{C-P}}$ = 7.0 Hz), 127.3, 124.6 (d, $J_{\text{C-P}}$ = 13.8 Hz), 112.6 ppm (d, $J_{\text{C-P}}$ = 3.9 Hz). ^{31}P NMR (C $_6$ D $_6$, 121 MHz): δ = 66.1 (d, $J_{\text{P-P}}$ = 167.3 Hz), -18.6 ppm (d, $J_{\text{P-P}}$ = 167.3 Hz). HRMS *calcd.* for C $_{26}$ H $_{22}$ N $_2$ P $_2$ Na $^+$: 447.114760, *found* 447.115045. IR $\tilde{\nu}$ = 419, 474, 498, 546, 616, 662, 693, 731, 766, 803, 100, 1057, 1074, 1176, 1241, 1262, 1292, 1389, 1434, 1449, 1478, 1555, 1582, 2924, 2961, 3063 cm $^{-1}$.

Compound **107a**

92b (36.4 mg, 0.038 mmol) and Mo(CO) $_6$ (10.0 mg, 0.038 mmol) was stirred in THF (2 ml) at 75 °C overnight. After cooling to r.t., the solvent was evaporated *in vacuo* and washed with CH $_2$ Cl $_2$ to afford the desired compound as a yellow solid (19.9 mg, 49%). Yellow crystals suitable for X-ray analysis were obtained from a saturated solution in CH $_3$ CN/Et $_2$ O at r.t. ^1H NMR (CD $_3$ CN, 400 MHz): δ = 8.15 – 8.07 (m, 1H), 8.04 – 7.89 (m, 3H), 7.68 – 7.27 (m, 10H), 4.01 (s, 8H), 3.14 – 2.92 (br, 12H). ^{13}C NMR (CD $_3$ CN, 125 Mz): δ = 213.6 (dd, $J_{\text{C-P}}$ = 32.5, $J_{\text{C-P}}$ = 10.0 Hz), δ = 213.1 (dd, $J_{\text{C-P}}$ = 23.8, $J_{\text{C-P}}$ = 7.6 Hz), 208.2 (m), 162.4 (d, $J_{\text{C-P}}$ = 22.7Hz), 144.9 (dd, $J_{\text{C-P}}$ = 42.2, $J_{\text{C-P}}$ = 35.1 Hz), 138.4 (d, $J_{\text{C-P}}$ = 15.6 Hz), 136.5 (d, $J_{\text{C-P}}$ =

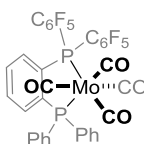
12.1 Hz), 136.2 (dd, $J_{C-P} = 4.7$ Hz, $J_{C-P} = 2.2$ Hz), 135.1 (dd, $J_{C-P} = 5.8$ Hz, $J_{C-P} = 1.7$ Hz), 134.4 (d, $J_{C-P} = 13.2$ Hz), 133.0 (m), 132.4, 130.3 (d, $J_{C-P} = 10.4$ Hz), 129.8 (dd, $J_{C-P} = 41.6$ Hz, 35.9 Hz), 53.5 (m), 53.5 ppm (m). ^{31}P NMR (CD_3CN , 162 MHz): $\delta = 60.1$ (d, $J_{P-P} = 13.7$ Hz), 40.2 ppm (d, $J_{P-P} = 13.77$ Hz). ^{19}F NMR (CD_3CN , 282 MHz): $\delta = -124.0$ ppm (sextet, $J_{F-Sb(I=5/2)} = 1933$ Hz, octet, $J_{F-Sb(I=7/2)} = 1049$ Hz). HRMS *calcd.* for $\text{C}_{32}\text{H}_{34}\text{N}_4\text{F}_6\text{MoP}_2\text{Sb}^+$: 933.004530, *found* 933.004662. IR $\tilde{\nu} = 514, 524, 657, 697, 796, 1016, 1090, 1259, 1297, 1572, 1847, 1938, 1973, 2403, 2963$ cm^{-1} .

Compound **107b**



(Dipyrrolylphosphino)-2-diphenylphosphine **106** (100.0 mg, 0.236 mmol) and $\text{Mo}(\text{CO})_6$ (62.2mg, 0.236 mmol) in THF (3 ml) was stirred overnight at 70 °C. After cooling to r.t., the solvent was evaporated *in vacuo* to afford the desired compound **107b** as a yellow solid (113.2 mg, 76%). ^1H NMR (CD_2Cl_2 , 400 MHz): $\delta = 7.57$ (m, 3H), 7.49 (m, 1H), 7.44 – 7.26 (m, 10H), 6.72 (dt, $J = 4.2, J = 2.1$ Hz, 4H), 6.32 ppm (td, $J = 2.1, J = 1.1$ Hz, 4H). ^{13}C NMR (CD_2Cl_2 , 100 Mz): $\delta = 215.7 - 214.8$ (m), 209.0 – 207.9 (m), 145.0 (dd, $J_{C-P} = 40.9, J_{C-P} = 33.8$ Hz), 143.1 (dd, $J_{C-P} = 42.9, J_{C-P} = 34.9$ Hz), 135.6 (dd, $J_{C-P} = 37.8, J_{C-P} = 2.9$ Hz), 133.9 (d, $J_{C-P} = 14.9$ Hz), 132.6 (dd, $J_{C-P} = 5.0$ Hz, $J_{C-P} = 2.0$ Hz), 132.6 (d, $J_{C-P} = 12.7$ Hz), 131.1 (d, $J_{C-P} = 5.5$ Hz), 130.6 (d, $J_{C-P} = 1.8$ Hz), 130.5 (d, $J_{C-P} = 2.1$ Hz), 129.0 (d, $J_{C-P} = 9.7$ Hz), 124.3 (d, $J_{C-P} = 7.5$ Hz), 113.0 ppm (d, $J_{C-P} = 5.7$ Hz). ^{31}P NMR (CD_2Cl_2 , 162 MHz): $\delta = 139.2$ (d, $J_{P-P} = 4.7$ Hz), 56.9 ppm (d, $J_{P-P} = 4.7$ Hz). HRMS *calcd.* for $\text{C}_{30}\text{H}_{22}\text{N}_2\text{O}_4\text{MoP}_2\text{Na}^+$: 656.999890, *found* 657.000215. IR $\tilde{\nu} = 416, 504, 525, 571, 585, 671, 732, 999, 1037, 1067, 1116, 1177, 1234, 1434, 1449, 1481, 1572, 1896, 1936, 2030, 3062, 3251$ cm^{-1} .

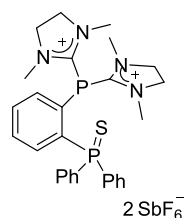
Compound **107c**



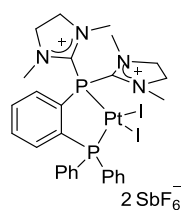
(Dipentafluorophenylphosphino)-2-diphenylphosphine **105** (100.0 mg, 0.160 mmol) and $\text{Mo}(\text{CO})_6$ (42.2mg, 0.160 mmol) in THF (3 ml) was stirred at 70 °C overnight. After cooling to r.t., the solvent was evaporated *in vacuo* to afford the desired compound **107c** as a white solid (114.6 mg, 86%). ^1H NMR (CD_2Cl_2 , 400 MHz): $\delta = 7.76 - 7.72$ (m, 1H), 7.61 – 7.56

(m, 4H), 7.43 – 7.40 ppm (m, 9H). ^{13}C NMR (CD_2Cl_2 , 100 MHz): $\delta = 216.6$ (dd, $J_{\text{C-P}} = 31.8$, $J_{\text{C-P}} = 8.7$ Hz), 215.1 (d, $J_{\text{C-P}} = 26.0$ Hz), 208.5 (m), 146.5 (dm, $J_{\text{C-F}} = 251.0$ Hz), 143.1 (dm, $J_{\text{C-F}} = 258.2$ Hz), 142.9 (dd, $J_{\text{C-P}} = 43.4$, $J_{\text{C-P}} = 35.0$ Hz), 139.5 (m), 137.0 (m), 135.9 (dd, $J_{\text{C-P}} = 37.4$, $J_{\text{C-P}} = 2.5$ Hz), 134.8 (d, $J_{\text{C-P}} = 15.6$ Hz), 133.4 (d, $J_{\text{C-P}} = 12.8$ Hz), 132.5 (d, $J_{\text{C-P}} = 12.7$ Hz), 131.7 (dd, $J_{\text{C-P}} = 16.5$, $J_{\text{C-P}} = 2.0$ Hz), 130.5 (d, $J = 2.0$ Hz), 128.9 (d, $J = 9.7$ Hz), 111.2 ppm (d, $J_{\text{C-P}} = 21.2$ Hz). ^{31}P NMR (CD_2Cl_2 , 162 MHz): $\delta = 60.5$ (d, $J_{\text{P-P}} = 7.3$ Hz), 31.1 ppm (q, $J_{\text{P-F}} = 10.6$, $J_{\text{P-F}} = 10.1$ Hz). ^{19}F NMR (CD_2Cl_2 , 282 MHz): $\delta = -128.6$ (m), -149.6 (m), -160.0 ppm (m). EI-MS *calcd.* for $\text{C}_{34}\text{H}_{14}\text{O}_4\text{F}_{10}\text{MoP}_2$: 834.37, *found* 834.25. IR $\tilde{\nu} = 424, 542, 585, 631, 665, 693, 729, 799, 976, 1009, 1086, 1190, 1260, 1287, 1322, 1384, 1436, 1470, 1514, 1639, 1911, 2028, 2072, 2963, 3058$ cm^{-1} .

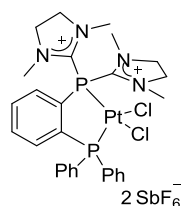
Compound 108



S_8 (2.0 mg, 0.063 mmol) and **92b** (30.0 mg, 0.031 mmol) in DCE (2 ml) were stirred at 70°C for 48 h. After removal of the solvent *in vacuo*, the remaining solid was washed with Et_2O and pentane to afford **108** as a white solid (23.6 mg, 76%). Colourless crystals suitable for X-ray crystallography were obtained from a saturated solution of the compound in $\text{CH}_2\text{Cl}_2/\text{Et}_2\text{O}$ at r.t. ^1H NMR (CD_3CN , 400 MHz): $\delta = 7.78 - 7.70$ (m, 9H), 7.63 – 7.61 (m, 4H), 7.37 – 7.30 (m, 1H), 3.97 – 3.91 (m, 8H), 2.79 ppm (s, 12H). ^{13}C NMR (CD_3CN , 100 MHz): $\delta = 166.0$ (d, $J = 45.2$ Hz), 141.7 (dd, $J = 83.4$ Hz, $J = 32.5$ Hz), 142.4 (dd, $J = 9.6$ Hz, $J = 2.0$ Hz), 135.8 (dd, $J = 8.4$ Hz, $J = 8.4$ Hz), 135.1 (d, $J = 10.5$ Hz), 134.9 (d, $J = 2.6$ Hz), 134.2 (d, $J = 3.0$ Hz), 133.7 (d, $J = 10.9$ Hz), 130.4 (d, $J = 13.0$ Hz), 129.7 (dd, $J = 86.7$ Hz, $J = 0.9$ Hz), 123.1 (dd, $J = 11.0$ Hz, $J = 9.6$ Hz), 55.3, 53.3, 36.3, 36.2 ppm. ^{31}P NMR (CD_3CN , 121 MHz): $\delta = 44.3$ (d, $J_{\text{P-P}} = 32.1$ Hz), -51.1 ppm (d, $J_{\text{P-P}} = 32.1$ Hz). ^{19}F NMR (CD_3CN , 282 MHz): $\delta = -122.4$ ppm (sextet, $J_{\text{F-Sb}(I=5/2)} = 1945$ Hz, octet, $J_{\text{F-Sb}(I=7/2)} = 1071$ Hz). HRMS *calcd.* for $\text{C}_{28}\text{H}_{34}\text{N}_4\text{SbF}_6\text{P}_2\text{S}^+$: 755.091860, *found* 755.091565. IR $\tilde{\nu} = 422, 437, 448, 474, 505, 521, 651, 690, 716, 738, 753, 767, 840, 929, 1000, 1105, 1187, 1293, 1329, 1409, 1441, 1484, 1518, 1572, 1715, 2962, 3066$ cm^{-1} .

Compound **109a**

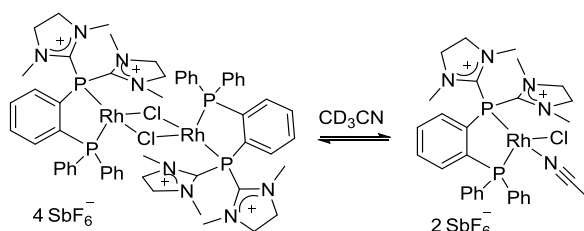
$\text{PtI}_2(\text{PhCN})_2$ (20.0 mg, 0.031 mmol) and **92b** (29.5 mg, 0.031 mmol) in CH_2Cl_2 (2 ml) was stirred overnight. After removal of the solvent *in vacuo*, the remaining solid was washed with pentane, affording the desired product as a yellow solid **109a** (40.3 mg, 95%). Yellow crystals suitable for X-ray crystallography were obtained from a saturated solution of $\text{CH}_3\text{COCH}_3/\text{Et}_2\text{O}$ at 0 °C. ^1H NMR (CD_3CN , 400 MHz): δ = 8.45 – 8.40 (m, 1H), 7.96 – 7.91 (m, 2H), 7.77 – 7.70 (m, 7H), 7.62 – 7.57 (m, 4H), 4.07 – 4.00 (m, 8H), 3.24 ppm (s, 12H). ^{13}C NMR (CD_3CN , 100 MHz): δ = 154.3 (d, J = 49.5 Hz), 138.7 (m), 138.5 (m), 136.3 (m), 136.2 (m), 136.1 (m), 135.9 (m), 135.1 (m), 134.9 (d, $J_{\text{C-P}}$ = 2.8 Hz), 134.5 (d, $J_{\text{C-P}}$ = 3.6 Hz), 127.6 (d, $J_{\text{C-P}}$ = 68.7 Hz), 54.5 (d, $J_{\text{C-P}}$ = 3.3 Hz), 39.6 ppm (d, $J_{\text{C-P}}$ = 3.0 Hz). ^{31}P NMR (CD_3CN , 121 MHz): δ = 39.2 (dt, $J_{\text{P-P}}$ = 4.6 Hz, $J_{\text{P-Pt}}$ = 2856.1 Hz), 5.4 ppm (d, $J_{\text{P-P}}$ = 4.6 Hz, $J_{\text{P-Pt}}$ = 3457.9 Hz). ^{19}F NMR (CD_3CN , 282 MHz): δ = – 122.4 ppm (sextet, $J_{\text{F-Sb}(I=5/2)}$ = 3890 Hz, octet, $J_{\text{F-Sb}(I=7/2)}$ = 1071 Hz). HRMS *calcd.* for $\text{C}_{28}\text{H}_{34}\text{N}_4\text{SbF}_6\text{P}_2\text{I}_2\text{Pt}^+$: 1171.893620, *found* 1171.893250. IR $\tilde{\nu}$ = 452, 503, 543, 598, 645, 689, 750, 922, 998, 1101, 1114, 1300, 1408, 1437, 1520, 1586, 1979, 2220, 3007, 3061 cm^{-1} .

Compound **109b**

CH_2Cl_2 (2 ml) was added to a mixture of $\text{PtCl}_2(\text{CH}_3\text{CN})_2$ (10.9 mg, 0.031 mmol) and **92b** (30.0 mg, 0.031 mmol) and the mixture stirred overnight. After removal of the solvent *in vacuo*, the solid left washed with pentane and dried, affording the desired product **109b** as a white solid (36.8 mg, 96%). ^1H NMR (CD_3CN , 400 MHz): δ = 8.28 – 8.23 (m, 1H), 8.05– 7.95 (m, 3H), 7.80 – 7.68 (m, 6H), 7.62 – 7.57 (m, 4H), 4.10 – 4.05 (m, 8H), 3.25 ppm (s, 12H). ^{13}C NMR (CD_3CN , 100 MHz): δ = 153.1 (d, J = 53.0 Hz), 143.0 (dd, J = 63.5 Hz, J = 40.9 Hz), 138.9 (dd, J = 7.8 Hz, J = 2.7 Hz), 138.2 (dd, J = 19.3 Hz, J = 4.1 Hz), 137.3 (dd, J = 9.2 Hz, J = 2.2 Hz), 136.6 (dd, J = 1.7 Hz, J = 3.6 Hz), 135.2 (dd, J = 19.9 Hz, J = 8.4 Hz), 134.7 (d, J = 3.0 Hz), 130.6 (d, J = 12.7 Hz), 128.0 (dd, J = 67.5 Hz, J = 22.5 Hz), 126.0 (d, J

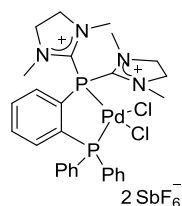
= 71.3 Hz), 54.5 (d, $J = 3.6$ Hz), 39.3 ppm (d, $J = 2.5$ Hz). ^{31}P NMR (CD_3CN , 121 MHz): $\delta = 39.5$ (t, $J_{\text{P-Pt}} = 3006.0$ Hz), 8.5 ppm (t, $J_{\text{P-Pt}} = 3893.4$ Hz). ^{19}F NMR (CD_3CN , 376 MHz): $\delta = -124.0$ ppm (sextet, $J_{\text{F-Sb}(I=5/2)} = 1933$ Hz, octet, $J_{\text{F-Sb}(I=7/2)} = 1049$ Hz). HRMS *calcd.* for $\text{C}_{28}\text{H}_{34}\text{N}_4\text{SbF}_6\text{P}_2\text{Cl}_2\text{Pt}^+$: 987.022430, *found* 988.022211. IR $\tilde{\nu} = 472, 505, 525, 654, 690, 735, 748, 767, 922, 997, 1102, 1117, 1205, 1294, 1437, 1521, 1581$ cm^{-1} .

Compound **109c** and **109d**



$[\text{RhCl}(\text{COD})]_2$ (5.0 mg, 0.013 mmol) and **92b** (24.7 mg, 0.026 mmol) in CH_2Cl_2 (2 ml) was stirred overnight. After removal of the solvent *in vacuo*, the solid left washed with pentane, affording the desired product **109c** as an orange solid (26.3 mg, 92%). The compound **109c** in CD_3CN is equilibrium between **109c** and **109d**, which can be proved by the related ^{31}P NMR Spectra. Mixing of the solution of **92b** and $[\text{RhCl}(\text{COD})]_2$ in CH_2Cl_2 at -78 $^\circ\text{C}$, orange crystals of **109c** suitable for X-ray crystallography were obtained by slowly warming up the solution. Orange crystals of **109d** suitable for X-ray crystallography were directly obtained from solutions of the title compound in $\text{CH}_3\text{CN}/\text{CH}_2\text{Cl}_2/\text{Et}_2\text{O}$ at r.t.

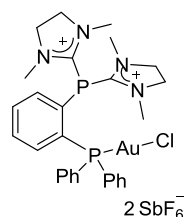
Compound **109e**



$\text{PdCl}_2(\text{PhCN})_2$ (7.2 mg, 0.019 mmol) and **92b** (18.0 mg, 0.019 mmol) in CH_2Cl_2 (2 ml) was stirred overnight. After removal of the solvent *in vacuo*, the solid left washed with pentane and dried, affording the desired product **109e** as a white solid (19.4 mg, 91%). ^1H NMR (CD_3CN , 400 MHz): $\delta = 8.28 - 8.23$ (m, 1H), 8.10 – 8.06 (m, 2H), 8.00 – 7.90 (m, 1H), 7.85 – 7.72 (m, 6H), 7.64 – 7.59 (m, 4H), 4.11 – 4.06 (m, 8H), 3.24 ppm (s, 12H). ^{13}C NMR (CD_3CN , 100 MHz): $\delta = 155.4$ (d, $J = 41.8$ Hz), 139.8 (dd, $J = 6.9$ Hz, $J = 2.2$ Hz), 138.6 (dd, $J = 23.6$ Hz, $J = 2.9$ Hz), 137.5 (d, $J = 1.7$ Hz), 137.4 (d, $J = 2.1$ Hz), 137.3 (d, $J = 1.5$ Hz), 137.2, 135.3 (d, $J = 11.5$ Hz), 135.0 (d, $J = 3.3$ Hz), 130.7 (d, $J = 12.8$ Hz), 126.9 (d, $J = 64.5$ Hz), 54.7 (d, $J = 3.4$ Hz), 39.4 ppm (d, $J = 2.8$ Hz). ^{31}P NMR (CD_3CN , 121 MHz): $\delta = 63.7$

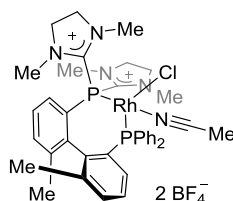
(d, $J_{P-P} = 5.9$ Hz), 22.8 ppm (d, $J_{P-P} = 5.9$ Hz). ^{19}F NMR (CD_3CN , 376 MHz): $\delta = -124.0$ ppm (sextet, $J_{F-Sb(I=5/2)} = 1933$ Hz, octet, $J_{F-Sb(I=7/2)} = 1049$ Hz). HRMS *calcd.* for $\text{C}_{28}\text{H}_{34}\text{N}_4\text{SbF}_6\text{P}_2\text{Cl}_2\text{Pd}^+$: 898.961130, *found* 898.960595. IR $\tilde{\nu} = 426, 452, 495, 507, 525, 678, 699, 746, 767, 938, 987, 1102, 1117, 1205, 1265, 1294, 1437, 1489, 1521, 1581, 2935$ cm^{-1} .

Compound **109f**



(Me_2S) AuCl (9.2 mg, 0.031 mmol) and **92b** (30.0 mg, 0.031 mmol) in CH_2Cl_2 (2 ml) were stirred overnight. After removal of the solvent *in vacuo*, the solid left washed with pentane and dried, affording the desired product **109f** as a white solid (34.6 mg, 93%). Colorless Crystals suitable for X-ray crystallography were obtained from $\text{CH}_3\text{CN}/\text{CH}_2\text{Cl}_2/\text{Et}_2\text{O}$. ^1H NMR (CD_3CN , 400 MHz): $\delta = 7.88 - 7.81$ (m, 2H), 7.75 - 7.70 (m, 3H), 7.70 - 7.61 (m, 8H), 7.36 - 7.30 (m, 1H), 4.01 (d, $J = 1.3$, 8H), 2.83 ppm (s, 12H). ^{13}C NMR (CD_3CN , 100 MHz): $\delta = 163.7$ (dd, $J = 39.6$ Hz, $J = 3.1$ Hz), 140.8 (dd, $J = 8.2$ Hz, $J = 1.8$ Hz), 138.6 (dd, $J = 59.6$ Hz, $J = 37.2$ Hz), 137.6 (dd, $J = 9.8$ Hz, $J = 6.0$ Hz), 136.9 (d, $J = 8.3$ Hz), 135.9 (d, $J = 14.2$ Hz), 135.5, 134.5 (d, $J = 2.8$ Hz), 131.1 (d, $J = 12.3$ Hz), 126.0 (dd, $J = 65.4$ Hz, $J = 3.0$ Hz), 120.6 (d, $J = 2.3$ Hz), 53.7, 36.3 ppm (d, $J = 9.1$ Hz). ^{31}P NMR (CD_3CN , 121 MHz): $\delta = 26.8$ (d, $J_{P-P} = 125.3$ Hz), -44.7 ppm (d, $J_{P-P} = 125.3$ Hz). ^{19}F NMR (CD_3CN , 282 MHz): $\delta = -122.4$ ppm (sextet, $J_{F-Sb(I=5/2)} = 1945$ Hz, octet, $J_{F-Sb(I=7/2)} = 1071$ Hz). HRMS *calcd.* for $\text{C}_{28}\text{H}_{34}\text{N}_4\text{P}_2\text{F}_6\text{ClSbAu}^+$: 955.054890, *found* 955.054898. IR $\tilde{\nu} = 454, 498, 509, 549, 645, 693, 796, 930, 1023, 1100, 1206, 1261, 1296, 1334, 1411, 1438, 1482, 1520, 1578, 2921, 2962$ cm^{-1} .

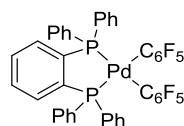
Compound **110**



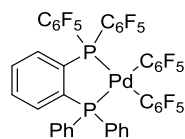
$[\text{RhCl}(\text{COD})]_2$ (6.4 mg, 0.013 mmol) and **101a** (20.0 mg, 0.026 mmol) in CH_3CN (2 ml) were stirred overnight. After removal of the solvent *in vacuo*, the solid left washed with CH_2Cl_2 and pentane, and dried, affording **110** as a yellow solid (21.6 mg, 86%). Yellow

crystals suitable for X-ray crystallography were obtained from CH₃CN/CH₂Cl₂/Et₂O at r.t. ¹H NMR (CD₃CN, 400 MHz): δ = 7.75 – 8.60 (m, 3H), 7.59 – 7.42 (m, 7H), 7.42 – 7.35 (m, 3H), 7.33 – 7.28 (m, 1H), 7.26 – 7.16 (m, 1H), 7.14 – 7.10 (m, 1H), 4.32 – 4.20 (m, 2H), 4.16 (s, 3H), 4.02 (s, 3H), 3.96 – 3.90 (m, 2H), 3.81 – 3.89 (m, 1H), 3.78 – 3.66 (m, 2H), 3.45 – 3.33 (m, 1H), 3.03 (s, 3H), 2.75 (s, 3H), 1.74 (s, 3H), 1.62 ppm (s, 3H). ¹³C NMR (CD₃CN, 125 MHz): δ = 164.8 (d, *J* = 33.6 Hz), 154.8, 143.1 (d, *J* = 9.5 Hz), 142.5 (d, *J* = 7.6 Hz), 140.5 (d, *J* = 18.2 Hz, *J* = 4.0 Hz), 137.0 (d, *J* = 52.9 Hz), 136.9 (dd, *J* = 11.5 Hz, *J* = 6.1 Hz), 135.9, 135.7 (d, *J*_{C-P} = 10.4 Hz), 135.5 (d, *J* = 12.9 Hz), 134.8, 132.7, 132.3 (d, *J* = 50.0 Hz), 132.0, 131.2 (d, *J* = 7.6 Hz), 130.1 (d, *J* = 9.3 Hz), 130.0 (d, *J* = 5.3 Hz), 129.6 (d, *J* = 10.6 Hz), 129.5 (d, *J* = 10.0 Hz), 129.4 (d, *J* = 9.7 Hz), 127.8 (d, *J* = 51.0 Hz), 121.7 (d, *J* = 59.1 Hz), 55.4, 53.7, 53.6, 51.5, 42.6 (d, *J* = 4.4 Hz), 39.4 (d, *J* = 11.0 Hz), 39.0, 37.4, 20.7, 19.8 ppm. ³¹P NMR (CD₃CN, 121 MHz): δ = 38.1 (dd, *J*_{P-Rh} = 153.9 Hz, *J*_{P-P} = 50.2 Hz), 11.9 ppm (dd, *J*_{P-Rh} = 215.7 Hz, *J*_{P-P} = 50.2 Hz). ¹¹B NMR (CD₃CN, 96 MHz): δ = - 1.2 ppm, ¹⁹F NMR (CD₃CN, 282 MHz): δ = - 151.9 ppm. IR $\tilde{\nu}$ = 463, 698, 754, 792, 868, 936, 1052, 1292, 1401, 1661, 2112, 2325, 3205, 3369 cm⁻¹.

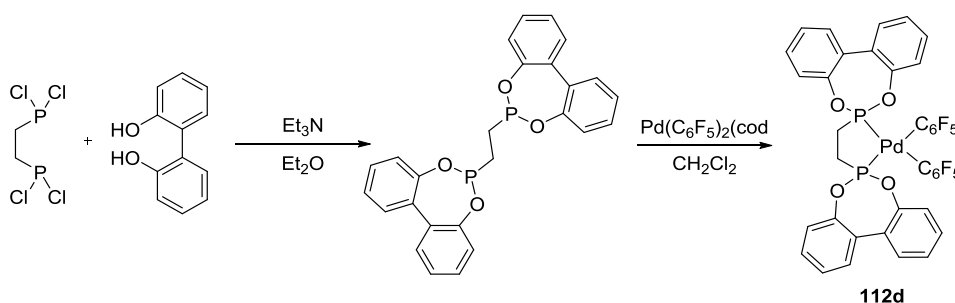
Compound **112b**



Pd(C₆F₅)₂(cod) (50.0 mg, 0.031 mmol) and 1,2-bis(diphenylphosphino)benzene (30.4 mg, 0.031 mmol) were stirred overnight in CH₂Cl₂ (2 ml). After removal of the solvent *in vacuo*, the solid left washed with pentane and dried, affording the desired product as a white solid **112b** (76.8 mg, 95%). Colorless crystals suitable for X-ray crystallography were obtained from CH₂Cl₂. ¹H NMR (CD₂Cl₂, 600 MHz): δ = 7.75 – 7.72 (m, 2H), 7.61 – 7.60 (m, 2H), 7.51 – 7.49 (m, 4H), 7.47 – 7.44 (m, 8H), 7.39 – 7.37 ppm (m, 8H). ¹³C NMR (CD₂Cl₂, 150 MHz): δ = 146.3 (dm, *J*_{C-F} = 230.4), 142.5 (t, *J*_{C-P} = 43.0 Hz), 137.5 (dm, *J*_{C-F} = 241.9 Hz), 136.5 (dm, *J*_{C-F} = 237.4 Hz), 133.9 (t, *J*_{C-P} = 8.6 Hz), 133.7 (t, *J*_{C-P} = 8.6 Hz), 133.1, 131.8, 130.6 (d, *J* = 47.9 Hz), 129.2 ppm (t, *J* = 4.5 Hz). ³¹P NMR (CD₂Cl₂, 121 MHz): δ = 52.3 ppm. ¹⁹F NMR (CD₂Cl₂, 282 MHz): δ = - 113.7 (m), - 161.2 (t, *J*_{F-F} = 20.7 Hz), - 163.1 (tm, *J*_{F-F} = 20.7 Hz) ppm. MS-EI *calcd.* for C₄₂H₂₄F₁₀P₂Pd: 886.02, *found* 886.90, IR $\tilde{\nu}$ = 411, 422, 445, 498, 544, 602, 617, 668, 687, 741, 760, 774, 950, 1000, 1027, 1055, 1098, 1159, 1186, 1254, 1281, 1308, 1346, 1432, 1496, 1608, 1633, 3062 cm⁻¹.

Compound **112c**

Pd(C₆F₅)₂(cod) (43.8 mg, 0.080 mmol) and the diphosphine **105** (50.0 mg, 0.080 mmol) were stirred overnight in CH₂Cl₂ (2 ml). After removal of the solvent *in vacuo*, the remaining solid was washed with pentane and dried, affording the desired product **112c** as a white solid (81.7 mg, 96%). ¹H NMR (CD₂Cl₂, 400 MHz): δ = 8.07 – 7.96 (m, 1H), 7.84 – 7.82 (m, 1H), 7.76 – 7.65 (m, 2H), 7.63 – 7.54 (m, 2H), 7.36 – 7.52 ppm (m, 8H). ¹³C NMR (CD₂Cl₂, 100 MHz): δ = 147.6 (dm, *J*_{C-F} = 81.4 Hz), 147.3 (dm, *J*_{C-F} = 252.3 Hz), 144.9, 144.4 (dm, *J*_{C-F} = 258.2 Hz), 141.4 (dd, *J*_{C-P} = 50.8 Hz, *J*_{C-P} = 44.5 Hz), 138.5 (dm, *J*_{C-F} = 243.4 Hz), 138.1 (dm, *J*_{C-F} = 216.5 Hz), 136.2 (*J*_{C-F} = 253.6 Hz), 134.7 (dd, *J*_{C-P} = 19.9 Hz, *J*_{C-P} = 1.1 Hz), 134.5 (dd, *J*_{C-P} = 5.5 Hz, *J*_{C-P} = 2.0 Hz), 134.3 (dd, *J*_{C-P} = 6.3 Hz, *J*_{C-P} = 1.8 Hz), 133.7 (d, *J*_{C-P} = 12.5 Hz), 133.3 (d, *J*_{C-P} = 15.7 Hz), 132.3 (d, *J*_{C-P} = 2.6 Hz), 129.8, 129.4 ppm (d, *J*_{C-P} = 11.1 Hz). ³¹P NMR (CD₂Cl₂, 121 MHz): δ = 51.0 (m), 16.9 ppm (m). ¹⁹F NMR (CD₂Cl₂, 282 MHz): δ = – 115.0 (m), – 118.1 (m), – 127.1 (m), – 145.7 (m), – 159.0 (m), – 160.7 (t, *J*_{F-F} = 19.7 Hz), – 161.4 (t, *J*_{F-F} = 19.7 Hz), – 163.5 (td, *J*_{F-F} = 20.1 Hz, *J*_{F-P} = 9.4 Hz), – 164.0 ppm (td, *J*_{F-F} = 20.1 Hz, *J*_{F-P} = 10.4 Hz). HRMS *calcd.* for C₄₂H₁₄F₂₀P₂PdNa⁺: 1088.917860, *found* 1088.917765. IR $\tilde{\nu}$ = 458, 483, 519, 536, 631, 670, 692, 745, 797, 954, 977, 1017, 1091, 1260, 1297, 1360, 1455, 1475, 1499, 1519, 1642, 2963 cm⁻¹.

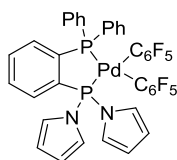
Compound **112d**

1,2-bis(dichlorophosphino)ethane (0.500 ml, 3.300 mmol) was added dropwise to a solution of 2,2'-biphenol (1.2 g, 6.600 mmol) and Et₃N (1.840 ml, 13.200 mmol) in Et₂O (30 ml) at – 78 °C, and the mixture allowed to warm to r.t. overnight. The reaction was then filtered and the filtrate evaporated *in vacuo* to give a white solid, which was washed with a small amount of CH₂Cl₂ and dried, affording bis(1,2-biphenylphosphino)ethane as a white solid (983.1 mg, 65%). ¹H NMR (CD₂Cl₂, 400 MHz): δ = 7.47 (dd, *J* = 7.5 Hz, *J* = 1.8 Hz, 4H), 7.37 (dt, *J* = 7.5 Hz, *J* = 1.8 Hz, 4H), 7.30 (dt, *J* = 7.5 Hz, *J* = 1.3 Hz, 4H), 7.12 (d, *J* = 7.9 Hz, 4H), 1.95

ppm (t, $J = 6.7$ Hz, 4H). ^{13}C NMR (CD_2Cl_2 , 100 MHz): $\delta = 151.4$ (t, $J = 3.1$ Hz), 132.2, 130.6, 129.7, 125.6, 122.2, 26.1 ppm (dd, $J = 42.1$ Hz, $J = 19.5$ Hz). ^{31}P NMR (CD_2Cl_2 , 121 MHz): $\delta = 207.2$ ppm. HRMS *calcd.* for $\text{C}_{26}\text{H}_{20}\text{O}_4\text{P}_2$: 458.083314, *found* 458.083689. IR $\tilde{\nu} = 416, 429, 480, 516, 591, 669, 703, 762, 883, 939, 978, 1036, 1060, 1094, 1202, 1245, 1268, 1400, 1435, 1474, 1496, 1595, 1713, 2404, 2943, 3023, 3070, 3185$ cm^{-1} .

$\text{Pd}(\text{C}_6\text{F}_5)_2(\text{cod})$ (53.8 mg, 0.098 mmol) and bis(1,2-biphenylphosphino)ethane (45.0 mg, 0.098 mmol) were dissolved in CH_2Cl_2 (2 ml) and stirred overnight. After removal of the solvent *in vacuo*, the solid left was washed with pentane and dried, affording **112d** as a white solid (82.1 mg, 93%). ^1H NMR (CD_2Cl_2 , 400 MHz): $\delta = 7.48 - 7.45$ (m, 4H), 7.36 – 7.34 (m, 8H), 7.15 – 7.13 (m, 4H), 2.41 ppm (d, $J = 23.0$ Hz, 4H). ^{13}C NMR (CD_2Cl_2 , 100 MHz): $\delta = 148.23$ (d, $J_{\text{C-P}} = 11.3$ Hz), 148.22, 146.1 (dm, $J = 226.3$ Hz), 137.4 (dm, $J_{\text{C-F}} = 245.2$ Hz), 136.1 (dm, $J_{\text{C-F}} = 252$ Hz), 130.5, 129.6, 129.2, 126.6, 121.0, 26.8 ppm (t, $J = 23.2$ Hz). ^{31}P NMR (CD_2Cl_2 , 121 MHz): $\delta = 202.2$ ppm (m). ^{19}F NMR (CD_2Cl_2 , 282 MHz): $\delta = -114.5$ (m), -161.9 (t, $J_{\text{F-F}} = 19.9$ Hz), -163.1 (td, $J_{\text{F-F}} = 19.9$ Hz, $J_{\text{F-P}} = 9.1$ Hz) ppm. HRMS *calcd.* for $\text{C}_{38}\text{H}_{20}\text{O}_4\text{F}_{10}\text{P}_2\text{PdNa}^+$: 920.960310, *found* 920.960340. IR $\tilde{\nu} = 435, 493, 523, 536, 595, 654, 716, 755, 772, 823, 871, 912, 954, 1012, 1045, 1094, 1191, 1248, 1274, 1361, 1403, 1456, 1498, 1532, 1606, 1633, 2916, 3067$ cm^{-1} .

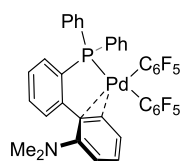
Compound 112e



(Dipyrrolylphosphino)-2-diphenylphosphine (38.7 mg, 0.091 mmol) and $\text{Pd}(\text{C}_6\text{F}_5)_2(\text{cod})$ (50.0 mg, 0.091 mmol) were dissolved in CH_2Cl_2 (1 ml) and stirred overnight. Then, the solvent was evaporated *in vacuo* and washed with Et_2O to afford the desired compound **112e** as a white solid (73.3 mg, 93%). ^1H NMR (CD_2Cl_2 , 500 MHz): $\delta = 7.50 - 7.91$ (m, 1H), 7.85 – 7.81 (m, 1H), 7.80 – 7.75 (m, 2H), 7.53 – 7.49 (m, 2H), 7.46 – 7.33 (m, 8H), 6.86 – 6.84 (m, 5H), 6.40 – 6.38 ppm (m, 4H). ^{13}C NMR (CD_2Cl_2 , 125 Mz): $\delta = 147.2$ (dm, $J_{\text{C-F}} = 68.6$ Hz), 145.3 (dm, $J_{\text{C-F}} = 72.8$ Hz), 141.8 (dd, $J_{\text{C-P}} = 49.6$, $J_{\text{C-P}} = 37.0$ Hz), 140.8 (dd, $J_{\text{C-P}} = 52.1$, $J_{\text{C-P}} = 43.2$ Hz), 138.1 (dm, $J_{\text{C-F}} = 241.6$ Hz), 136.8 (d, $J_{\text{C-F}} = 250.6$ Hz), 135.62 (d, $J_{\text{C-P}} = 6.0$ Hz), 134.23 (d, $J_{\text{C-P}} = 19.3$ Hz), 133.59 (d, $J_{\text{C-P}} = 12.6$ Hz), 133.3 (dd, $J_{\text{C-P}} = 5.9$ Hz, $J_{\text{C-P}} = 1.6$ Hz), 132.2 (d, $J_{\text{C-P}} = 2.5$ Hz), 132.1 (dd, $J_{\text{C-P}} = 15.8$, $J_{\text{C-P}} = 2.4$ Hz), 129.4 (d, $J_{\text{C-P}} = 10.9$ Hz), 128.9 (d, $J_{\text{C-P}} = 49.7$ Hz), 124.1 (d, $J_{\text{C-P}} = 8.2$ Hz), 114.8 ppm (d, $J_{\text{C-P}} = \text{Hz}$). ^{31}P NMR

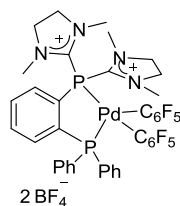
(CD₂Cl₂, 162 MHz): δ = 109.1 (br), 47.9 ppm (br). ¹⁹F NMR (CD₂Cl₂, 282 MHz): δ = -115.02 (m), -161.59 (m), -163.57 (dm, J_{F-P} = 139.0 Hz). HRMS *calcd.* for C₃₈H₂₂N₂F₁₀P₂PdNa⁺: 887.002710, *found* 887.002477. IR $\tilde{\nu}$ = 421, 450, 478, 511, 537, 566, 608, 627, 672, 702, 725, 776, 953, 1001, 1055, 1100, 1115, 1237, 1350, 1360, 1436, 1498, 1531, 3060 cm⁻¹.

Compound **112f**



2-Diphenylphosphino-2'-(N,N-dimethylamino)biphenyl (30.0 mg, 0.055 mmol) and Pd(C₆F₅)₂(cod) (20.8 mg, 0.055 mmol) were stirred in CH₂Cl₂ (2 ml) for 2 d. Then the solvent was evaporated *in vacuo* and washed with Et₂O to afford compound **112f** as a pale yellow solid (41.4 mg, 92%). Yellow crystals suitable for X-ray analysis were obtained from saturated CH₂Cl₂/pentane solution. ¹H NMR (CD₂Cl₂, 300 MHz): δ = 8.05 – 7.99 (m, 2H), 7.70 – 7.65 (m, 1H), 7.55 – 7.46 (m, 4H), 7.42 – 7.32 (m, 2H), 7.23 – 7.16 (m, 3H), 6.98 – 6.75 (m, 5H), 6.59 – 6.56 (m, 1H), 3.04 ppm (s, 6H). ¹³C NMR (CD₂Cl₂, 125 Mz): δ = 155.33 (m), 150.5 (d, J_{C-P} = 22.0 Hz), 147.2 (m), 145.8 (m), 144.6 (m), 138.2 (m), 135.5 (d, J_{C-P} = 13.3 Hz), 133.7, 132.5 (m), 131.9, 131.6, 131.4 (d, J_{C-P} = 11.4 Hz), 130.5, 129.4 (d, J_{C-P} = 10.6 Hz), 128.4 (d, J_{C-P} = 10.2 Hz), 128.2 (d, J_{C-P} = 5.6 Hz), 122.4 (br), 116.6 (br), 47.3 ppm (m). ³¹P NMR (CD₂Cl₂, 162 MHz): δ = 23.2 ppm (m). ¹⁹F NMR (CD₂Cl₂, 282 MHz): δ = -112.92 (m), -114.28 (m), -115.26 (m), -117.93 (m), -162.35 (t, J_{F-F} = 19.8 Hz), -162.95 (t, J_{F-F} = 19.8 Hz), -163.64 (m), -163.88, -164.43 (m), -164.94 ppm (m). HRMS *calcd.* for C₃₈H₂₄NF₁₀PPdNa⁺: 844.041910, *found* 884.041289. IR $\tilde{\nu}$ = 433, 450, 494, 538, 692, 760, 788, 852, 949, 1041, 1058, 1099, 1213, 1274, 1344, 1362, 1435, 1493, 1577, 2965, 3067 cm⁻¹.

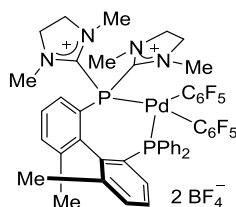
Compound **112g**



Pd(C₆F₅)₂(cod) (100.0 mg, 0.182 mmol) and **92a** (120.3 mg, 0.182 mmol) were dissolved in CH₂Cl₂ (4 ml) and stirred overnight. After removal of the solvent *in vacuo*, the remaining solid was washed with CH₂Cl₂ and pentane, and dried, affording **112g** as a white solid (168.8

mg, 84%). Colorless crystals suitable for X-ray crystallography were obtained from saturated CH₃CN/CH₂Cl₂/Et₂O solutions of the title compound. ¹H NMR (CD₃CN, 400 MHz): δ = 8.25 – 8.20 (m, 1H), 8.16 – 8.11(m, 1H), 8.10 – 8.05 (m, 2H), 7.68 – 7.65 (m, 2H), 7.53 – 7.50 (m, 8H), 4.14 – 4.10 (m, 8H), 3.03 ppm (s, 12H). ¹³C NMR (CD₃CN, 125 MHz): δ = 157.2 (dd, $J_{C-P} = 26.2$ Hz, $J_{C-P} = 1.1$ Hz), 147.6 (dm, $J_{C-F} = 194.2$ Hz), 146.0 (dm, $J_{C-F} = 191.3$ Hz), 144.2 (dd, $J_{C-P} = 52.0$ Hz, $J_{C-P} = 44.5$ Hz), 140.6 (br), 138.8 (dd, $J_{C-P} = 5.6$ Hz, $J_{C-P} = 2.3$ Hz), 138.3 (d, $J_{C-P} = 20.2$ Hz), 137.8 (dm, $J_{C-F} = 256.1$ Hz), 137.5 (d, $J_{C-P} = 13.4$ Hz), 137.2 (dd, $J_{C-P} = 7.2$ Hz, $J_{C-P} = 1.7$ Hz), 134.4 (d, $J_{C-P} = 12.5$ Hz), 134.1 (d, $J_{C-P} = 2.8$ Hz), 130.6 (d, $J_{C-P} = 11.4$ Hz), 127.9 (d, $J_{C-P} = 53.4$ Hz), 126.3 (dd, $J_{C-P} = 50.3$ Hz, $J_{C-P} = 33.7$ Hz), 54.3 (d, $J_{C-P} = 2.1$ Hz), 38.3 ppm (d, $J_{C-P} = 3.4$ Hz). ³¹P NMR (CD₃CN, 121 MHz): δ = 49.0 (m), 11.9 ppm (m). ¹¹B NMR (CD₃CN, 96 MHz): δ = – 1.1 ppm. ¹⁹F NMR (CD₃CN, 282 MHz): δ = – 116.8 (m), – 117.6 (m), – 157.9 (t, $J_{F-F} = 19.7$ Hz), – 159.9 (t, $J_{F-F} = 19.2$ Hz), – 161.8 (dt, $J_{F-F} = 19.7$, $J_{F-P} = 8.7$ Hz), – 163.6 ppm (dt, $J_{F-F} = 20.3$, $J_{F-P} = 8.3$ Hz). HRMS *calcd.* for C₄₀H₃₄N₄BF₁₄P₂Pd⁺: 1015.119220, *found* 1015.115674. IR $\tilde{\nu} = 465, 499, 518, 536, 643, 691, 735, 775, 1300, 1363, 1440, 1458, 1501, 1589, 1600$ cm⁻¹.

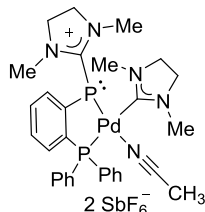
Compound **112h**



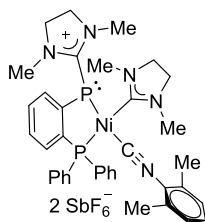
Pd(C₆F₅)₂(cod) (50.0 mg, 0.065 mmol) and **101a** (35.8 mg, 0.065 mmol) were dissolved in CH₃COCH₃ (3 ml) and stirred for 48 h. After removal of the solvent *in vacuo*, the solid left was washed with CH₂Cl₂ and pentane, and dried, to afford **112h** as a light yellow solid (57.5 mg, 73%). ¹H NMR (CD₃COCD₃, 400 MHz): δ = 8.08 – 8.04 (m, 1H), 7.97 (d, $J = 7.8$ Hz, 1H), 7.93 – 7.78 (m, 3H), 7.71 – 7.62 (m, 2H), 7.56 – 7.44 (m, 3H), 7.43 – 4.40 (m, 1H), 7.36 – 7.29 (m, 3H), 7.20 – 7.12 (m, 2H), 4.49 – 4.31 (m, 4H), 3.84 – 3.74 (m, 8H), 3.59 – 3.54 (m, 2H), 3.25 (s, 3H), 3.23 (s, 3H), 1.89 (s, 3H), 1.50 ppm (s, 3H). ¹³C NMR (CD₃COCD₃, 100 MHz): δ = 158.3 (dd, $J_{C-P} = 24.4$ Hz, $J_{C-P} = 3.6$ Hz), 156.6 (d, $J_{C-P} = 14.3$ Hz), 144.3 (d, $J_{C-P} = 8.3$ Hz), 144.0 (d, $J_{C-P} = 10.8$ Hz), 142.3 (dd, $J_{C-P} = 23.3$ Hz, d, $J_{C-P} = 3.0$ Hz), 138.1 (d, $J_{C-P} = 2.0$ Hz), 137.7 (dd, $J_{C-P} = 13.5$ Hz, $J_{C-P} = 5.5$ Hz), 136.8 (dd, $J_{C-P} = 12.5$ Hz, $J_{C-P} = 2.8$ Hz), 136.4 (d, $J_{C-P} = 2.2$ Hz), 134.7 (d, $J_{C-P} = 10.0$ Hz), 134.2 (d, $J_{C-P} = 4.5$ Hz), 133.9 (d, $J_{C-P} = 2.4$ Hz), 132.1 (d, $J_{C-P} = 7.3$ Hz), 131.9 (d, $J_{C-P} = 2.5$ Hz), 131.6 (d, $J_{C-P} = 41.8$ Hz), 131.3 (d, $J_{C-P} = 8.7$ Hz), 130.5 (d, $J_{C-P} = 8.6$ Hz), 130.4 (d, $J_{C-P} = 11.3$ Hz), 129.2 (d, $J_{C-P} =$

10.7 Hz), 128.6 (t, $J_{C-P} = 24.6$ Hz), 126.5 (dd, $J_{C-P} = 51.8$ Hz, $J_{C-P} = 1.8$ Hz), 125.3 (d, $J_{C-P} = 48.6$ Hz), 56.1 (d, $J_{C-P} = 1.5$ Hz), 54.1 (d, $J_{C-P} = 2.2$ Hz), 53.6 (d, $J_{C-P} = 2.2$ Hz), 53.4, 42.5 (dd, $J_{C-P} = 6.2$ Hz, $J_{C-P} = 5.1$ Hz), 39.7 (t, $J_{C-P} = 9.4$ Hz), 37.6, 37.3 (d, $J_{C-P} = 6.3$ Hz), 20.9 (d, $J_{C-P} = 2.5$ Hz), 19.9 ppm (d, $J_{C-P} = 1.6$ Hz). ^{31}P NMR (CD_3COCD_3 , 121 MHz): $\delta = 15.3$ (m), 12.6 ppm (m). ^{11}B NMR (CD_3COCD_3 , 96 MHz): $\delta = -1.0$ ppm. ^{19}F NMR (CD_3COCD_3 , 282 MHz): $\delta = -110.8$ (m), -111.0 (m), -113.7 (m), -114.2 (m), -156.7 (t, $J_{F-F} = 19.9$ Hz), -160.7 (m), -161.6 (t, $J_{F-F} = 19.9$ Hz), -163.4 (m), -163.9 ppm (m). HRMS *calcd.* for $\text{C}_{48}\text{H}_{42}\text{N}_4\text{BF}_{14}\text{P}_2\text{Pd}^+$: 1119.178050, *found* 1119.178274. IR $\tilde{\nu} = 420, 458, 468, 501, 521, 544, 696, 747, 766, 783, 924, 956, 1056, 1298, 1442, 1504, 1580\text{ cm}^{-1}$.

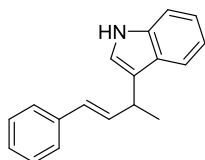
Compound 113



Compound **92b** (20.0 mg, 0.021 mmol) and $\text{Pd}(\text{dba})_2$ (12.0 mg, 0.021 mmol) in CH_2Cl_2 (2 ml) were stirred at r.t. for 2 h and then the solvent was evaporated *in vacuo*. The resulting solid was extracted with CH_3CN and recrystallized from CH_3CN , CH_2Cl_2 and Et_2O to afford the desired compound **113** as a yellow solid (4.9 mg, 21%). The colorless crystals suitable for X-ray analysis were obtained from $\text{CH}_3\text{CN}/\text{CH}_2\text{Cl}_2/\text{Et}_2\text{O}$. ^1H NMR ($\text{CD}_3\text{CN}/\text{CH}_2\text{Cl}_2/\text{Et}_2\text{O}$, 600 MHz): $\delta = 7.69 - 7.55$ (m, 13H), $7.55 - 7.50$ (m, 1H), $3.90 - 3.84$ (m, 2H), $3.83 - 3.76$ (m, 2H), $3.75 - 3.66$ (m, 4H), 3.35 (s, 3H), 3.04 (s, 3H), 2.94 ppm (s, 6H). ^{13}C NMR (CD_3CN , 125 Mz): $\delta = 196.5$ (dd, $J_{C-P} = 126.7$ Hz, $J_{C-P} = 16.4$ Hz), 176.6 (dd, $J_{C-P} = 80.7$ Hz, $J_{C-P} = 1.7$ Hz), 146.2 (dd, $J_{C-P} = 40.9$ Hz, $J_{C-P} = 20.9$ Hz), 135.4 (dd, $J_{C-P} = 56.0$ Hz, $J_{C-P} = 15.8$ Hz), 135.1 (d, $J_{C-P} = 2.4$ Hz), 134.6 (dd, $J_{C-P} = 4.4$ Hz, $J_{C-P} = 1.8$ Hz), $134.21, 134.20$ (d, $J_{C-P} = 9.3$ Hz), 134.1 (d, $J_{C-P} = 11.3$ Hz), 134.0 (d, $J_{C-P} = 21.8$ Hz), 133.4 (d, $J_{C-P} = 2.6$ Hz), 130.8 (dd, $J_{C-P} = 11.0$ Hz, $J_{C-P} = 2.4$ Hz), 130.7 (d, $J_{C-P} = 1.7$ Hz), 130.4 (d, $J_{C-P} = 47.5$ Hz), 129.7 (d, $J_{C-P} = 96.8$ Hz), 128.6 (d, $J_{C-P} = 48.2$ Hz), 52.8 (d, $J_{C-P} = 5.2$ Hz), 52.5 (d, $J_{C-P} = 4.6$ Hz), 52.4 (d, $J_{C-P} = 1.0$ Hz), $37.7, 37.6, 37.4, 37.3, 37.2$ ppm (m). ^{31}P NMR (CD_3CN , 162 MHz): $\delta = 49.4, 15.9$ ppm. ^{19}F NMR (CD_3CN , 282 MHz): $\delta = -124.0$ ppm (sextet, $J_{F-Sb(I=5/2)} = 1933$ Hz, octet, $J_{F-Sb(I=7/2)} = 1049$ Hz). HRMS *calcd.* for $\text{C}_{28}\text{H}_{34}\text{N}_4\text{F}_6\text{P}_2\text{SbPd}^+$: 829.022380, *found* 829.022889. IR $\tilde{\nu} = 426, 495, 507, 534, 591, 652, 699, 752, 774, 920, 940, 1103, 1203, 1291, 1333, 1407, 1438, 1546, 1567, 2301, 2929\text{ cm}^{-1}$.

Compound **114**

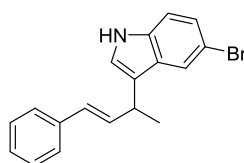
Compound **92b** (50.0 mg, 0.052 mmol) and Ni(cod)₂ (14.3 mg, 0.052 mmol) were stirred overnight in CH₂Cl₂ (2 ml). A yellow precipitate was separated from the solution. 2,6-dimethylphenyl isocyanide (16.7 mg, 0.128 mmol) was added in CH₂Cl₂ (2 ml) and the mixture stirred overnight. After evaporation of the solvent, the solid was washed with Et₂O and recrystallized from CH₂Cl₂/Et₂O to afford the desired compound **114** as a yellow solid (22.1 mg, 37%). The yellow crystal suitable for X-ray analysis was obtained from a saturated solution of the title compound in CH₂Cl₂/Et₂O. ¹H NMR (CD₂Cl₂, 600 MHz): δ = 7.74 – 7.48 (m, 13H), 7.37 (t, *J* = 8.2 Hz, 1H), 7.32 (t, *J* = 7.7 Hz, 1H), 7.14 (d, *J* = 7.7 Hz, 2H), 3.98 (s, *J* = 4H), 3.88 – 3.71 (m, 4H), 3.33 (s, 6H), 3.01 (s, 6H), 1.98 (s, 6H). ¹³C NMR (CD₂Cl₂, 125 Mz): δ = 199.2 (dd, *J*_{C-P} = 71.0 Hz, , *J*_{C-P} = 22.3 Hz), 176.7 (dd, *J*_{C-P} = 76.9 Hz, *J*_{C-P} = 3.7 Hz), 146.2 (m), 144.7 (dd, *J*_{C-P} = 39.7 Hz, , *J*_{C-P} = 15.4 Hz), 136.2, 135.4 (dd, *J*_{C-P} = 59.0 Hz, *J*_{C-P} = 20.0 Hz), 135.0, 134.1, 133.5, 133.3, 133.2, 132.8 (dd, *J*_{C-P} = 35.4 Hz, , *J*_{C-P} = 17.5 Hz), 131.7, 130.7 (d, *J*_{C-P} = 11.4 Hz), 130.4 (d, *J*_{C-P} = 8.3 Hz), 129.0, 125.6, 52.7, 51.7, 37.43, 37.41, 37.34, 37.28, 18.3 ppm (m). ³¹P NMR (CD₂Cl₂, 162 MHz): δ = 56.9 (d, *J*_{P-P} = 4.3 Hz), 23.7 ppm (d, *J*_{P-P} = 4.3 Hz). ¹⁹F NMR (CD₂Cl₂, 282 MHz): δ = – 124.0 ppm (sextet, *J*_{F-Sb(I=5/2)} = 1933 Hz, octet, *J*_{F-Sb(I=7/2)} = 1049 Hz). HRMS *calcd.* for C₃₇H₄₃N₅F₆P₂Sb⁺: 912.128170, *found* 912.128332. IR $\tilde{\nu}$ = 442, 487, 515, 530, 651, 693, 713, 752, 773, 791, 939, 957, 1097, 1205, 1287, 1438, 1536, 1566, 2164 cm⁻¹.

Compound **118**

Indole (25.8 mg, 0.220 mmol) and phenyl 1,3-butadiene (26.0 mg, 0.200 mmol) were added to a solution of **92b** (9.6 mg, 0.010 mmol), [RhCl(CO)₂]₂ (1.9 mg, 0.005 mmol) and KB(Ar^F)₄ (14.3 mg, 0.020) in DCE (1 ml), and the reaction was stirred at 70 °C for 18 h. The resulting oil was purified by column chromatography (SiO₂, Hexane:EtOAc = 20:1) to afford the desired compound **118** as a colorless oil (41.0 mg, 86% yield). ¹H NMR (CDCl₃, 400 MHz): δ

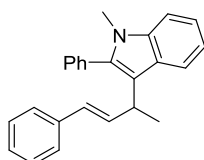
= 7.95 (br, 1H), 7.69 (dd, $J = 7.9$ Hz, $J = 0.6$ Hz, 1H), 7.40 – 7.35 (m, 3H), 7.31 – 7.27 (m, 2H), 7.23 – 7.17 (m, 2H), 7.10 (ddd, $J = 7.9$ Hz, $J = 7.8$ Hz, $J = 0.6$ Hz, 1H), 7.03 (dd, $J = 2.3$ Hz, $J = 0.6$ Hz, 1H), 6.51 – 6.48 (m, 2H), 3.95 (p, $J = 6.8$ Hz, 1H), 1.58 ppm (d, $J = 7.0$ Hz, 3H). ^{13}C NMR (CDCl_3 , 100 MHz): $\delta = 137.9, 136.7, 135.6, 128.6, 128.3, 127.0, 126.9, 126.3, 122.1, 120.6, 120.5, 119.8, 119.4, 111.2, 34.4, 20.8$ ppm. HRMS *calcd.* for $\text{C}_{18}\text{H}_{18}\text{N}^+$: 248.143420, *found* 248.143374. IR $\tilde{\nu} = 424, 497, 581, 693, 742, 765, 807, 928, 966, 1009, 1095, 1221, 1244, 1337, 1417, 1455, 1492, 1598, 1618, 2869, 2927, 2963, 3024, 3055, 3417$ cm^{-1} .

Compound 119



5-Bromoindole (43.1 mg, 0.220 mmol) and phenyl 1,3-butadiene^[165] (26.0 mg, 0.200 mmol) were added to a solution of **92b** (9.6 mg, 0.010 mmol), $[\text{RhCl}(\text{CO})_2]_2$ (1.9 mg, 0.005 mmol) and $\text{KB}(\text{Ar}^{\text{F}})_4$ (14.3 mg, 0.020) in DCE (1 ml), and the reaction mixture was stirred at 70 °C for 18 h. The resulting oil was purified by column chromatography (SiO_2 , Hexane:EtOAc = 20:1) to afford the desired compound **119** as a light yellow oil (53.5 mg, 82% yield). ^1H NMR (CDCl_3 , 400 MHz): $\delta = 8.00$ (br, 1H), 7.78 (m, 1H), 7.40 – 7.35 (m, 2H), 7.31 – 7.28 (m, 2H), 7.27 – 7.25 (m, 2H), 7.23 – 7.17 (m, 2H), 7.03 (d, $J = 2.0$ Hz, 1H), 6.51 – 6.39 (m, 1H), 3.88 (p, $J = 6.7$ Hz, 1H), 1.55 ppm (d, $J = 7.0$ Hz, 3H). ^{13}C NMR (CDCl_3 , 100 MHz): $\delta = 137.7, 135.3, 135.0, 128.7, 128.6, 128.6, 127.1, 126.3, 125.0, 122.3, 121.8, 120.4, 112.7, 34.2, 20.9$ ppm. HRMS *calcd.* for $\text{C}_{18}\text{H}_{15}\text{NBr}^+$: 324.039610, *found* 324.039349. IR $\tilde{\nu} = 421, 488, 583, 696, 749, 795, 865, 996, 1045, 1096, 1260, 1373, 1458, 1493, 1599, 1721, 2927, 2962, 3025, 3421$ cm^{-1} .

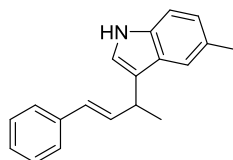
Compound 120



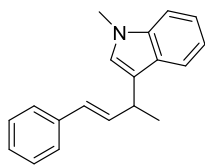
1-Methyl-2-phenylindole (45.6 mg, 0.220 mmol) and diene (26.0 mg, 0.200 mmol) were added to a solution of **92b** (9.6 mg, 0.010 mmol), $[\text{RhCl}(\text{CO})_2]_2$ (1.9 mg, 0.005 mmol) and $\text{KB}(\text{Ar}^{\text{F}})_4$ (14.3 mg, 0.020) in DCE (1 ml), and the reaction mixture was stirred at 70 °C for

18 h. The resulting oil was purified by column chromatography (SiO₂, Hexane:EtOAc = 20:1) to afford the desired compound **120** as a colorless oil (39.1 mg, 57% yield). ¹H NMR (CDCl₃, 400 MHz): δ = 7.76 (dm, *J* = 8.0 Hz, 1H), 7.53 – 7.45 (m, 3H), 7.44 – 7.40 (m, 2H), 7.37 (dm, *J* = 8.0 Hz, 1H), 7.34 – 7.30 (m, 2H), 7.28 (m, 3H), 7.17 (tm, *J* = 7.1 Hz, 1H), 7.11 (tm, *J* = 7.4 Hz, 1H), 6.62 (dd, *J* = 15.9 Hz, *J* = 5.8 Hz, 1H), 6.39 (dd, *J* = 15.9 Hz, *J* = 1.5 Hz, 1H), 3.80 (m, 1H), 3.58 (s, 3H), 1.56 ppm (d, *J* = 7.2 Hz, 3H). ¹³C NMR (CDCl₃, 100 MHz): δ = 138.1, 137.5, 135.7, 132.3, 131.0, 128.6, 128.5, 128.4, 128.3, 128.0, 126.9, 126.4, 126.2, 121.6, 120.7, 119.2, 116.3, 116.2, 109.6, 34.4, 30.9, 21.1 ppm. HRMS *calcd.* for C₂₅H₂₃NNa⁺: 360.172400, *found* 360.172268. IR $\tilde{\nu}$ = 435, 486, 520, 592, 582, 601, 722, 735, 805, 921, 964, 1017, 1098, 1135, 1157, 1247, 1264, 1335, 1362, 1397, 1429, 1466, 1492, 1600, 2926, 2963, 3025 cm⁻¹.

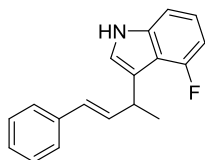
Compound **121**



5-Methylindol (28.9 mg, 0.220 mmol) and phenyl 1,3-butadiene (26.0 mg, 0.200 mmol) were added to a solution of **92b** (9.6 mg, 0.010 mmol), [RhCl(CO)₂]₂ (1.9 mg, 0.005 mmol) and KB(Ar^F)₄ (14.3 mg, 0.020) in DCE (1 ml), and the reaction mixture was stirred at 70 °C for 18 h. The resulting oil was purified by column chromatography (SiO₂, Hexane:EtOAc = 100:1 to 20:1) to afford the desired compound **121** as a light yellow oil (41.2 mg, 76% yield). ¹H NMR (CDCl₃, 400 MHz): δ = 7.86 (br, 1H), 7.45 (m, 1H), 7.38 – 7.35 (m, 2H), 7.30 – 7.25 (m, 3H), 7.19 (tm, *J* = 8.4 Hz, 1H), 7.2 (dd, *J* = 8.3 Hz, *J* = 1.2 Hz, 1H), 7.00 (d, *J* = 2.3 Hz, 1H), 6.49 – 6.43 (m, 2H), 3.95 – 3.88 (m, 1H), 2.44 (s, 3H), 1.56 ppm (d, *J* = 7.0 Hz, 3H). ¹³C NMR (CDCl₃, 100 MHz): δ = 138.0, 135.7, 135.0, 128.6, 128.2, 127.1, 127.0, 126.3, 126.9, 123.7, 120.7, 120.1, 119.3, 110.9, 34.3, 21.7, 20.9 ppm. HRMS *calcd.* for C₁₉H₁₉NNa⁺: 284.141150, *found* 284.140968. IR $\tilde{\nu}$ = 423, 460, 493, 589, 696, 748, 793, 698, 920, 996, 1012, 1029, 1073, 1096, 1182, 1224, 1320, 1369, 1419, 1448, 1493, 1580, 1598, 2867, 2925, 2962, 3023, 3414 cm⁻¹.

Compound **122**

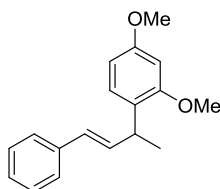
1-Methylindol (28.8 mg, 0.220 mmol) and phenyl 1,3-butadiene (26.0 mg, 0.200 mmol) were added to a solution of **92b** (9.6 mg, 0.010 mmol), $[\text{RhCl}(\text{CO})_2]_2$ (1.9 mg, 0.005 mmol) and $\text{KB}(\text{Ar}^{\text{F}})_4$ (14.3 mg, 0.020) in DCE (1 ml), and the reaction mixture was stirred at 70 °C for 18 h. The resulting oil was purified by column chromatography (SiO_2 , Hexane:EtOAc = 20:1) to afford the desired compound **122** as colorless oil (32.1 mg, 63% yield). ^1H NMR (CDCl_3 , 400 MHz): δ = 7.67 (dm, J = 7.9 Hz, 1H), 7.38 – 7.25 (m, 2H), 7.31 – 7.27 (m, 2H), 7.24 – 7.21 (m, 1H), 7.21 – 7.16 (m, 1H), 7.01 – 7.06 (m, 1H), 6.88 (s, 1H), 6.54 – 6.43 (m, 2H), 3.93 (p, J = 6.8 Hz, 1H), 3.76 (s, 3H), 1.56 ppm (d, J = 7.0 Hz, 3H). ^{13}C NMR (CDCl_3 , 100 MHz): δ = 137.9, 137.4, 135.7, 128.6, 128.1, 127.3, 127.0, 126.3, 125.4, 121.7, 119.8, 119.0, 118.8, 109.3, 34.3, 32.8, 21.0 ppm. HRMS *calcd.* for $\text{C}_{19}\text{H}_{19}\text{NNa}^+$: 284.141100, *found* 284.140968. IR $\tilde{\nu}$ = 424, 497, 581, 698, 746, 968, 992, 1093, 1242, 1373, 1470, 1493, 1528, 1613, 1712, 1778, 2930, 2961, 3026, 3055 cm^{-1} .

Compound **123**

5-Fluoroindole (29.7 mg, 0.220 mmol) and phenyl 1,3-butadiene (26.0 mg, 0.200 mmol) were added to a solution of **122b** (9.6 mg, 0.010 mmol), $[\text{RhCl}(\text{CO})_2]_2$ (1.9 mg, 0.005 mmol) and $\text{KB}(\text{Ar}^{\text{F}})_4$ (14.3 mg, 0.020) in DCE (1 ml), and the reaction mixture was stirred at 70 °C for 18 h. The resulting oil was purified by column chromatography (SiO_2 , Hexane:EtOAc = 100:1 to 20:1) to afford the desired compound **123** as light yellow oil (34.4 mg, 65% yield). ^1H NMR (CDCl_3 , 400 MHz): δ = 8.00 (br, 1H), 7.36 – 7.33 (m, 2H), 7.28 – 7.25 (m, 2H), 7.18 – 7.17 (m, 1H), 7.14 – 7.11 (m, 1H), 7.09 – 7.05 (m, 1H), 6.96 – 6.95 (m, 1H), 6.76 – 7.1 (m, 1H), 6.54 – 6.42 (m, 2H), 4.08 (p, J = 6.8 Hz, 1H), 1.53 ppm (d, J = 6.9 Hz, 3H). ^{13}C NMR (CDCl_3 , 100 MHz): δ = 152.3 (d, J = 247.0 Hz), 139.4 (d, J = 11.9), 138.1, 135.6 (d, J = 0.8), 128.6, 128.4 (d, J = 7.6), 128.2 (d, J = 1.0), 127.0, 126.3, 125.8 (d, J = 35.1), 122.7 (d, J = 8.0), 120.5 (d, J = 1.3), 120.3 (d, J = 3.9 Hz), 115.7 (d, J = 20.2), 115.7 (d, J = 20.2),

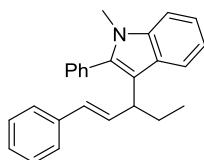
107.3 (d, $J = 3.6$), 104.9 (d, $J = 20.2$), 34.8 (d, $J = 1.4$), 21.5 ppm (d, $J = 1.9$). ^{19}F NMR (CDCl_3 , 282 MHz): $\delta = -120.8$ ppm. HRMS *calcd.* for $\text{C}_{18}\text{H}_{15}\text{NF}^+$: 264.119600, *found* 264.119402. IR $\tilde{\nu} = 483, 649, 696, 732, 780, 908, 996, 1035, 1224, 1348, 1446, 1494, 1578, 1628, 1628, 1694, 2962, 3025, 3416\text{ cm}^{-1}$.

Compound **124**



1,3-Dimethoxybenzene (30.4 mg, 0.220 mmol) and phenyl 1,3-butadiene (26.0 mg, 0.200 mmol) were added to a solution of **92b** (9.6 mg, 0.010 mmol), $[\text{RhCl}(\text{CO})_2]_2$ (1.9 mg, 0.005 mmol) and $\text{KB}(\text{Ar}^{\text{F}})_4$ (14.3 mg, 0.020) in DCE (1 ml), and the reaction mixture was stirred at 70 °C for 18 h. The resulting oil was purified by column chromatography (SiO_2 , Hexane:EtOAc = 20:1) to afford the desired compound **124** as colorless oil (33.6 mg, 63% yield). ^1H NMR (CDCl_3 , 400 MHz): $\delta = 7.37 - 7.34$ (m, 2H), 7.30 - 7.27 (m, 2H), 7.20 - 7.15 (m, 1H), 7.10 (d, $J = 8.2$ Hz, 1H), 6.47 - 6.40 (m, 4H), 4.00 - 3.97 (m, 1H), 3.83 (s, 3H), 3.80 (s, 3H), 1.39 ppm (d, $J = 7.0$ Hz, 3H). ^{13}C NMR (CDCl_3 , 100 MHz): $\delta = 159.3, 157.9, 138.1, 135.4, 128.6, 128.1, 128.0, 126.9, 126.7, 126.2, 104.3, 98.9, 55.6, 55.5, 34.8, 20.3$ ppm. HRMS *calcd.* for $\text{C}_{18}\text{H}_{21}\text{O}_2^+$: 269.153580, *found* 269.135605. IR $\tilde{\nu} = 495, 634, 692, 737, 798, 909, 966, 1034, 1117, 1156, 1179, 1206, 1259, 1290, 1417, 1453, 1503, 1586, 1610, 2835, 2928, 2959, 3024\text{ cm}^{-1}$.

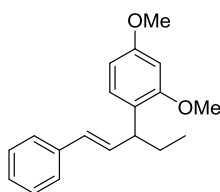
Compound **125**



1-Methyl-2-phenylindole (45.6 mg, 0.220 mmol) and 1-phenyl-1,3-pentadiene (E/Z = 1:1, 26.0 mg, 0.200 mmol)^[165] were added to a solution of **92b** (9.6 mg, 0.010 mmol), $[\text{RhCl}(\text{CO})_2]_2$ (1.9 mg, 0.005 mmol) and $\text{KB}(\text{Ar}^{\text{F}})_4$ (14.3 mg, 0.020) in DCE (1 ml), and the reaction mixture was stirred at 70 °C for 18 h. The resulting oil was purified by column chromatography (SiO_2 , Hexane:EtOAc = 100:1 to 20:1) to afford the desired compound **125** as colorless yellow oil (23.1 mg, 33% yield). ^1H NMR (CDCl_3 , 400 MHz): $\delta = 7.72$ (d, $J = 8.0$ Hz, 1H), 7.49 - 7.38 (m, 3H), 7.38 - 7.30 (m, 3H), 7.28 - 7.25 (m, 2H), 7.24 - 7.19 (m,

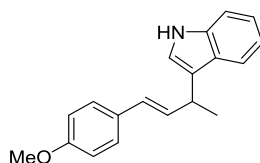
3H), 7.15 – 7.04 (m, 2H), 6.58 (dd, $J = 15.8$, $J = 7.0$ Hz, 1H), 6.30 (d, $J = 15.8$ Hz, 1H), 3.52 (s, 3H), 3.43 (q, $J = 8.1$, 7.6 Hz, 1H), 1.92 (qt, $J = 13.7$, $J = 7.1$ Hz, 2H), 0.75 ppm (t, $J = 7.4$ Hz, 3H). ^{13}C NMR (CDCl_3 , 100 MHz): $\delta = 138.45$, 138.12, 134.56, 132.45, 131.11, 128.75, 128.49, 128.43, 128.27, 126.84, 126.37, 126.22, 121.54, 120.68, 119.07, 114.70, 109.59, 42.66, 30.92, 28.17, 12.83. HRMS *calcd.* for $\text{C}_{26}\text{H}_{25}\text{NNa}^+$: 374.187880, *found* 374.187918. IR $\tilde{\nu} = 701$, 741, 808, 908, 964, 1019, 1072, 1134, 1157, 1246, 1334, 1365, 1397, 1429, 1446, 1467, 1601, 2869, 2928, 2959, 3025, 3056 cm^{-1} .

Compound 126



1,3-Dimethoxybenzene (30.4 mg, 0.220 mmol) and 1-phenyl-1,3-pentadiene (E/Z = 1:1, 28.8 mg, 0.200 mmol)^[165] were added to a solution of **92b** (9.6 mg, 0.010 mmol), $[\text{RhCl}(\text{CO})_2]_2$ (1.9 mg, 0.005 mmol) and $\text{KB}(\text{Ar}^{\text{F}})_4$ (14.3 mg, 0.020) in DCE (1 ml), and the reaction mixture was stirred at 70 °C for 18 h. The resulting oil was purified by column chromatography (SiO_2 , Hexane:EtOAc = 20:1) to afford the desired compound **126** as colorless oil (24.3 mg, 43% yield). ^1H NMR (CDCl_3 , 400 MHz): $\delta = 7.28 - 7.25$ (m, 2H), 7.21 – 7.17 (m, 2H), 7.11 – 7.07 (m, 1H), 7.03 – 7.01 (m, 1H), 6.41 – 6.38 (m, 2H), 6.29 – 6.28 (m, 2H), 3.74 (s, 3H), 3.73 (s, 3H), 3.63 (p, $J = 6.4$ Hz, 1H), 1.70 (m, 2H), 0.82 ppm (t, $J = 7.4$, 3H). ^{13}C NMR (CDCl_3 , 100 MHz): $\delta = 159.1$, 158.2, 138.1, 134.3, 129.1, 128.5, 128.3, 126.9, 126.2, 125.5, 104.3, 98.8, 55.6, 55.5, 43.0, 28.1, 12.4 ppm. HRMS *calcd.* for $\text{C}_{19}\text{H}_{23}\text{O}_2^+$: 283.169380, *found* 283.169255. IR $\tilde{\nu} = 634$, 694, 747, 797, 834, 936, 966, 1037, 1133, 1157, 1179, 1207, 1259, 1289, 1438, 1463, 1504, 1586, 1610, 2834, 2871, 2931, 2959, 2998, 3024 cm^{-1} .

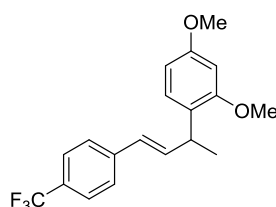
Compound 127



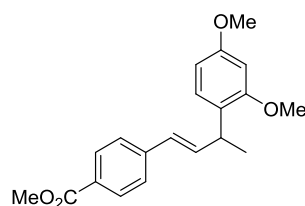
Indole (25.8 mg, 0.220 mmol) and 1-(*p*-methoxyphenyl)-1,3-butadiene (E/Z = 2.1:1, 32.0 mg, 0.200 mmol)^[165] were added to a solution of **92b** (9.6 mg, 0.010 mmol), $[\text{RhCl}(\text{CO})_2]_2$ (1.9 mg, 0.005 mmol) and $\text{KB}(\text{Ar}^{\text{F}})_4$ (14.3 mg, 0.020) in DCE (1 ml), and the reaction mixture

was stirred at 70 °C for 18 h. The resulting oil was purified by column chromatography (SiO₂, Hexane:EtOAc = 20:1) to afford the desired compound **127** as colorless yellow oil (19.4 mg, 35% yield). ¹H NMR (CD₂Cl₂, 400 MHz): δ = 8.10 (s, 1H), 7.66 (dd, *J* = 7.9, 1.0 Hz, 1H), 7.37 (dt, *J* = 8.2, 1.0 Hz, 1H), 7.32 – 7.27 (m, 2H), 7.16 (ddd, *J* = 8.2, 7.0, 1.2 Hz, 1H), 7.10 – 7.04 (m, 2H), 6.85 – 6.79 (m, 2H), 6.51 – 6.41 (m, 1H), 6.32 (dd, *J* = 15.8, 7.0 Hz, 1H), 3.91 (tt, *J* = 7.1, 1.1 Hz, 1H), 3.78 (s, 3H), 1.55 ppm (d, *J* = 7.0 Hz, 3H). ¹³C NMR (CD₂Cl₂, 100 MHz): δ = 159.17, 136.98, 133.75, 130.89, 129.60, 127.77, 127.49, 122.19, 120.84, 120.82, 119.83, 119.43, 114.19, 111.47, 55.59, 34.67, 20.98 ppm. HRMS *calcd.* for C₁₉H₁₉NONa⁺: 300.135910, *found* 300.135883, IR $\tilde{\nu}$ = 424, 488, 743, 815, 850, 967, 1010, 1032, 1096, 1175, 1246, 1298, 1337, 1418, 1456, 4510, 1606, 2838, 2930, 2960, 3415 cm⁻¹.

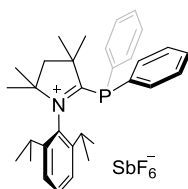
Compound **128**



1,3-Dimethoxybenzene (30.4 mg, 0.220 mmol) and 1-(*p*-trifluoromethylphenyl)-1,3-butadiene (E/Z = 1.8:1, 39.6 mg, 0.200 mmol)^[166] were added to a solution of **92b** (9.6 mg, 0.010 mmol), [RhCl(CO)₂]₂ (1.9 mg, 0.005 mmol) and KB(Ar^F)₄ (14.3 mg, 0.020) in DCE (1 ml), and the reaction mixture was stirred at 70 °C for 18 h. The resulting oil was purified by column chromatography (SiO₂, Hexane:EtOAc = 100:1 to 20:1) to afford the desired compound **128** as a colorless yellow oil (14.1 mg, 21% yield). ¹H NMR (CDCl₃, 400 MHz): δ = 7.52 (d, *J* = 8.2 Hz, 2H), 7.43 (d, *J* = 8.1 Hz, 2H), 7.13 – 7.04 (m, 1H), 6.56 – 6.44 (m, 3H), 6.44 – 6.35 (m, 1H), 4.01 (p, *J* = 6.3 Hz, 1H), 3.83 (s, 3H), 3.80 (s, 3H), 1.40 ppm (d, *J* = 7.0 Hz, 3H). ¹³C NMR (CDCl₃, 100 MHz): δ = 159.44, 157.85, 141.62 (d, *J*_{C-F} = 1.5 Hz), 138.28, 128.73 (q, *J*_{C-F} = 32.4 Hz), 127.93, 126.86, 126.32, 126.02, 125.81, 125.50 (q, *J*_{C-F} = 3.8 Hz), 104.33, 98.90, 55.60, 55.51, 34.98, 20.03 ppm. ¹⁹F NMR (CDCl₃, 376 MHz): δ = -62.35 ppm. HRMS *calcd.* for C₁₉H₁₉O₂F₃Na⁺: 359.122850, *found* 359.122934. IR $\tilde{\nu}$ = 502, 596, 636, 798, 820, 864, 969, 1015, 1036, 1066, 1106, 1116, 1157, 1207, 1322, 1415, 1464, 1504, 1586, 1612, 2837, 2935, 2962 cm⁻¹.

Compound **129**

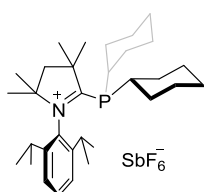
1,3-Dimethoxybenzene (*E/Z* = 1:1, 30.4 mg, 0.220 mmol) and 4-(1*E* or *Z*)-1,3-butadien-1-yl-methyl ester^[165] (37.6 mg, 0.200 mmol) were added to a solution of **92b** (9.6 mg, 0.010 mmol), [RhCl(CO)₂]₂ (1.9 mg, 0.005 mmol) and KB(Ar^F)₄ (14.3 mg, 0.020) in DCE (1 ml), and the reaction mixture was stirred at 70 °C for 18 h. The resulting oil was purified by column chromatography (SiO₂, Hexane:EtOAc = 100:1 to 20:1) to afford the desired compound **129** as a colorless yellow oil (15.0 mg, 23% yield). ¹H NMR (CD₂Cl₂, 400 MHz): δ = 7.89 – 7.79 (m, 2H), 7.37 – 7.29 (m, 2H), 7.00 (dt, *J* = 8.0, 0.6 Hz, 1H), 6.47 (dd, *J* = 16.0, 6.4 Hz, 1H), 6.41 – 6.29 (m, 3H), 3.95 – 3.86 (m, 1H), 3.78 (s, 3H), 3.74 (s, 3H), 3.69 (s, 3H), 1.30 ppm (d, *J* = 7.1 Hz, 3H). ¹³C NMR (CD₂Cl₂, 100 MHz): δ = 167.10, 159.74, 158.13, 142.91, 138.69, 130.07, 128.77, 128.09, 127.39, 126.25, 126.14, 104.59, 98.89, 55.81, 55.66, 52.23, 35.37, 20.04 ppm. HRMS *calcd.* for C₂₀H₂₂O₄Na⁺: 349.141170, *found* 349.141029. IR $\tilde{\nu}$ = 699, 768, 833, 871, 936, 970, 1016, 1157, 1178, 1207, 1276, 1414, 1435, 1455, 1504, 1586, 1607, 1644, 1717, 2836, 2954, 2996 cm⁻¹.

Compound **133a**

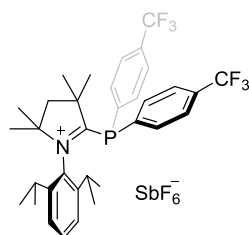
To a solution of carbene **137** (1 g, 2.260 mmol) in THF (10 ml), Ph₂PCl (0.418 ml, 2.26 mmol) was added and the resulting mixture stirred at r.t. overnight. The initial pale yellow solution changed to a bright yellow suspension. Then the solution was filtered off and the remaining yellow solid washed with Et₂O and dried *in vacuo*. The yellow solid thus obtained was dissolved in CH₃CN, NaSbF₆ (1.020 g, 3.95 mmol) was added to that solution and the resulting suspension stirred overnight at r.t. Removal of the solvents and the extraction with CH₂Cl₂ afforded the desired product **138a** as a yellow solid, which can be further purified by recrystallization from CH₂Cl₂/Et₂O (1.03 g, 66%). ¹H NMR (400 MHz, CD₂Cl₂): δ = 7.59 – 7.51 (m, 3H), 7.50 – 7.44 (m, 4H), 7.43 – 7.31 (m, 6H), 2.54 – 2.43 (m, 4H), 1.59 (s, 6H), 1.41 (s, 6H), 1.31 (d, *J* = 6.5 Hz, 6H), 0.90 ppm (d, *J* = 6.5 Hz, 6H). ¹³C NMR (100 MHz,

CD₂Cl₂): δ = 215.3 (d, J = 58.5 Hz), 144.7 (d, J = 2.4 Hz), 136.2 (d, J = 23.5 Hz), 132.4, 132.8 (d, J = 4.9 Hz), 132.5 (d, J = 0.94 Hz), 130.4 (d, J = 9.4 Hz), 128.8 (d, J = 6.6 Hz), 127.2, 83.1 (d, J = 3.4 Hz), 56.5 (d, J = 4.6 Hz), 52.7, 30.2, 29.6 (d, J = 2.2 Hz), 29.1 (d, J = 1.1 Hz), 26.1, 24.7 ppm (d, J = 5.9 Hz). ³¹P NMR (162 MHz, CD₂Cl₂): δ = 0.0 ppm. ¹⁹F NMR (CD₃CN, 282 MHz): δ = - 122.4 ppm (sextet, $J_{F-Sb(I=5/2)}$ = 1945 Hz, octet, $J_{F-Sb(I=7/2)}$ = 1071 Hz). HRMS *calcd.* for C₃₂H₄₁NP⁺: 470.296970, *found*: 470.297113. IR $\tilde{\nu}$ = 427, 481, 499, 569, 651, 696, 752, 807, 931, 999, 1052, 1090, 1130, 1197, 1338, 1377, 1391, 1437, 1469, 1520, 1586, 2944, 2977 cm⁻¹.

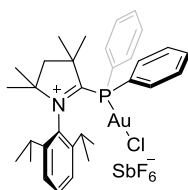
Compound **138b**



To a solution of carbene **137** (1 g, 2.26 mmol) in THF (10 ml), Cy₂PCl (0.5 ml, 2.26 mmol) was added and the resulting mixture stirred at r.t. overnight. The pale yellow solution changed to a bright yellow suspension. Then the solution was filtered off and the remaining yellow solid washed with diethyl ether and dried *in vacuo*. The yellow solid was dissolved in CH₃CN, NaSbF₆ (1.27 g, 4.92 mmol) was added to the solution and the resulting suspension stirred overnight at r.t. Removal of the solvents and extraction with CH₂Cl₂ afforded the desired product **138b** as a yellow solid, which was purified by recrystallization from CH₂Cl₂/Et₂O (1.06 g, 65%). ¹H NMR (500 MHz, CD₂Cl₂) δ = 7.60 (t, J = 7.8 Hz, 1H), 7.41 (d, J = 7.8 Hz, 2H), 2.53 (hept, J = 6.5 Hz, 2H), 2.40 (s, 2H), 2.25 – 2.15 (m, 2H), 1.89 – 1.81 (m, 8H), 1.80 (s, 6H), 1.76 – 1.69 (m, 2H), 1.56 – 1.47 (m, 5H), 1.46 (s, 6H), 1.37 (d, J = 6.5 Hz, 6H), 1.29 (d, J = 6.6 Hz, 6H), 1.28 – 1.21 ppm (m, 5H). ¹³C NMR (126 MHz, CD₂Cl₂) δ = 214.5 (d, J = 70.7 Hz), 144.9 (d, J = 2.7 Hz), 132.1, 131.7 (d, J = 2.5 Hz), 126.5, 83.1 (d, J = 2.7 Hz), 57.5 (d, J = 4.0 Hz), 52.1, 35.8 (d, J = 19.0 Hz), 32.9 (d, J = 13.1 Hz), 29.7, 29.5 (d, J = 2.9 Hz), 27.7 (d, J = 11.5 Hz), 26.7 (d, J = 3.6 Hz), 25.9, 24.7 ppm. ³¹P NMR (122 MHz, CDCl₃) δ = 21.6 ppm. ¹⁹F NMR (CD₃CN, 282 MHz): δ = - 122.4 ppm (sextet, $J_{F-Sb(I=5/2)}$ = 1945 Hz, octet, $J_{F-Sb(I=7/2)}$ = 1071 Hz). HRMS *calcd.* for C₃₂H₅₃NP⁺: 482.391013, *found*: 482.391350. IR $\tilde{\nu}$ = 420, 463, 567, 606, 654, 774, 808, 849, 996, 1051, 1130, 1201, 1337, 1389, 1459, 1518, 2866, 2935, 2971 cm⁻¹.

Compound **138c**

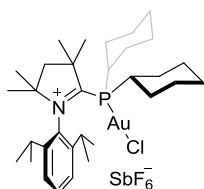
To a solution of carbene **137** (0.500 g, 1.132 mmol) in THF (5 ml), [(*p*-CF₃)Ph]₂PCl (403.9 mg, 1.132 mmol) was added and the resulting mixture stirred at r.t. overnight. The initial pale yellow solution changed to a bright yellow suspension. Then the solvent was removed *in vacuo* and the remaining yellow solid washed with pentane and dried *in vacuo*. The solid thus obtained was dissolved in CH₂Cl₂ (20 ml) and NaSbF₆ (732.6 g, 2.831 mmol) was added to a yellow suspension and stirred overnight at r.t. After that the solvent was filtered and the remaining solid was extracted with CH₂Cl₂. Evaporation of the organic solvents *in vacuo* afforded a yellow solid, which was purified by recrystallization from CH₂Cl₂/Et₂O to afford the desired product **138c** (610.0 mg, 64%). ¹H NMR (CD₂Cl₂, 300 MHz, 298 K): δ = 7.82 – 7.72 (m, 4H), 7.65 – 7.48 (m, 5H), 7.36 (d, *J* = 7.8 Hz, 2H), 2.53 (s, 2H), 2.48 (p, *J* = 6.5 Hz, 2H), 1.63 (s, 6H), 1.46 (d, *J* = 0.7 Hz, 6H), 1.34 (d, *J* = 6.5 Hz, 6H), 0.92 ppm (d, *J* = 6.6 Hz, 6H). ¹³C NMR (CD₂Cl₂, 100 MHz, 298 K): δ = 213.03 (d, *J*_{C-P} = 57.2 Hz), 144.69 (d, *J*_{C-P} = 2.3 Hz), 136.63 (d, *J* = 23.8 Hz), 134.40 (q, *J*_{C-F} = 33.4 Hz), 133.36 – 132.58 (m), 132.52 – 132.11 (m), 128.48 – 126.53 (m), 123.69 (d, *J*_{C-F} = 272.9 Hz), 84.34 (d, *J*_{C-P} = 3.2 Hz), 56.79 (d, *J*_{C-P} = 4.7 Hz), 52.56, 30.22, 29.69 (d, *J*_{C-P} = 1.9 Hz), 29.21, 25.97, 24.86 ppm (d, *J*_{C-P} = 5.7 Hz). ³¹P NMR (CD₂Cl₂, 121 MHz, 298K): δ = – 4.29 ppm. ¹⁹F NMR (CD₂Cl₂, 282 MHz, 298K): δ = – 63.81 ppm. HRMS *calcd.* for C₃₄H₃₉NF₆P⁺ 606.272470, *found*: 606.271884. IR $\tilde{\nu}$ = 413, 514, 602, 654, 695, 711, 807, 836, 954, 1014, 1059, 1110, 1127, 1170, 1262, 1320, 1396, 1461, 1607, 2966 cm⁻¹.

Compound **139a**

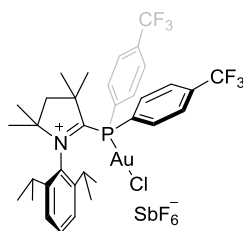
(Me₂S)AuCl (42.0 mg, 0.140 mmol) was added to a solution of compound **138a** (100.2 mg, 0.140 mmol) in CH₂Cl₂ (2 ml) and the resulting suspension stirred for 1 hour at r.t. After evaporation of the solvent, the resulting solid was dissolved in CH₃CN and filtered. Removal of the solvent *in vacuo* afforded the desired product **139a** as a yellow solid, which could be

further purified by recrystallization from $\text{CH}_2\text{Cl}_2/\text{Et}_2\text{O}$ (95.8 mg, 72%). ^1H NMR (300 MHz, CD_3CN): $\delta = 7.81 - 7.64$ (m, 11H), 7.52 (d, $J = 7.8$ Hz, 2H), 1.66 (s, 6H), 2.64 – 2.49 (m, 4H), 1.35 (d, $J = 6.6$ Hz, 12H), 1.19 ppm (d, $J = 6.6$ Hz, 6H). ^{13}C NMR (126 MHz, CD_3CN): $\delta = 202.3$ (d, $J = 12.8$ Hz), 145.4, 135.8 (d, $J = 15.2$ Hz), 135.4 (d, $J = 2.8$ Hz), 133.7, 131.4 (d, $J = 12.7$ Hz), 128.6, 124.4 (d, $J = 60.0$ Hz), 90.3 (d, $J = 1.9$ Hz), 59.5 (d, $J = 2.2$ Hz), 50.5 (d, $J = 2.2$ Hz), 30.4 (d, $J = 7.4$ Hz), 29.8, 27.4, 25.0 ppm. ^{31}P NMR (122 MHz, CD_2Cl_2): $\delta = 29.5$ ppm. ^{19}F NMR (CD_3CN , 282 MHz): $\delta = -122.4$ ppm (sextet, $J_{\text{F-Sb}(I=5/2)} = 1945$ Hz, octet, $J_{\text{F-Sb}(I=7/2)} = 1071$ Hz). HRMS *calcd.* for $\text{C}_{32}\text{H}_{41}\text{AuClINP}^+$: 702.232519, *found*: 702.232490. IR $\tilde{\nu} = 426, 452, 504, 537, 562, 609, 648, 657, 692, 744, 800, 999, 1052, 1091, 1191, 1342, 1378, 1392, 1438, 1464, 1481, 1538, 1588, 2962$ cm^{-1} .

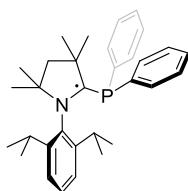
Compound **139b**



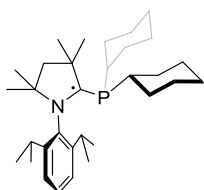
$(\text{Me}_2\text{S})\text{AuCl}$ (42.0 mg, 0.140 mmol) was added to a solution of compound **138b** (101.1 mg, 0.140 mmol) in CH_2Cl_2 (2 ml) and the resulting suspension stirred for 1 hour at r.t. After evaporation of the solvent, the resulting solid dissolved in CH_3CN and filtered. Removal of the solvents afforded the desired solid **139b** dried *in vacuo* to yield the new gold complex (90.0 mg, 90%). ^1H NMR (300 MHz, CD_3CN) $\delta = 7.63$ (t, $J = 7.8$ Hz, 1H), 7.41 (d, $J = 7.9$ Hz, 2H), 2.74 – 2.58 (m, 2H), 2.34 (hept, $J = 6.6$ Hz, 2H), 2.43 (s, 2H), 2.22 – 2.09 (m, 2H), 1.82 (m, , 3H), 1.78 (s, 6H), 1.72 – 1.47 (m, 9H), 1.43 (d, $J = 6.6$ Hz, 6H), 1.41 – 1.38 (m, 6H), 1.35 (d, $J = 12.0$ Hz, 3H), 1.28 (d, $J = 6.3$ Hz, 6H), 1.26 – 1.16 ppm (m, 3H). ^{13}C NMR (150 MHz, CD_3CN) $\delta = 204.7$ (d, $J = 3.4$ Hz), 145.3, 27.0 (d, $J = 14.1$ Hz), 133.5, 128.2, 90.2, 58.9 (d, $J = 1.6$ Hz), 50.9 (d, $J = 2.3$ Hz), 38.7 (d, $J = 23.9$ Hz), 34.9 (d, $J = 3.4$ Hz), 32.7 (d, $J = 2.2$ Hz), 30.2 (d, $J = 16.3$ Hz), 29.0 (d, $J = 17.3$ Hz), 27.4 (d, $J = 15.3$ Hz), 25.9 (d, $J = 2.1$ Hz), 25.0 ppm. ^{31}P NMR (121 MHz, CD_3CN) $\delta = 54.97$ ppm. ^{19}F NMR (CD_3CN , 282 MHz): $\delta = -122.4$ ppm (sextet, $J_{\text{F-Sb}(I=5/2)} = 1945$ Hz, octet, $J_{\text{F-Sb}(I=7/2)} = 1071$ Hz). HRMS *calcd.* for $\text{C}_{32}\text{H}_{53}\text{AuClINP}^+$: 714.326419, *found*: 714.326670. IR $\tilde{\nu} = 431, 472, 527, 561, 605, 654, 771, 799, 814, 851, 885, 919, 999, 1053, 1128, 1187, 1264, 1341, 1378, 1452, 1520, 2858, 2932$ cm^{-1} .

Compound **139c**

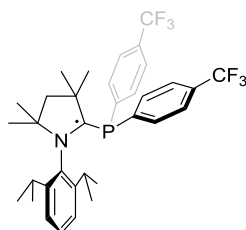
(Me₂S)AuCl (17.5 mg, 0.059 mmol) was added to a solution of compound **138c** (50.0 mg, 0.059 mmol) in CH₂Cl₂ (1 ml) and the resulting suspension stirred for 1 hour at r.t. After evaporation of the solvent, the resulting solid was recrystallized from CH₂Cl₂/Et₂O to afford the desired compound **139c** as a yellow solid (45.6 mg, 70%). ¹H NMR (CD₂Cl₂, 300 MHz, 298 K): δ = 7.99 (m, 4H), 7.94 – 7.75 (m, 5H), 7.50 (d, *J* = 7.9 Hz, 2H), 2.72 (s, 2H), 2.53 (p, *J* = 6.6 Hz, 2H), 1.75 (s, 6H), 1.44 (s, 6H), 1.40 (d, *J* = 6.4 Hz, 6H), 1.22 ppm (d, *J* = 6.6 Hz, 6H). ¹³C NMR (CD₂Cl₂, 100 MHz, 298 K): δ = 200.1 (d, *J*_{C-P} = 14.3 Hz), 144.8, 136.78 (qd, *J*_{C-F} = 33.8, *J*_{C-P} = 2.9 Hz), 135.9 (d, *J*_{C-P} = 15.9 Hz), 134.0, 132.5 (d, *J*_{C-P} = 6.6 Hz), 128.5, 128.1 (dq, *J*_{C-F} = 13.0, *J*_{C-P} = 3.6 Hz), 127.4 (d, *J*_{C-P} = 1.7 Hz), 123.4 (q, *J*_{C-F} = 273.3 Hz), 90.6 (d, *J*_{C-P} = 1.8 Hz), 59.4 (d, *J*_{C-P} = 2.1 Hz), 50.5 (d, *J*_{C-P} = 2.2 Hz), 30.7, 30.4, 30.1, 27.5, 25.3 ppm. ³¹P NMR (CD₂Cl₂, 121 MHz, 298K): δ = 27.40 ppm. ¹⁹F NMR (CD₂Cl₂, 282 MHz, 298K): δ = - 64.02 ppm. HRMS *calcd.* for C₃₂H₅₃AuClNP⁺: 838.207200, *found*: 838.207290. IR $\tilde{\nu}$ = 421, 437, 517, 539, 563, 605, 652, 710, 771, 802, 833, 954, 1011, 1062, 1117, 1138, 1318, 1337, 1399, 1464, 2308, 2854, 2925, 2962, 3104 cm⁻¹.

Compound **140a**

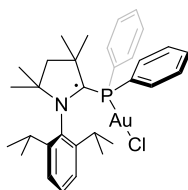
Potassium graphite (74.6 mg, 0.552 mmol) was added to a solution of **138a** (390.0 mg, 0.552 mmol) in THF (2 ml) at - 78 °C and the resulting suspension stirred for 5 min. Then the reaction was allowed to warm up to r.t and further stirred for 1 h. The solvent was removed *in vacuo* and the resulting solid extracted with pentane to afford, after the evaporation of pentane, the desired product **140a** as a black solid (81%, 212.0 mg). Crystals suitable for X-ray analysis were obtained from a saturated solution of **140a** in pentane at - 20 °C. Elemental analysis *calcd.* for C₃₂H₄₁NP: C: 81.66%, H: 8.78%, N: 2.98%, *found*: C: 81.75%, H: 8.84%, N: 2.97%. UV-visible absorption bands *found* at 213 and 265 nm (in CH₂Cl₂). HRMS *calcd.* for C₃₂H₄₁NP⁺: 470.296830, *found*: 470.297113.

Compound **140b**

Potassium graphite (21.5 mg, 0.159 mmol) was added to a solution of **138b** (114.0 mg, 0.159 mmol) in THF (2 ml) at $-78\text{ }^{\circ}\text{C}$ and the resulting suspension stirred for 5 min. Then the reaction was allowed to warm up to r.t and further stirred for 1 h. The solvent was removed *in vacuo* and the resulting solid extracted with pentane to afford, after the evaporation of the solvent, the desired product **140b** as a orange solid (70%, 54.0 mg). UV–visible absorption bands *found* at 285 and 321 nm (in CH_2Cl_2). HRMS *calcd.* for $\text{C}_{32}\text{H}_{53}\text{NP}^+$: 482.391500, *found*: 482.391013.

Compound **140c**

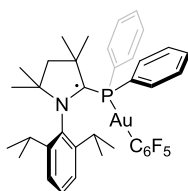
Potassium graphite (18.8 mg, 0.126 mmol) was added to a solution of **138c** (106.0 mg, 0.126 mmol) in THF (2 ml) at $-78\text{ }^{\circ}\text{C}$ and the resulting suspension stirred for 5 min. Then the reaction was allowed to warm up to r.t and further stirred for 1 h. The solvent was removed *in vacuo* and the resulting solid extracted with pentane to afford, after the evaporation of pentane, the desired product **140c** as a black solid (60%, 46.0 mg). Crystals suitable for X–ray analysis were obtained from a saturated solution of **140c** in pentane at $-20\text{ }^{\circ}\text{C}$. UV–visible absorption bands *found* at 250 and 276 nm (in CH_2Cl_2). HRMS *calcd.* for $\text{C}_{34}\text{H}_{39}\text{NPF}^+$: 606.272470, *found*: 606.271884.

Compound **141**

$(\text{Me}_2\text{S})\text{AuCl}$ (12.5 mg, 0.043 mmol) was added to a solution of **140a** (20.0 mg, 0.043 mmol) in THF (1 ml) at $-78\text{ }^{\circ}\text{C}$ and the resulting solution stirred for 5 min. Then, the reaction was

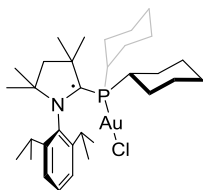
warmed up to r.t and further stirred for 1 h. Removal of the solvents *in vacuo* afforded a red solid, which was washed with pentane to afford the desired product **141** as red solid (87%, 24.0 mg). Red crystals suitable for X-ray analysis were obtained from CH₂Cl₂/pentane at r.t. Elemental analysis *calcd.* for C₃₂H₄₁NPAuCl: C: 54.67%, H: 5.88%, N: 1.99%, *found*: C: 51.99%, H: 6.09%, N: 2.02%. UV– visible absorption bands *found* at 234 and 246 nm (in CH₂Cl₂). HRMS *calcd.* for C₃₂H₄₁NPAuCl⁺: 702.233360, *found*: 702.232519.

Compound 142

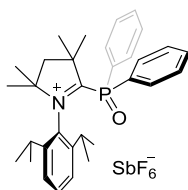


(THT)Au(C₆F₅) (19.2 mg, 0.043 mmol) was added to **140a** (20.0 mg, 0.043 mmol) in THF (1 ml) at – 78 °C and the resulting mixture was stirred for 5 min. Then the reaction was warmed up to r.t and further stirred for 1 h. Removal of the solvents *in vacuo* and afforded a red solid, which was washed with pentane to afford the desired product **142** as yellow solid (76%, 27.0 mg). Red crystals suitable for X– ray analysis were obtained from a solution of **142** in benzene/pentane at r.t. UV– visible absorption bands *found* at 234 and 246 nm (in CH₂Cl₂). HRMS *calcd.* for C₃₈H₄₁NPAuF₅⁺: 834.256130, *found*: 834.255683.

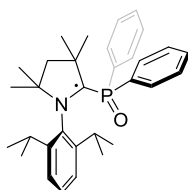
Compound 143



(Me₂S)AuCl (12.2 mg, 0.041 mmol) was added to **140b** (20.0 mg, 0.041 mmol) in THF (1 ml) at – 78 °C and the mixture stirred for 5 min. Then the reaction was warmed up to r.t and further stirred for 1 h. Removal of the solvents *in vacuo* afforded a solid, which was washed with pentane to afford the desired product **143** as a red solid (88%, 26.0 mg). Red crystals suitable for X– ray analysis were obtained from a solution of **143** in benzene/pentane at 4 °C. Elemental analysis *calcd.* for C₃₂H₄₁NPAuCl: C: 57.54%, H: 7.50%, N: 1.77%, *found*: C: 54.49%, H: 7.21%, N: 1.69%. UV– visible absorption bands *found* at 229 and 276 nm (in CH₂Cl₂). HRMS *calcd.* for C₃₂H₄₁AuClNP⁺: 702.232514, *found*: 702.232490.

Compound **146**

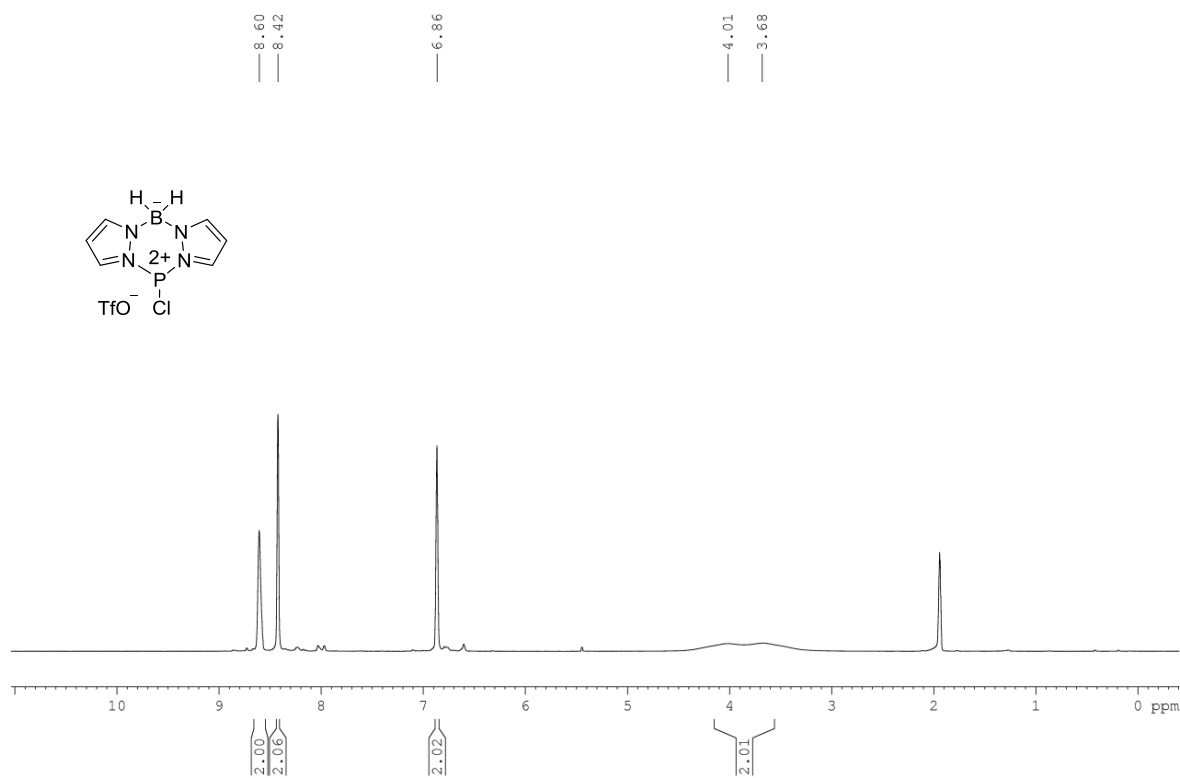
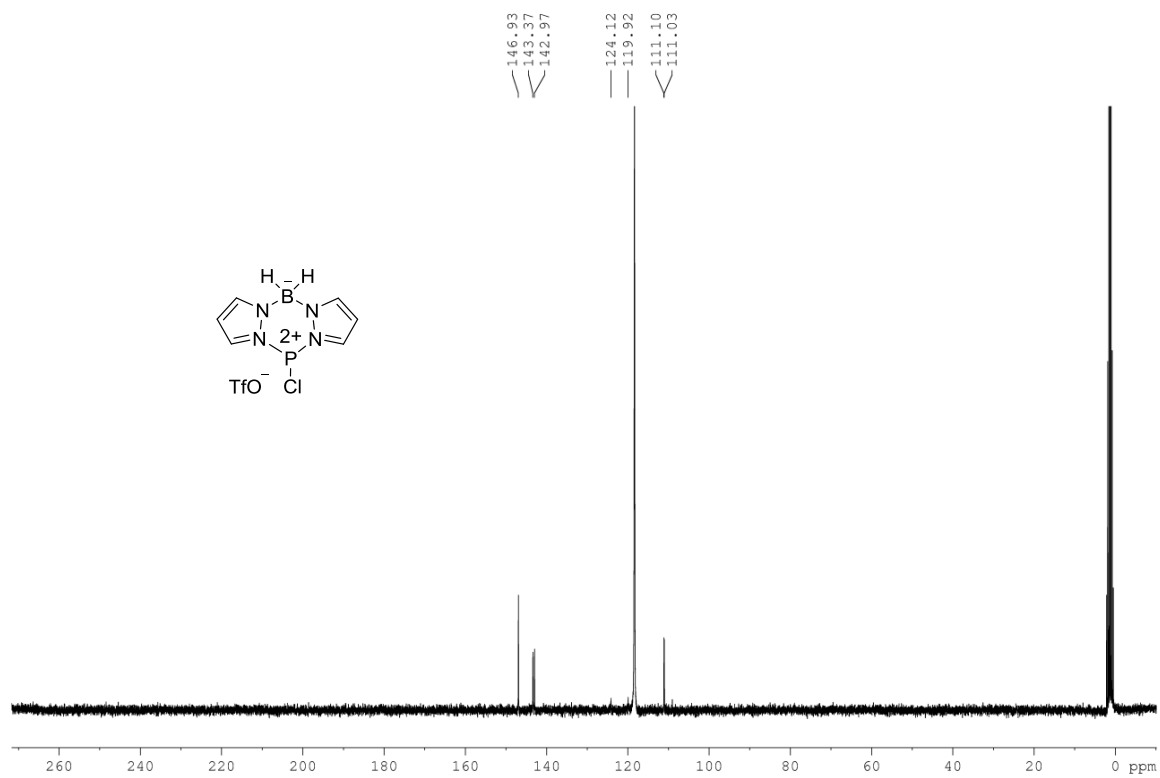
m-CPBA (63.5 mg, 0.283 mmol) was added to a solution of phosphine **138a** (200.0 mg, 0.283 mmol) in CH₂Cl₂ (2 ml), and the resulting mixture stirred for 1 h. Partly removal of the solvent to approximately 2 ml and addition of Et₂O (10 ml) resulted in precipitation of the desired product, which was further washed with Et₂O to afford clean **146** as a white solid (97%, 200.0 mg). ¹H NMR (CD₃CN, 300 MHz): δ = 7.91 – 7.63 (m, 10H), 7.53 (dd, *J* = 8.5, 7.0 Hz, 1H), 7.44 – 7.35 (m, 2H), 2.67 (p, *J* = 6.5 Hz, 2H), 2.56 (s, 2H), 1.53 (s, 6H), 1.38 (d, *J* = 6.4 Hz, 6H), 1.27 (s, 6H), 1.00 ppm (d, *J* = 6.6 Hz, 6H), ¹³C NMR (CD₃CN, 100 MHz): δ = 202.6 (d, *J* = 43.3 Hz), 143.5, 134.5 (d, *J* = 3.0 Hz), 132.9 (d, *J* = 11.2 Hz), 130.7, 130.5, 129.2 (d, *J* = 13.3 Hz), 128.2 (d, *J* = 110.1 Hz), 125.2, 87.7 (d, *J* = 5.2 Hz), 54.2 (d, *J* = 8.4 Hz), 48.8 (d, *J* = 3.8 Hz), 29.3, 28.4, 27.9, 25.5, 22.9 ppm. ³¹P NMR (CD₃CN, 121 MHz) δ = 24.50 ppm. ¹⁹F NMR (CD₃CN, 282 MHz): δ = – 122.4 ppm (sextet, *J*_{F-Sb(*I*=5/2)} = 1945 Hz, octet, *J*_{F-Sb(*I*=7/2)} = 1071 Hz). HRMS *calcd.* for C₃₂H₄₁ONP⁺: 486.292280, *found*: 486.292028. IR $\tilde{\nu}$ = 447, 472, 502, 536, 655, 697, 732, 754, 799, 807, 1098, 1114, 1219, 1378, 1438, 1471, 2979 cm⁻¹.

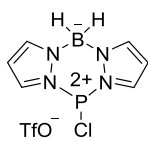
Compound **147**

Potassium graphite (10.3 mg, 0.069 mmol) was added to **146** (50.0 mg, 0.069 mmol) in THF (2 ml) at – 78 °C and the resulting suspension stirred for 5 min. Then, the reaction was warmed up to r.t and further stirred for 1 h. Removal of the solvents *in vacuo*, followed by extraction with pentane afforded the desired product **147** as a black solid (84%, 28.3 mg). Crystals suitable for X-ray analysis were obtained from a solution of **147** in pentane at – 20 °C. Elemental analysis *calcd.* for C₃₂H₄₁NOP: C: 78.98%, H: 8.48%, N: 2.88%, *found*: C: 77.34%, H: 8.86%, N: 2.68%. UV– visible absorption bands *found* at 228 and 270 nm (in CH₂Cl₂). HRMS *calcd.* for C₃₂H₄₁NOP⁺: 486.292230, *found*: 486.292028.

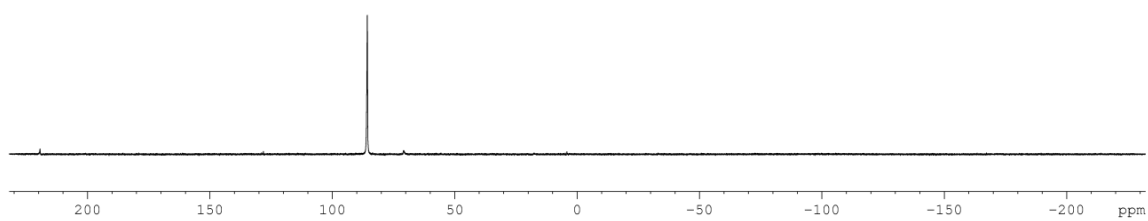
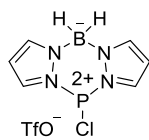
6 Appendix

6.1 NMR Spectra of Representative Compounds

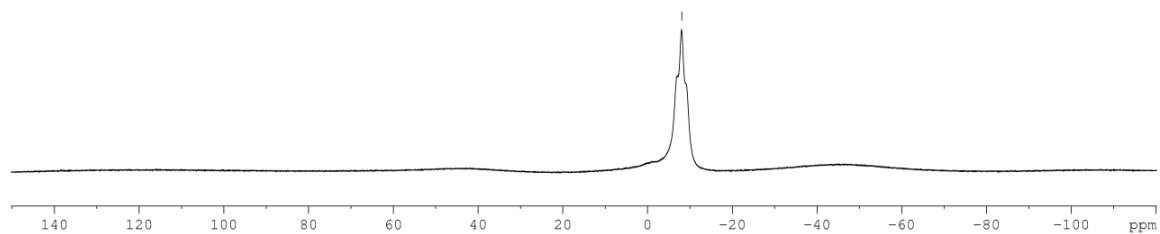
^1H NMR (CD₃CN, 300 MHz) (Compound 62) **^{13}C NMR (CD₃CN, 75 MHz) (Compound 62)**

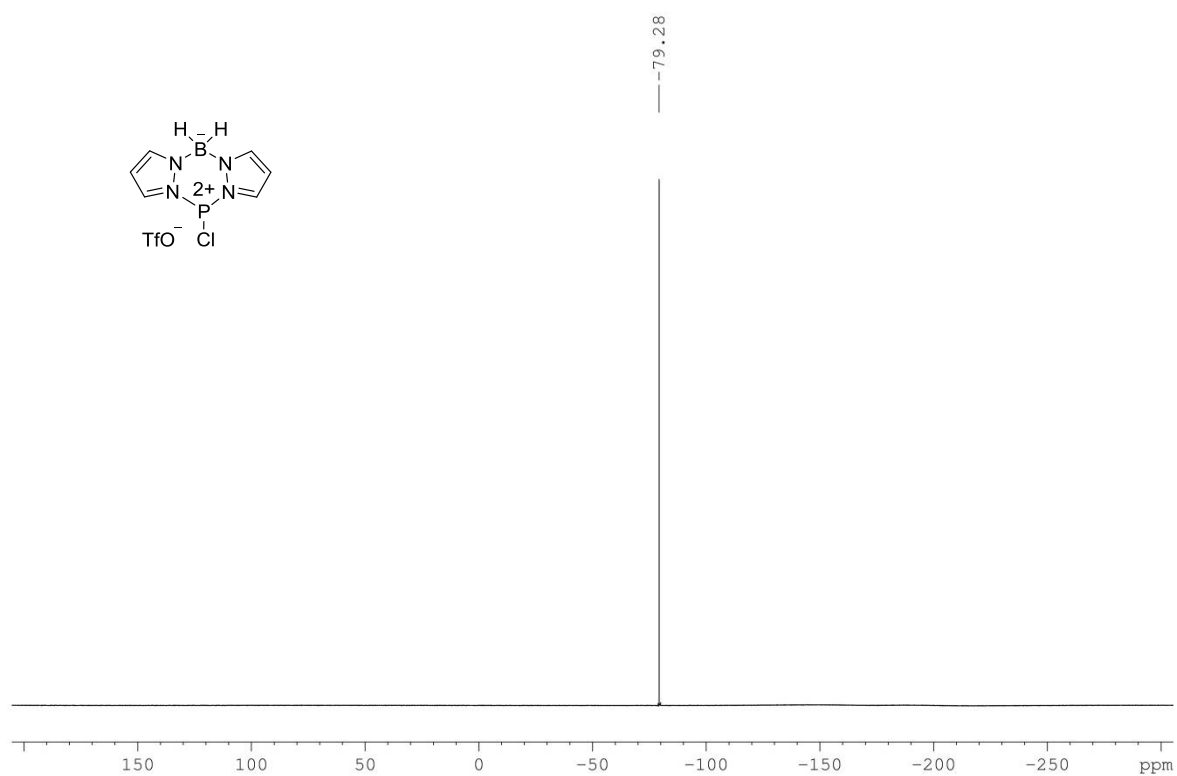
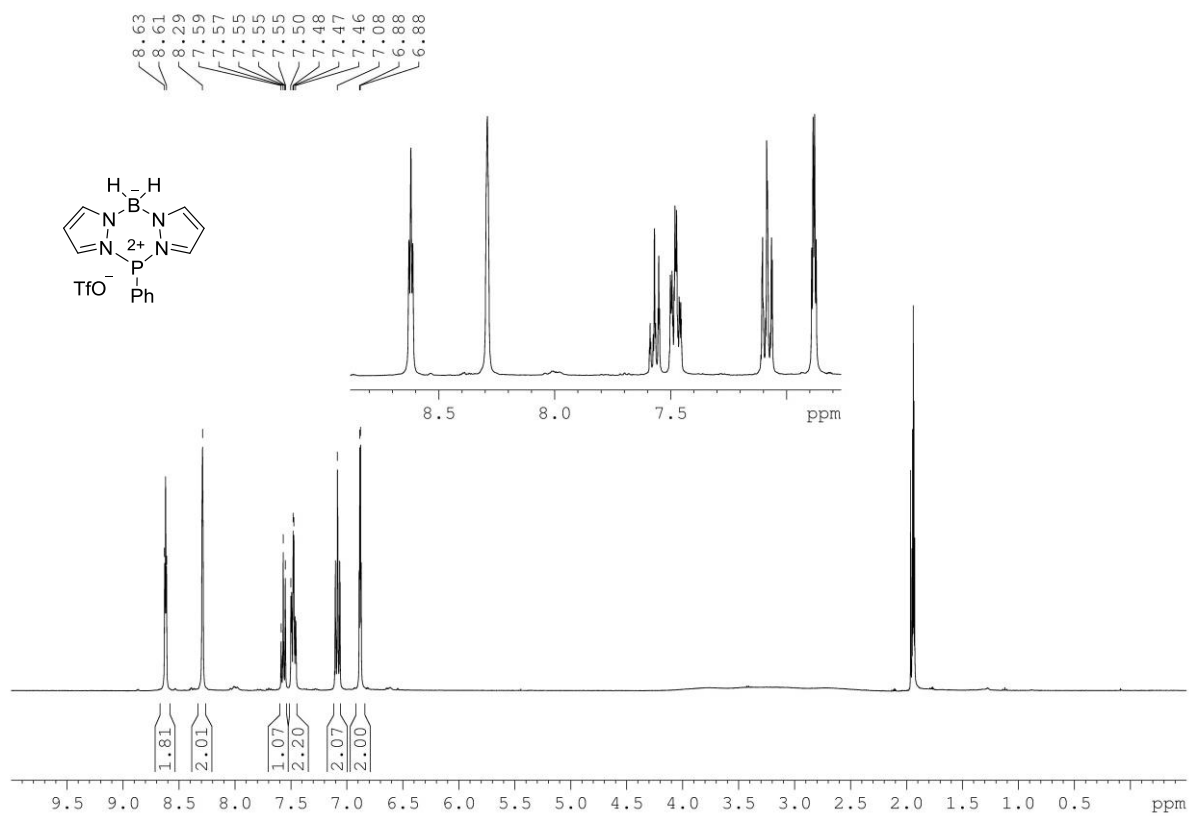
^{31}P NMR (CD_3CN , 162 MHz) (Compound 62)

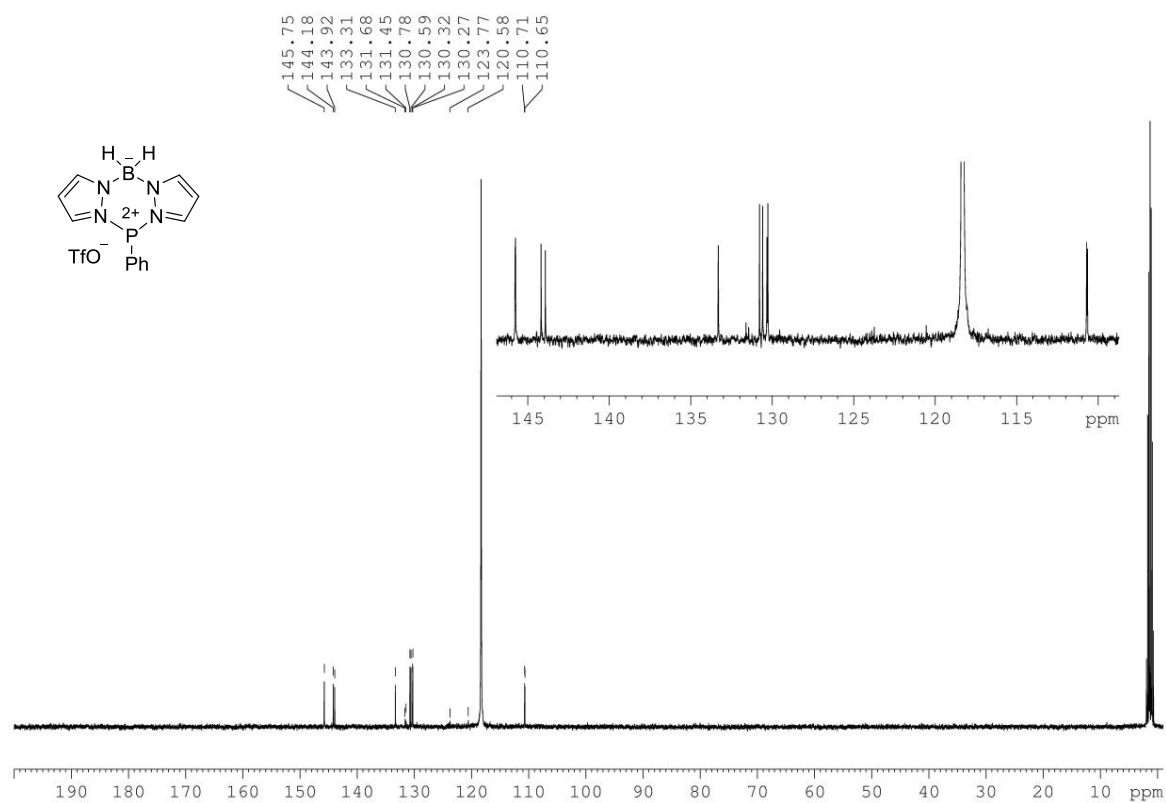
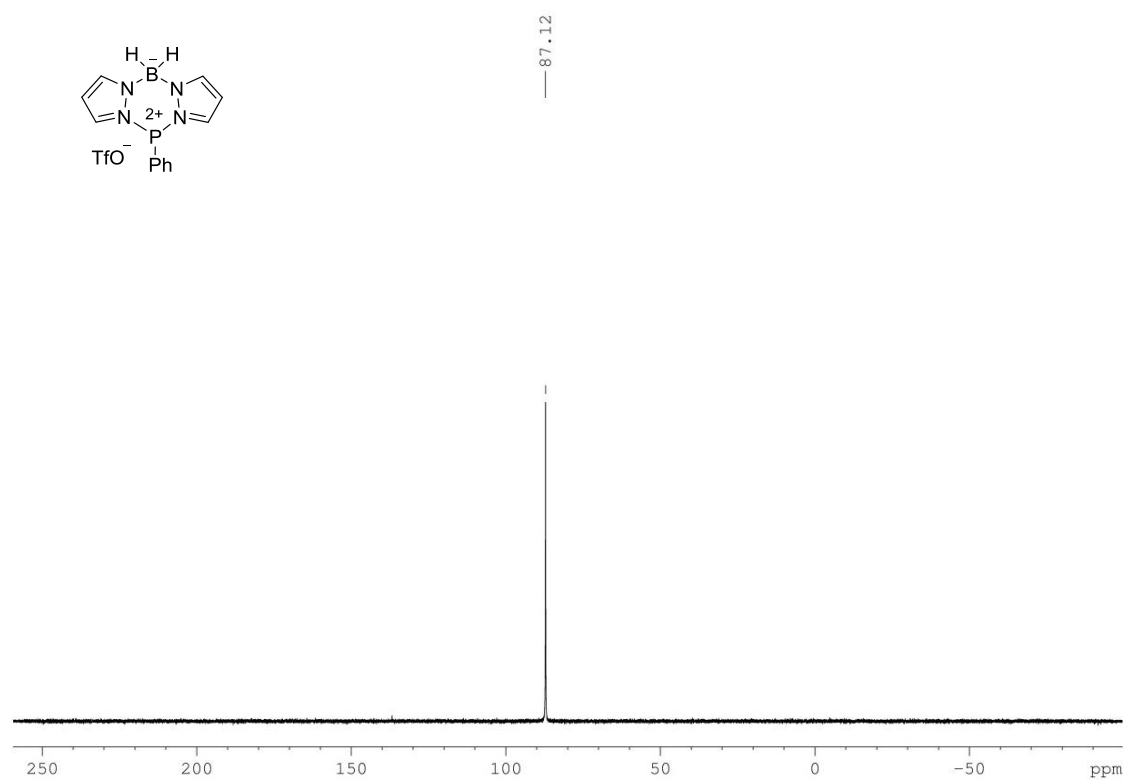
— 85.72

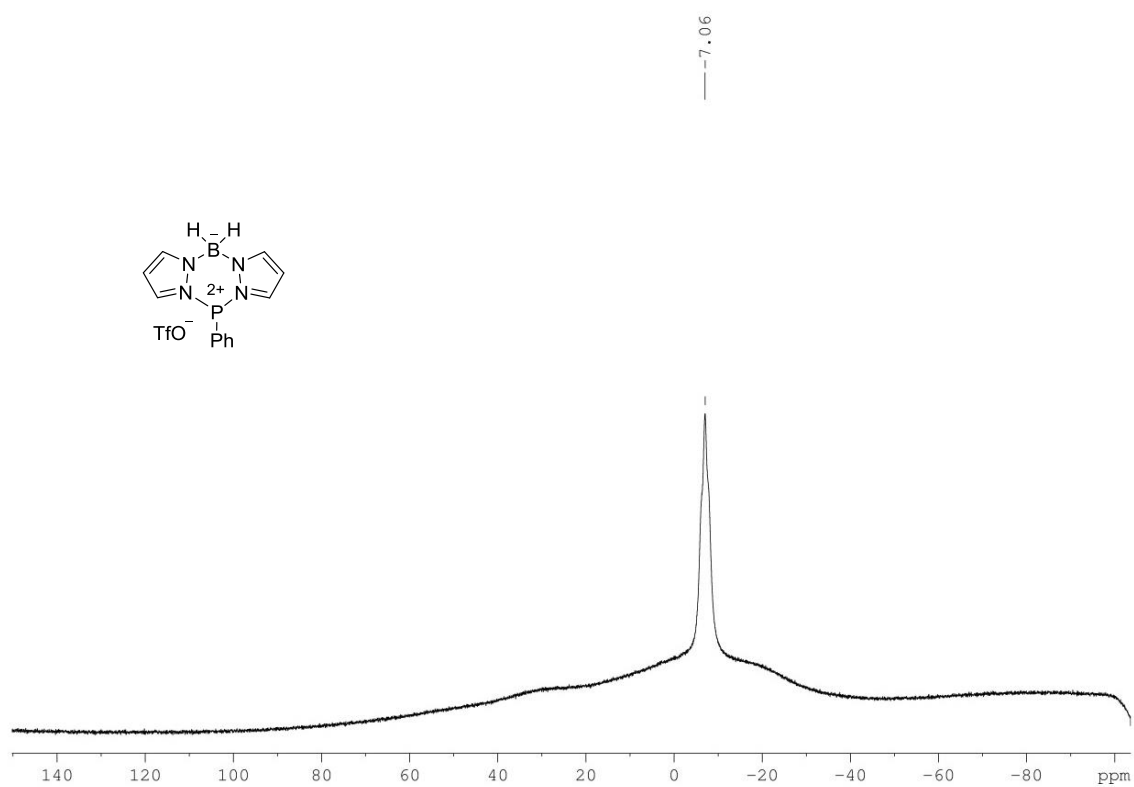
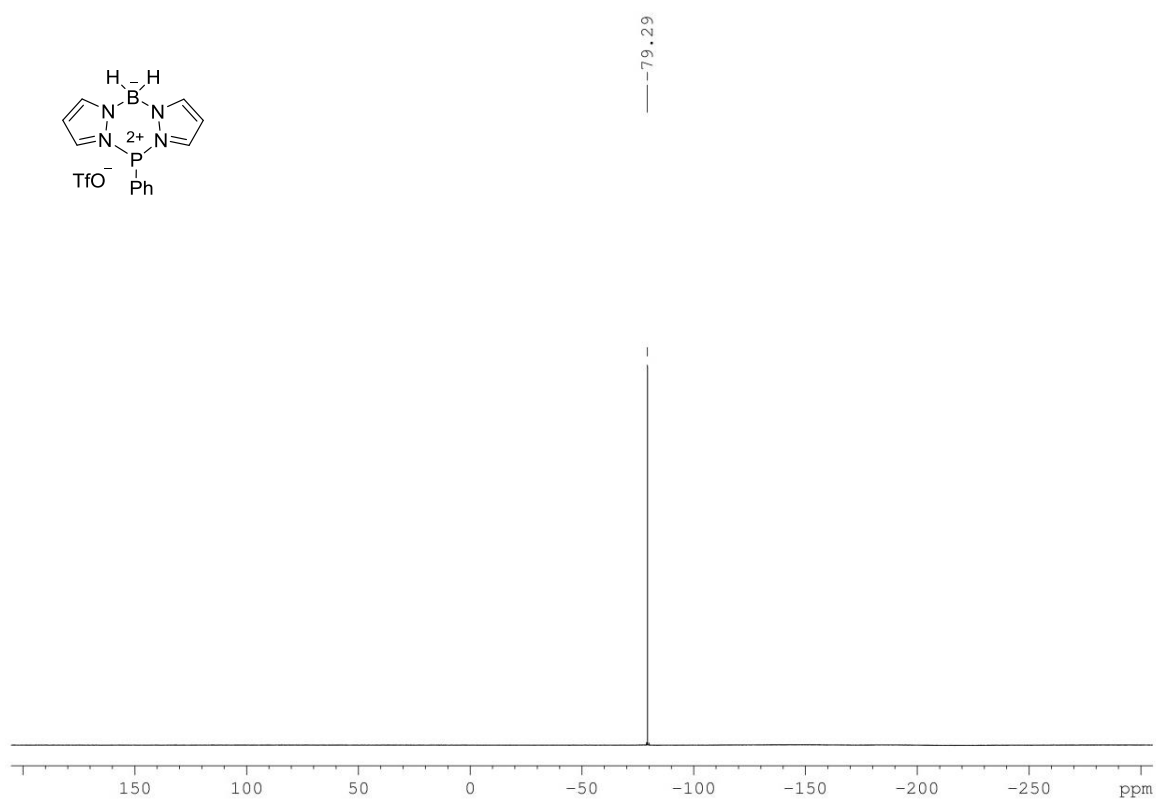
 **^{11}B NMR (CD_3CN , 128 MHz) (Compound 62)**

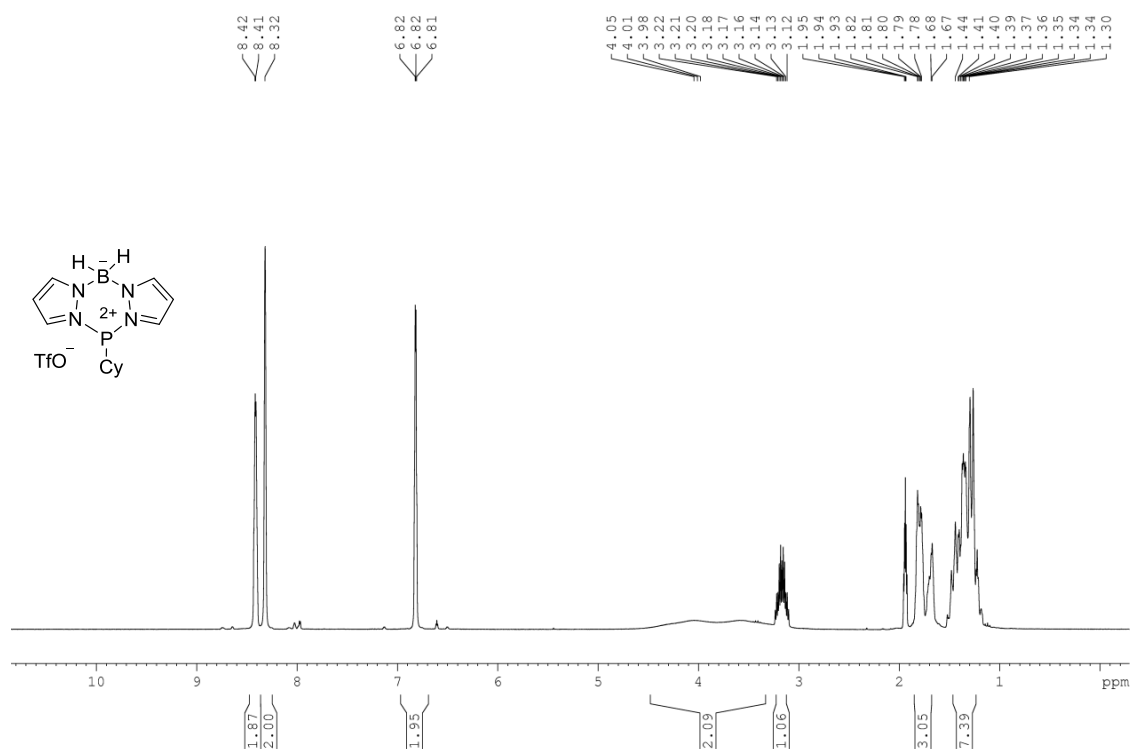
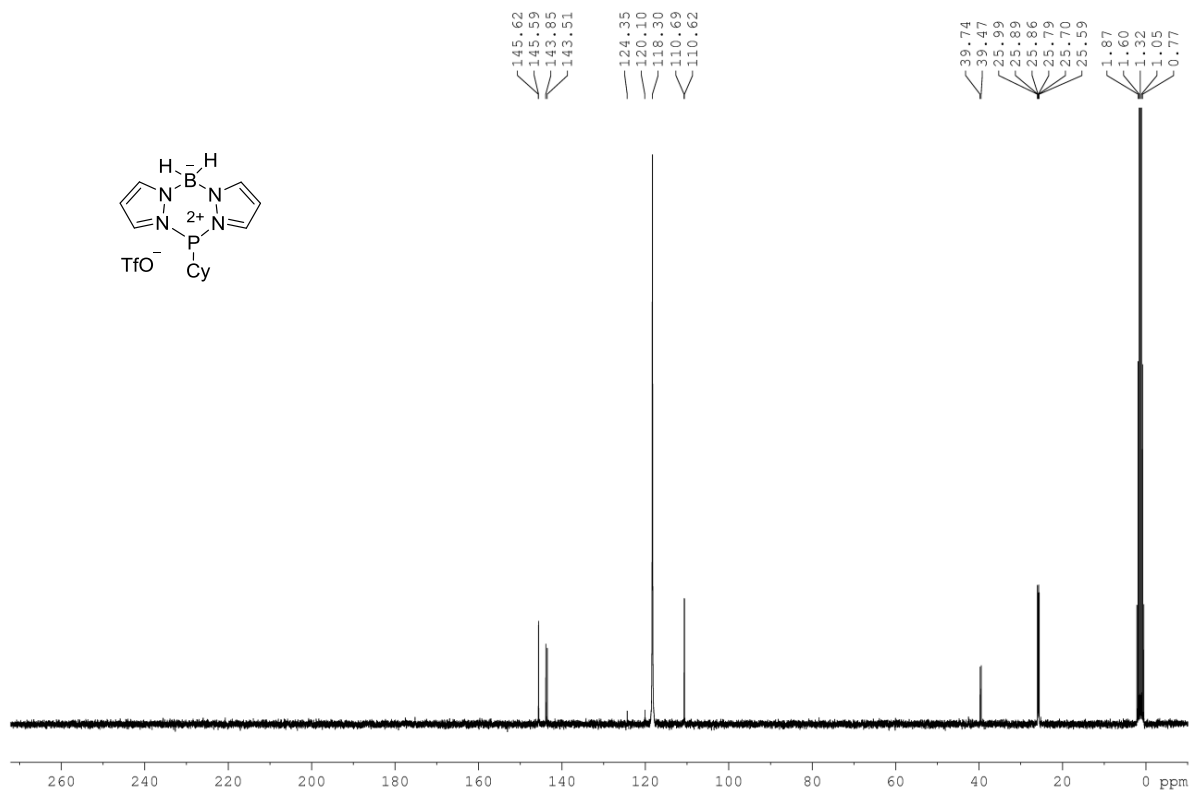
— 8.06

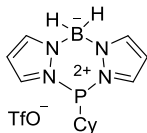
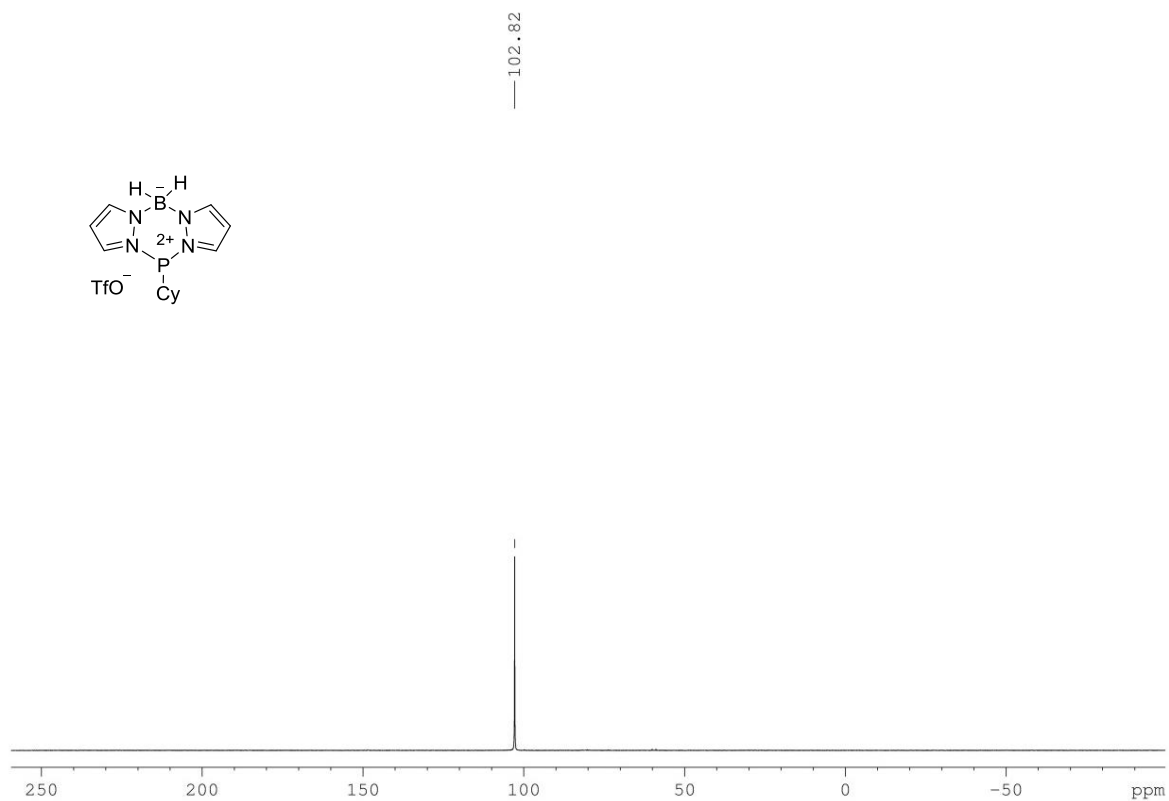
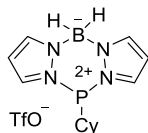
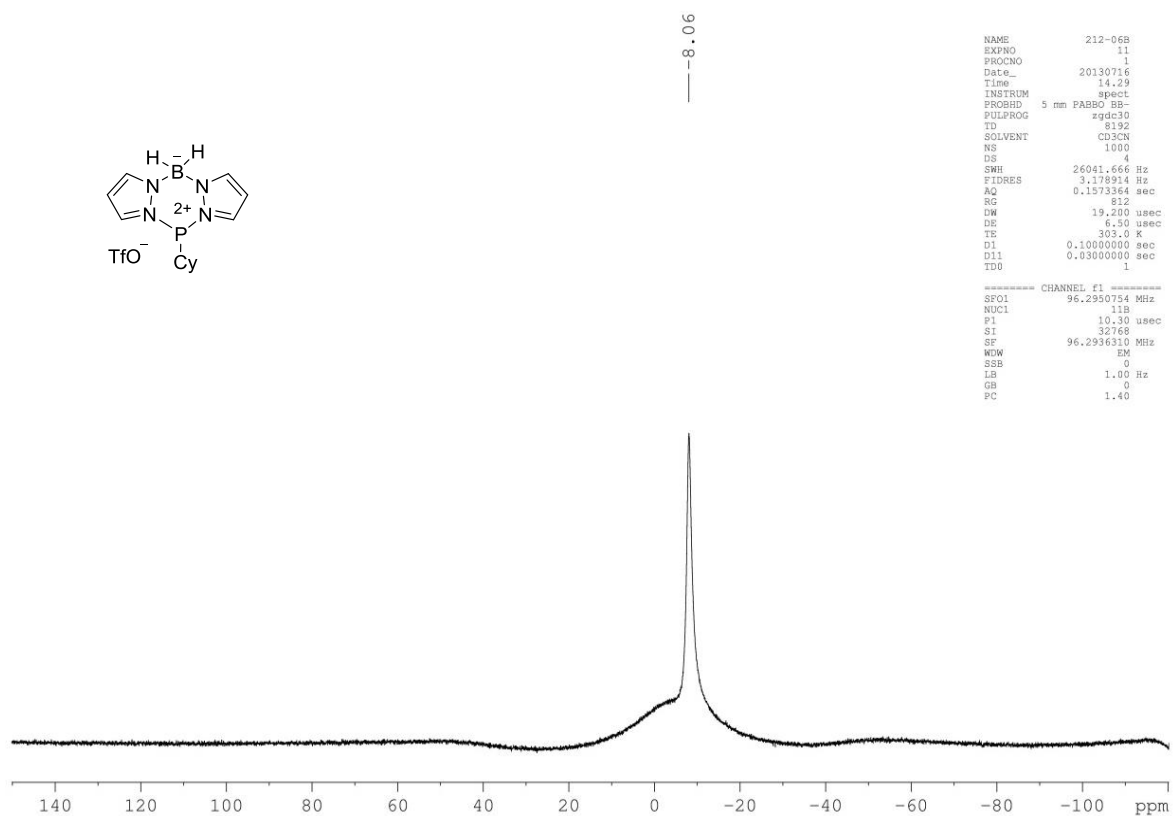


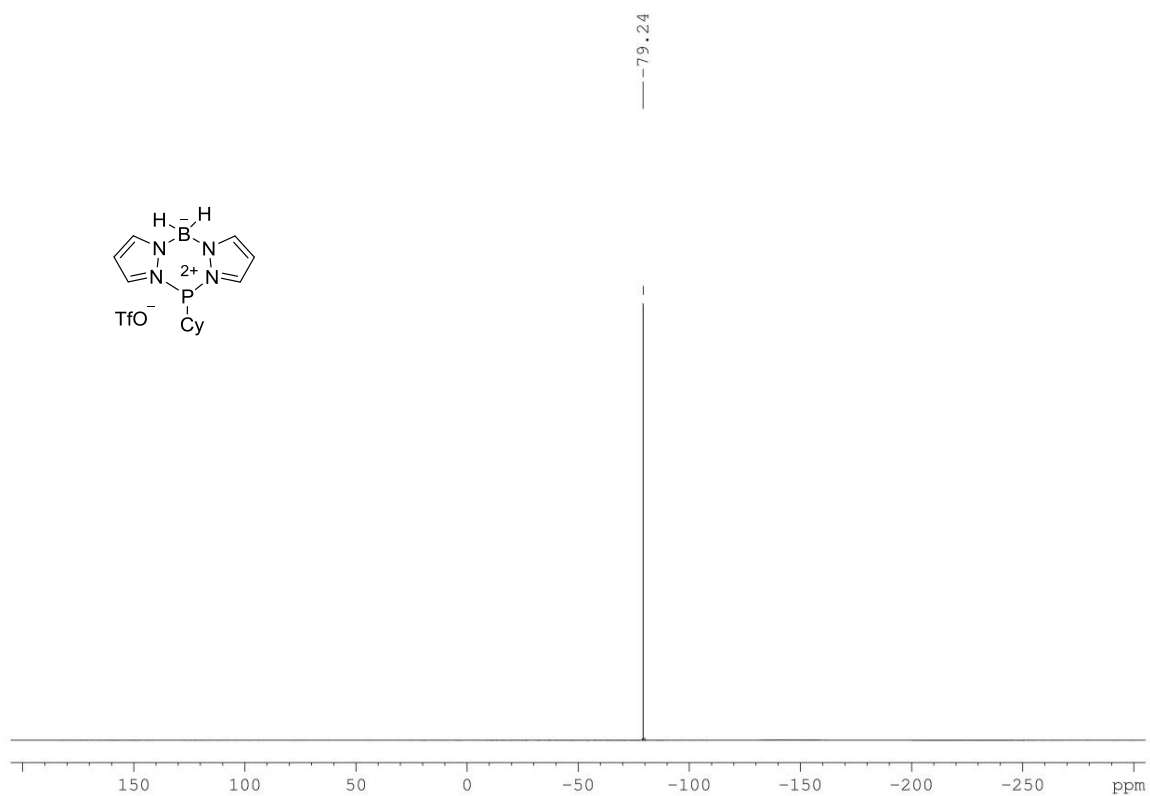
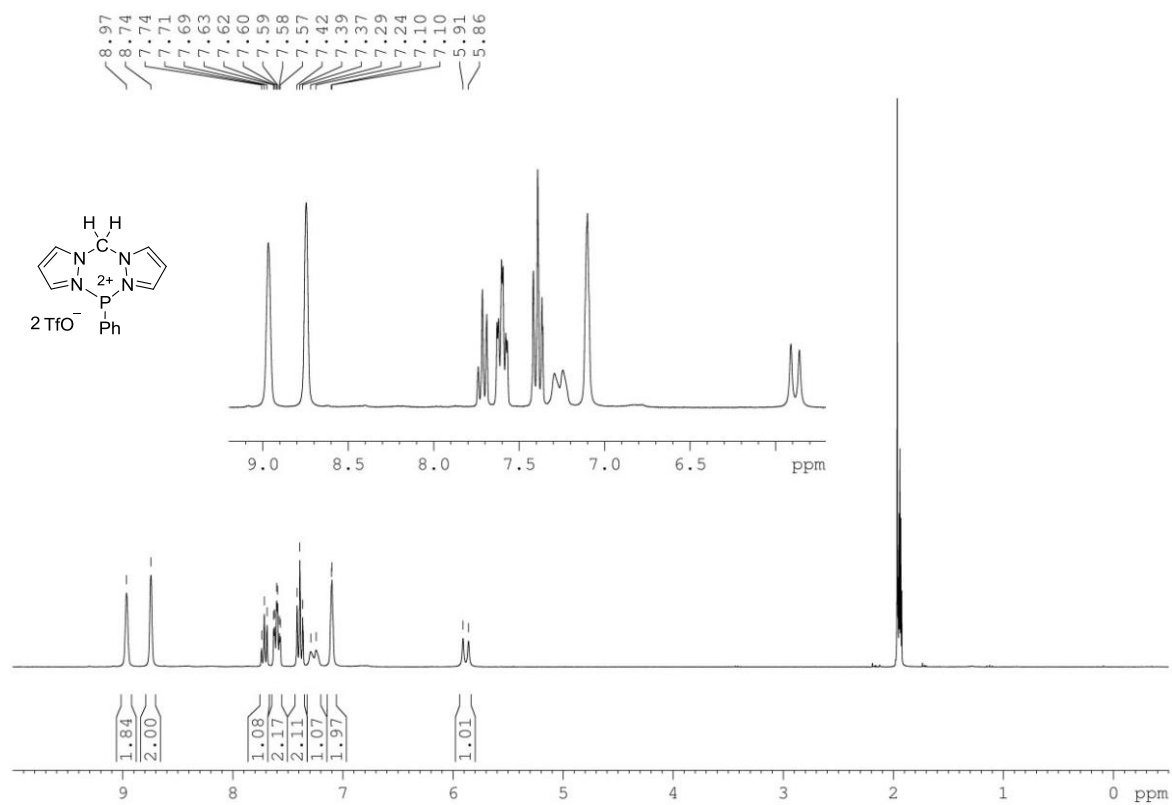
^{19}F NMR (CD_3CN , 282 MHz) (Compound 62) **^1H NMR (CD_3CN , 400 MHz) (Compound 63)**

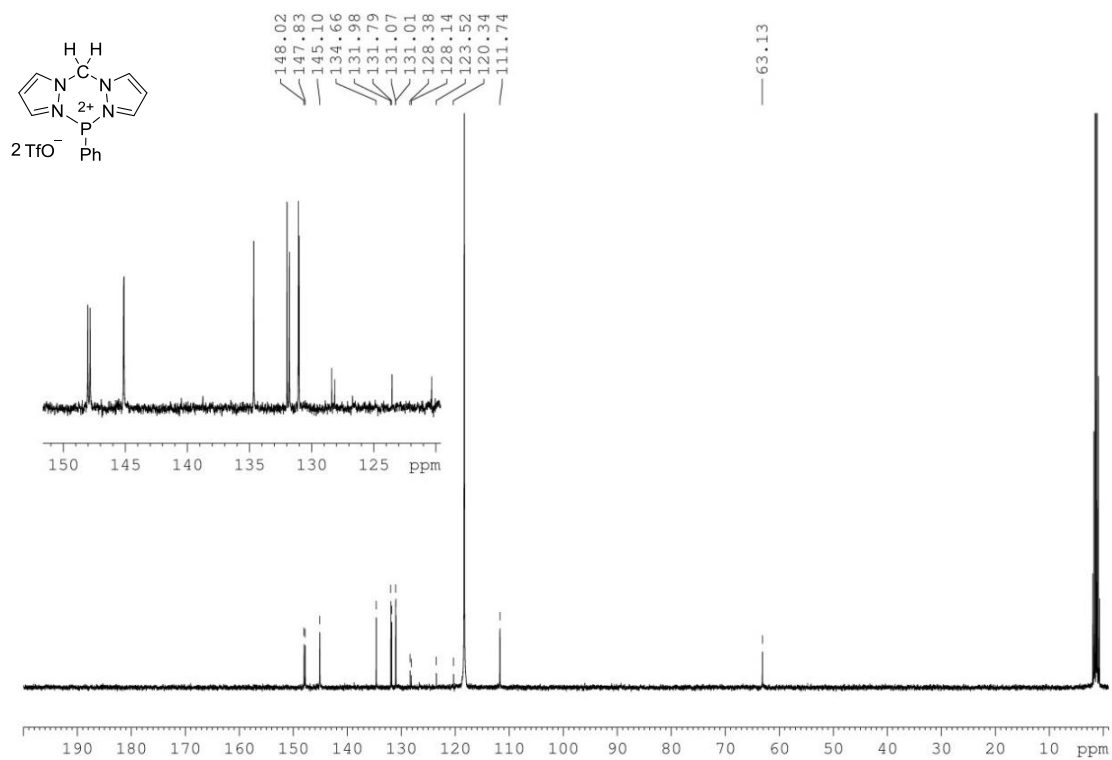
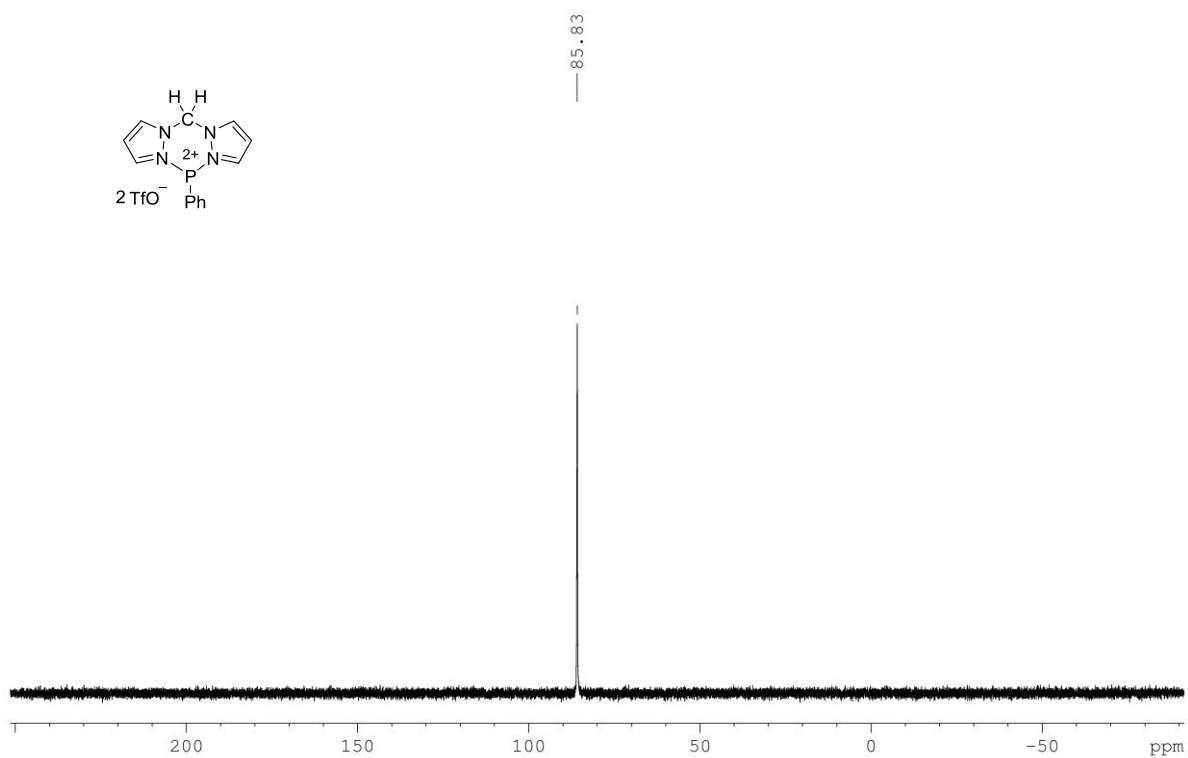
^{13}C NMR (CD₃CN, 101 MHz) (Compound 63) **^{31}P NMR (CD₃CN, 162 MHz) (Compound 63)**

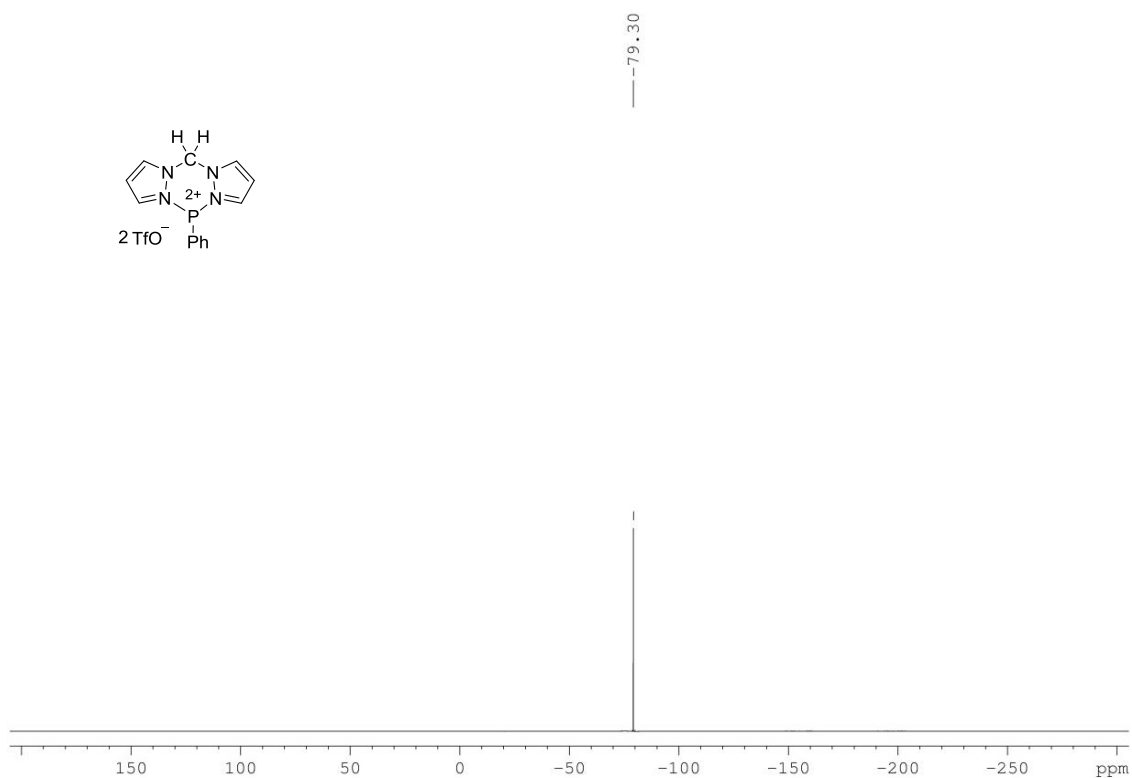
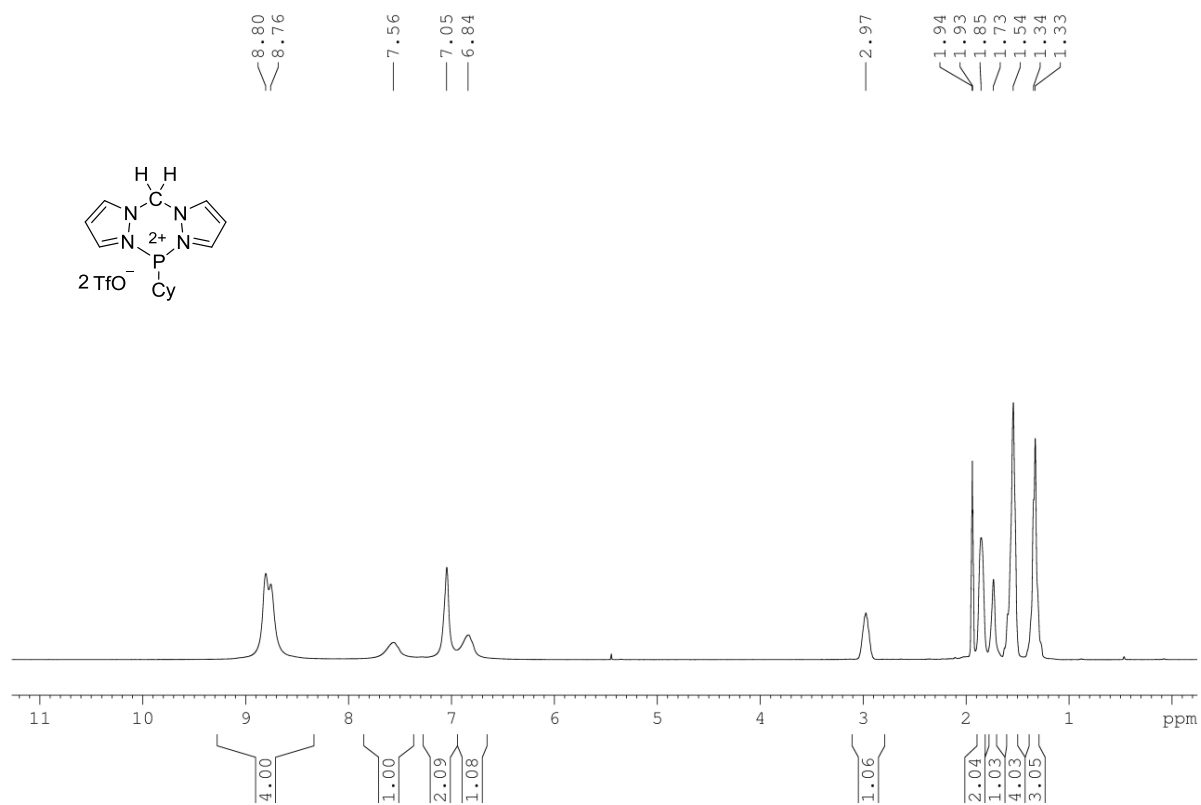
^{11}B NMR (CD₃CN, 128 MHz) (Compound 63) **^{19}F NMR (CD₃CN, 282 MHz) (Compound 63)**

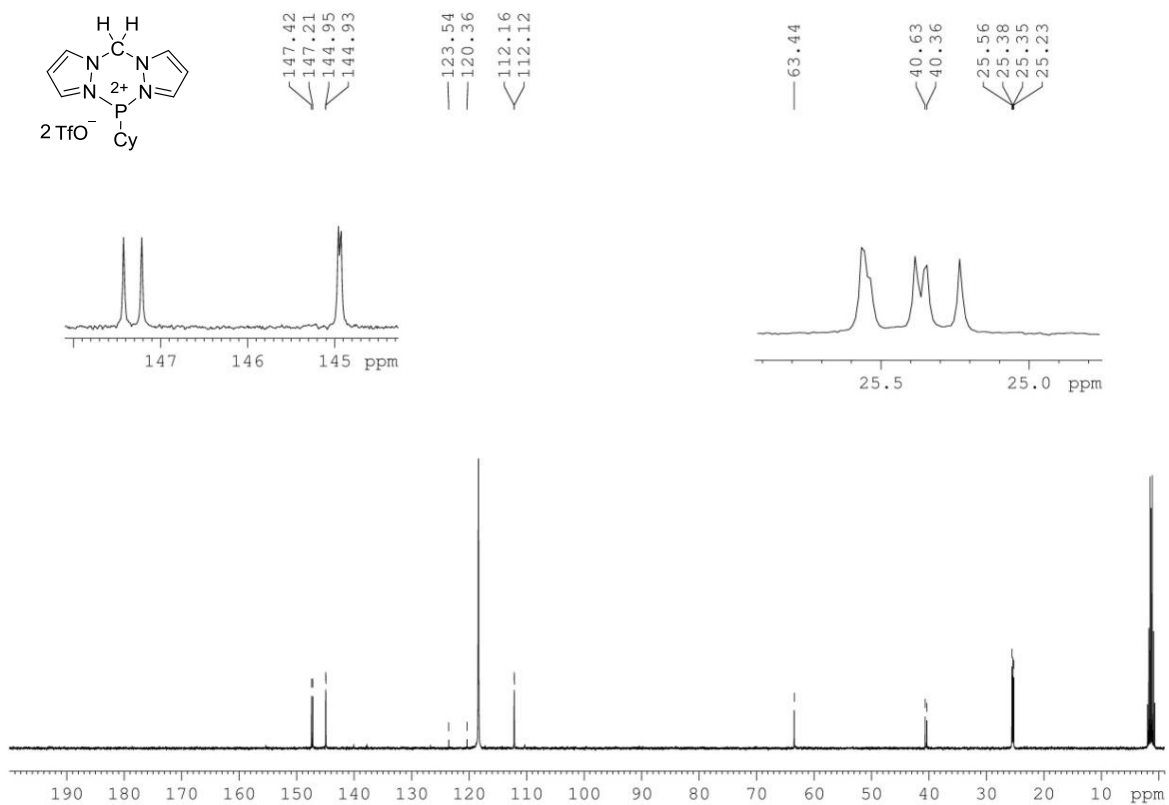
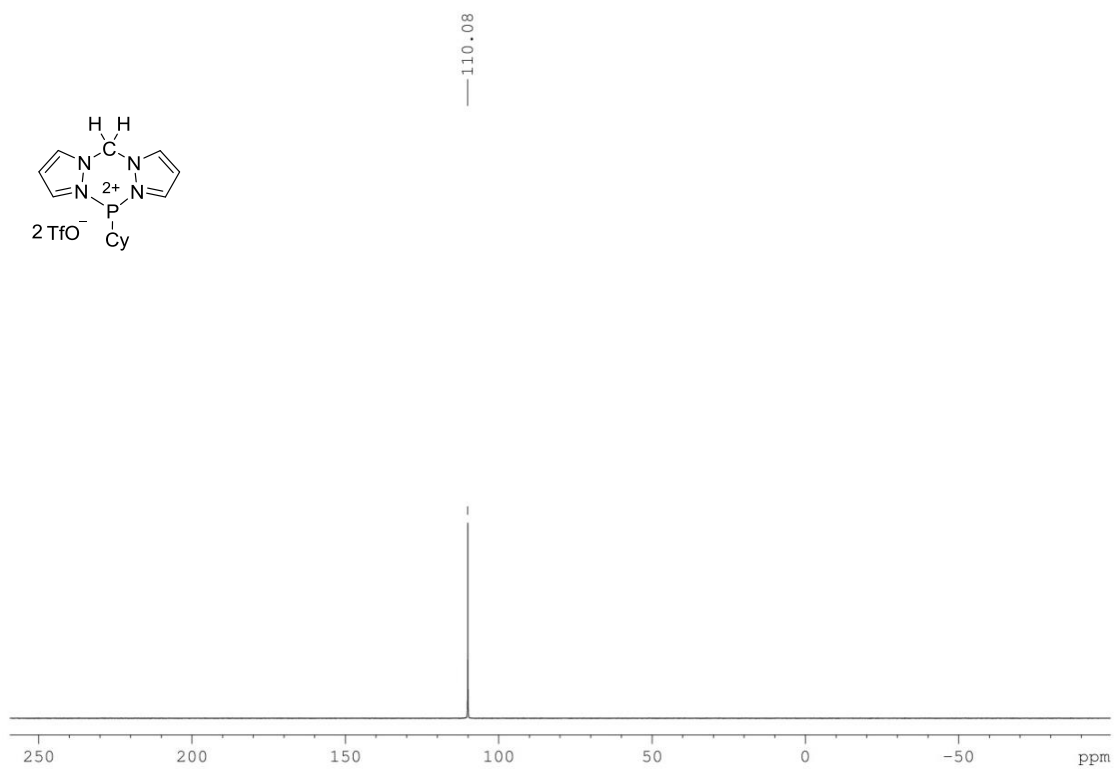
^1H NMR (CD₃CN, 400 MHz) (Compound 64) **^{13}C NMR (CD₃CN, 100 MHz) (Compound 64)**

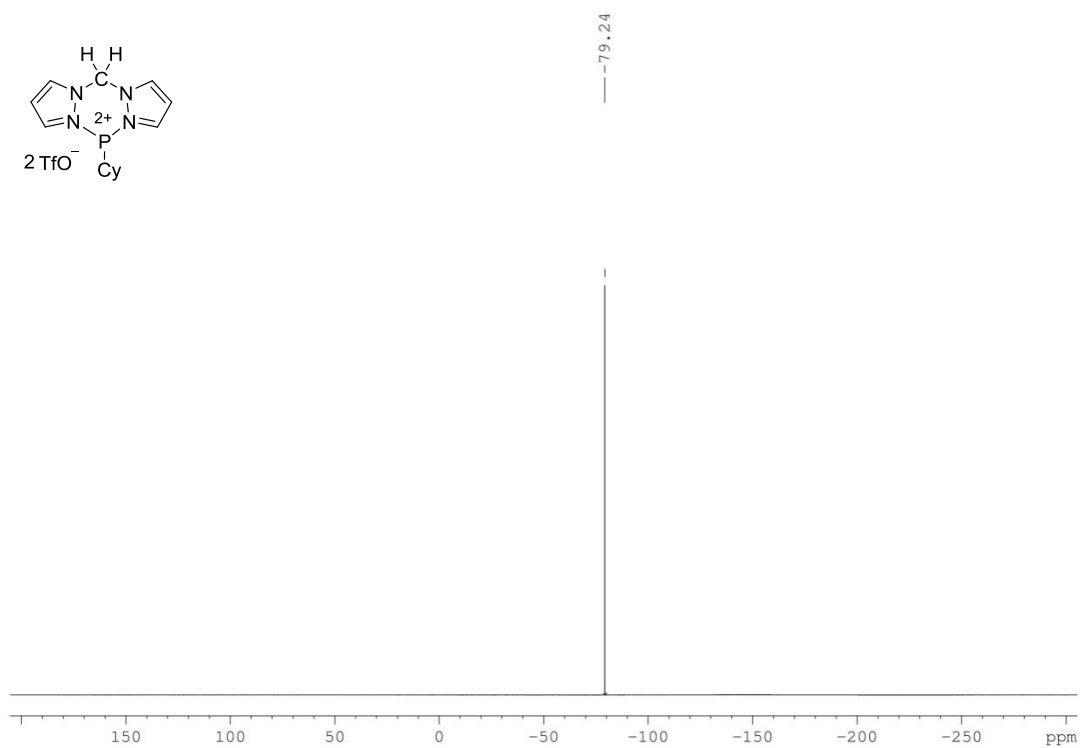
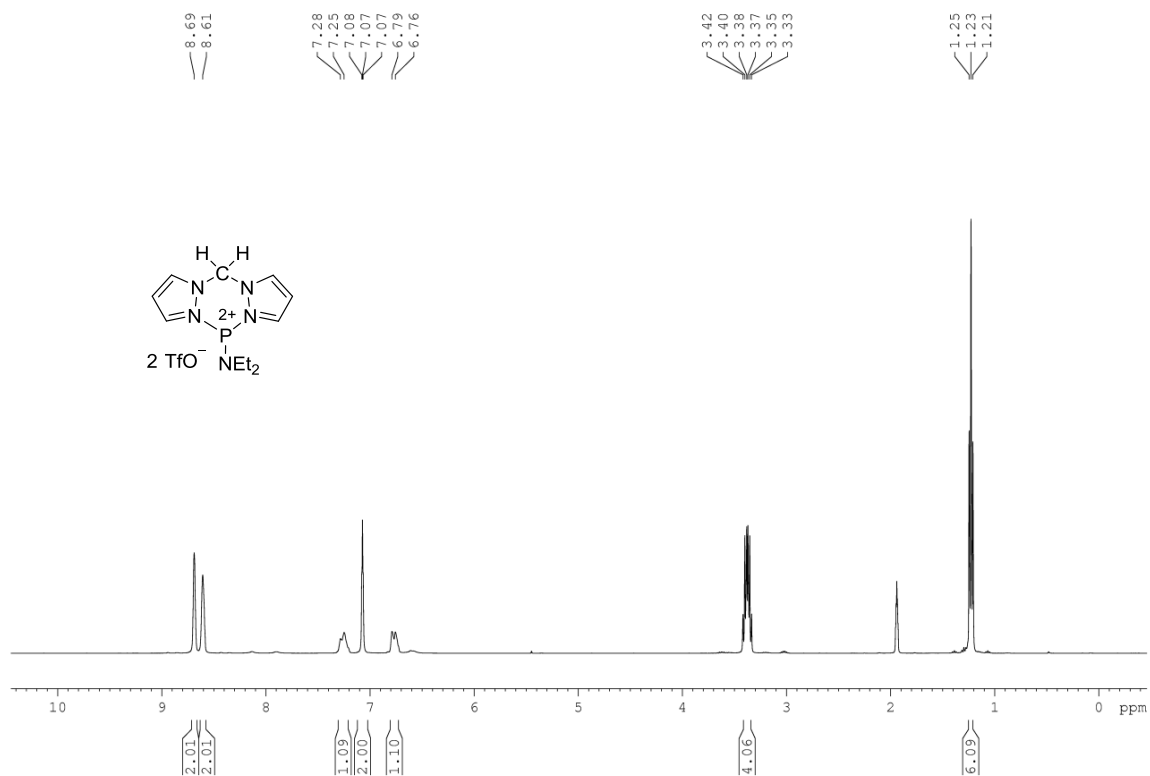
^{31}P NMR (CD₃CN, 162 MHz) (Compound 64) **^{11}B NMR (CD₃CN, 128 MHz) (Compound 64)**

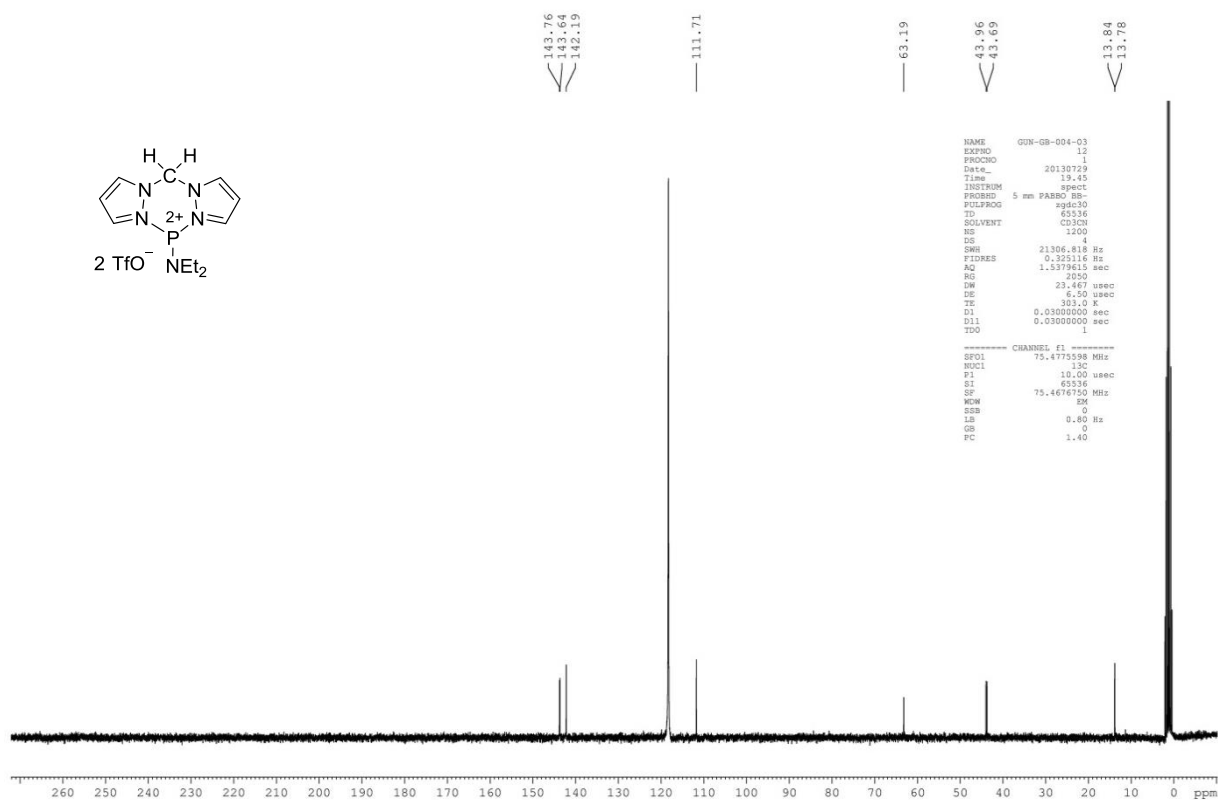
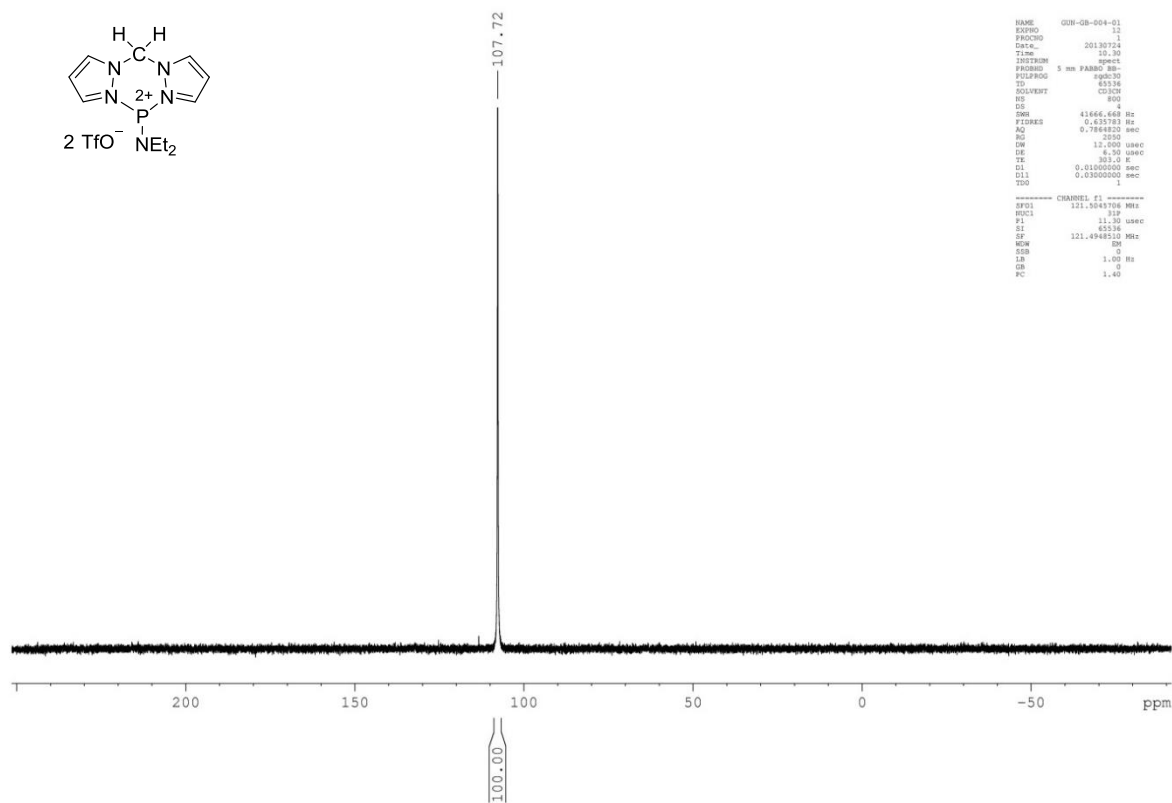
^{19}F NMR (CD_3CN , 282 MHz) (Compound 64) **^1H NMR (CD_3CN , 400 MHz) (Compound 67)**

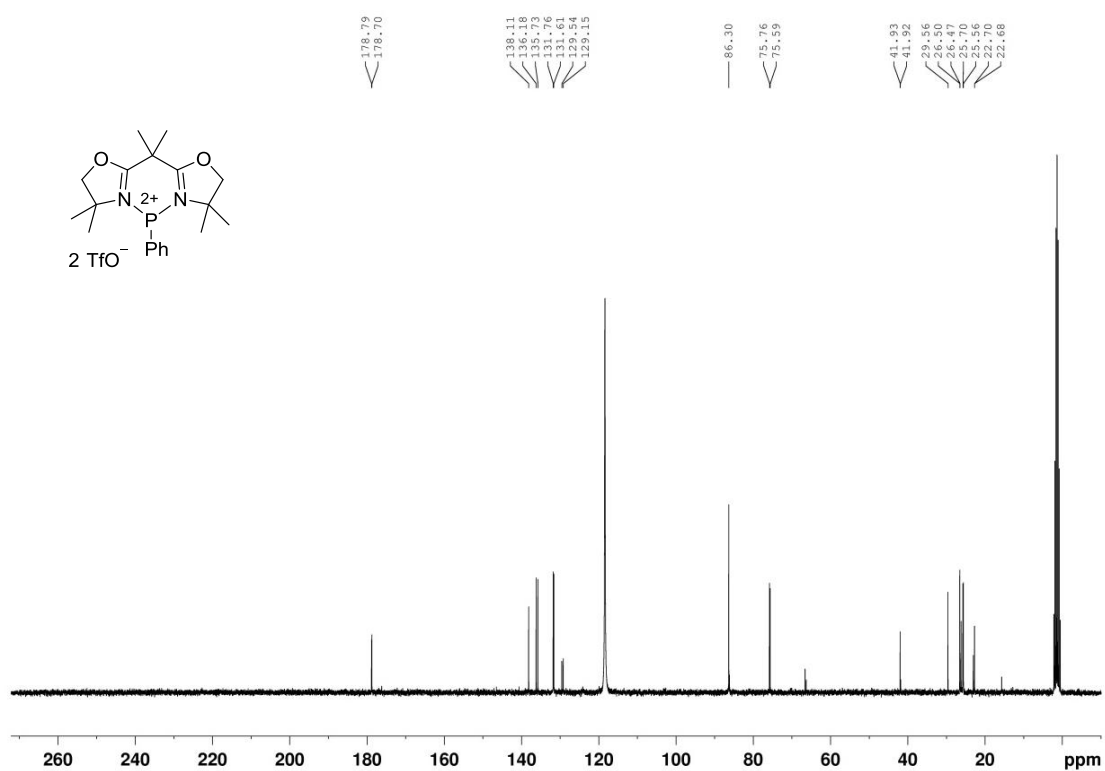
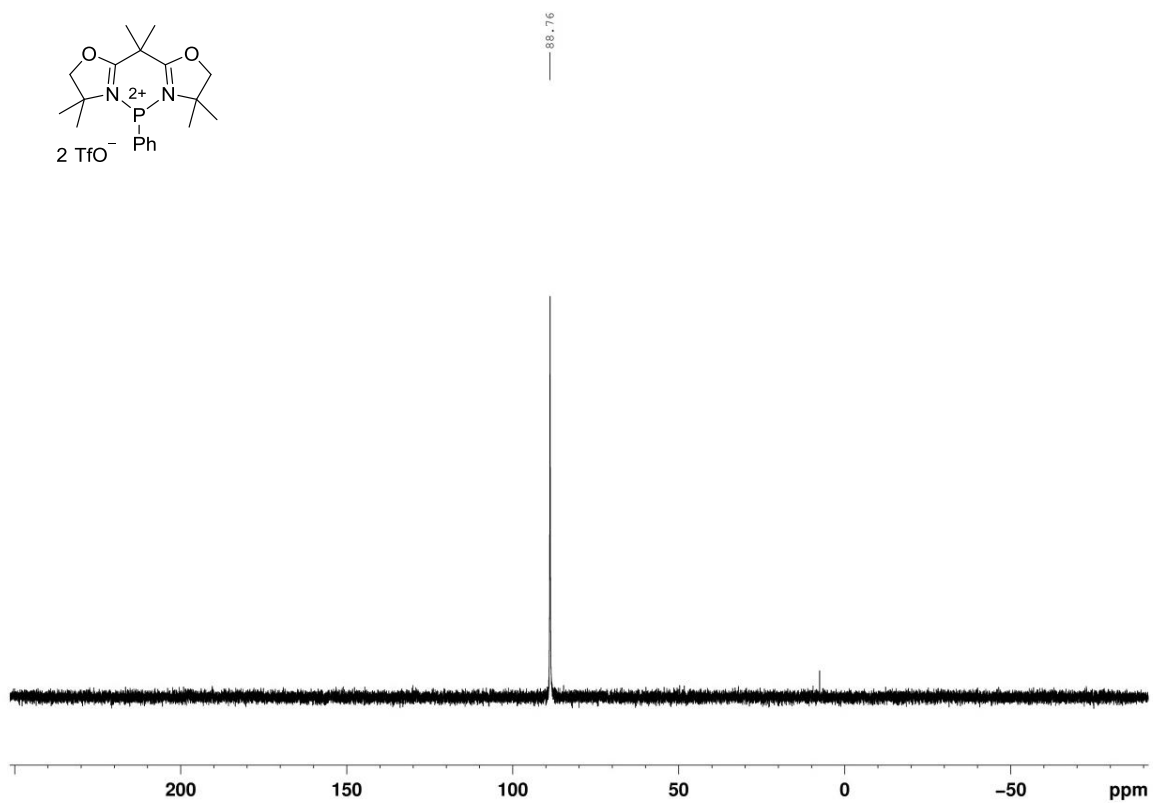
^{13}C NMR (CD₃CN, 100 MHz) (Compound 67) **^{31}P NMR (CD₃CN, 162 MHz) (Compound 67)**

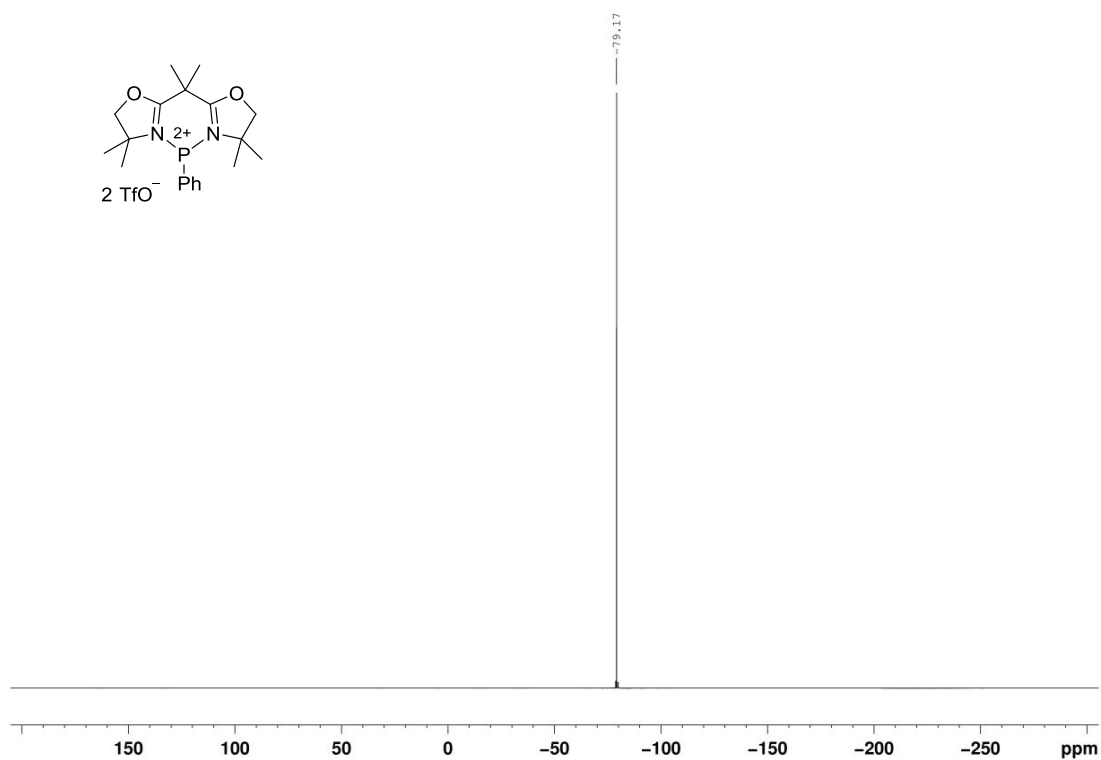
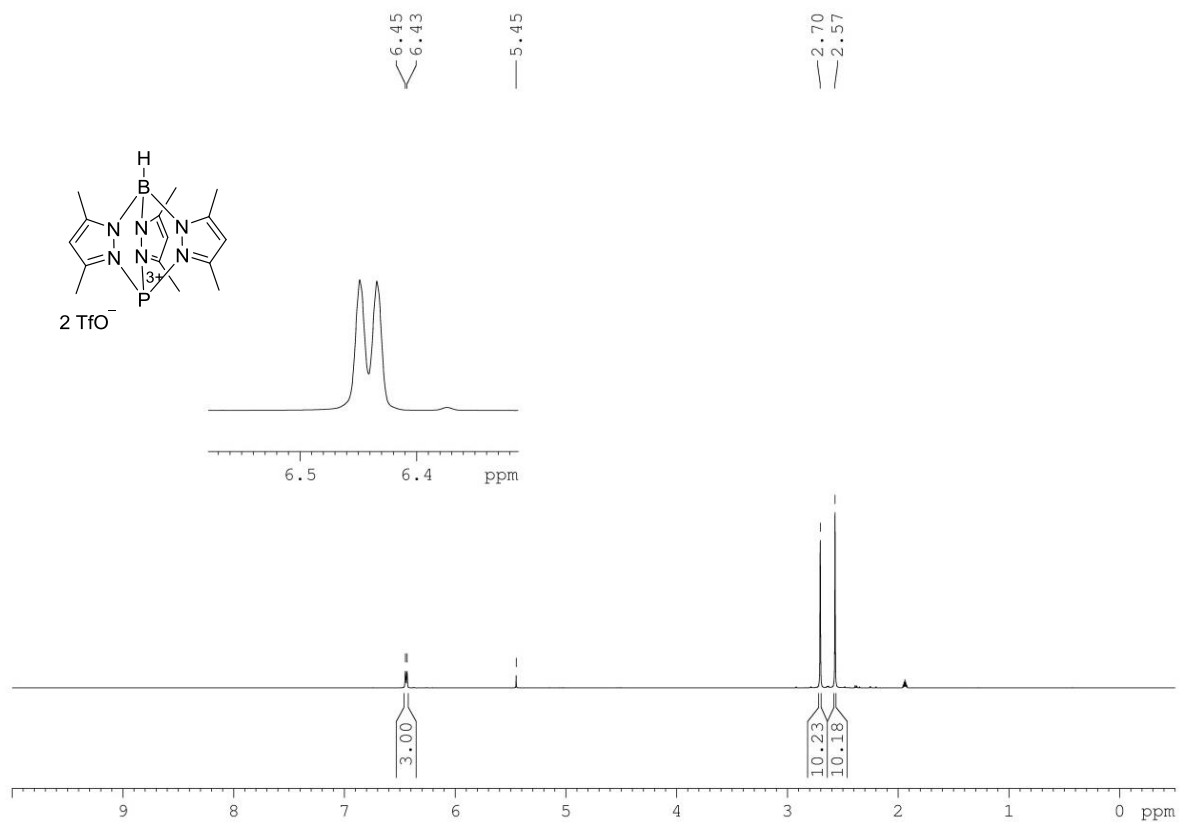
^{19}F NMR (CD_3CN , 282 MHz) (Compound 67) **^1H NMR (CD_3CN , 400 MHz) (Compound 68)**

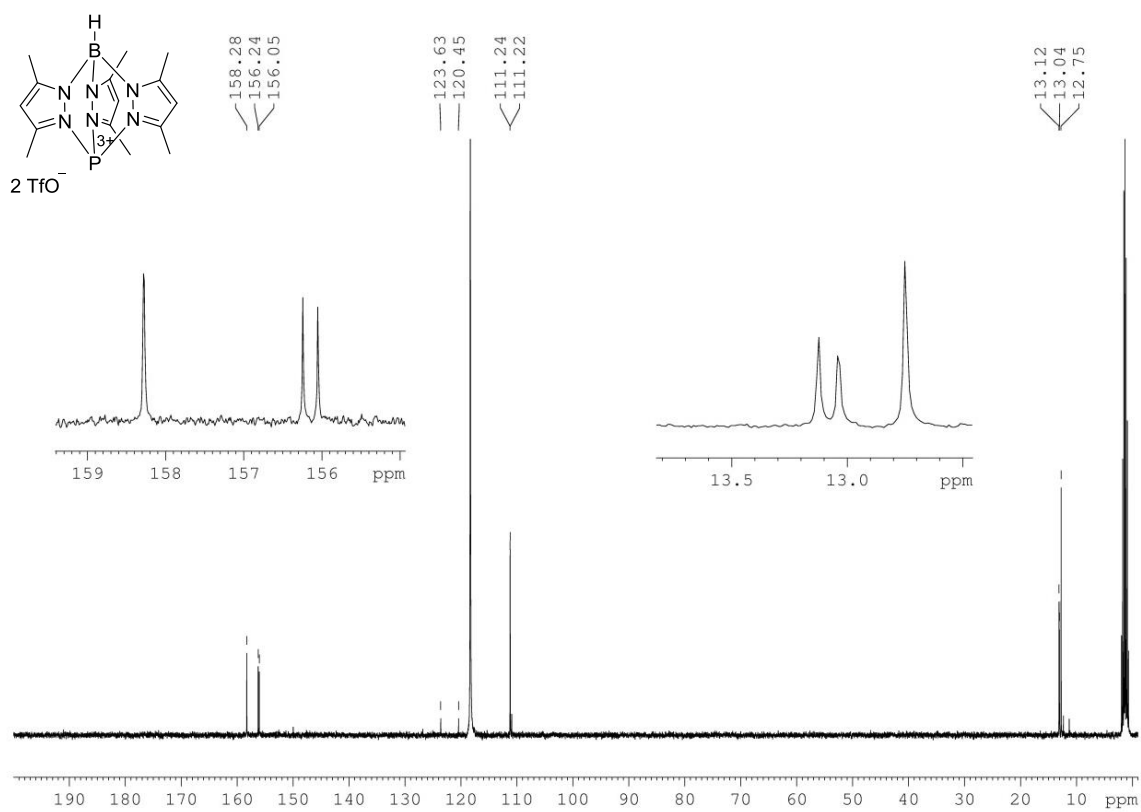
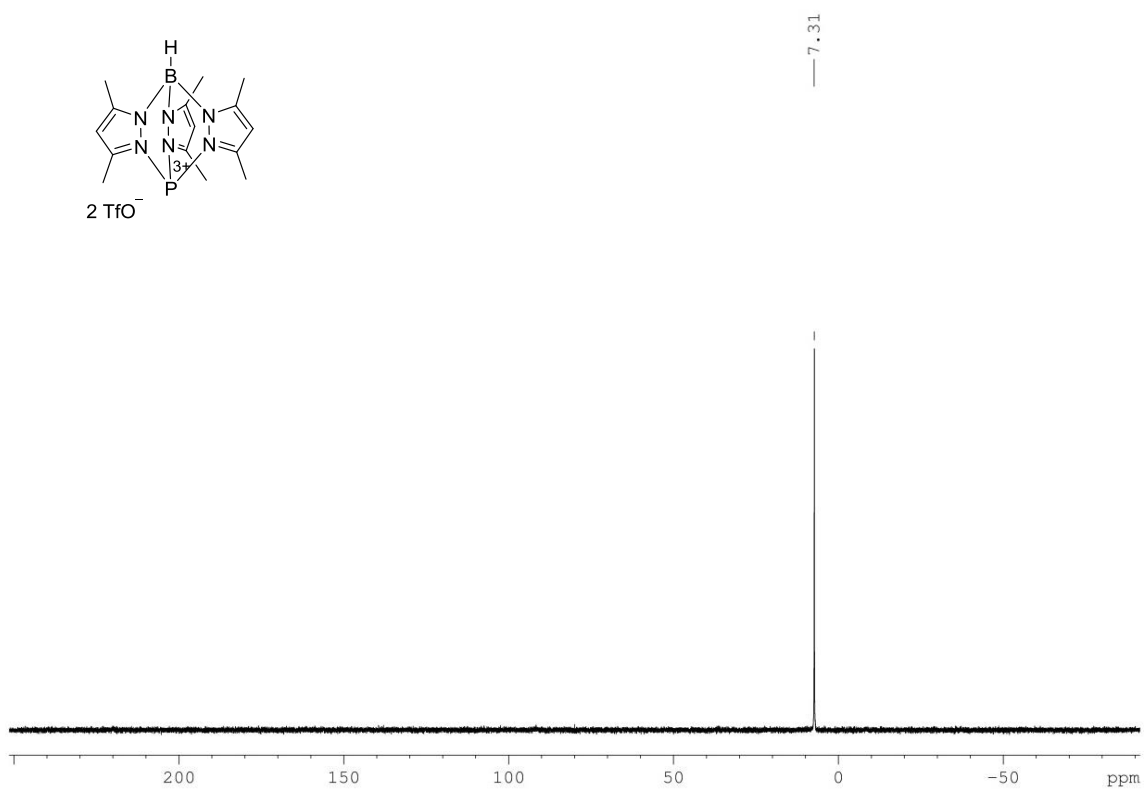
^{13}C NMR (CD₃CN, 100 MHz) (Compound 68) **^{31}P NMR (CD₃CN, 162 MHz) (Compound 68)**

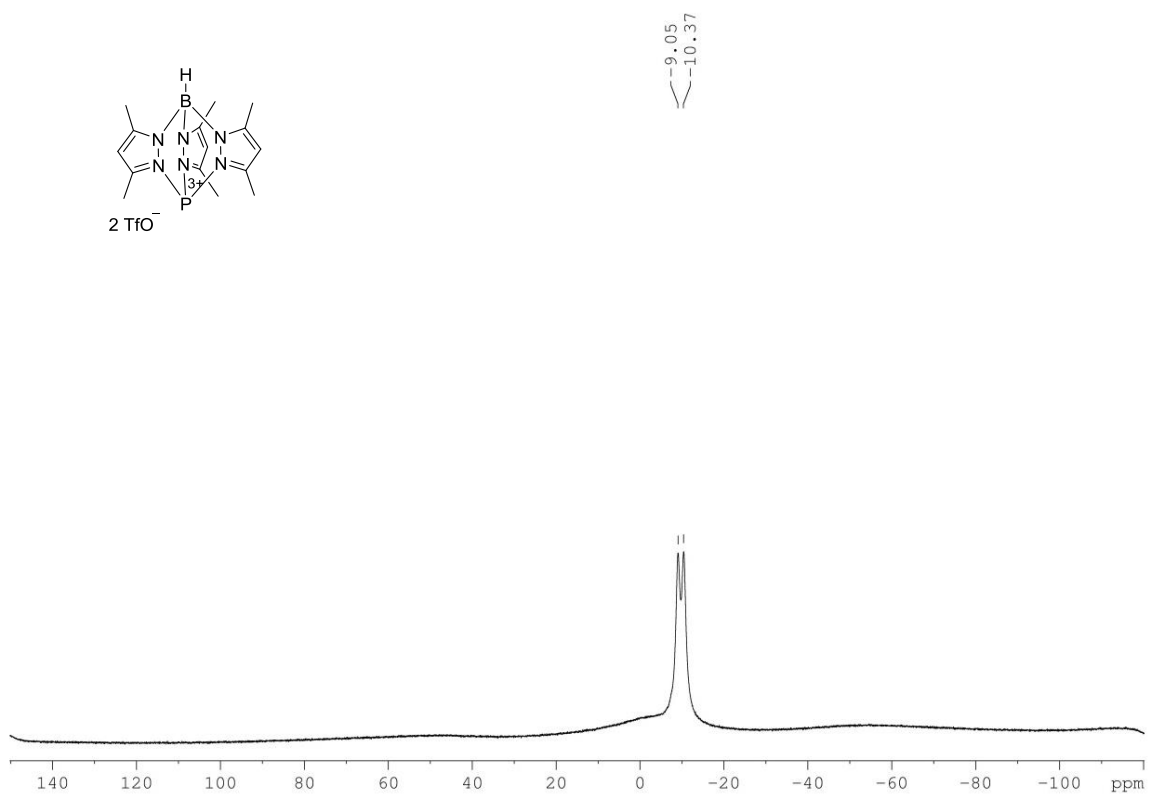
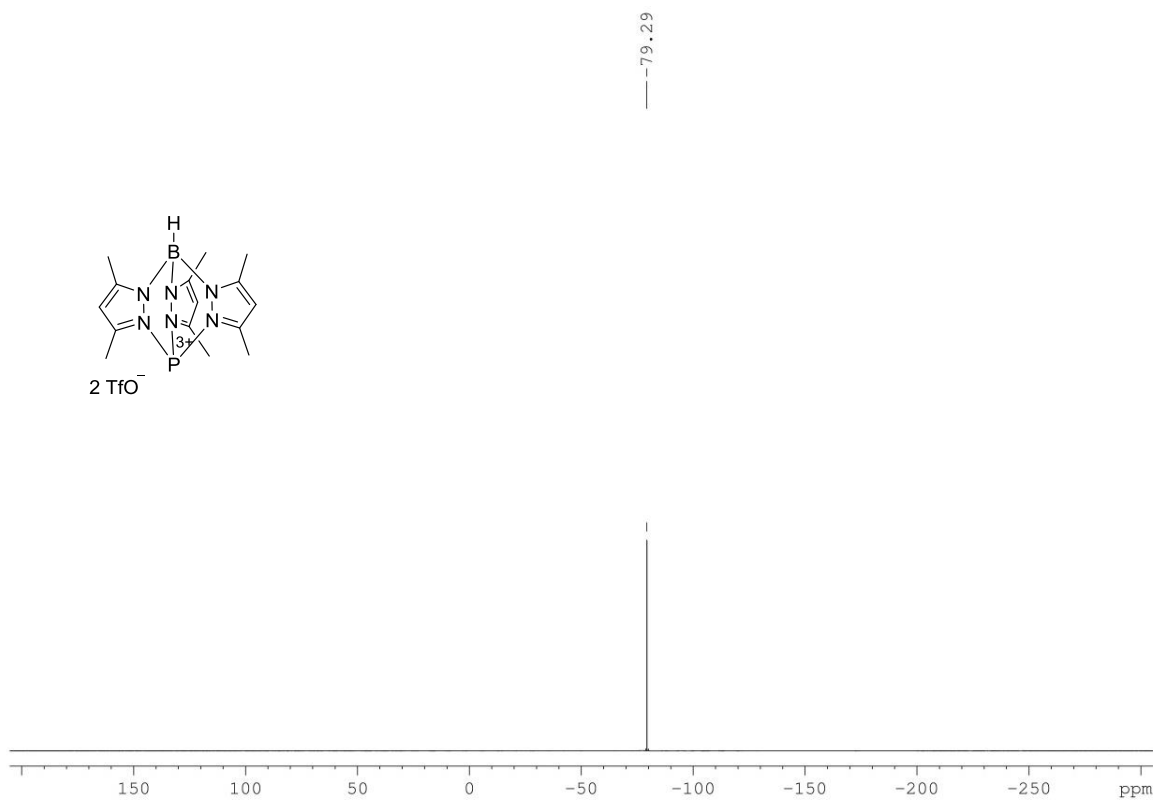
^{19}F NMR (CD_3CN , 282 MHz) (Compound 68) **^1H NMR (CD_3CN , 300 MHz) (Compound 69)**

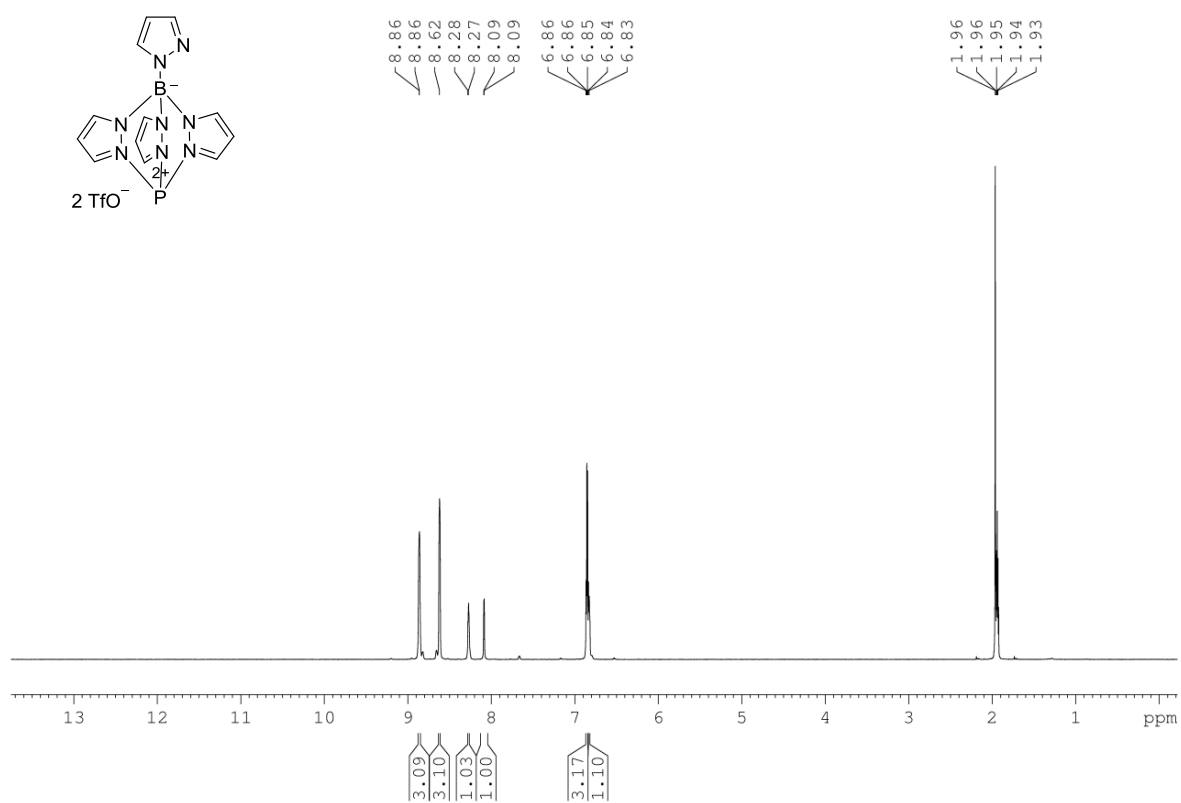
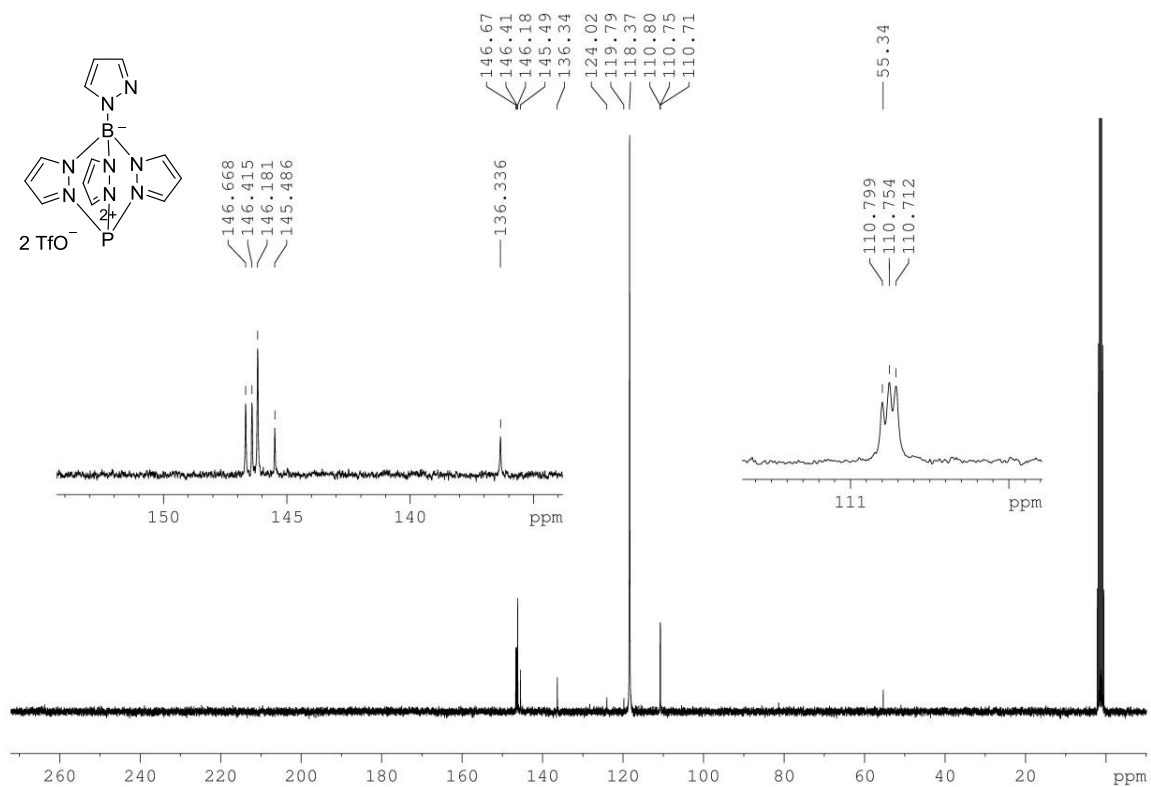
^{13}C NMR (CD₃CN, 75 MHz) (Compound 69) **^{31}P NMR (CD₃CN, 121 MHz) (Compound 69)**

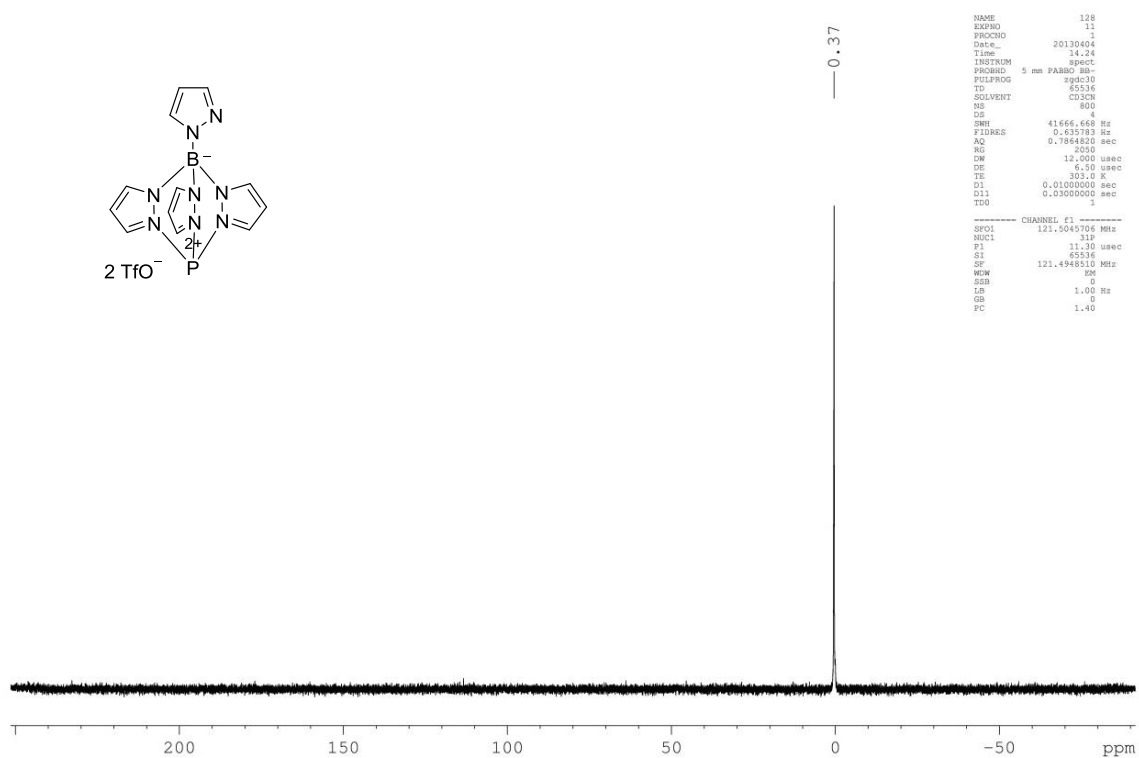
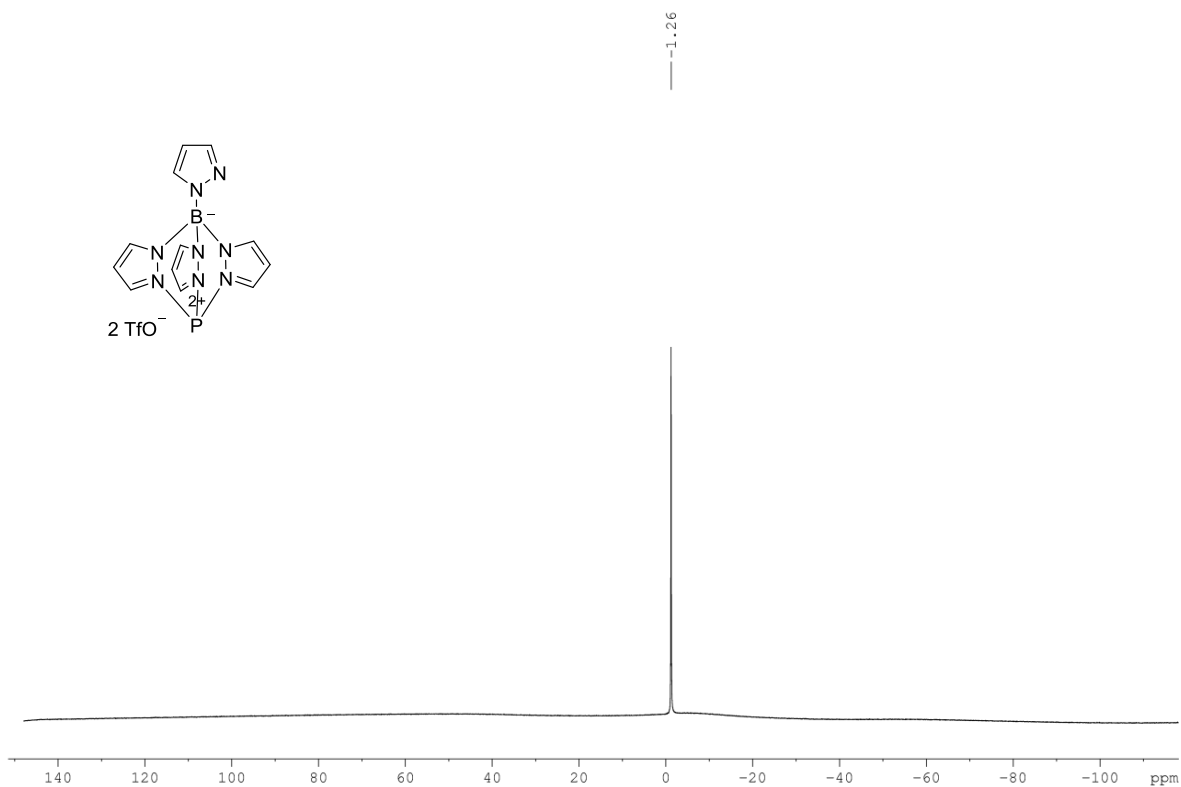
^{13}C NMR (CD₃CN, 100 MHz) (Compound 73) **^{31}P NMR (CD₃CN, 162 MHz) (Compound 73)**

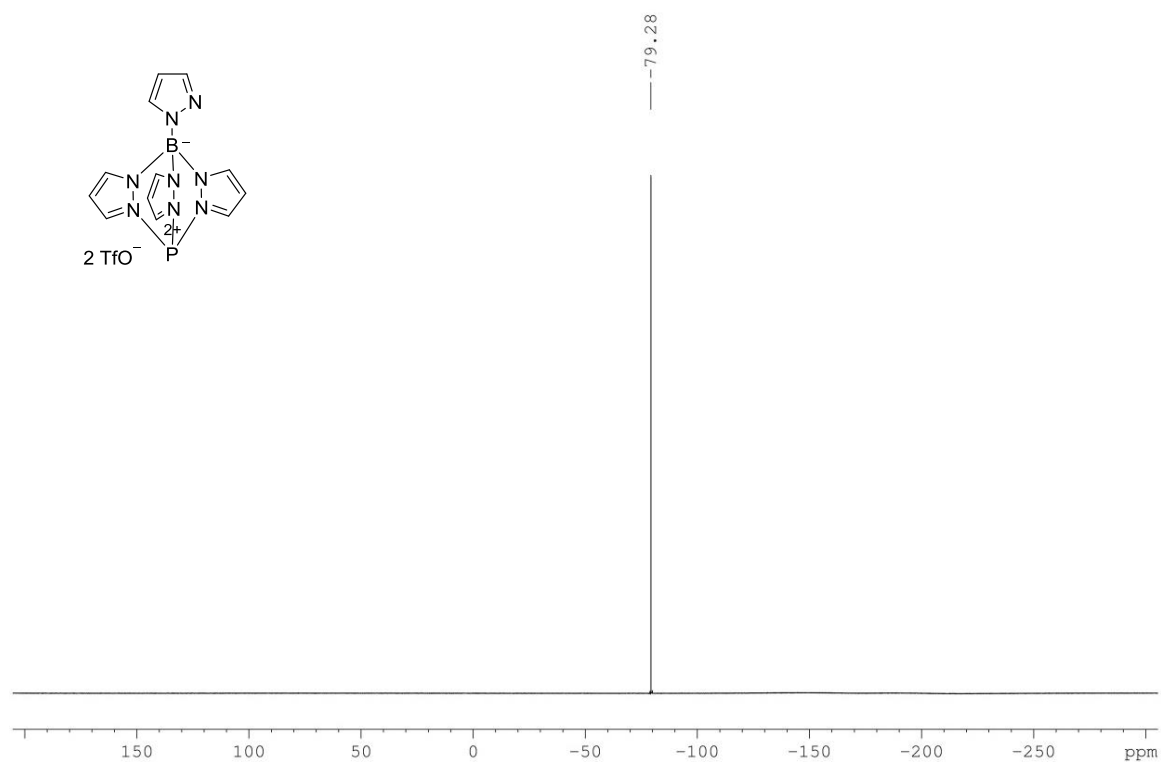
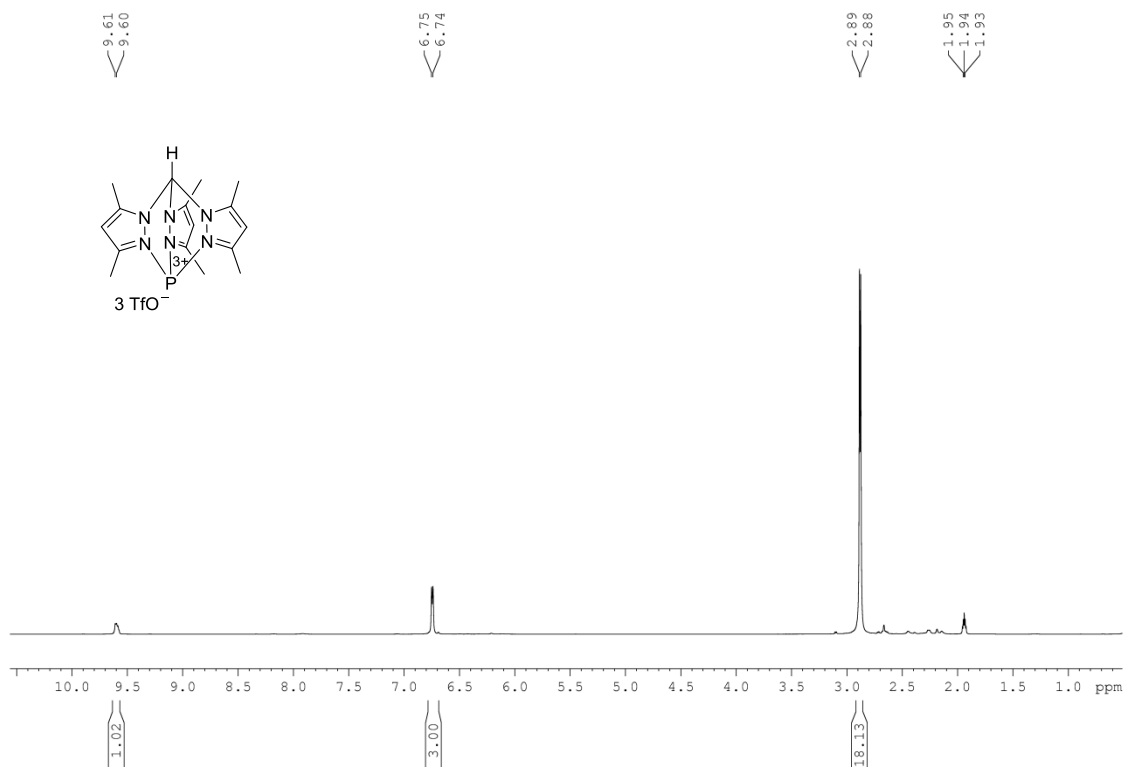
^{19}F NMR (CD_3CN , 282 MHz) (Compound 73) **^1H NMR (CD_3CN , 400 MHz) (Compound 76)**

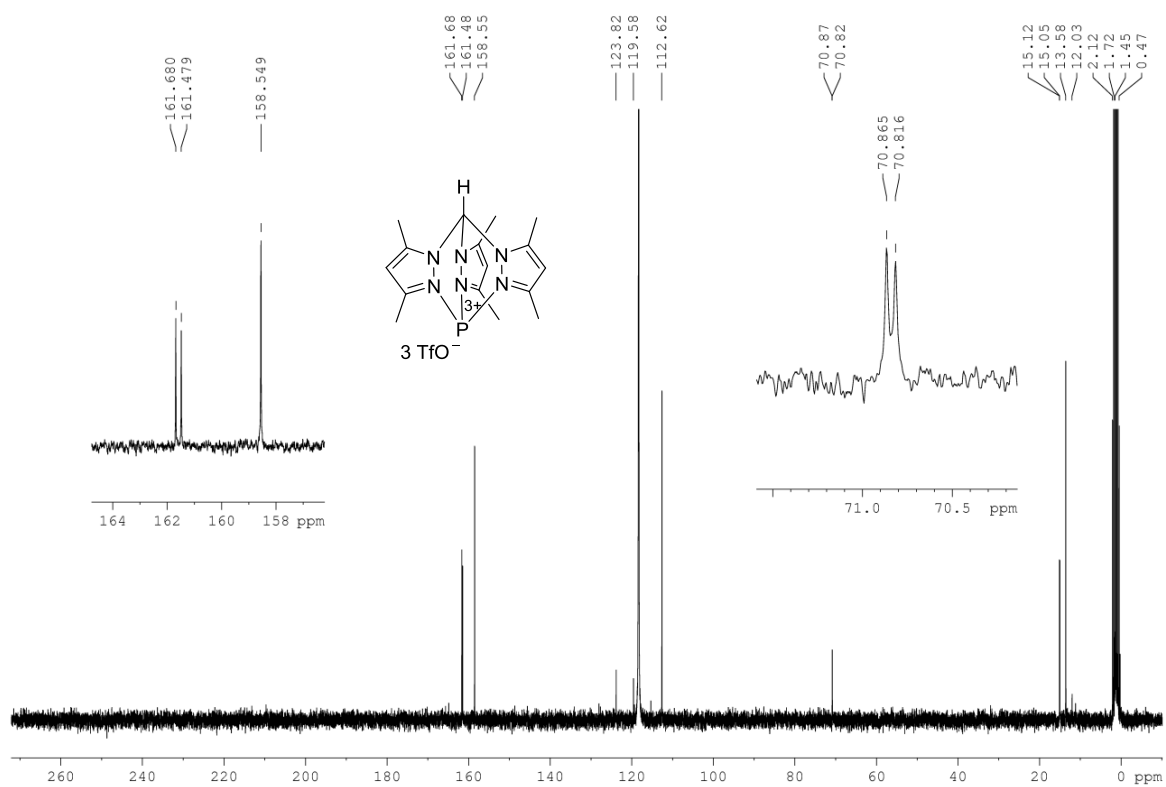
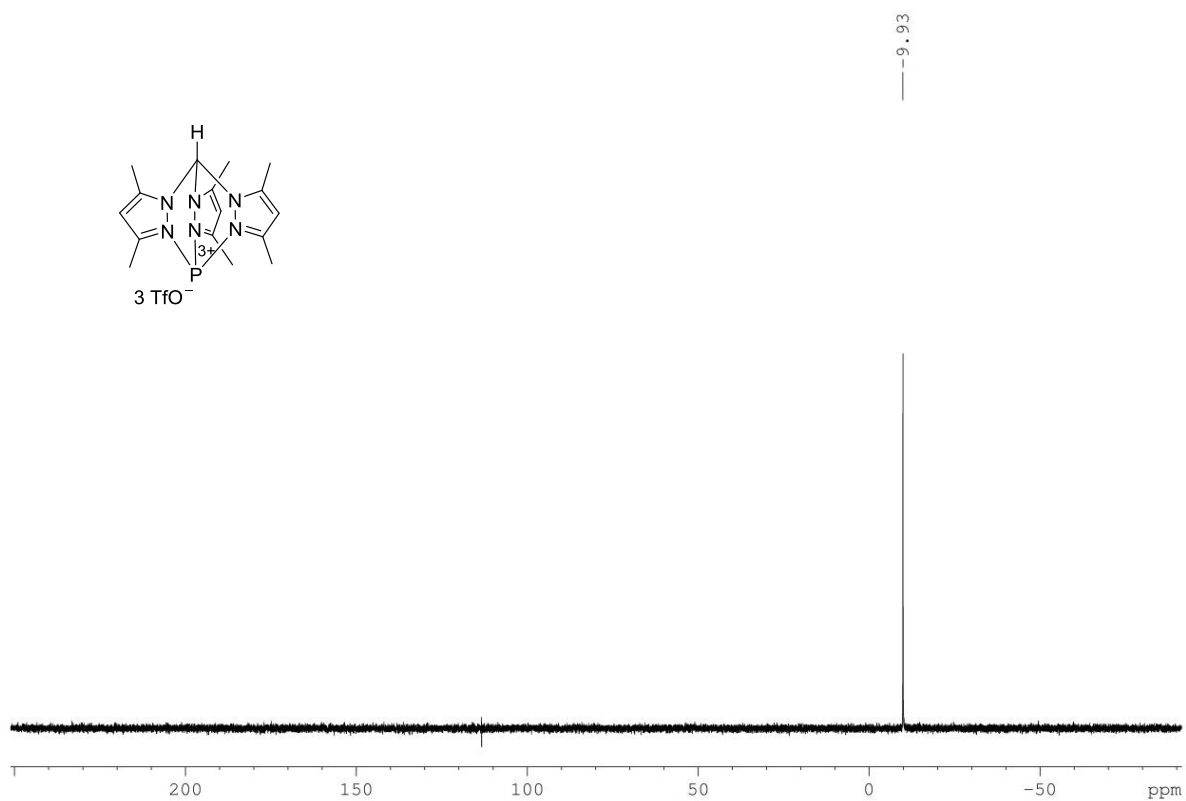
^{13}C NMR (CD₃CN, 100 MHz) (Compound 76) **^{31}P NMR (CD₃CN, 162 MHz) (Compound 76)**

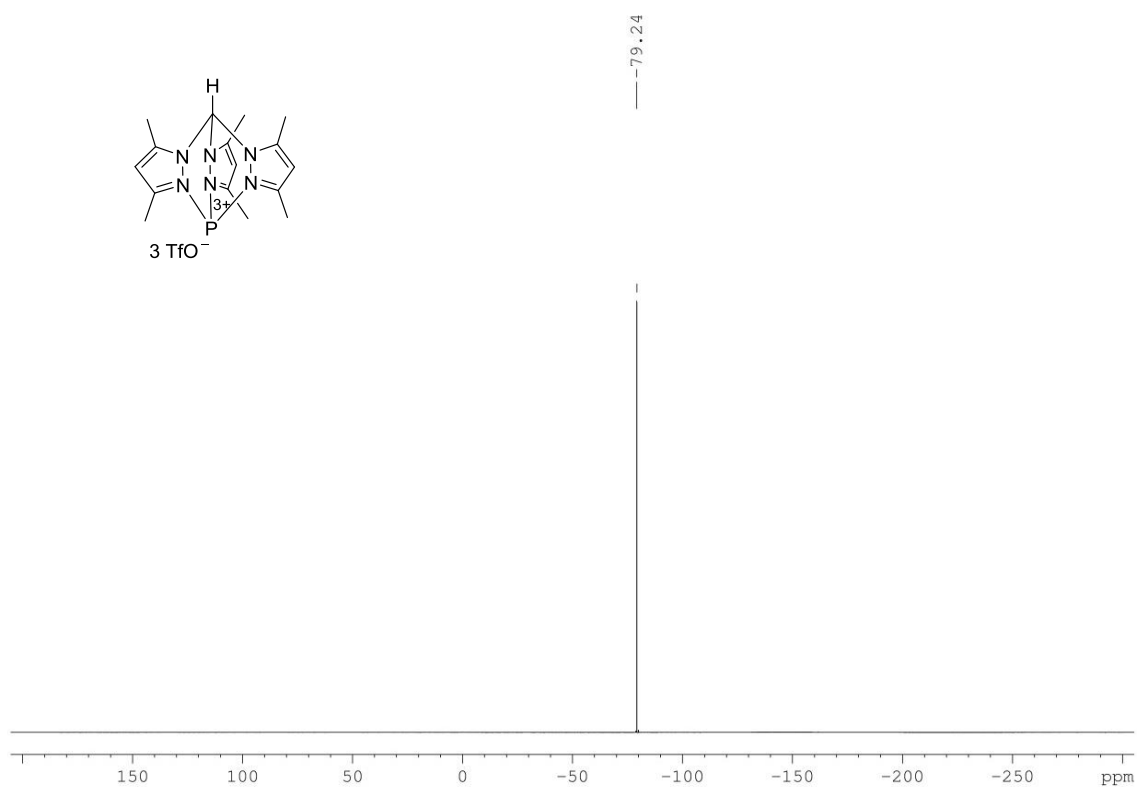
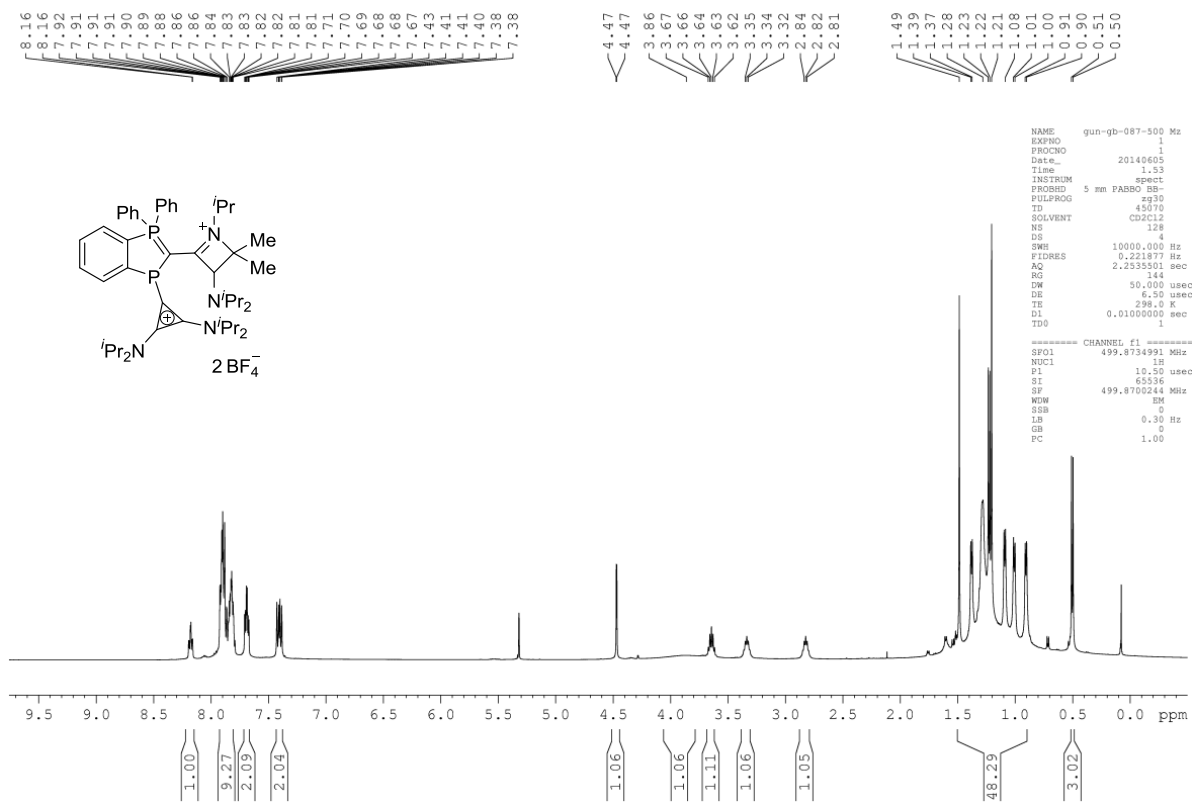
^{11}B NMR (CD_3CN , 128 MHz) (Compound 76) **^{19}F NMR (CD_3CN , 282 MHz) (Compound 76)**

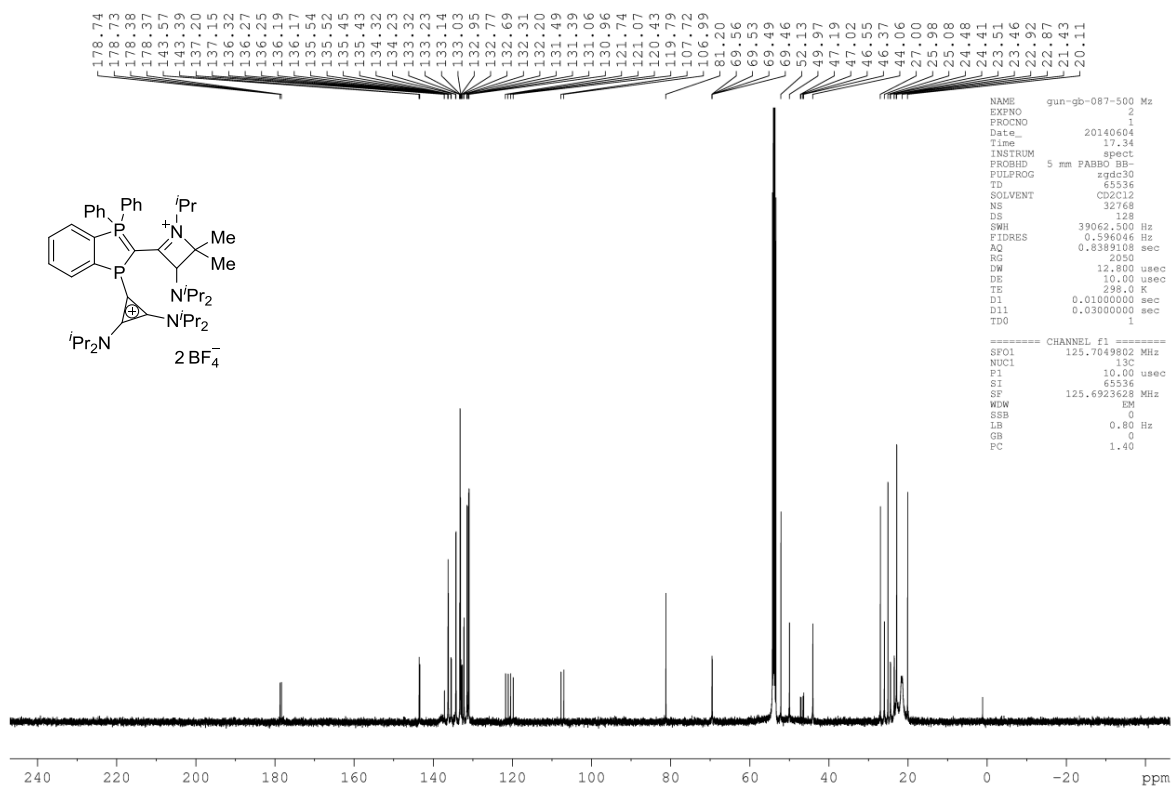
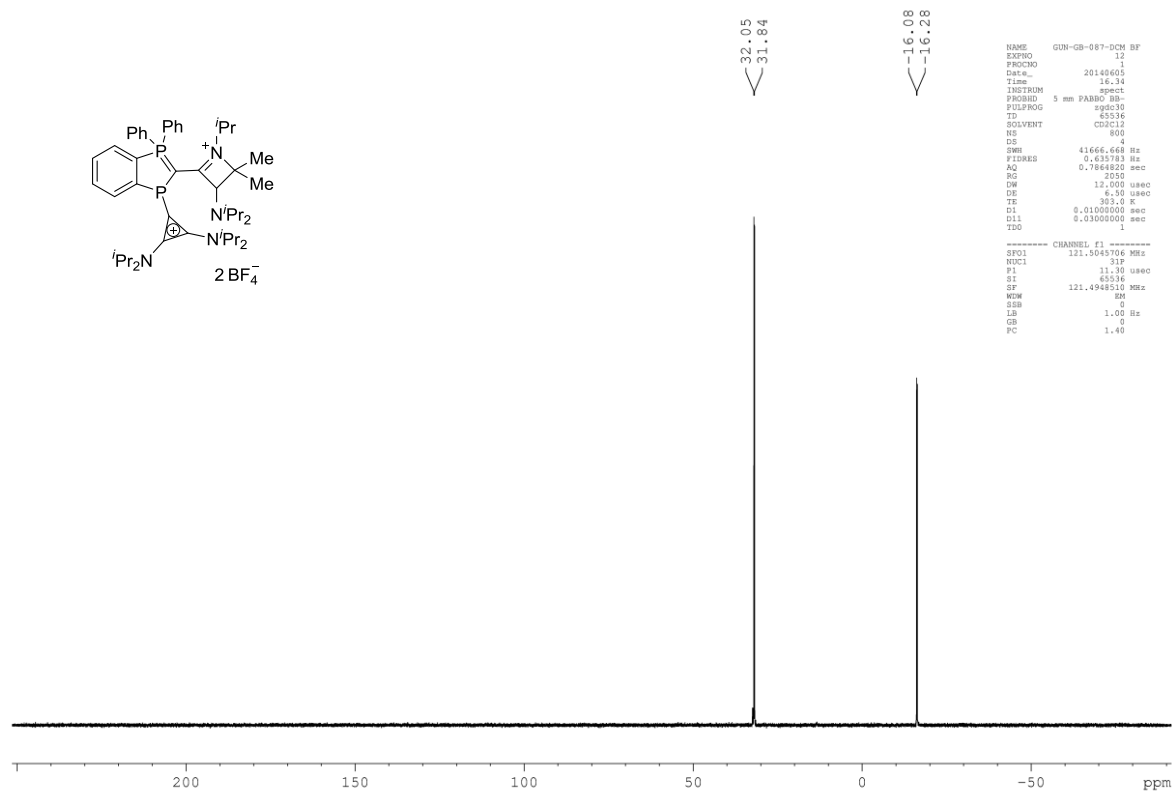
^1H NMR (CD₃CN, 300 MHz) (Compound 79) **^{13}C NMR (CD₃CN, 75 MHz) (Compound 79)**

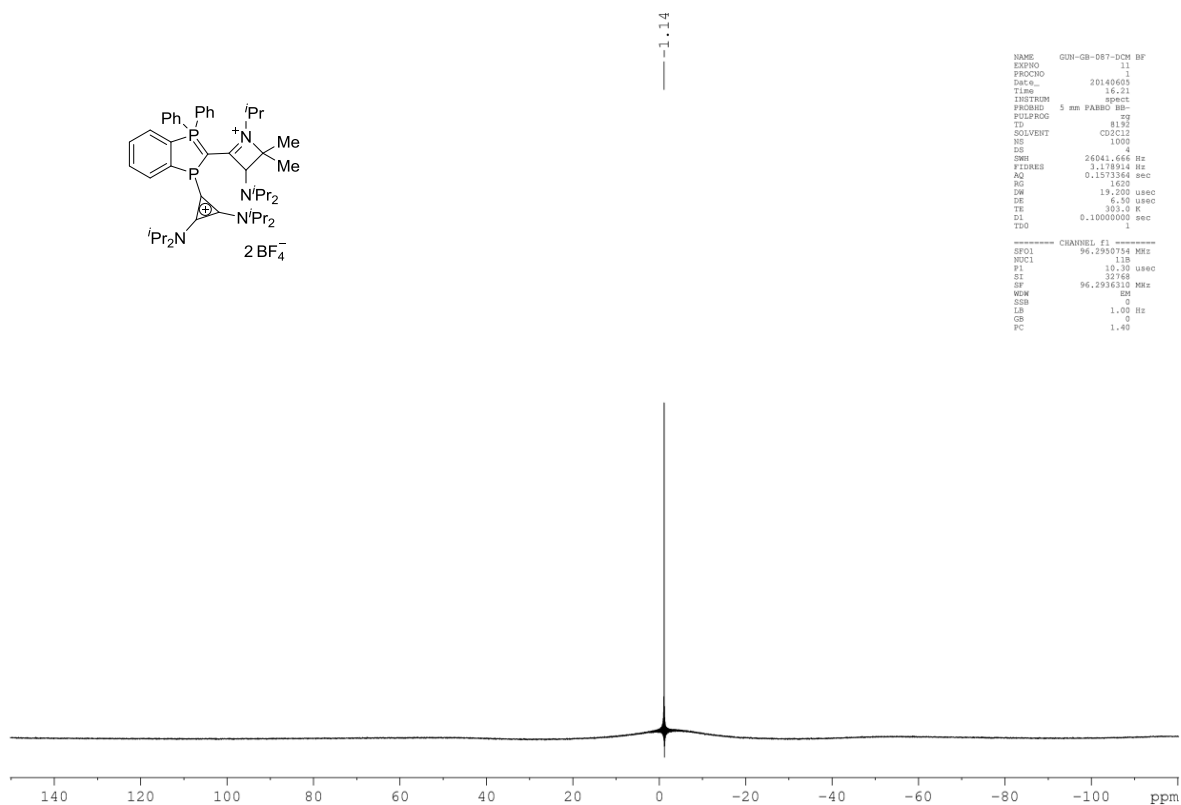
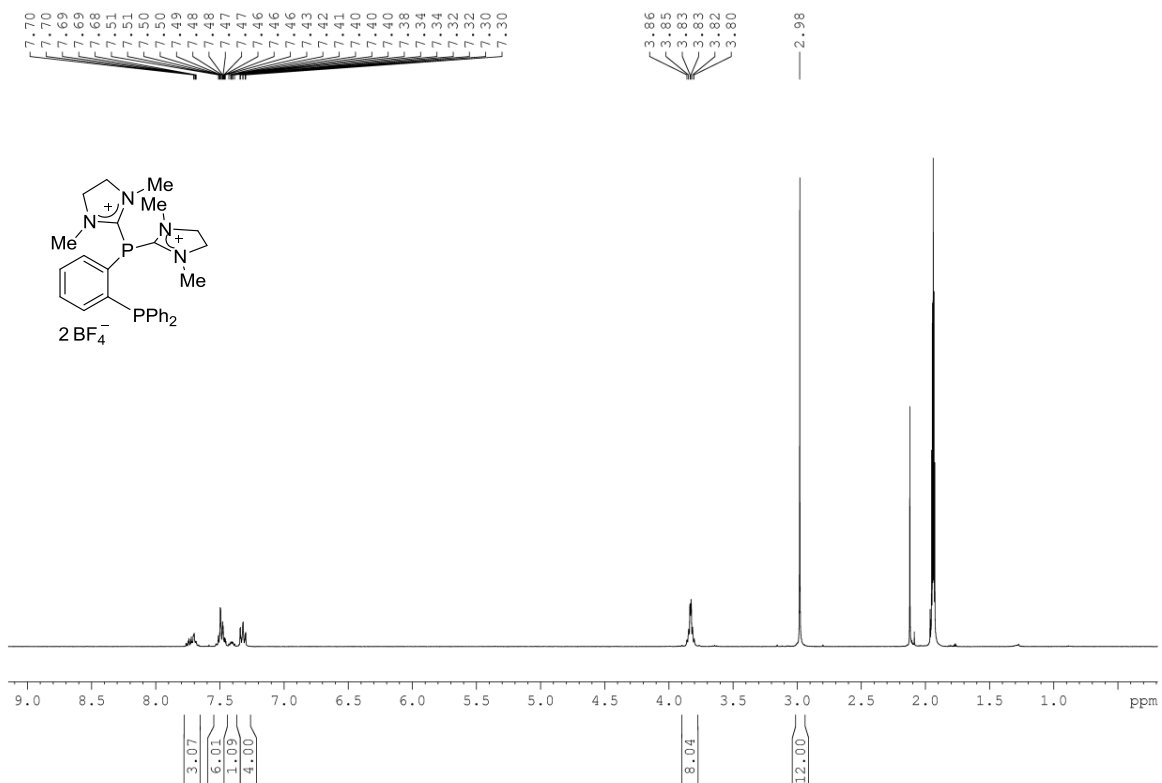
^{31}P NMR (CD₃CN, 121 MHz) (Compound 79) **^{11}B NMR (CD₃CN, 96 MHz) (Compound 79)**

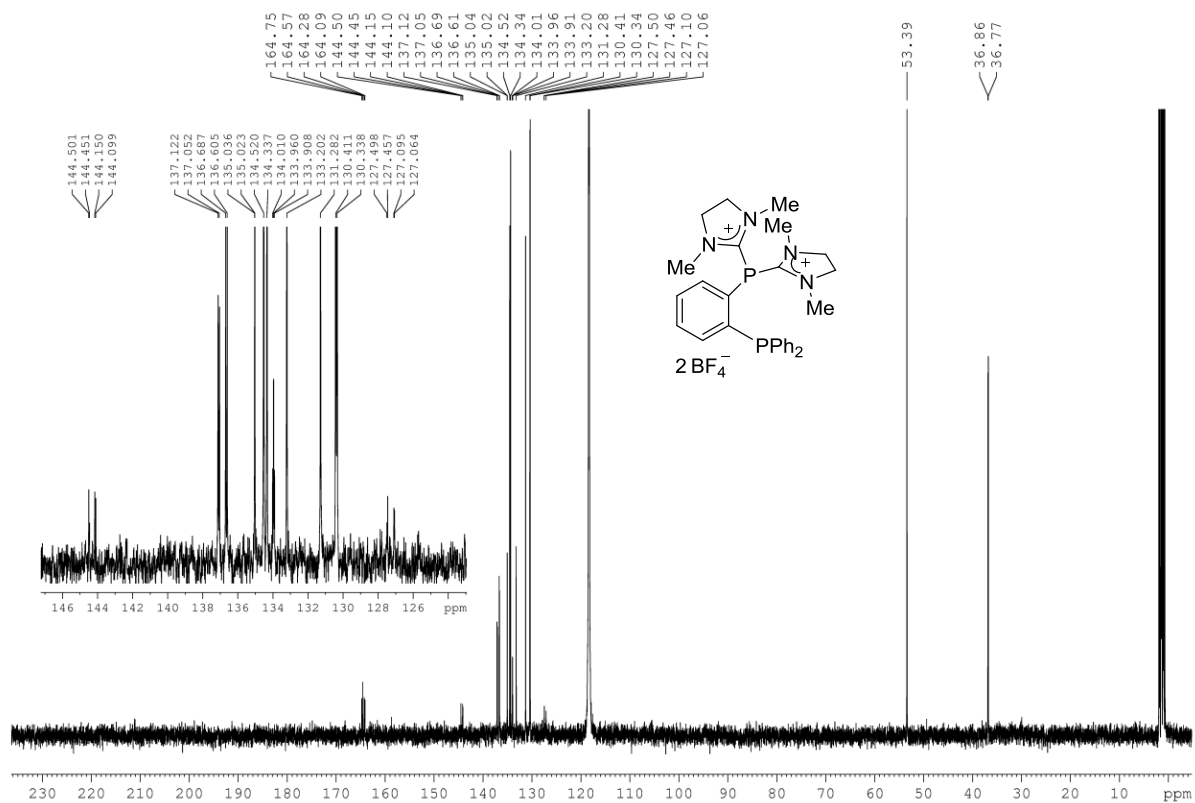
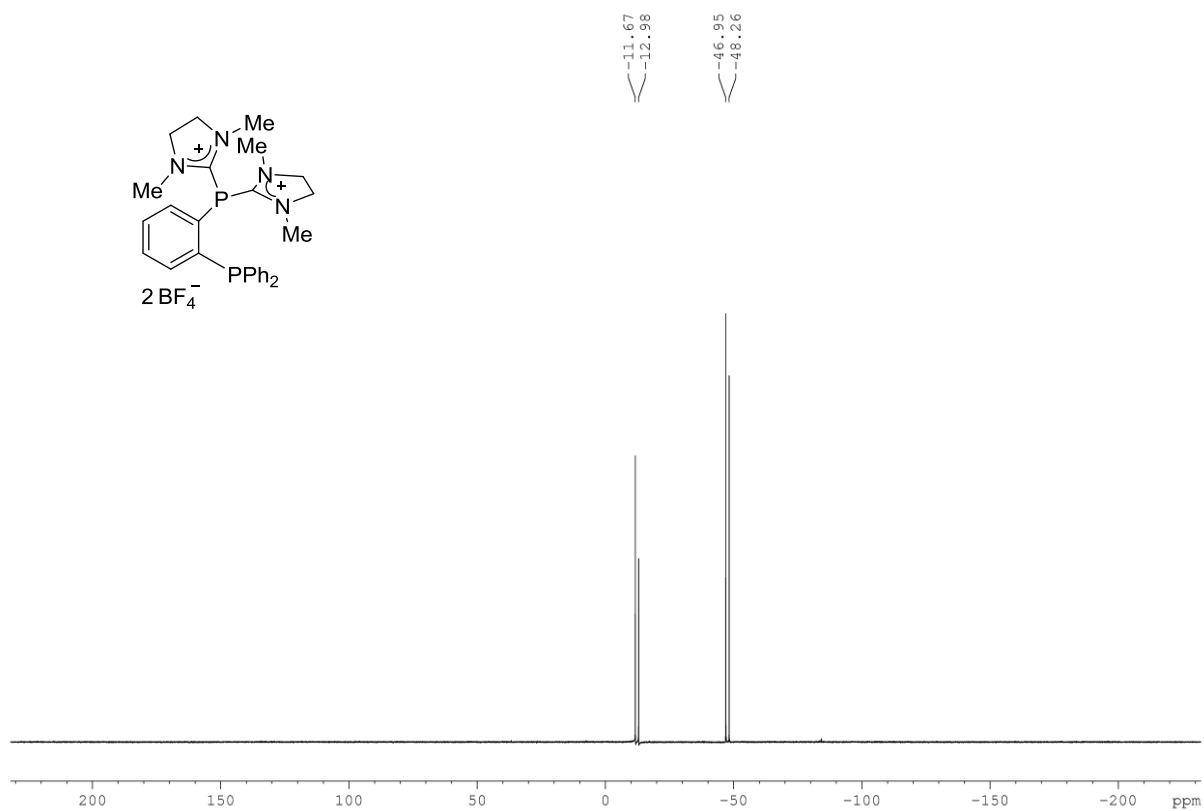
^{11}F NMR (CD₃CN, 282 MHz) (Compound 79) **^1H NMR (CD₃CN, 300 MHz) (Compound 82)**

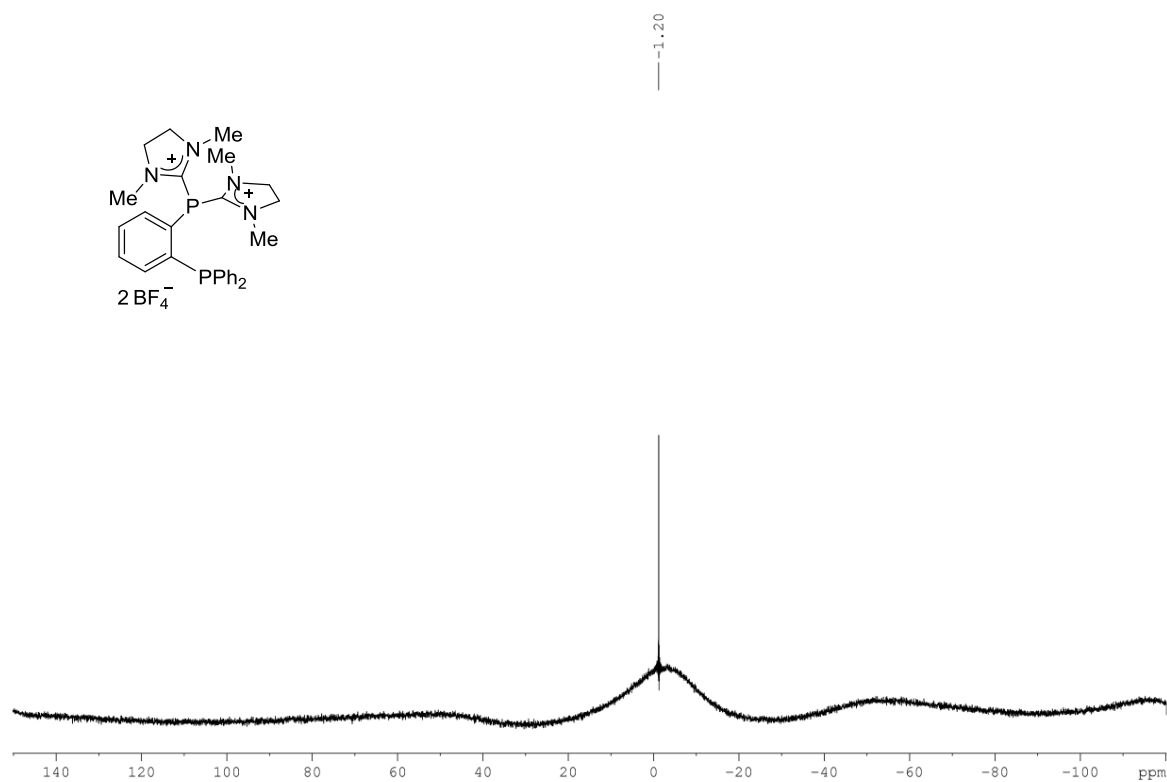
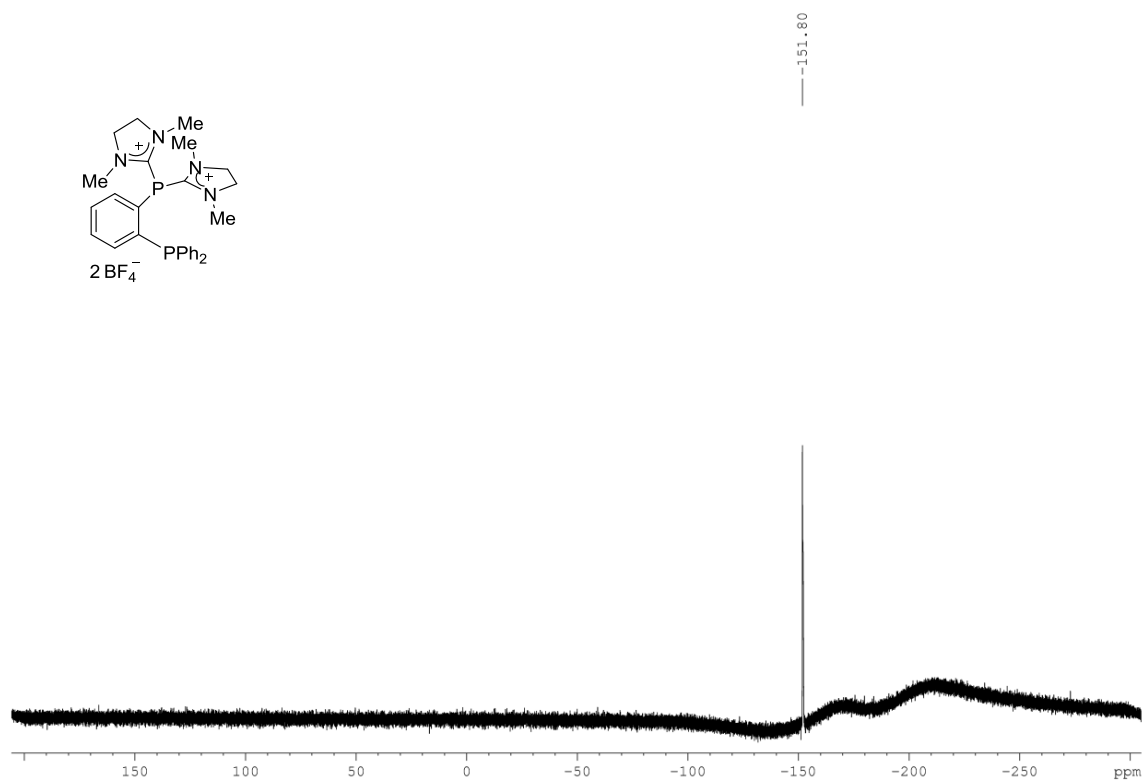
^{13}C NMR (CD₃CN, 100 MHz) (Compound 82) **^{31}P NMR (CD₃CN, 121 MHz) (Compound 82)**

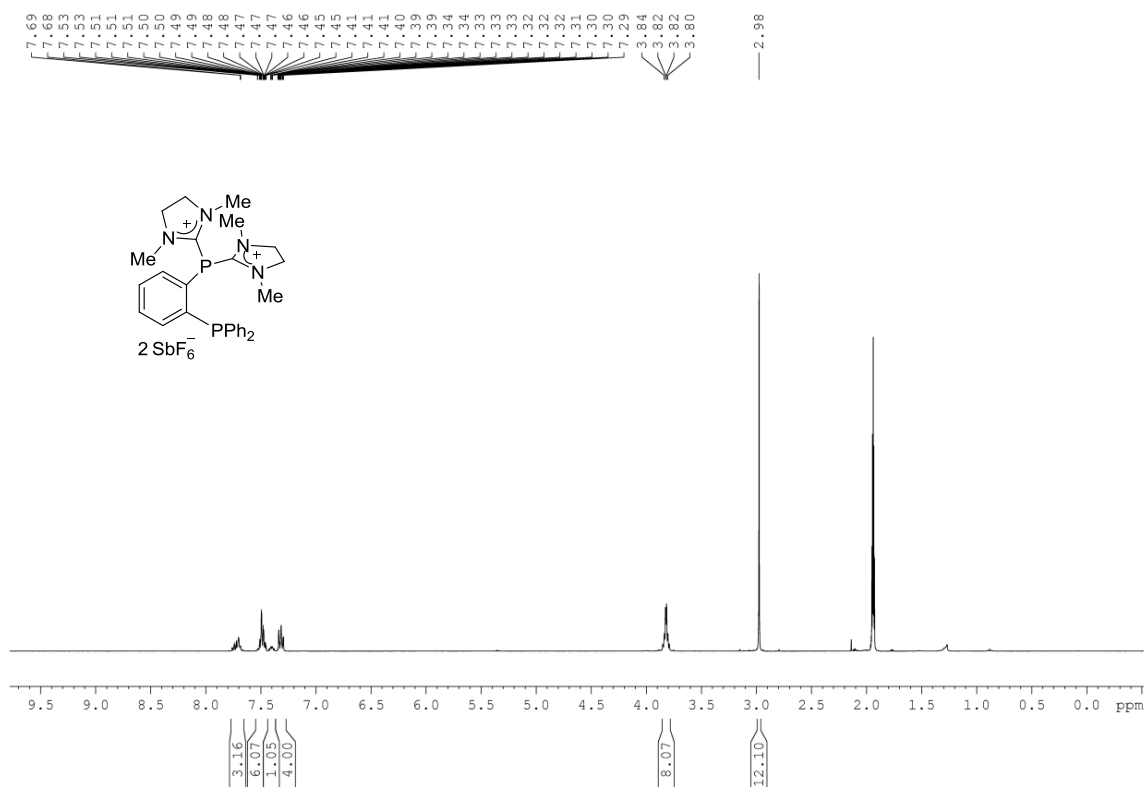
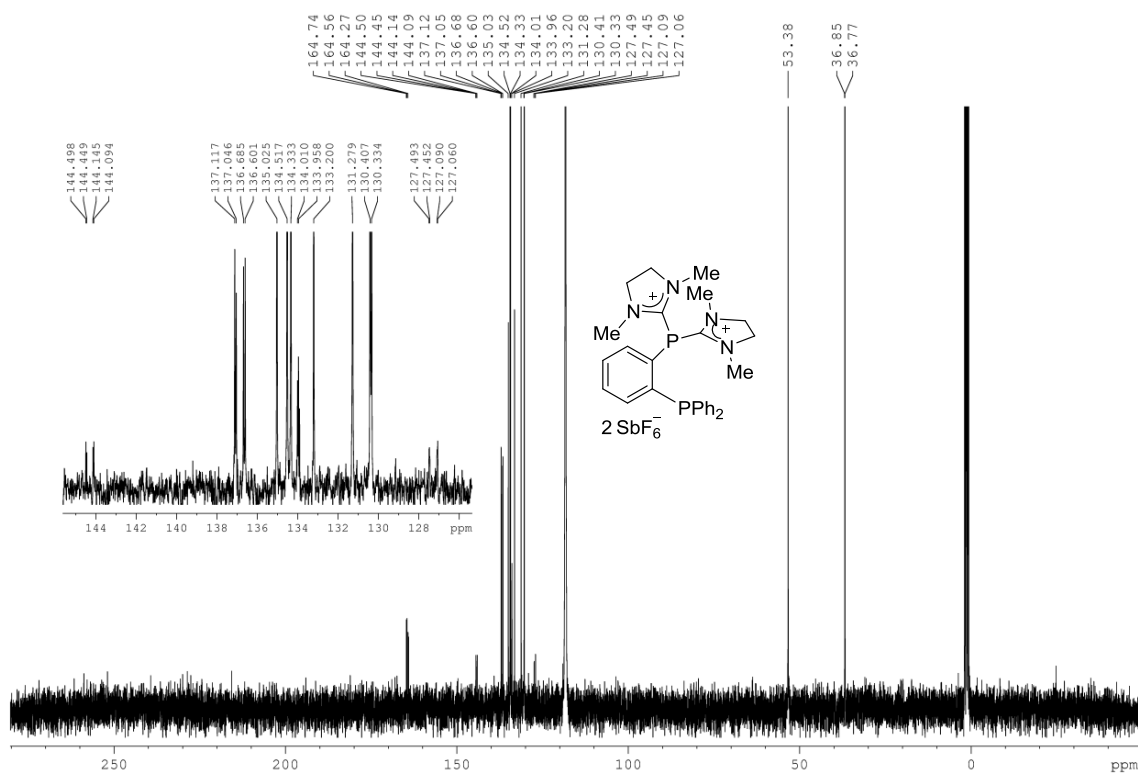
^{19}F NMR (CD₃CN, 282 MHz) (Compound 82) **^1H NMR (CD₂Cl₂, 500 MHz) (Compound 91)**

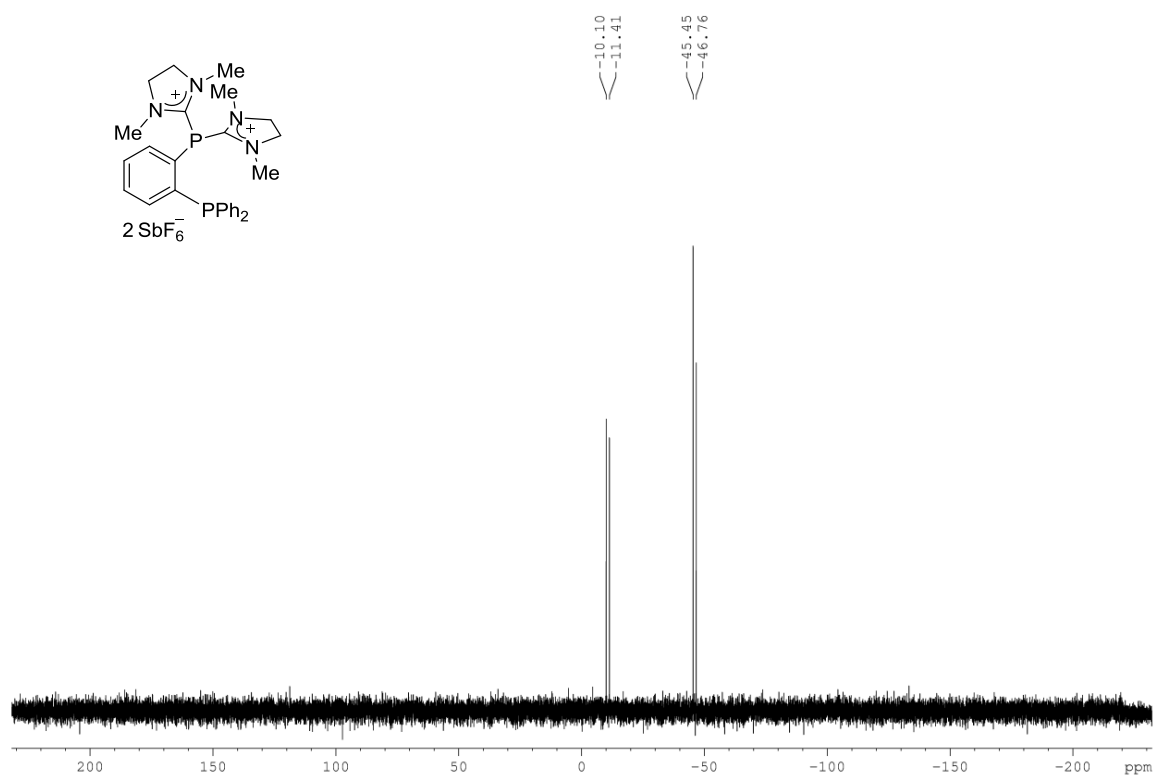
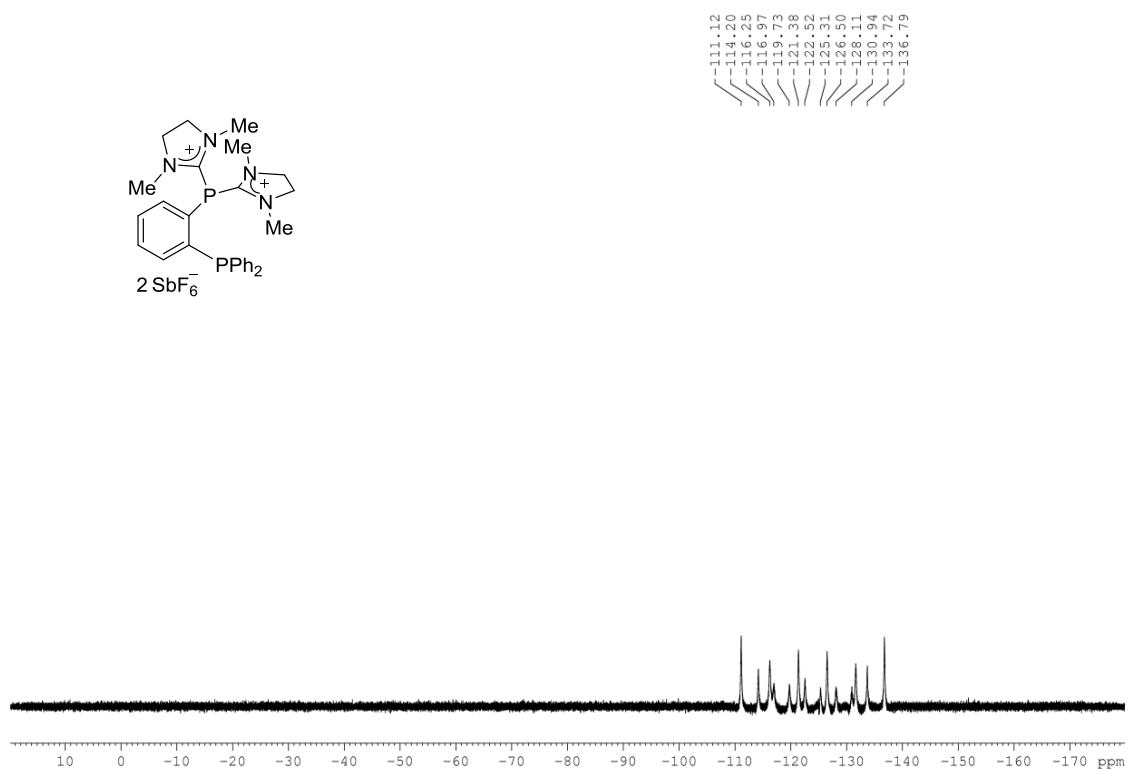
¹³C NMR (CD₃CN, 125 MHz) (Compound 91)**³¹P NMR (CD₃CN, 121 MHz) (Compound 91)**

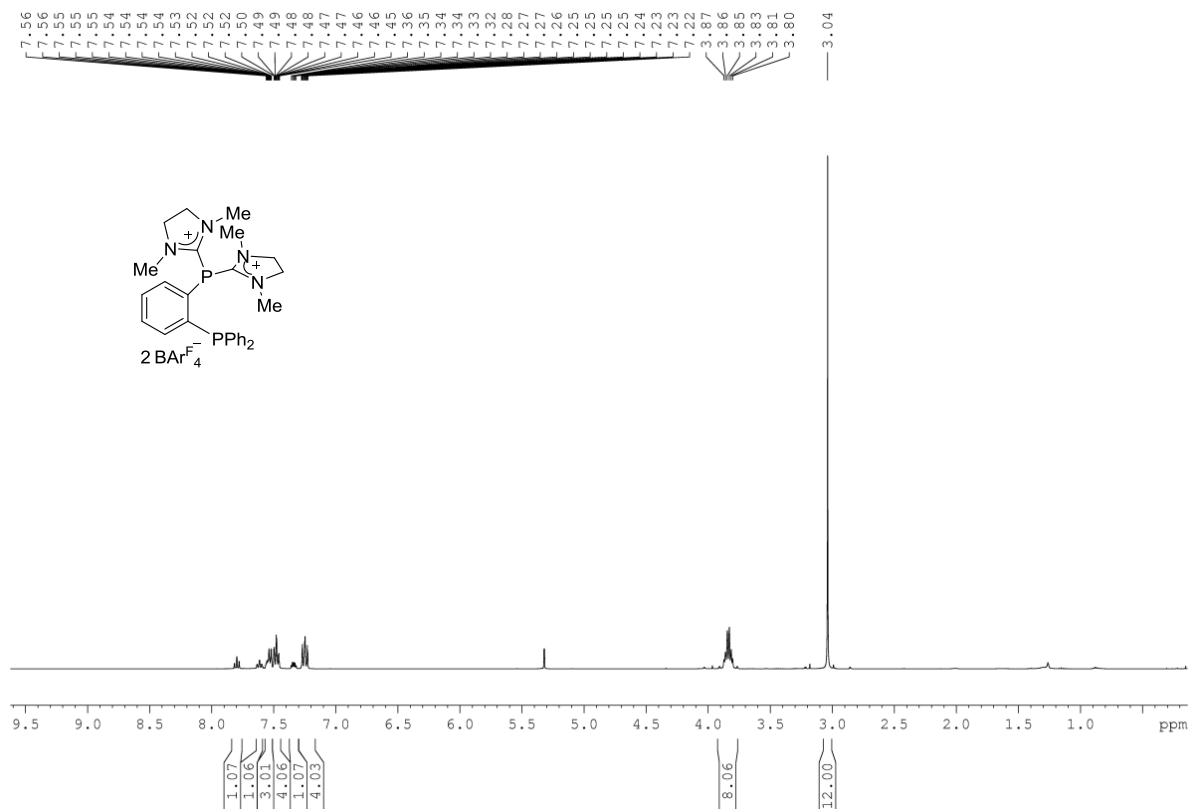
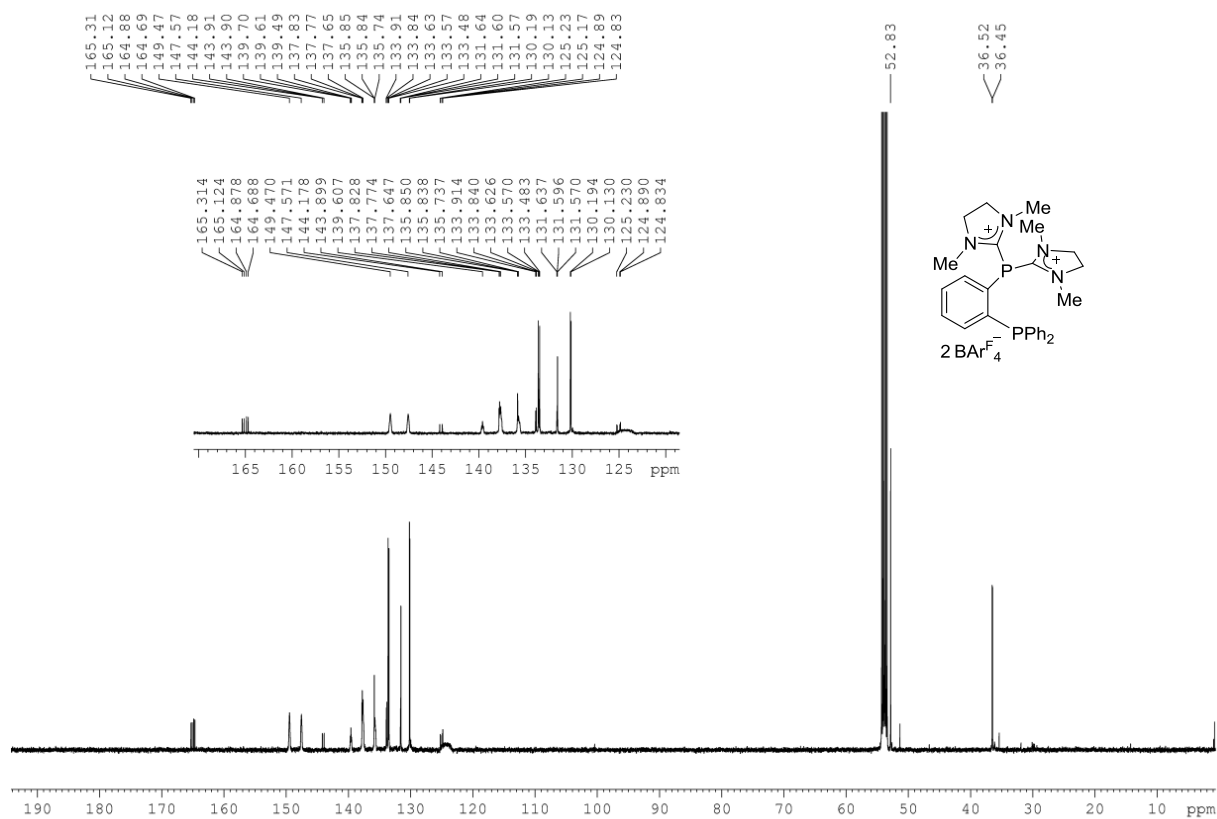
^{11}B NMR (CD₃CN, 96 MHz) (Compound 91) **^1H NMR (CD₃CN, 400 MHz) (Compound 92a)**

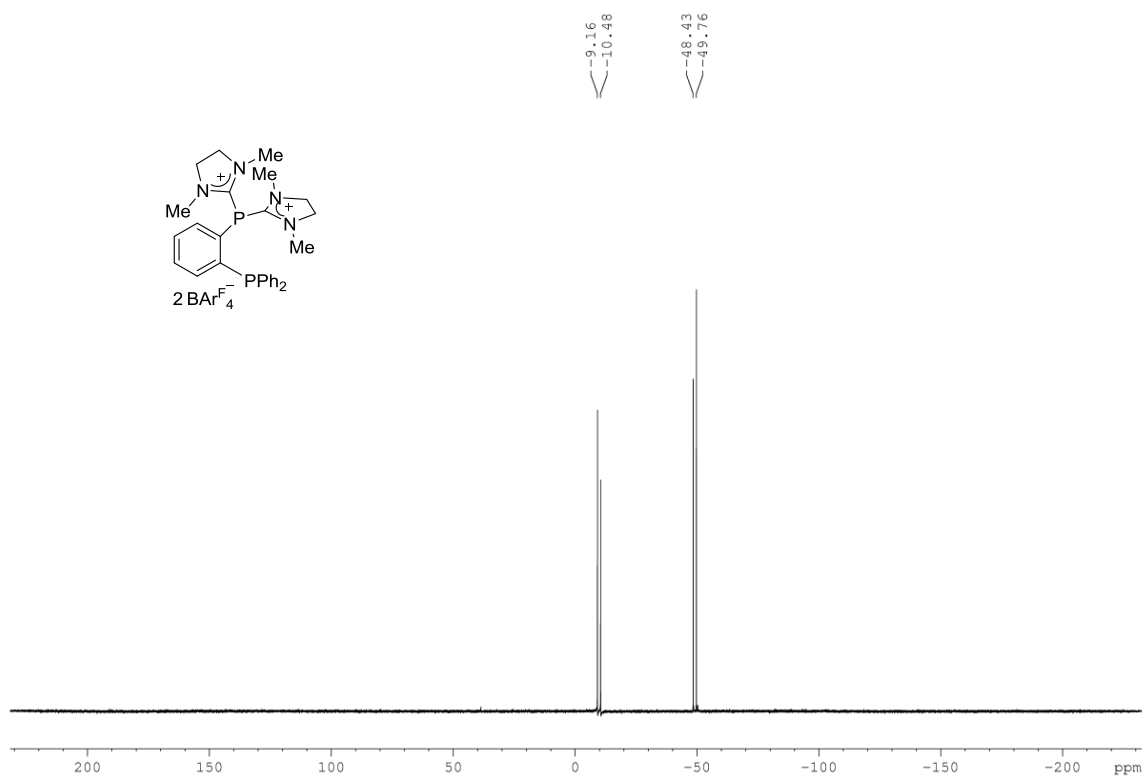
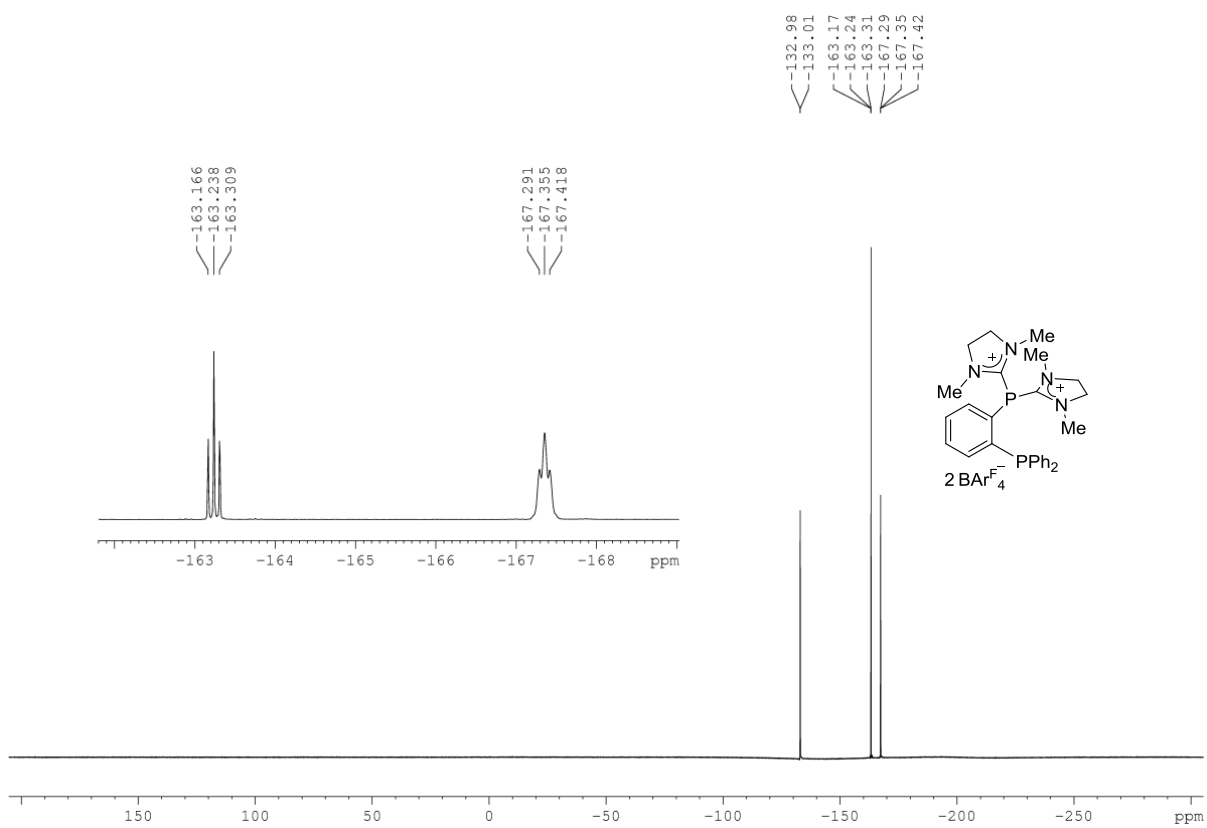
¹³C NMR (CD₃CN, 100 MHz) (Compound 92a)**³¹P NMR (CDCl₃, 121 MHz) (Compound 92a)**

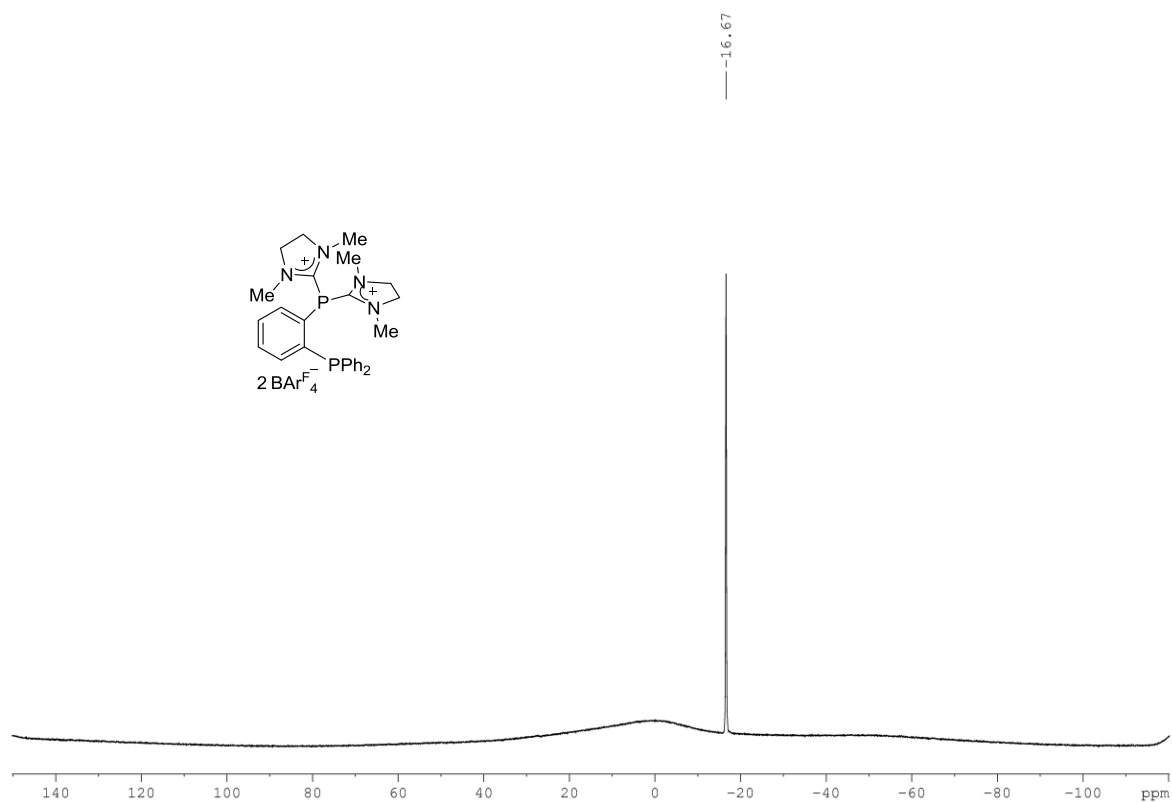
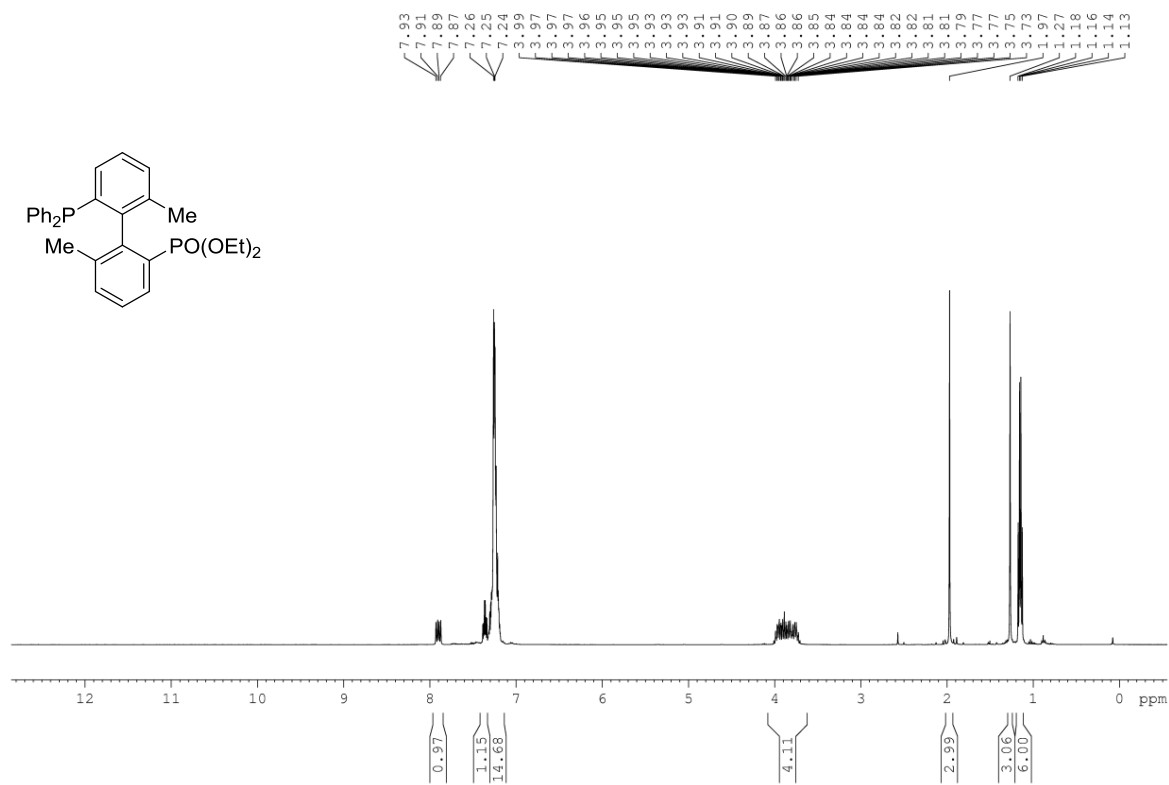
^{11}B NMR (CD_3CN , 96 MHz) (Compound 92a) **^{19}F NMR (CD_3CN , 282 MHz) (Compound 92a)**

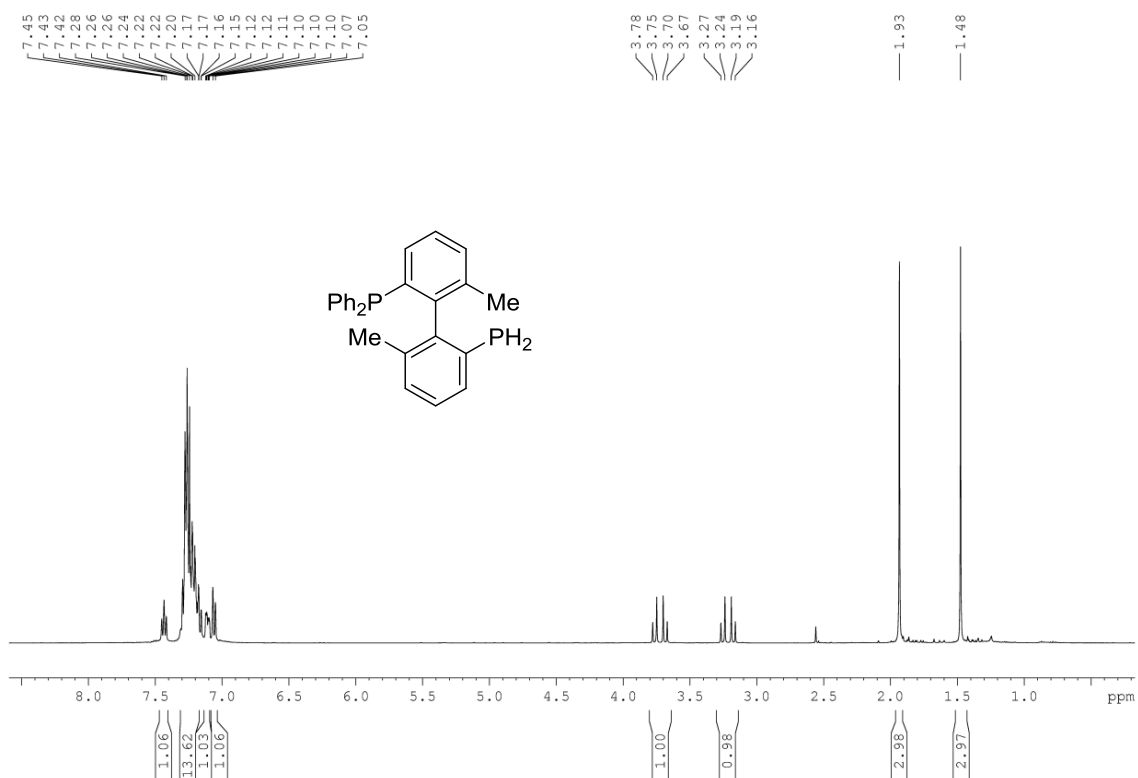
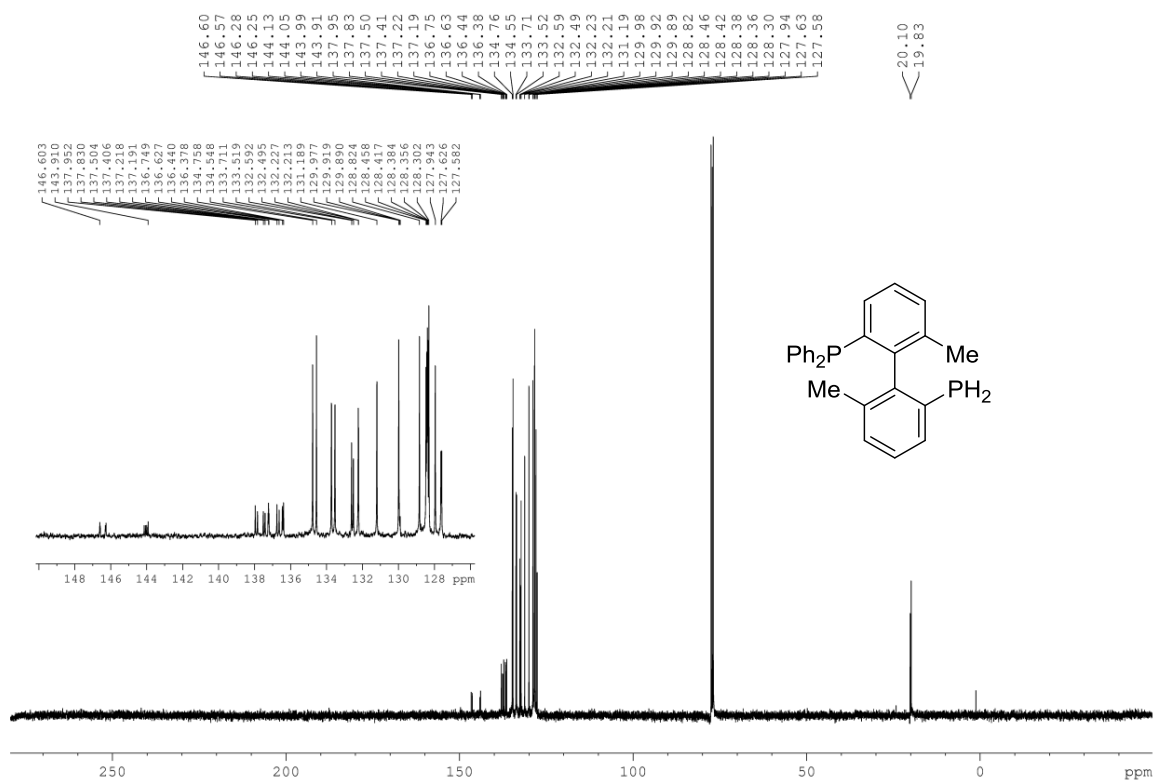
^1H NMR (CD₃CN, 400 MHz) (Compound 92b) **^{13}C NMR (CD₃CN, 100 MHz) (Compound 92b)**

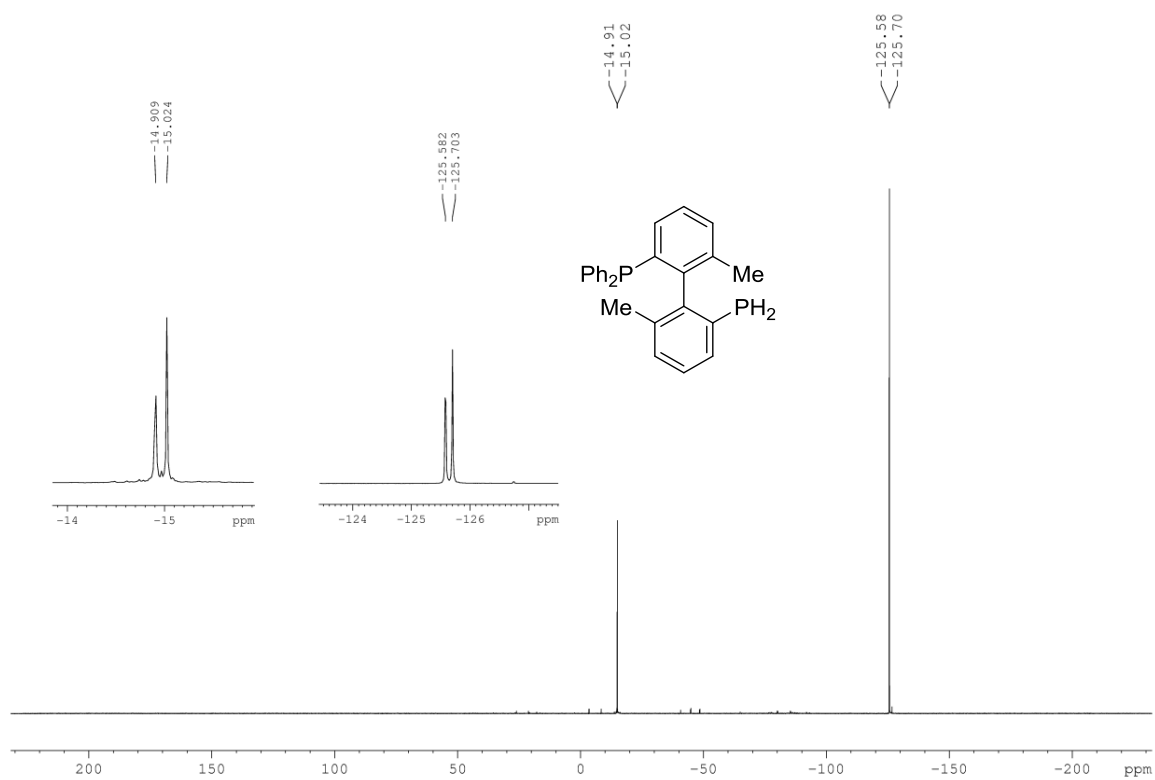
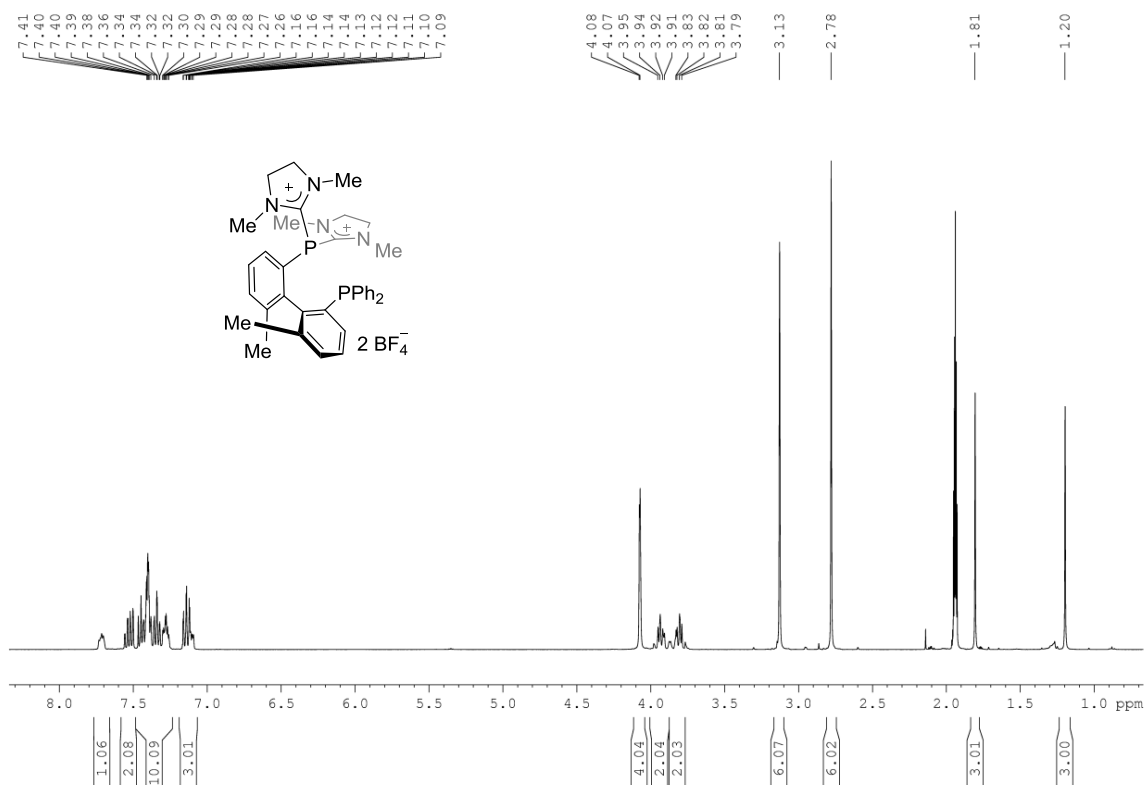
^{31}P NMR (CD_3CN , 121 MHz) (Compound 92b) ^{19}F NMR (CD_3CN , 282 MHz) (Compound 92b)

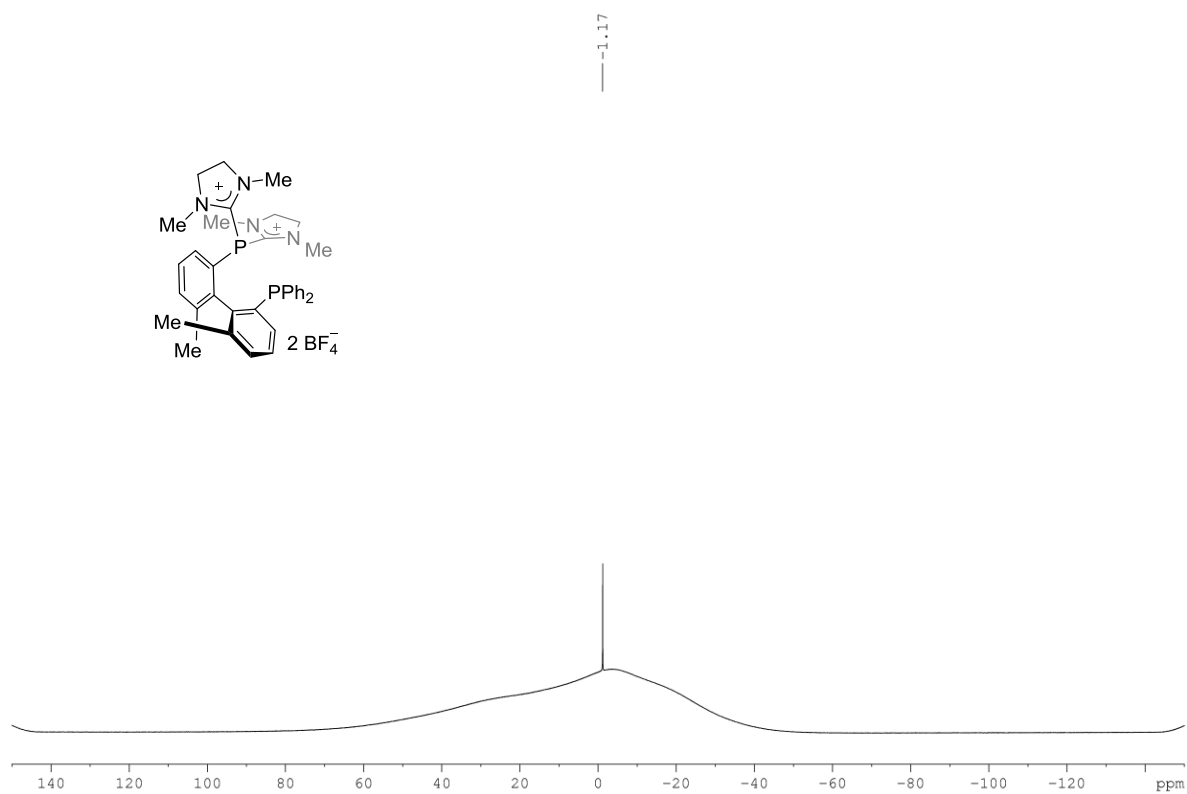
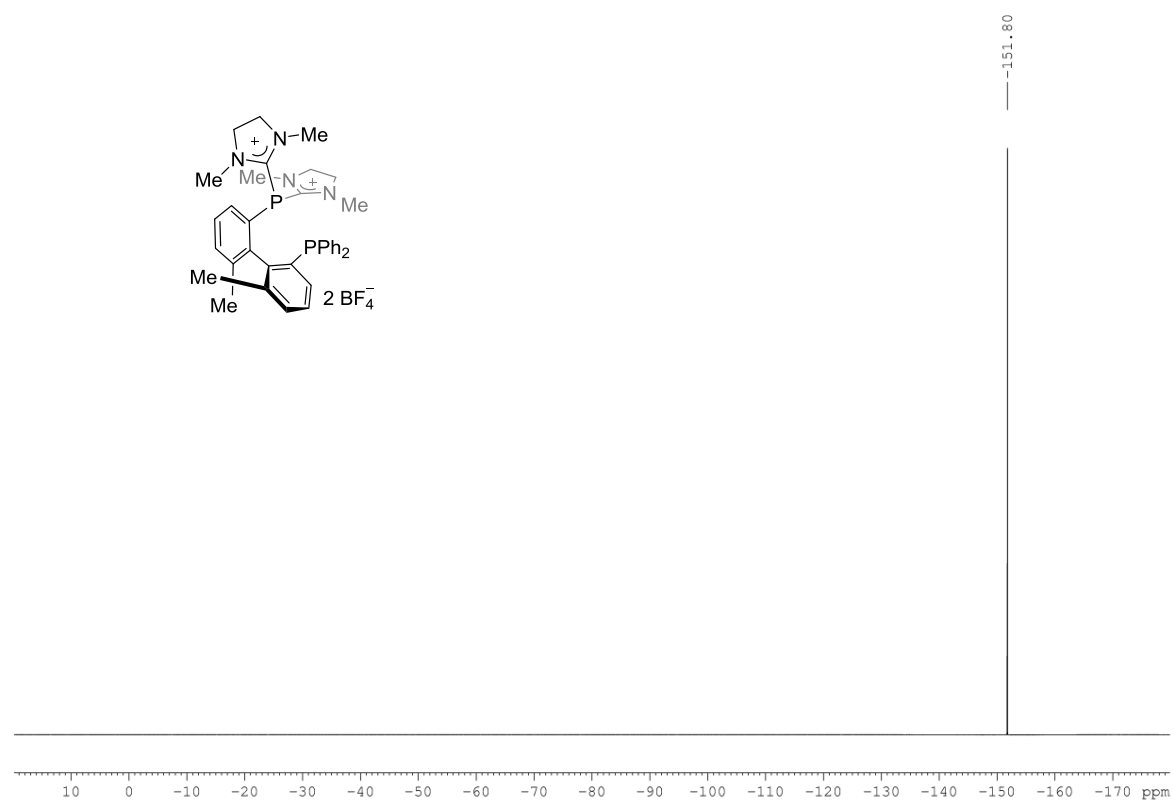
^1H NMR (CD_2Cl_2 , 400 MHz) (Compound 92c) **^{13}C NMR (CD_2Cl_2 , 125 Mz) (Compound 92c)**

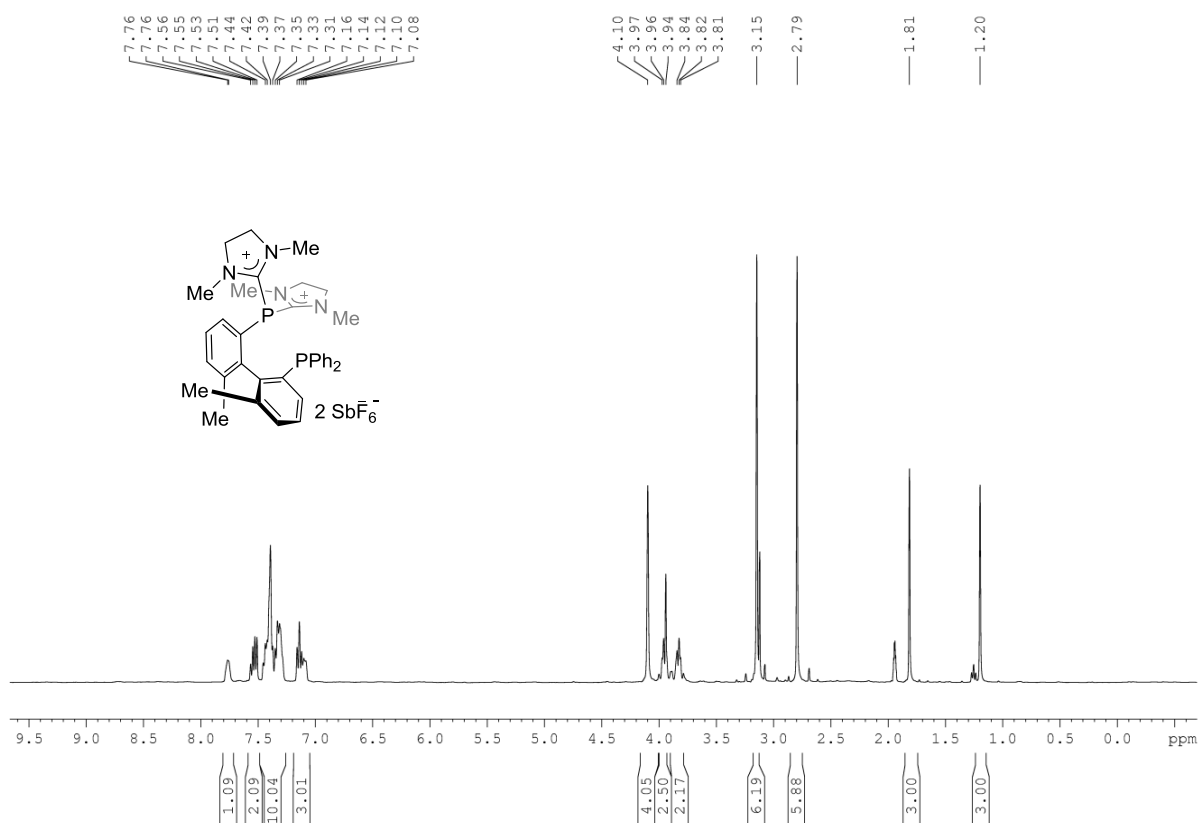
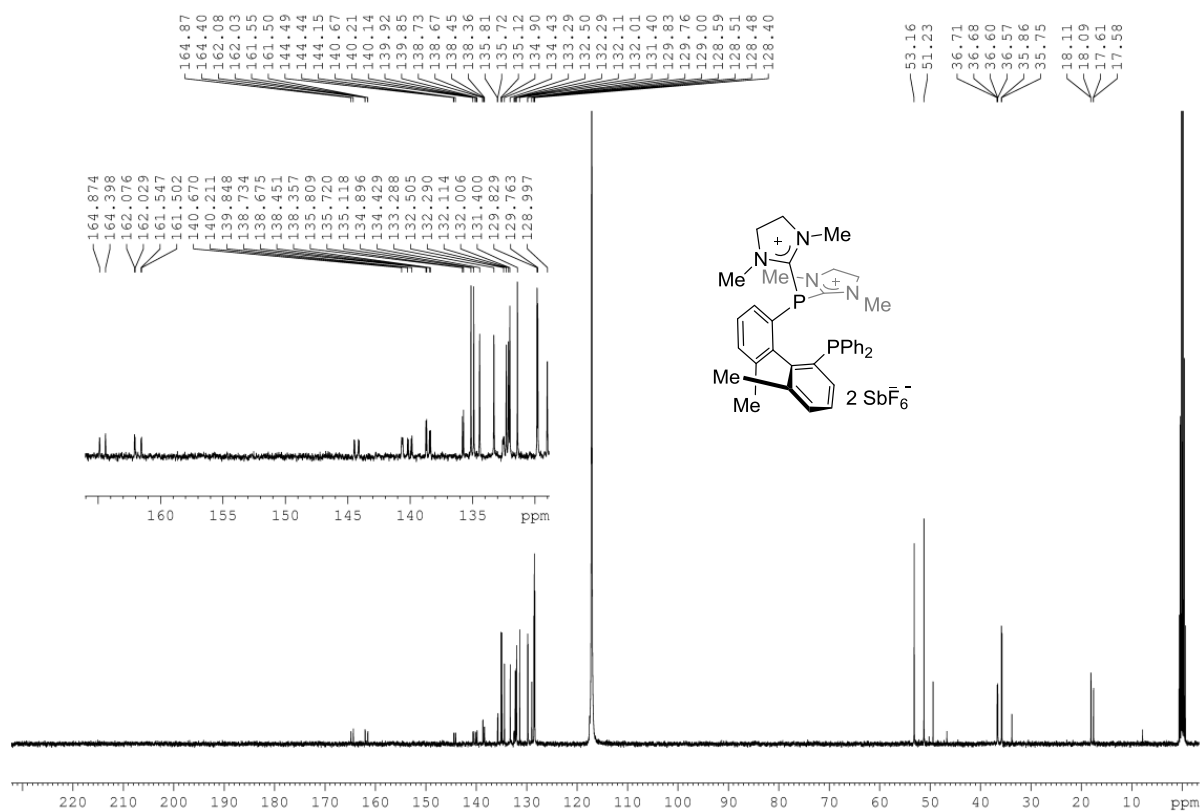
^{31}P NMR (CD_2Cl_2 , 162 MHz) (Compound 92c) **^{19}F NMR (CD_2Cl_2 , 282 MHz) (Compound 92c)**

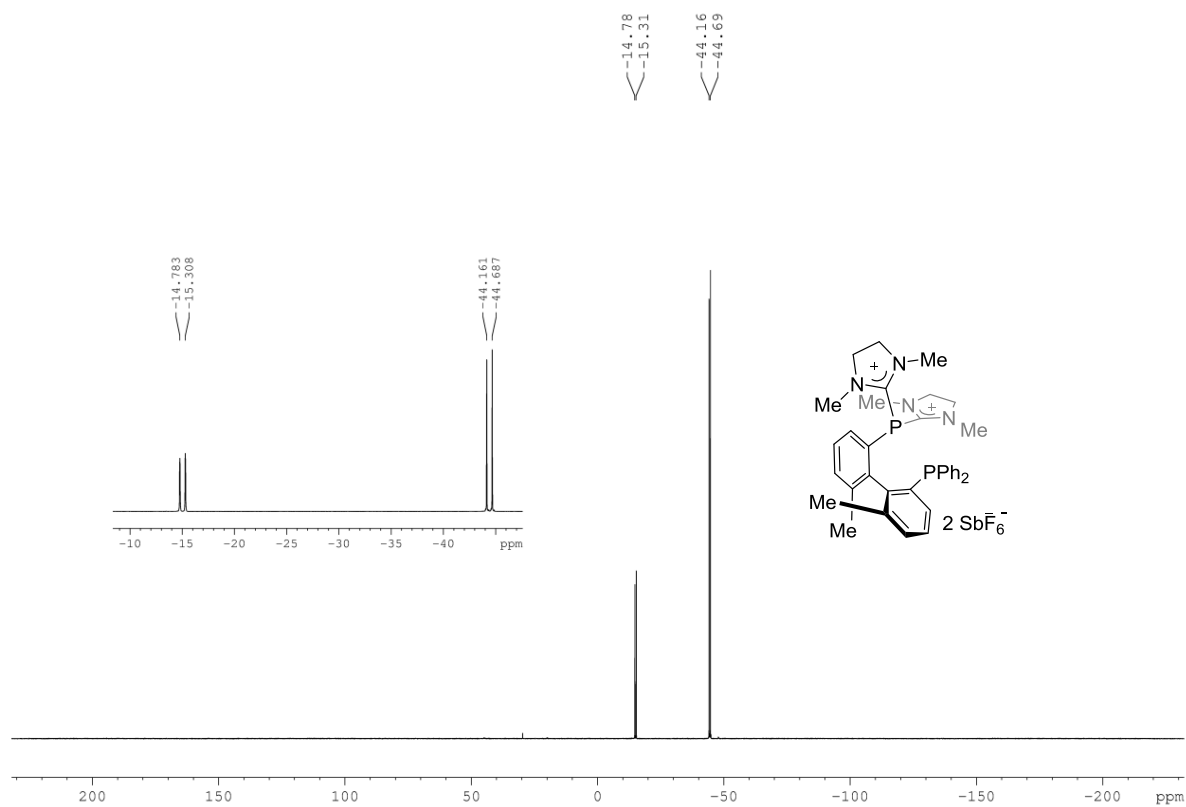
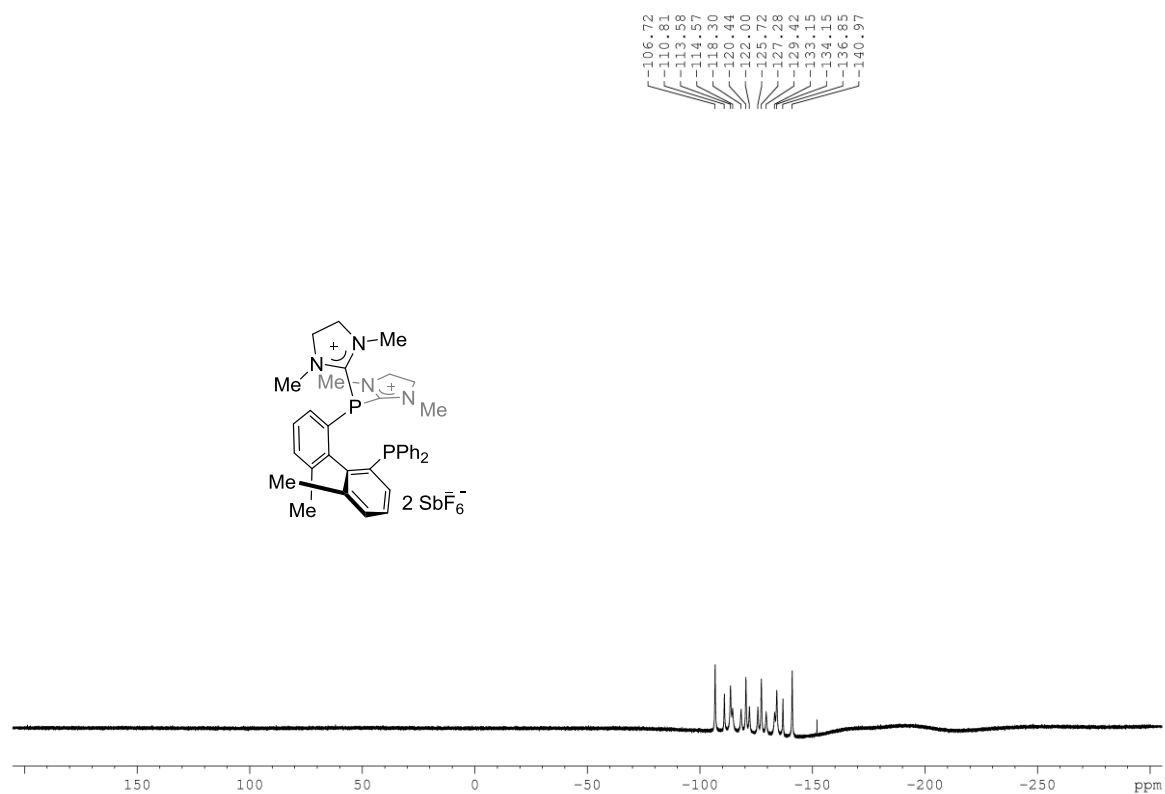
^{11}B NMR (CD_2Cl_2 , 96 MHz) (Compound 92c) ^1H NMR (CDCl_3 , 400 MHz) (Compound 99)

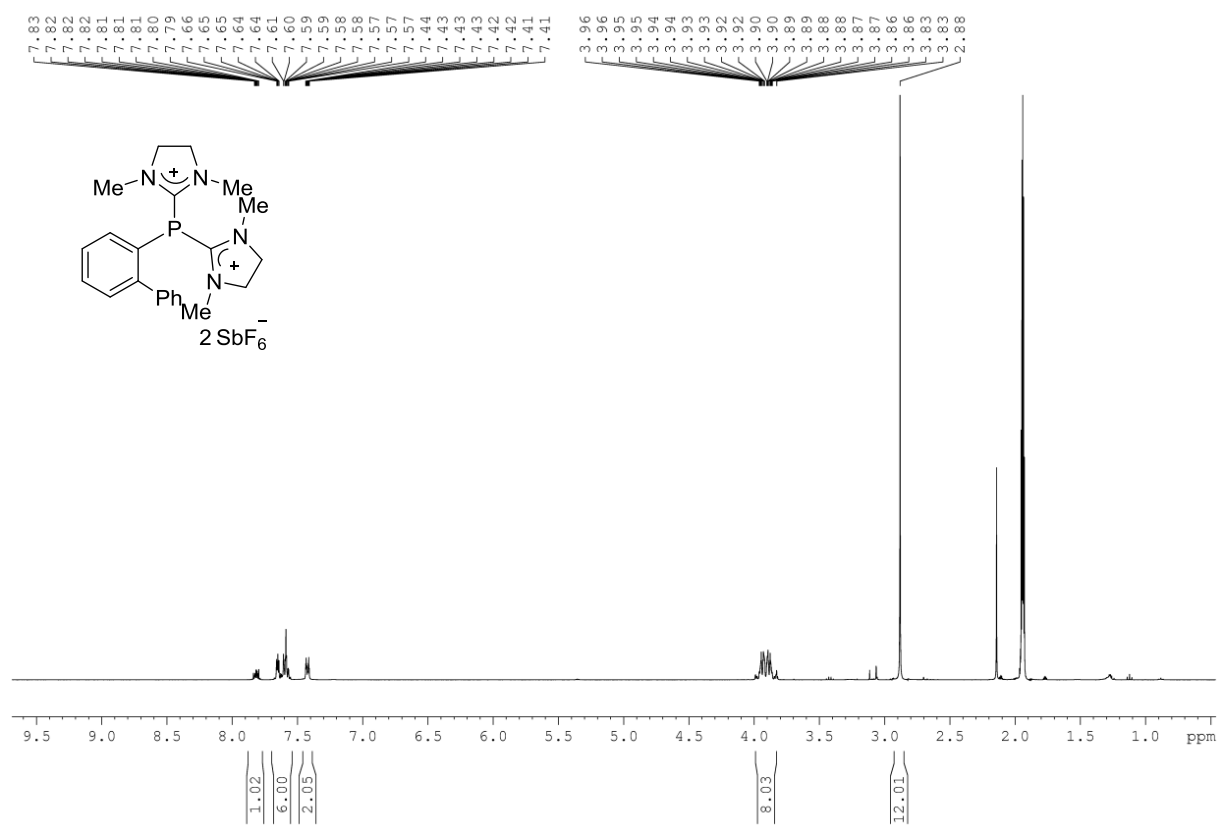
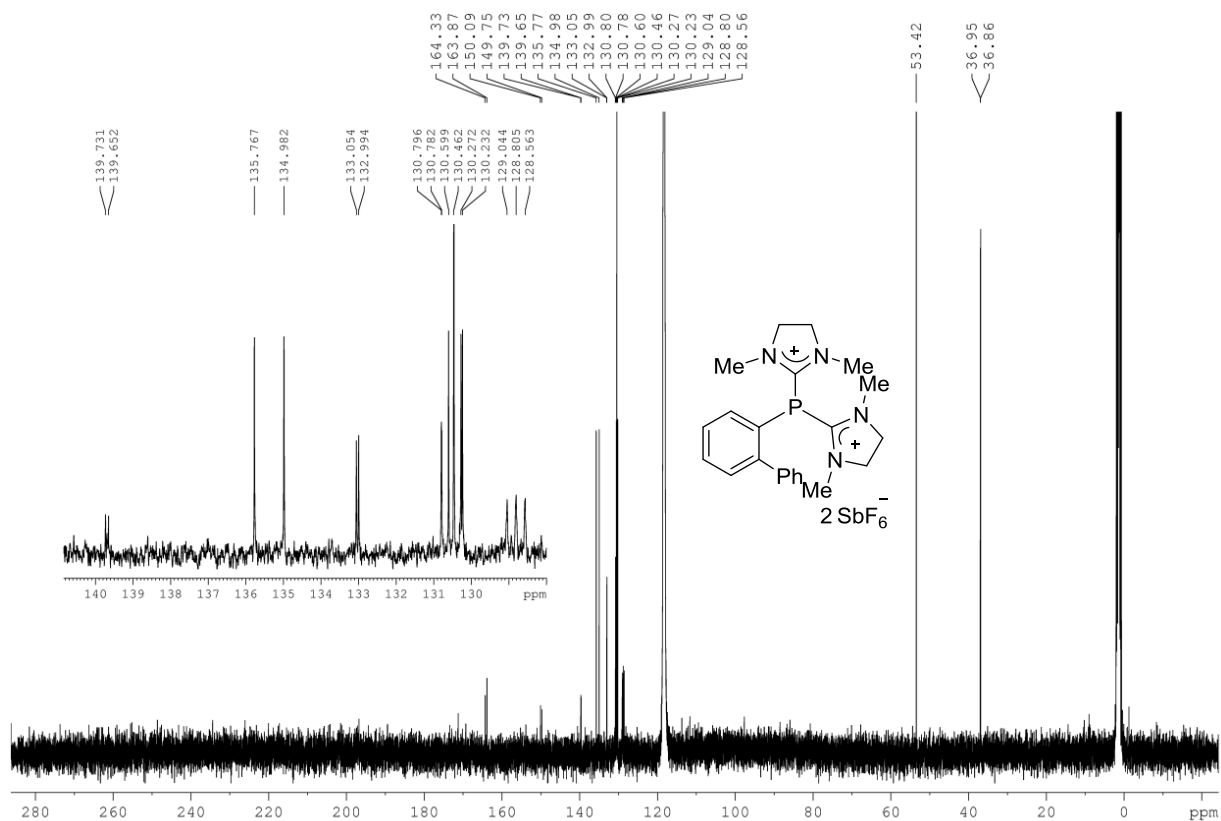
^1H NMR (CDCl_3 , 400 MHz) (Compound 100) ^{13}C NMR (CDCl_3 , 100 MHz) (Compound 100)

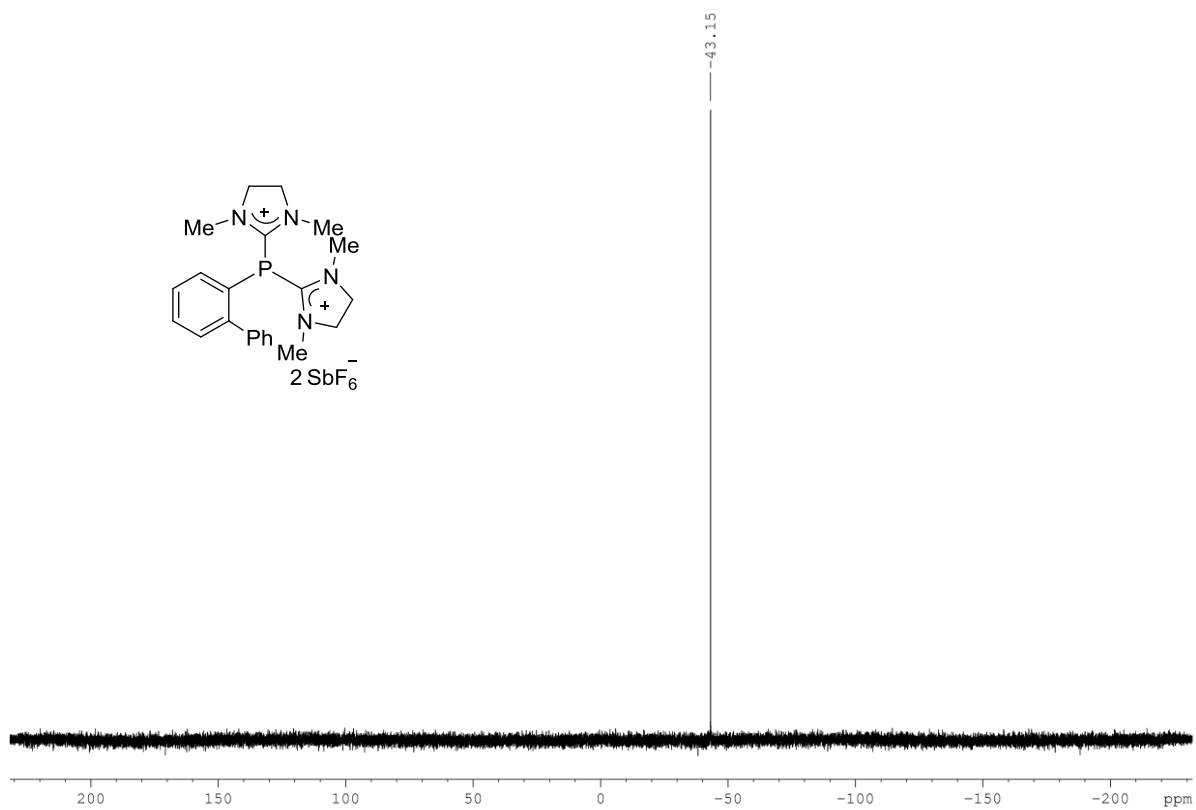
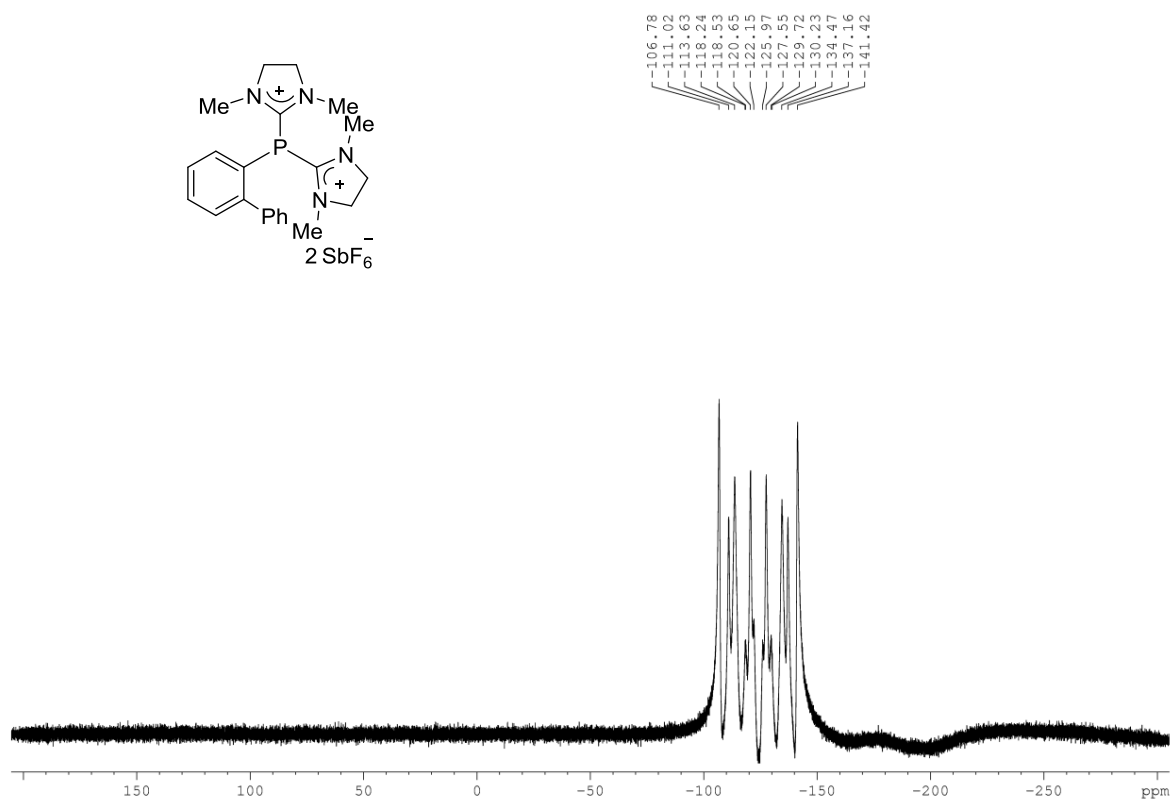
^{31}P NMR (CDCl_3 , 121 MHz) (Compound 100) **^1H NMR (CD_3CN , 400 MHz) (Compound 101a)**

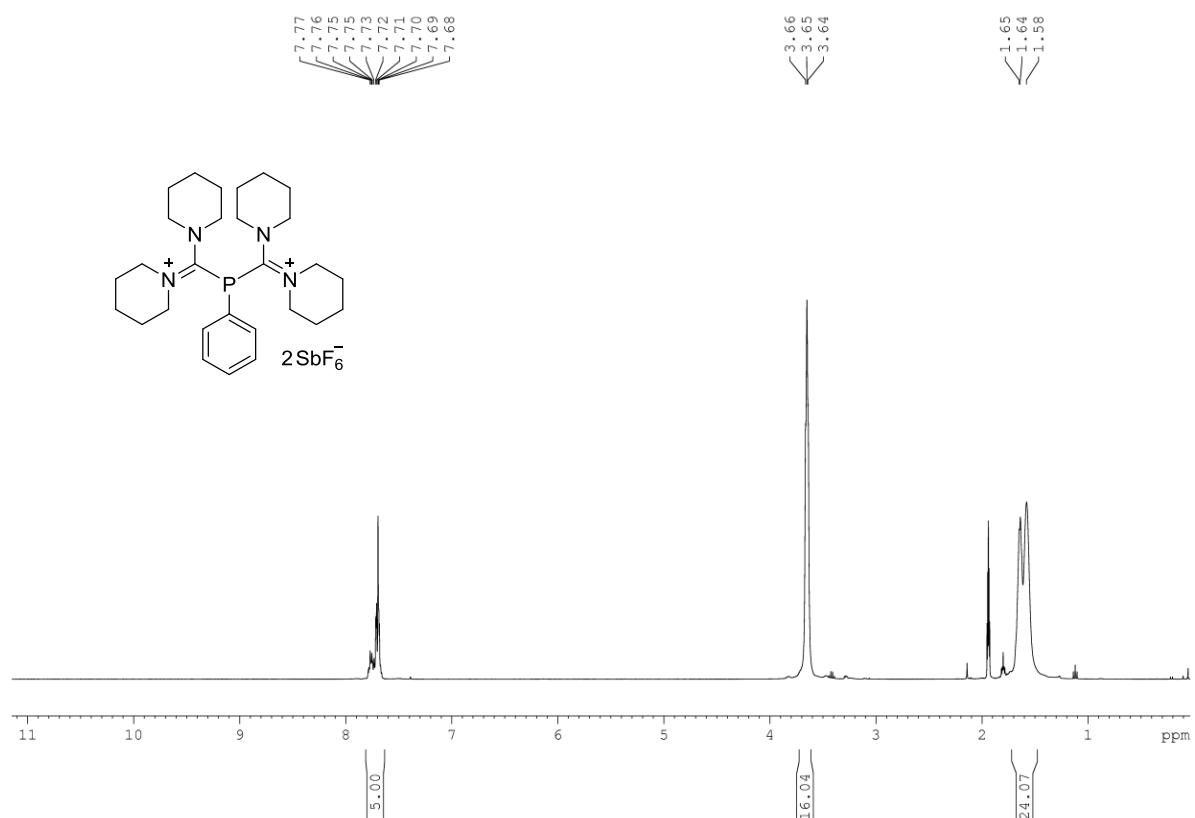
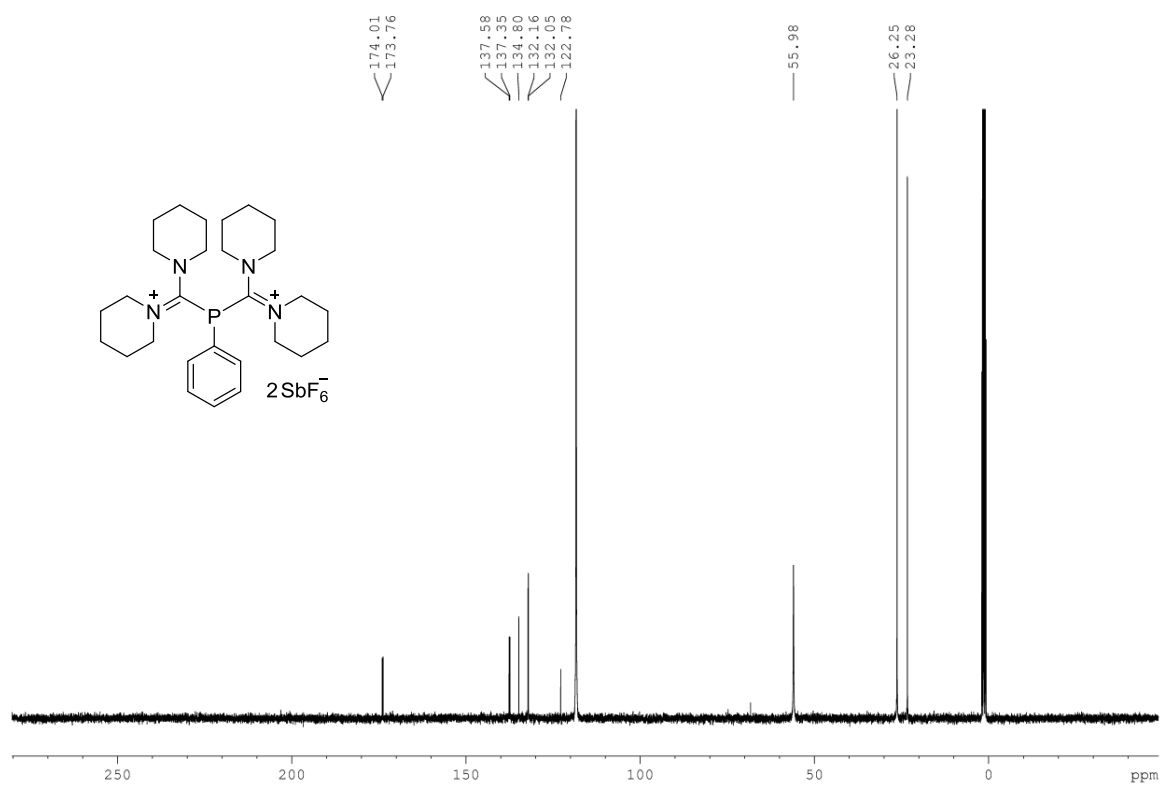
^{11}B NMR (CD₃CN, 96 MHz) (Compound 101a) **^{19}F NMR (CD₃CN, 282 MHz) (Compound 101a)**

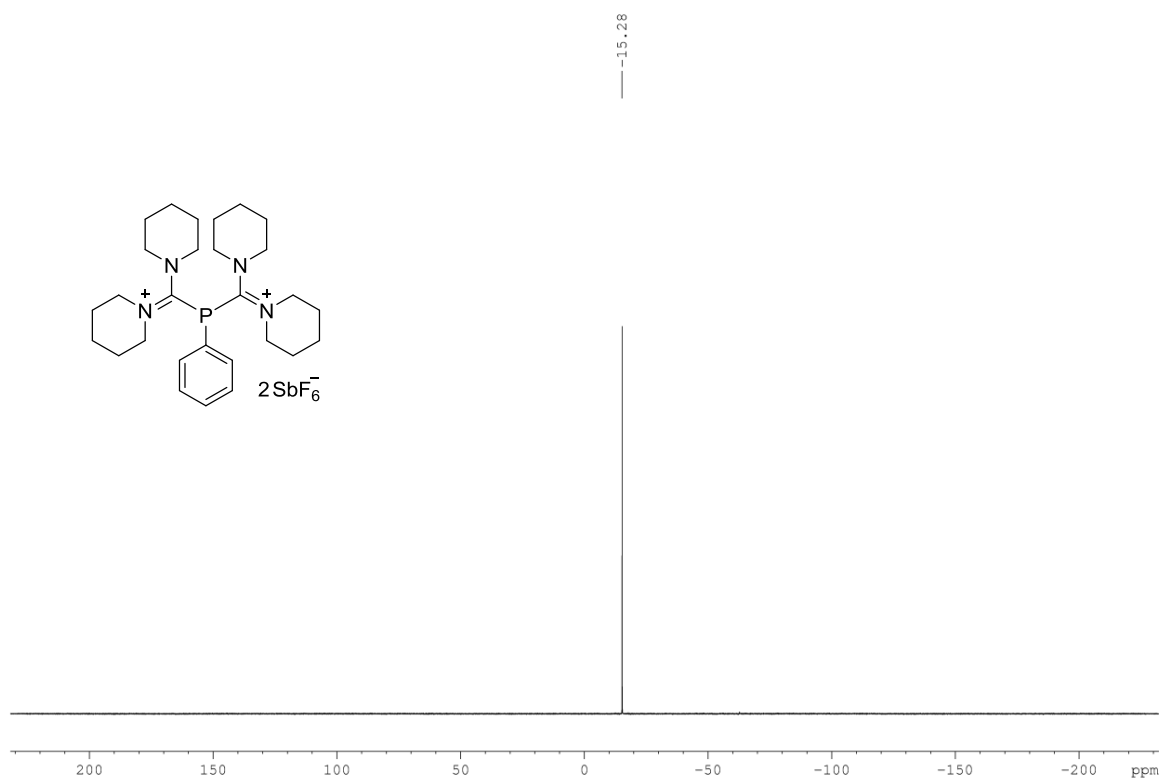
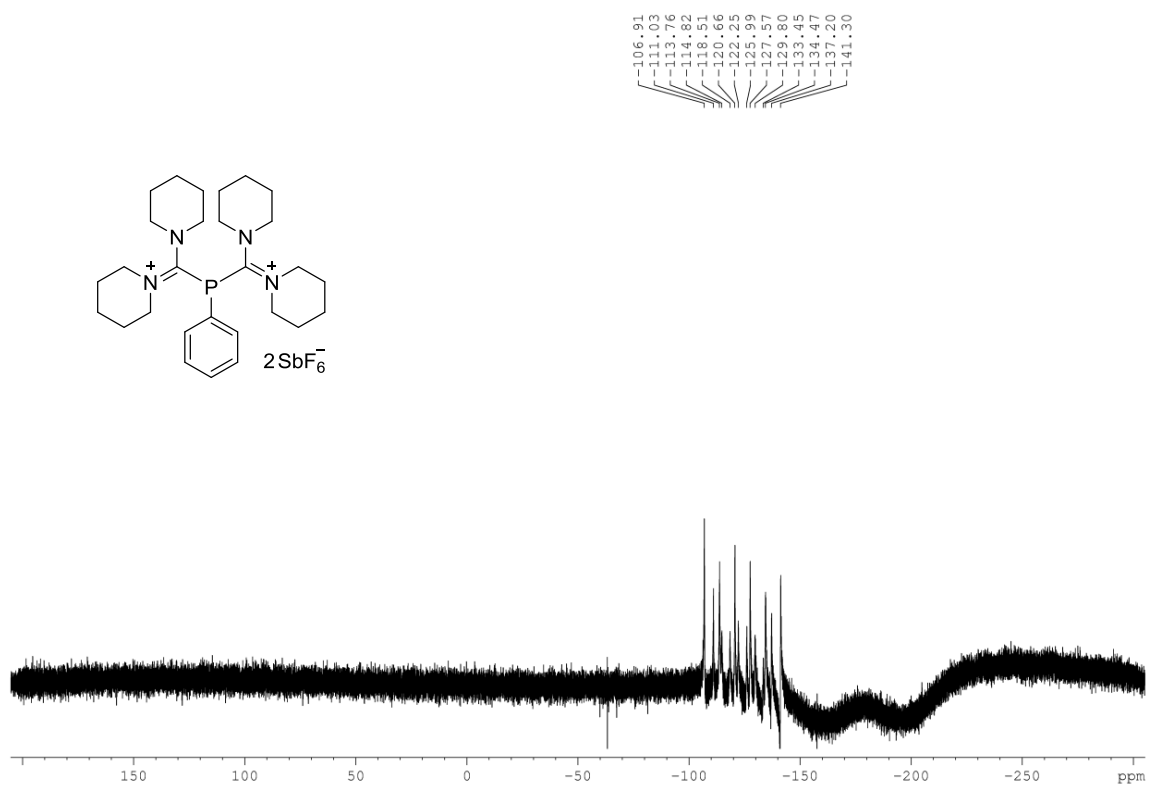
^1H NMR (CD₃CN, 400 MHz) (Compound 101b) **^{13}C NMR (CD₃CN, 100 MHz) (Compound 101b)**

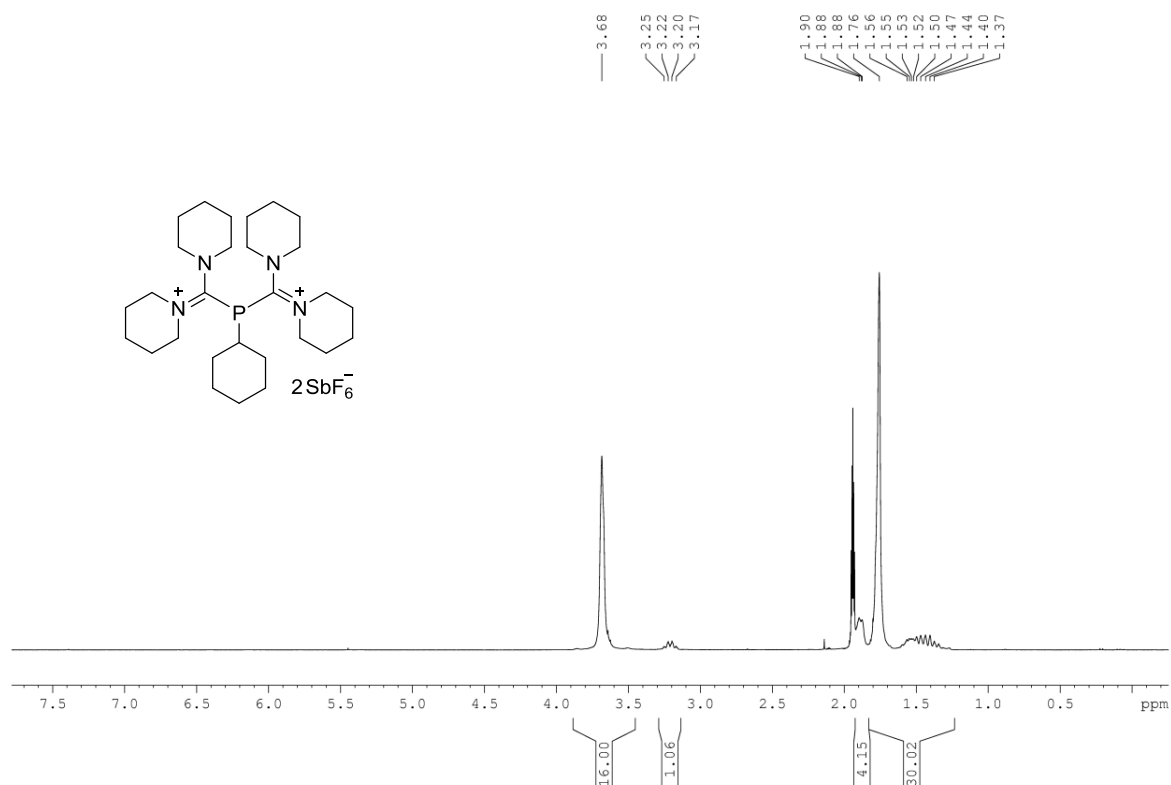
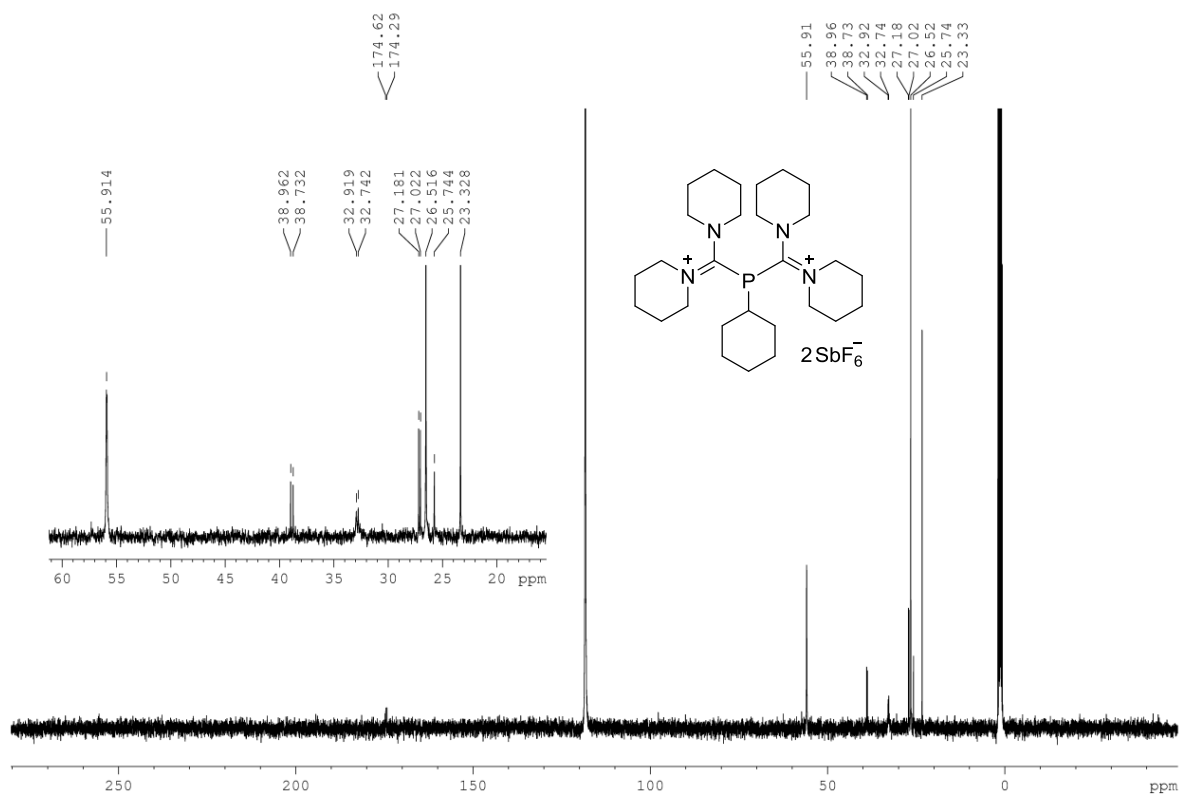
^{31}P NMR (CD₃CN, 121 MHz) (Compound 101b) **^{19}F NMR (CD₃CN, 282 MHz) (Compound 101b)**

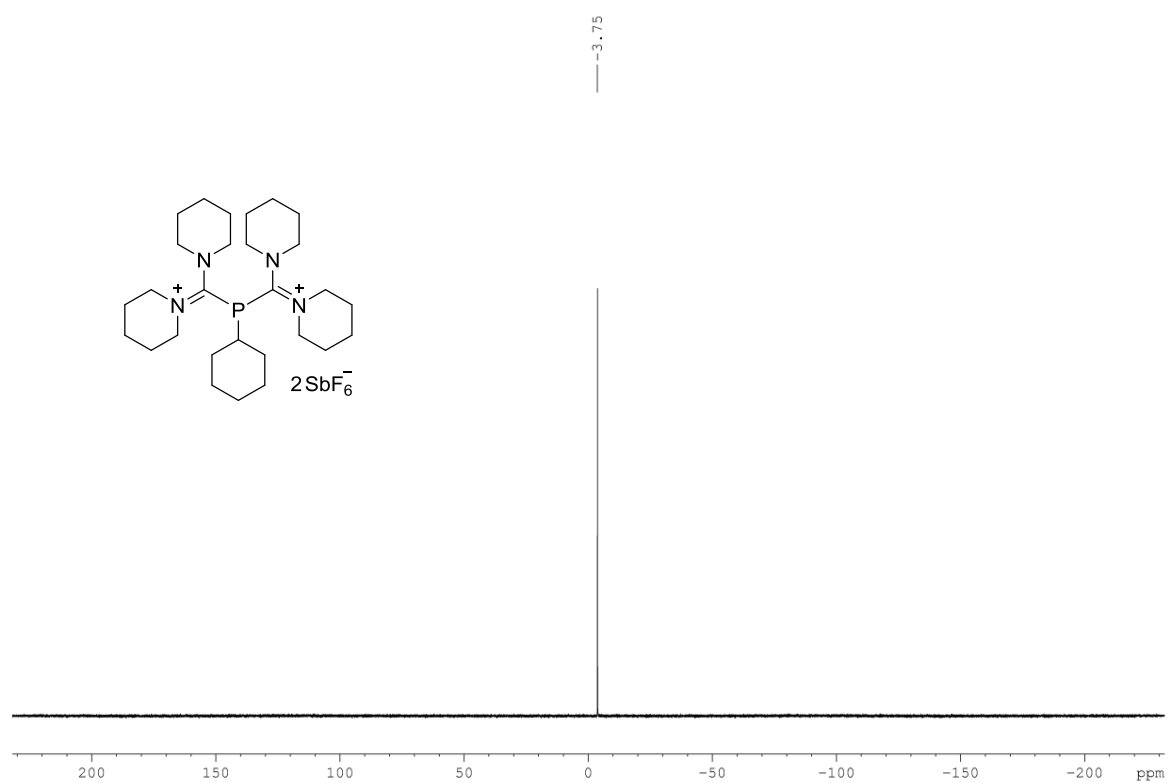
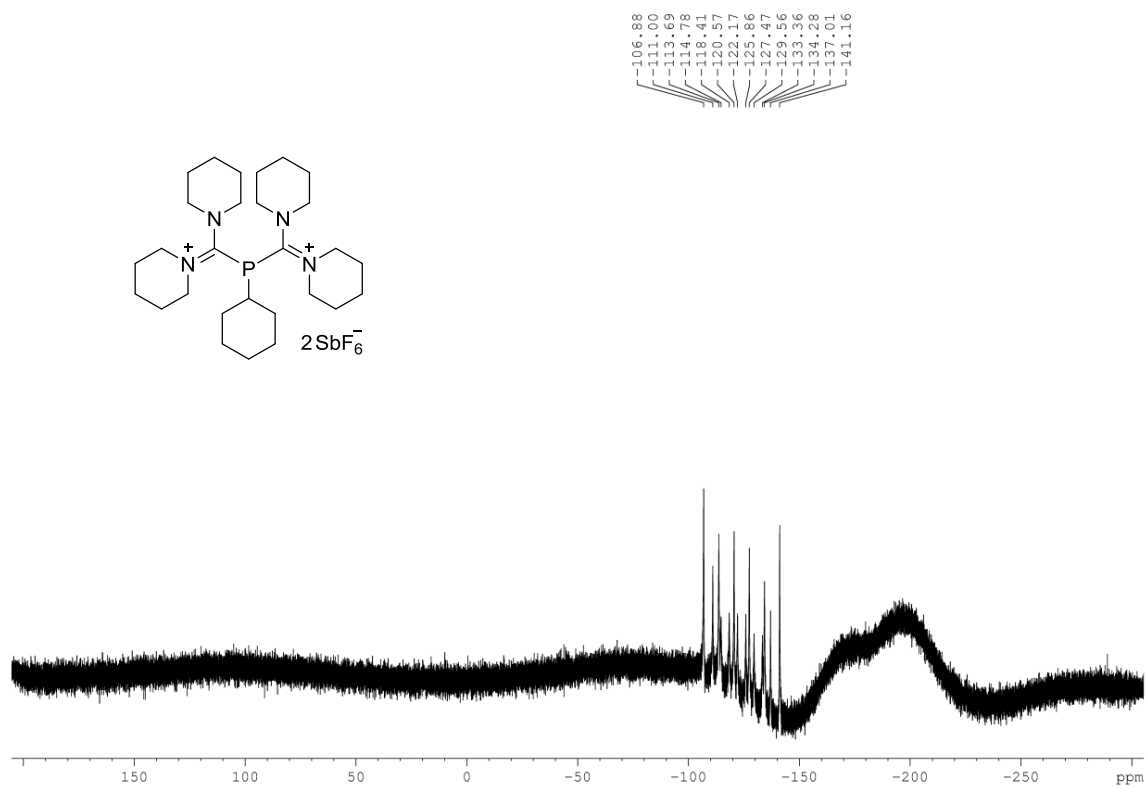
^1H NMR (CD₃CN, 400 MHz) (Compound 102) **^{13}C NMR (CD₃CN, 100 MHz) (Compound 102)**

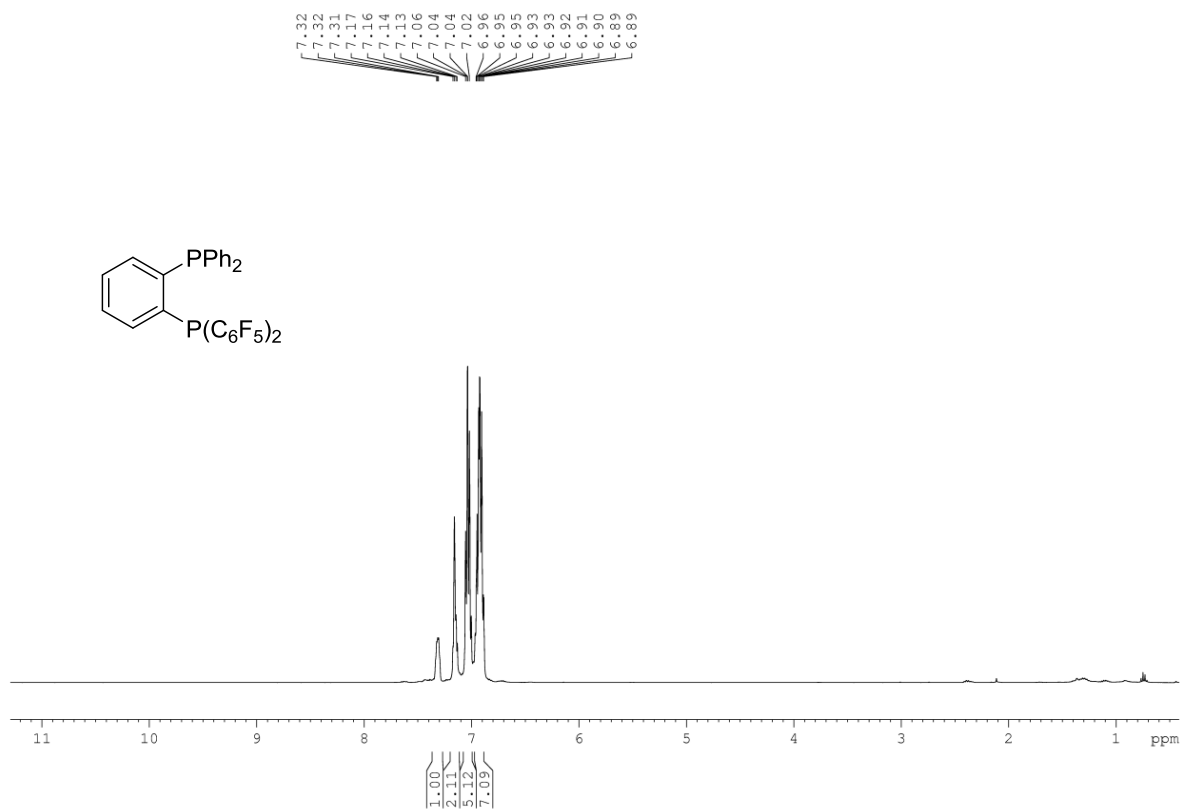
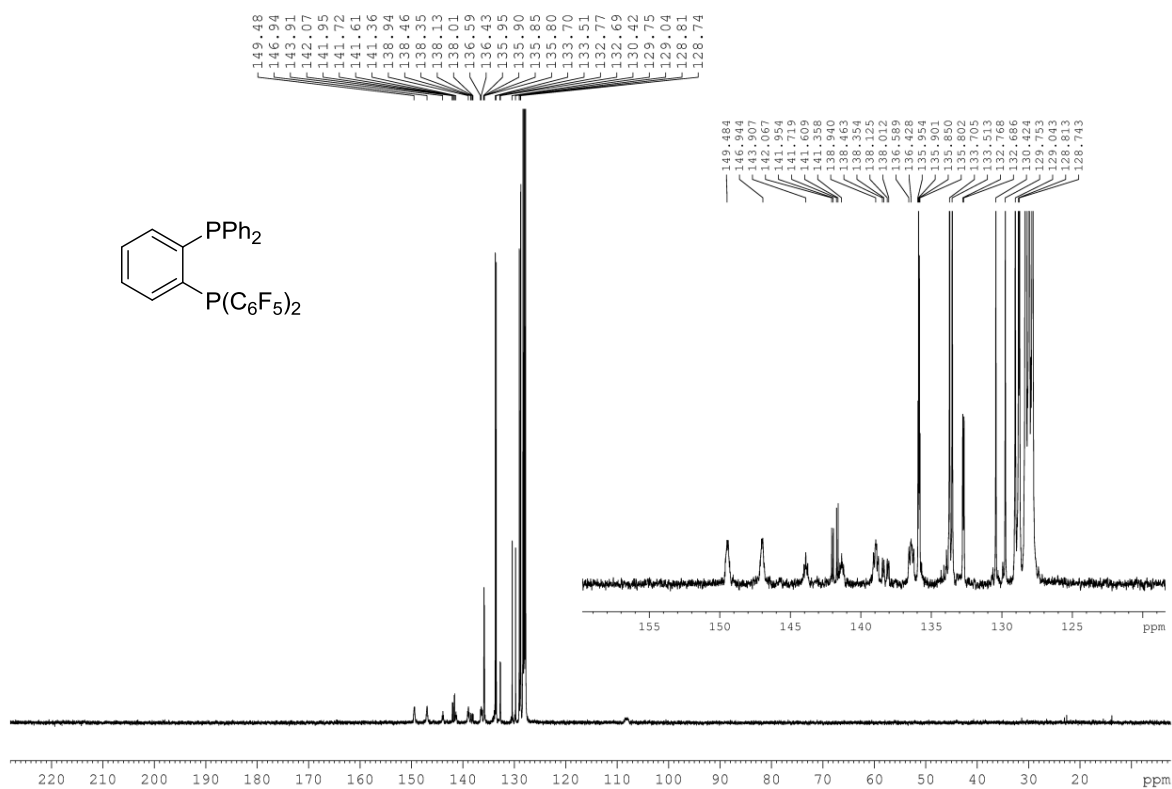
^{31}P NMR (CD_3CN , 121 MHz) (Compound 102) **^{19}F NMR (CD_3CN , 282 MHz) (Compound 102)**

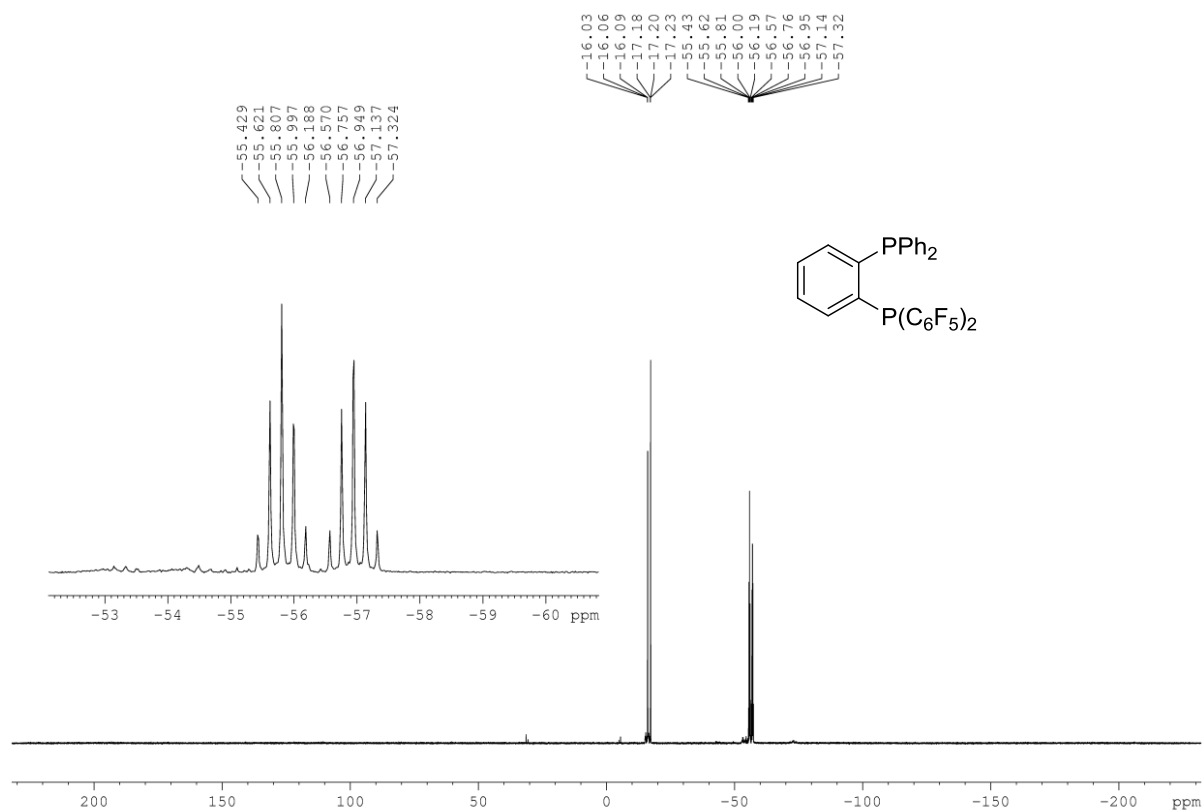
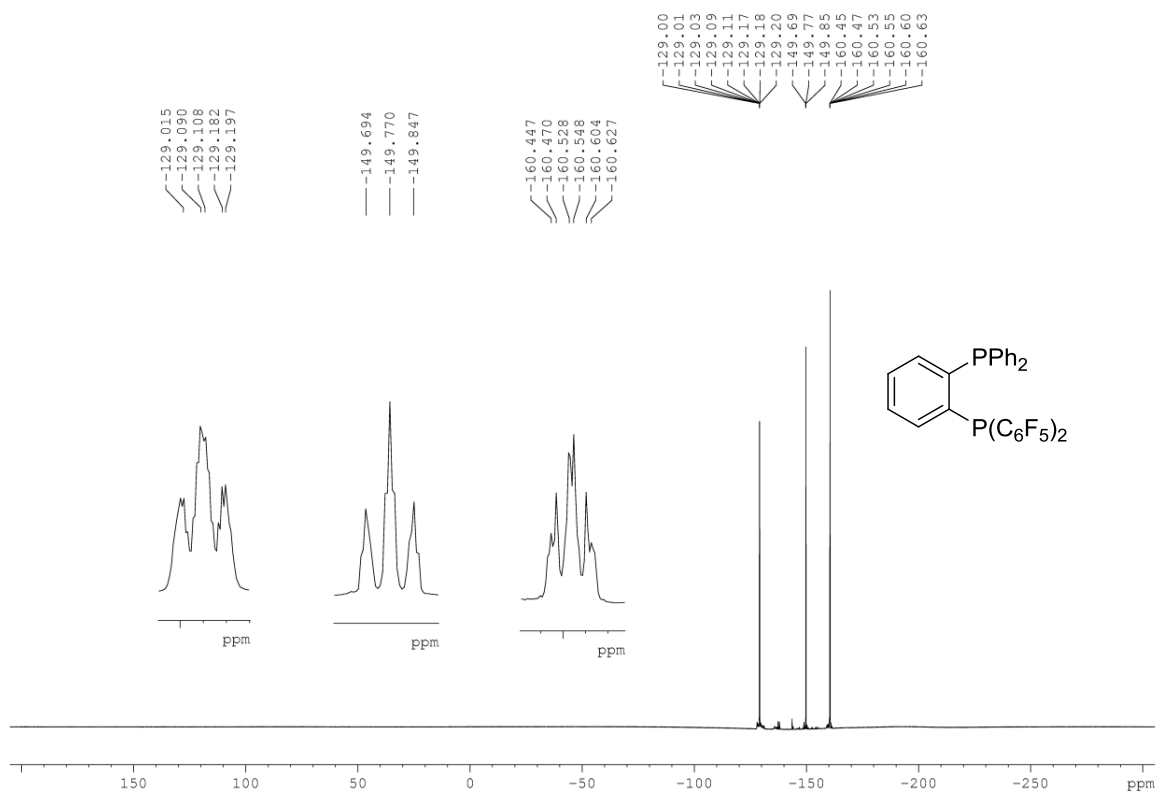
^1H NMR (CD₃CN, 400 MHz) (Compound 103) **^{13}C NMR (CD₃CN, 100 MHz) (Compound 103)**

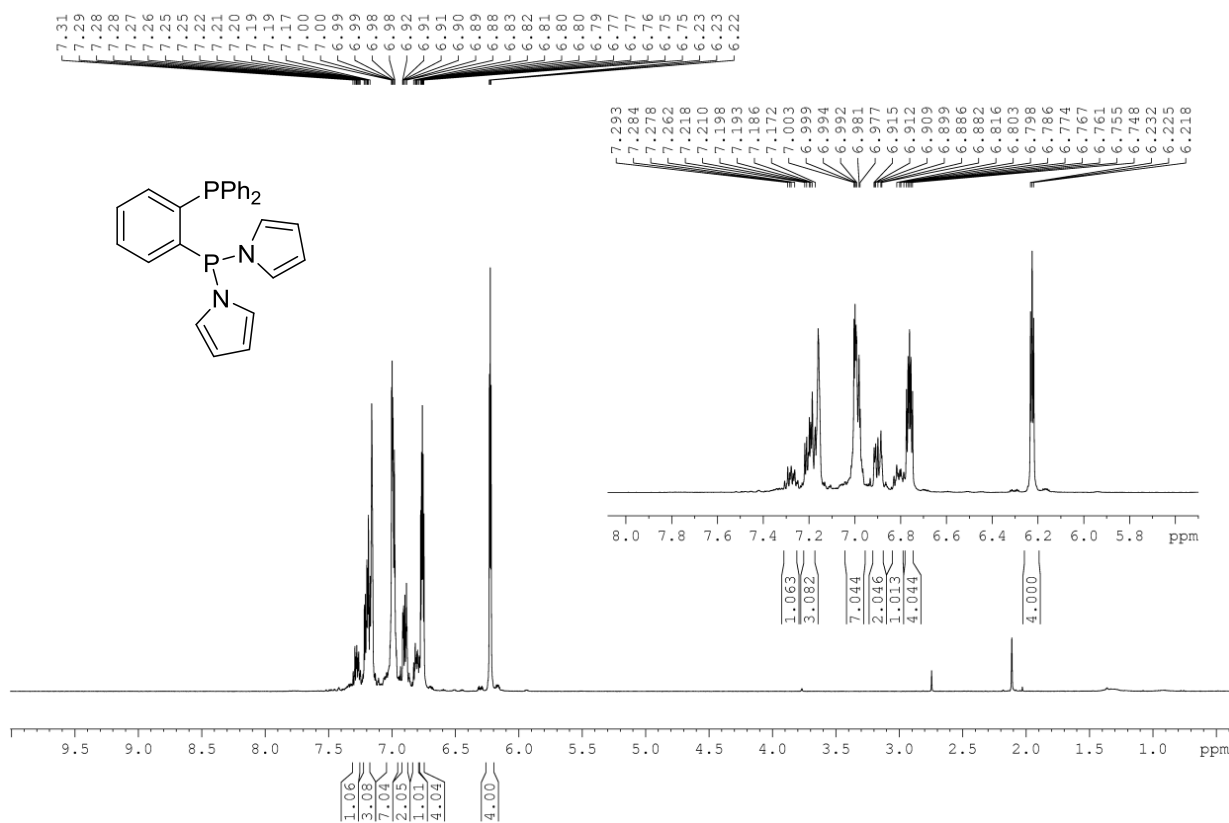
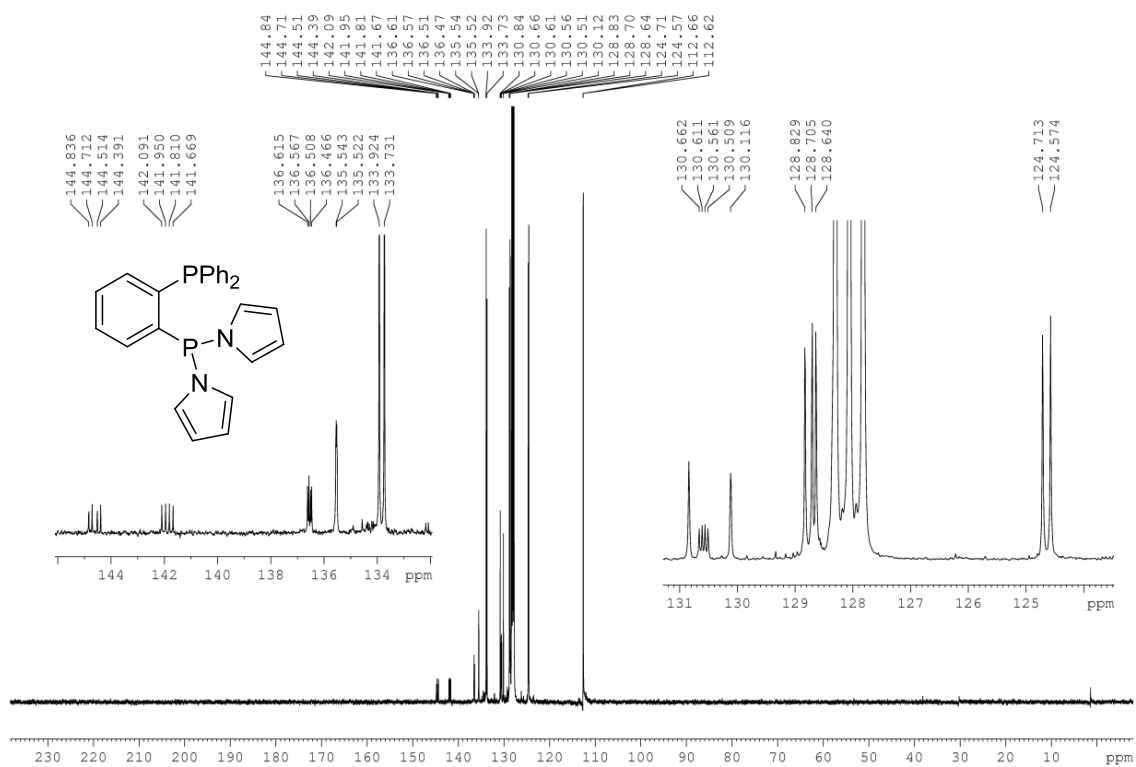
^{31}P NMR (CD_3CN , 121 MHz) (Compound 103) **^{19}F NMR (CD_3CN , 282 MHz) (Compound 103)**

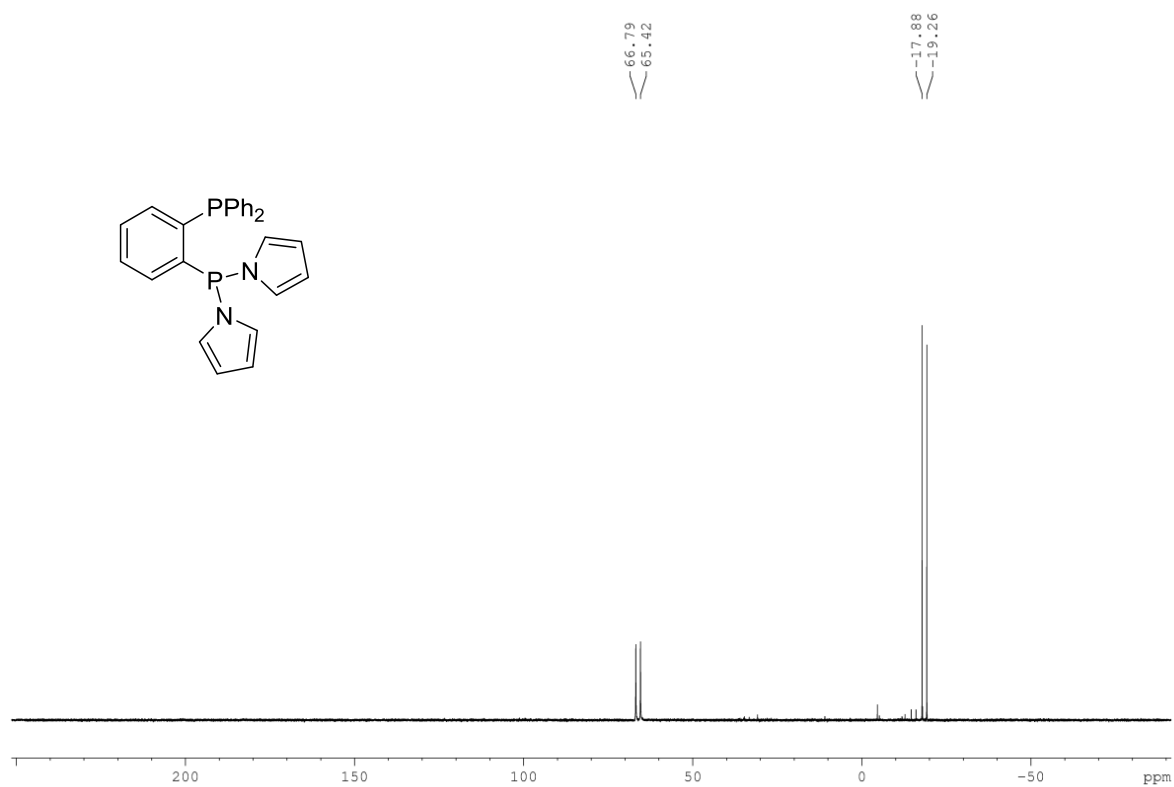
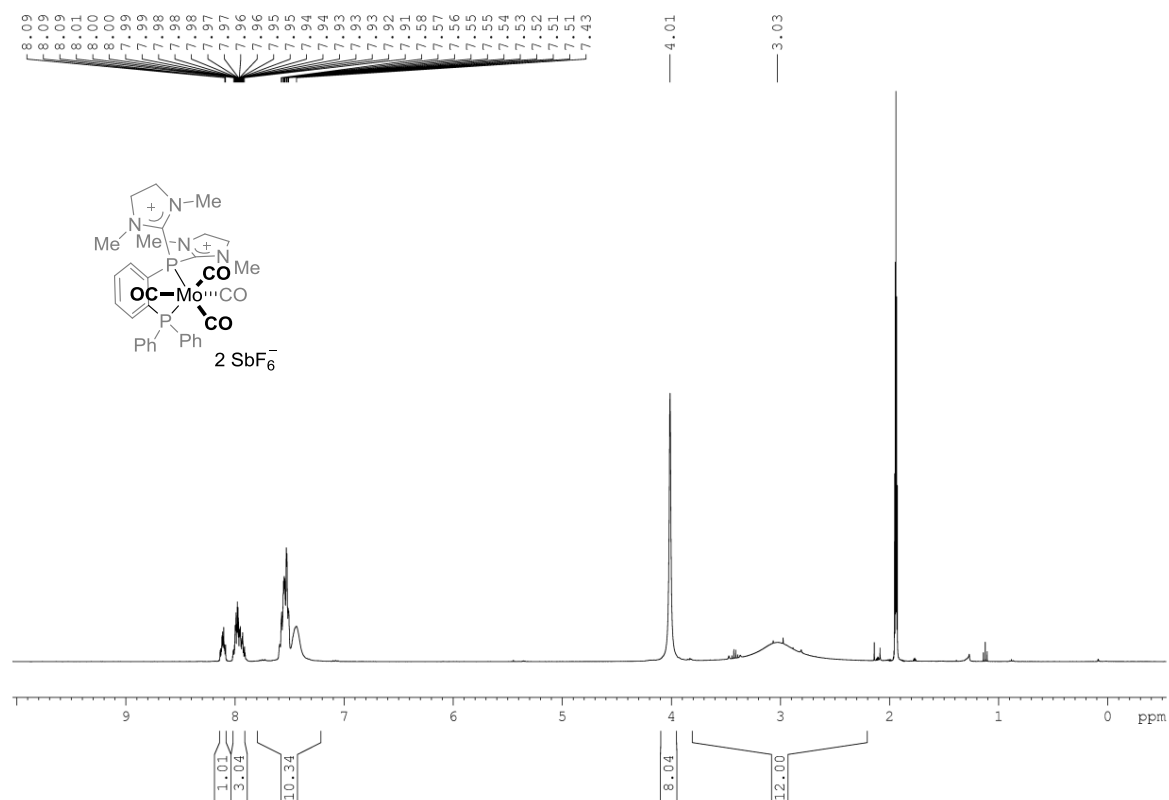
^1H NMR (CD_3CN , 400 MHz) (Compound 104) ^{13}C NMR (CD_3CN , 100 MHz) (Compound 104)

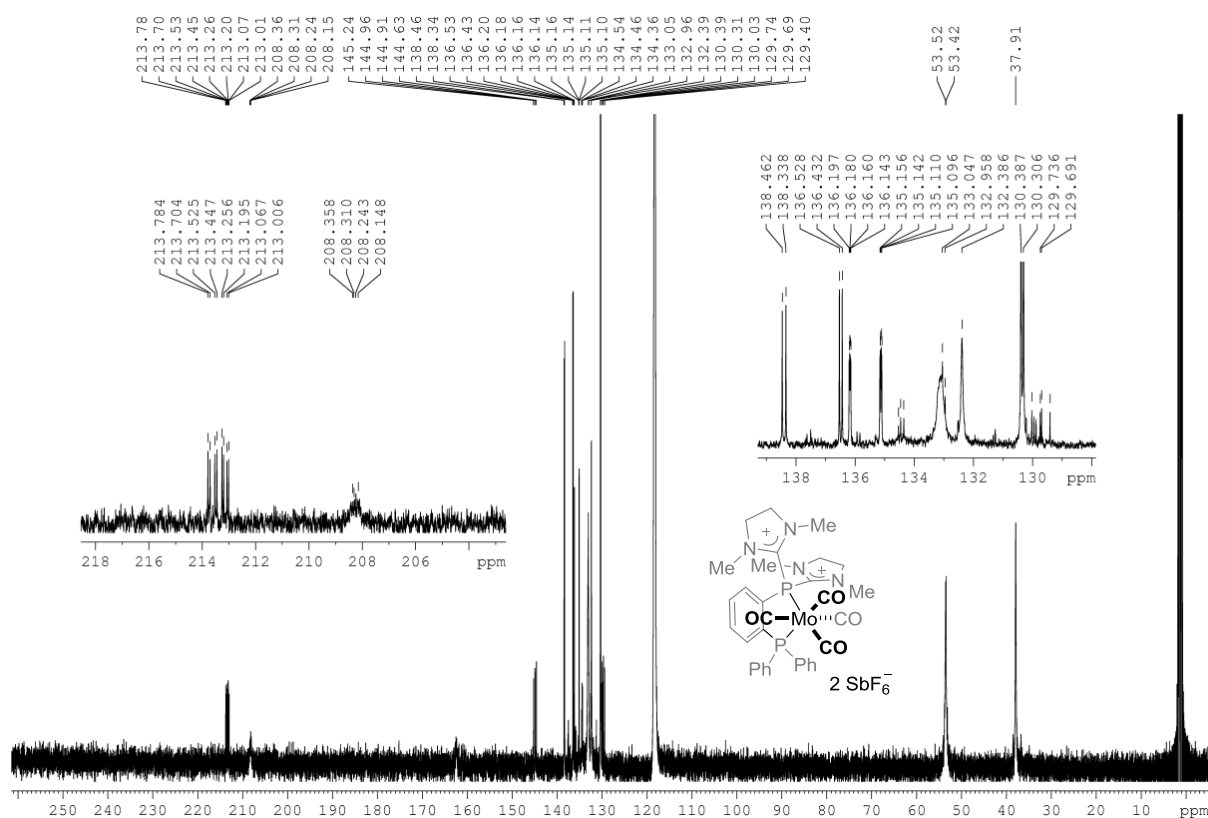
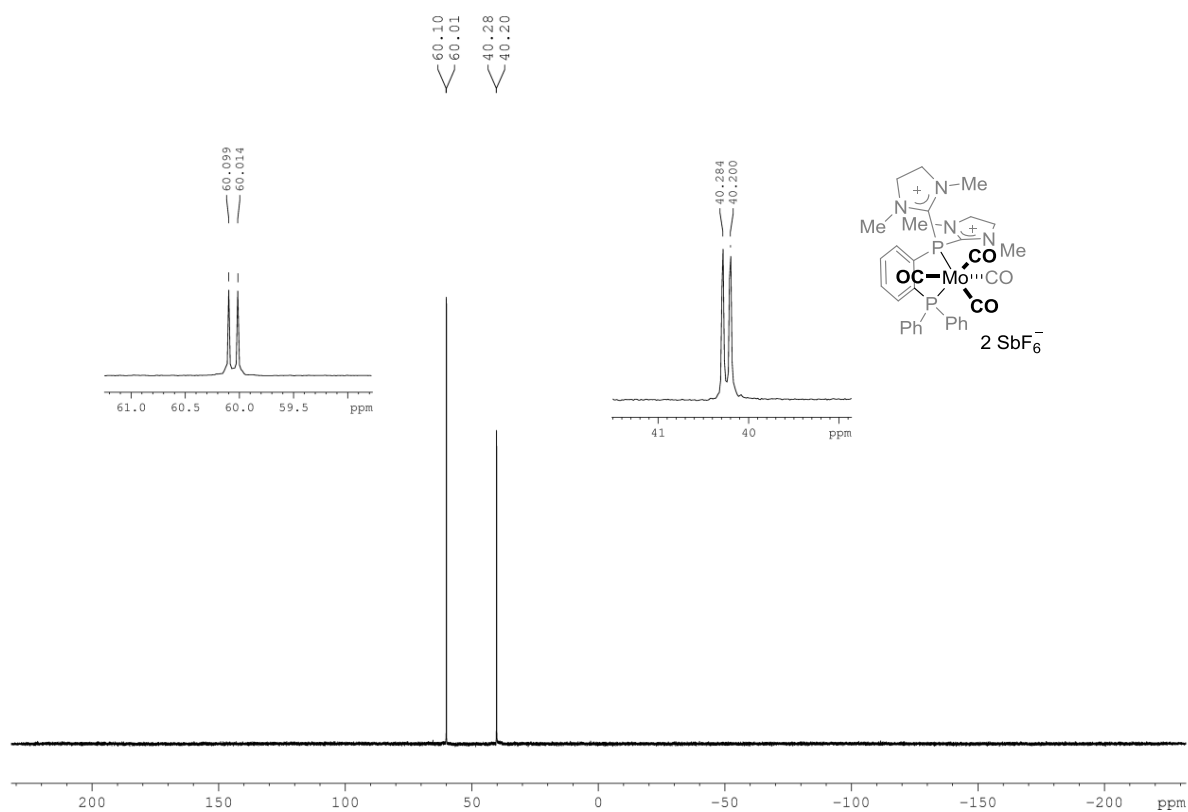
^{31}P NMR (CD₃CN, 121 MHz) (Compound 104) **^{19}F NMR (CD₃CN, 282 MHz) (Compound 104)**

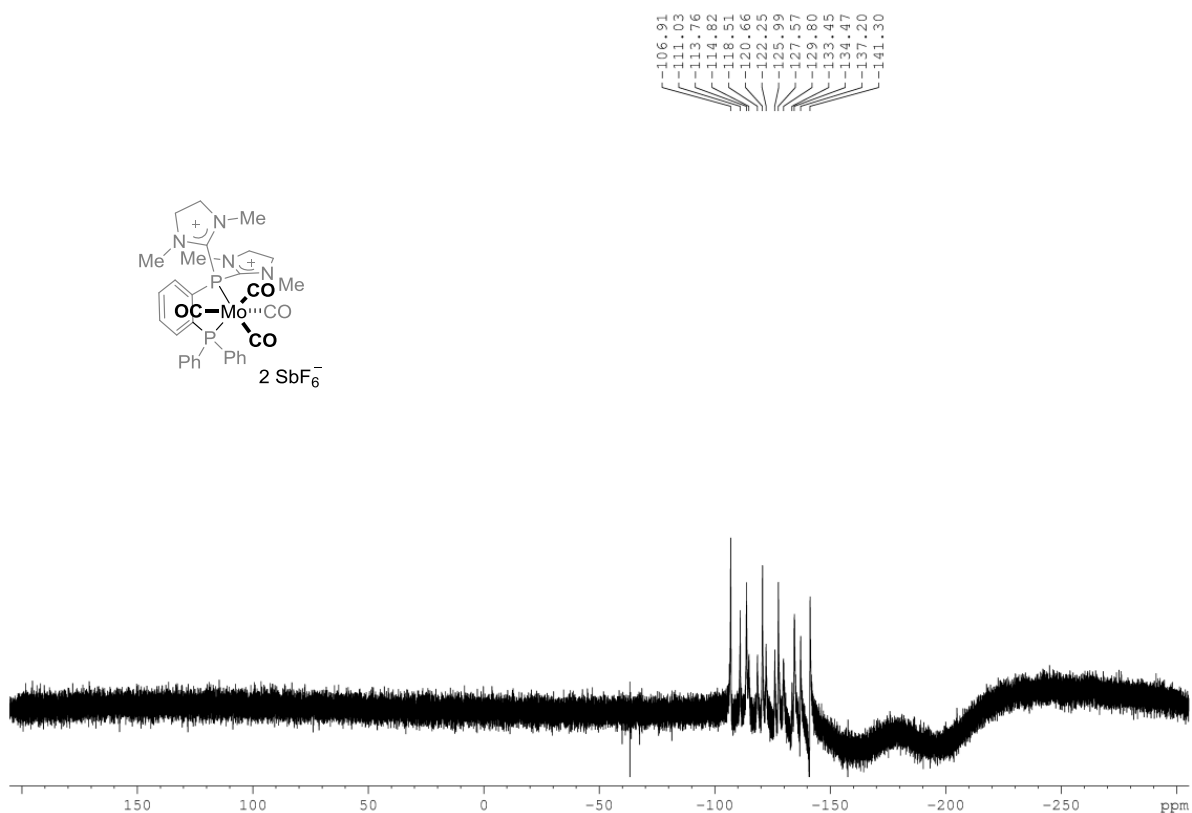
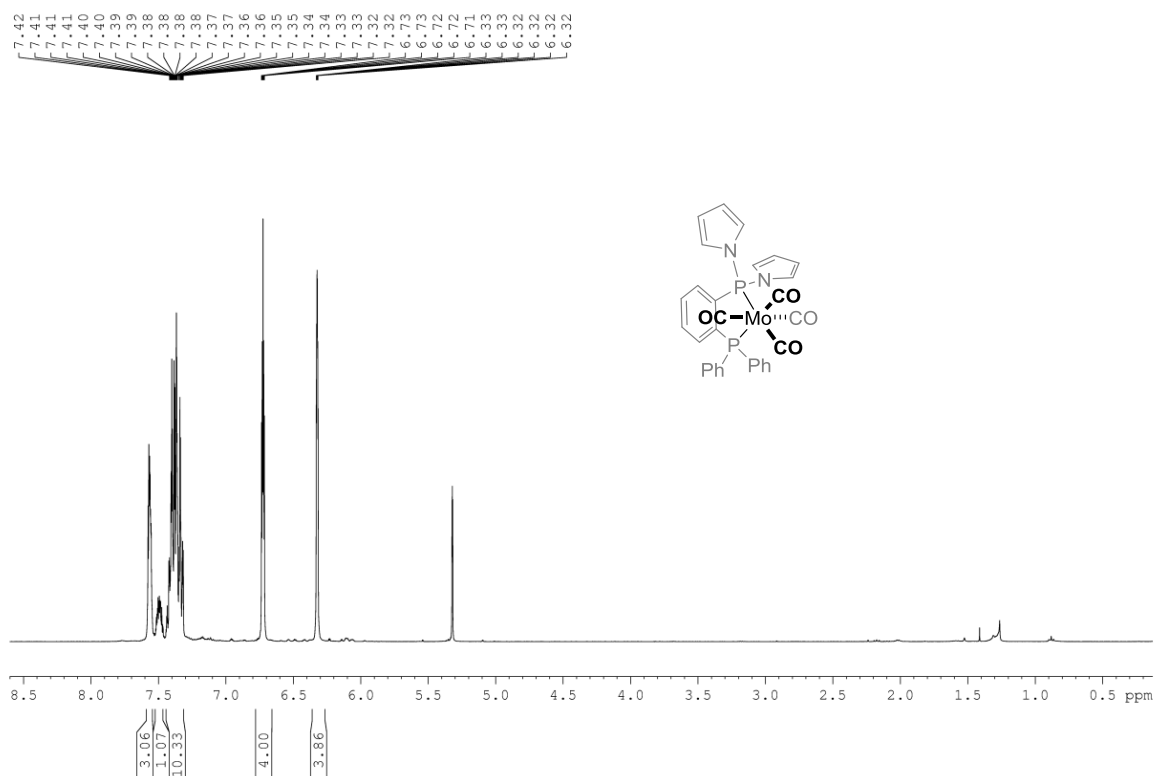
^1H NMR (C_6D_6 , 400 MHz) (Compound 105) ^{13}C NMR (C_6D_6 , 100 MHz) (Compound 105)

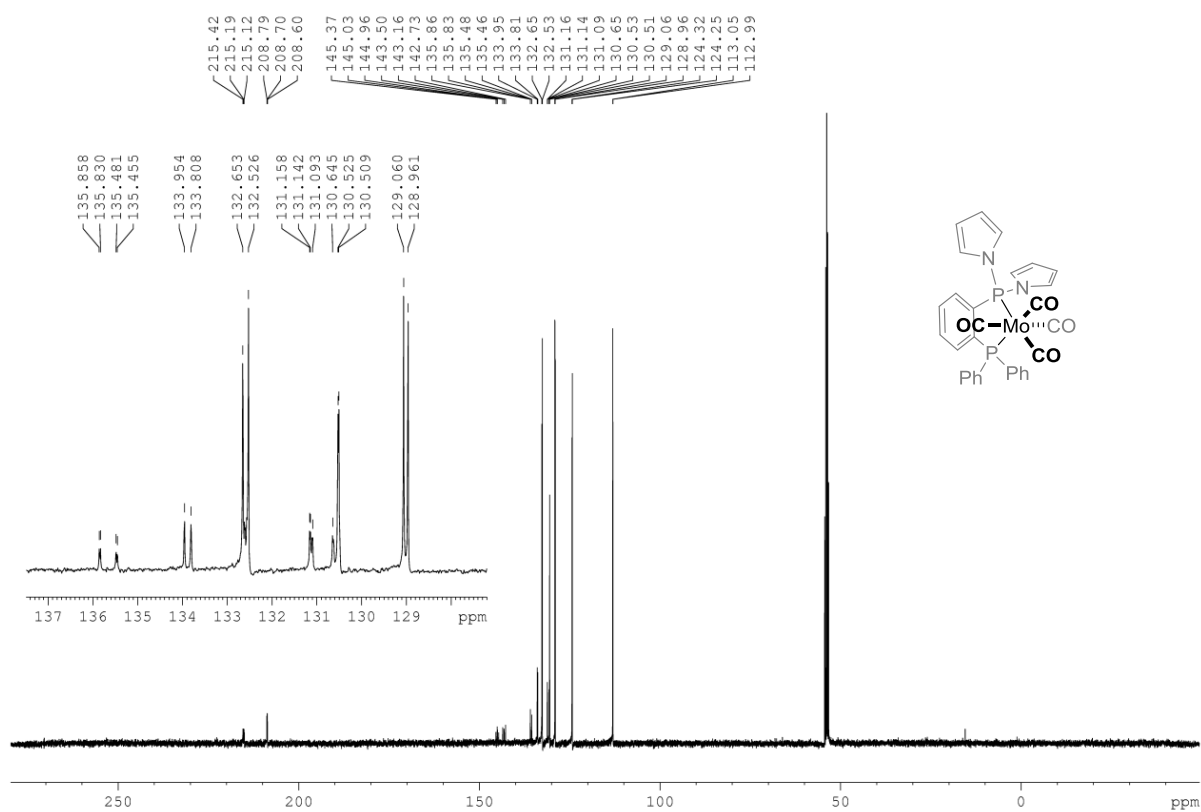
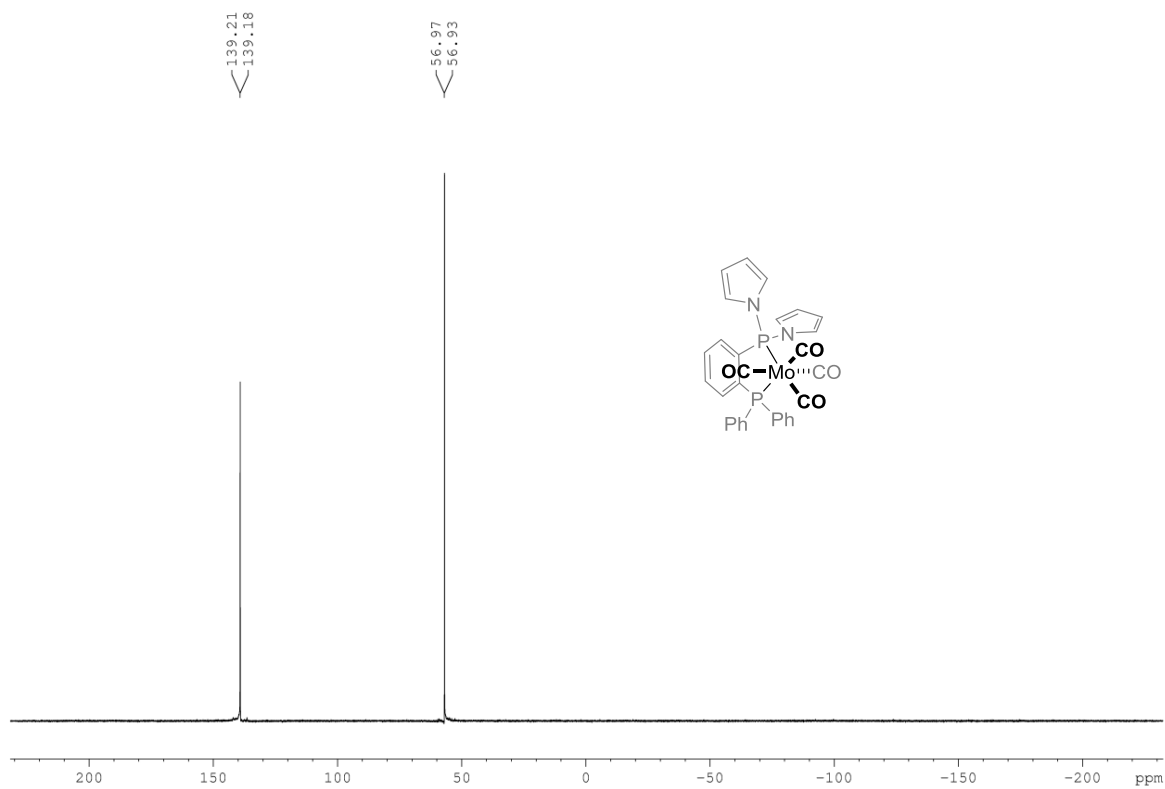
^{31}P NMR (C_6D_6 , 121 MHz) (Compound 105) **^{19}F NMR (C_6D_6 , 282 MHz) (Compound 105)**

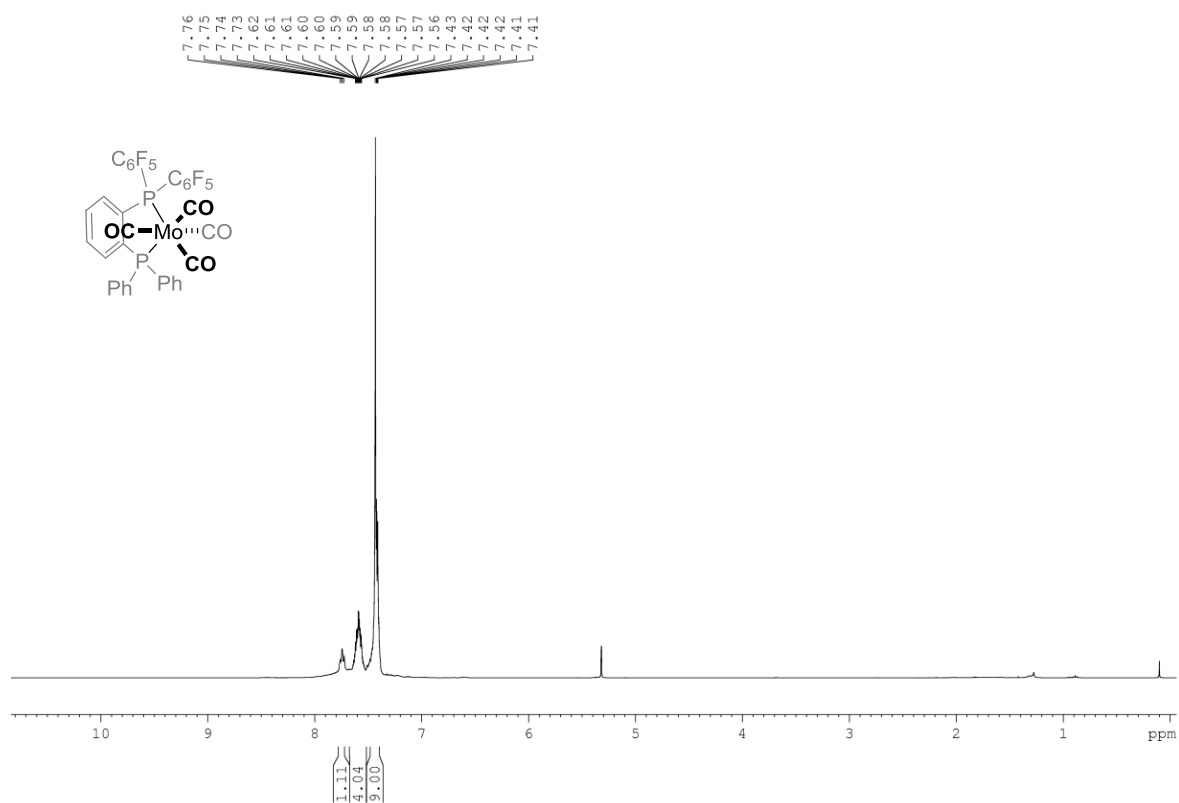
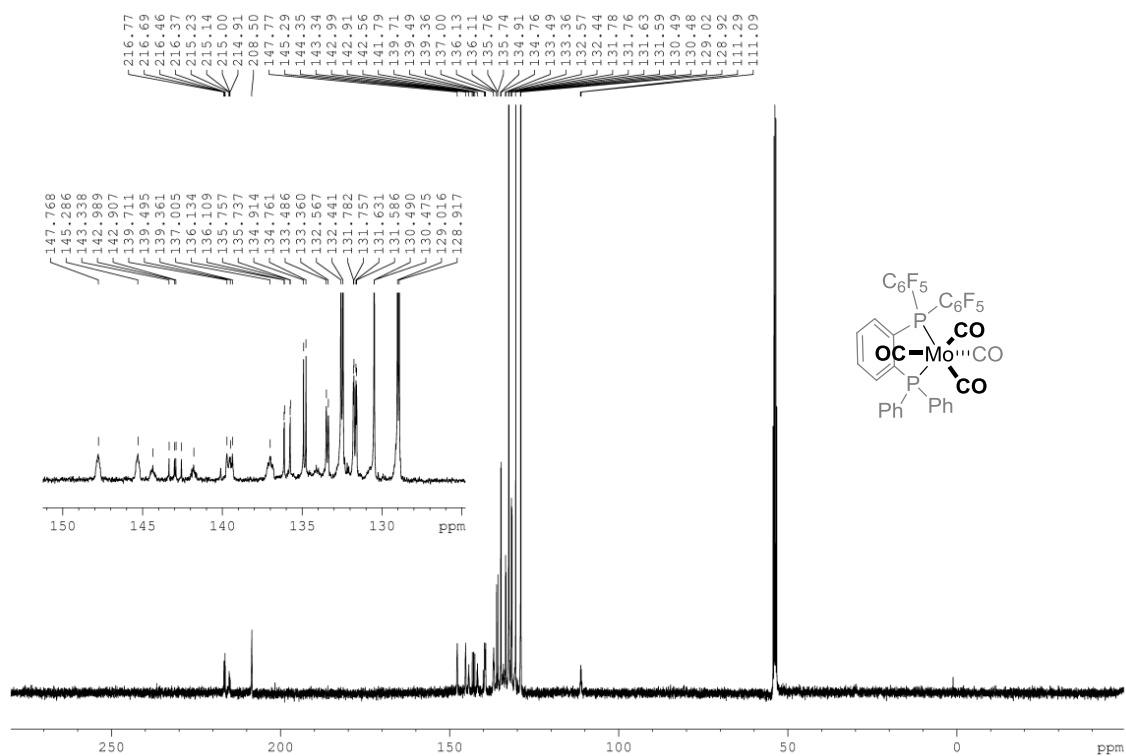
^1H NMR (C_6D_6 , 300 MHz) (Compound 106) ^{13}C NMR (C_6D_6 , 100 Mz) (Compound 106)

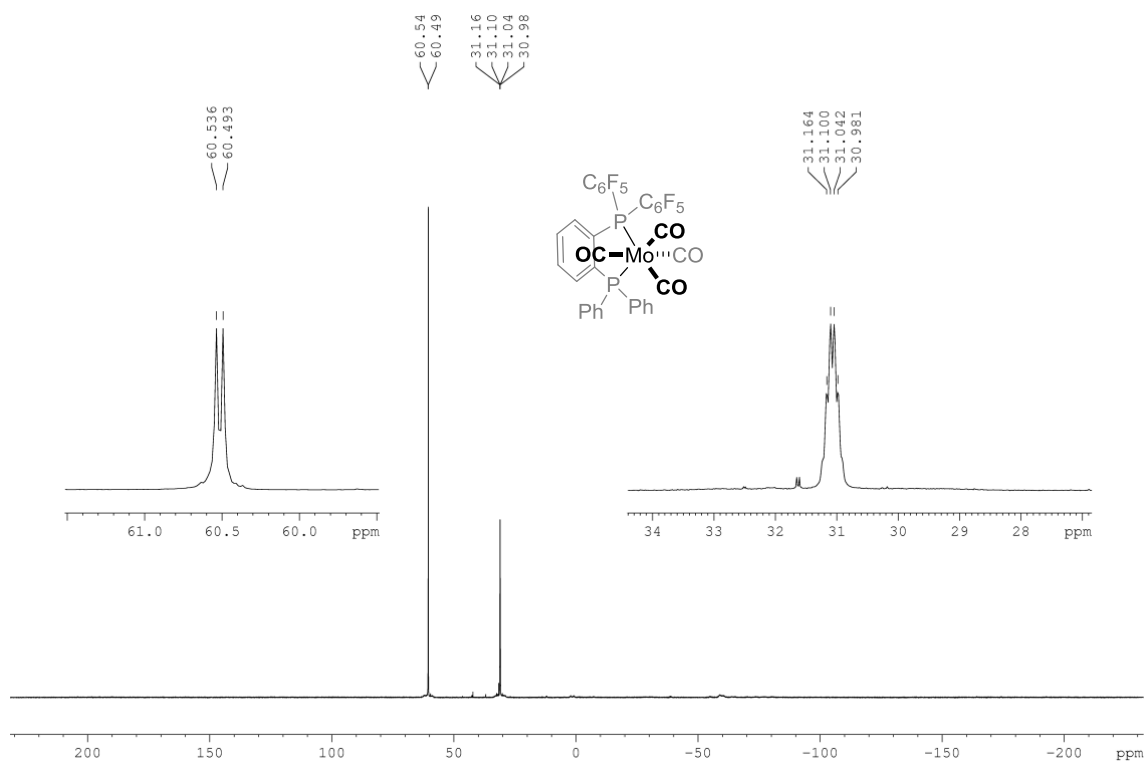
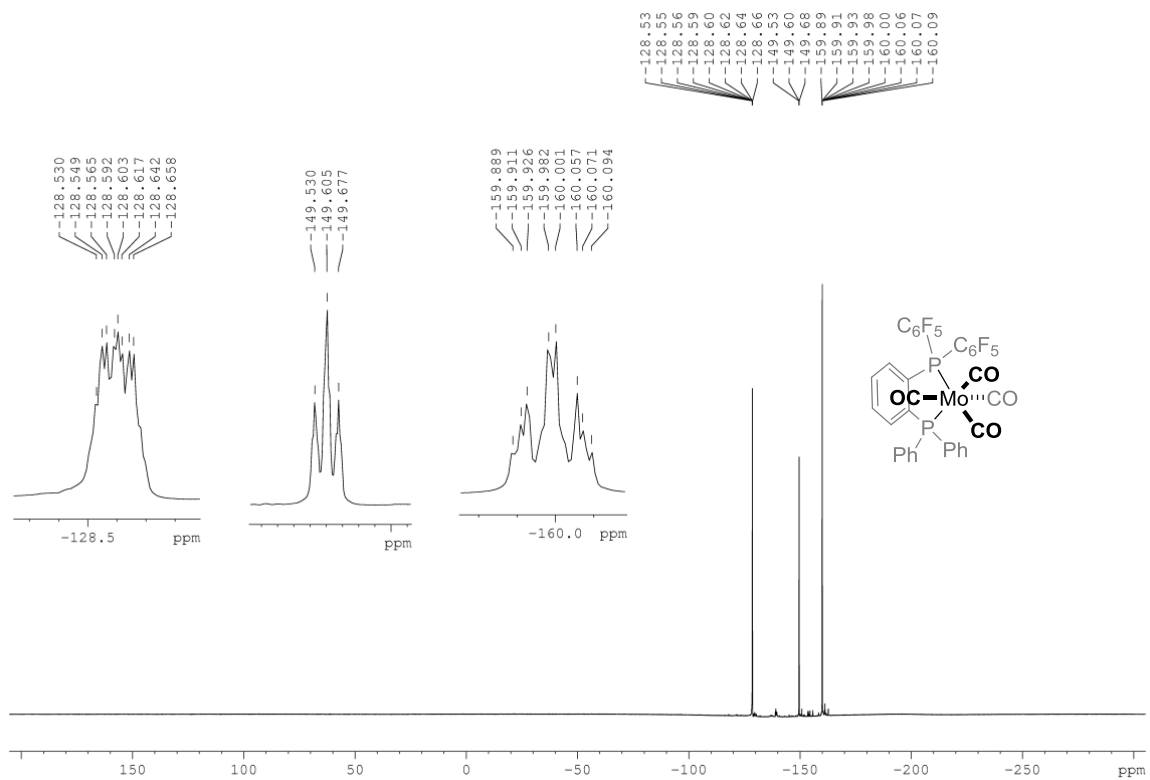
^{31}P NMR (C_6D_6 , 121 MHz) (Compound 106) **^1H NMR (CD_3CN , 400 MHz) (Compound 107a)**

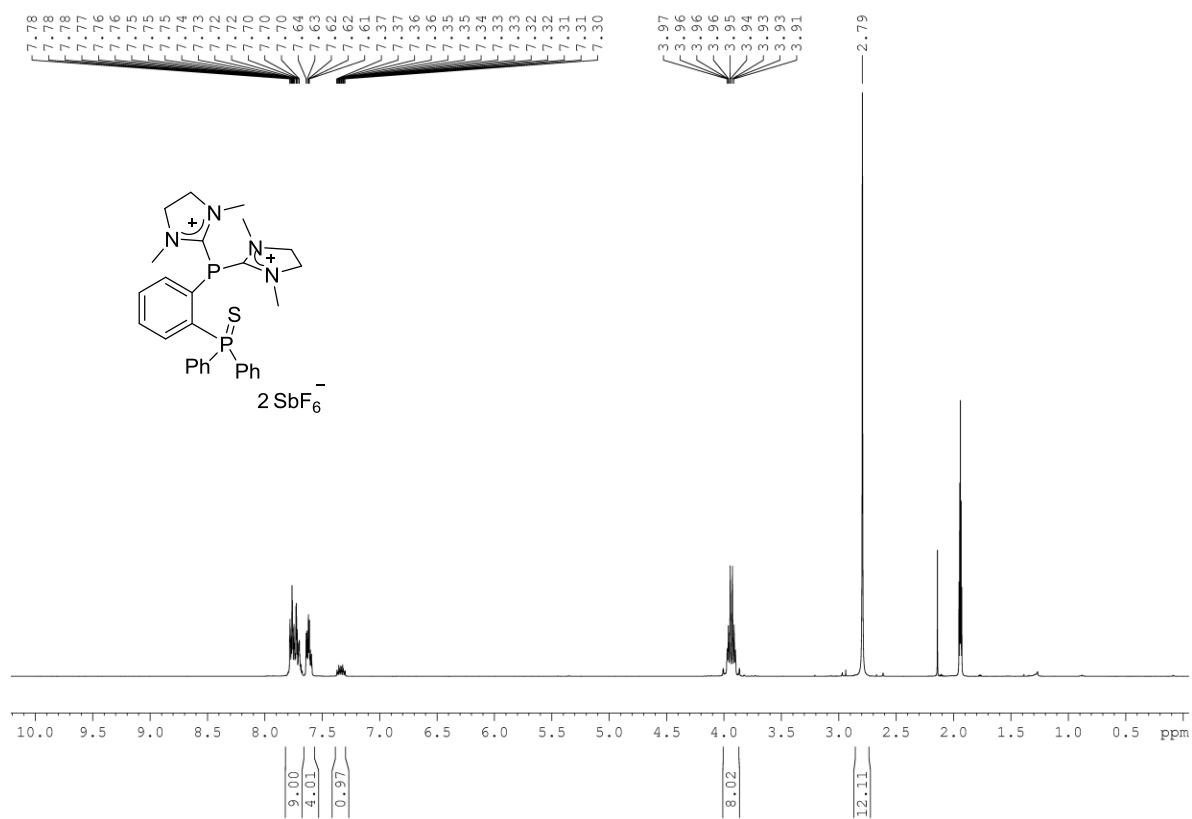
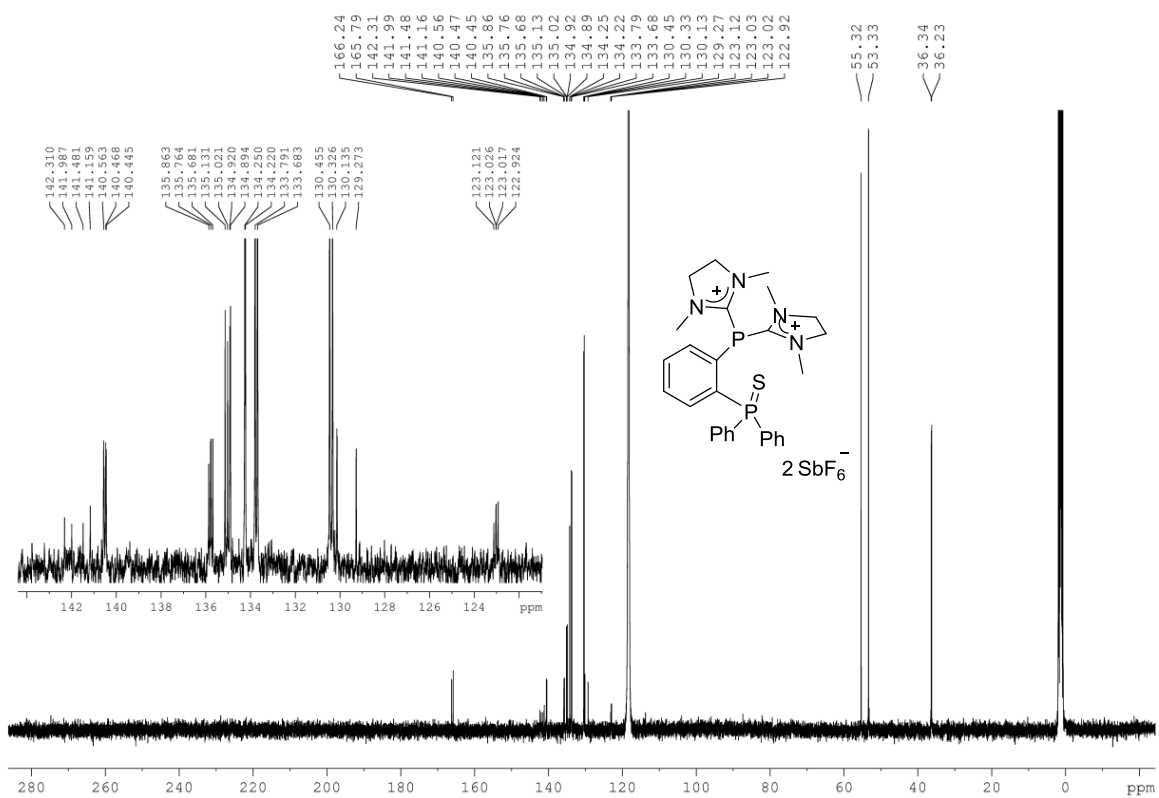
^{13}C NMR (CD₃CN, 125 Mz) (Compound 107a) ^{31}P NMR (CD₃CN, 162 MHz) (Compound 107a)

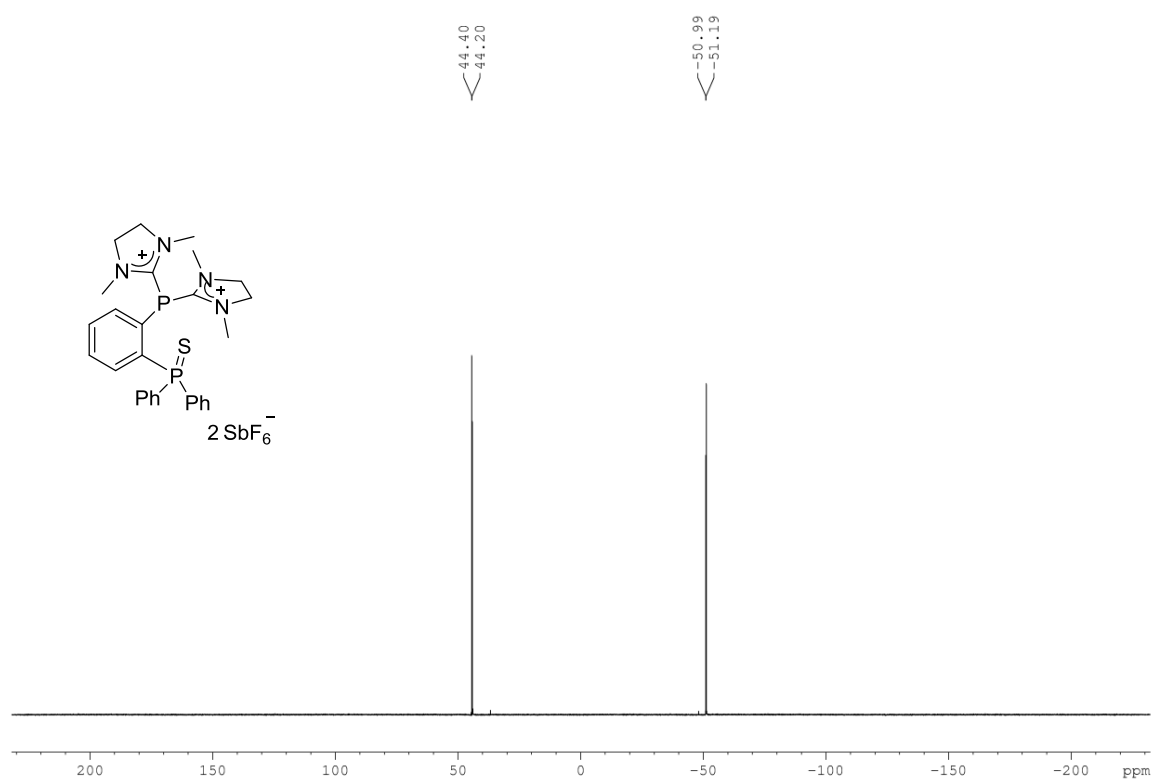
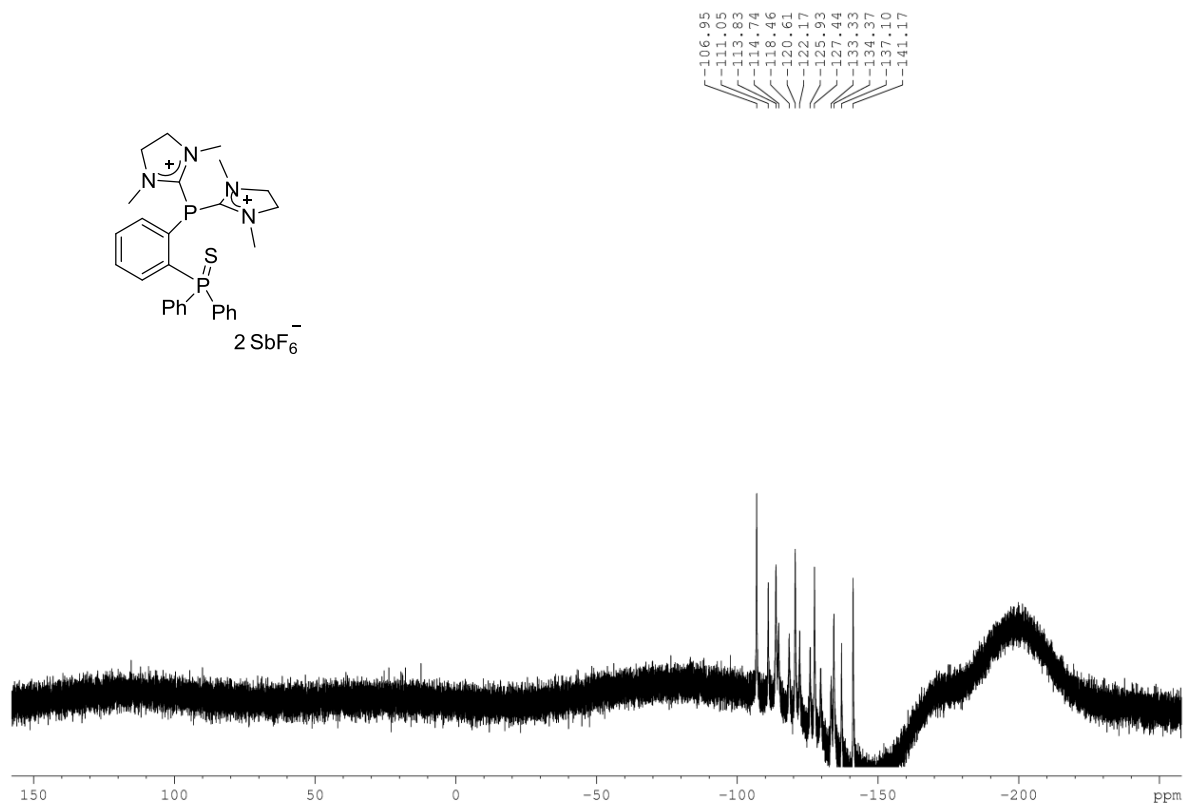
^{19}F NMR (CD_3CN , 282 MHz) (Compound 107a) **^1H NMR (CD_2Cl_2 , 400 MHz) (Compound 107b)**

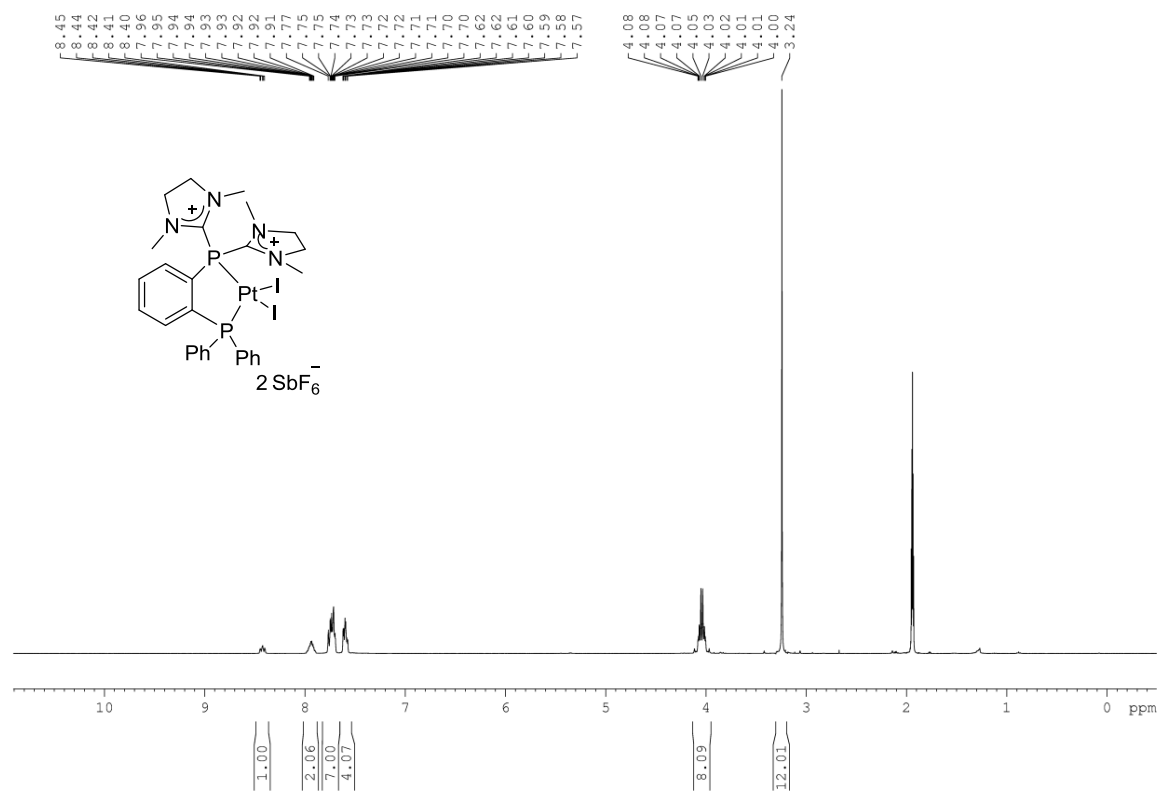
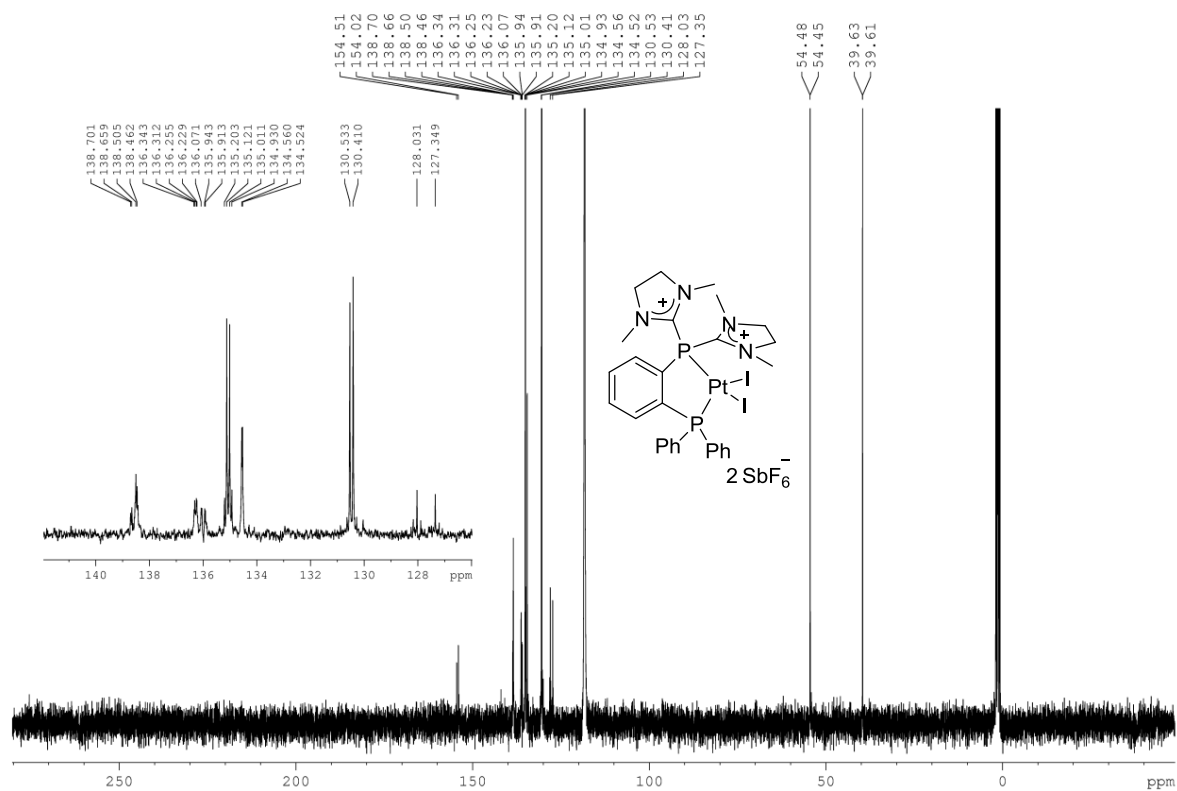
^{13}C NMR (CD_2Cl_2 , 100 Mz) (Compound 107b) **^{31}P NMR (CD_2Cl_2 , 162 MHz) (Compound 107b)**

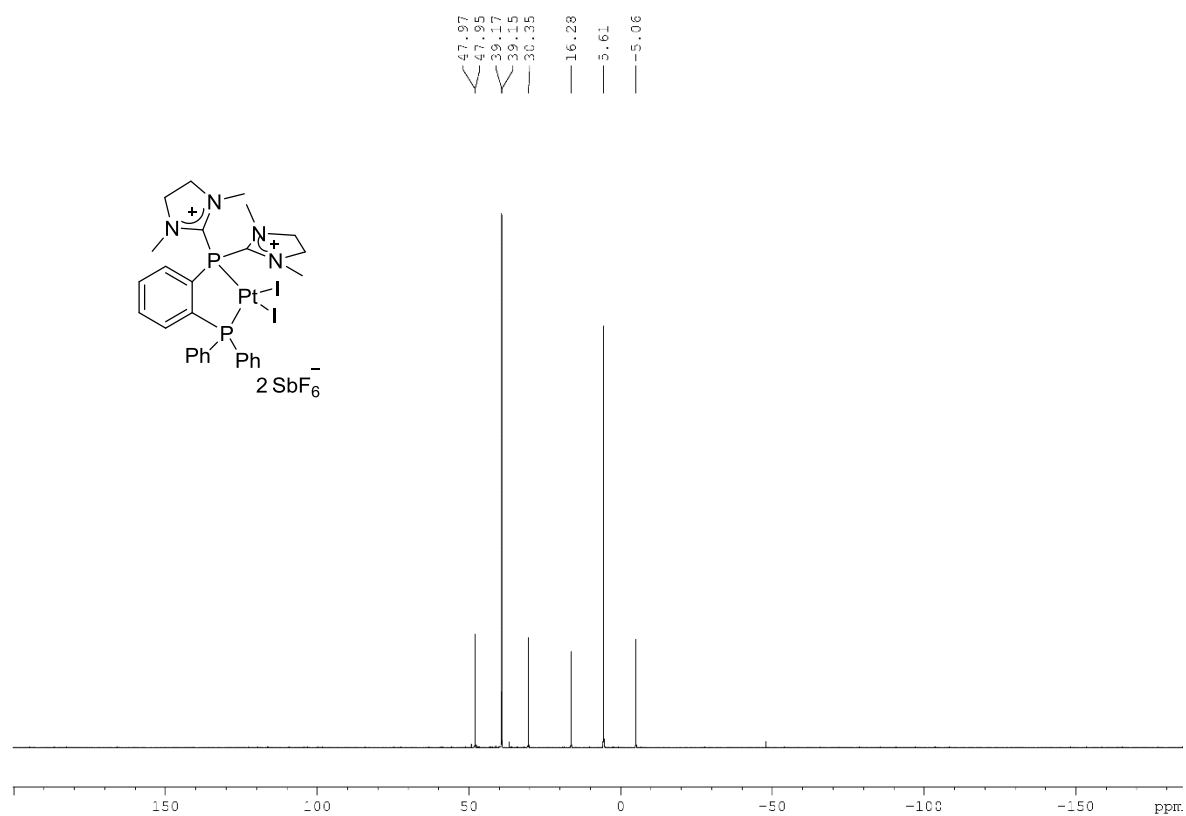
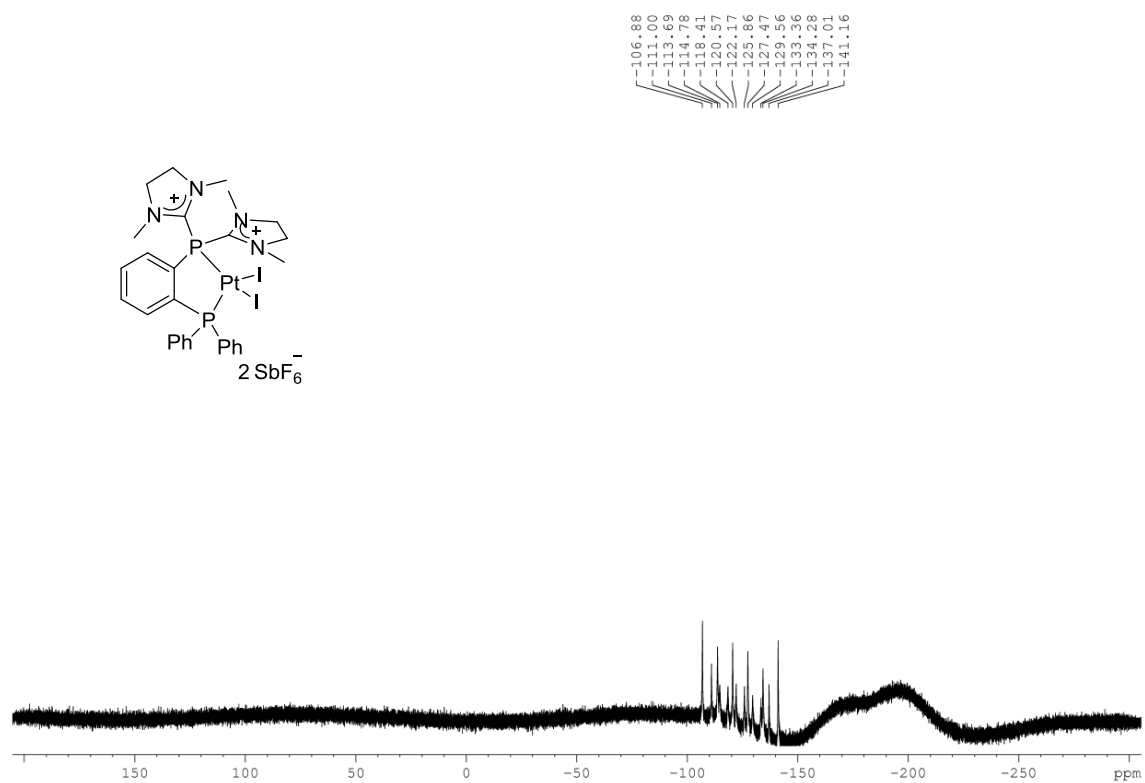
^1H NMR (CD_2Cl_2 , 400 MHz) (Compound 107c) **^{13}C NMR (CD_2Cl_2 , 100 Mz) (Compound 107c)**

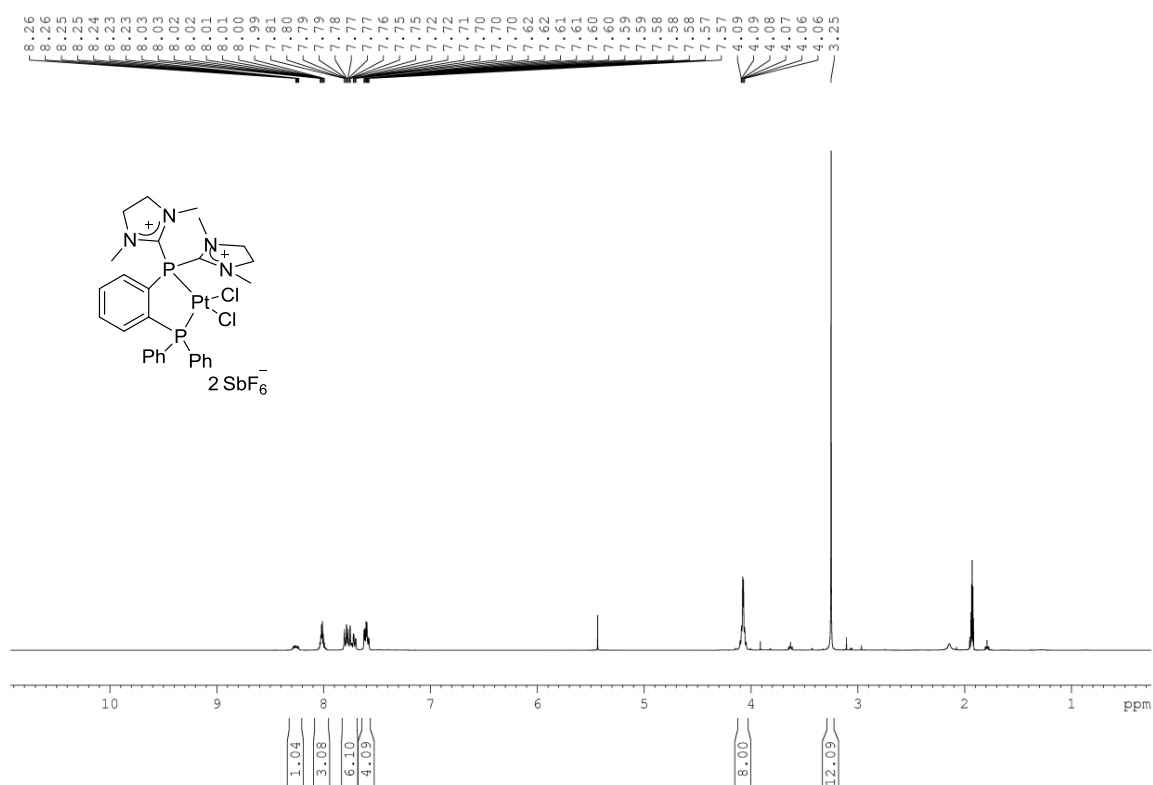
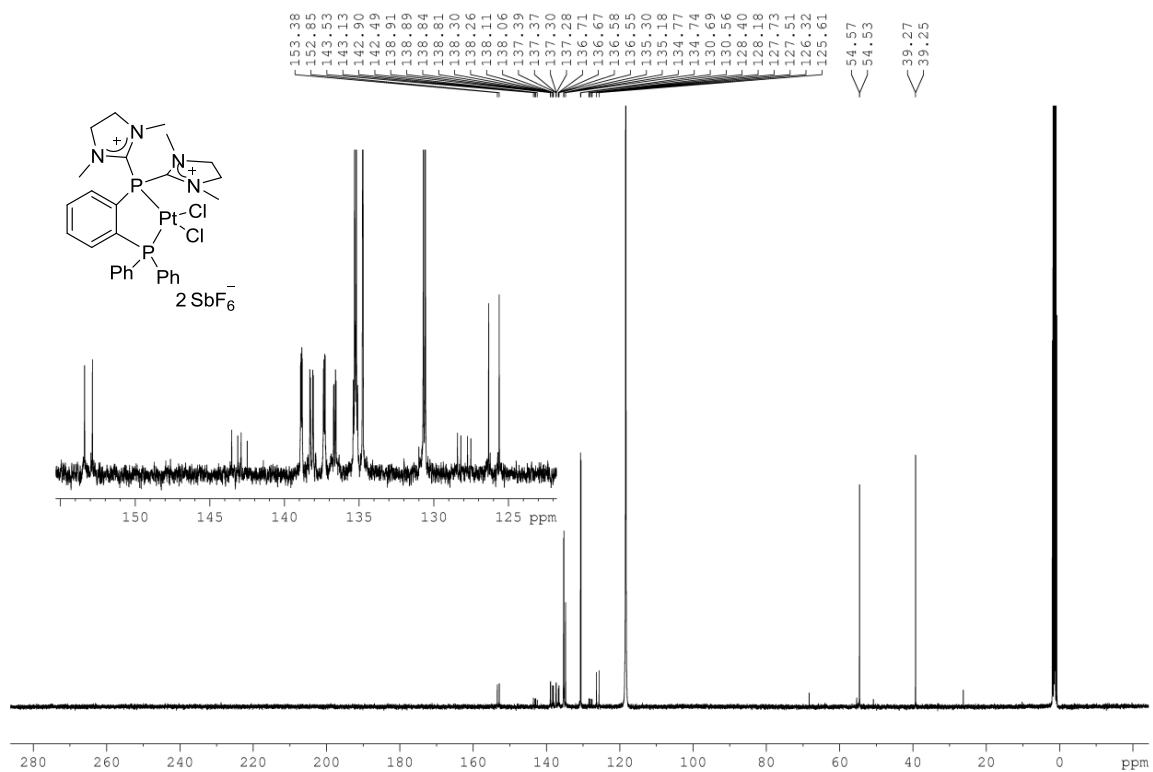
^{31}P NMR (CD_2Cl_2 , 162 MHz) (Compound 107c) **^{19}F NMR (CD_2Cl_2 , 282 MHz) (Compound 107c)**

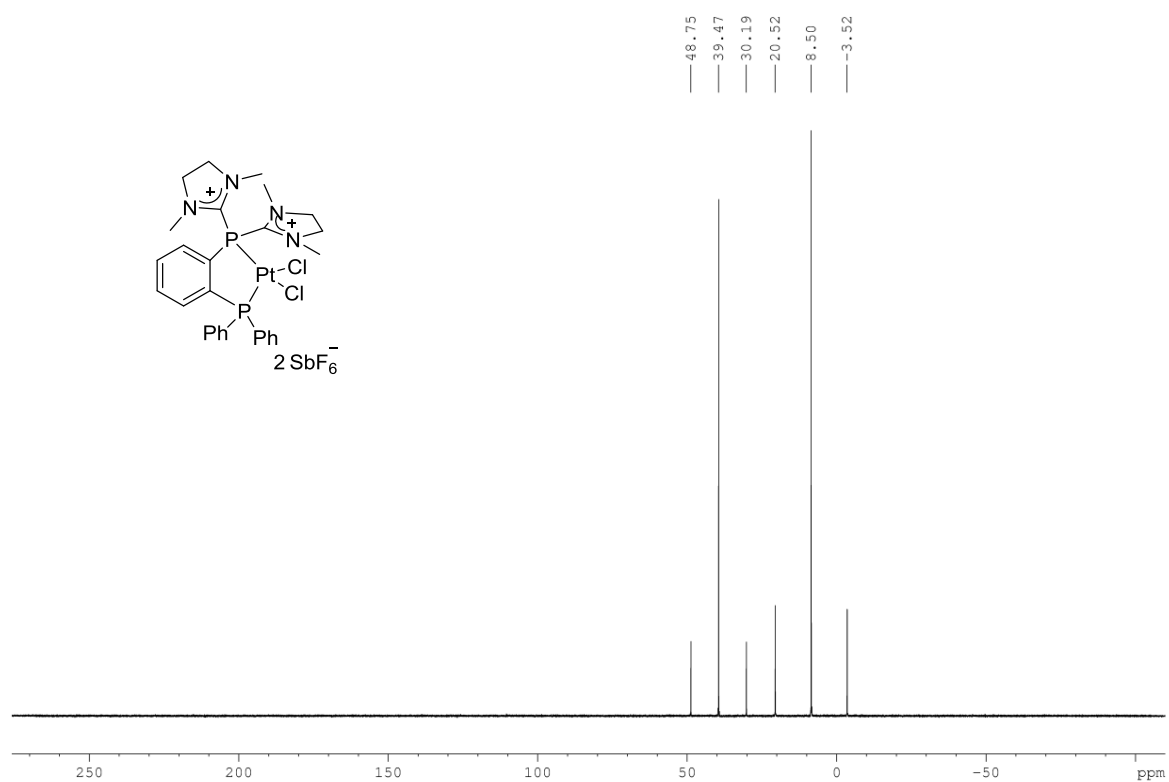
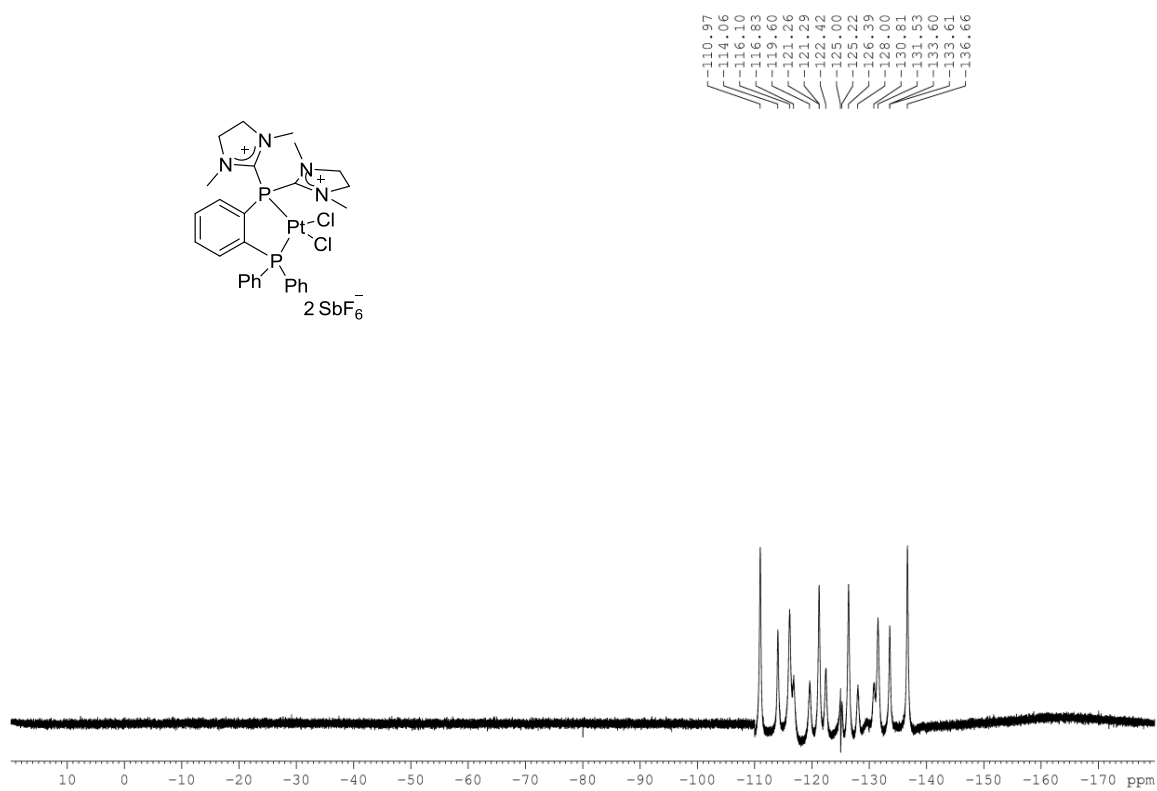
^{13}H NMR (CD₃CN, 400 MHz) (Compound 108) **^{13}C NMR (CD₃CN, 100 MHz) (Compound 108)**

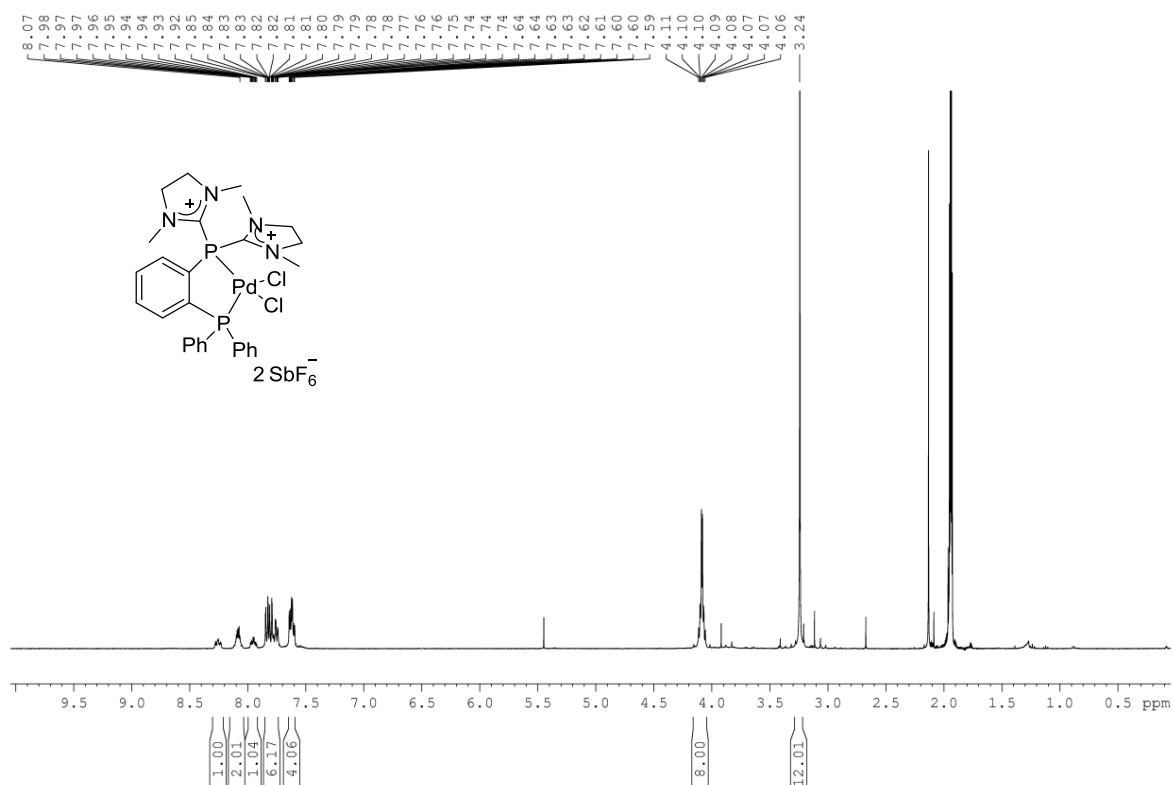
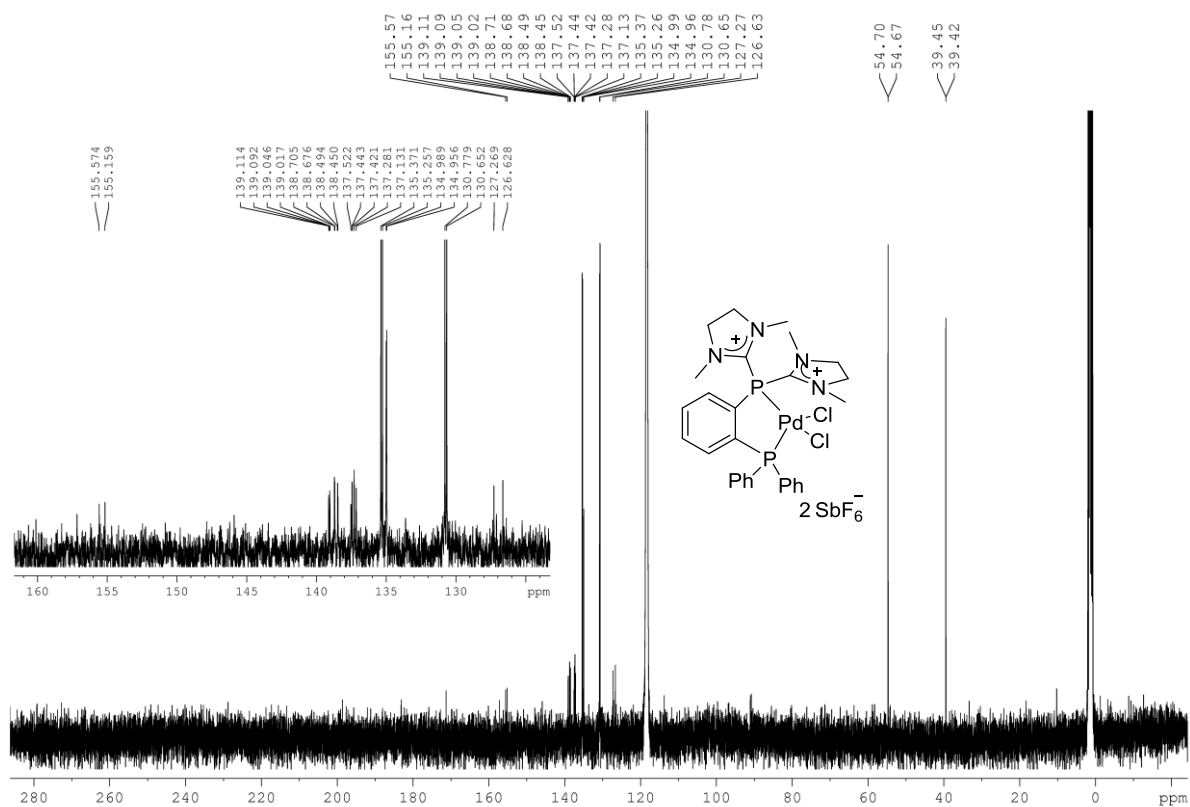
^{31}P NMR (CD₃CN, 121 MHz) (Compound 108) **^{19}F NMR (CD₃CN, 282 MHz) (Compound 108)**

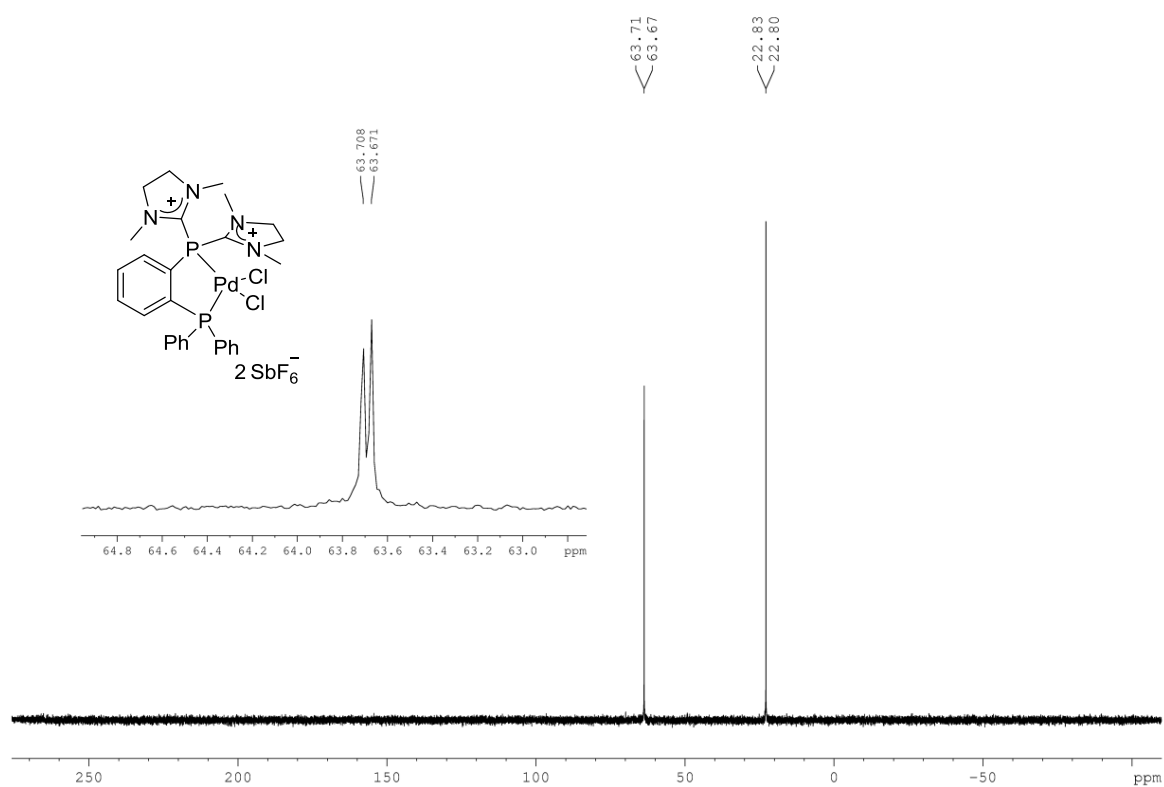
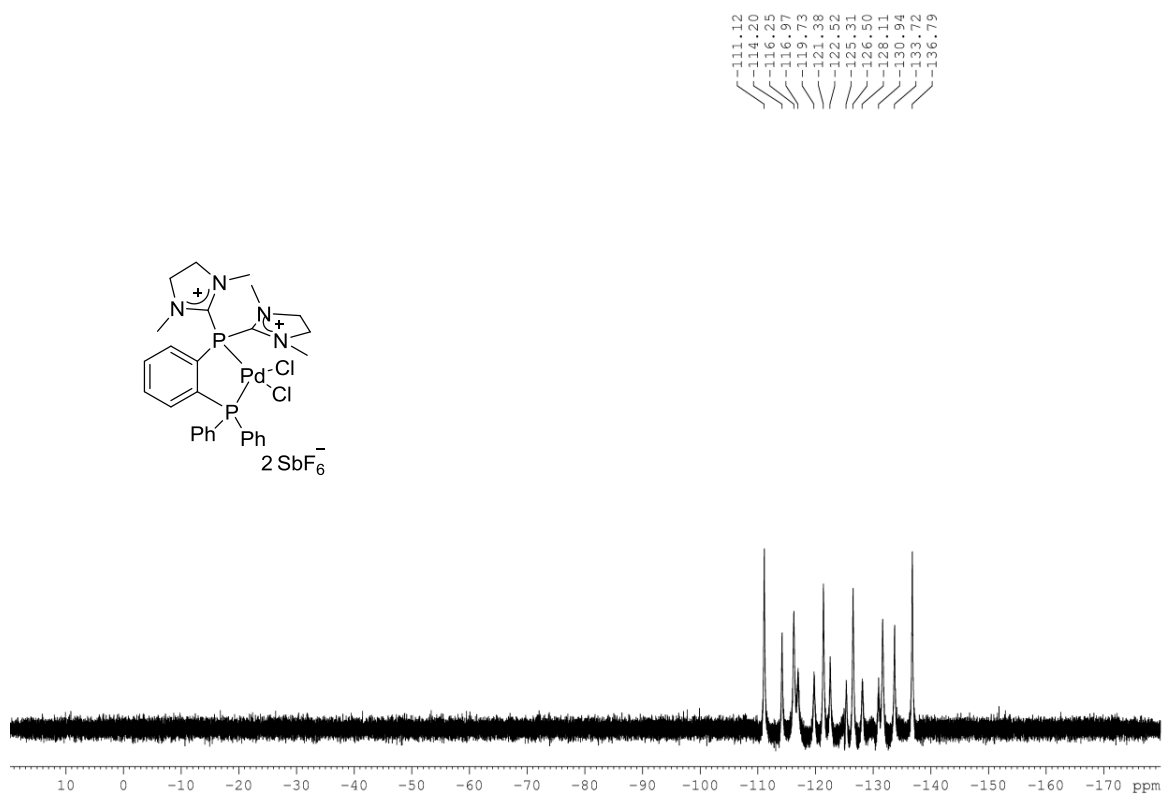
^1H NMR (CD₃CN, 400 MHz) (Compound 109a) **^{13}C NMR (CD₃CN, 100 MHz) (Compound 109a)**

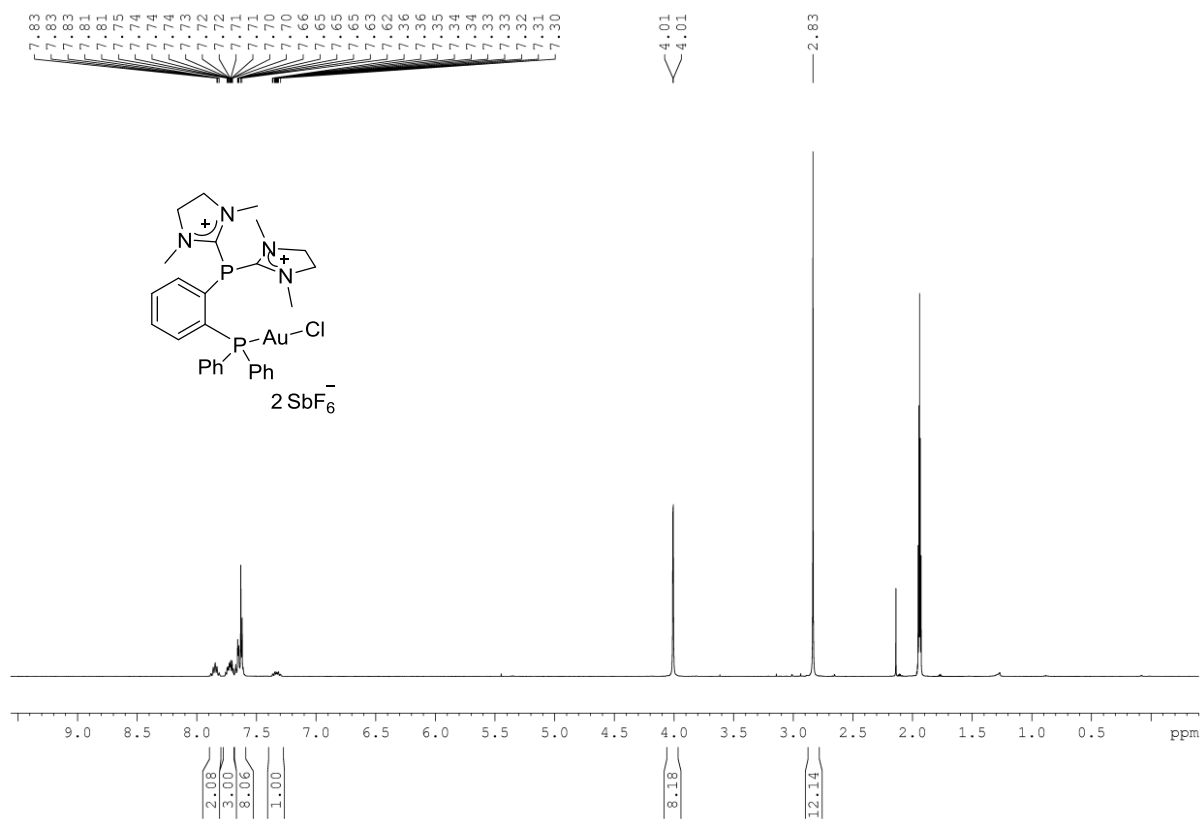
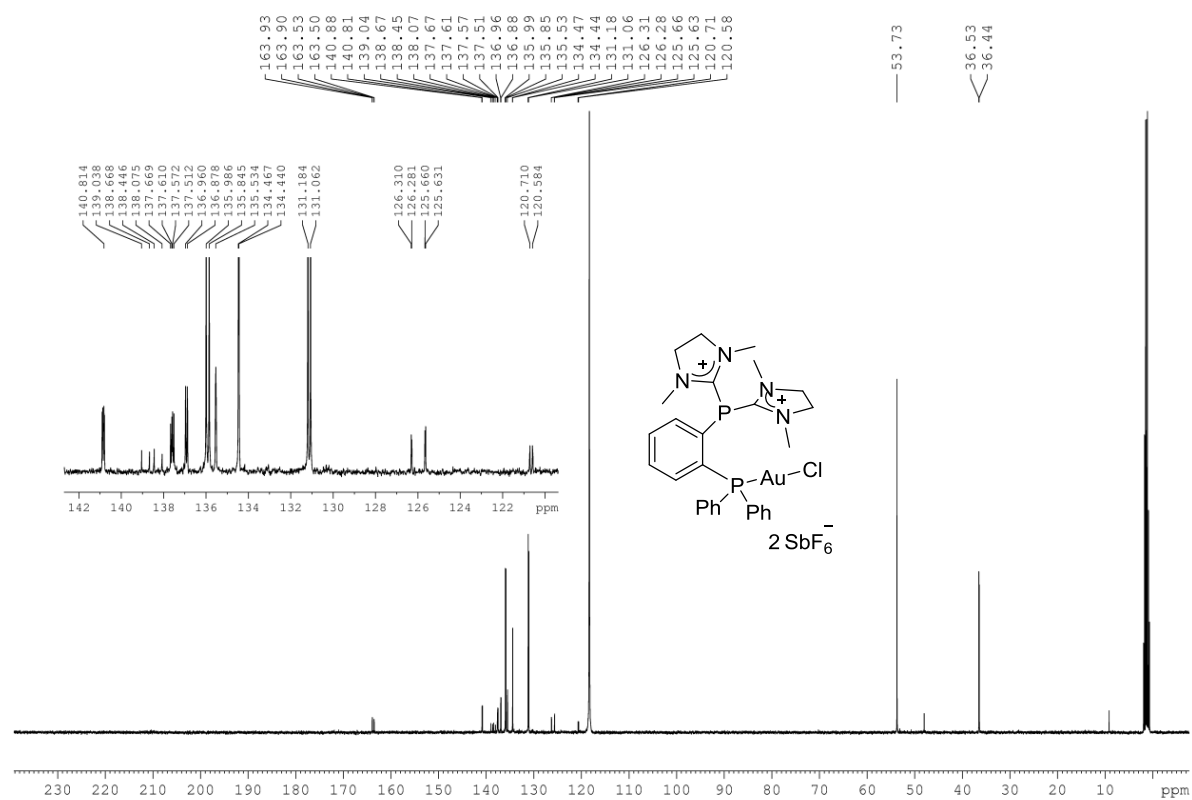
^{31}P NMR (CD₃CN, 121 MHz) (Compound 109a) **^{19}F NMR (CD₃CN, 282 MHz) (Compound 109a)**

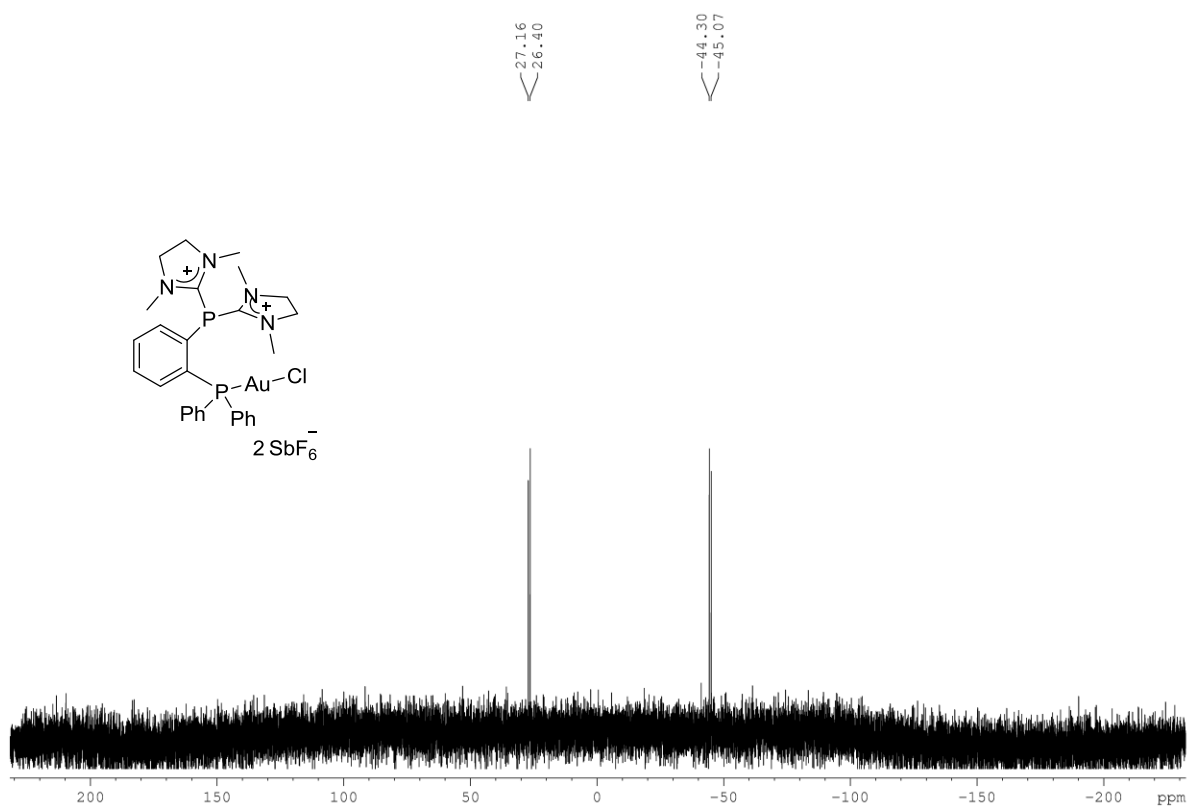
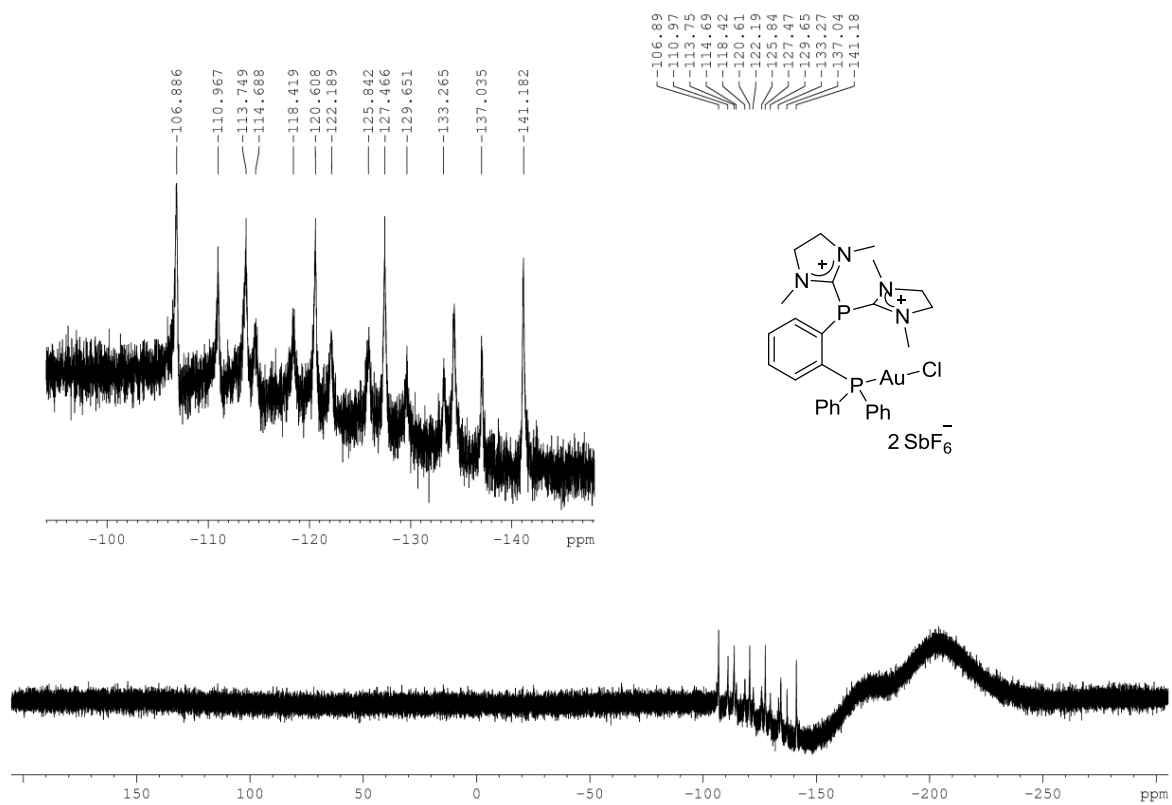
^1H NMR (CD₃CN, 400 MHz) (Compound 109b) **^{13}C NMR (CD₃CN, 100 MHz) (Compound 109b)**

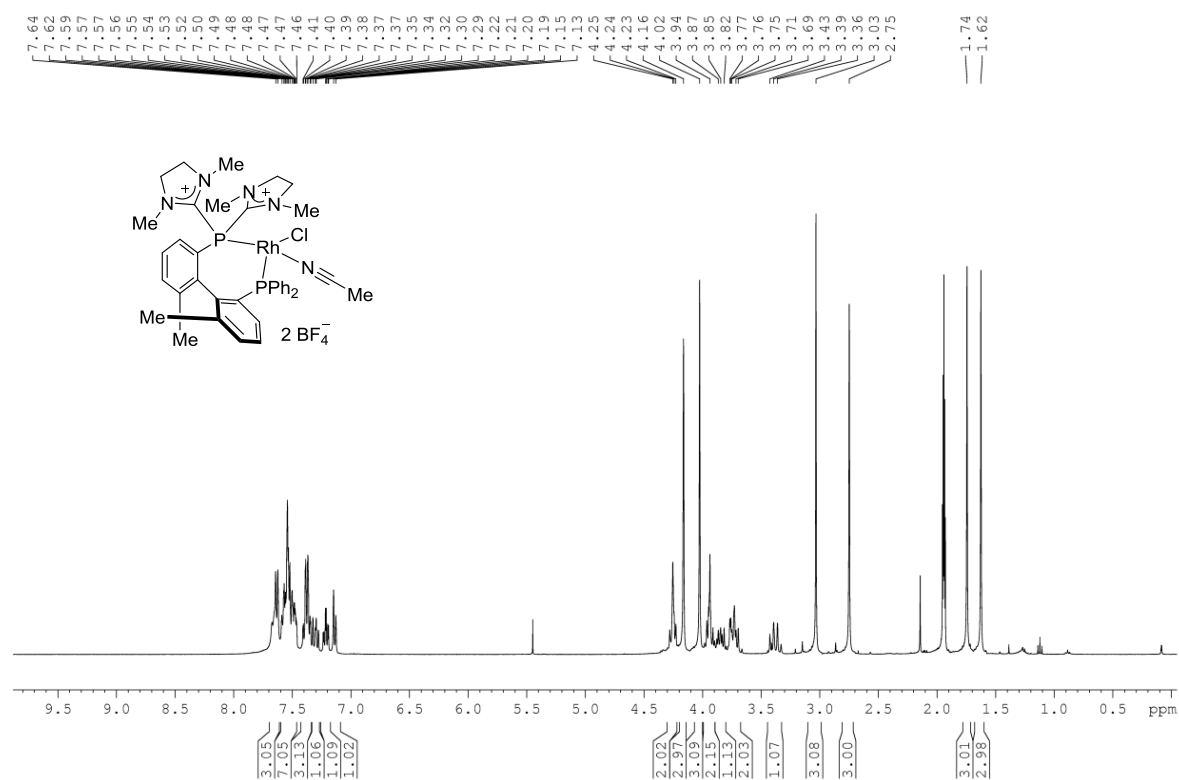
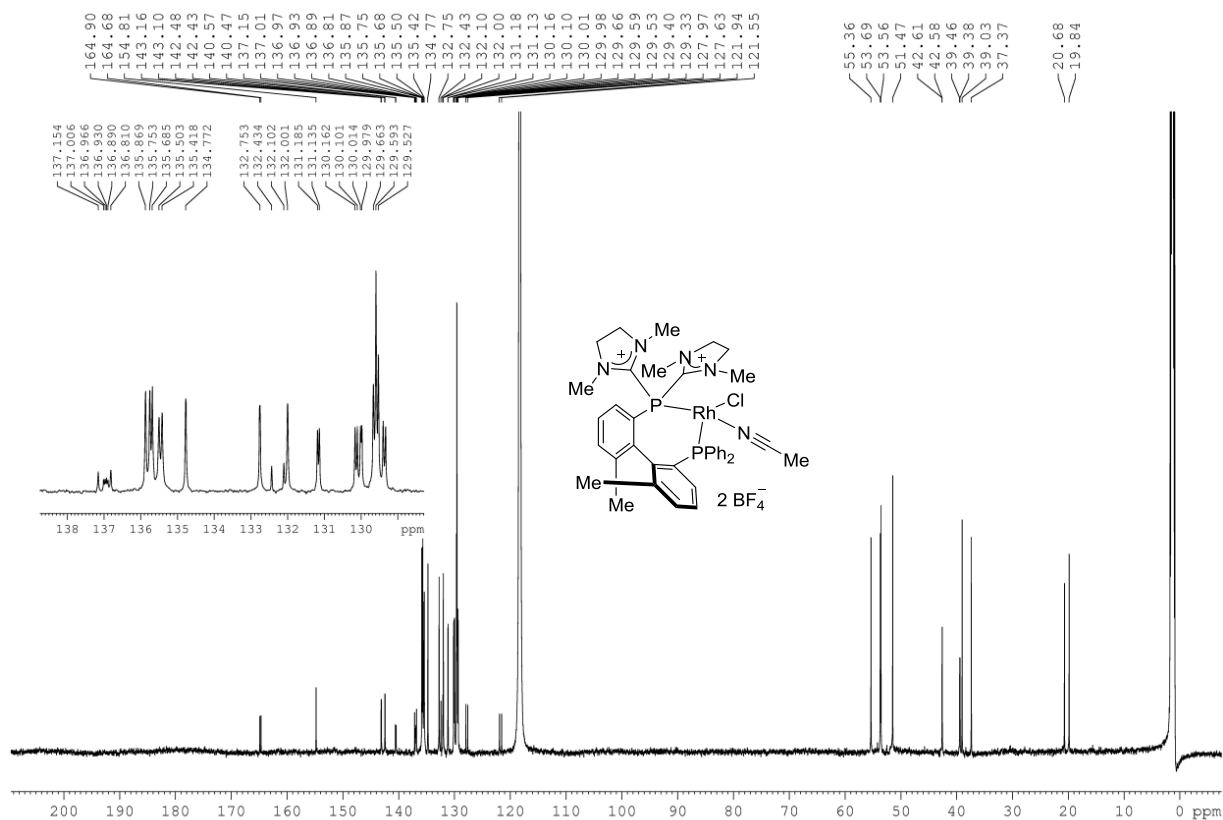
^{31}P NMR (CD₃CN, 121 MHz) (Compound 109b) **^{19}F NMR (CD₃CN, 376 MHz) (Compound 109b)**

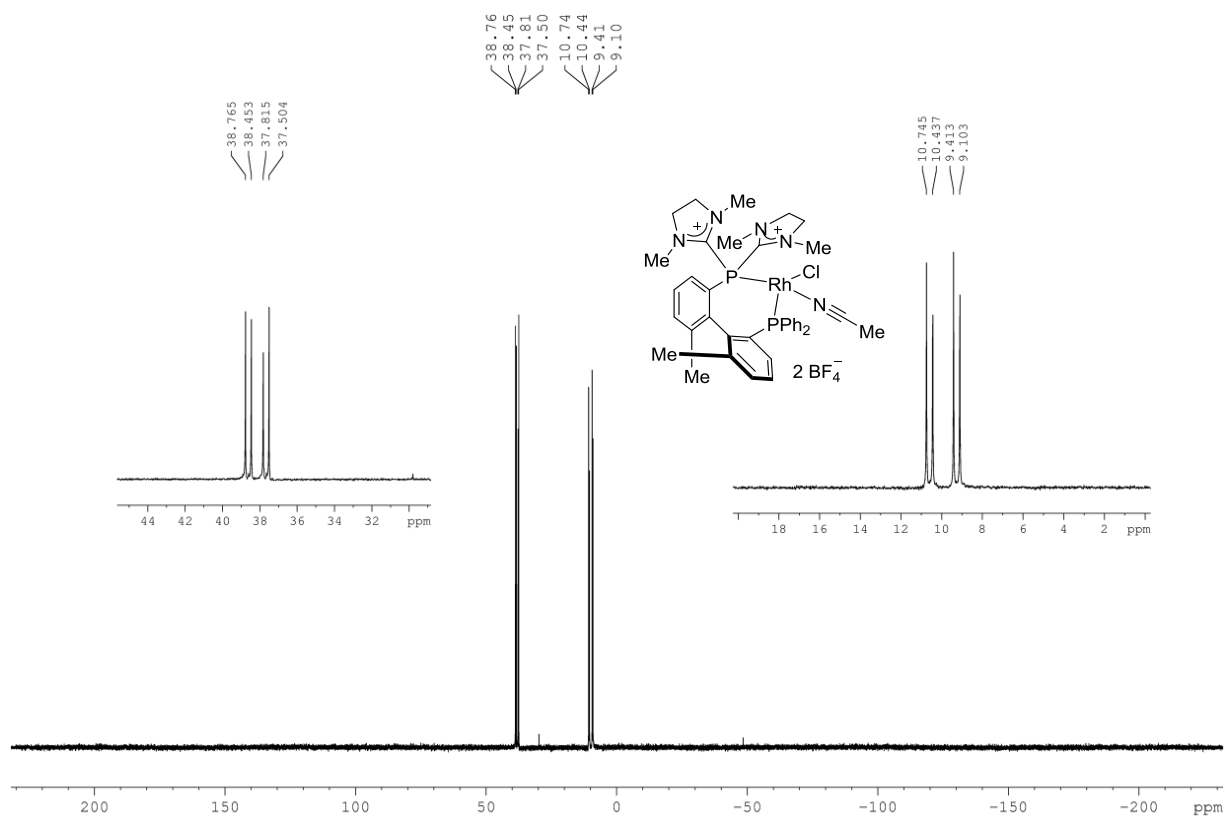
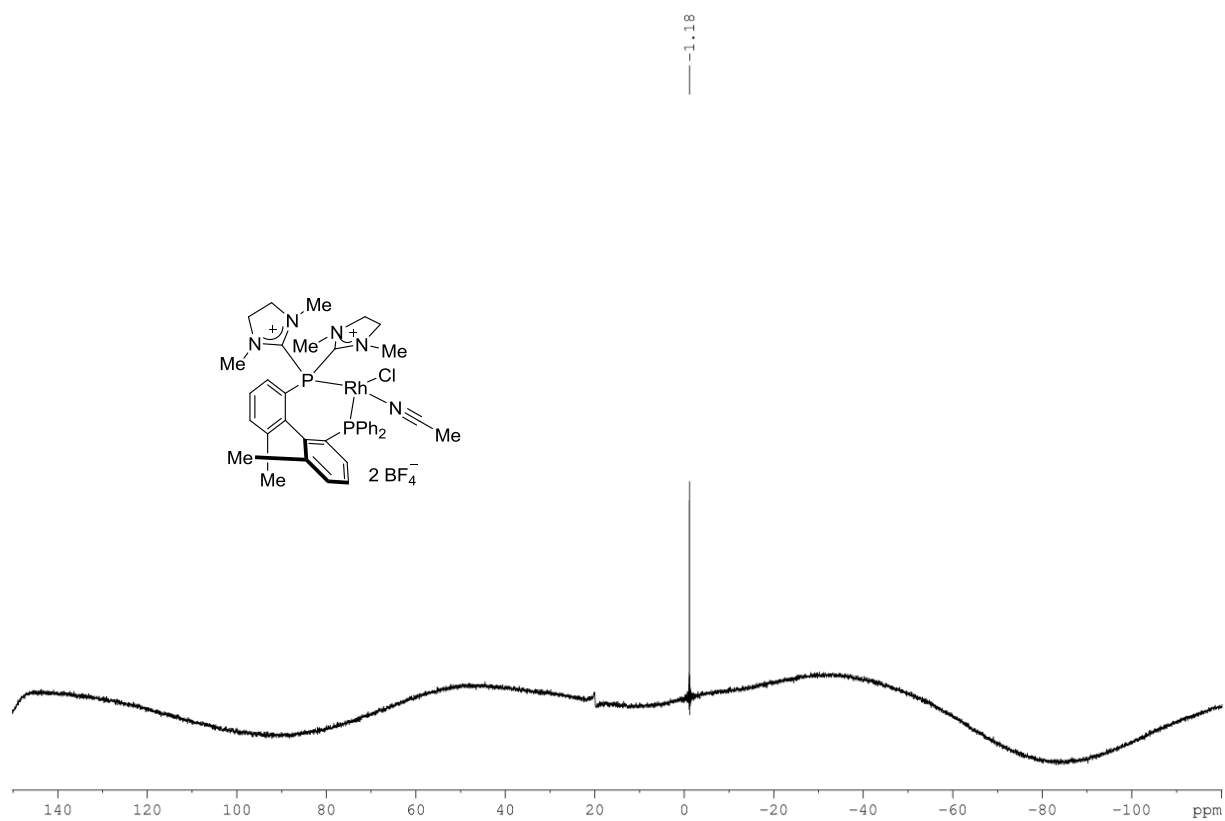
^1H NMR (CD₃CN, 400 MHz) (Compound 109e) **^{13}C NMR (CD₃CN, 100 MHz) (Compound 109e)**

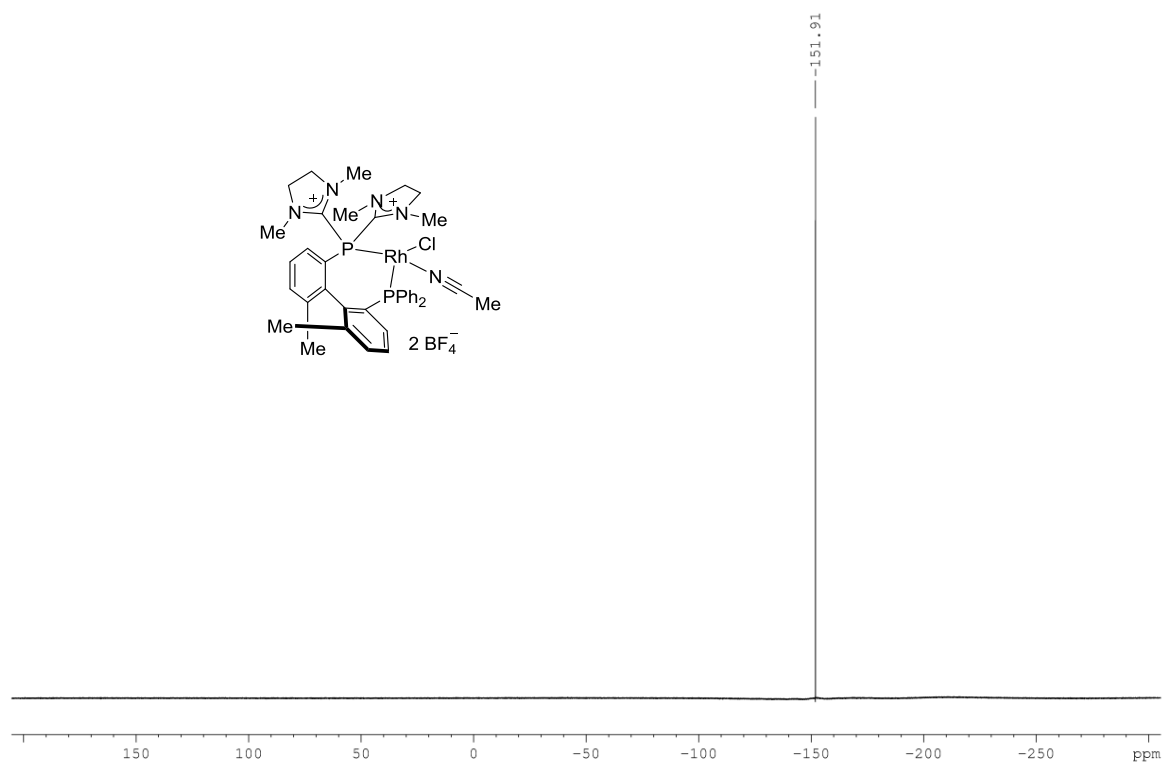
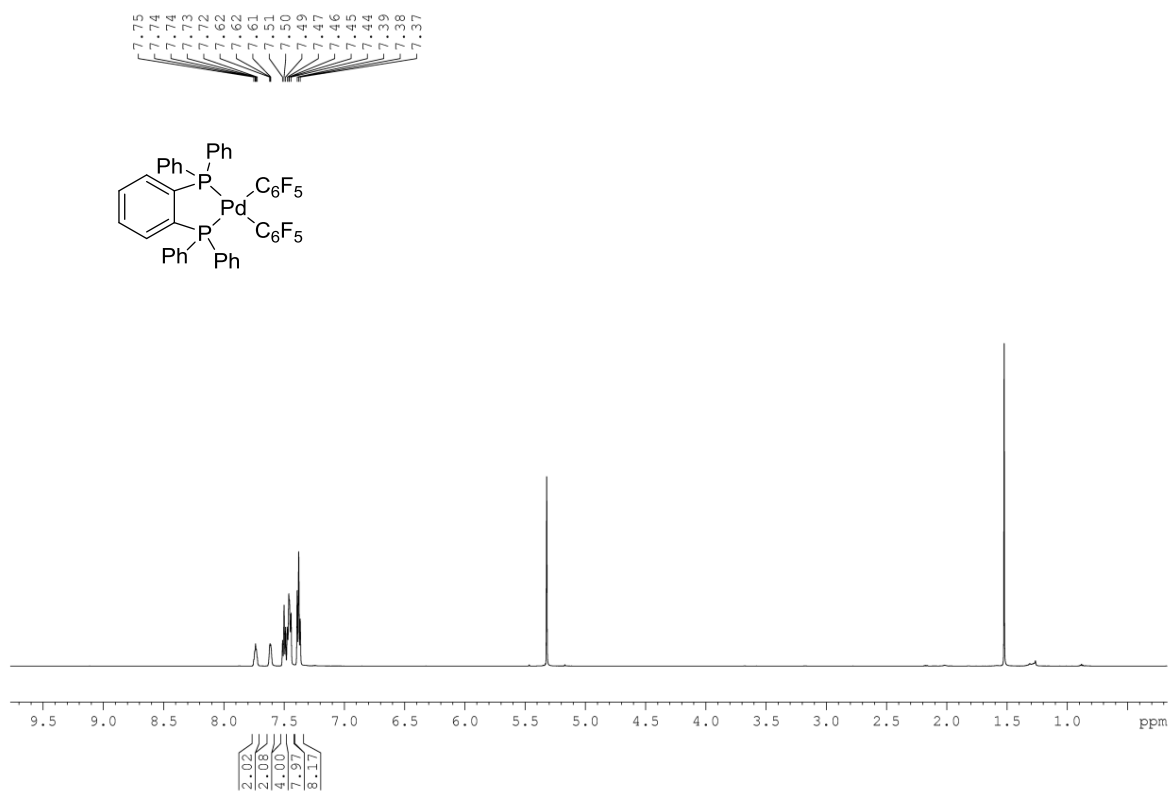
^{31}P NMR (CD_3CN , 121 MHz) (Compound 109e) **^{19}F NMR (CD_3CN , 376 MHz) (Compound 109e)**

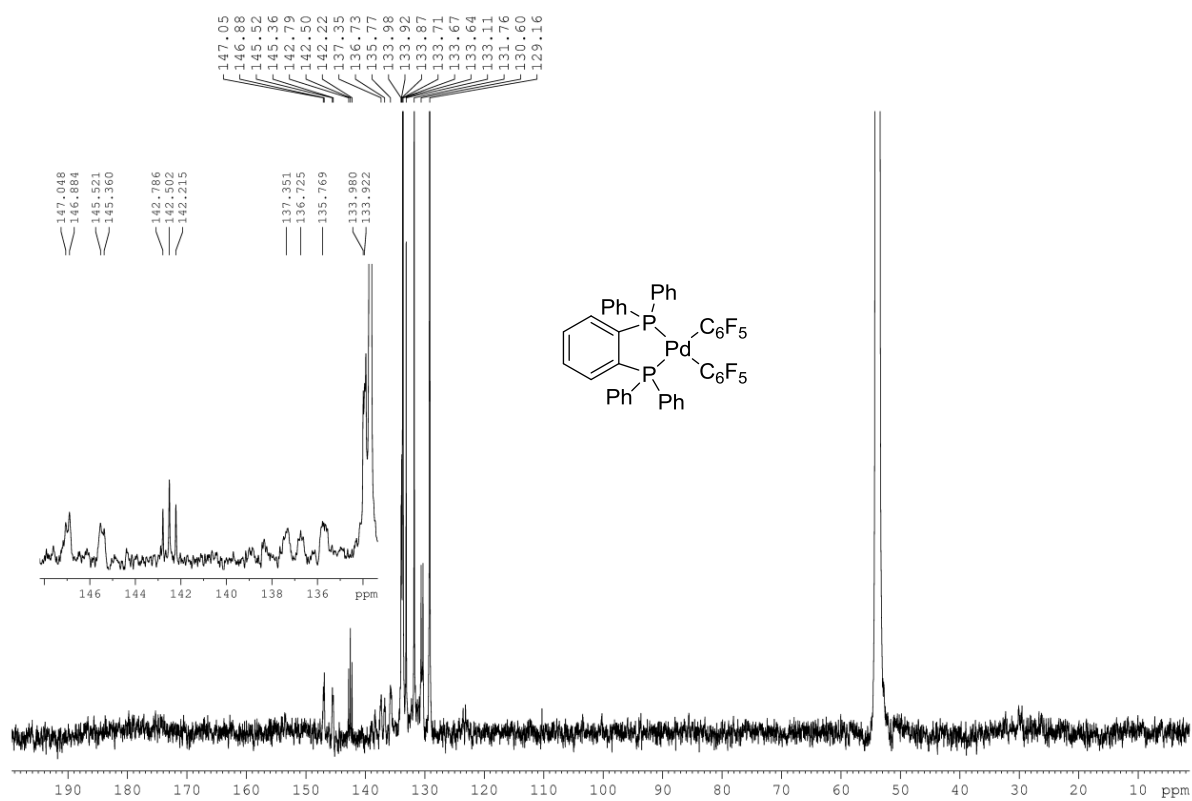
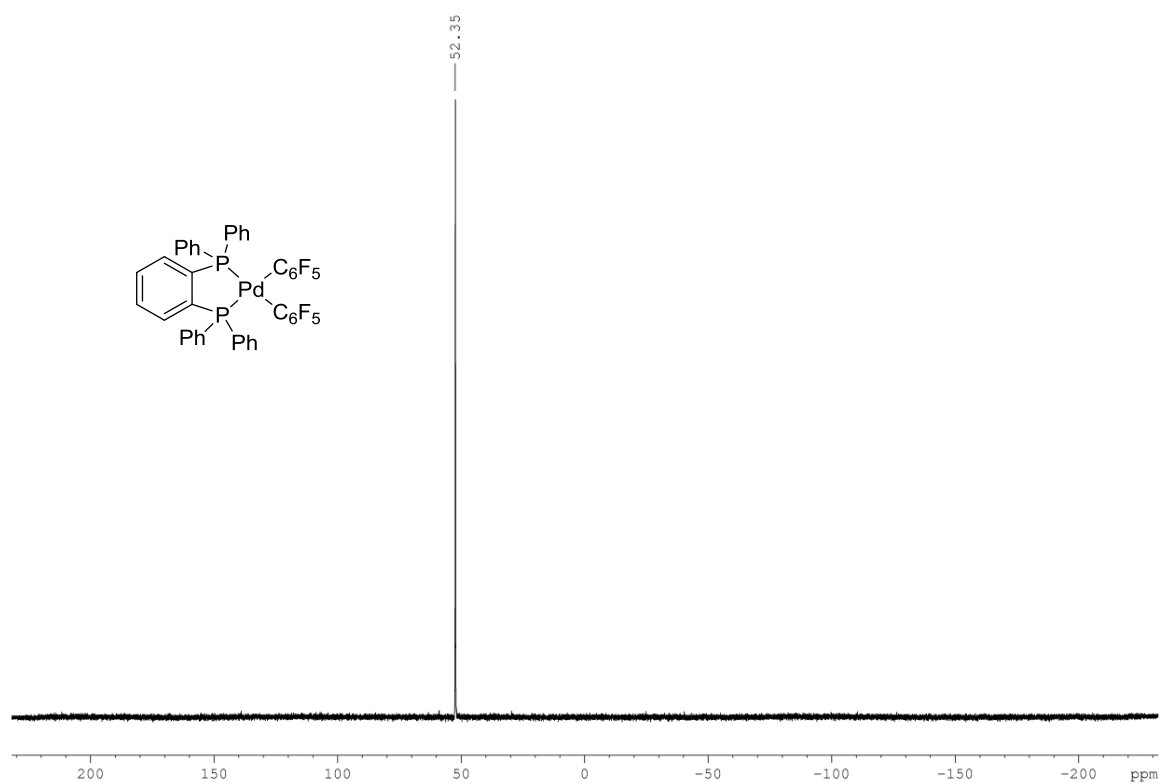
¹H NMR (CD₃CN, 400 MHz) (Compound 109f)**¹³C NMR (CD₃CN, 150 MHz) (Compound 109f)**

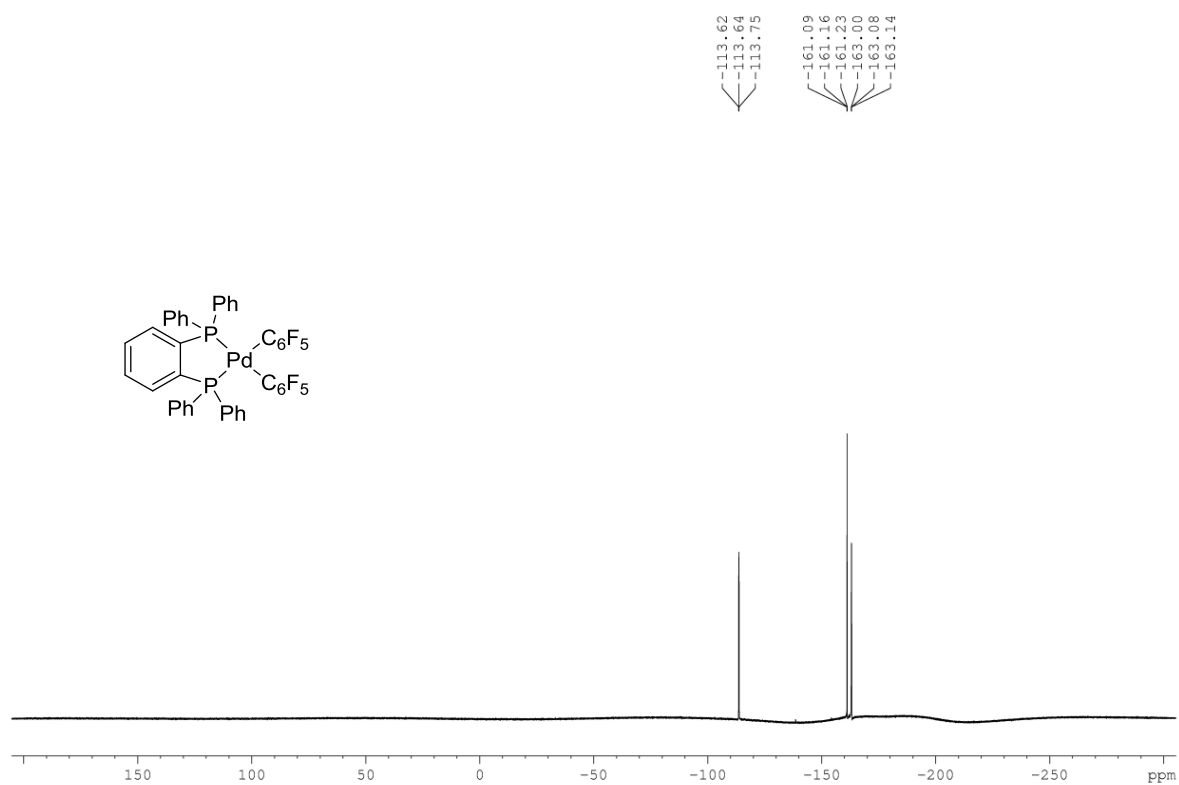
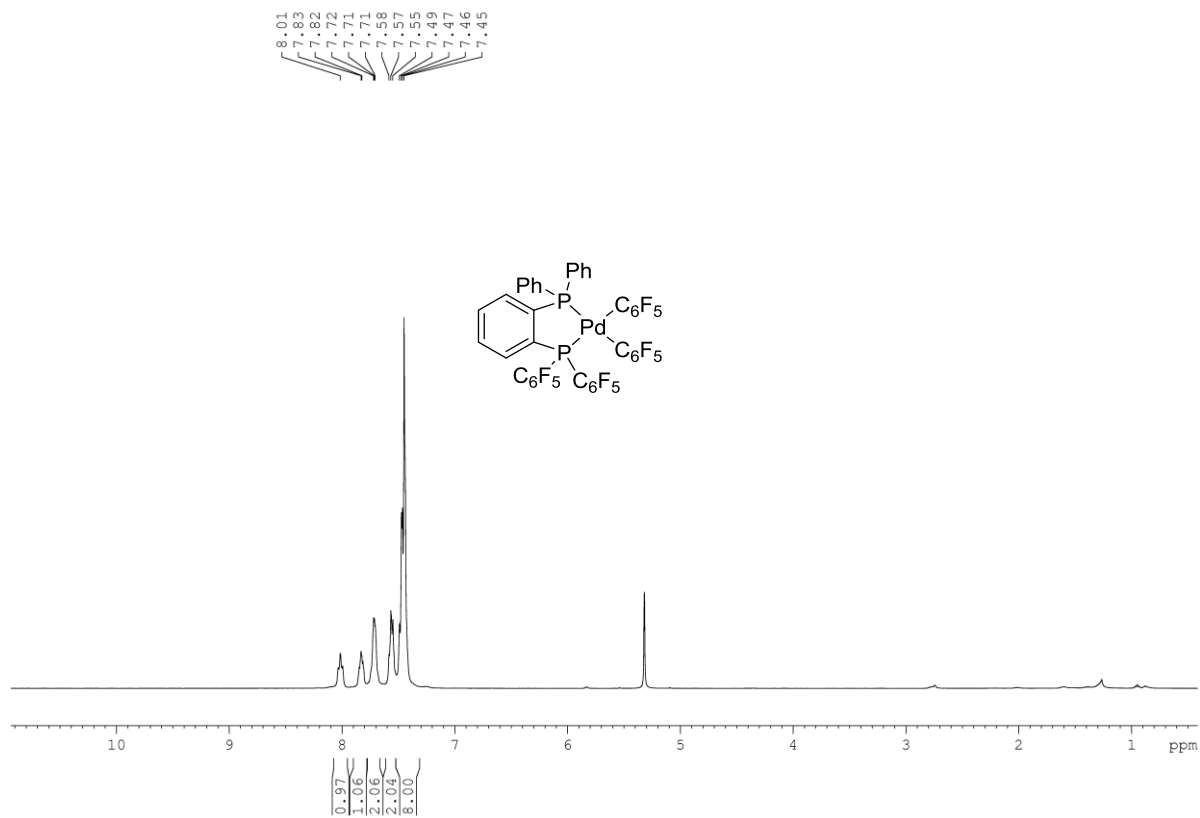
^{31}P NMR (CD₃CN, 121 MHz) (Compound 109f) **^{19}F NMR (CD₃CN, 282 MHz) (Compound 109f)**

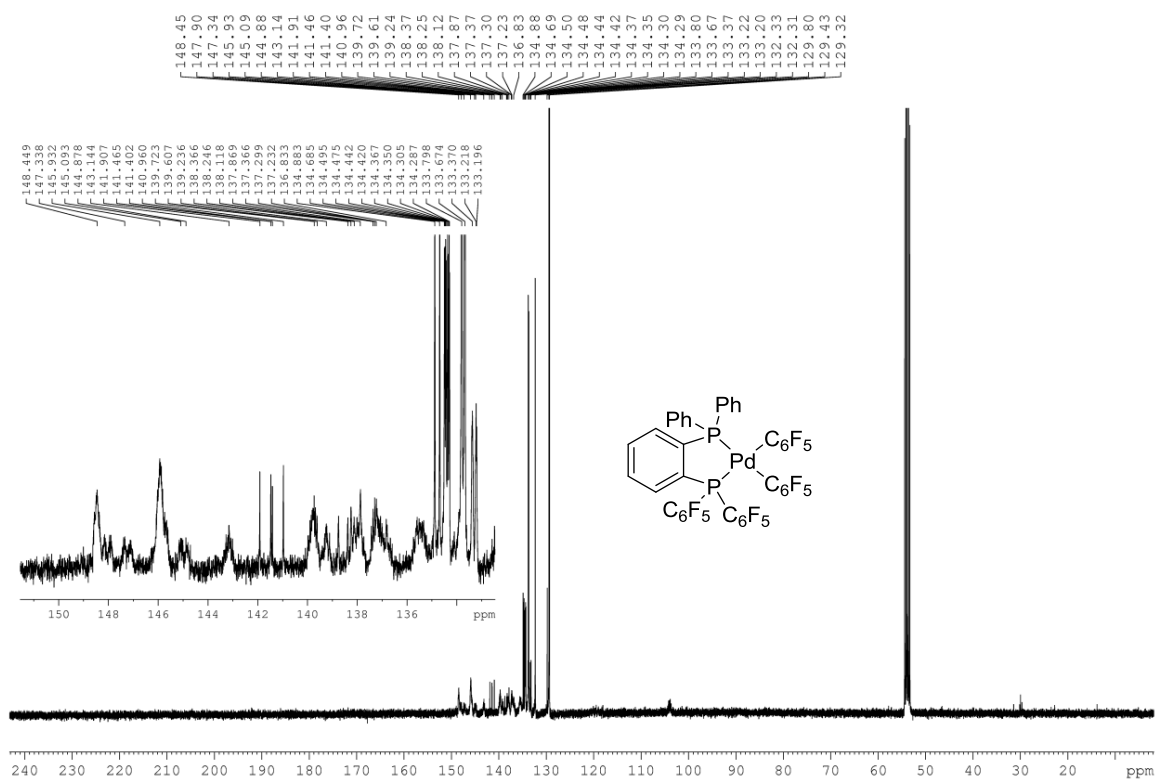
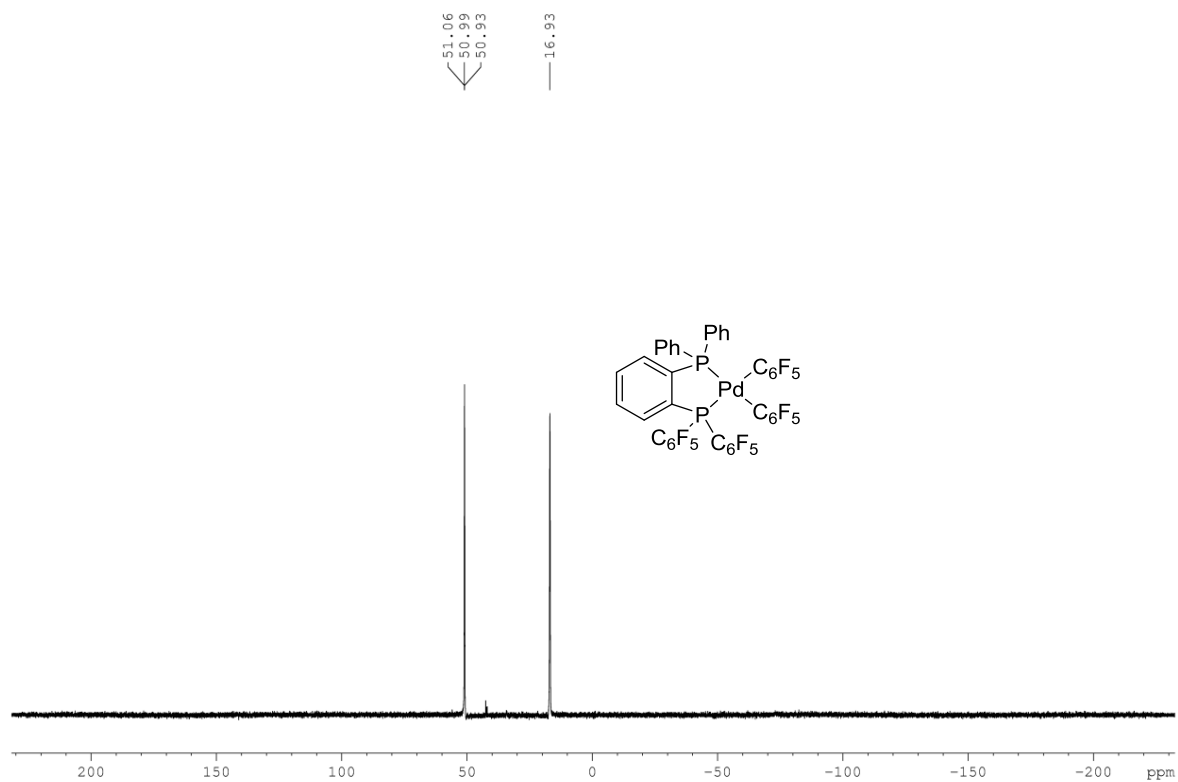
^1H NMR (CD₃CN, 400 MHz) (Compound 110) **^{13}C NMR (CD₃CN, 150 MHz) (Compound 110)**

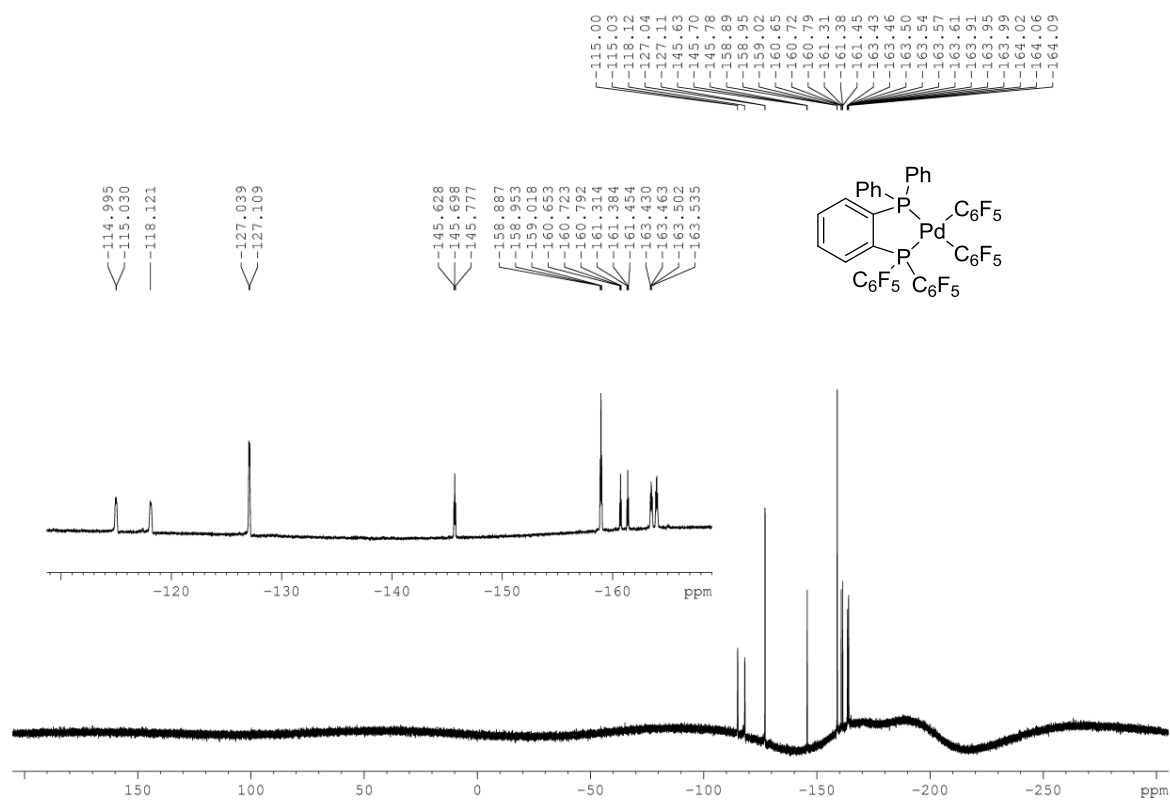
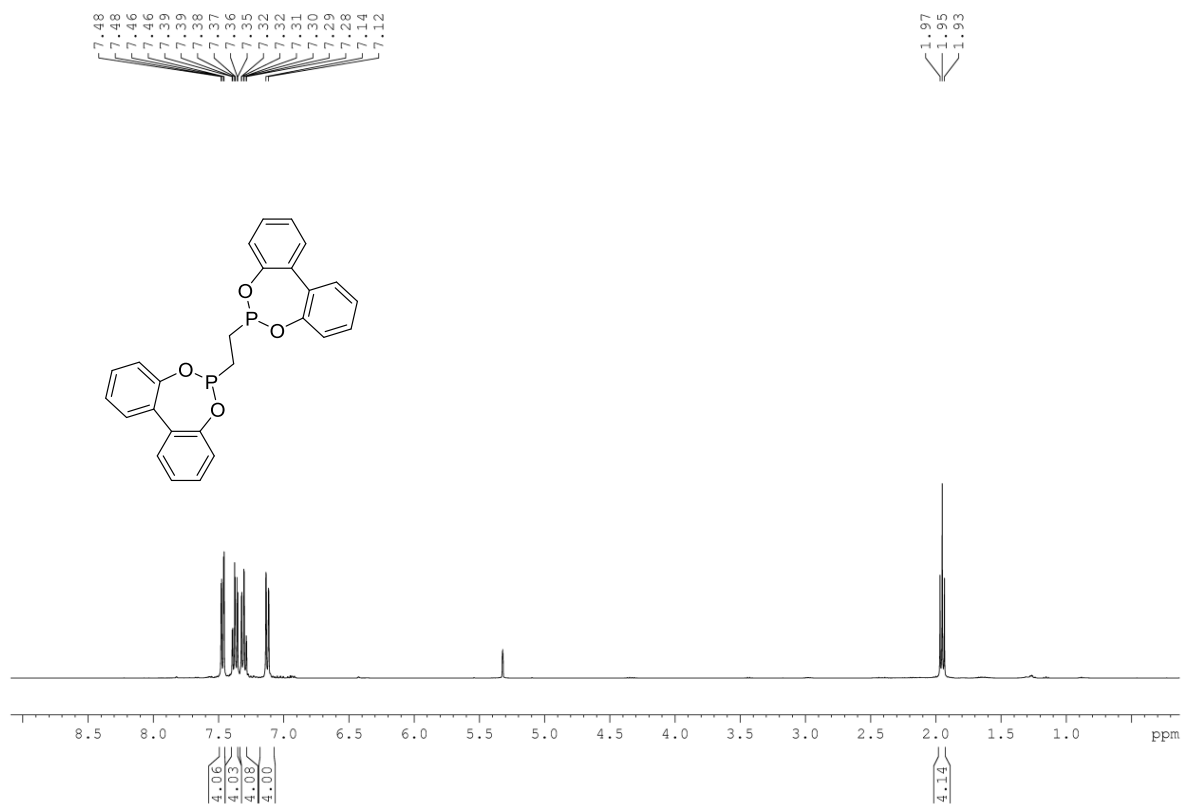
^{31}P NMR (CD_3CN , 121 MHz) (Compound 110) **^{11}B NMR (CD_3CN , 96 MHz) (Compound 110)**

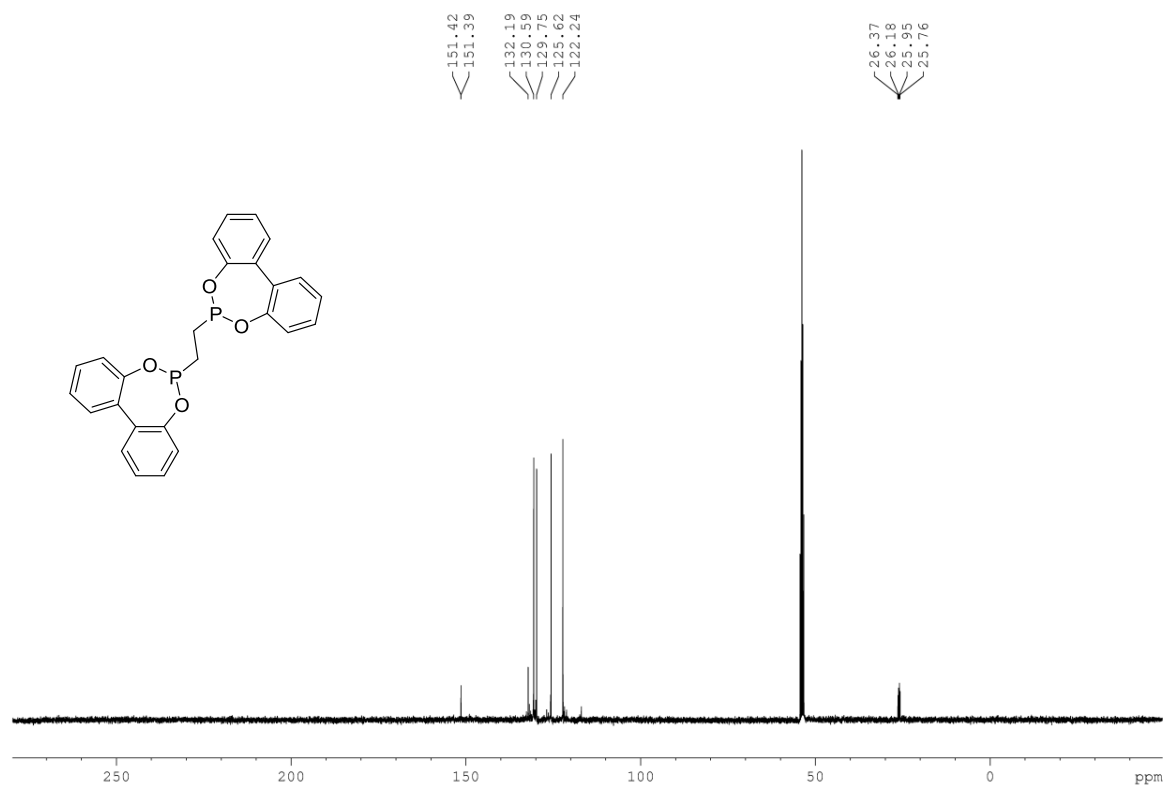
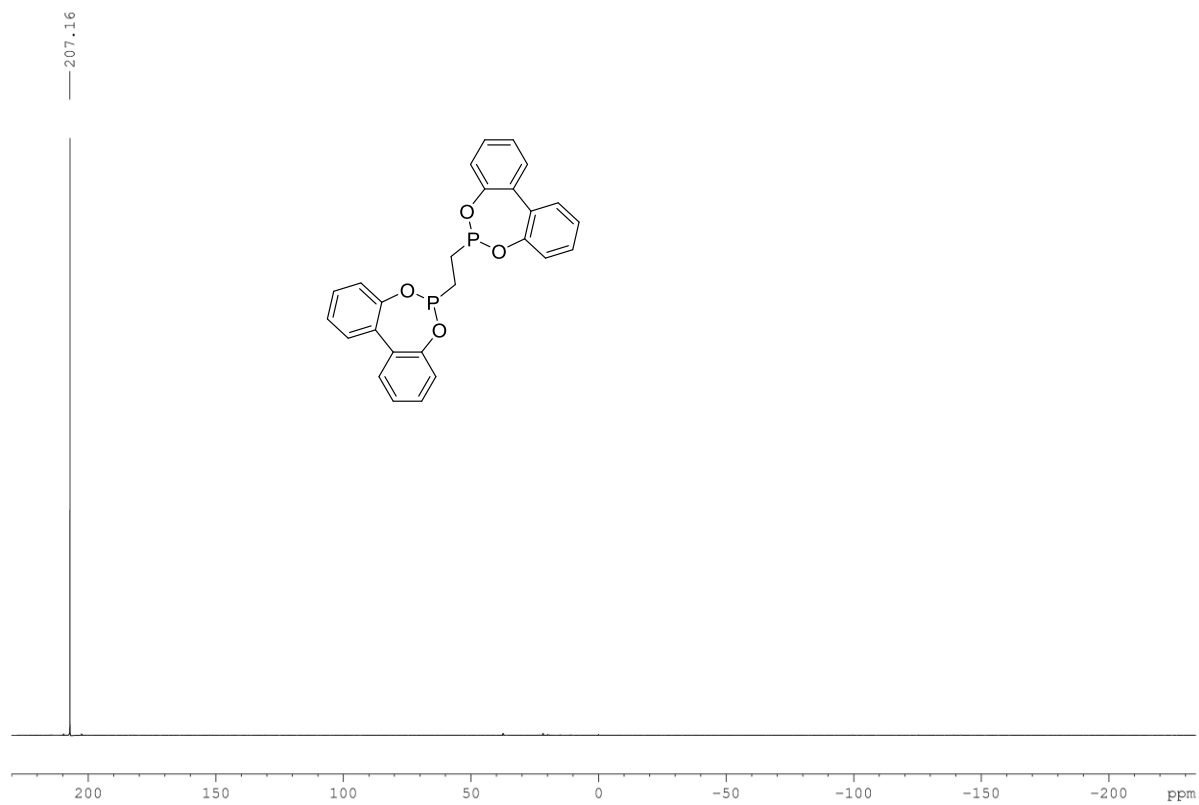
^{19}F NMR (CD_3CN , 282 MHz) (Compound 110) **^1H NMR (CD_2Cl_2 , 600 MHz): (Compound 112b)**

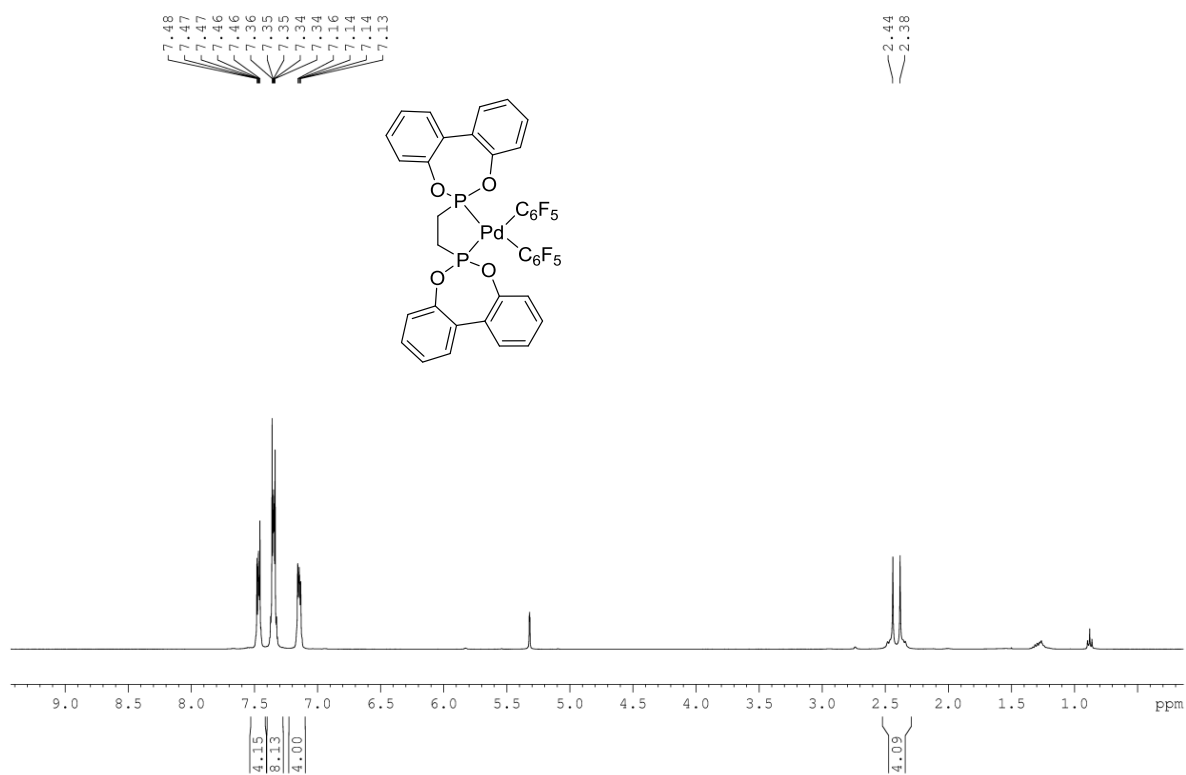
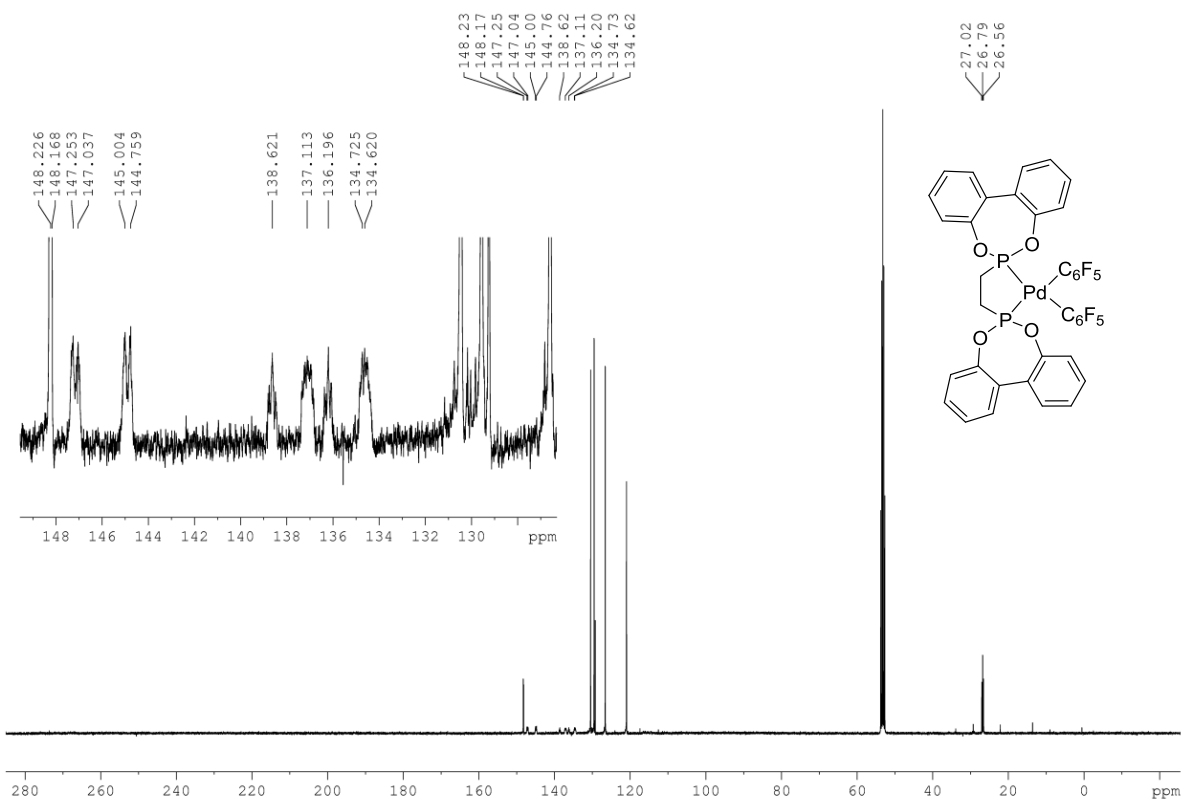
^{13}C NMR (CD_2Cl_2 , 150 MHz) (Compound 112b) **^{31}P NMR (CD_2Cl_2 , 121 MHz) (Compound 112b)**

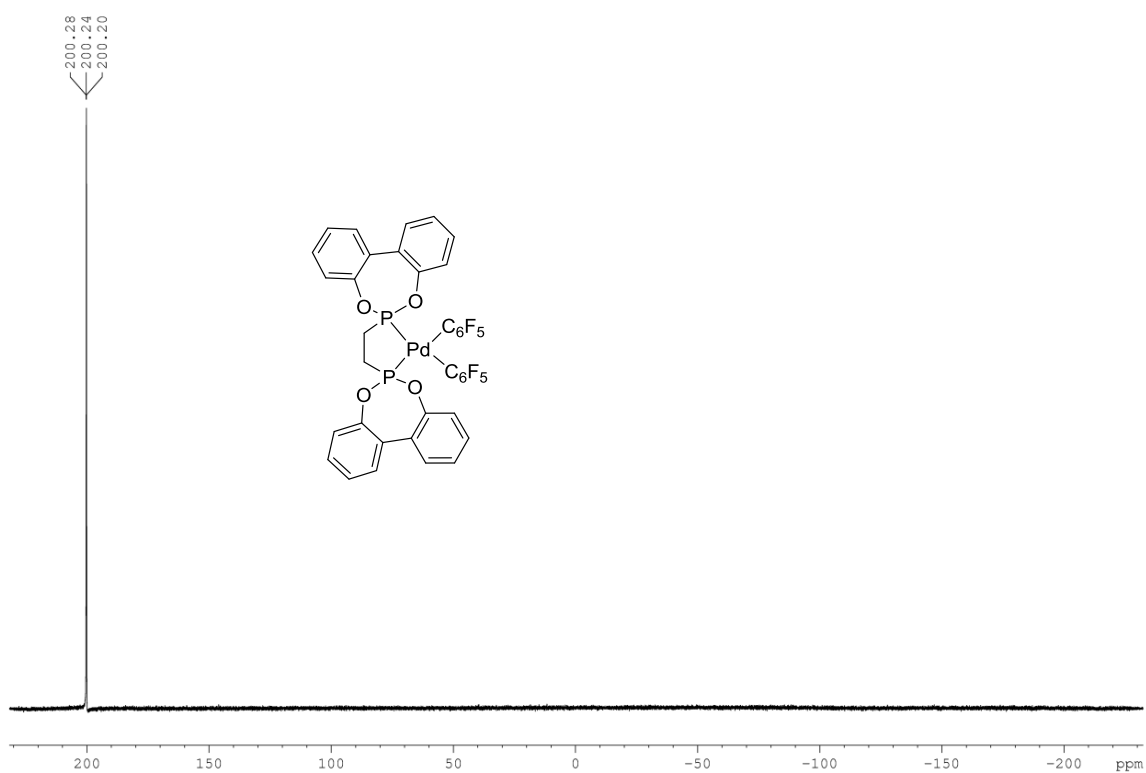
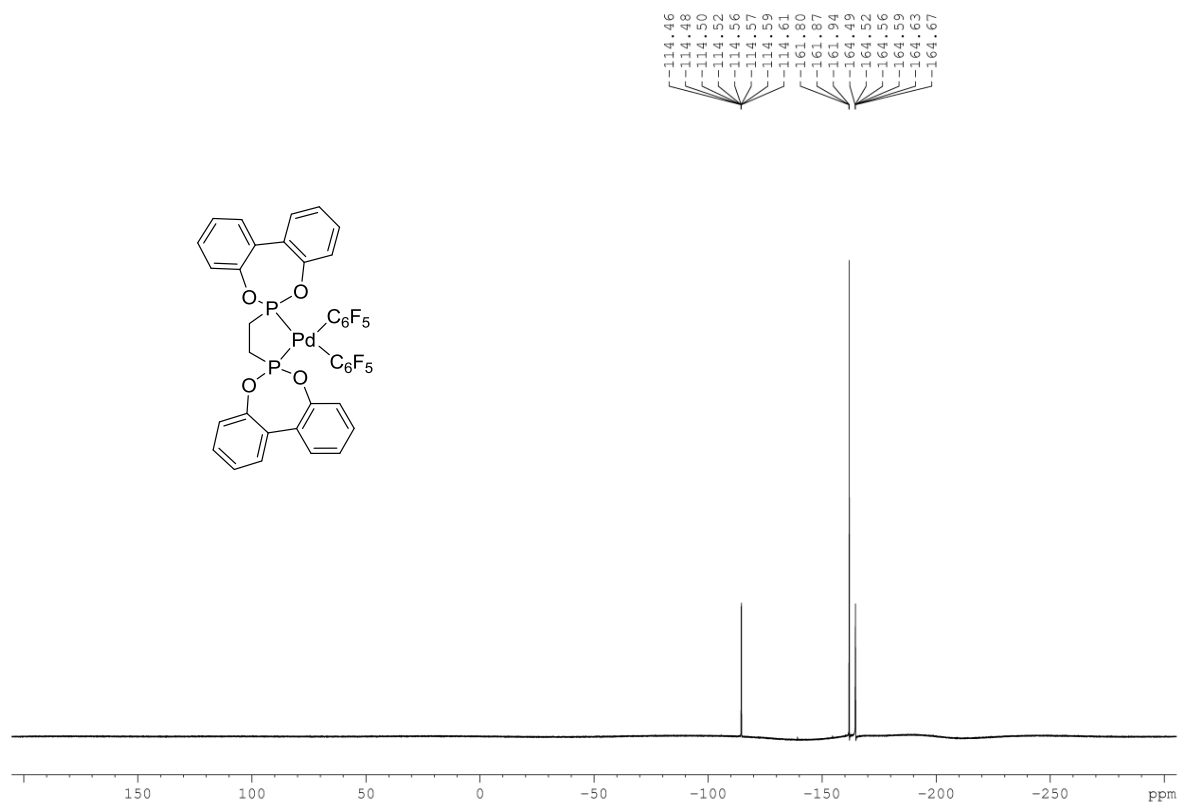
^{19}F NMR (CD_2Cl_2 , 282 MHz) (Compound 112b) **^1H NMR (CD_2Cl_2 , 400 MHz) (Compound 112c)**

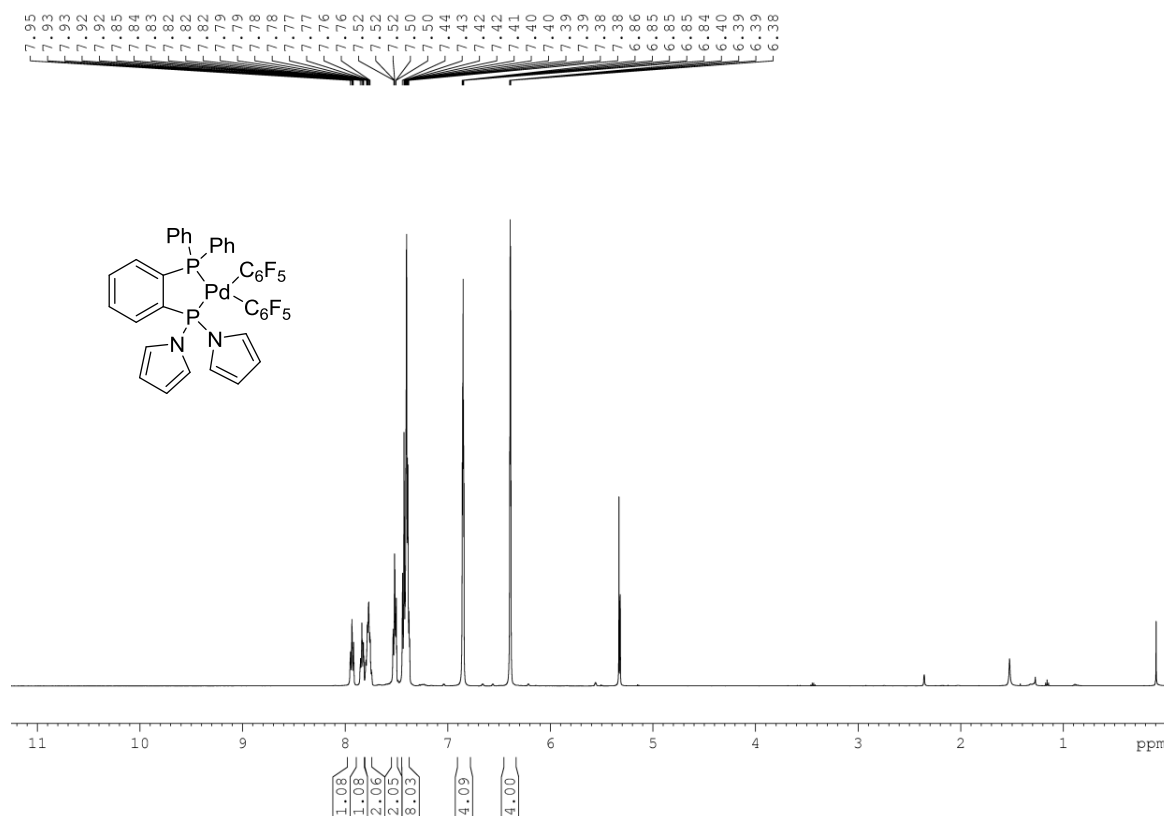
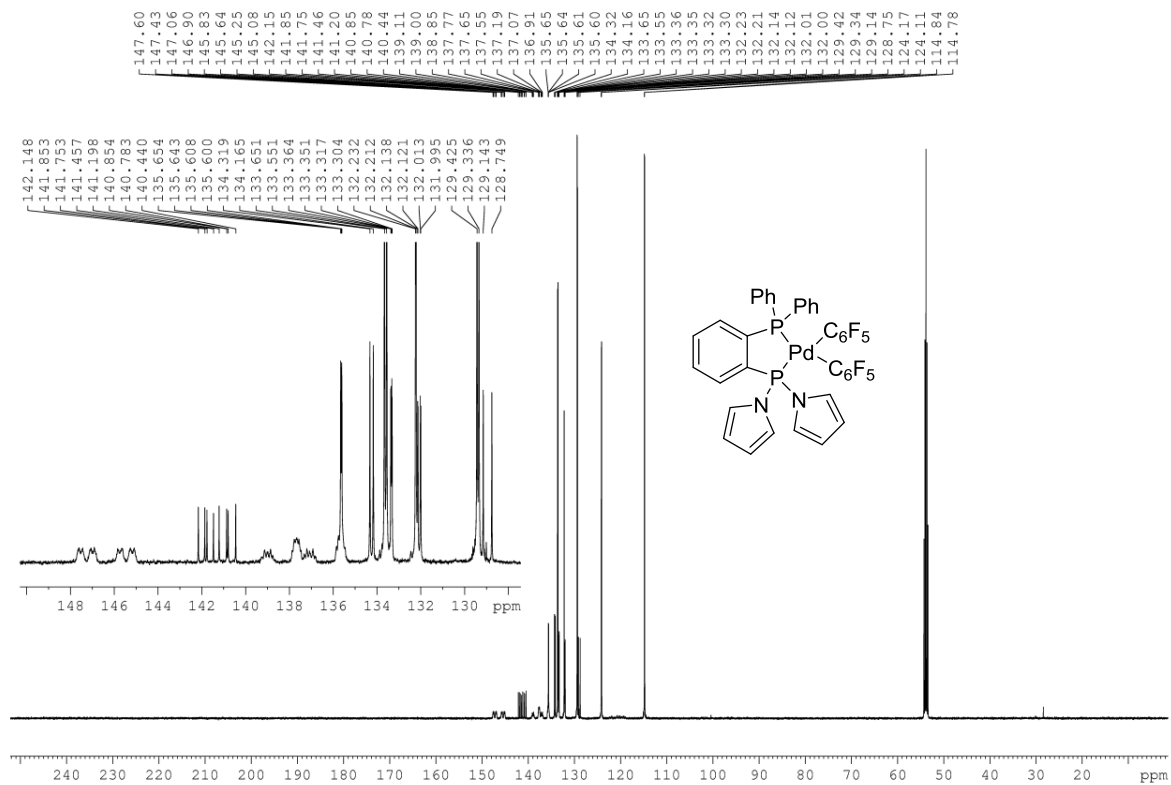
^{13}C NMR (CD_2Cl_2 , 100 MHz) (Compound 112c) **^{31}P NMR (CD_2Cl_2 , 121 MHz) (Compound 112c)**

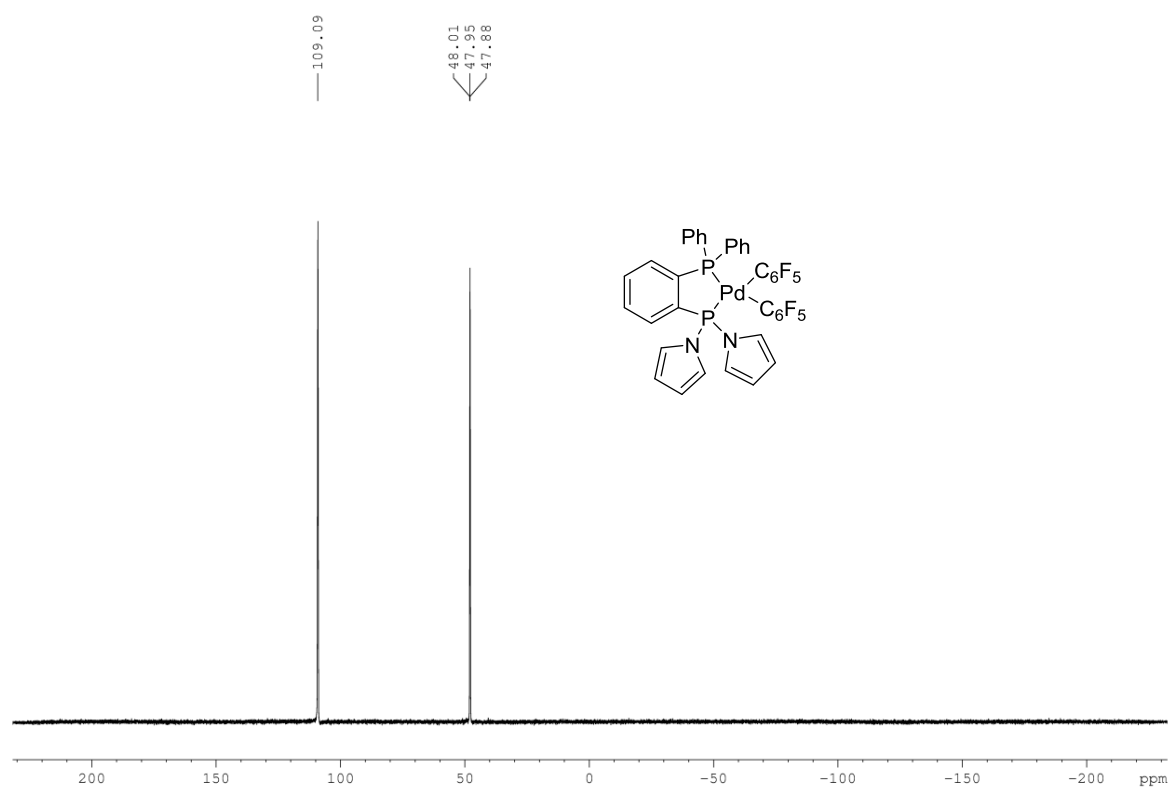
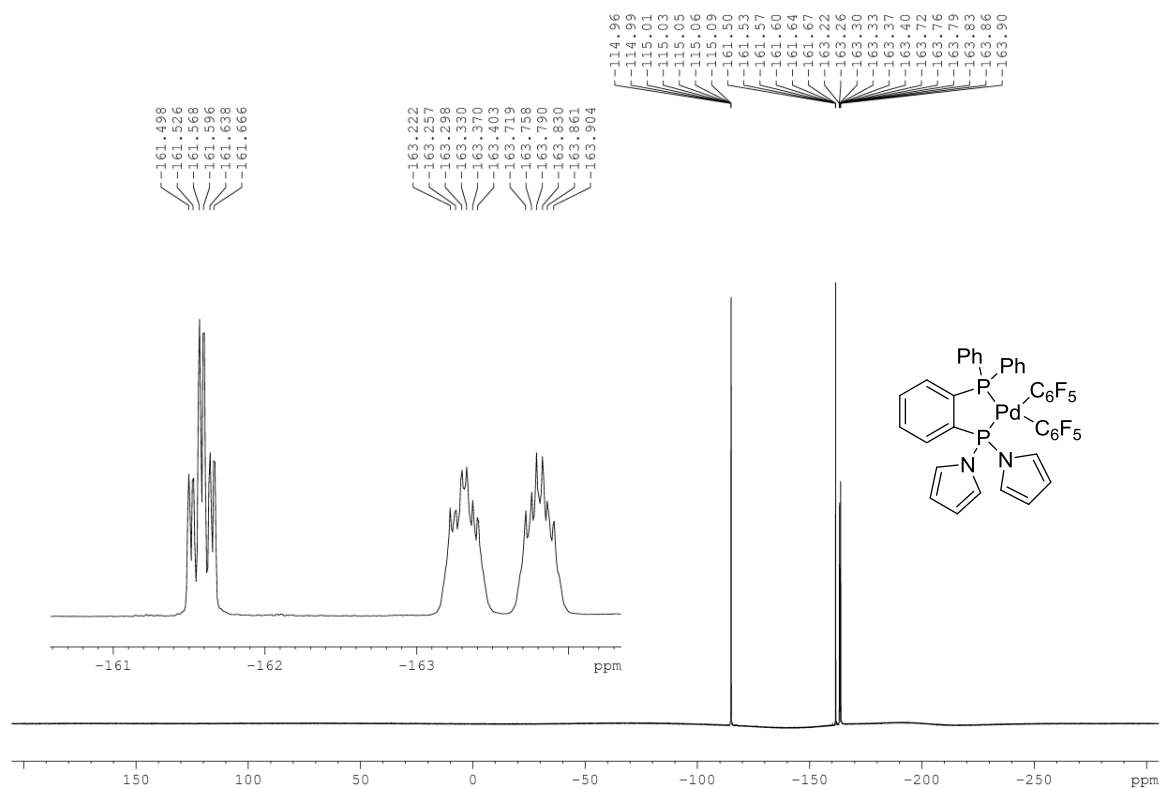
^{19}F NMR (CD_2Cl_2 , 282 MHz) (Compound 112c) **^1H NMR (CD_2Cl_2 , 400 MHz)**

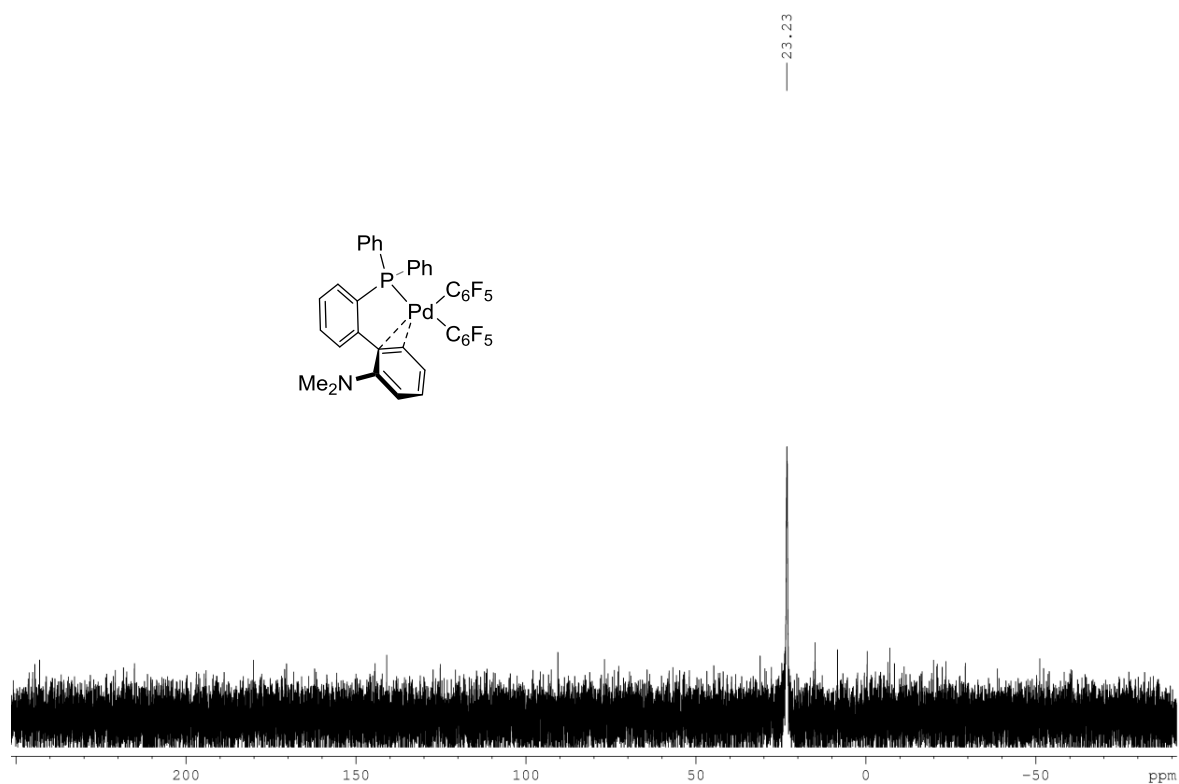
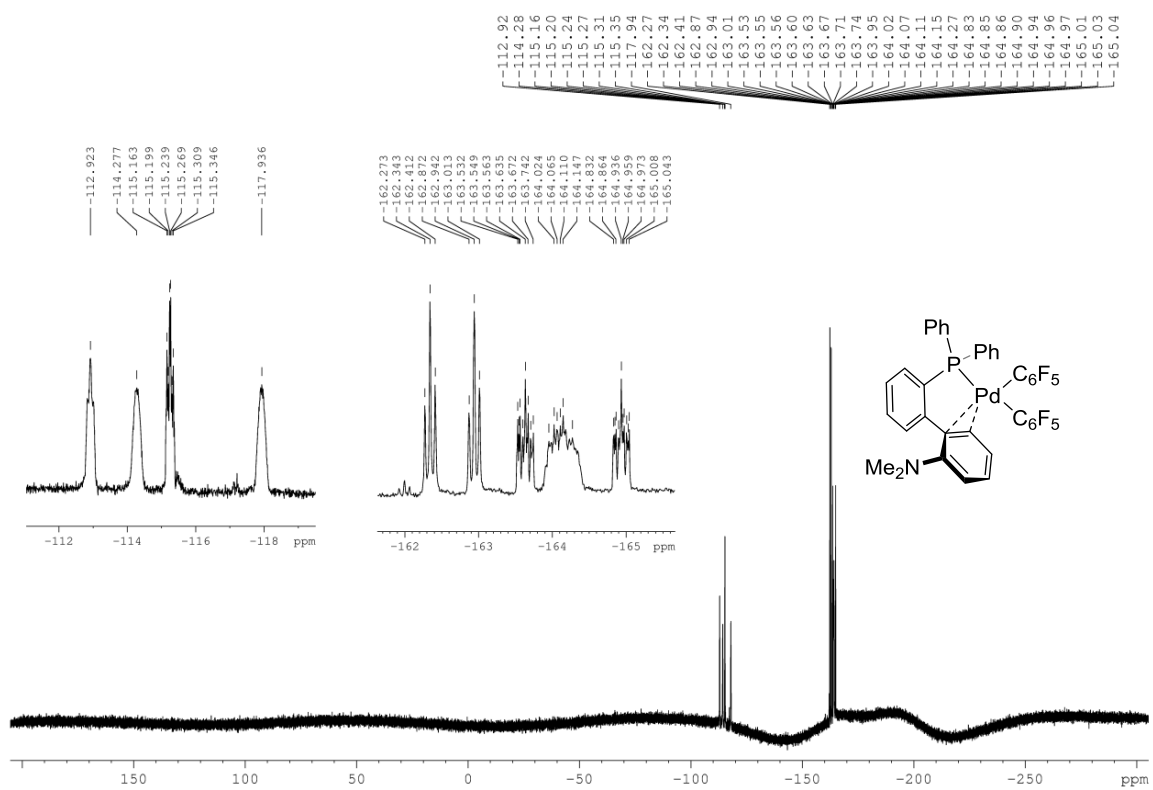
^{13}C NMR (CD₂Cl₂, 100 MHz) **^{31}P NMR (CD₂Cl₂, 121 MHz)**

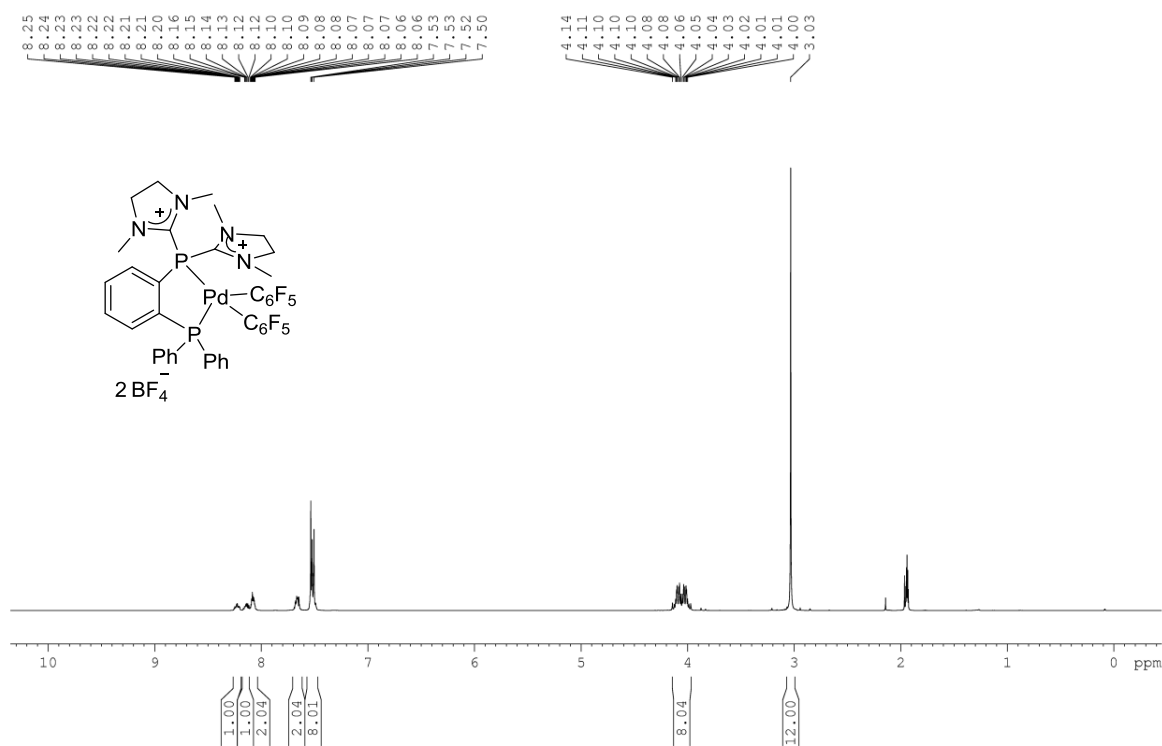
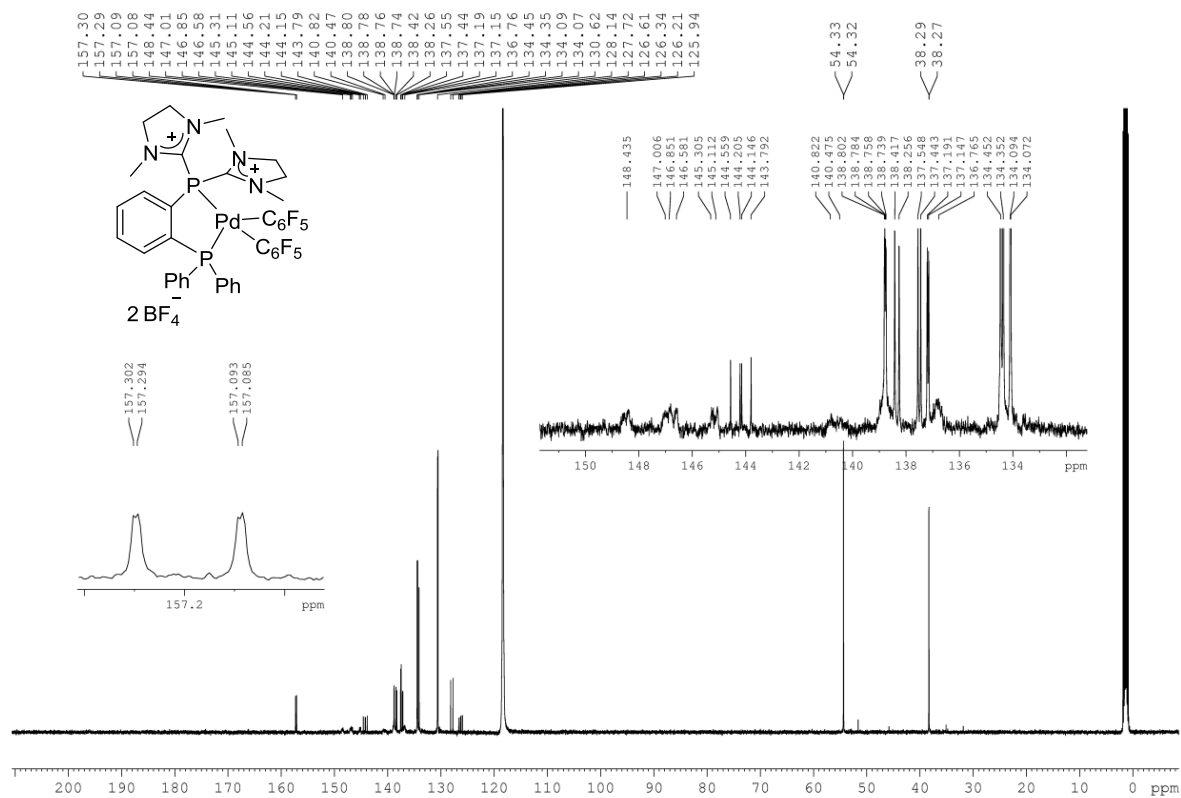
^1H NMR (CD_2Cl_2 , 400 MHz) (Compound 112d) **^{13}C NMR (CD_2Cl_2 , 100 MHz) (Compound 112d)**

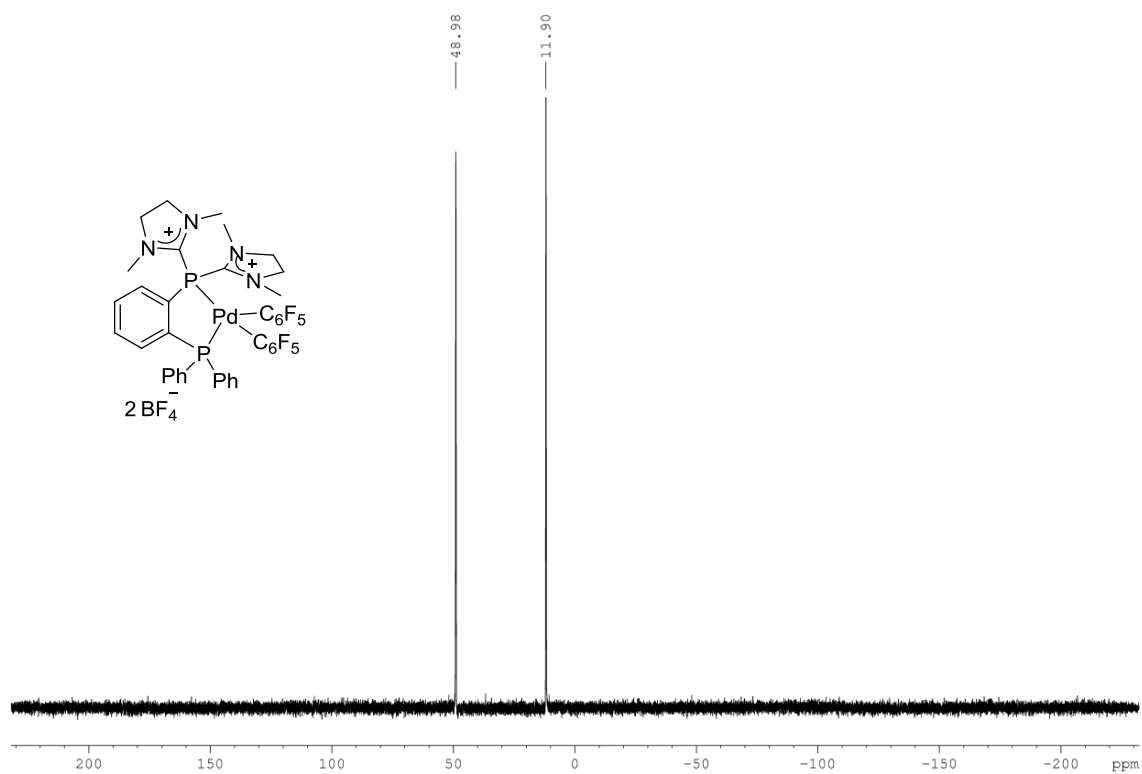
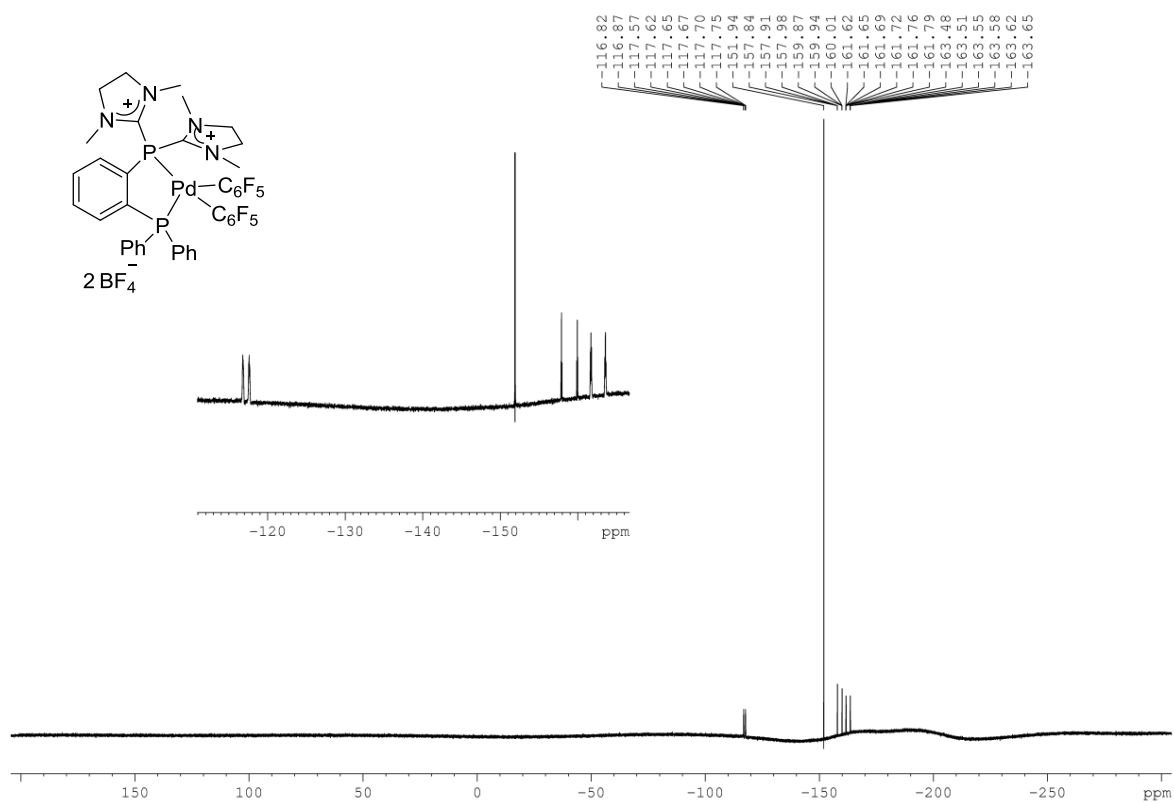
^{31}P NMR (CD_2Cl_2 , 121 MHz) (Compound 112d) **^{19}F NMR (CD_2Cl_2 , 282 MHz) (Compound 112d)**

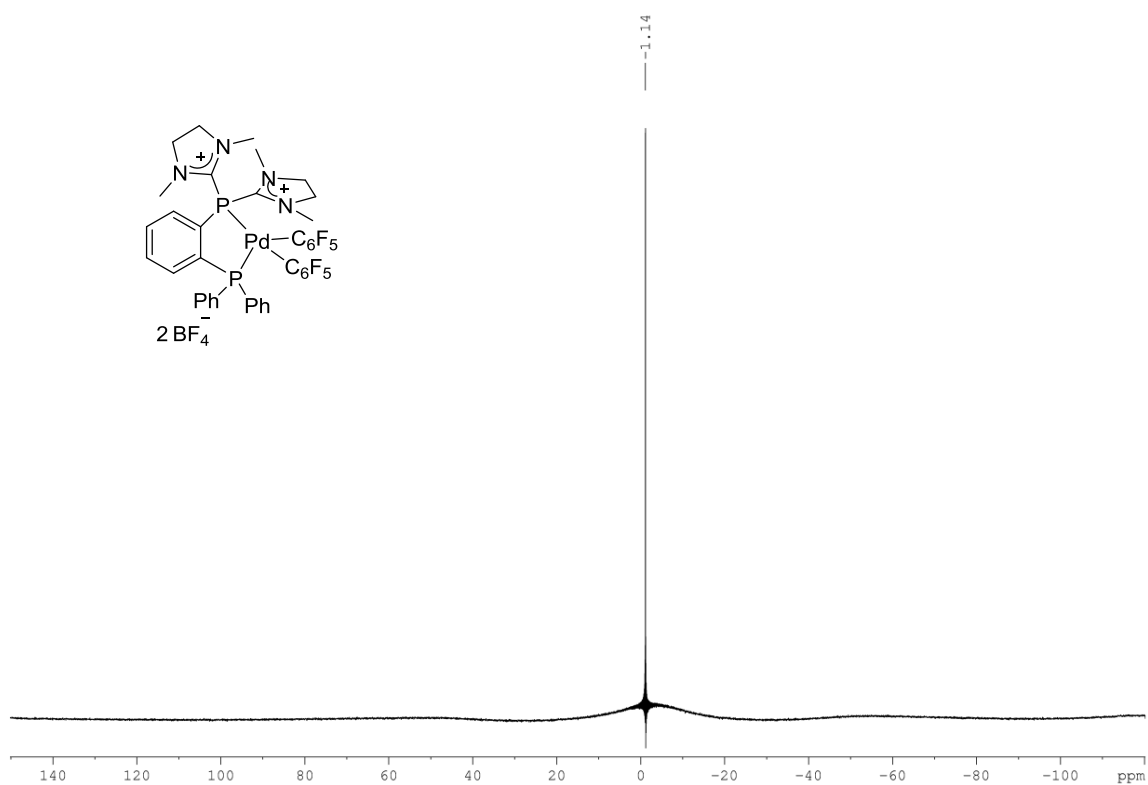
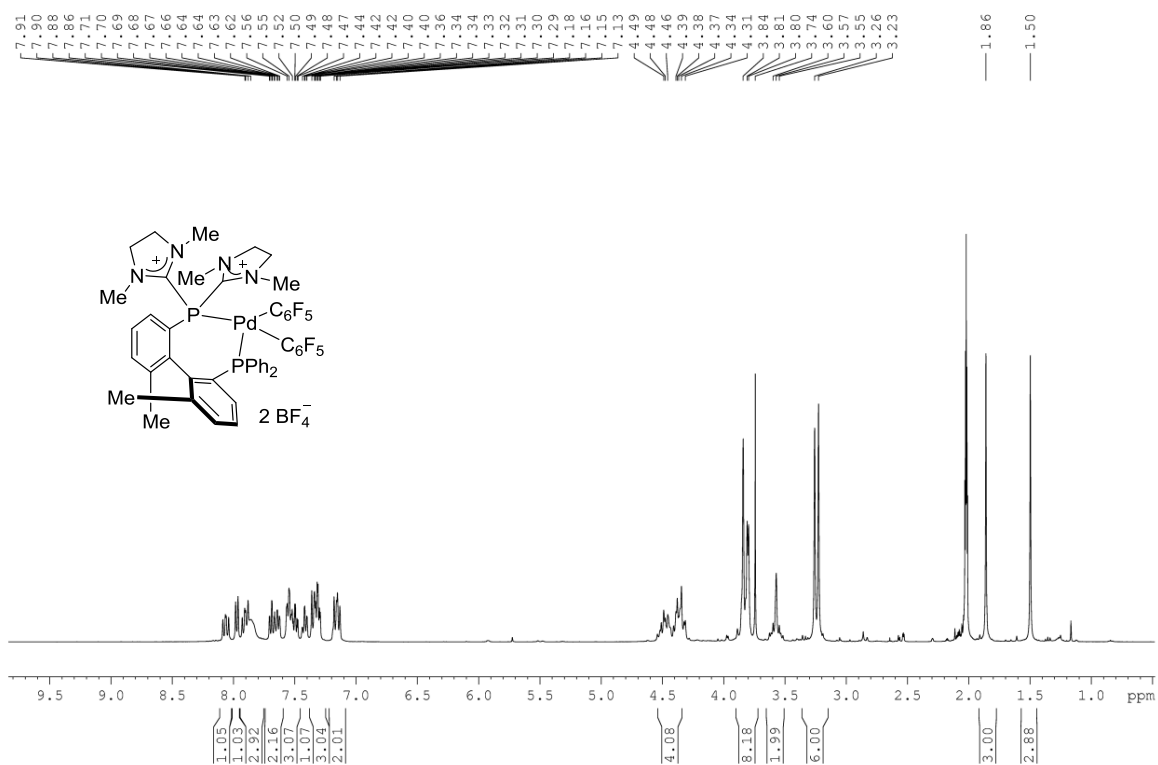
^1H NMR (CD₂Cl₂, 500 MHz) (Compound 112e) **^{13}C NMR (CD₂Cl₂, 125 Mz) (Compound 112e)**

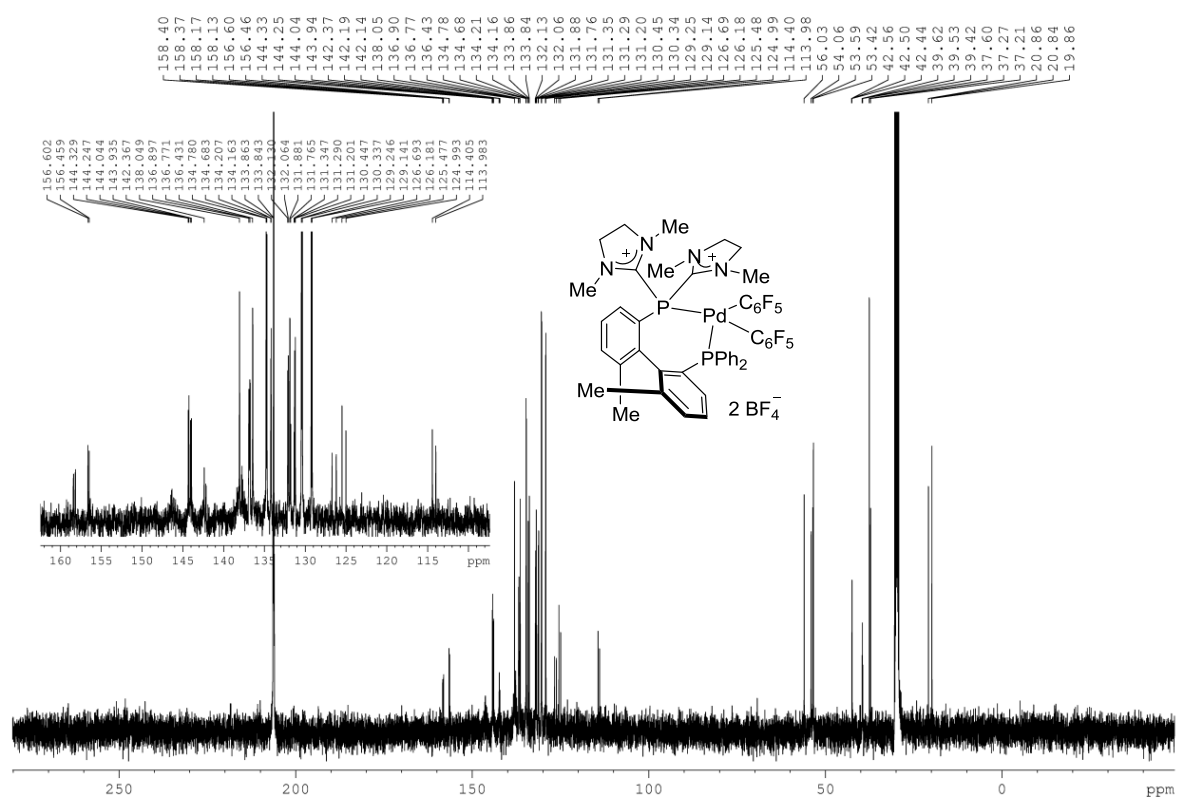
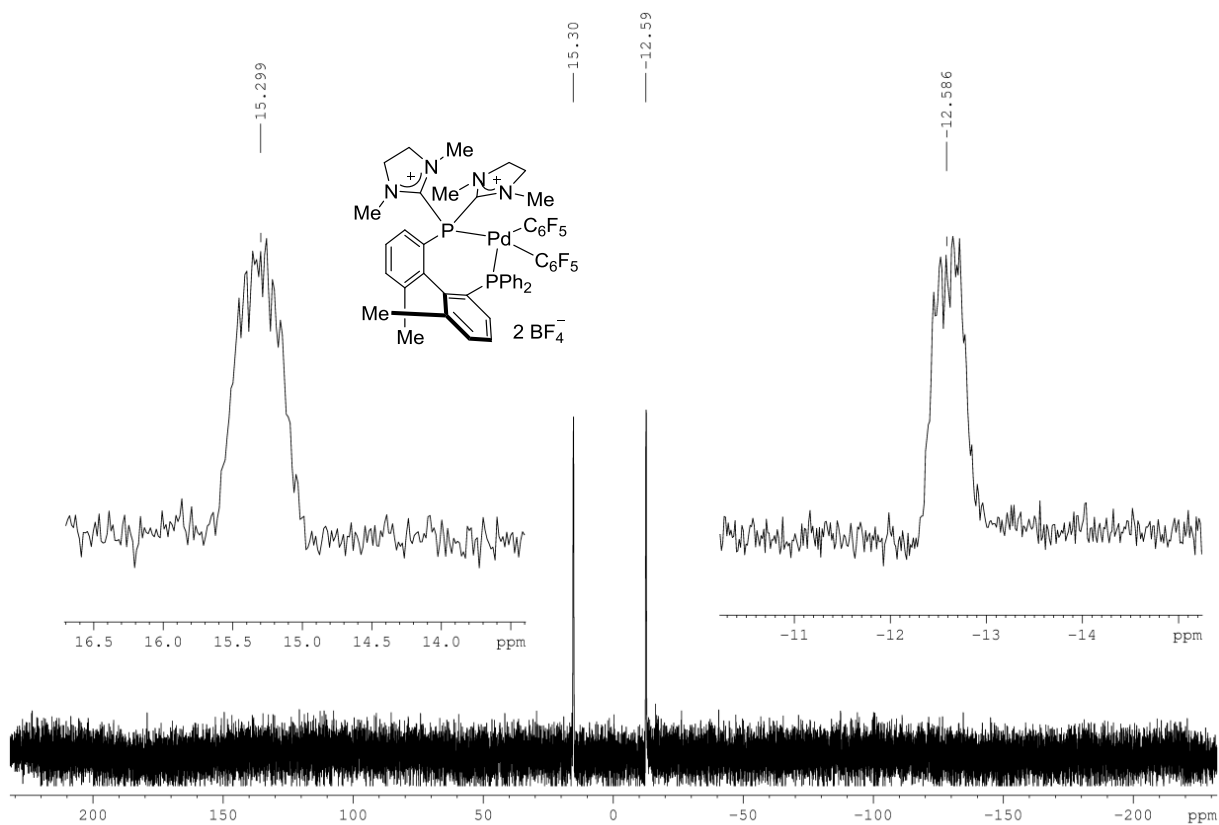
^{31}P NMR (CD_2Cl_2 , 162 MHz) (Compound 112e) **^{19}F NMR (CD_2Cl_2 , 282 MHz) (Compound 112e)**

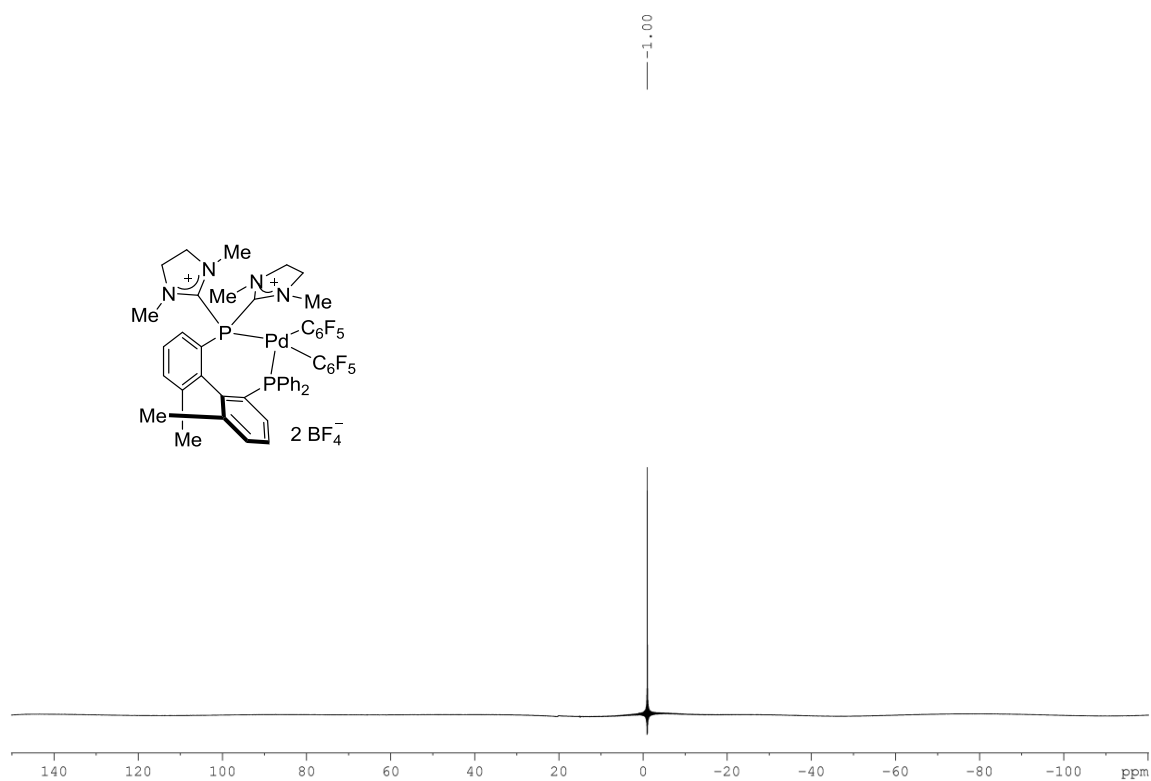
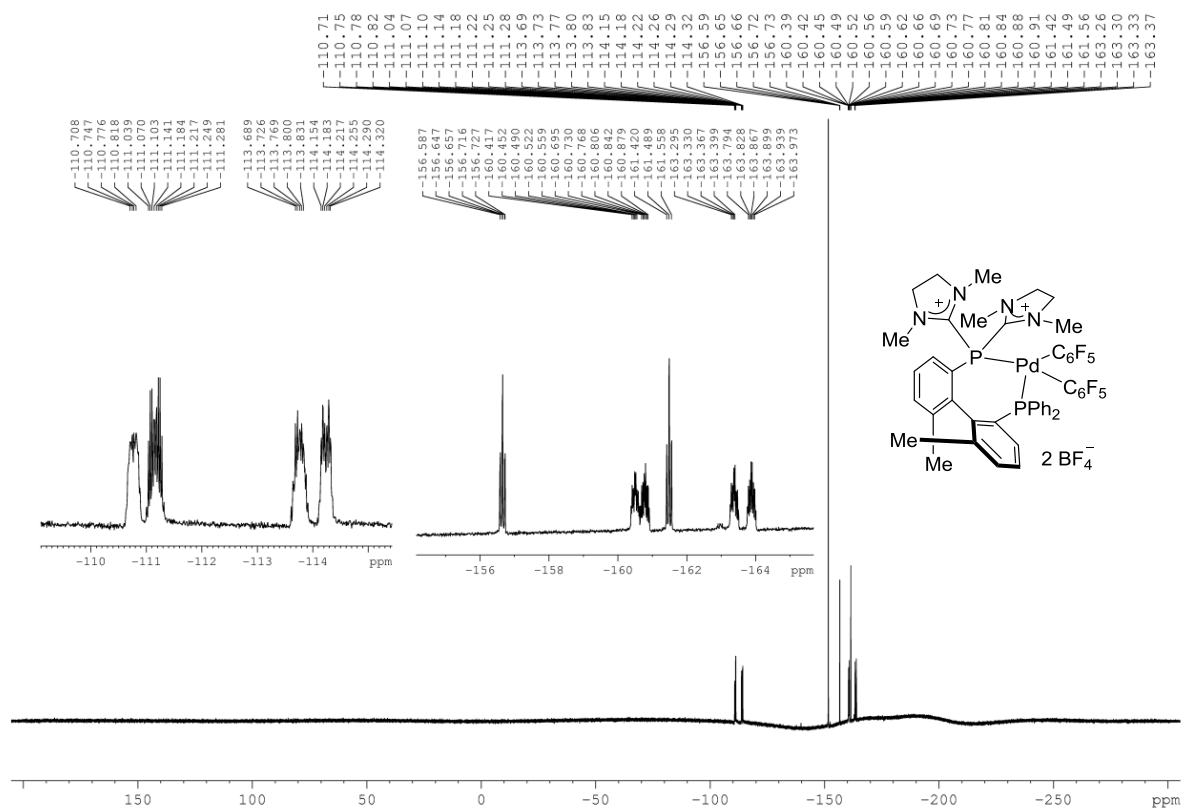
^{31}P NMR (CD_2Cl_2 , 162 MHz) (Compound 112f) **^{19}F NMR (CD_2Cl_2 , 282 MHz) (Compound 112f)**

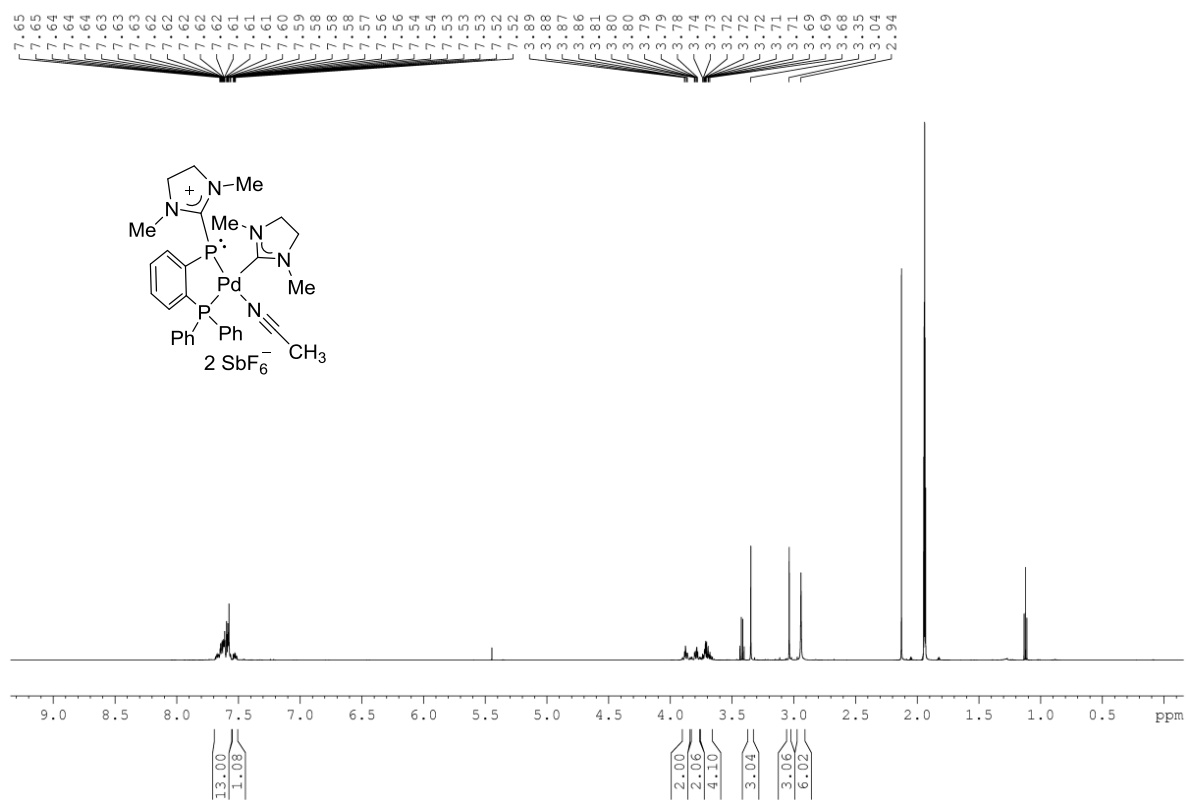
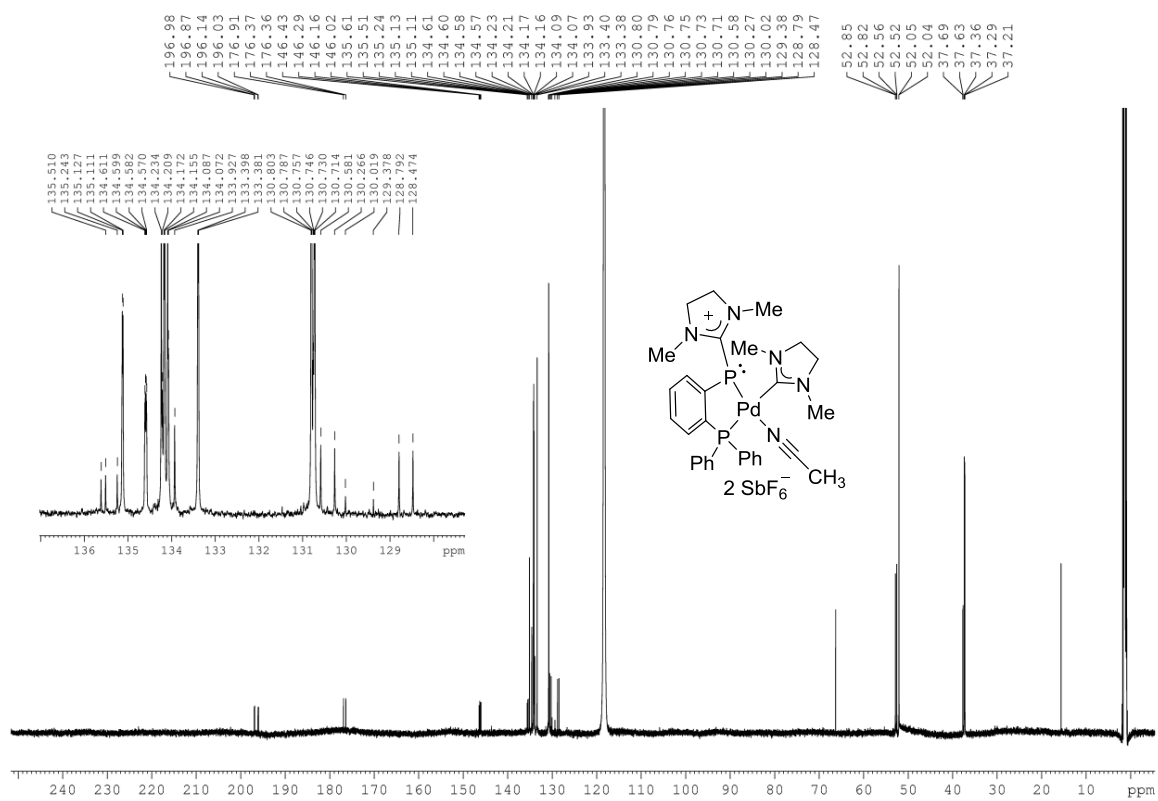
¹H NMR (CD₃CN, 400 MHz) (Compound 112g)**¹³C NMR (CD₃CN, 100 MHz) (Compound 112g)**

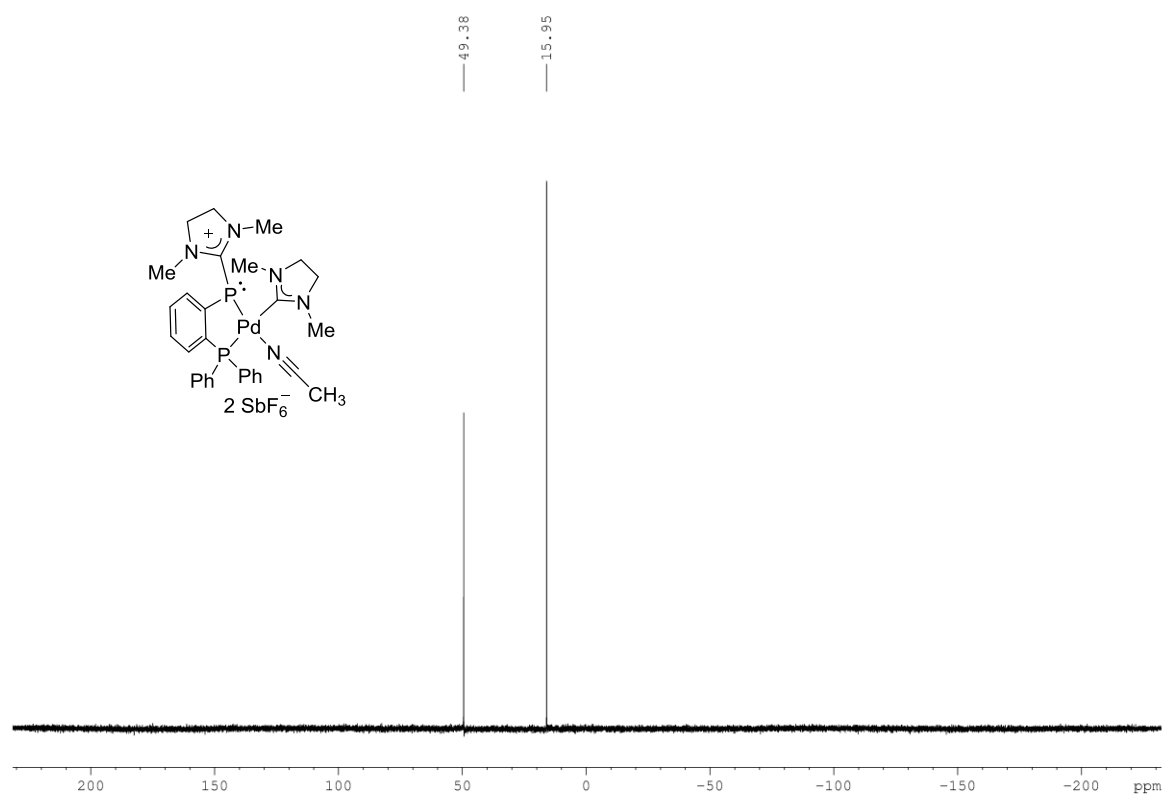
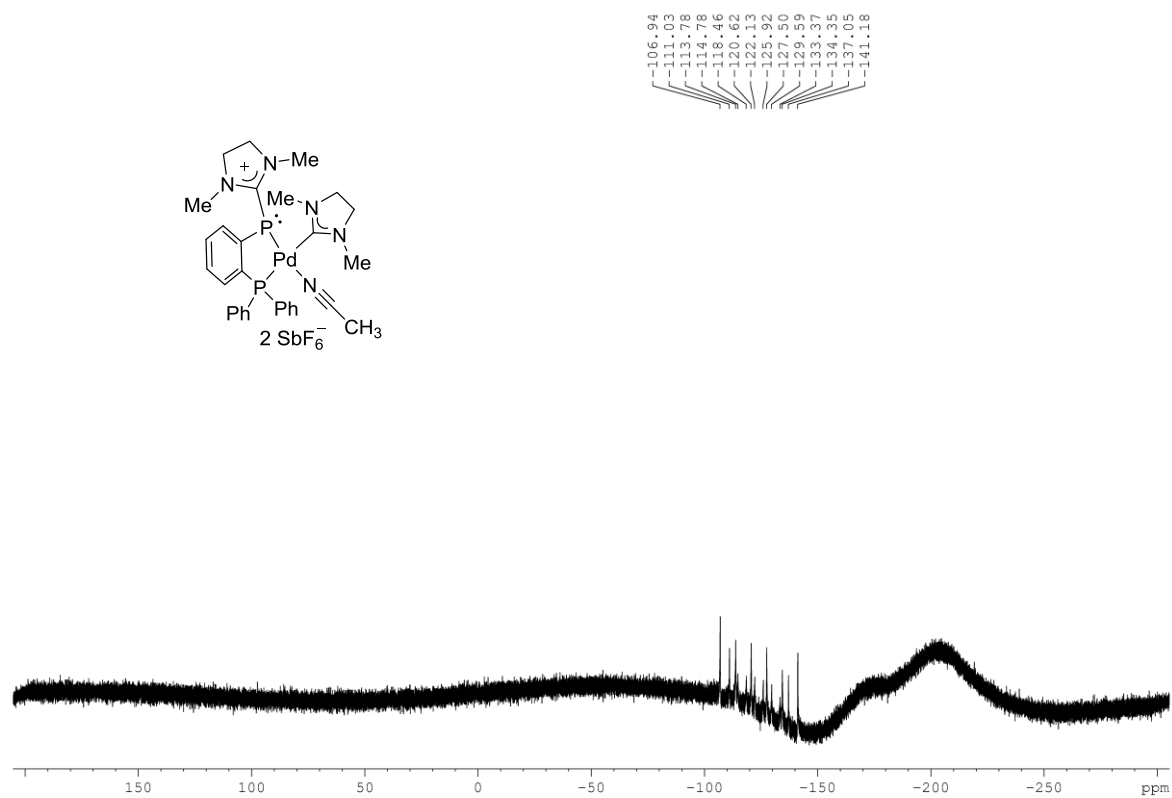
^{31}P NMR (CD_3CN , 121 MHz) (Compound 112g) **^{19}F NMR (CD_3CN , 282 MHz) (Compound 112g)**

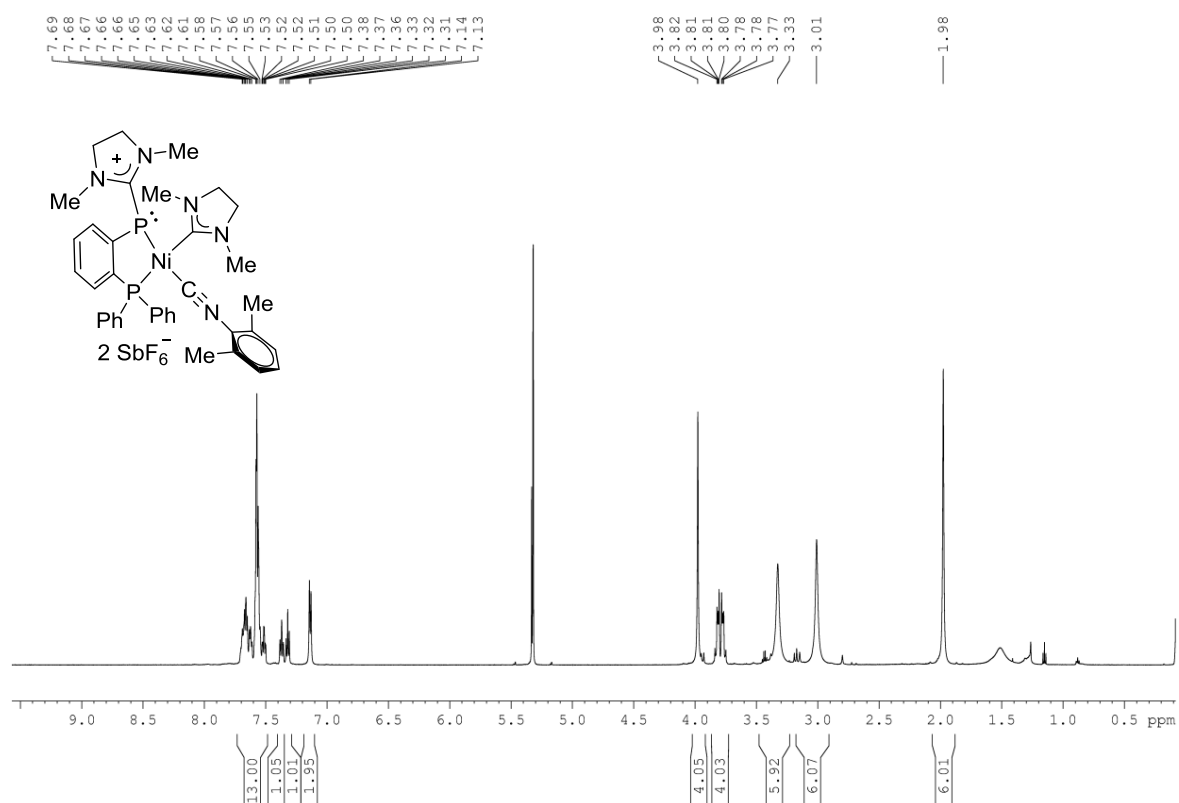
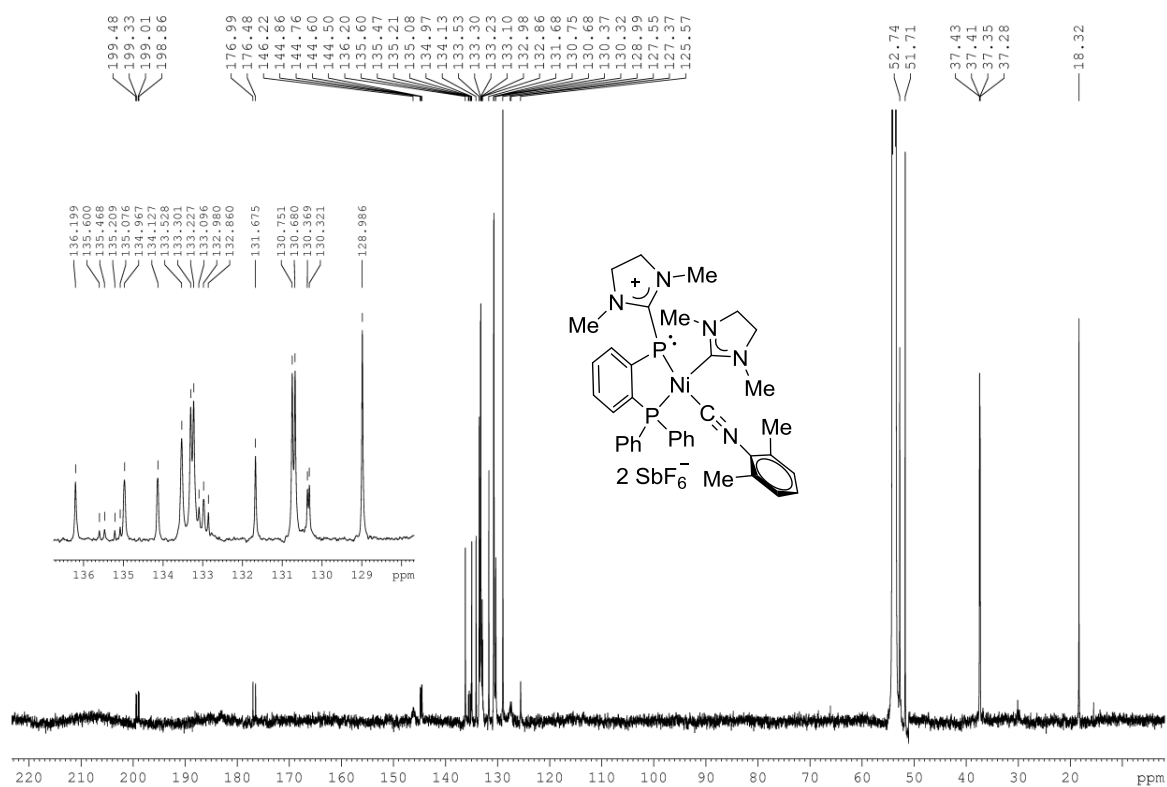
^{11}B NMR (CD₃CN, 96 MHz) (Compound 112g) **^1H NMR (CD₃COCD₃, 400 MHz) (Compound 112h)**

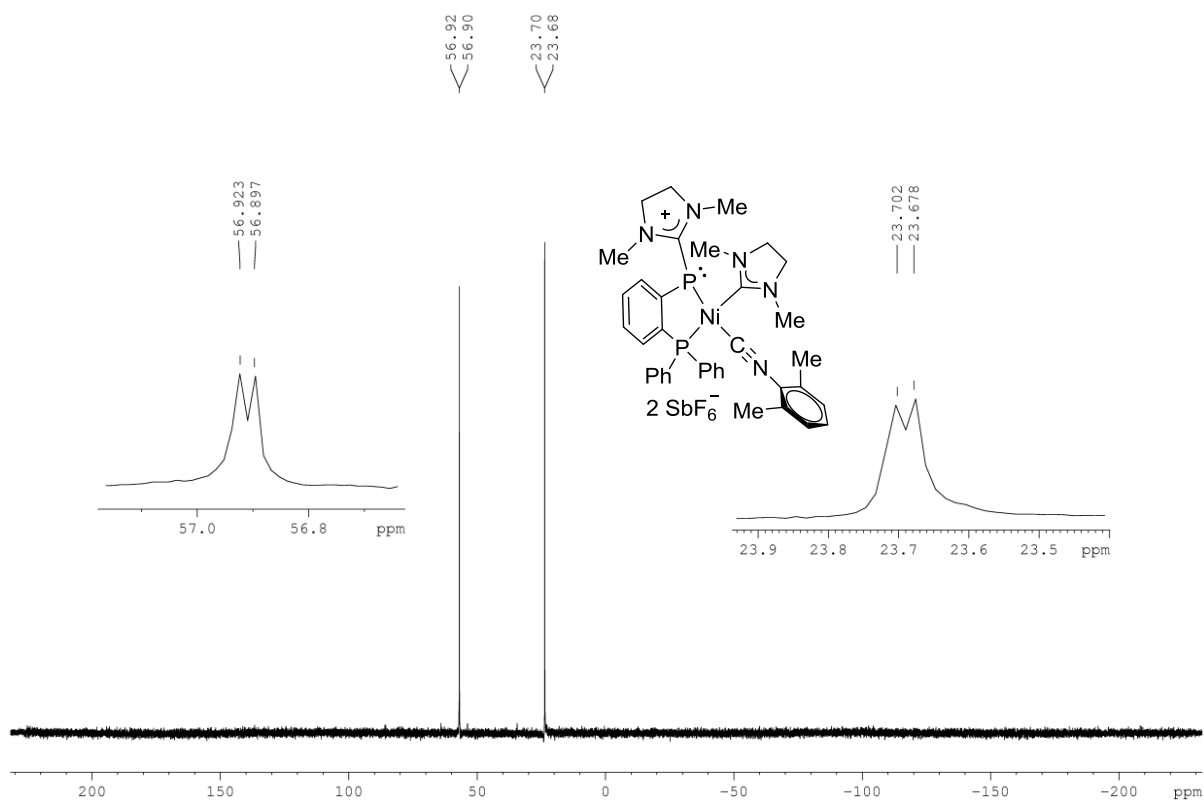
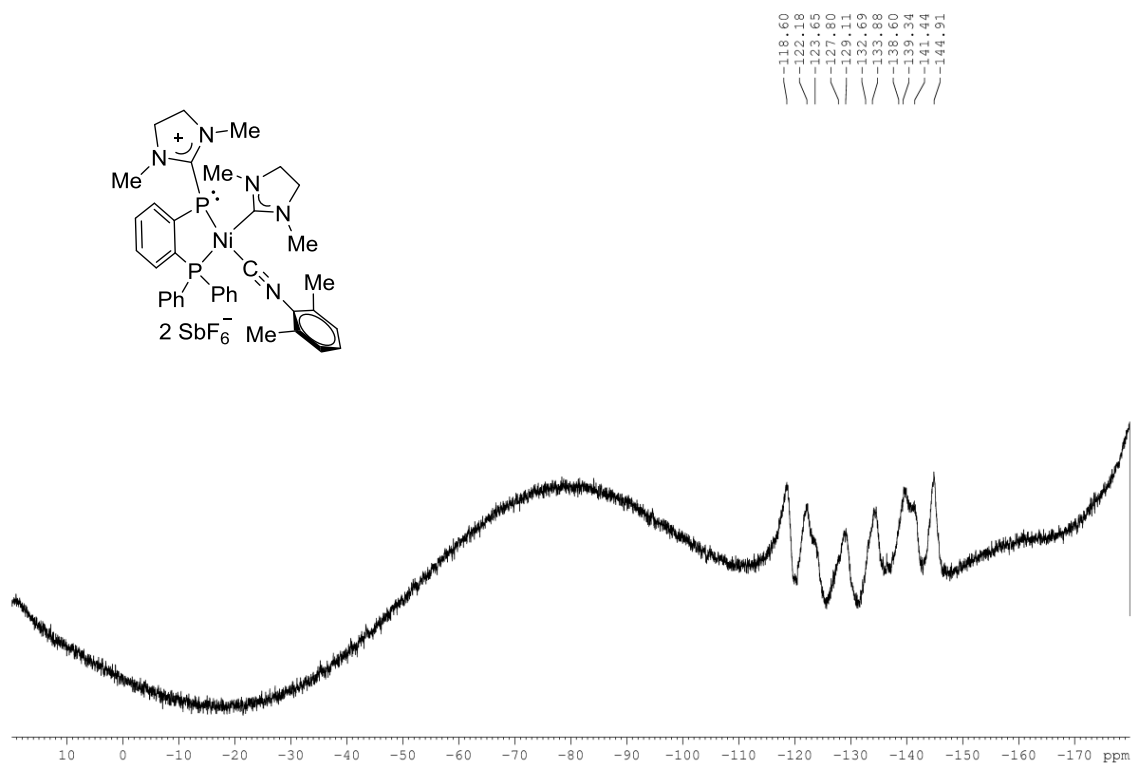
^{13}C NMR (CD_3COCD_3 , 100 MHz) (Compound 112h) **^{31}P NMR (CD_3COCD_3 , 121 MHz) (Compound 112h)**

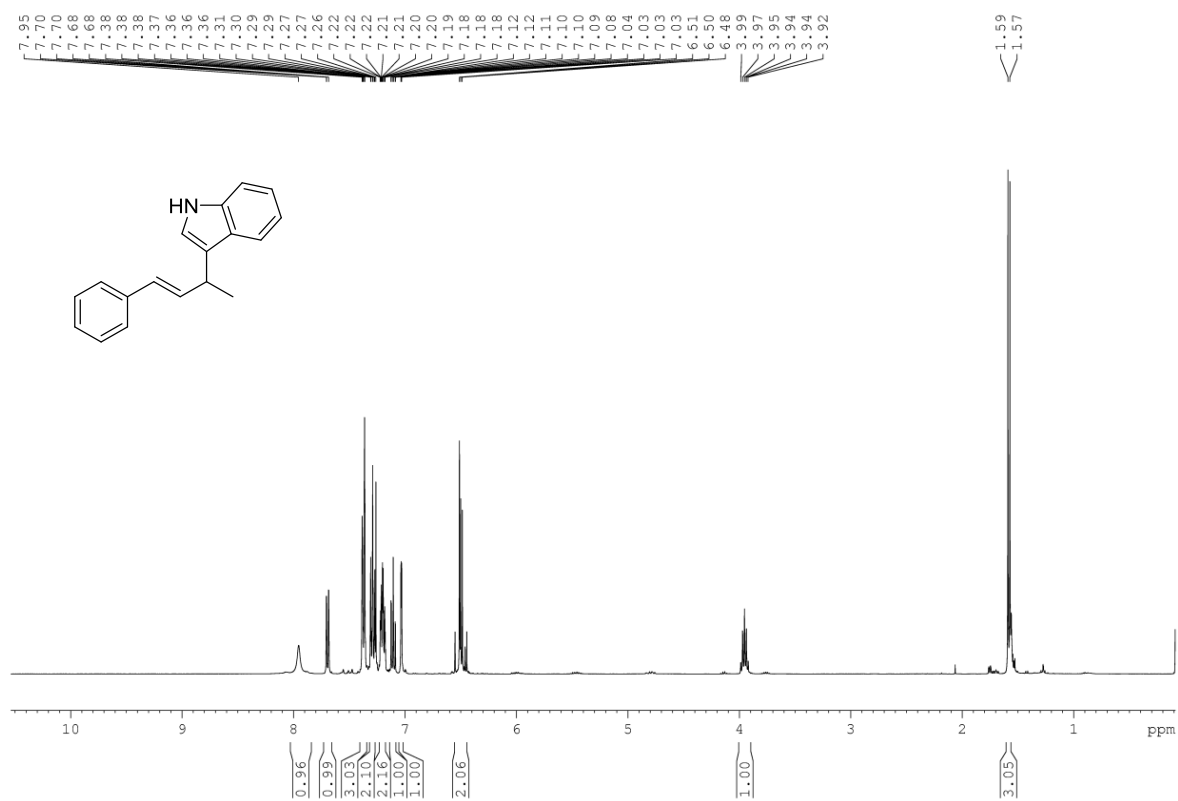
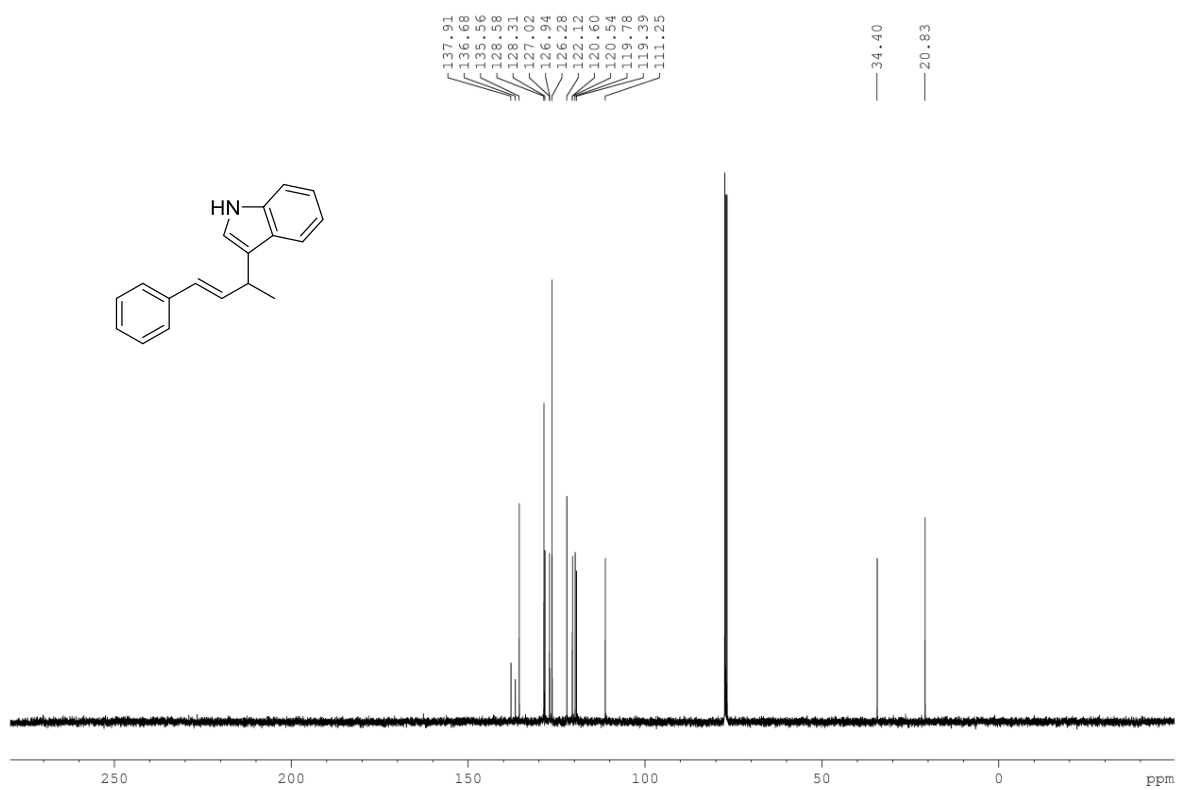
^{11}B NMR (CD₃COCD₃, 96 MHz) (Compound 112h) **^{19}F NMR (CD₃COCD₃, 282 MHz) (Compound 112h)**

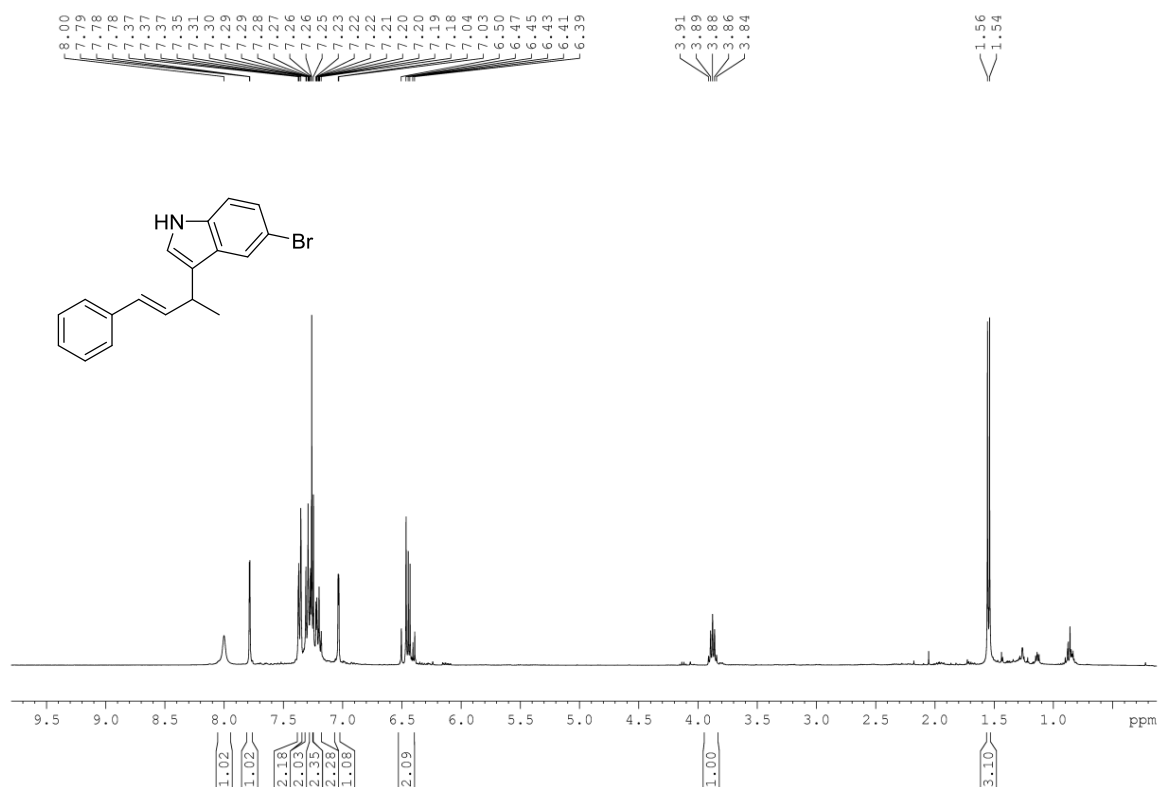
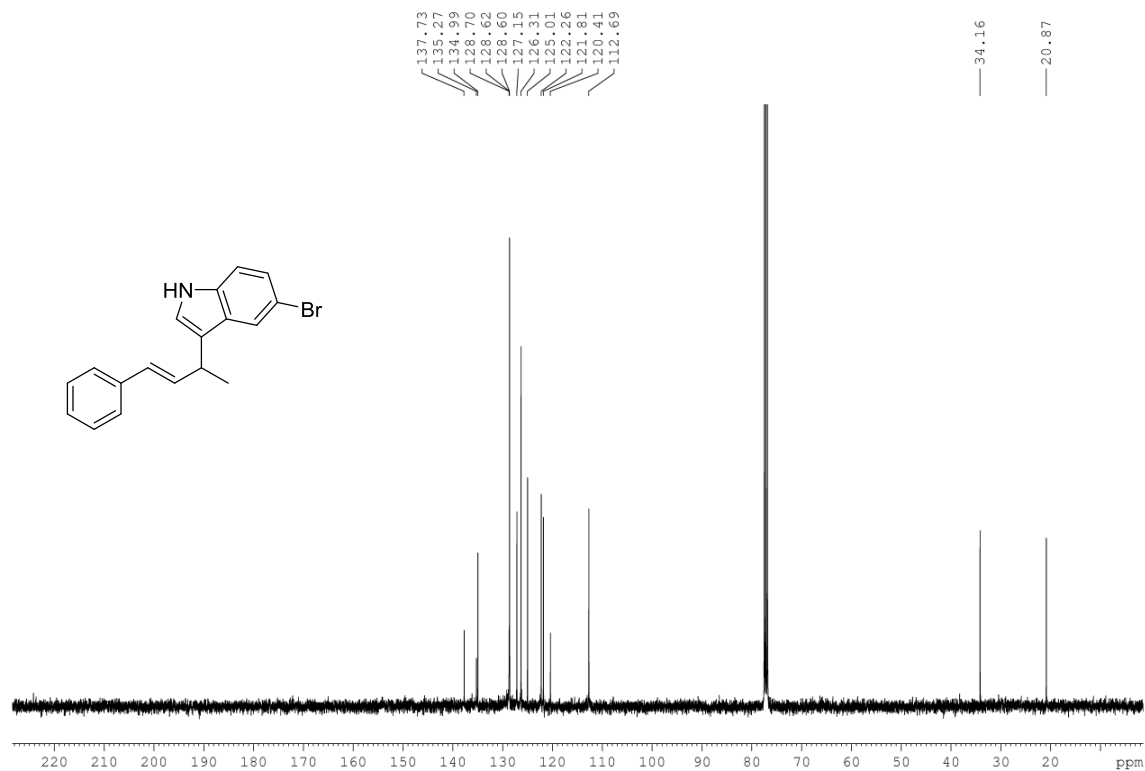
^1H NMR (CD₃CN, 600 MHz) (Compound 113) **^{13}C NMR (CD₃CN, 125 Mz) (Compound 113)**

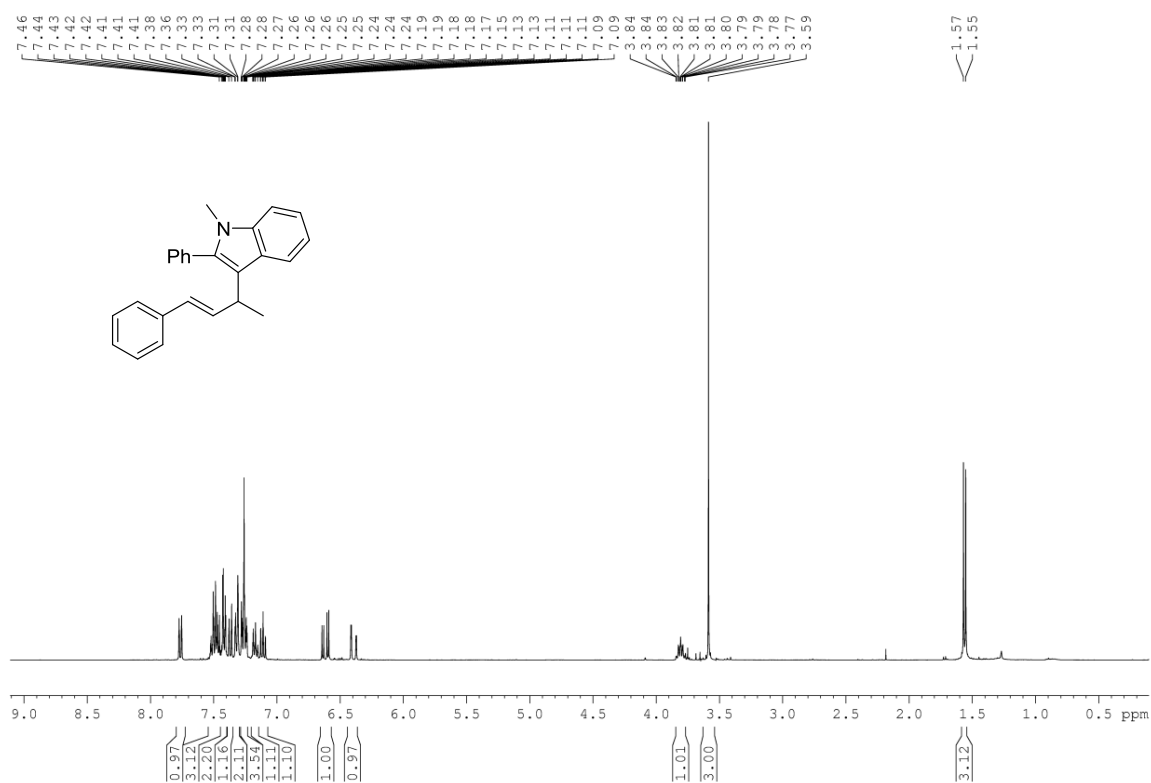
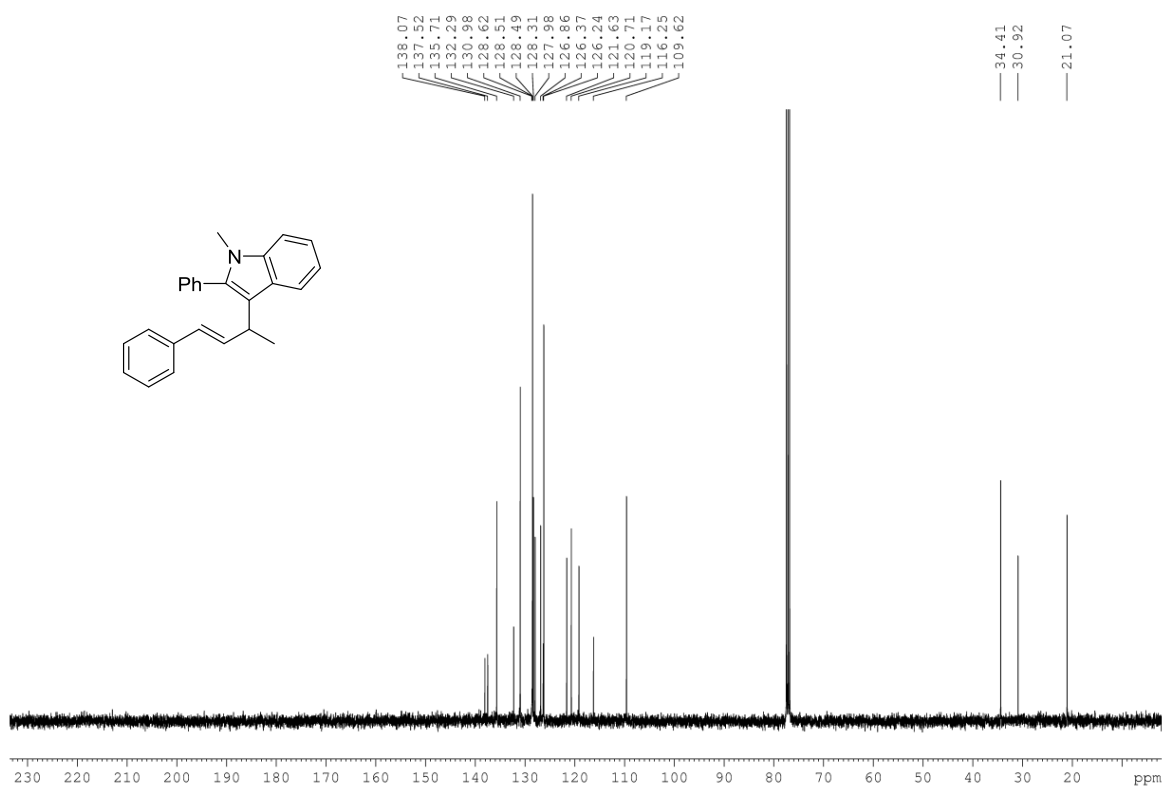
^{31}P NMR (CD_3CN , 162 MHz) (Compound 113) **^{19}F NMR (CD_3CN , 282 MHz) (Compound 113)**

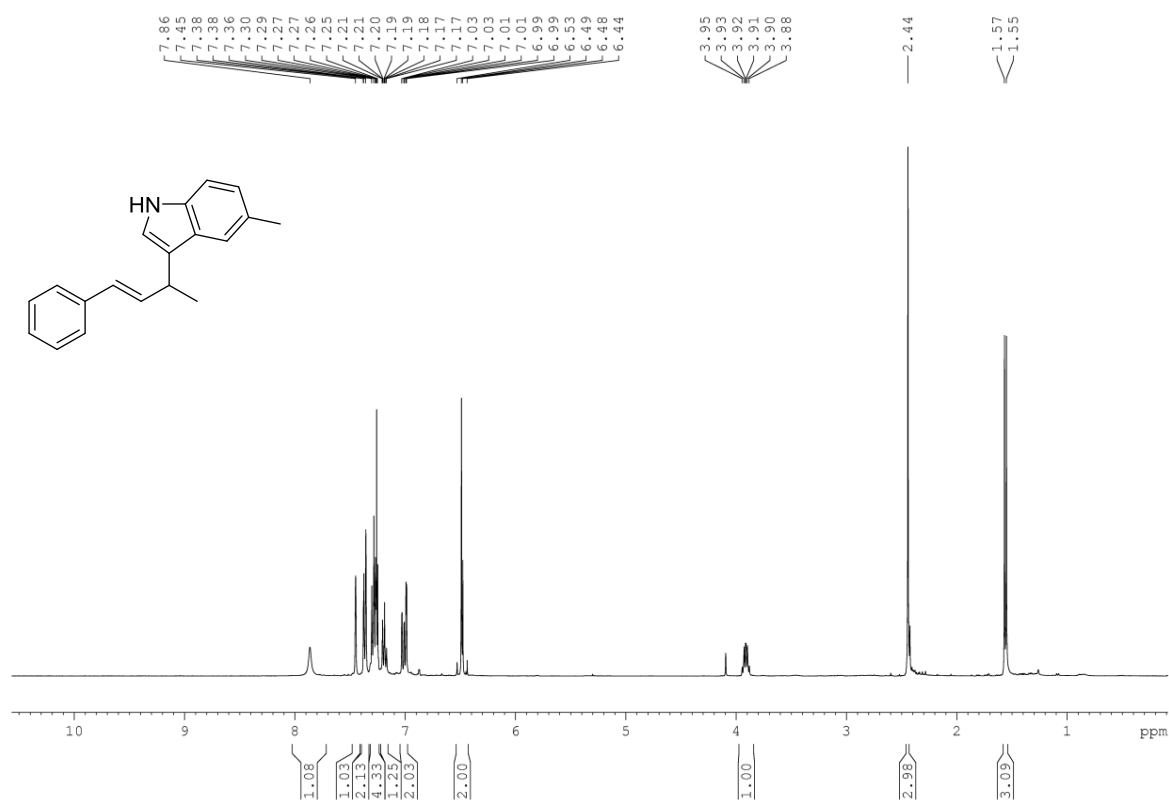
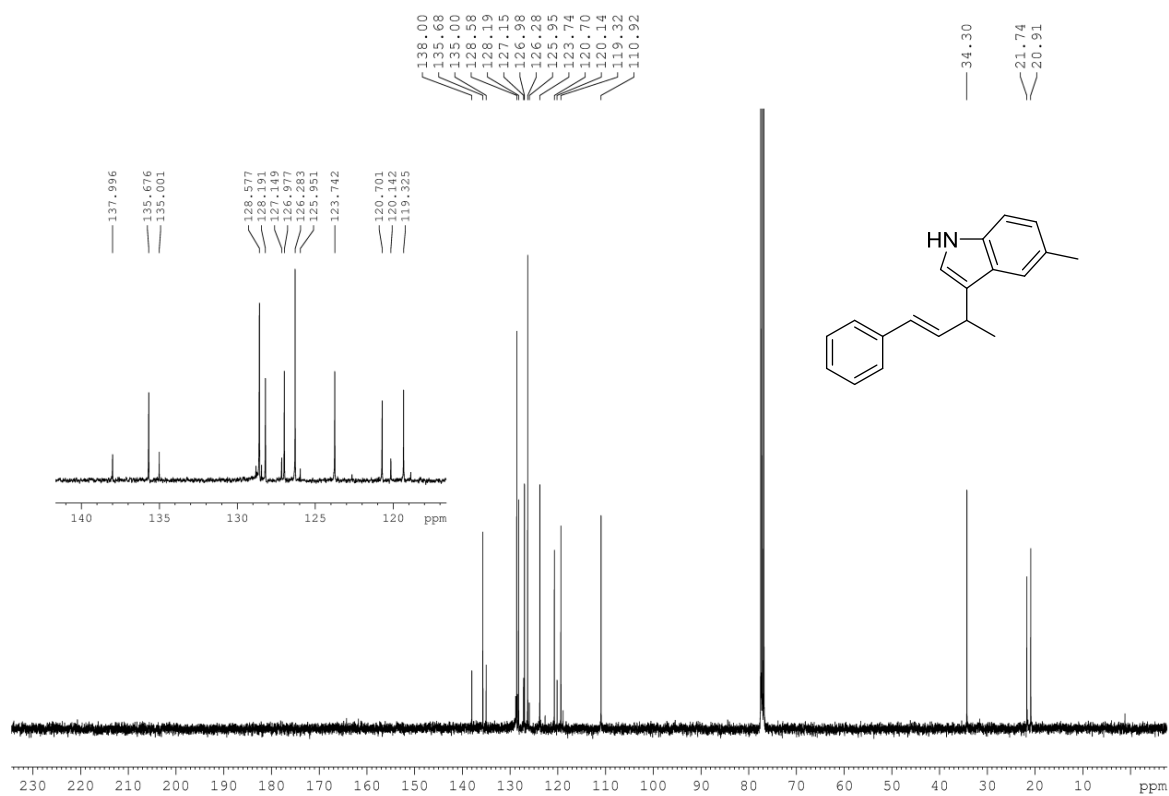
^1H NMR (CD_2Cl_2 , 600 MHz) (Compound 114) **^{13}C NMR (CD_2Cl_2 , 125 Mz) (Compound 114)**

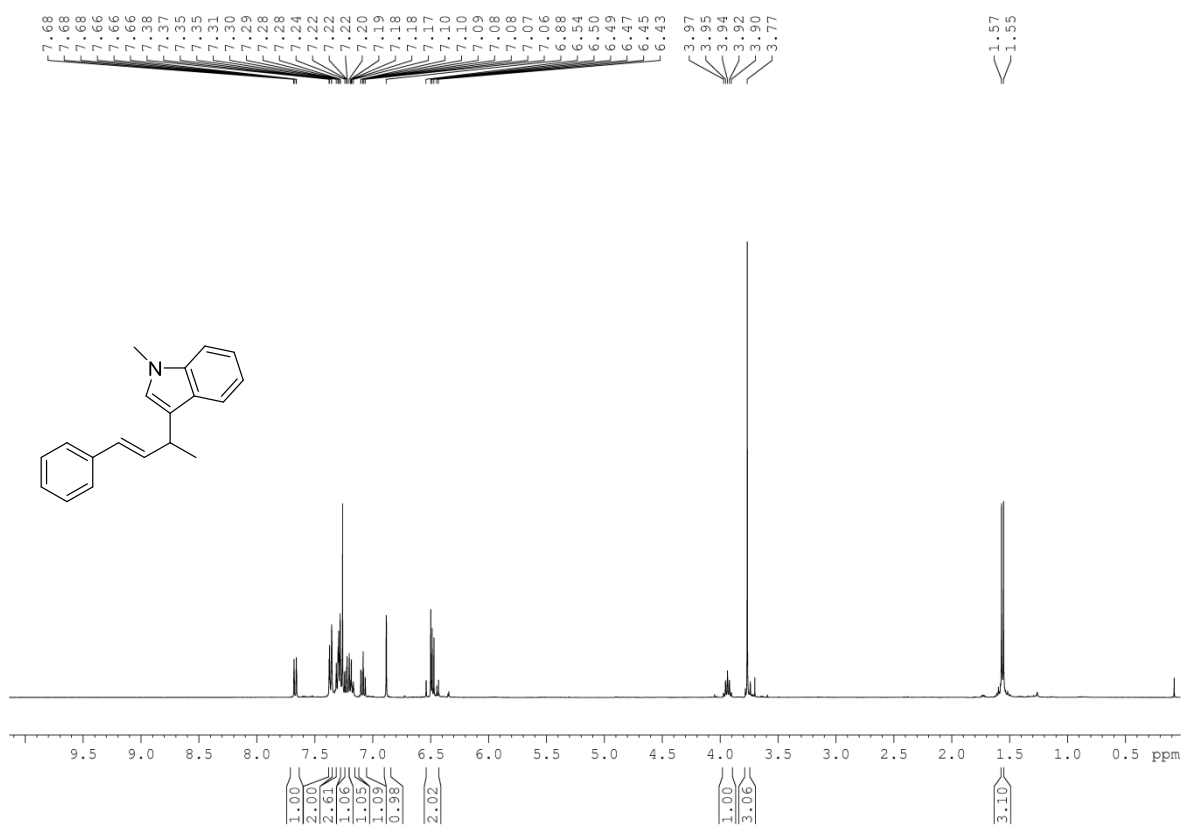
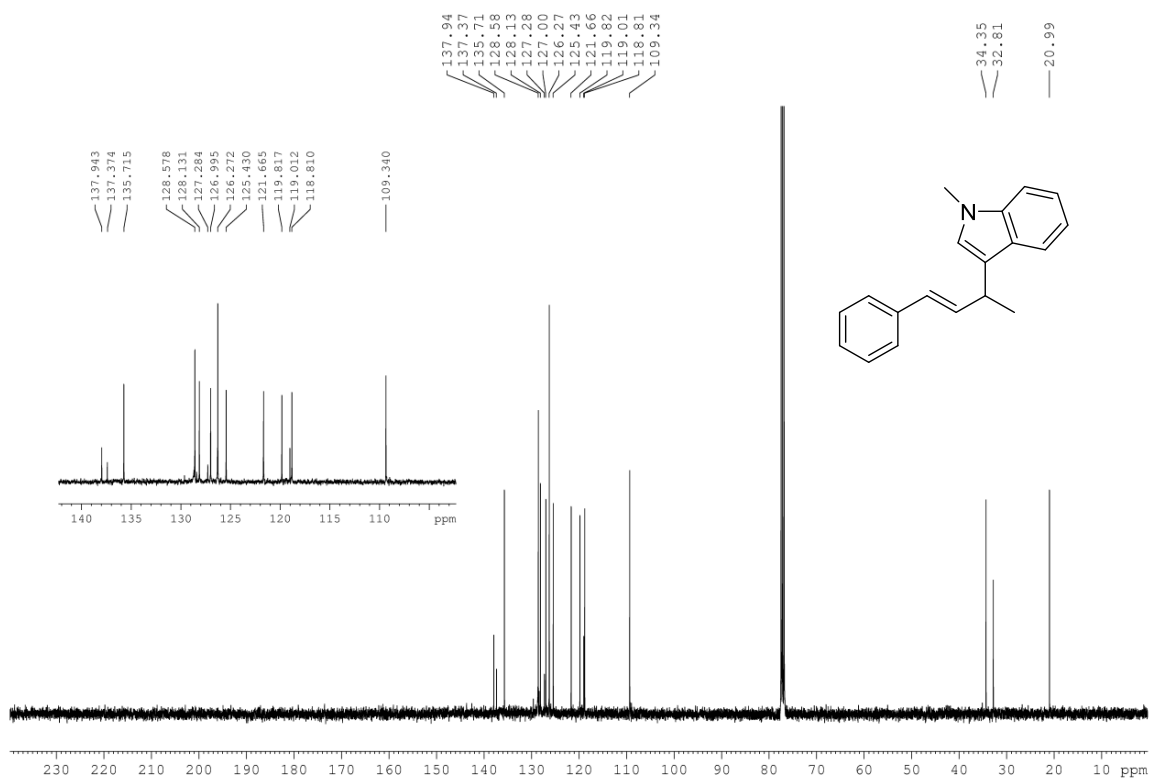
^{31}P NMR (CD_2Cl_2 , 162 MHz) (Compound 114) **^{19}F NMR (CD_2Cl_2 , 282 MHz) (Compound 114)**

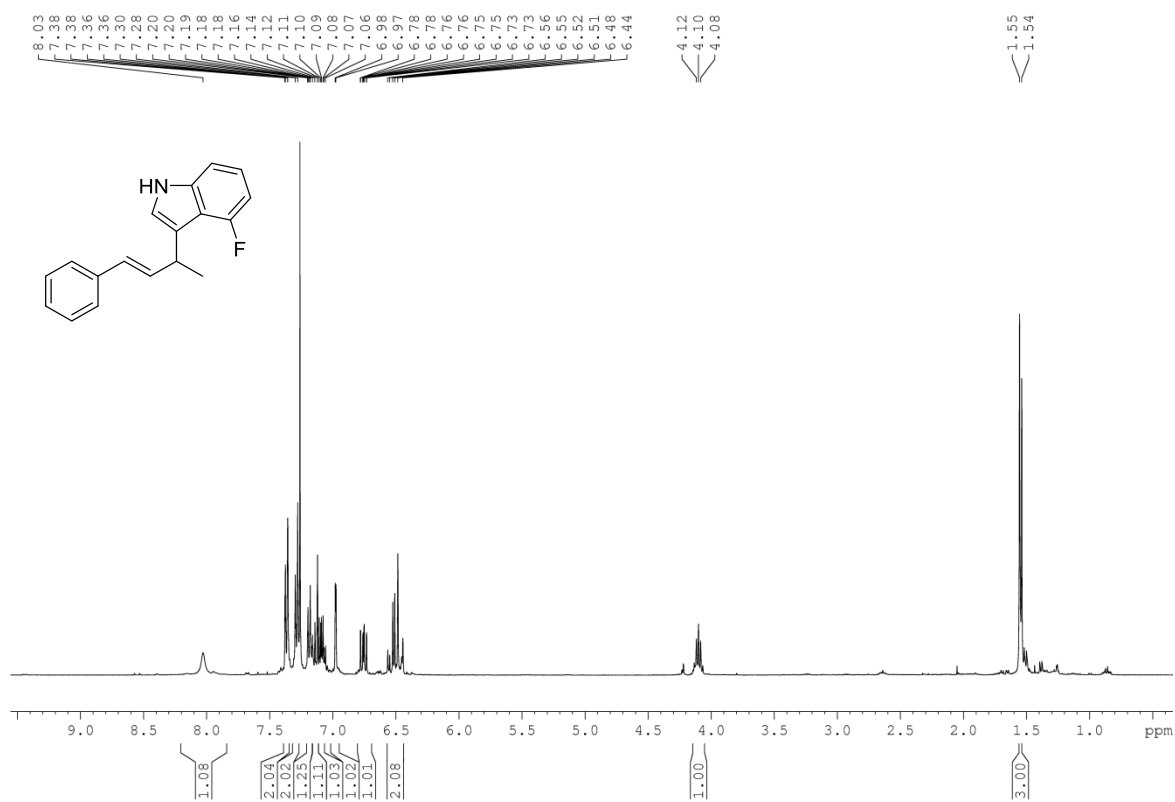
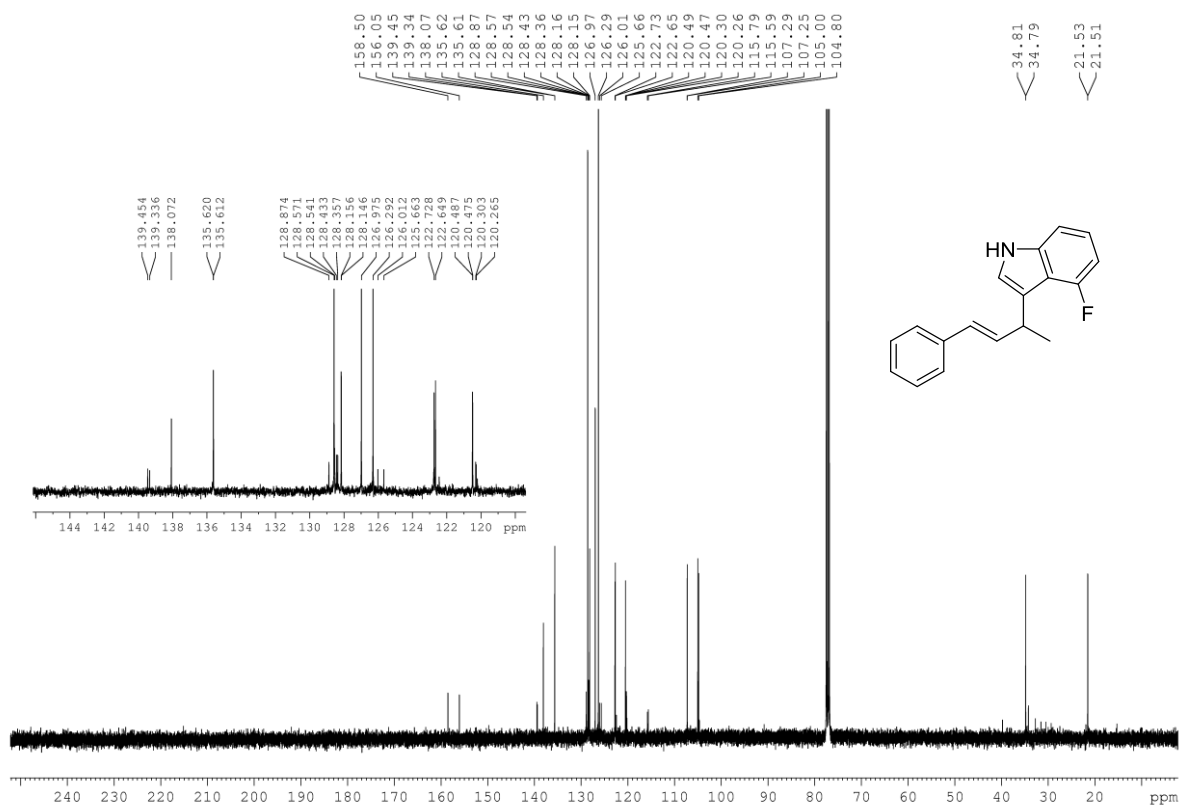
^1H NMR (CDCl₃, 400 MHz) (Compound 118) **^{13}C NMR (CDCl₃, 100 MHz) (Compound 118)**

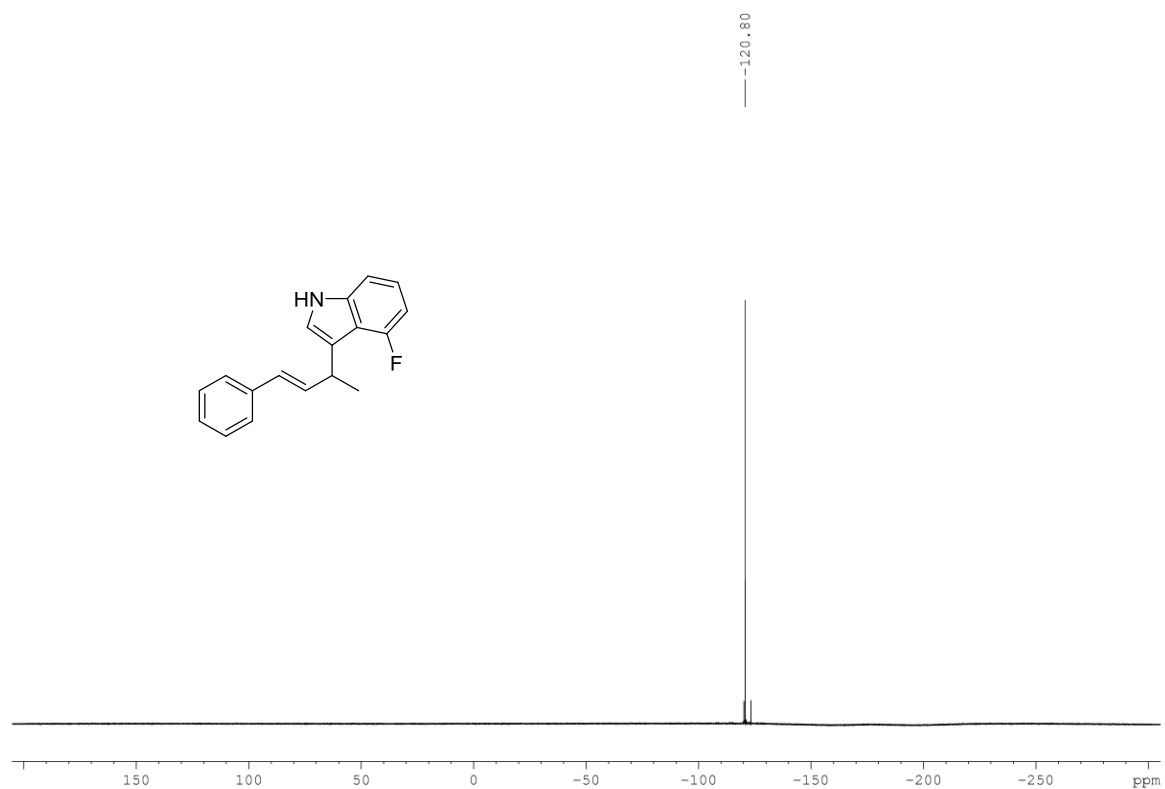
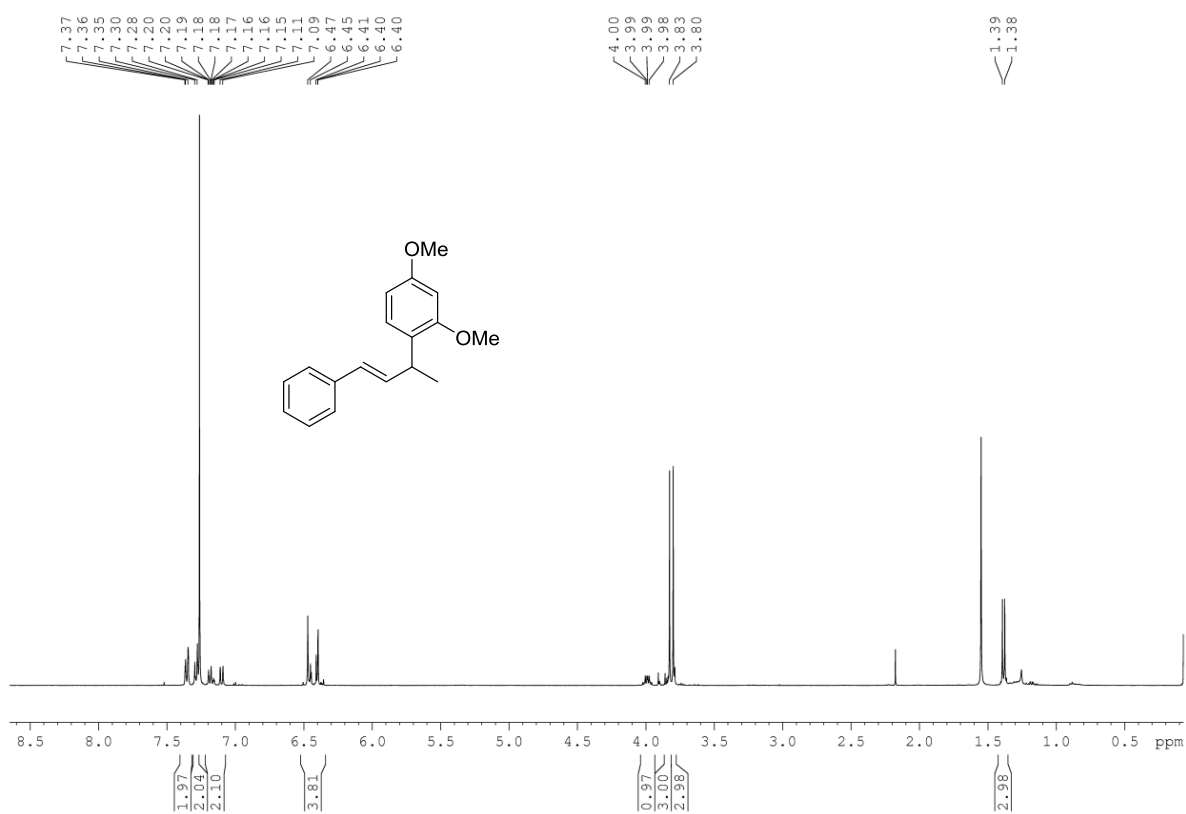
^1H NMR (CDCl₃, 400 MHz) (Compound 119) **^{13}C NMR (CDCl₃, 100 MHz) (Compound 119)**

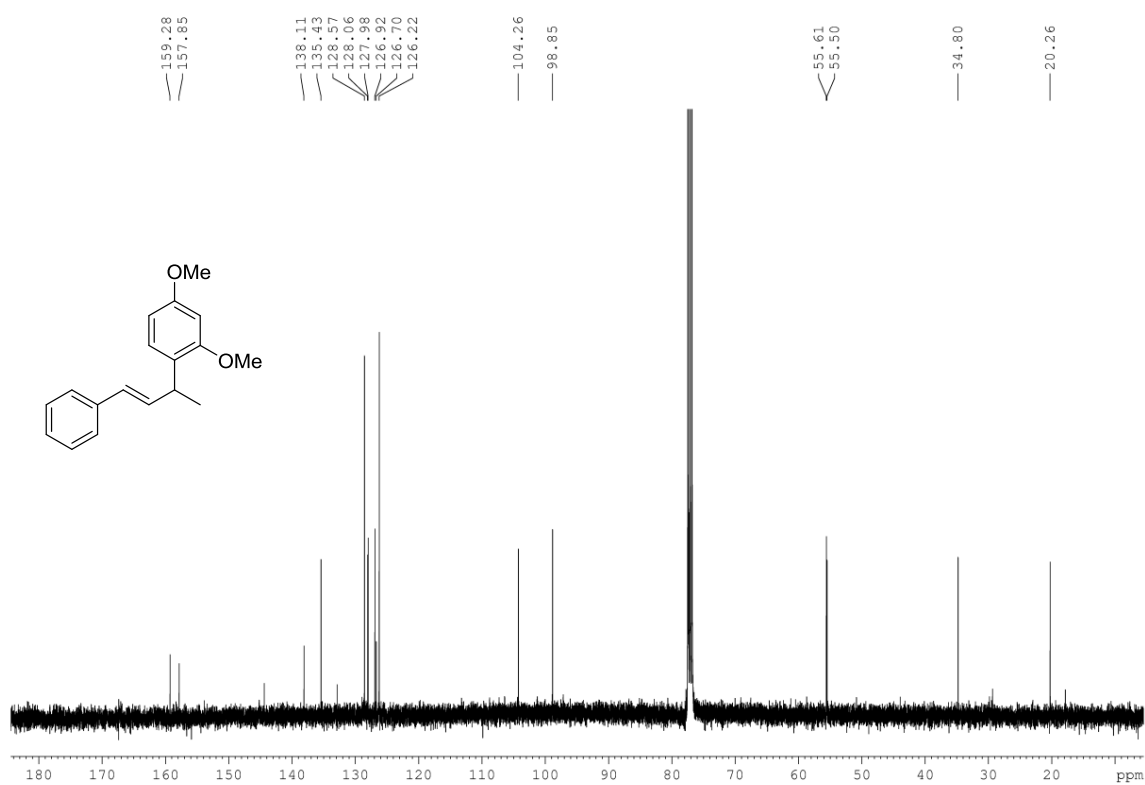
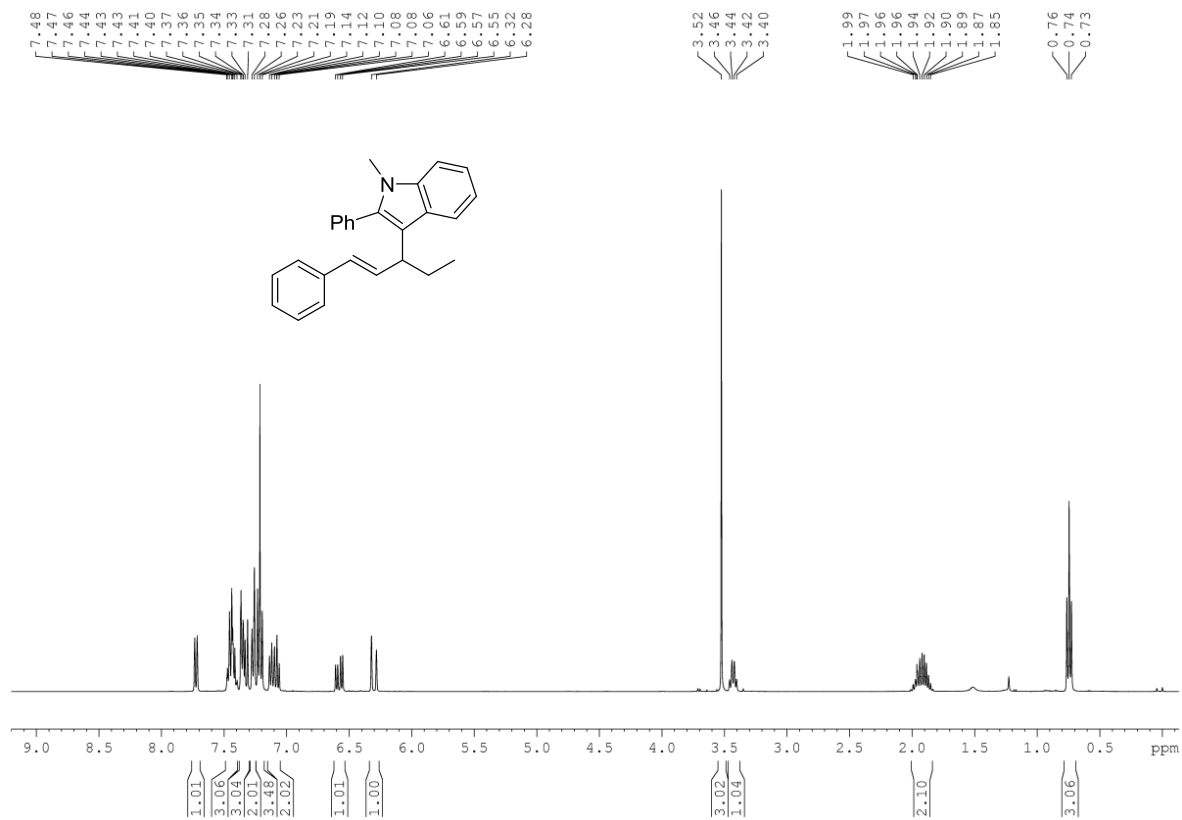
^1H NMR (CDCl₃, 400 MHz) (Compound 120) **^{13}C NMR (CDCl₃, 100 MHz) (Compound 120)**

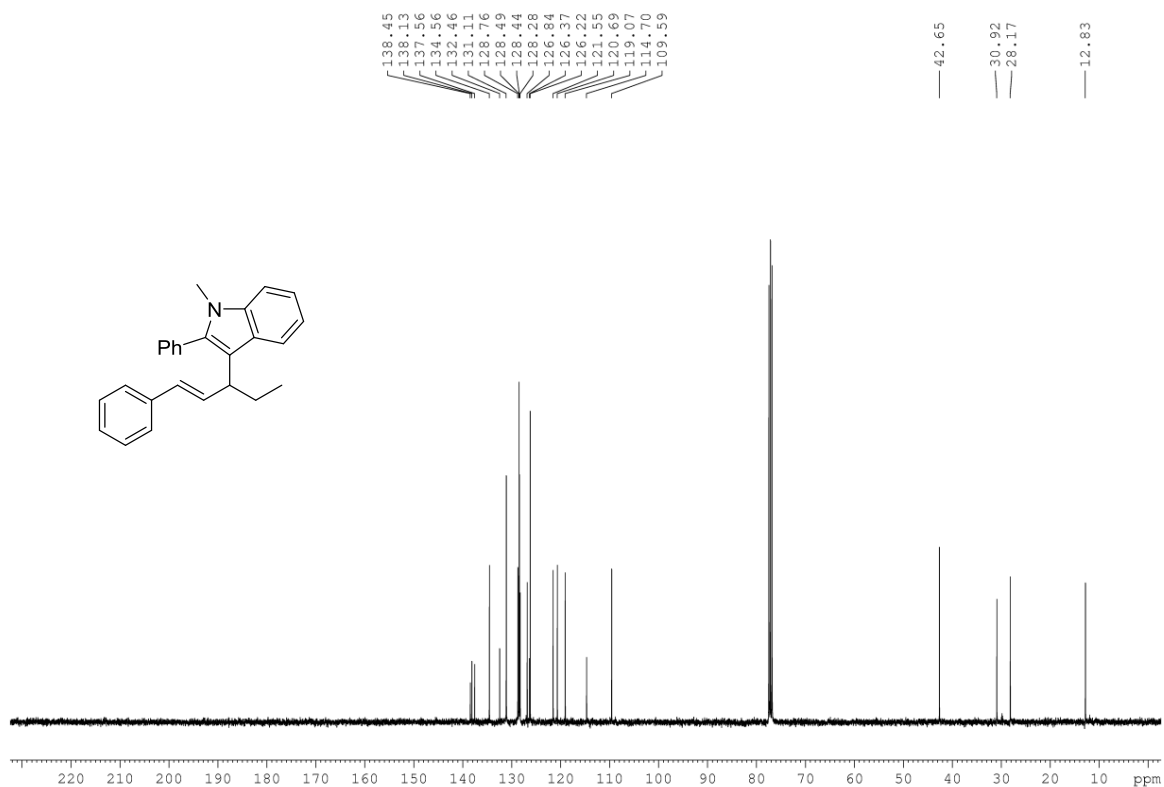
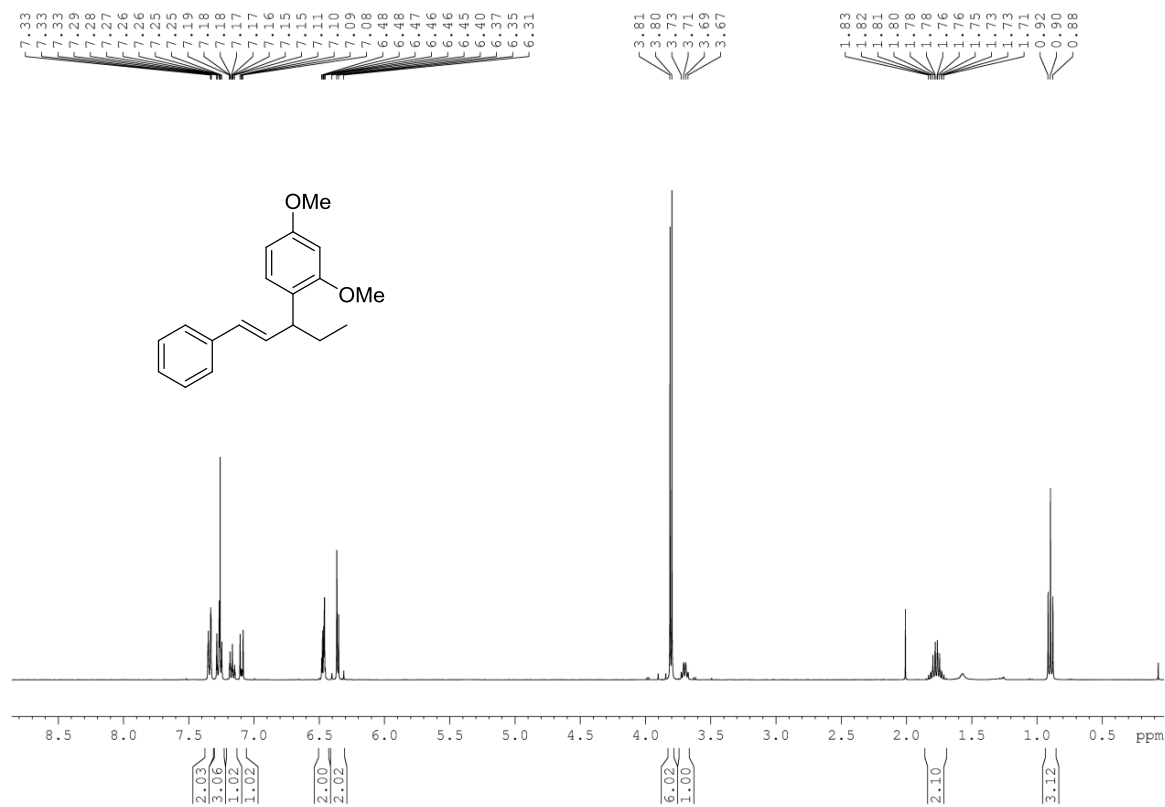
^1H NMR (CDCl₃, 400 MHz) (Compound 121) **^{13}C NMR (CDCl₃, 100 MHz) (Compound 121)**

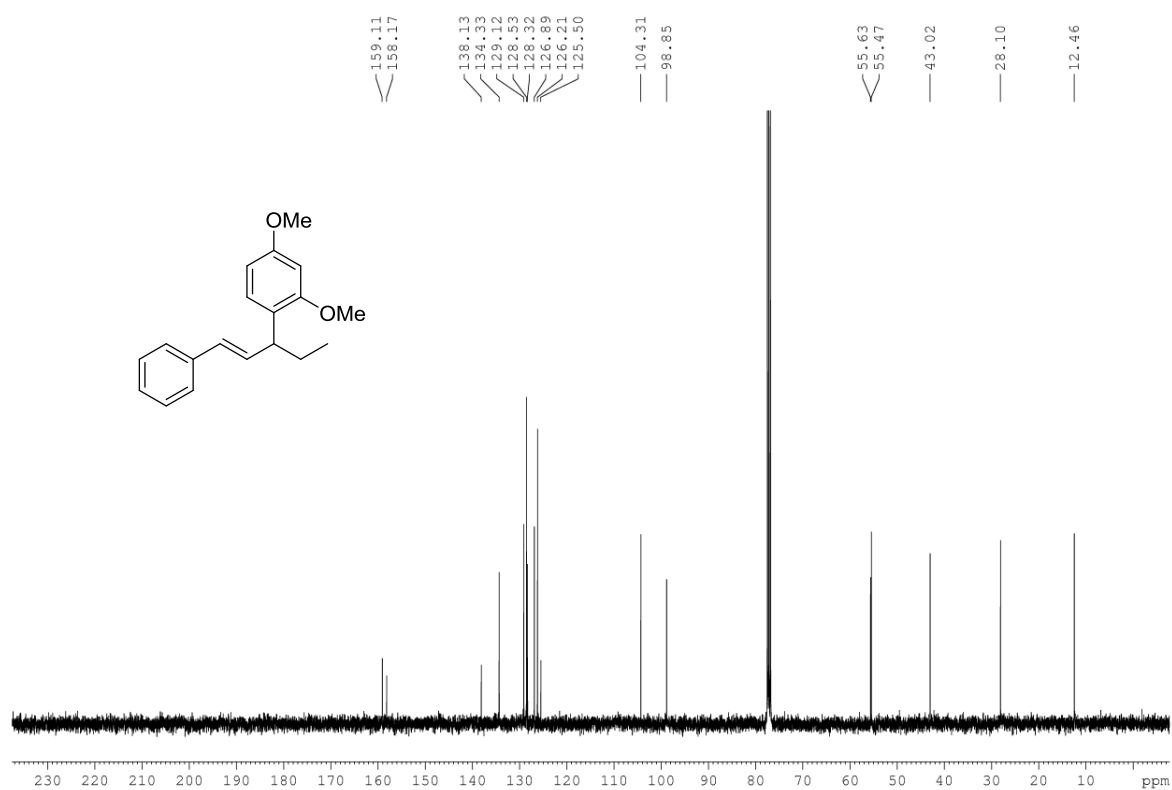
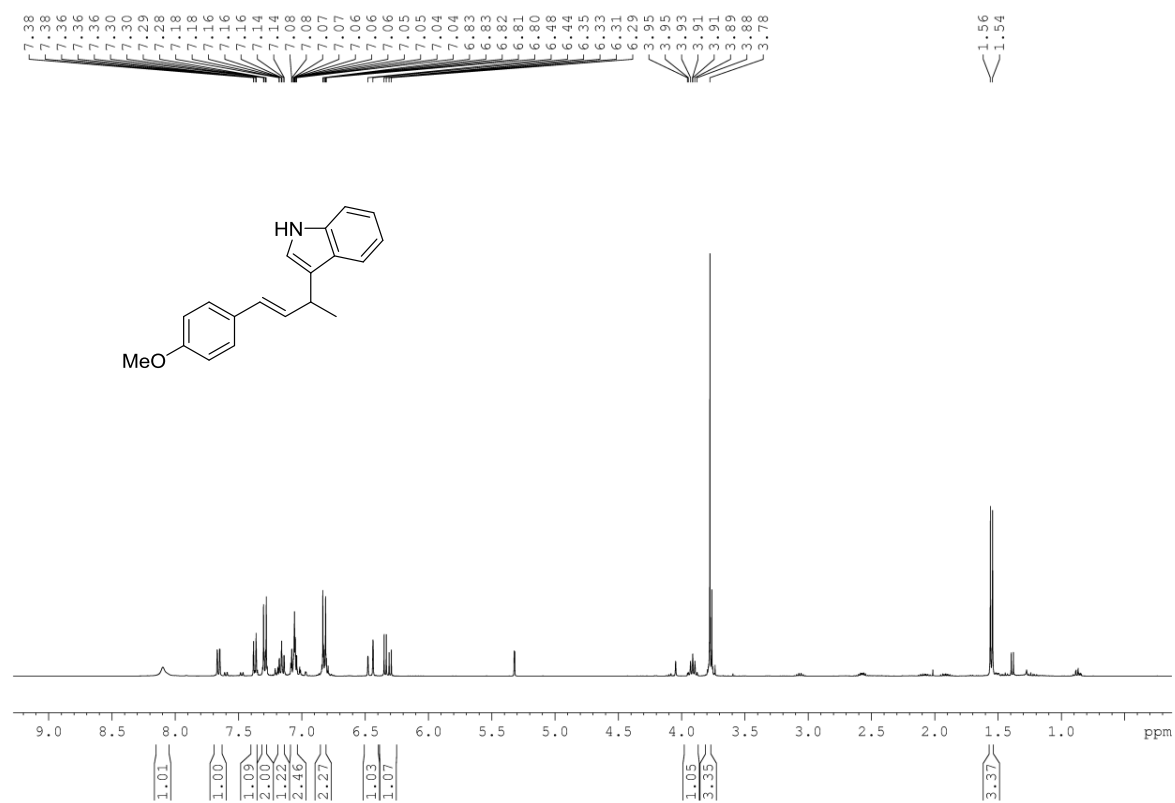
^1H NMR (CDCl₃, 400 MHz) (Compound 122) **^{13}C NMR (CDCl₃, 100 MHz) (Compound 122)**

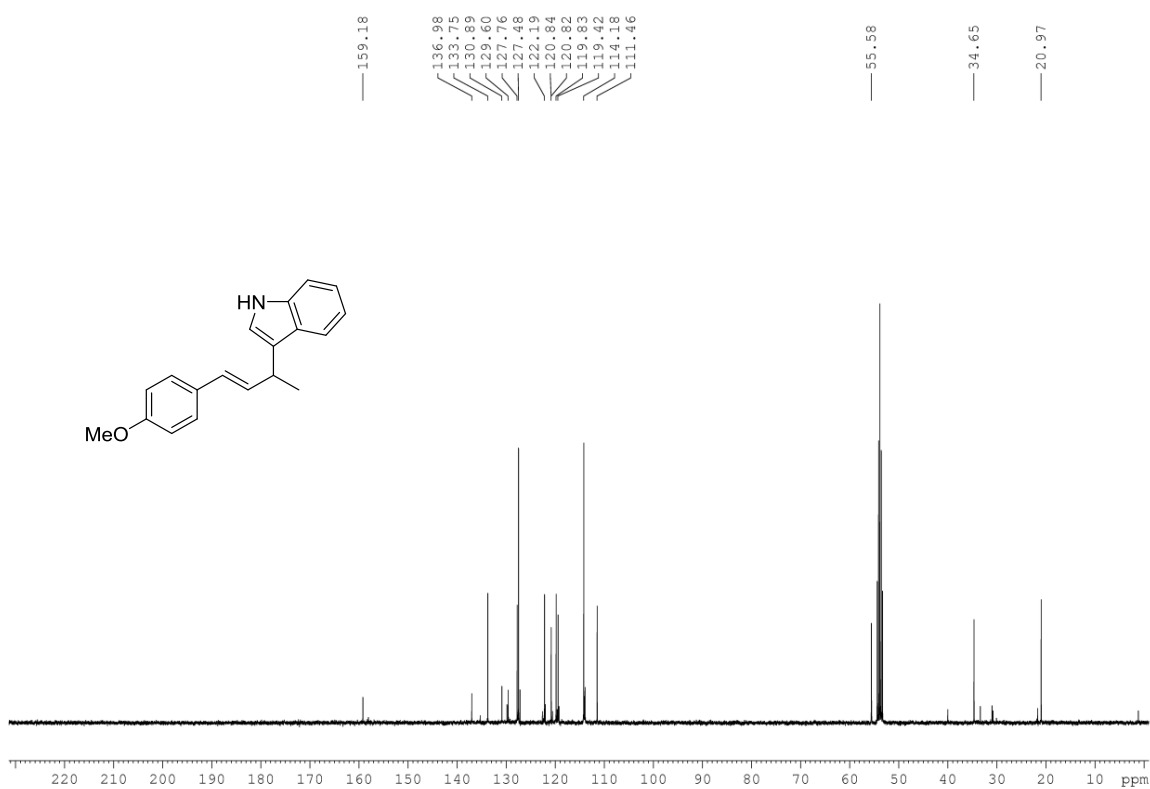
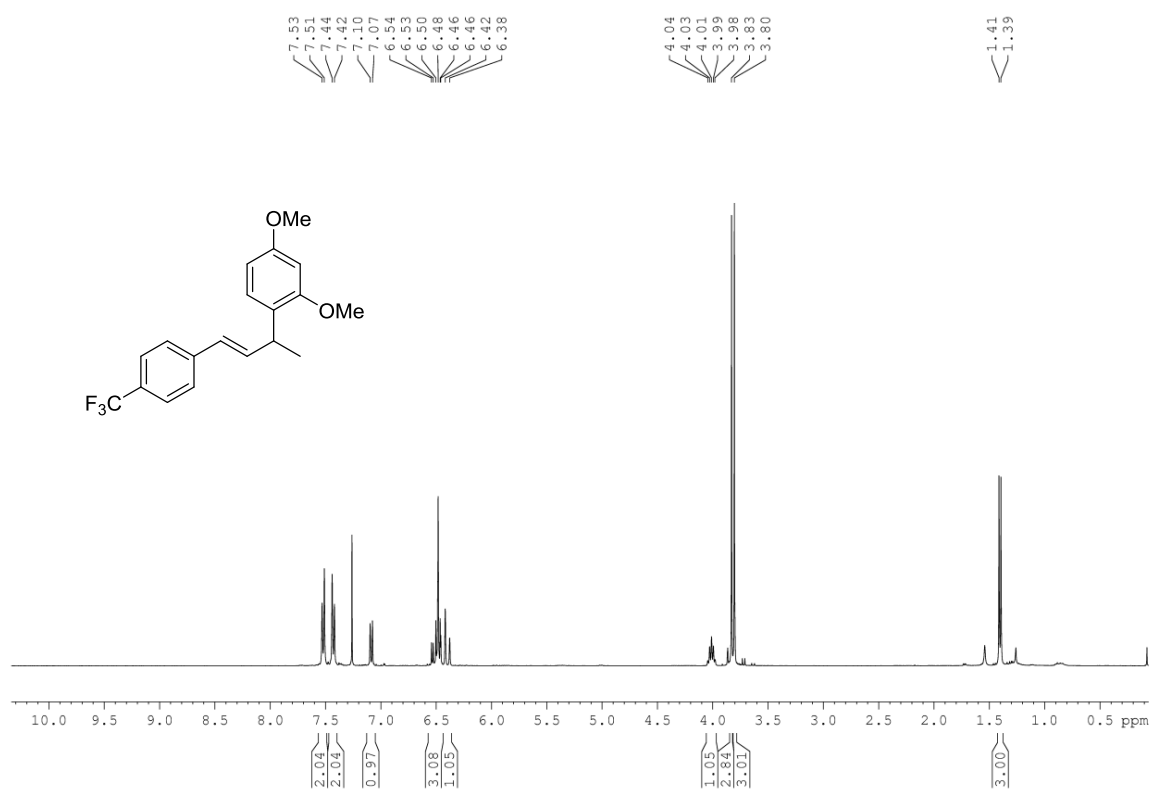
^1H NMR (CDCl₃, 400 MHz) (Compound 123) **^{13}C NMR (CDCl₃, 100 MHz) (Compound 123)**

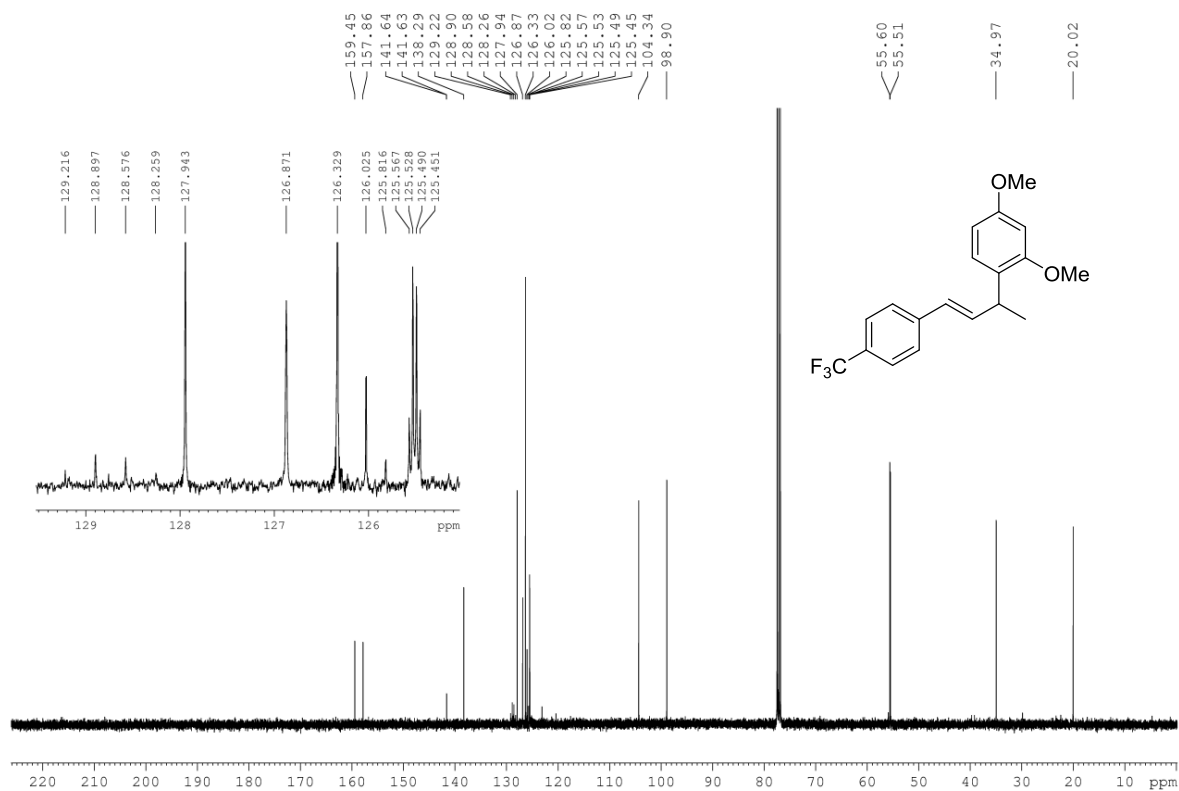
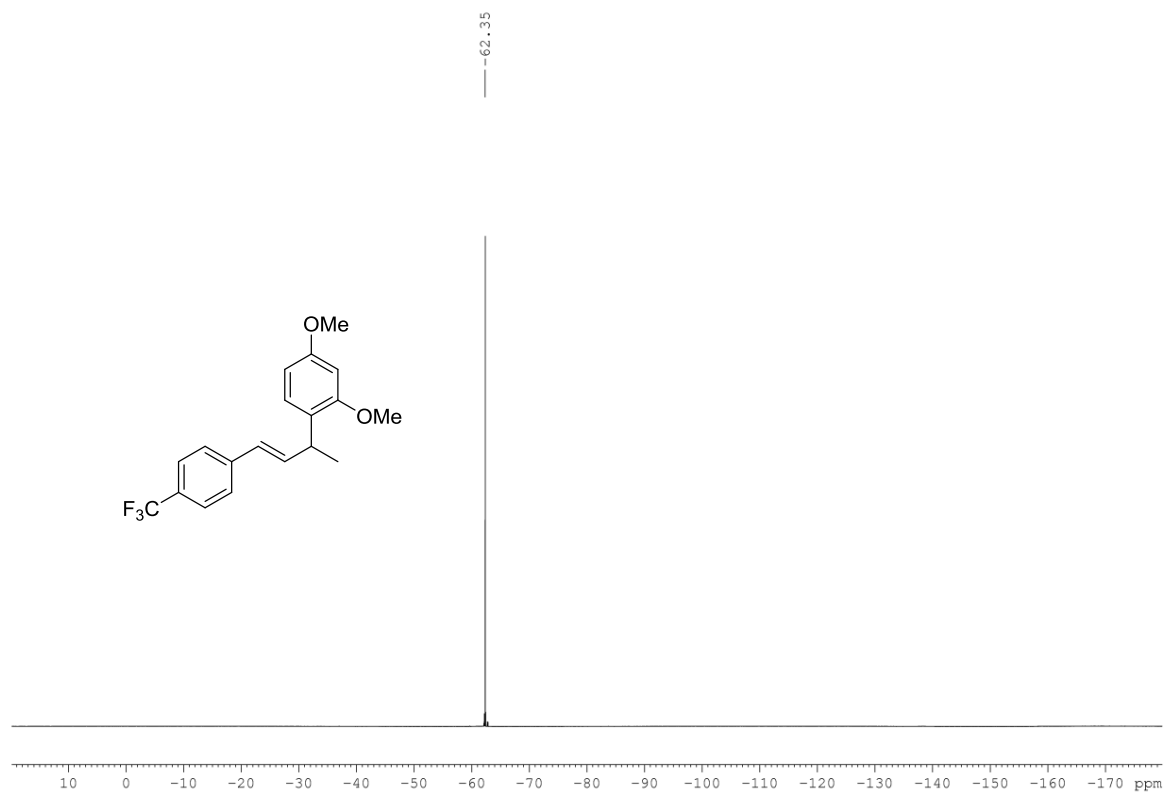
^{19}F NMR (CDCl₃, 282 MHz) (Compound 123) **^1H NMR (CDCl₃, 400 MHz) (Compound 124)**

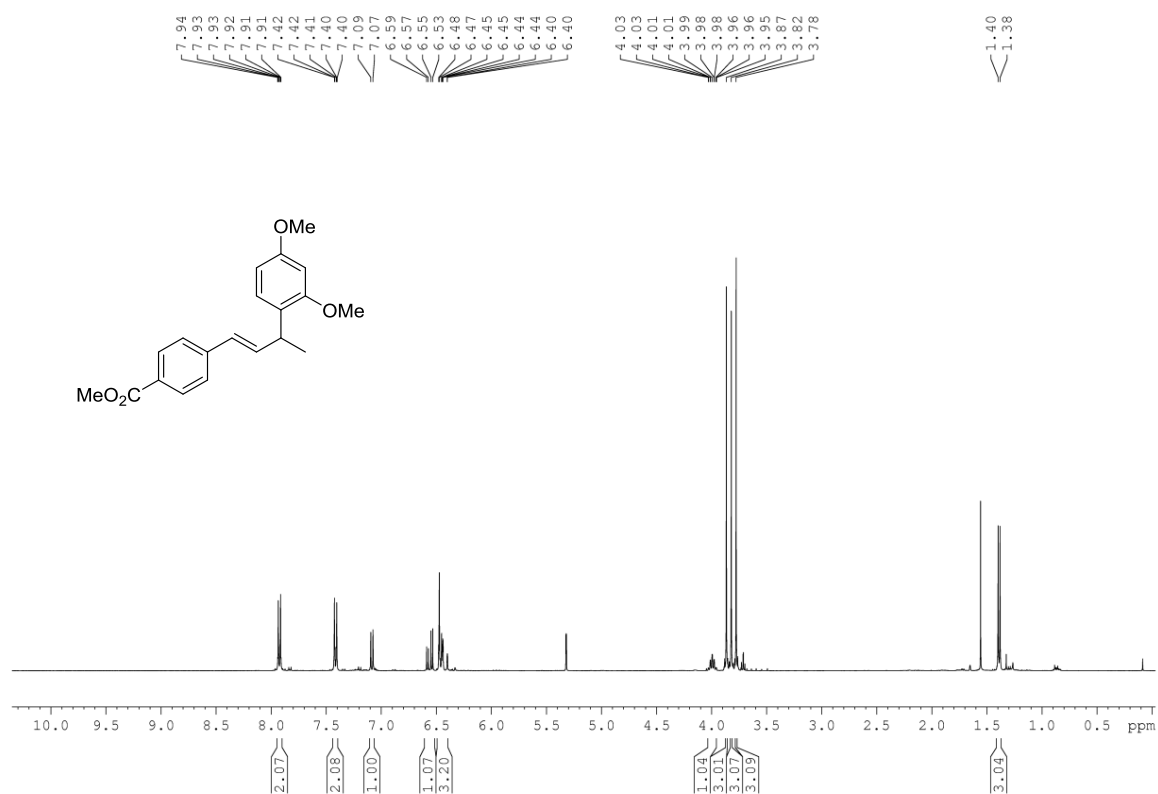
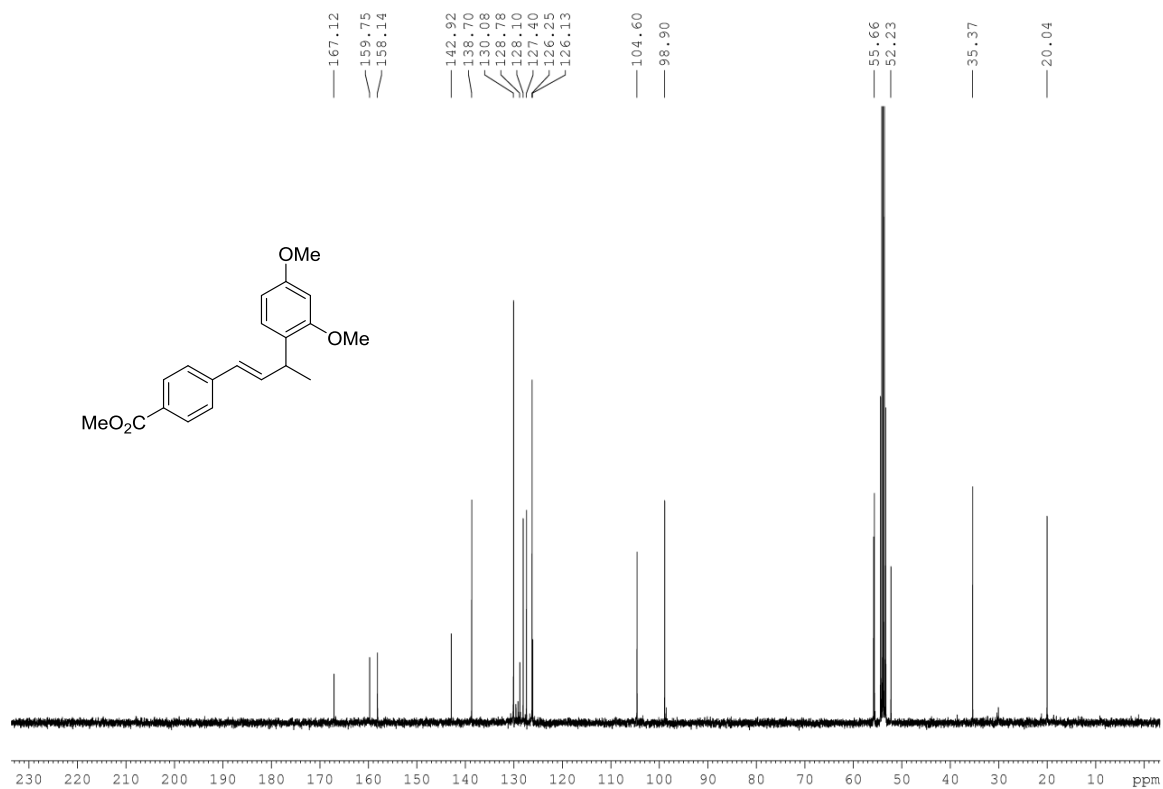
^{13}C NMR (CDCl₃, 100 MHz) (Compound 124) **^1H NMR (CDCl₃, 400 MHz) (Compound 125)**

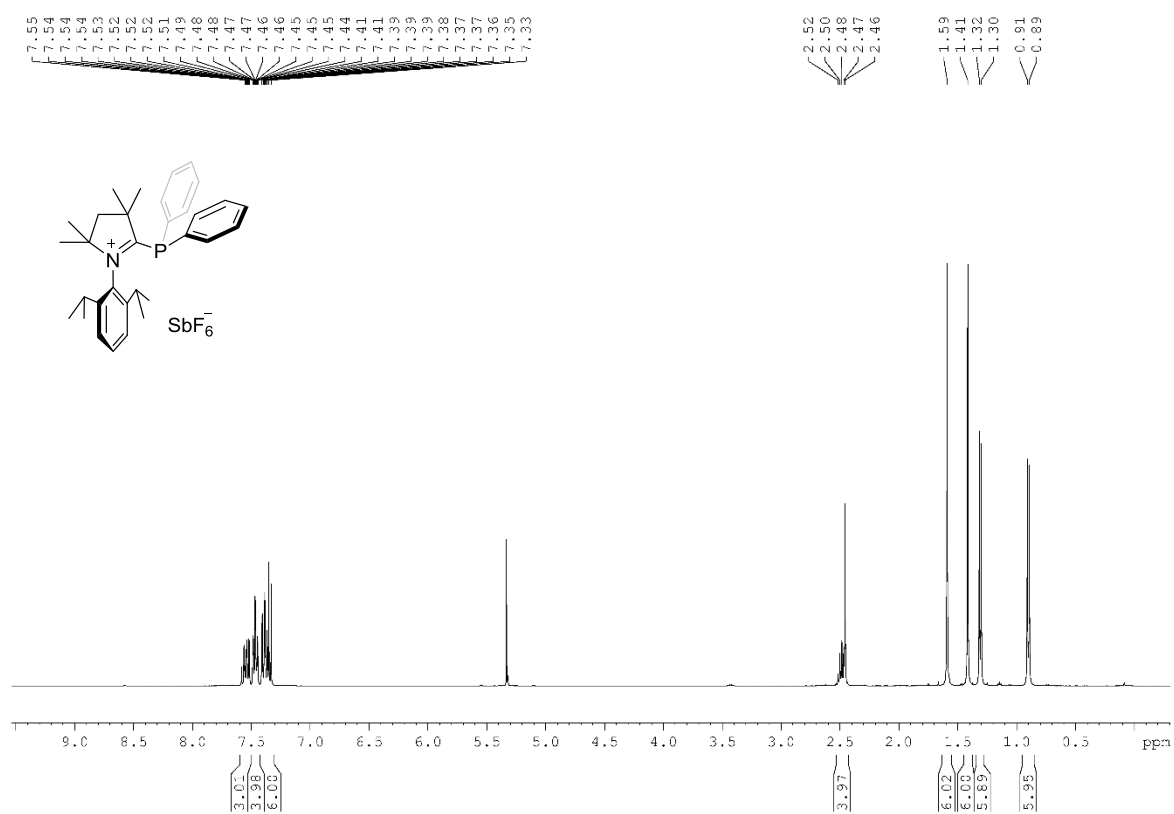
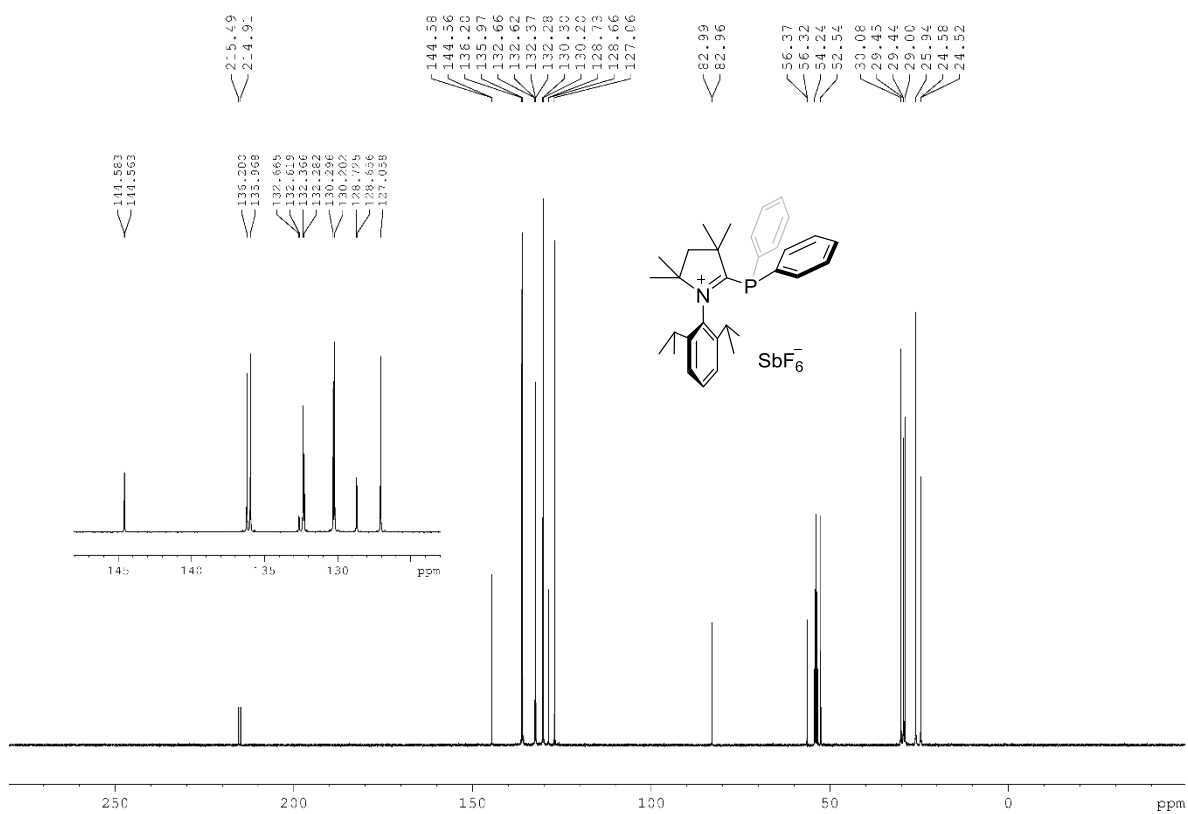
^{13}C NMR (CDCl₃, 100 MHz) (Compound 125) **^1H NMR (CDCl₃, 400 MHz) (Compound 126)**

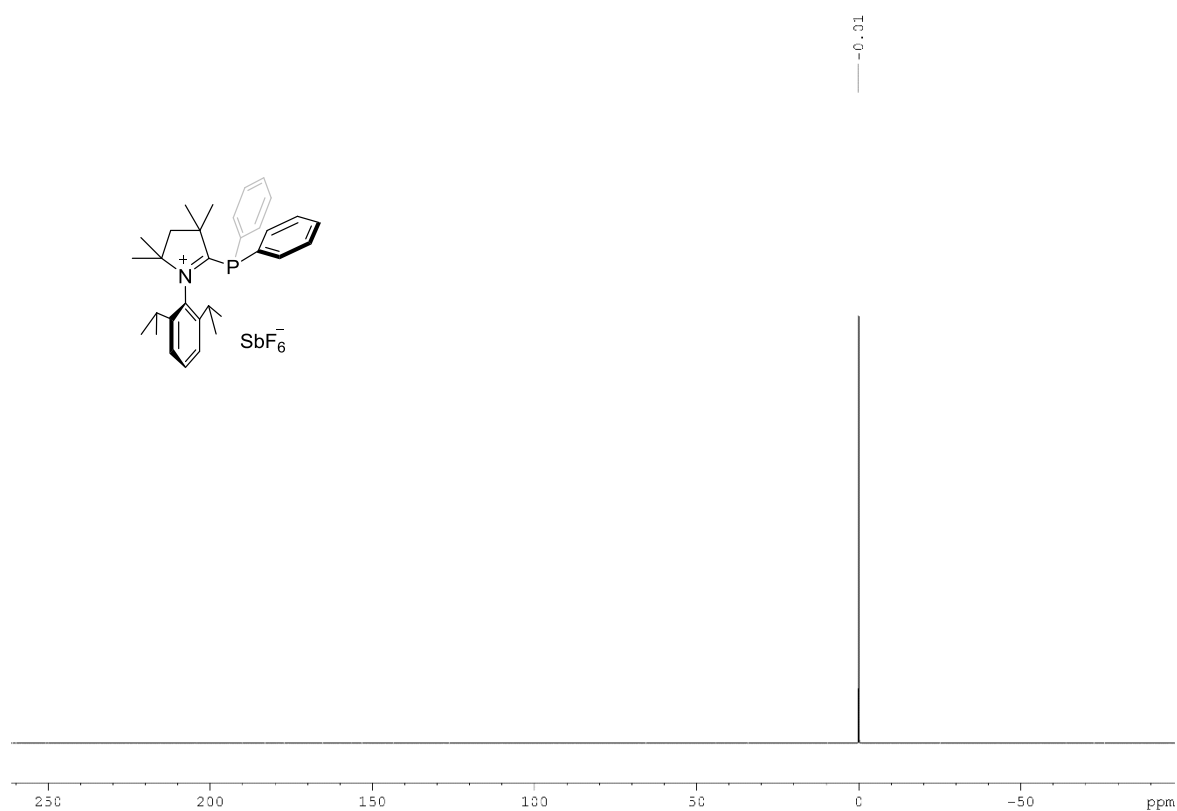
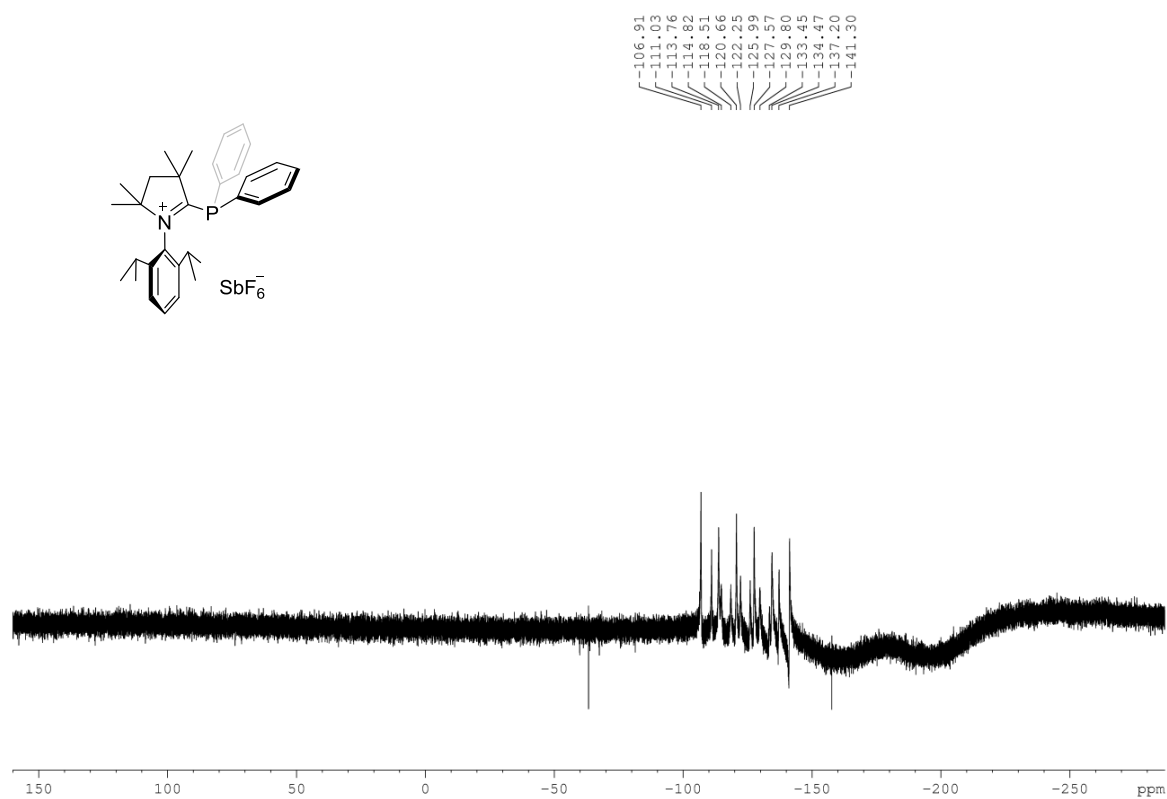
^{13}C NMR (CDCl_3 , 100 MHz) (Compound 126) ^1H NMR (CD_2Cl_2 , 400 MHz) (Compound 127)

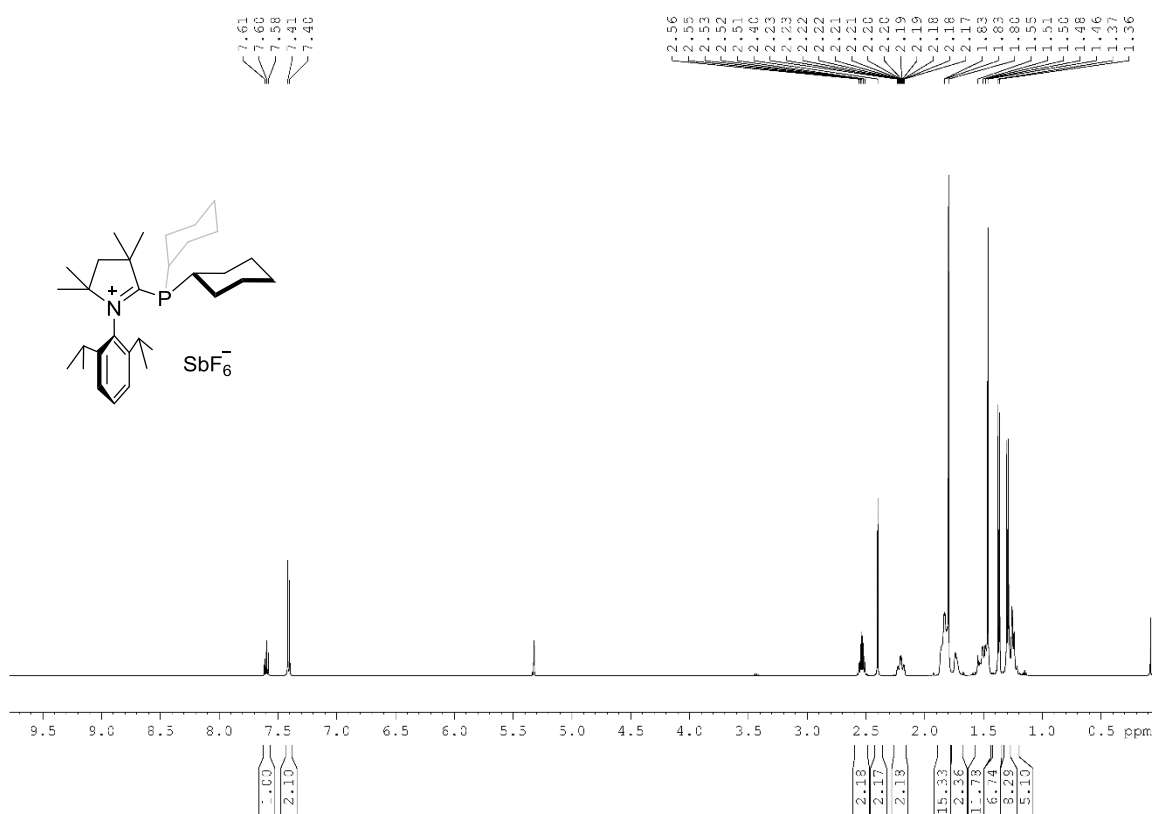
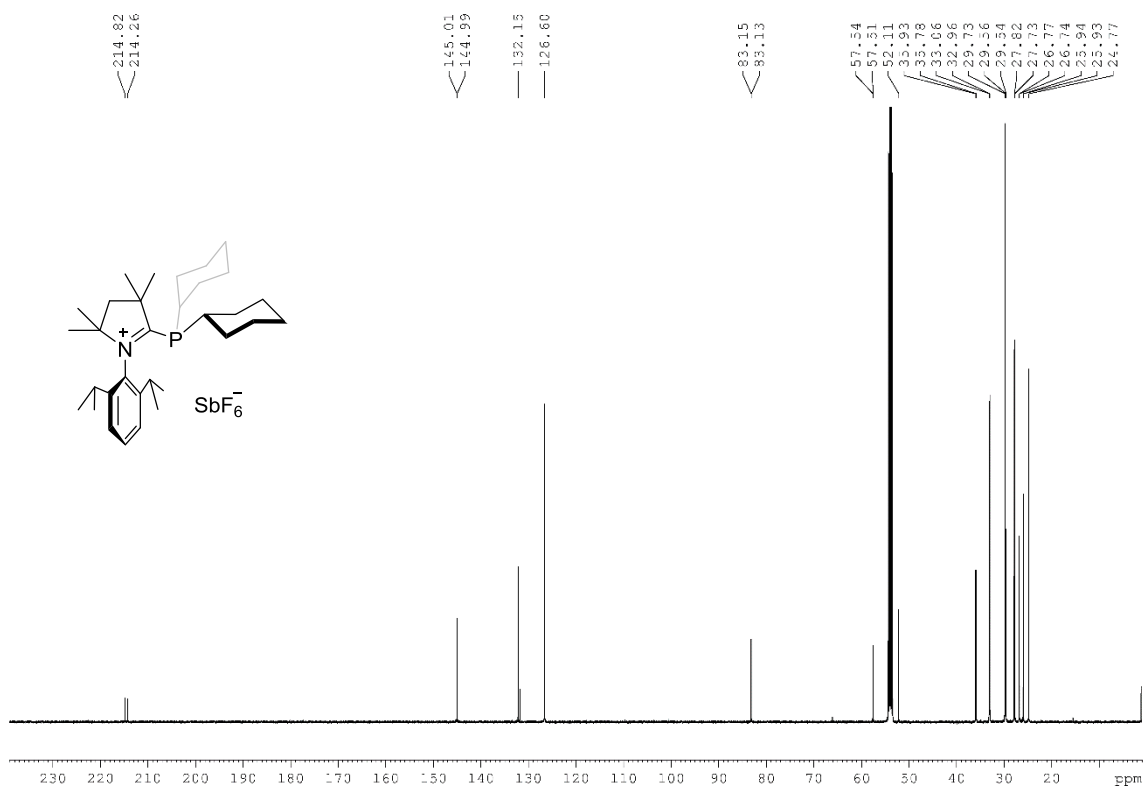
^{13}C NMR (CD₂Cl₂, 100 MHz) (Compound 127) **^1H NMR (CDCl₃, 400 MHz) (Compound 128)**

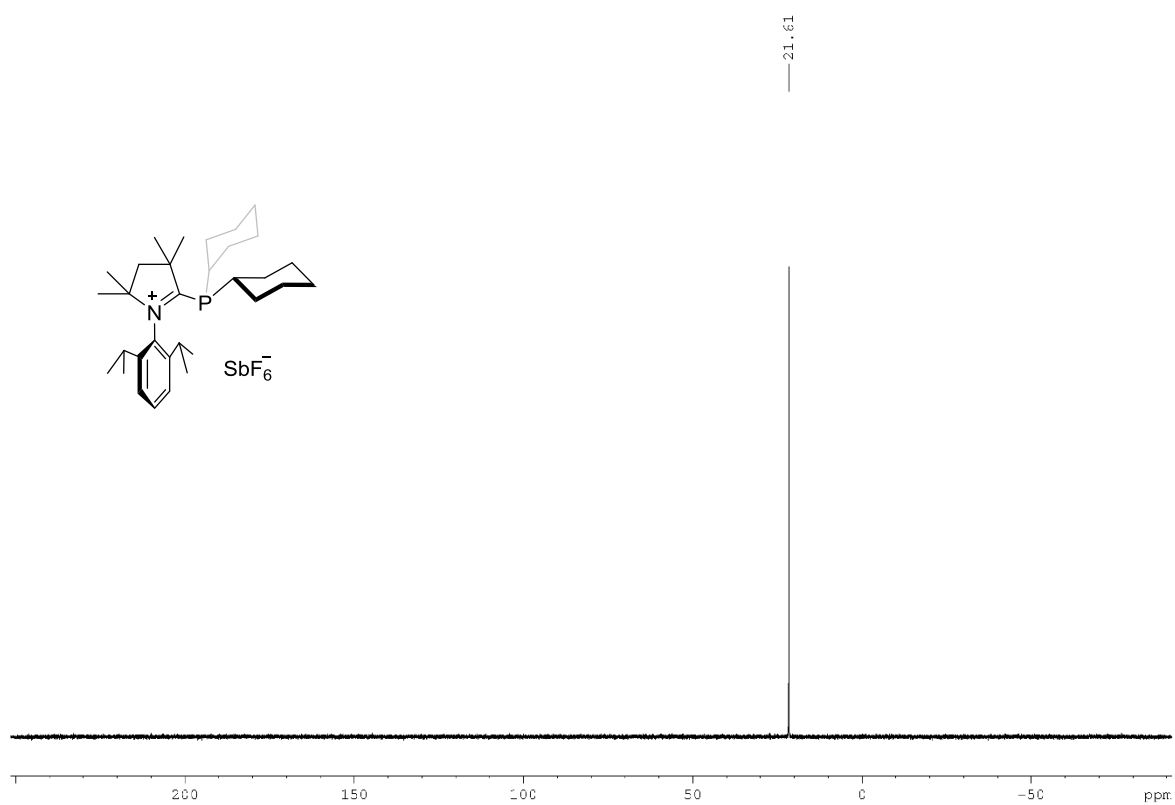
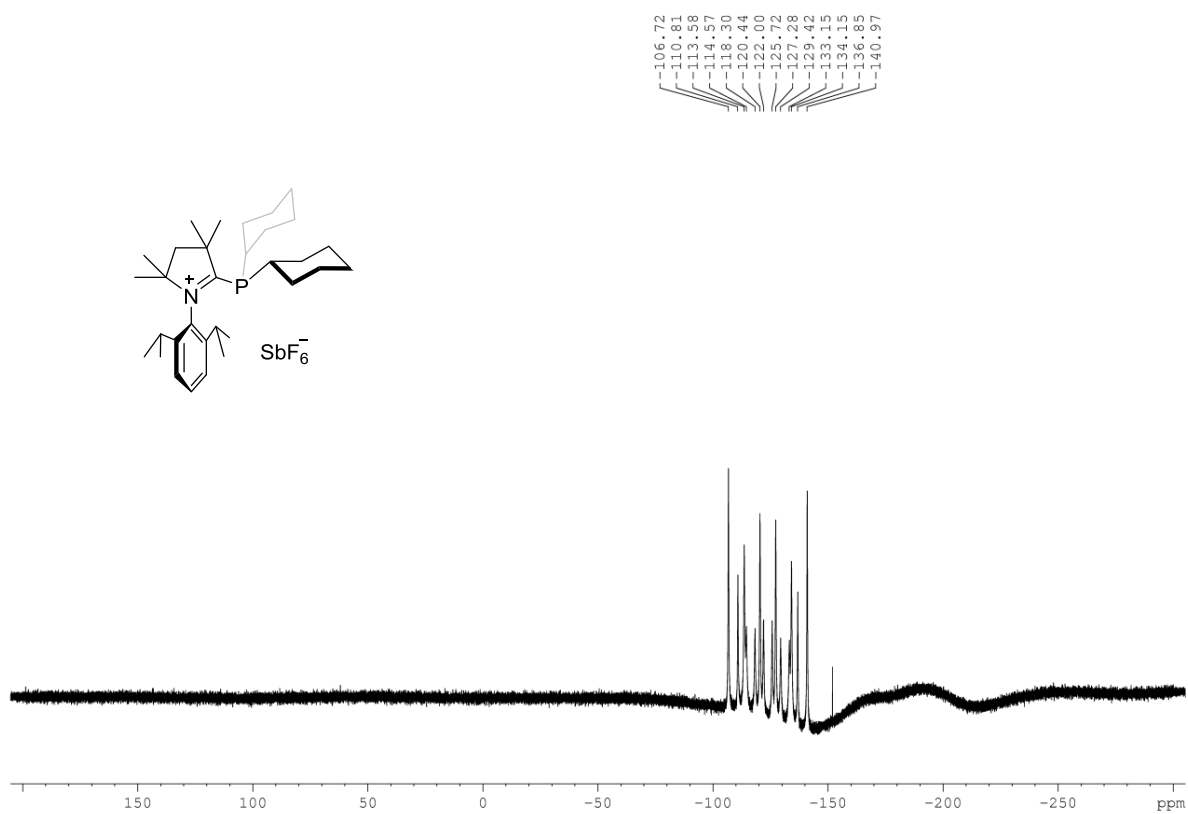
^{13}C NMR (CDCl₃, 100 MHz) (Compound 128) **^{19}F NMR (CDCl₃, 376 MHz) (Compound 128)**

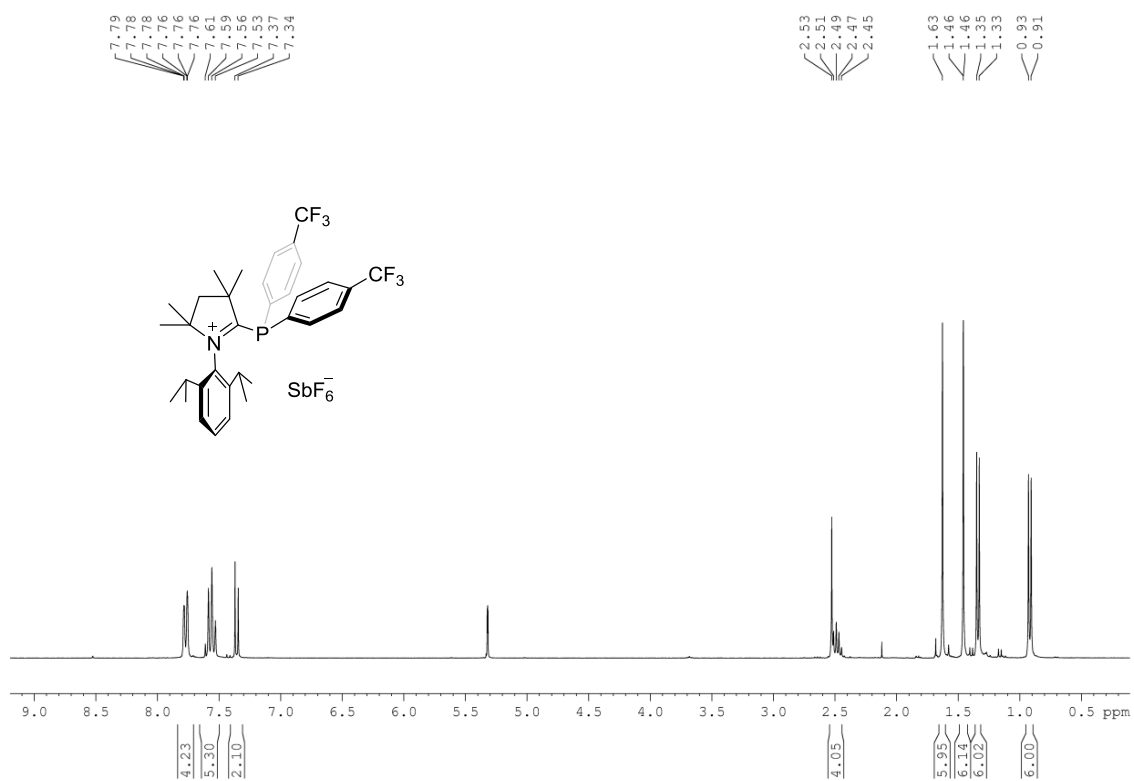
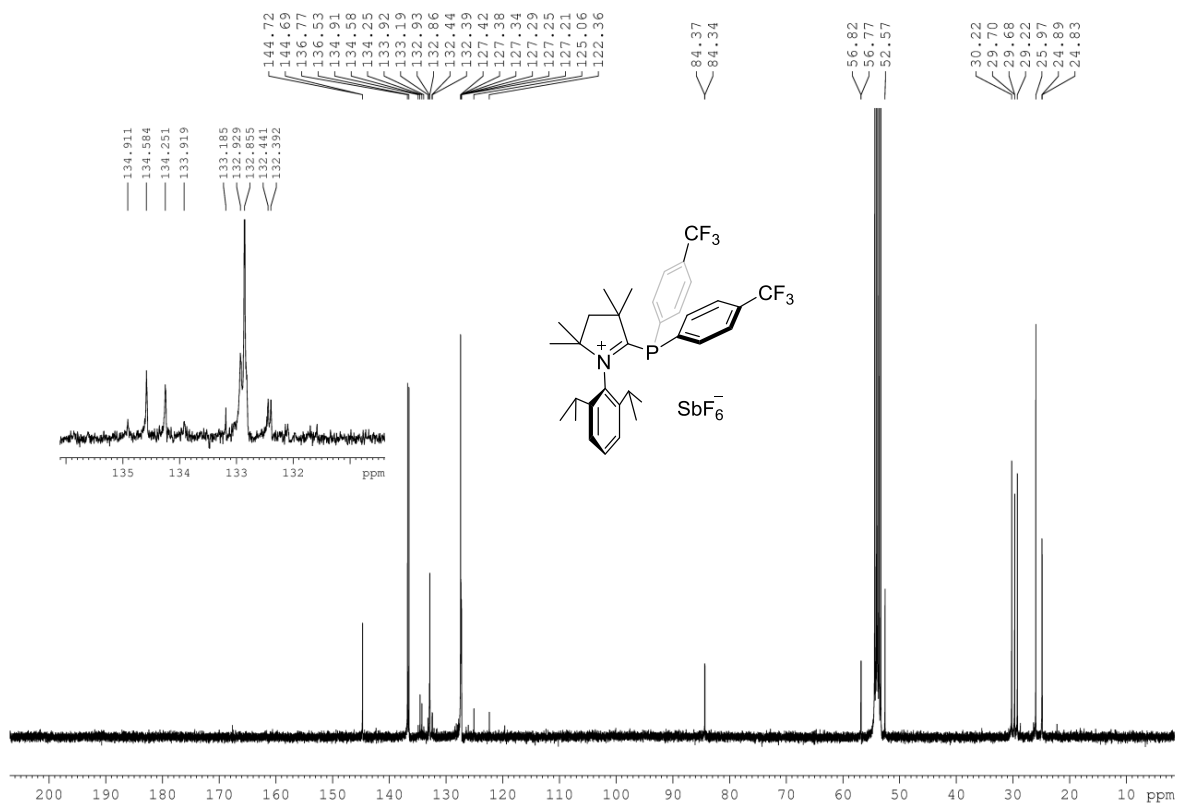
^1H NMR (CD_2Cl_2 , 400 MHz) (Compound 129) **^{13}C NMR (CD_2Cl_2 , 100 MHz) (Compound 129)**

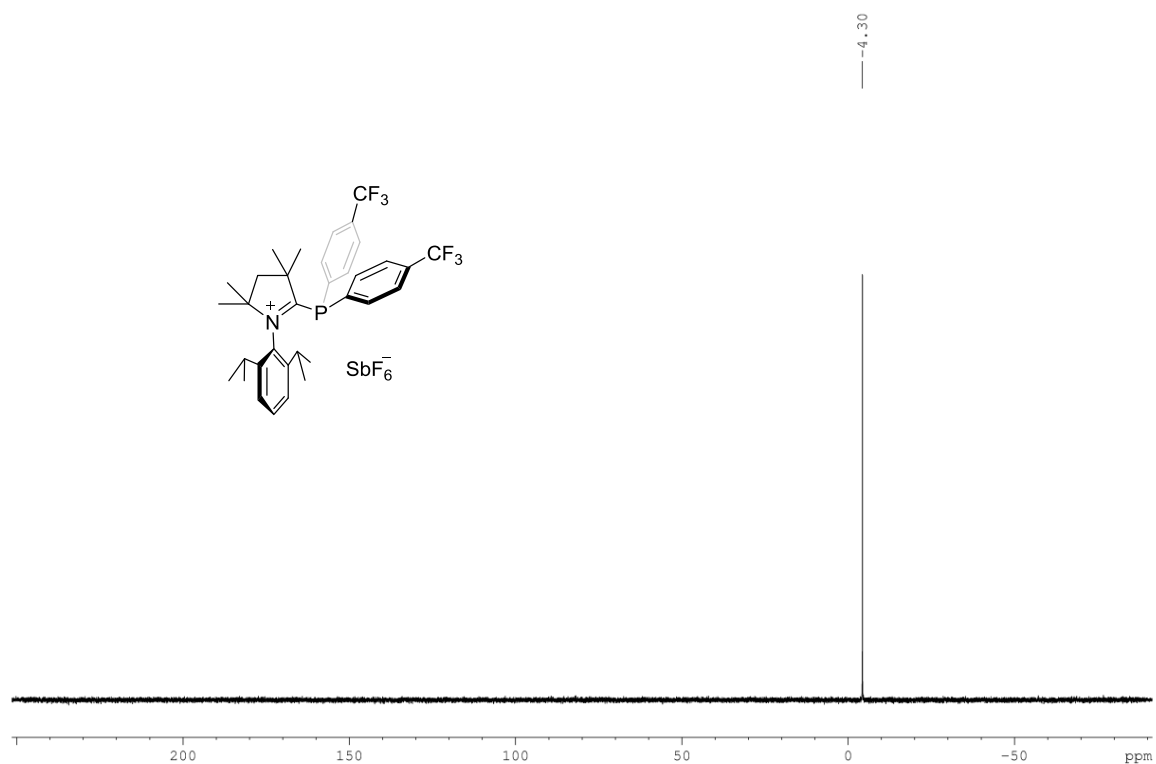
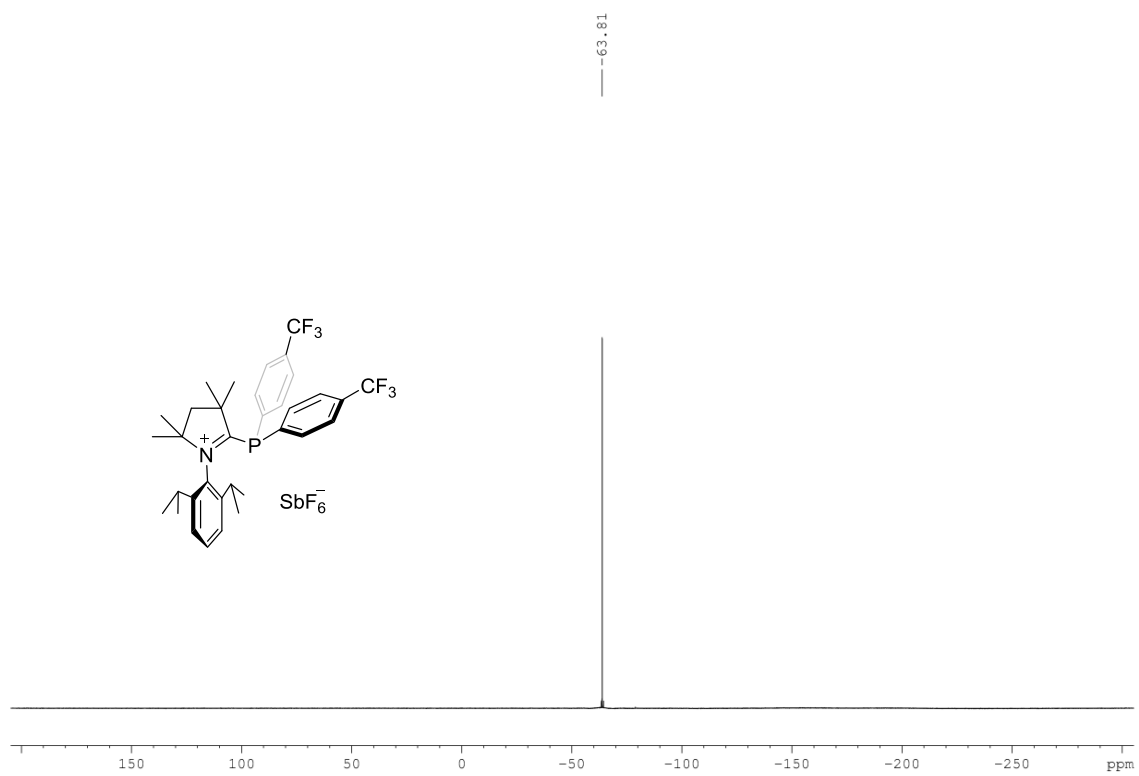
^1H NMR (CD_2Cl_2 , 400 MHz) (Compound 138a) **^{13}C NMR (CD_2Cl_2 , 100 MHz) (Compound 138a)**

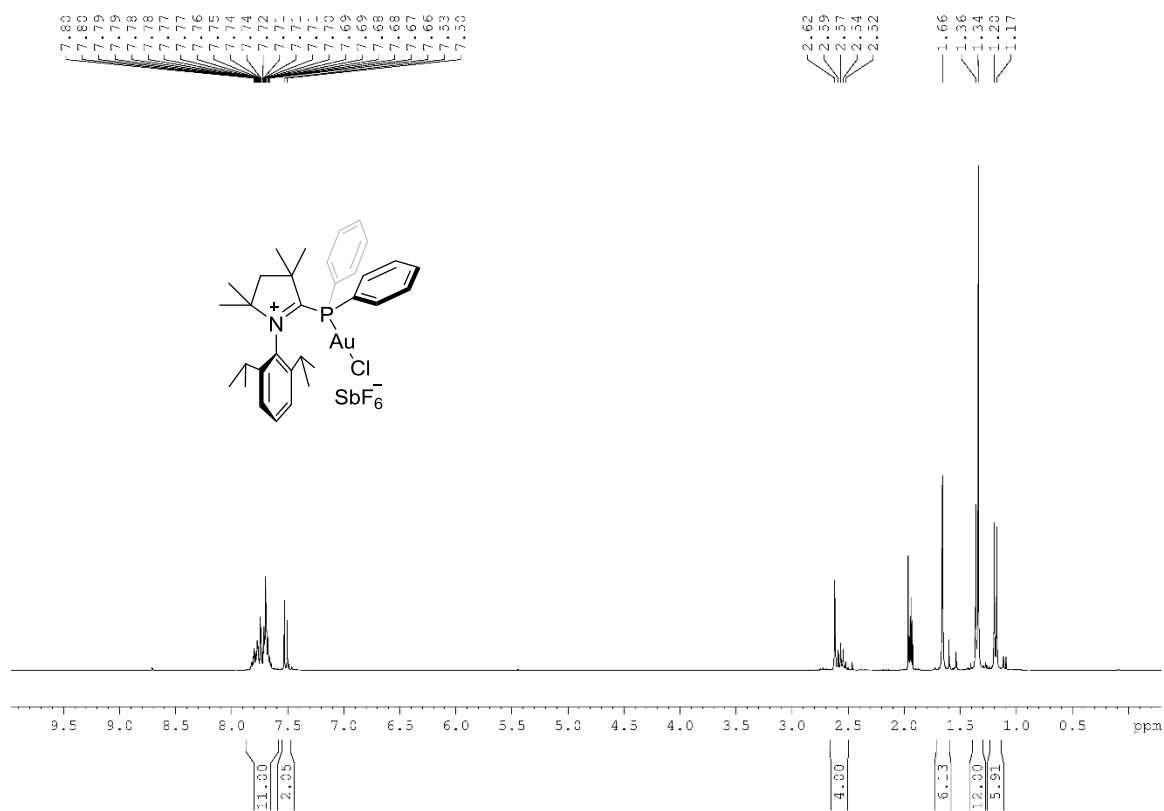
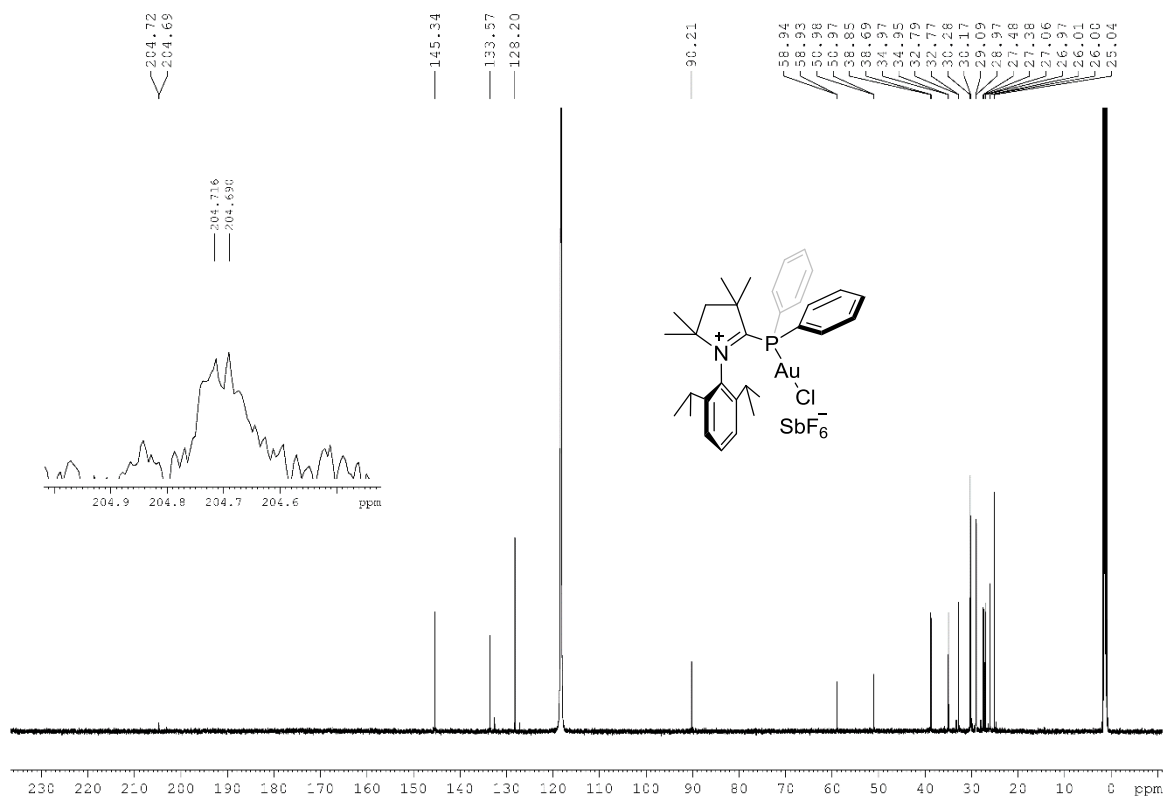
^{31}P NMR (CD_2Cl_2 , 162 MHz) (Compound 138a) **^{19}F NMR (CD_3CN , 282 MHz) (Compound 138a)**

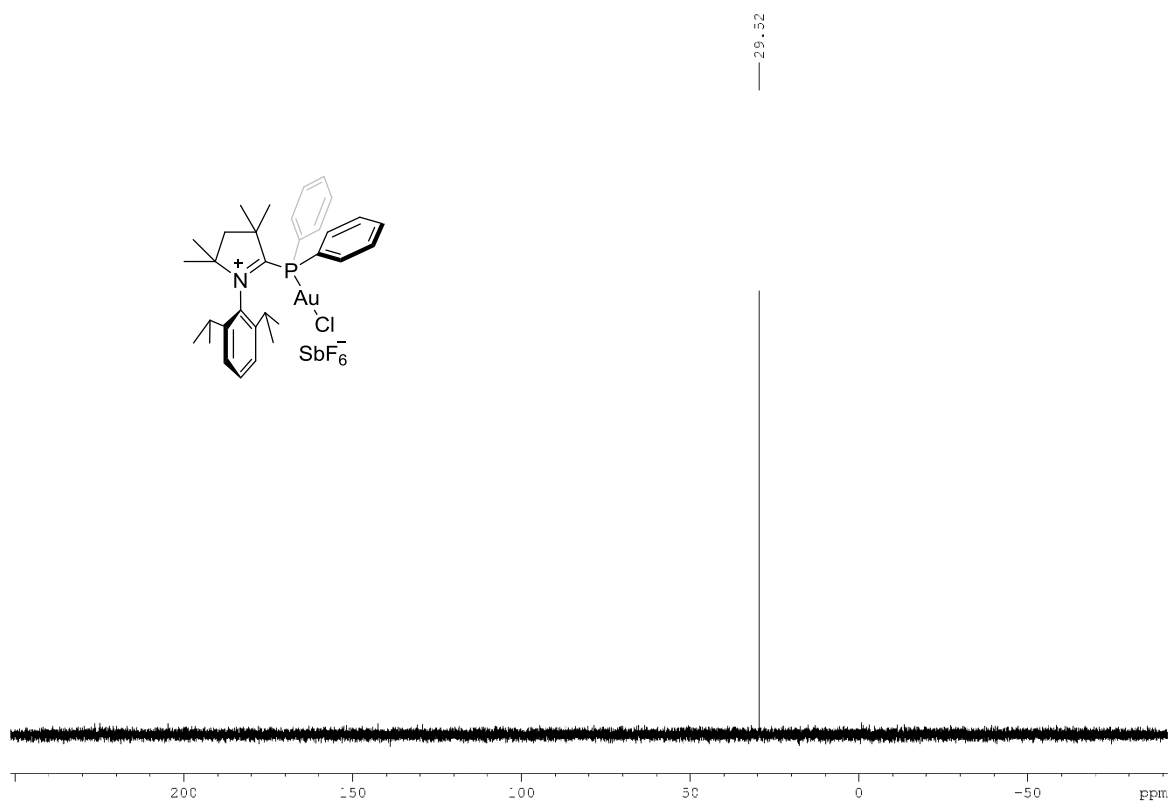
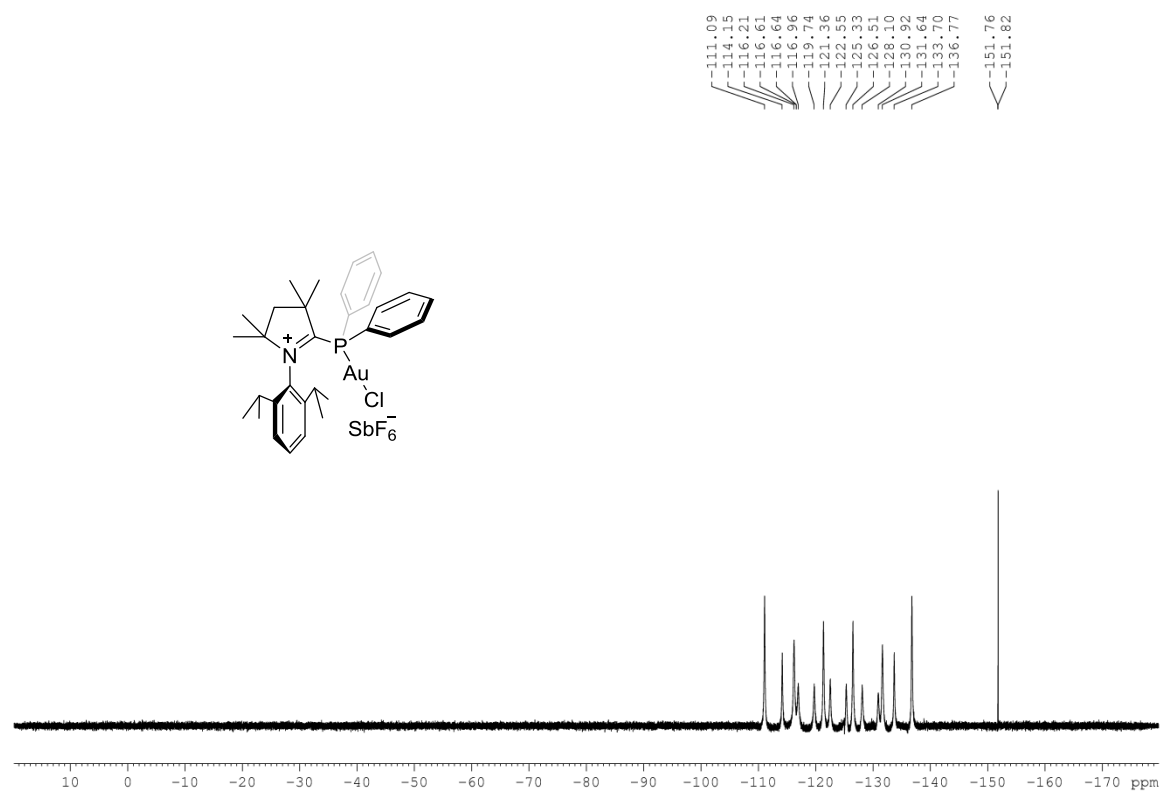
^1H NMR (CD₂Cl₂, 400 MHz) (Compound 138b) **^{13}C NMR (CD₂Cl₂, 125 MHz) (Compound 138b)**

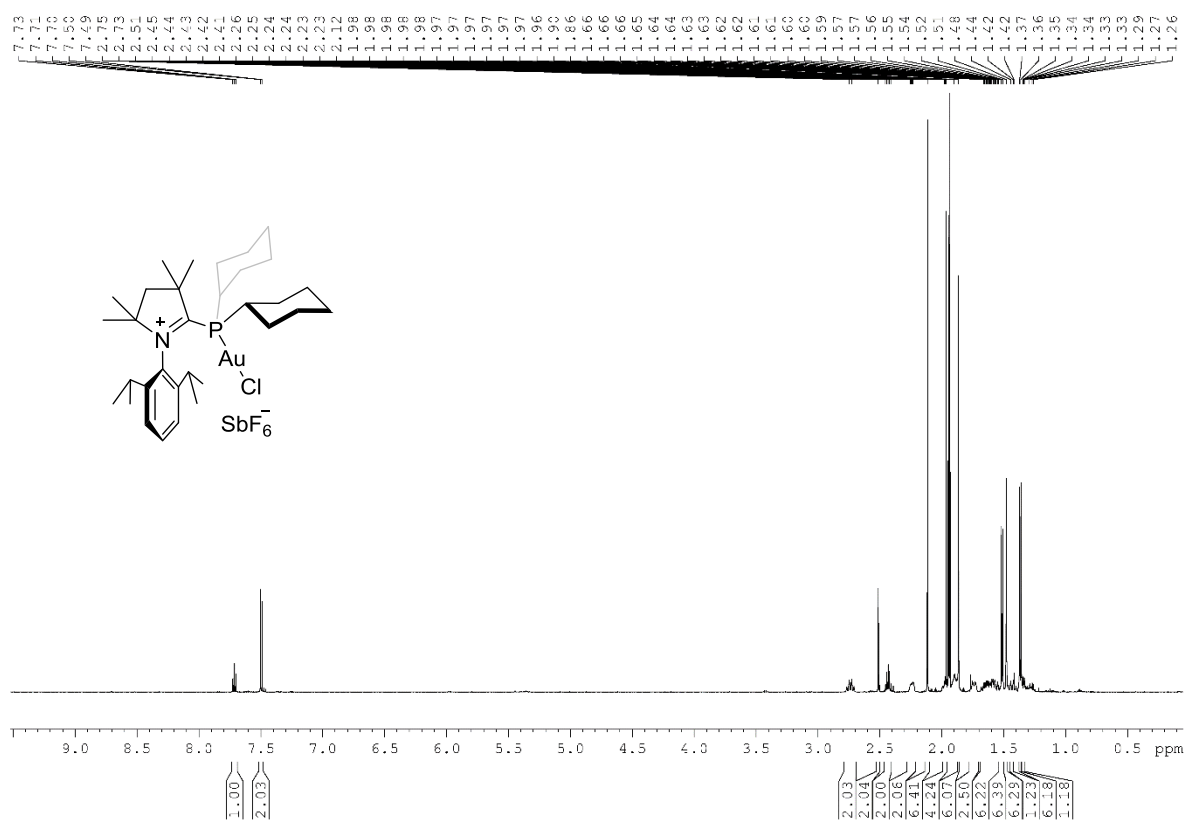
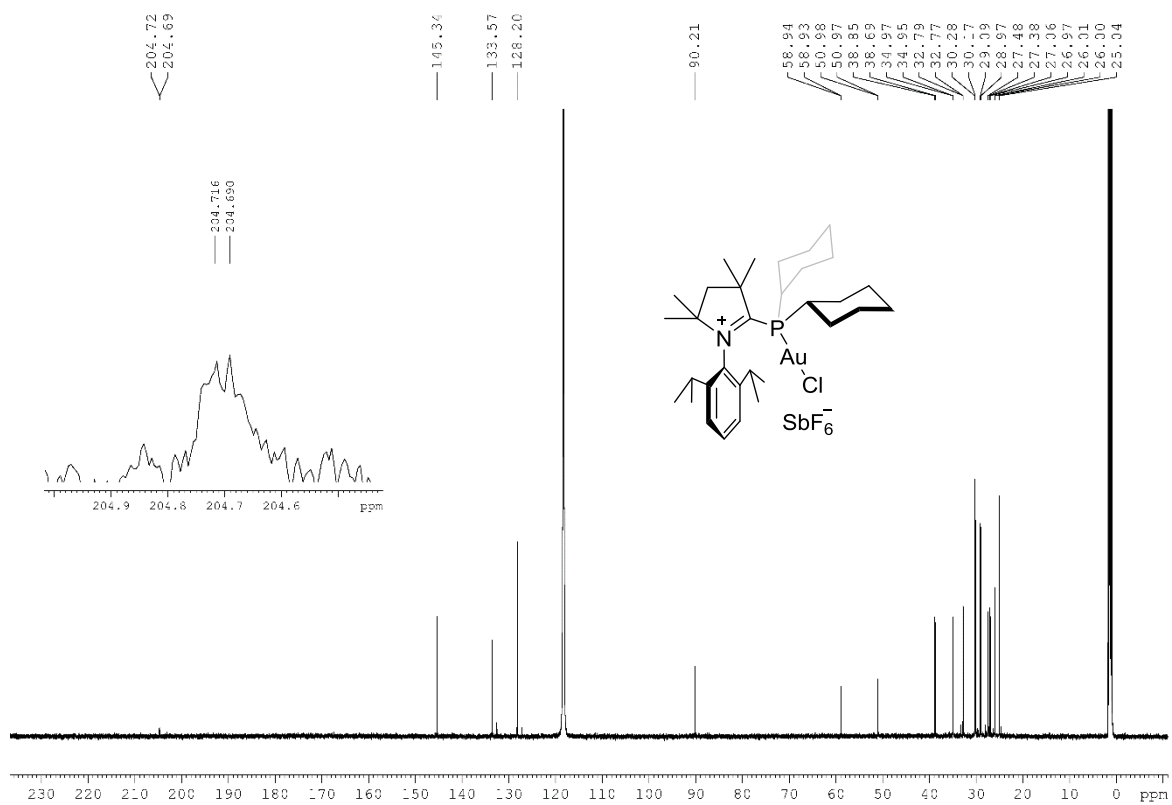
^{31}P NMR (CD_2Cl_2 , 162 MHz) (Compound 138b) **^{19}F NMR (CD_2Cl_2 , 282 MHz) (Compound 138b)**

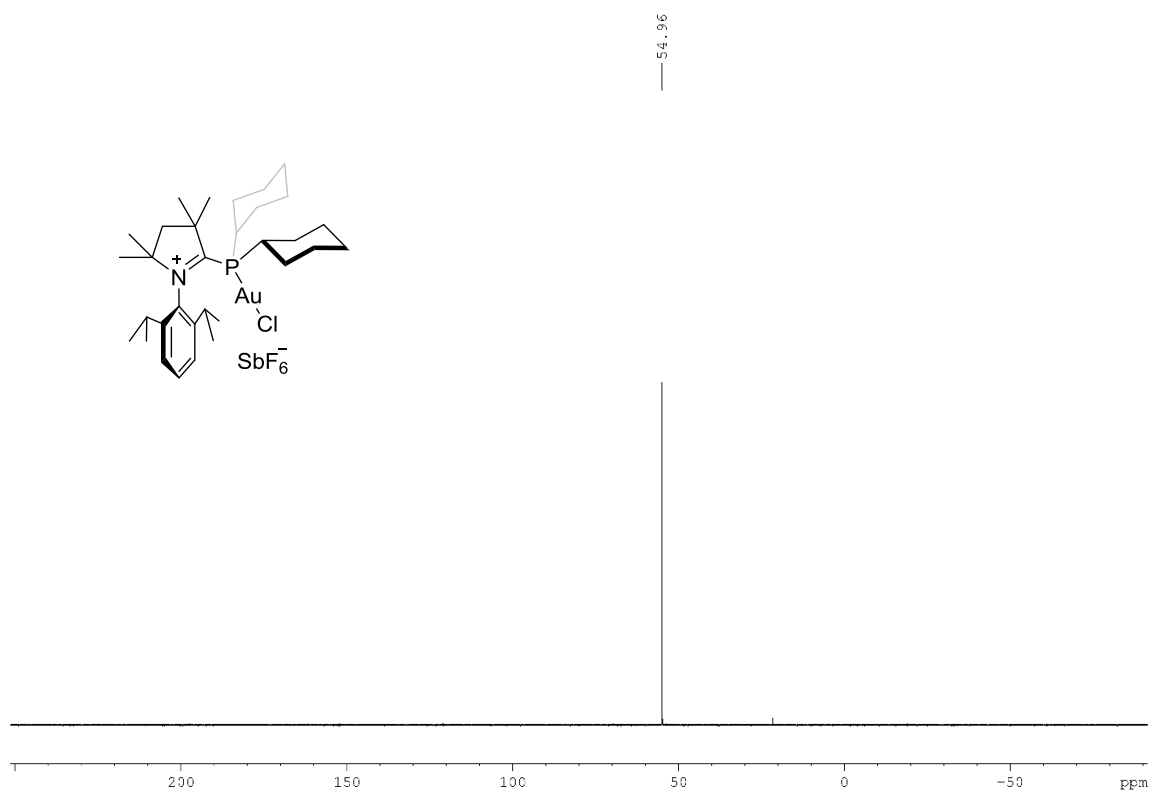
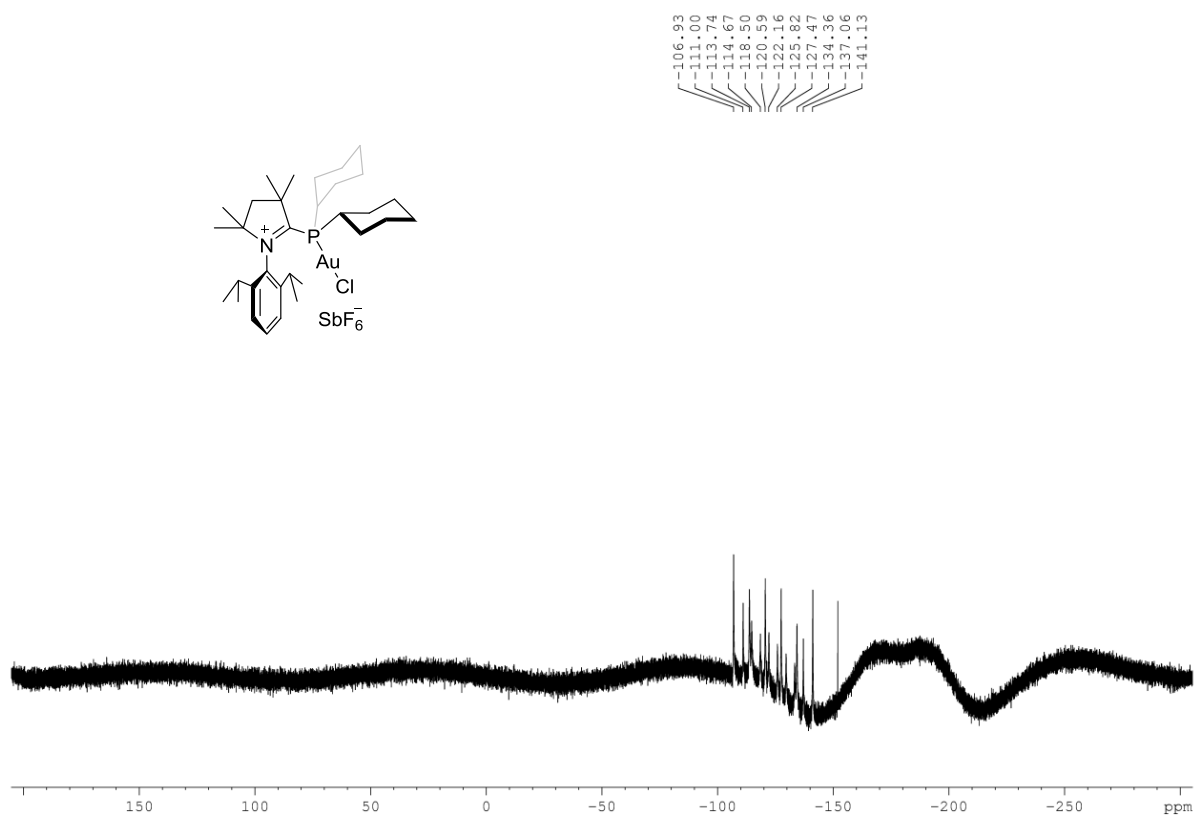
^1H NMR (CD_2Cl_2 , 300 MHz) (Compound 138c) ^{13}C NMR (CD_2Cl_2 , 100 MHz) (Compound 138c)

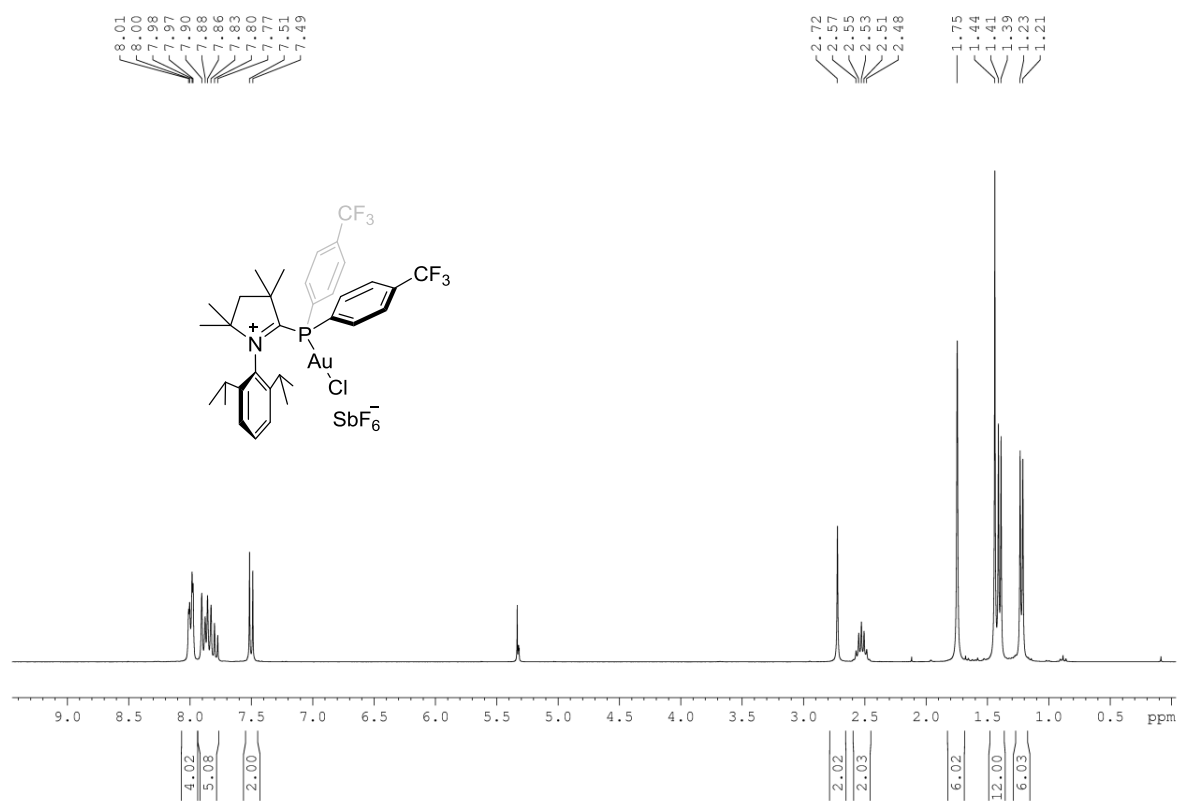
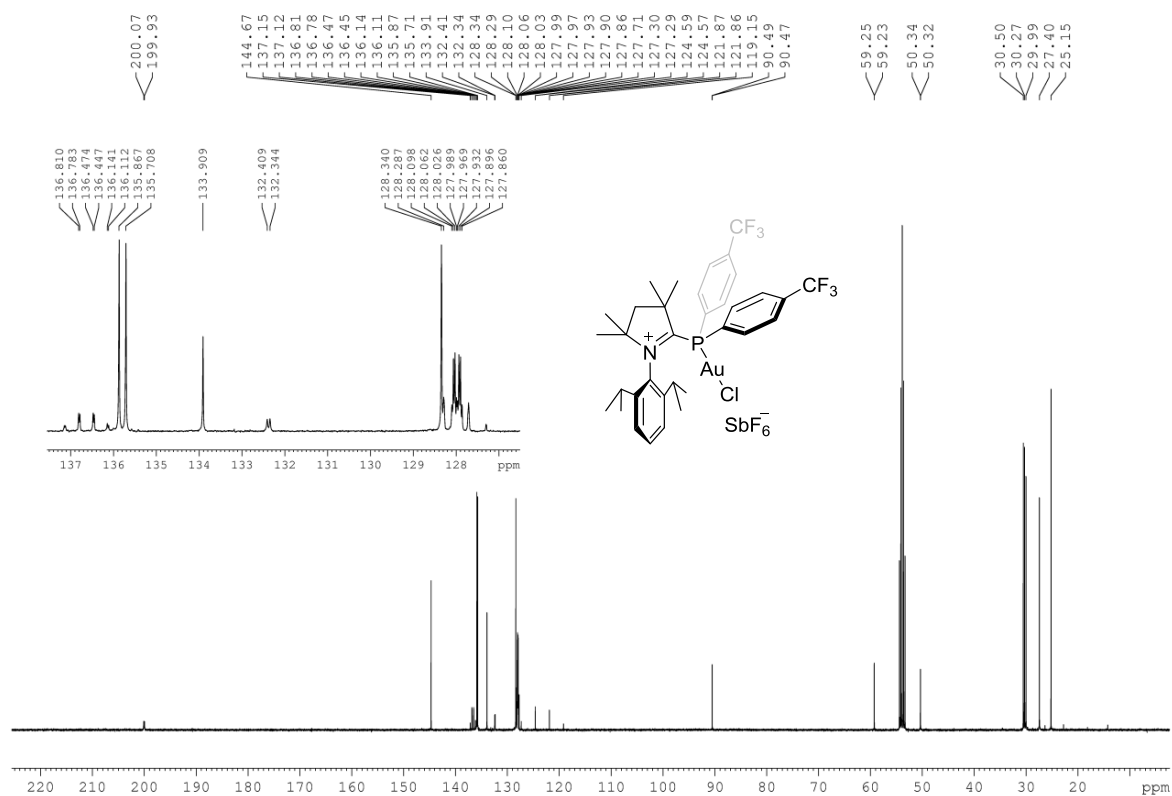
^{31}P NMR (CD_2Cl_2 , 121 MHz) (Compound 138c) **^{19}F NMR (CD_2Cl_2 , 282 MHz) (Compound 138c)**

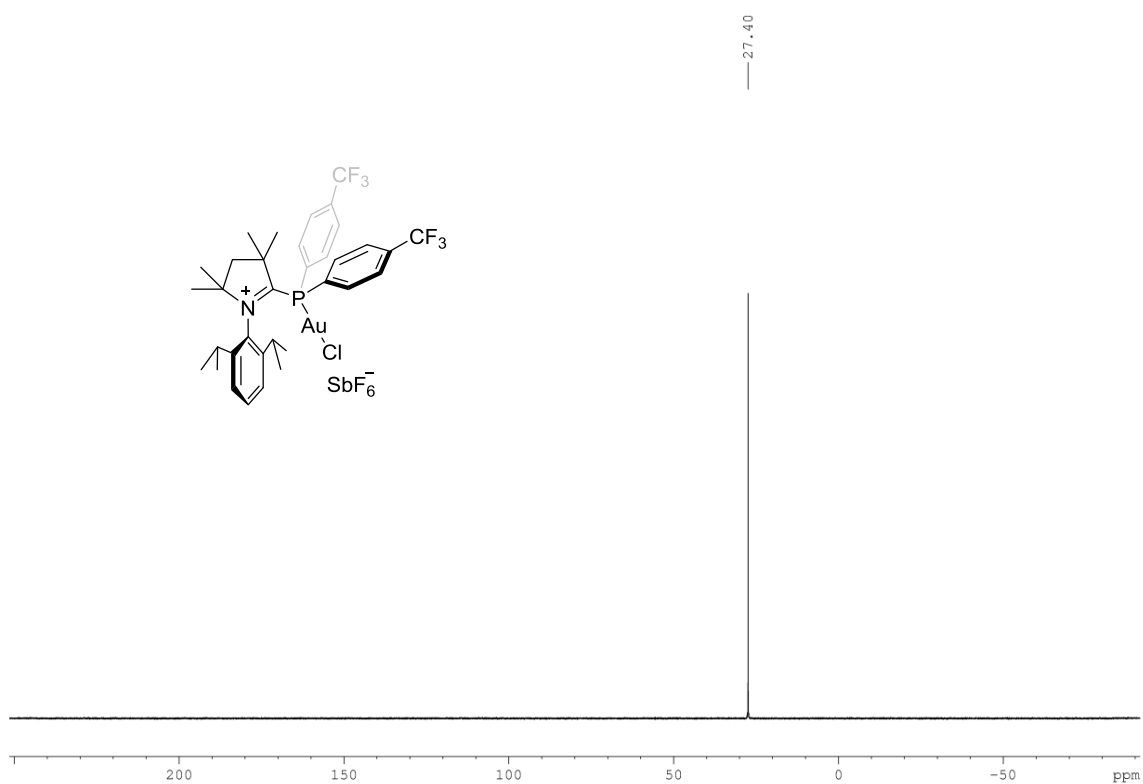
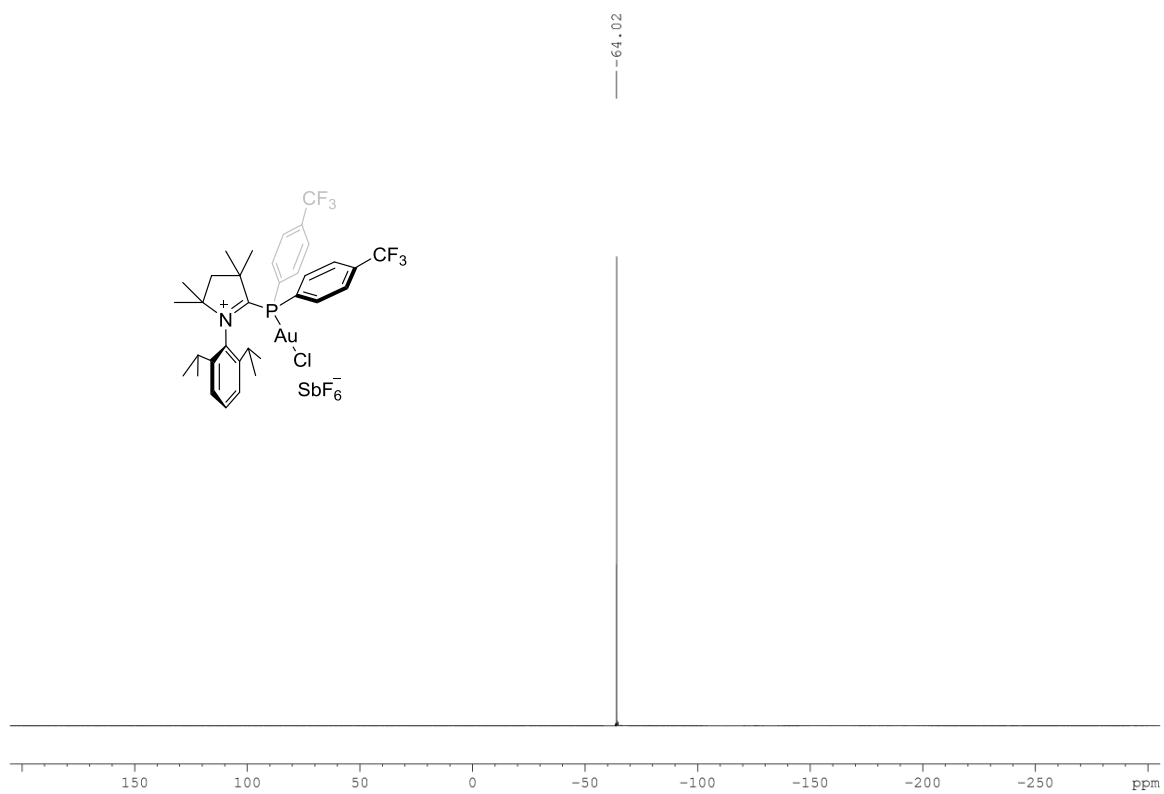
^1H NMR (CD₃CN, 300 MHz) (Compound 139a) **^{13}C NMR (CD₃CN, 125 MHz) (Compound 139a)**

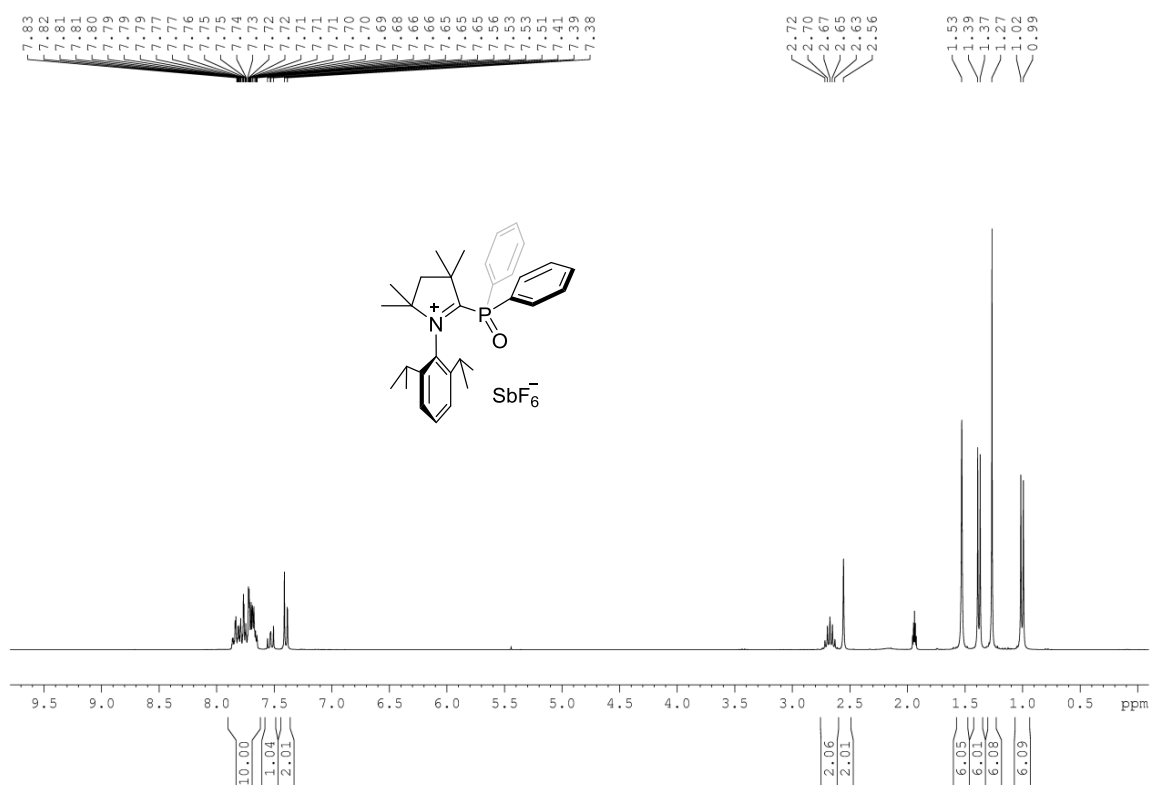
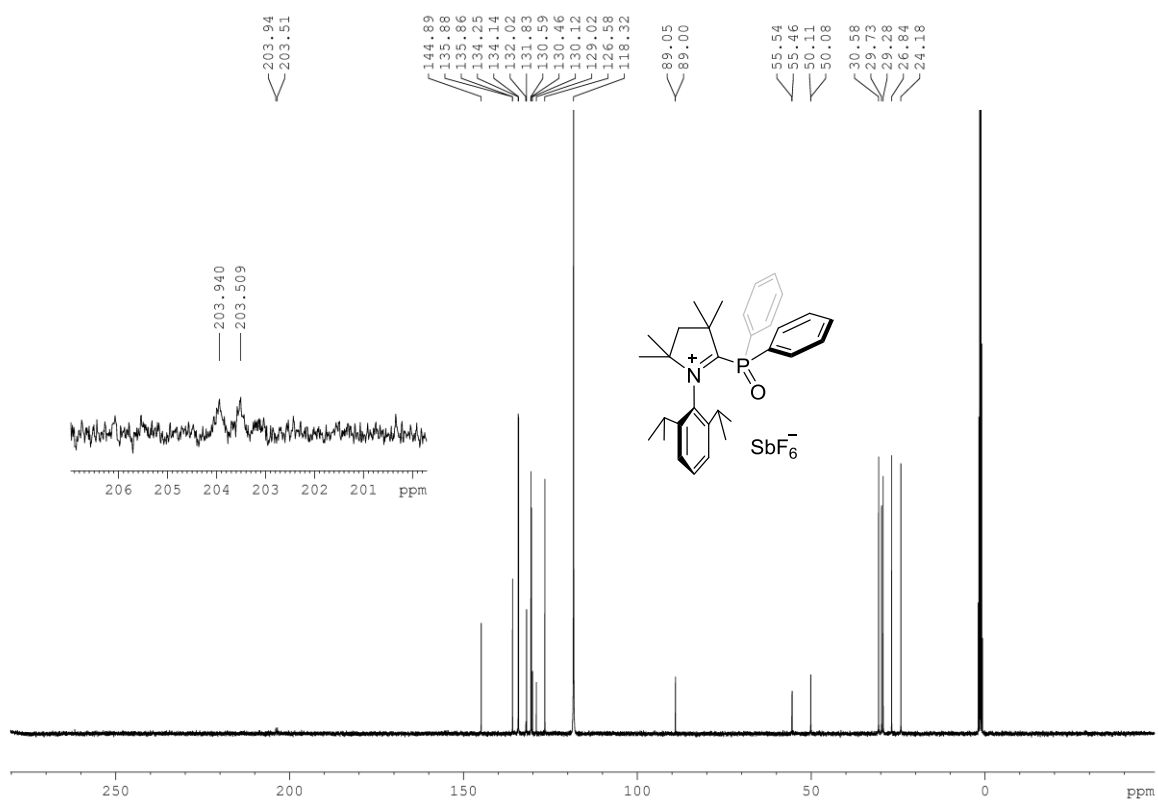
^{31}P NMR (CD_3CN , 121 MHz, 298K) (Compound 139a) **^{19}F NMR (CD_3CN , 282 MHz) (Compound 139a)**

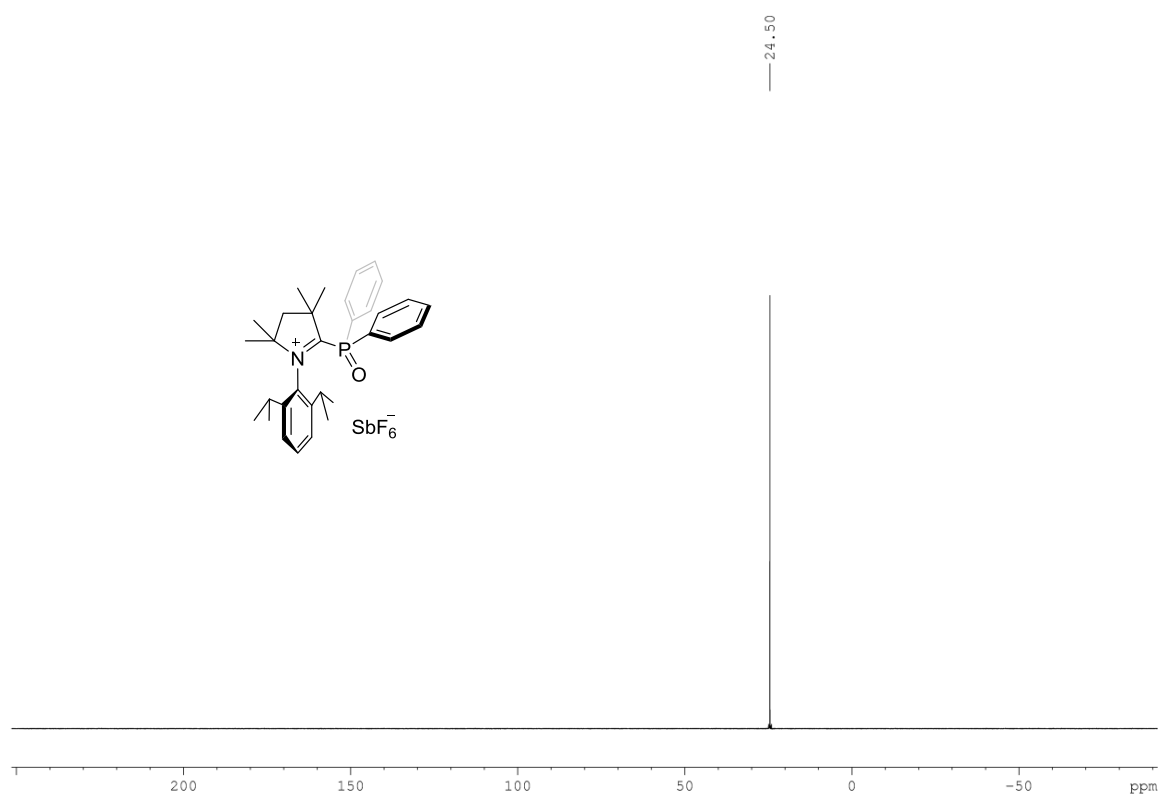
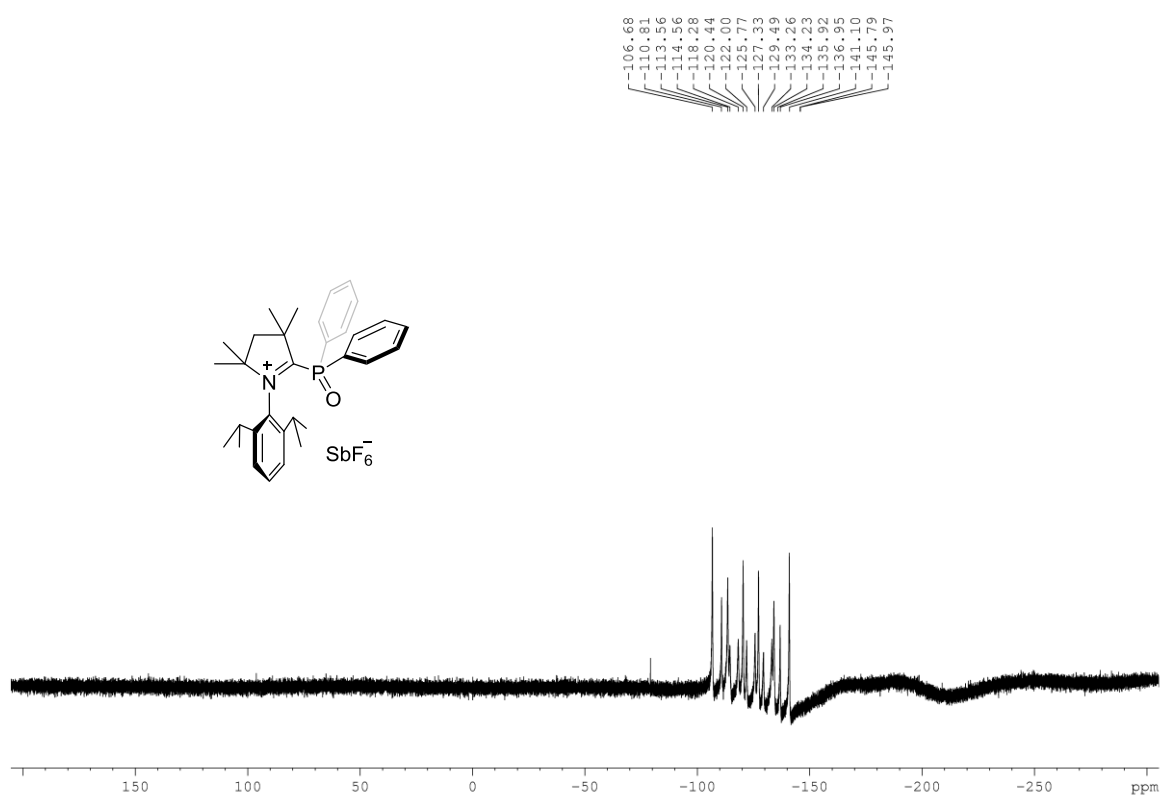
^1H NMR (CD₃CN, 300 MHz) (Compound 139b) **^{13}C NMR (CD₃CN, 125 MHz) (Compound 139b)**

^{31}P NMR (CD_3CN , 121 MHz) (Compound 139b) **^{19}F NMR (CD_3CN , 282 MHz) (Compound 139b)**

^1H NMR (CH_2Cl_2 , 300 MHz) (Compound 139c) **^{13}C NMR (CH_2Cl_2 , 100 MHz) (Compound 139c)**

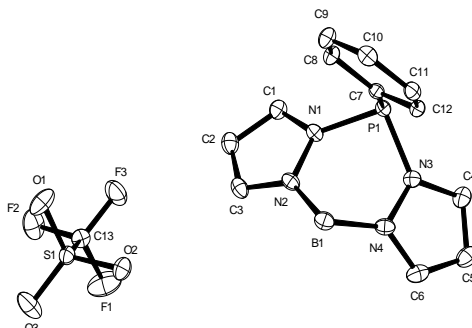
^{31}P NMR (CH_2Cl_2 , 121 MHz) (Compound 139c) **^{19}F NMR (CH_2Cl_2 , 282 MHz) (Compound 139c)**

¹H NMR (CD₃CN, 300 MHz) (Compound 146)**¹³C NMR (CD₃CN, 100 MHz) (Compound 146)**

^{31}P NMR (CD_3CN , 161 MHz) (Compound 146) **^{19}F NMR (CD_3CN , 282 MHz) (Compound 146)**

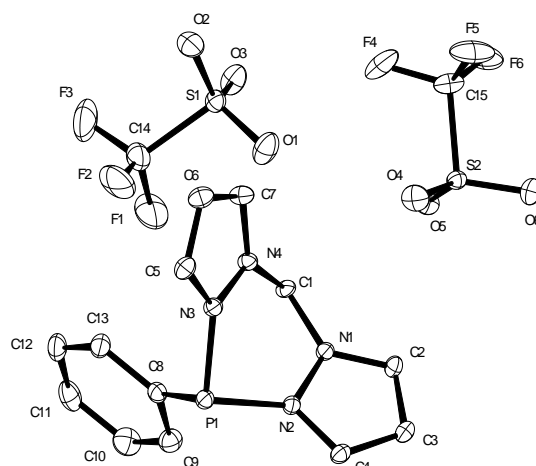
6.2 X-ray Structures

6.2.1 Crystal Data and Structure Refinement of Compound 63



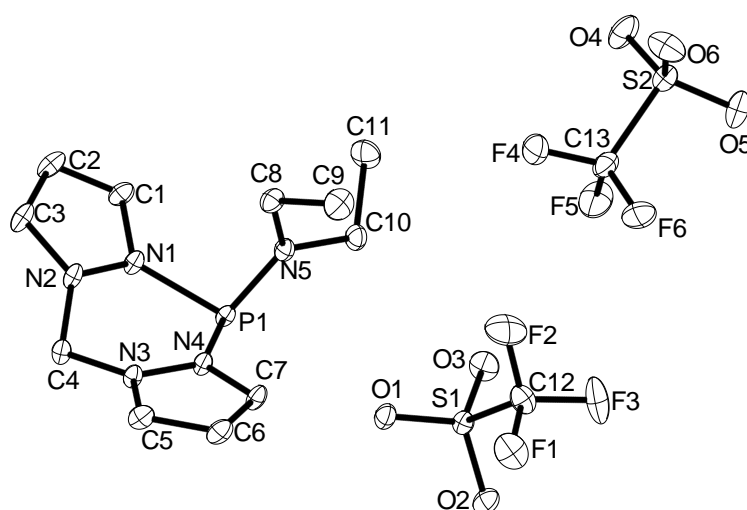
Empirical formula	$C_{13}H_{13}BF_3N_4O_3PS$	
Color	colourless	
Formula weight	404.11 g · mol ⁻¹	
Temperature	100 K	
Wavelength	0.71073 Å	
Crystal system	ORTHORHOMBIC	
Space group	Pna2₁ , (no. 33)	
Unit cell dimensions	a = 20.258(2) Å b = 10.0335(10) Å c = 8.2844(8) Å	$\alpha = 90^\circ$ $\beta = 90^\circ$ $\gamma = 90^\circ$
Volume	1683.9(3) Å ³	
Z	4	
Density (calculated)	1.594 mg · m ⁻³	
Absorption coefficient	0.341 mm ⁻¹	
F(000)	824 e	
Crystal size	0.48 x 0.07 x 0.05 mm ³	
θ range for data collection	2.01 to 28.39° .	
Index ranges	$-27 \leq h \leq 27$, $-13 \leq k \leq 13$, $-11 \leq l \leq 11$	
Reflections collected	39971	
Independent reflections	4204 [Rint = 0.0253]	
Reflections with I > 2s(I)	4118	
Completeness to $\theta = 27.50^\circ$	100.00%	
Absorption correction	Gaussian	
Max. and min. transmission	0.98 and 0.91	
Refinement method	Full-matrix least-squares on F ²	
Data / restraints / parameters	4204 / 1 / 243	
Goodness-of-fit on F ²	1.063	
Final R indices [I > 2s(I)]	R1 = 0.0222	wR2 = 0.0599
R indices (all data)	R1 = 0.0229	wR2 = 0.0604
Absolute structure parameter	-0.03(5)	
Largest diff. peak and hole	0.3 and -0.2 e · Å ⁻³	

6.2.2 Crystal Data and Structure Refinement of Compound 65



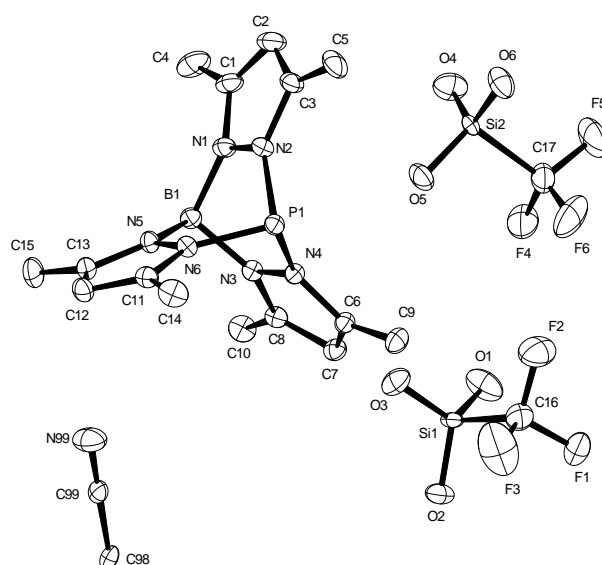
Empirical formula	$C_{15}H_{13}F_6N_4O_6PS_2$	
Color	colourless	
Formula weight	554.38 g · mol ⁻¹	
Temperature	100 K	
Wavelength	0.71073 Å	
Crystal system	TRICLINIC	
Space group	P$\bar{1}$, (no. 2)	
Unit cell dimensions	a = 9.1777(11) Å b = 9.9125(12) Å c = 13.419(2) Å	$\alpha = 102.624(3)^\circ$ $\beta = 98.632(3)^\circ$ $\gamma = 112.612(2)^\circ$
Volume	1061.9(3) Å ³	
Z	2	
Density (calculated)	1.734 mg · m ⁻³	
Absorption coefficient	0.421 mm ⁻¹	
F(000)	560 e	
Crystal size	0.11 x 0.07 x 0.03 mm ³	
θ range for data collection	2.34 to 31.16°	
Index ranges	-13 ≤ h ≤ 13, -14 ≤ k ≤ 14, -19 ≤ l ≤ 19	
Reflections collected	31528	
Independent reflections	6834 [Rint = 0.0306]	
Reflections with I > 2s(I)	5721	
Completeness to $\theta = 31.16^\circ$	99.50%	
Absorption correction	Gaussian	
Max. and min. transmission	0.99 and 0.95	
Refinement method	Full-matrix least-squares on F ²	
Data / restraints / parameters	6834 / 0 / 307	
Goodness-of-fit on F ²	1.035	
Final R indices [I > 2s(I)]	R1 = 0.0385	wR2 = 0.0975
R indices (all data)	R1 = 0.0491	wR2 = 0.1039
Largest diff. peak and hole	1.2 and -0.6 e · Å ⁻³	

6.2.3 Crystal Data and Structure Refinement of Compound 67



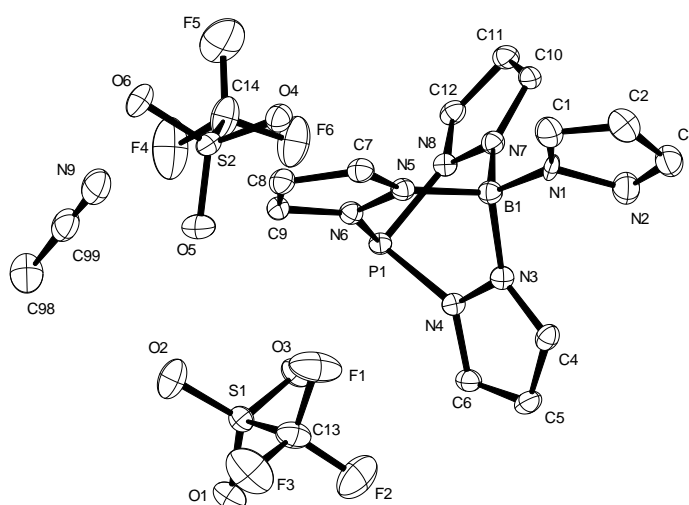
Empirical formula	$C_{13} H_{18} F_6 N_5 O_6 P S_2$	
Color	colourless	
Formula weight	$549.41 \text{ g}\cdot\text{mol}^{-1}$	
Temperature	100 K	
Wavelength	0.71073 \AA	
Crystal system	MONOCLINIC	
Space group	$p 2_1/n$, (no. 14)	
Unit cell dimensions	$a = 12.814(3) \text{ \AA}$ $b = 12.704(3) \text{ \AA}$ $c = 14.321(3) \text{ \AA}$	$\alpha = 90^\circ$ $\beta = 113.697(4)^\circ$ $\gamma = 90^\circ$
Volume	$2134.8(9) \text{ \AA}^3$	
Z	4	
Density (calculated)	$1.709 \text{ mg}\cdot\text{m}^{-3}$	
Absorption coefficient	0.419 mm^{-1}	
F(000)	1120 e	
Crystal size	$0.31 \times 0.27 \times 0.20 \text{ mm}^3$	
θ range for data collection	1.80 to 31.38°	
Index ranges	$-18 \leq h \leq 18$, $-18 \leq k \leq 18$, $-20 \leq l \leq 20$	
Reflections collected	58788	
Independent reflections	6998 [$R_{\text{int}} = 0.0543$]	
Reflections with $I > 2s(I)$	5519	
Completeness to $\theta = 31.38^\circ$	99.60%	
Absorption correction	Gaussian	
Max. and min. transmission	0.92807 and 0.86261	
Refinement method	Full-matrix least-squares on F^2	
Data / restraints / parameters	6998 / 0 / 300	
Goodness-of-fit on F^2	1.075	
Final R indices [$I > 2s(I)$]	$R_1 = 0.0342$	$wR_2 = 0.0847$
R indices (all data)	$R_1 = 0.0524$	$wR_2 = 0.09$
Largest diff. peak and hole	0.733 and $-0.555 \text{ e}\cdot\text{\AA}^{-3}$	

6.2.4 Crystal Data and Structure Refinement of Compound 76



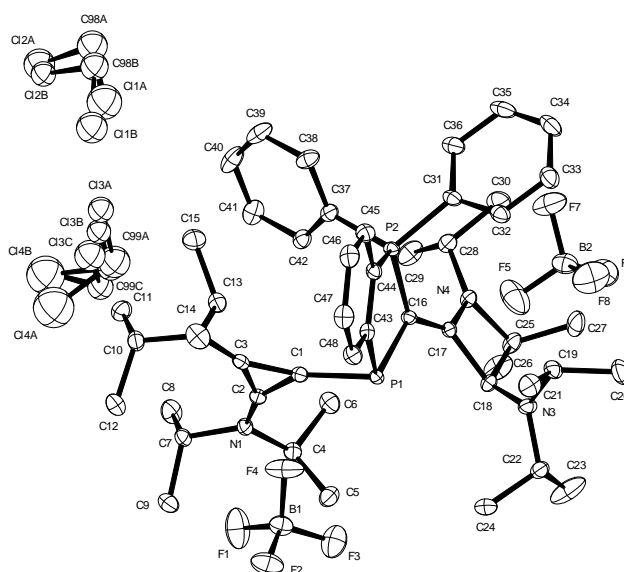
Empirical formula	$C_{18}H_{23.50}BF_6N_{6.50}O_6PS_2$	
Color	colourless	
Formula weight	646.83 g · mol ⁻¹	
Temperature	100 K	
Wavelength	0.71073 Å	
Crystal system	MONOCLINIC	
Space group	P2₁/n, (no. 14)	
Unit cell dimensions	a = 12.9893(16) Å b = 10.6028(13) Å c = 21.575(3) Å	α = 90°. β = 94.762(2)°. γ = 90°.
Volume	2961.1(6) Å ³	
Z	4	
Density (calculated)	1.451 mg · m ⁻³	
Absorption coefficient	0.315 mm ⁻¹	
F(000)	1324 e	
Crystal size	0.33 x 0.26 x 0.16 mm ³	
θ range for data collection	1.89 to 36.32°.	
Index ranges	-21 ≤ h ≤ 21, -17 ≤ k ≤ 17, -35 ≤ l ≤ 35	
Reflections collected	111154	
Independent reflections	14234 [R _{int} = 0.0235]	
Reflections with I > 2σ(I)	12489	
Completeness to θ = 27.50°	99.60%	
Absorption correction	Gaussian	
Max. and min. transmission	0.95 and 0.78	
Refinement method	Full-matrix least-squares on F ²	
Data / restraints / parameters	14234 / 0 / 390	
Goodness-of-fit on F ²	1.081	
Final R indices [I > 2σ(I)]	R ₁ = 0.0511	wR ₂ = 0.1672
R indices (all data)	R ₁ = 0.0573	wR ₂ = 0.1752
Largest diff. peak and hole	2.0 and -0.6 e · Å ⁻³	

6.2.5 Crystal Data and Structure Refinement of Compound 79



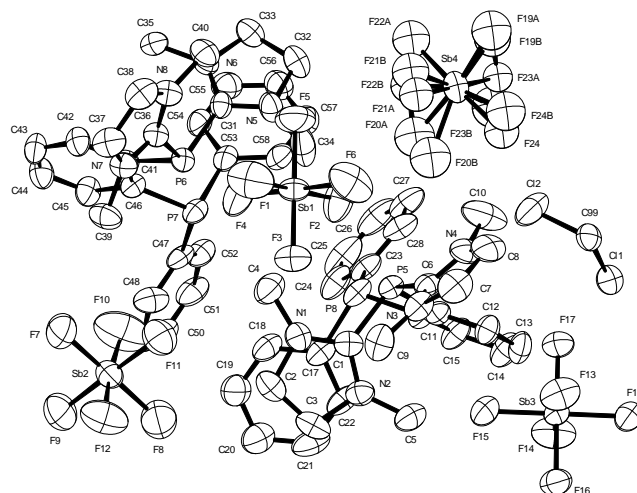
Empirical formula	$C_{16}H_{15}BF_6N_9O_6PS_2$	
Color	colourless	
Formula weight	649.27 g · mol ⁻¹	
Temperature	100 K	
Wavelength	1.54178 Å	
Crystal system	TRICLINIC	
Space group	P$\bar{1}$, (no. 2)	
Unit cell dimensions	a = 11.615(15) Å b = 11.639(9) Å c = 11.913(9) Å	$\alpha = 115.626(15)^\circ$ $\beta = 102.37(2)^\circ$ $\gamma = 105.87(2)^\circ$
Volume	1290(2) Å ³	
Z	2	
Density (calculated)	1.672 mg · m ⁻³	
Absorption coefficient	3.361 mm ⁻¹	
F(000)	656 e	
Crystal size	0.58 x 0.34 x 0.12 mm ³	
θ range for data collection	4.28 to 63.68°	
Index ranges	-13 ≤ h ≤ 13, -13 ≤ k ≤ 13, -13 ≤ l ≤ 13	
Reflections collected	34084	
Independent reflections	4161 [Rint = 0.0469]	
Reflections with I > 2s(I)	4028	
Completeness to $\theta = 63.68^\circ$	97.70%	
Absorption correction	Gaussian	
Max. and min. transmission	0.68 and 0.17	
Refinement method	Full-matrix least-squares on F ²	
Data / restraints / parameters	4161 / 0 / 371	
Goodness-of-fit on F ²	1.054	
Final R indices [I > 2s(I)]	R1 = 0.0357	wR2 = 0.0916
R indices (all data)	R1 = 0.0366	wR2 = 0.0922
Largest diff. peak and hole	0.484 and -0.433 e · Å ⁻³	

6.2.6 Crystal Data and Structure Refinement of Compound 91



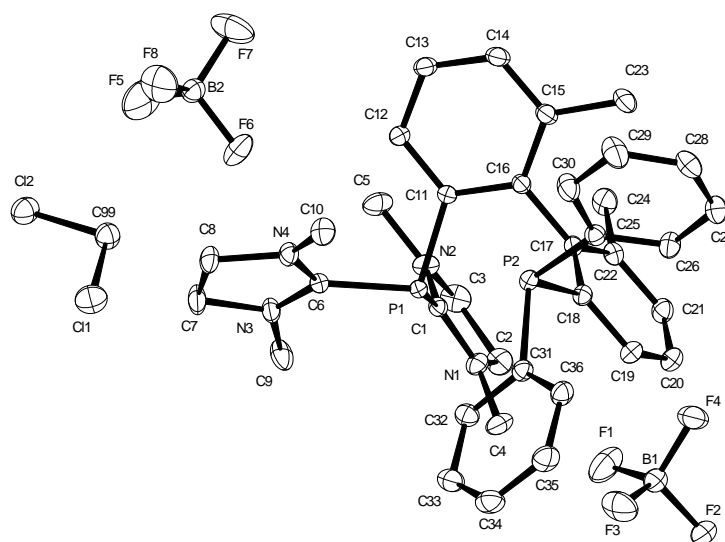
Empirical formula	$C_{50}H_{74}B_2Cl_4F_8N_4P_2$	
Color	yellow	
Formula weight	1109.05 g · mol ⁻¹	
Temperature	100 K	
Wavelength	0.71073 Å	
Crystal system	MONOCLINIC	
Space group	P2₁/n, (no. 14)	
Unit cell dimensions	a = 15.178(3) Å b = 10.0356(17) Å c = 36.990(6) Å	$\alpha = 90^\circ$ $\beta = 97.184(3)^\circ$ $\gamma = 90^\circ$
Volume	5590.0(16) Å ³	
Z	4	
Density (calculated)	1.318 mg · m ⁻³	
Absorption coefficient	0.334 mm ⁻¹	
F(000)	2329 e	
Crystal size	0.17 x 0.16 x 0.07 mm ³	
θ range for data collection	1.110 to 27.498°	
Index ranges	-19 ≤ h ≤ 19, -13 ≤ k ≤ 13, -48 ≤ l ≤ 48	
Reflections collected	127328	
Independent reflections	12834 [R _{int} = 0.0371]	
Reflections with I > 2σ(I)	11133	
Completeness to $\theta = 25.242^\circ$	100.00%	
Absorption correction	Gaussian	
Max. and min. transmission	0.99 and 0.96	
Refinement method	Full-matrix least-squares on F ²	
Data / restraints / parameters	12834 / 10 / 653	
Goodness-of-fit on F ²	1.033	
Final R indices [I > 2 σ (I)]	R1 = 0.0744	wR2 = 0.1719
R indices (all data)	R1 = 0.0843	wR2 = 0.1801
Largest diff. peak and hole	2.0 and -2.9 e · Å ⁻³	

6.2.7 Crystal Data and Structure Refinement of Compound 92b



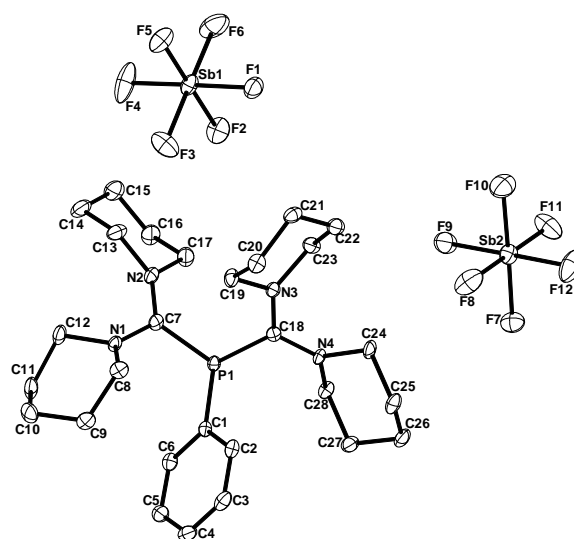
Empirical formula	$C_{28}H_{34}F_{12}N_4P_2Sb_2 \cdot 0.25 CH_2Cl_2$	
Color	colorless	
Formula weight	981.26 g · mol ⁻¹	
Temperature	150 K	
Wavelength	1.54178 Å	
Crystal system	MONOCLINIC	
Space group	P2₁/c, (no. 14)	
Unit cell dimensions	a = 15.3374(6) Å b = 37.0863(14) Å c = 13.4231(5) Å	$\alpha = 90^\circ$ $\beta = 104.8921(17)^\circ$ $\gamma = 90^\circ$
Volume	7378.7(5) Å ³	
Z	8	
Density (calculated)	1.767 mg · m ⁻³	
Absorption coefficient	13.564 mm ⁻¹	
F(000)	3844 e	
Crystal size	0.20 x 0.11 x 0.03 mm ³	
θ range for data collection	2.383 to 65.082°	
Index ranges	-18 ≤ h ≤ 17, -43 ≤ k ≤ 43, -15 ≤ l ≤ 15	
Reflections collected	172322	
Independent reflections	12440 [R _{int} = 0.0844]	
Reflections with I > 2σ(I)	10497	
Completeness to $\theta = 67.679^\circ$	93.10%	
Absorption correction	Gaussian	
Max. and min. transmission	0.68 and 0.08	
Refinement method	Full-matrix least-squares on F ²	
Data / restraints / parameters	12440 / 0 / 895	
Goodness-of-fit on F ²	1.028	
Final R indices [I > 2σ(I)]	R ₁ = 0.0724	wR ₂ = 0.1879
R indices (all data)	R ₁ = 0.0840	wR ₂ = 0.1972
Extinction coefficient	0.00034(3)	
Largest diff. peak and hole	1.8 and -1.6 e · Å ⁻³	

6.2.8 Crystal Data and Structure Refinement of Compound 101a



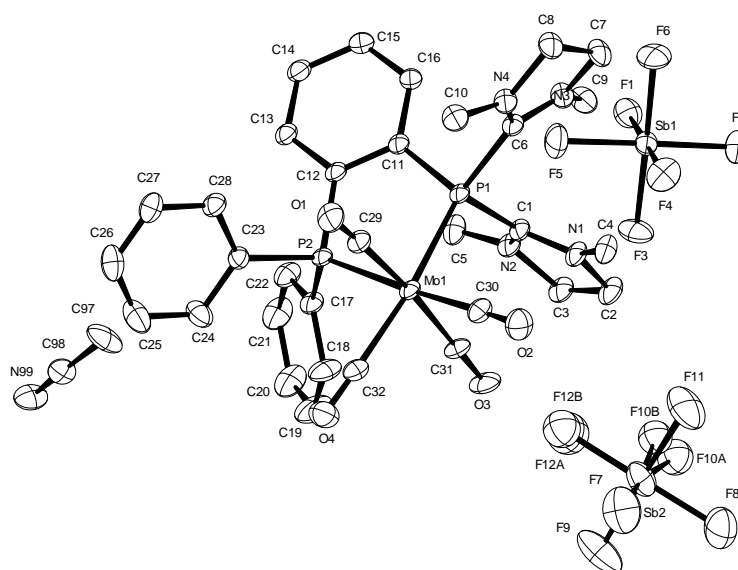
Empirical formula	$C_{37}H_{44}B_2Cl_2F_8N_4P_2$	
Color	yellow	
Formula weight	851.22 g · mol ⁻¹	
Temperature	100.15 K	
Wavelength	0.71073 Å	
Crystal system	MONOCLINIC	
Space group	P2₁/c, (no. 14)	
Unit cell dimensions	$a = 19.5245(8)$ Å	$\alpha = 90^\circ$.
	$b = 12.1720(11)$ Å	$\beta = 102.298(4)^\circ$.
	$c = 17.6079(10)$ Å	$\gamma = 90^\circ$.
Volume	4088.5(5) Å ³	
Z	4	
Density (calculated)	1.383 mg · m ⁻³	
Absorption coefficient	0.306 mm ⁻¹	
F(000)	1760 e	
Crystal size	0.18 x 0.18 x 0.17 mm ³	
θ range for data collection	2.713 to 33.139°.	
Index ranges	$-30 \leq h \leq 30, -18 \leq k \leq 18, -27 \leq l \leq 27$	
Reflections collected	123046	
Independent reflections	15544 [Rint = 0.0289]	
Reflections with $I > 2\sigma(I)$	13476	
Completeness to $\theta = 25.242^\circ$	99.60%	
Absorption correction	Gaussian	
Max. and min. transmission	0.75 and 0.68	
Refinement method	Full-matrix least-squares on F ²	
Data / restraints / parameters	15544 / 0 / 502	
Goodness-of-fit on F ²	1.052	
Final R indices [$I > 2\sigma(I)$]	R1 = 0.0342	wR2 = 0.0892
R indices (all data)	R1 = 0.0420	wR2 = 0.0949
Largest diff. peak and hole	0.6 and -0.5 e · Å ⁻³	

6.2.9 Crystal Data and Structure Refinement of Compound 103



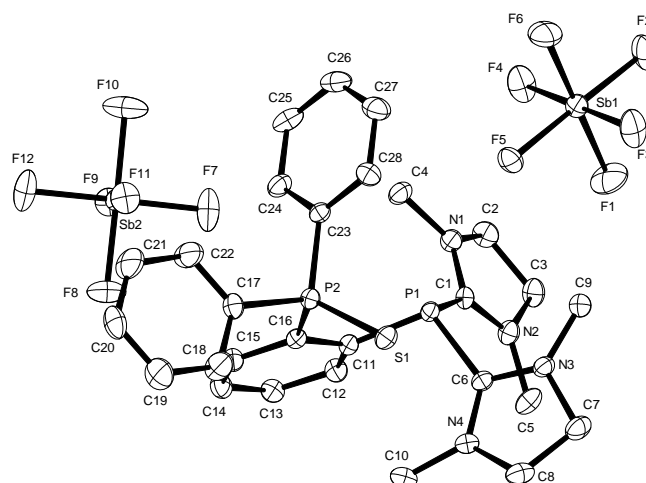
Empirical formula	$C_{28} H_{45} F_{12} N_4 P Sb_2$	
Color	colourless	
Formula weight	940.15 g·mol ⁻¹	
Temperature	100 K	
Wavelength	1.54178 Å	
Crystal system	TRICLINIC	
Space group	<i>p</i> -1, (no. 2)	
Unit cell dimensions	<i>a</i> = 10.2341(2) Å <i>b</i> = 11.9121(3) Å <i>c</i> = 14.5106(3) Å	$\alpha = 82.3872(10)^\circ$ $\beta = 82.2212(9)^\circ$ $\gamma = 87.2389(10)^\circ$
Volume	1736.43(7) Å ³	
<i>Z</i>	2	
Density (calculated)	1.798 mg·m ⁻³	
Absorption coefficient	13.602 mm ⁻¹	
<i>F</i> (000)	932 e	
Crystal size	0.26 x 0.12 x 0.04 mm ³	
θ range for data collection	3.099 to 67.509°.	
Index ranges	-12 ≤ <i>h</i> ≤ 12, -14 ≤ <i>k</i> ≤ 14, -16 ≤ <i>l</i> ≤ 17	
Reflections collected	41228	
Independent reflections	6054 [Rint = 0.0676]	
Reflections with <i>I</i> > 2σ(<i>I</i>)	5404	
Completeness to $\theta = 67.679^\circ$	96.30%	
Absorption correction	Gaussian	
Max. and min. transmission	0.60027 and 0.11584	
Refinement method	Full-matrix least-squares on <i>F</i> ²	
Data / restraints / parameters	6054 / 0 / 424	
Goodness-of-fit on <i>F</i> ²	1.021	
Final <i>R</i> indices [<i>I</i> > 2σ(<i>I</i>)]	<i>R</i> 1 = 0.0320	<i>wR</i> 2 = 0.0778
<i>R</i> indices (all data)	<i>R</i> 1 = 0.0380	<i>wR</i> 2 = 0.0815
Extinction coefficient	n/a	
Largest diff. peak and hole	0.661 and -1.106 e·Å ⁻³	

6.2.10 Crystal Data and Structure Refinement of Compound 107a



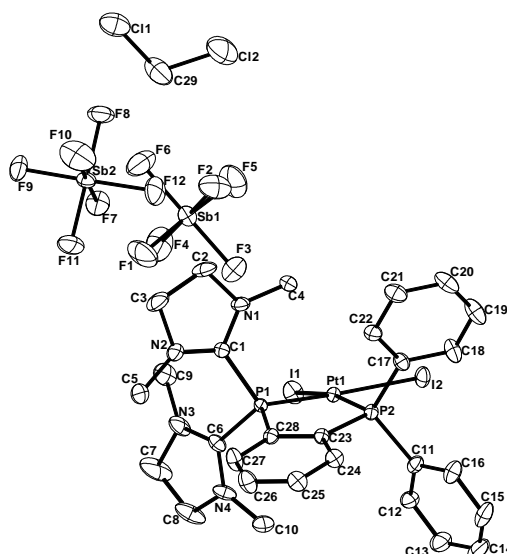
Empirical formula	$C_{33}H_{35.50}F_{12}MoN_{4.50}O_4P_2Sb_2$	
Color	yellow	
Formula weight	1188.54 g · mol ⁻¹	
Temperature	100 K	
Wavelength	0.71073 Å	
Crystal system	TRICLINIC	
Space group	P⁻1, (no. 2)	
Unit cell dimensions	a = 10.5620(5) Å b = 14.8442(13) Å c = 14.9641(14) Å	$\alpha = 99.497(8)^\circ$ $\beta = 92.181(6)^\circ$ $\gamma = 92.074(6)^\circ$
Volume	2310.2(3) Å ³	
Z	2	
Density (calculated)	1.709 mg · m ⁻³	
Absorption coefficient	1.584 mm ⁻¹	
F(000)	1158 e	
Crystal size	0.15 x 0.08 x 0.03 mm ³	
θ range for data collection	2.633 to 32.031°	
Index ranges	$15 \leq h \leq -15, 21 \leq k \leq -22, 22 \leq l \leq 0$	
Reflections collected	53813	
Independent reflections	15951 [Rint = 0.0520]	
Reflections with $I > 2\sigma(I)$	14303	
Completeness to $\theta = 25.242^\circ$	99.20%	
Absorption correction	Gaussian	
Max. and min. transmission	0.75 and 0.44	
Refinement method	Full-matrix least-squares on F ²	
Data / restraints / parameters	15951 / 0 / 544	
Goodness-of-fit on F ²	1.042	
Final R indices [$I > 2\sigma(I)$]	R1 = 0.0631	wR2 = 0.1740
R indices (all data)	R1 = 0.0683	wR2 = 0.1784
Largest diff. peak and hole	7.060 and -3.420 e · Å ⁻³	

6.2.11 Crystal Data and Structure Refinement of Compound 108



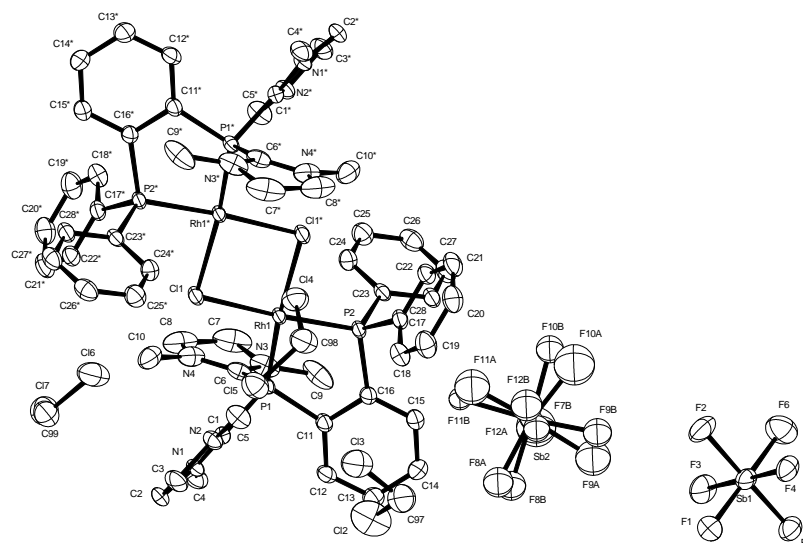
Empirical formula	$C_{28}H_{34}F_{12}N_4P_2S Sb_2$	
Color	colorless	
Formula weight	992.09 g · mol ⁻¹	
Temperature	100.15 K	
Wavelength	0.71073 Å	
Crystal system	MONOCLINIC	
Space group	C2/c, (no. 15)	
Unit cell dimensions	$a = 39.801(4)$ Å $b = 12.189(5)$ Å $c = 17.500(6)$ Å	$\alpha = 90^\circ$. $\beta = 112.724(12)^\circ$. $\gamma = 90^\circ$.
Volume	7831(4) Å ³	
Z	8	
Density (calculated)	1.683 mg · m ⁻³	
Absorption coefficient	1.597 mm ⁻¹	
F(000)	3888 e	
Crystal size	0.10 x 0.04 x 0.04 mm ³	
θ range for data collection	2.640 to 33.168°.	
Index ranges	$-61 \leq h \leq 61$, $-18 \leq k \leq 18$, $-25 \leq l \leq 26$	
Reflections collected	77801	
Independent reflections	14892 [Rint = 0.0550]	
Reflections with $I > 2\sigma(I)$	11755	
Completeness to $\theta = 25.242^\circ$	99.90%	
Absorption correction	Gaussian	
Max. and min. transmission	0.95 and 0.86	
Refinement method	Full-matrix least-squares on F ²	
Data / restraints / parameters	14892 / 0 / 446	
Goodness-of-fit on F ²	1.056	
Final R indices [$I > 2\sigma(I)$]	R1 = 0.0365	wR2 = 0.0829
R indices (all data)	R1 = 0.0530	wR2 = 0.0888
Extinction coefficient	n/a	
Largest diff. peak and hole	0.7 and -1.3 e · Å ⁻³	

6.2.12 Crystal Data and Structure Refinement of Compound 109a



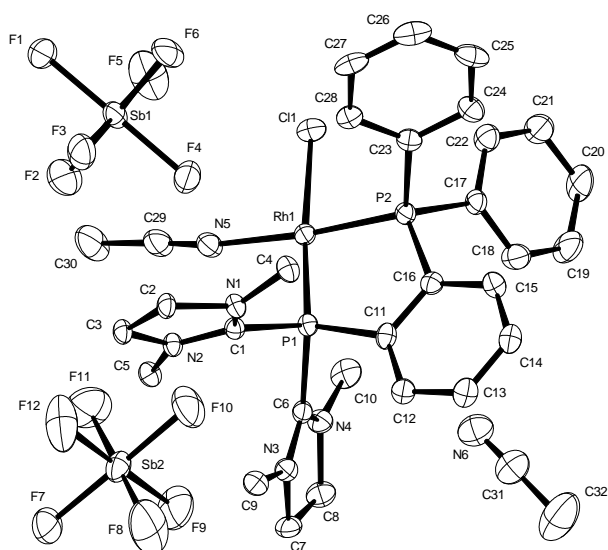
Empirical formula	$C_{29} H_{36} Cl_2 F_{12} I_2 N_4 P_2 Pt Sb_2$	
Color	yellow	
Formula weight	1493.85 g·mol ⁻¹	
Temperature	293(2) K	
Wavelength	0.71073 Å	
Crystal system	MONOCLINIC	
Space group	p 21/c, (no. 14)	
Unit cell dimensions	a = 17.976(6) Å b = 14.1503(12) Å c = 17.202(5) Å	$\alpha = 90^\circ$ $\beta = 100.40(3)^\circ$ $\gamma = 90^\circ$
Volume	4303.5(19) Å ³	
Z	4	
Density (calculated)	2.306 mg·m ⁻³	
Absorption coefficient	6.202 mm ⁻¹	
F(000)	2784 e	
Crystal size	0.16 x 0.10 x 0.01 mm ³	
θ range for data collection	2.717 to 33.132°	
Index ranges	-27 ≤ h ≤ 27, -21 ≤ k ≤ 21, -26 ≤ l ≤ 26	
Reflections collected	135279	
Independent reflections	16334 [R _{int} = 0.0675]	
Reflections with I > 2 σ (I)	14409	
Completeness to $\theta = 26.000^\circ$	99.90%	
Absorption correction	Gaussian	
Max. and min. transmission	0.94105 and 0.50116	
Refinement method	Full-matrix least-squares on F ²	
Data / restraints / parameters	16334 / 0 / 491	
Goodness-of-fit on F ²	1.051	
Final R indices [I > 2 σ (I)]	R ₁ = 0.0342	wR ₂ = 0.0832
R indices (all data)	R ₁ = 0.0420	wR ₂ = 0.0883
Extinction coefficient	n/a	
Largest diff. peak and hole	3.007 and -3.217 e·Å ⁻³	

6.2.13 Crystal Data and Structure Refinement of Compound 109c



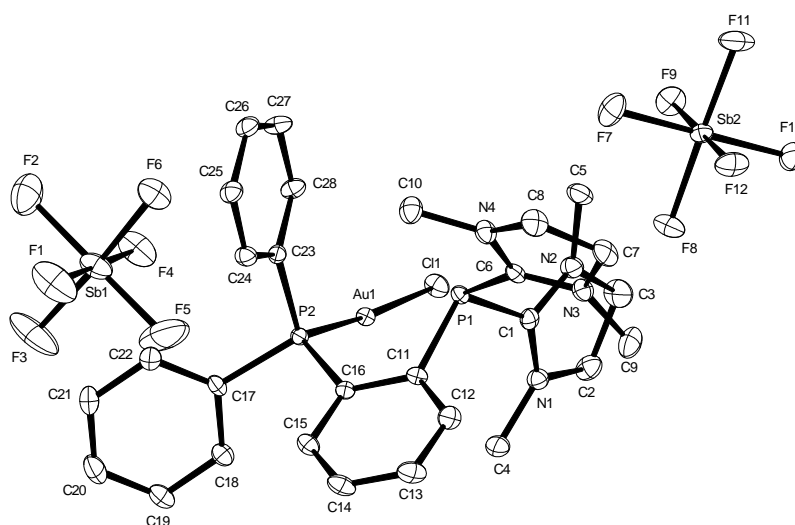
Empirical formula	$C_{62}H_{80}Cl_{14}F_{24}N_8P_4Rh_2Sb_4$	
Color	orange	
Formula weight	2706.38 g · mol ⁻¹	
Temperature	100.15 K	
Wavelength	0.71073 Å	
Crystal system	MONOCLINIC	
Space group	P2₁/n, (no. 14)	
Unit cell dimensions	a = 13.2883(12) Å b = 13.0485(16) Å c = 26.3951(12) Å	$\alpha = 90^\circ$ $\beta = 92.308(7)^\circ$ $\gamma = 90^\circ$
Volume	4573.0(7) Å ³	
Z	2	
Density (calculated)	1.965 mg · m ⁻³	
Absorption coefficient	2.088 mm ⁻¹	
F(000)	2632 e	
Crystal size	0.10 x 0.07 x 0.04 mm ³	
θ range for data collection	2.727 to 27.500°	
Index ranges	-17 ≤ h ≤ 17, -16 ≤ k ≤ 16, -34 ≤ l ≤ 34	
Reflections collected	87023	
Independent reflections	10476 [R _{int} = 0.0536]	
Reflections with I > 2σ(I)	9134	
Completeness to $\theta = 25.242^\circ$	99.60%	
Absorption correction	Gaussian	
Max. and min. transmission	0.94 and 0.83	
Refinement method	Full-matrix least-squares on F ²	
Data / restraints / parameters	10476 / 0 / 530	
Goodness-of-fit on F ²	1.054	
Final R indices [I > 2 σ(I)]	R ₁ = 0.0593	wR ₂ = 0.1638
R indices (all data)	R ₁ = 0.0672	wR ₂ = 0.1762
Largest diff. peak and hole	3.6 and -1.8 e · Å ⁻³	

6.2.14 Crystal Data and Structure Refinement of Compound 109d



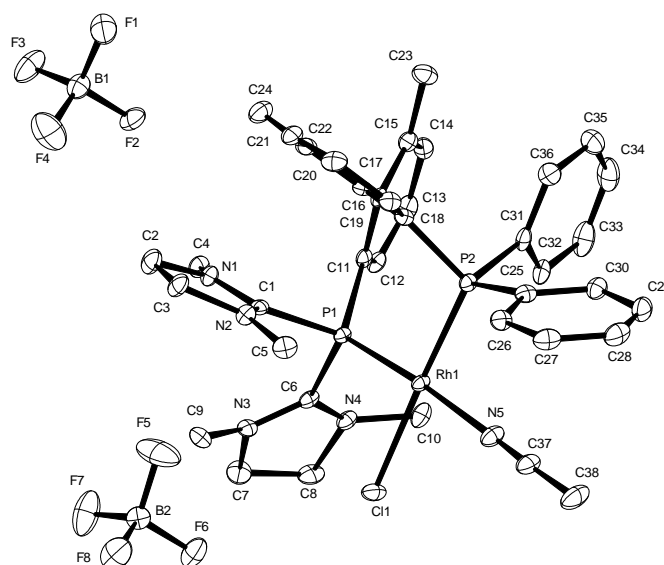
Empirical formula	$C_{32}H_{34}Cl_2D_6F_{12}N_6P_2RhSb_2$	
Color	orange	
Formula weight	1186.53 g · mol ⁻¹	
Temperature	100.15 K	
Wavelength	0.71073 Å	
Crystal system	MONOCLINIC	
Space group	P2₁/c, (no. 14)	
Unit cell dimensions	a = 17.492(2) Å b = 15.774(2) Å c = 17.985(2) Å	$\alpha = 90^\circ$ $\beta = 111.088(2)^\circ$ $\gamma = 90^\circ$
Volume	4629.8(11) Å ³	
Z	4	
Density (calculated)	1.702 mg · m ⁻³	
Absorption coefficient	1.716 mm ⁻¹	
F(000)	2304 e	
Crystal size	0.1 x 0.1 x 0.1 mm ³	
θ range for data collection	2.296 to 31.082°	
Index ranges	-25 ≤ h ≤ 25, -22 ≤ k ≤ 22, -26 ≤ l ≤ 26	
Reflections collected	129694	
Independent reflections	14793 [R _{int} = 0.0730]	
Reflections with I > 2 σ (I)	11201	
Completeness to $\theta = 25.242^\circ$	99.60%	
Absorption correction	Gaussian	
Max. and min. transmission	0.89 and 0.83	
Refinement method	Full-matrix least-squares on F ²	
Data / restraints / parameters	14793 / 0 / 511	
Goodness-of-fit on F ²	1.059	
Final R indices [I > 2 σ (I)]	R ₁ = 0.0511	wR ₂ = 0.1030
R indices (all data)	R ₁ = 0.0748	wR ₂ = 0.1098
Largest diff. peak and hole	3.4 and -2.0 e · Å ⁻³	

6.2.15 Crystal Data and Structure Refinement of Compound 109f



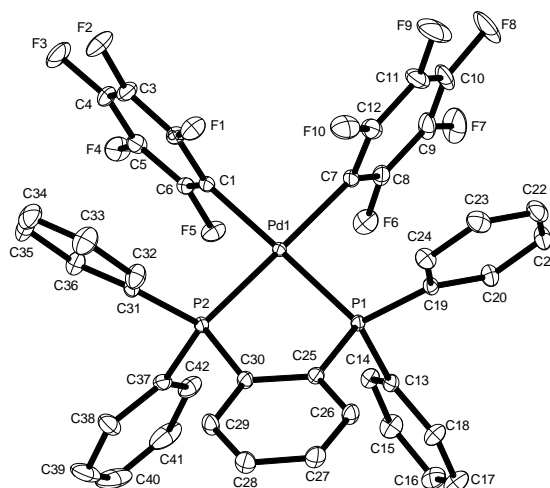
Empirical formula	$C_{28}H_{34}AuClF_{12}N_4P_2Sb_2$	
Color	colorless	
Formula weight	1192.45 g · mol ⁻¹	
Temperature	100 K	
Wavelength	0.71073 Å	
Crystal system	MONOCLINIC	
Space group	C 2/c, (no. 15)	
Unit cell dimensions	a = 36.725(5) Å b = 12.1334(15) Å c = 17.956(2) Å	$\alpha = 90^\circ$ $\beta = 108.584(2)^\circ$ $\gamma = 90^\circ$
Volume	7584.1(16) Å ³	
Z	8	
Density (calculated)	2.089 mg · m ⁻³	
Absorption coefficient	5.514 mm ⁻¹	
F(000)	4528 e	
Crystal size	0.06 x 0.05 x 0.03 mm ³	
θ range for data collection	2.393 to 31.060°	
Index ranges	-53 ≤ h ≤ 53, -17 ≤ k ≤ 17, -25 ≤ l ≤ 26	
Reflections collected	110234	
Independent reflections	12111 [R _{int} = 0.0641]	
Reflections with I > 2σ(I)	10022	
Completeness to $\theta = 25.242^\circ$	99.90%	
Absorption correction	Gaussian	
Max. and min. transmission	0.83 and 0.65	
Refinement method	Full-matrix least-squares on F ²	
Data / restraints / parameters	12111 / 0 / 455	
Goodness-of-fit on F ²	1.021	
Final R indices [I > 2σ(I)]	R ₁ = 0.0253	wR ₂ = 0.0464
R indices (all data)	R ₁ = 0.0387	wR ₂ = 0.0501
Largest diff. peak and hole	2.3 and -1.4 e · Å ⁻³	

6.2.16 Crystal Data and Structure Refinement of Compound 110



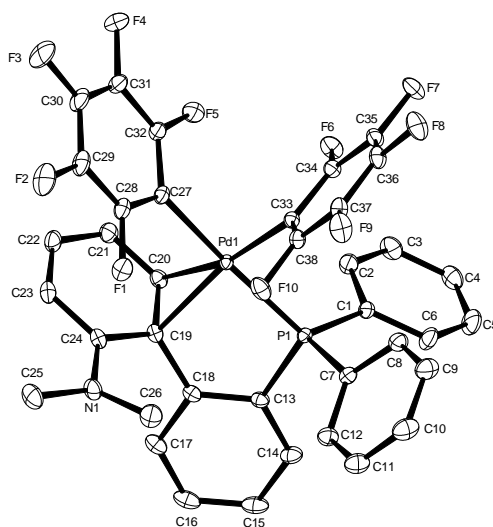
Empirical formula	$C_{38}H_{45}B_2ClF_8N_5P_2Rh$	
Color	yellow	
Formula weight	945.71 g · mol ⁻¹	
Temperature	100 K	
Wavelength	0.71073 Å	
Crystal system	MONOCLINIC	
Space group	P2₁/n, (no. 14)	
Unit cell dimensions	a = 17.7583(18) Å b = 12.1947(12) Å c = 18.3067(18) Å	$\alpha = 90^\circ$ $\beta = 91.115(2)^\circ$ $\gamma = 90^\circ$
Volume	3963.7(7) Å ³	
Z	4	
Density (calculated)	1.585 mg · m ⁻³	
Absorption coefficient	0.654 mm ⁻¹	
F(000)	1928 e	
Crystal size	0.34 x 0.10 x 0.03 mm ³	
θ range for data collection	1.582 to 26.818°	
Index ranges	-22 ≤ h ≤ 22, -15 ≤ k ≤ 15, -23 ≤ l ≤ 23	
Reflections collected	76406	
Independent reflections	8461 [R _{int} = 0.0750]	
Reflections with I > 2σ(I)	6803	
Completeness to $\theta = 25.242^\circ$	100.00%	
Absorption correction	Gaussian	
Max. and min. transmission	0.99 and 0.87	
Refinement method	Full-matrix least-squares on F ²	
Data / restraints / parameters	8461 / 0 / 521	
Goodness-of-fit on F ²	1.138	
Final R indices [I > 2 σ (I)]	R ₁ = 0.0332	wR ₂ = 0.0890
R indices (all data)	R ₁ = 0.0517	wR ₂ = 0.1114
Largest diff. peak and hole	0.8 and -0.9 e · Å ⁻³	

6.2.17 Crystal Data and Structure Refinement of Compound 112b



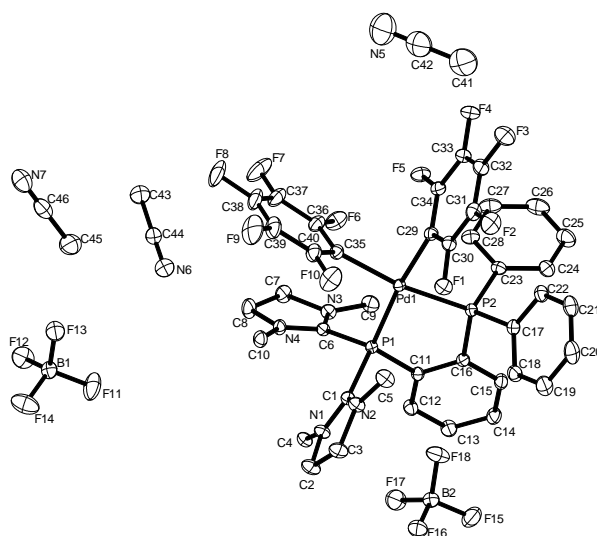
Empirical formula	$C_{42} H_{24} F_{10} P_2 Pd$	
Color	colourless	
Formula weight	886.95 g·mol ⁻¹	
Temperature	100 K	
Wavelength	0.71073 Å	
Crystal system	monoclinic	
Space group	$P 2_1/n$, (no. 14)	
Unit cell dimensions	$a = 15.061(3)$ Å $b = 14.768(3)$ Å $c = 16.339(4)$ Å	$\alpha = 90^\circ$ $\beta = 102.298(4)^\circ$ $\gamma = 90^\circ$
Volume	3550.9(13) Å ³	
Z	4	
Density (calculated)	1.659 mg·m ⁻³	
Absorption coefficient	0.698 mm ⁻¹	
F(000)	1768 e	
Crystal size	0.07 x 0.06 x 0.04 mm ³	
θ range for data collection	3.039 to 33.647°	
Index ranges	$-23 \leq h \leq 23$, $-22 \leq k \leq 22$, $-25 \leq l \leq 25$	
Reflections collected	117912	
Independent reflections	14026 [R _{int} = 0.0724]	
Reflections with $I > 2\sigma(I)$	11056	
Completeness to $\theta = 25.242^\circ$	99.80%	
Absorption correction	Gaussian	
Max. and min. transmission	0.97433 and 0.95301	
Refinement method	Full-matrix least-squares on F ²	
Data / restraints / parameters	14026 / 0 / 496	
Goodness-of-fit on F ²	1.02	
Final R indices [$I > 2 \sigma(I)$]	R ₁ = 0.0303	wR ₂ = 0.0651
R indices (all data)	R ₁ = 0.0483	wR ₂ = 0.0706
Extinction coefficient	0	
Largest diff. peak and hole	0.839 and -0.716 e·Å ⁻³	

6.2.18 Crystal Data and Structure Refinement of Compound 112f



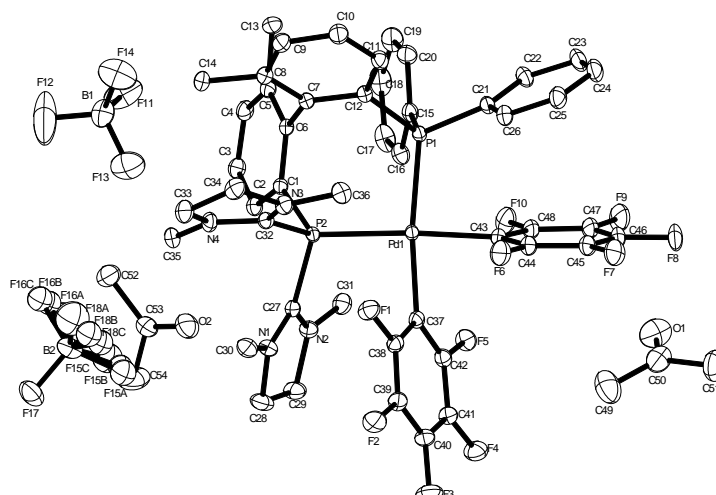
Empirical formula	$C_{38}H_{24}F_{10}NPd$	
Color	yellow	
Formula weight	821.95 g·mol ⁻¹	
Temperature	100 K	
Wavelength	0.71073 Å	
Crystal system	MONOCLINIC	
Space group	p 21/c, (no. 14)	
Unit cell dimensions	a = 11.0106(11) Å b = 14.0190(14) Å c = 21.167(2) Å	$\alpha = 90^\circ$ $\beta = 96.5422(19)^\circ$ $\gamma = 90^\circ$
Volume	3246.0(6) Å ³	
Z	4	
Density (calculated)	1.682 mg·m ⁻³	
Absorption coefficient	0.709 mm ⁻¹	
F(000)	1640 e	
Crystal size	0.22 x 0.21 x 0.19 mm ³	
θ range for data collection	2.421 to 37.341°	
Index ranges	-18 ≤ h ≤ 18, -23 ≤ k ≤ 23, -35 ≤ l ≤ 35	
Reflections collected	127102	
Independent reflections	16348 [R _{int} = 0.0252]	
Reflections with I > 2σ(I)	14984	
Completeness to $\theta = 25.242^\circ$	99.90%	
Absorption correction	Gaussian	
Max. and min. transmission	0.90265 and 0.82904	
Refinement method	Full-matrix least-squares on F ²	
Data / restraints / parameters	16348 / 0 / 462	
Goodness-of-fit on F ²	1.058	
Final R indices [I > 2σ(I)]	R ₁ = 0.0214	wR ₂ = 0.0575
R indices (all data)	R ₁ = 0.0250	wR ₂ = 0.0596
Extinction coefficient	n/a	
Largest diff. peak and hole	0.687 and -0.528 e·Å ⁻³	

6.2.19 Crystal Data and Structure Refinement of Compound 112g



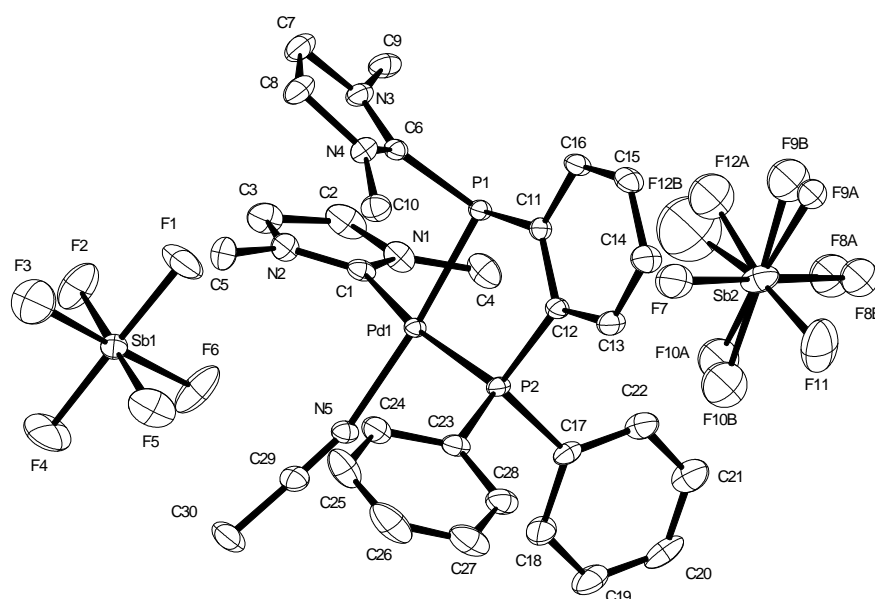
Empirical formula	$C_{46} H_{43} B_2 F_{18} N_7 P_2 Pd$	
Color	colourless	
Formula weight	1225.83 g·mol ⁻¹	
Temperature	100 K	
Wavelength	0.71073 Å	
Crystal system	MONOCLINIC	
Space group	<i>p</i> 21/ <i>c</i> , (no. 14)	
Unit cell dimensions	<i>a</i> = 18.3894(13) Å <i>b</i> = 14.7845(14) Å <i>c</i> = 20.6566(7) Å	$\alpha = 90^\circ$ $\beta = 114.994(4)^\circ$ $\gamma = 90^\circ$
Volume	5090.2(7) Å ³	
Z	4	
Density (calculated)	1.600 mg·m ⁻³	
Absorption coefficient	0.535 mm ⁻¹	
F(000)	2464 e	
Crystal size	0.15 x 0.09 x 0.04 mm ³	
θ range for data collection	2.609 to 35.008°	
Index ranges	-29 ≤ <i>h</i> ≤ 29, -23 ≤ <i>k</i> ≤ 23, -32 ≤ <i>l</i> ≤ 33	
Reflections collected	124759	
Independent reflections	22373 [R _{int} = 0.0428]	
Reflections with <i>I</i> > 2σ(<i>I</i>)	18998	
Completeness to $\theta = 25.242^\circ$	99.80%	
Absorption correction	Gaussian	
Max. and min. transmission	0.98046 and 0.93073	
Refinement method	Full-matrix least-squares on F ²	
Data / restraints / parameters	22373 / 0 / 692	
Goodness-of-fit on F ²	1.048	
Final R indices [<i>I</i> > 2σ(<i>I</i>)]	R ₁ = 0.0361	wR ₂ = 0.0924
R indices (all data)	R ₁ = 0.0465	wR ₂ = 0.0988
Extinction coefficient	0	
Largest diff. peak and hole	2.507 and -1.787 e·Å ⁻³	

6.2.20 Crystal Data and Structure Refinement of Compound 112h



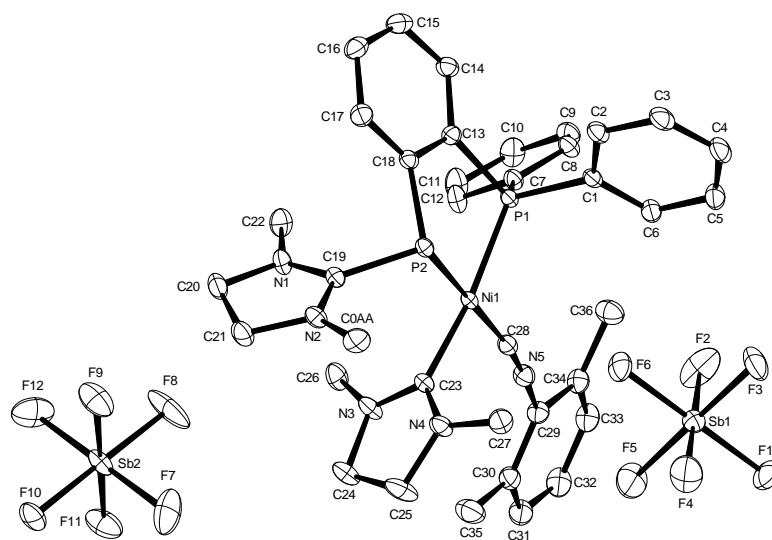
Empirical formula	C ₅₄ H ₅₄ B ₂ F ₁₈ N ₄ O ₂ P ₂ Pd	
Color	yellow	
Formula weight	1322.97 g·mol ⁻¹	
Temperature	100 K	
Wavelength	0.71073 Å	
Crystal system	TRICLINIC	
Space group	<i>P</i> -1, (no. 2)	
Unit cell dimensions	<i>a</i> = 12.5325(6) Å <i>b</i> = 13.8883(13) Å <i>c</i> = 18.2445(18) Å	$\alpha = 93.239(6)^\circ$ $\beta = 103.518(7)^\circ$ $\gamma = 115.502(6)^\circ$
Volume	2741.7(4) Å ³	
<i>Z</i>	2	
Density (calculated)	1.603 mg·m ⁻³	
Absorption coefficient	0.505 mm ⁻¹	
<i>F</i> (000)	1340 e	
Crystal size	0.14 x 0.14 x 0.09 mm ³	
θ range for data collection	2.607 to 35.056°	
Index ranges	-20 ≤ <i>h</i> ≤ 20, -22 ≤ <i>k</i> ≤ 22, -29 ≤ <i>l</i> ≤ 29	
Reflections collected	78461	
Independent reflections	24146 [<i>R</i> _{int} = 0.0279]	
Reflections with <i>I</i> > 2σ(<i>I</i>)	21322	
Completeness to $\theta = 25.242^\circ$	99.60%	
Absorption correction	Gaussian	
Max. and min. transmission	0.96402 and 0.92959	
Refinement method	Full-matrix least-squares on <i>F</i> ²	
Data / restraints / parameters	24146 / 0 / 767	
Goodness-of-fit on <i>F</i> ²	1.047	
Final <i>R</i> indices [<i>I</i> > 2σ(<i>I</i>)]	<i>R</i> ₁ = 0.0352	<i>wR</i> ₂ = 0.0900
<i>R</i> indices (all data)	<i>R</i> ₁ = 0.0425	<i>wR</i> ₂ = 0.0946
Extinction coefficient	0	
Largest diff. peak and hole	1.251 and -1.121 e·Å ⁻³	

6.2.21 Crystal Data and Structure Refinement of Compound 113



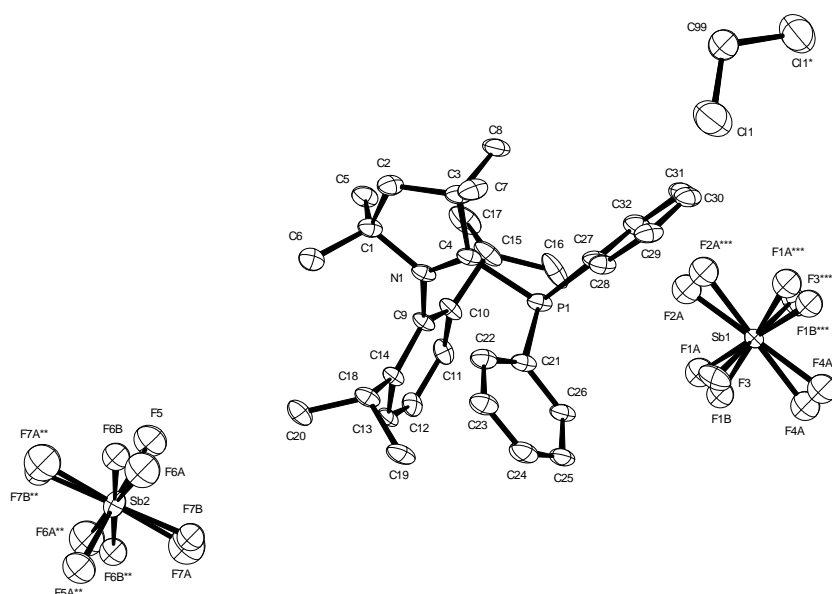
Empirical formula	$C_{30}H_{37}F_{12}N_5P_2PdSb_2$	
Color	yellow	
Formula weight	1107.48 g · mol ⁻¹	
Temperature	100 K	
Wavelength	0.71073 Å	
Crystal system	TRICLINIC	
Space group	P$\bar{1}$, (no. 2)	
Unit cell dimensions	$a = 10.3416(10)$ Å $b = 13.4178(13)$ Å $c = 15.5829(15)$ Å	$\alpha = 77.0009(18)^\circ$ $\beta = 79.6302(17)^\circ$ $\gamma = 80.8707(17)^\circ$
Volume	2056.7(3) Å ³	
Z	2	
Density (calculated)	1.788 mg · m ⁻³	
Absorption coefficient	1.897 mm ⁻¹	
F(000)	1076 e	
Crystal size	0.19 x 0.05 x 0.04 mm ³	
q range for data collection	1.570 to 31.543°	
Index ranges	$-15 \leq h \leq 15, -19 \leq k \leq 19, -22 \leq l \leq 22$	
Reflections collected	61748	
Independent reflections	13489 [R _{int} = 0.0329]	
Reflections with I > 2σ(I)	11188	
Completeness to q = 25.242°	99.90%	
Absorption correction	Gaussian	
Max. and min. transmission	0.93 and 0.78	
Refinement method	Full-matrix least-squares on F ²	
Data / restraints / parameters	13489 / 0 / 470	
Goodness-of-fit on F ²	1.079	
Final R indices [I > 2σ(I)]	R ₁ = 0.0359	wR ₂ = 0.0837
R indices (all data)	R ₁ = 0.0457	wR ₂ = 0.0873
Largest diff. peak and hole	4.0 and -3.1 e · Å ⁻³	

6.2.22 Crystal Data and Structure Refinement of Compound 114



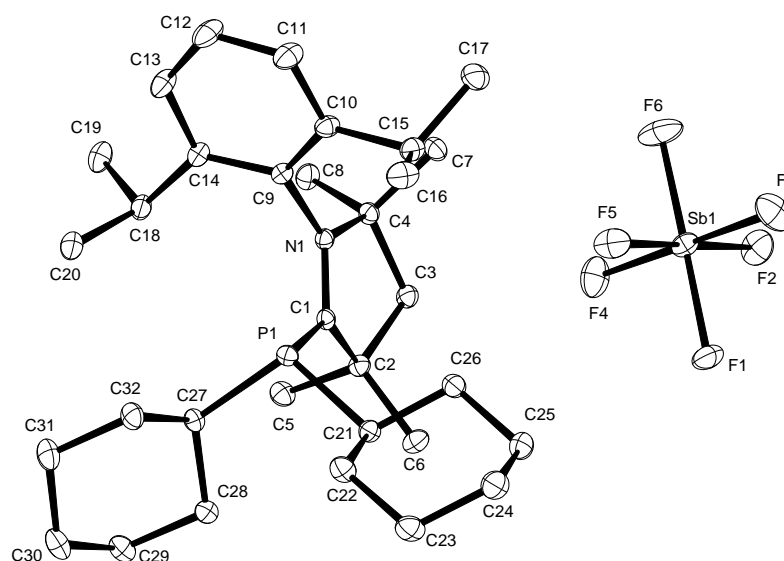
Empirical formula	$C_{37}H_{43}F_{12}N_5NiP_2Sb_2$	
Color	yellow	
Formula weight	1149.91 g·mol ⁻¹	
Temperature	100.15 K	
Wavelength	0.71073 Å	
Crystal system	MONOCLINIC	
Space group	p 21/n, (no. 14)	
Unit cell dimensions	a = 11.903(2) Å b = 12.036(2) Å c = 33.183(4) Å	$\alpha = 90^\circ$ $\beta = 97.511(13)^\circ$ $\gamma = 90^\circ$
Volume	4713.2(14) Å ³	
Z	4	
Density (calculated)	1.621 mg·m ⁻³	
Absorption coefficient	1.680 mm ⁻¹	
F(000)	2272 e	
Crystal size	0.26 x 0.22 x 0.08 mm ³	
θ range for data collection	2.696 to 33.092°	
Index ranges	-18 ≤ h ≤ 18, -18 ≤ k ≤ 18, -50 ≤ l ≤ 50	
Reflections collected	64200	
Independent reflections	16882 [Rint = 0.0373]	
Reflections with I > 2σ(I)	14536	
Completeness to $\theta = 25.242^\circ$	97.50%	
Absorption correction	Gaussian	
Max. and min. transmission	0.87772 and 0.69551	
Refinement method	Full-matrix least-squares on F ²	
Data / restraints / parameters	16882 / 0 / 538	
Goodness-of-fit on F ²	1.123	
Final R indices [I > 2σ(I)]	R1 = 0.0338	wR2 = 0.0963
R indices (all data)	R1 = 0.0427	wR2 = 0.1028
Extinction coefficient	n/a	
Largest diff. peak and hole	0.846 and -2.010 e·Å ⁻³	

6.2.23 Crystal Data and Structure Refinement of Compound 138a



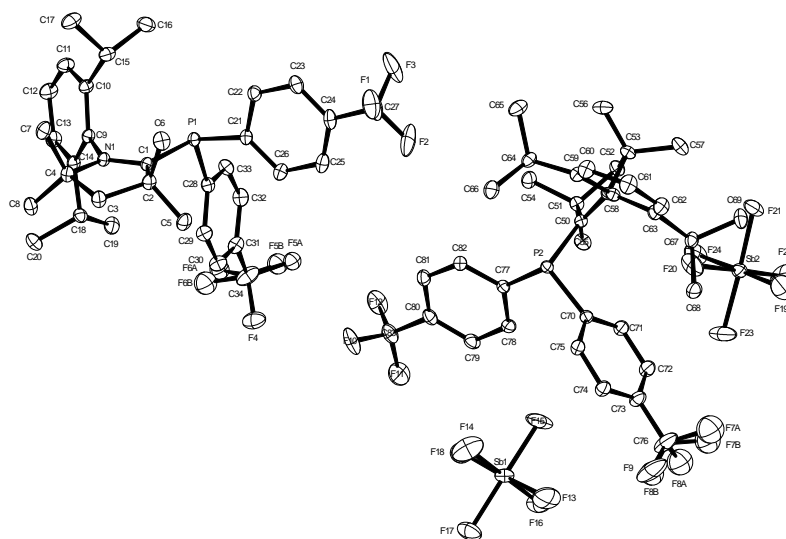
Empirical formula	$C_{32.50}H_{41.50}ClF_6NP Sb$	
Color	yellow	
Formula weight	748.33 g · mol ⁻¹	
Temperature	100.15 K	
Wavelength	0.71073 Å	
Crystal system	MONOCLINIC	
Space group	P2/c, (no. 13)	
Unit cell dimensions	a = 21.327(4) Å b = 10.399(2) Å c = 15.717(3) Å	$\alpha = 90^\circ$ $\beta = 111.57(3)^\circ$ $\gamma = 90^\circ$
Volume	3241.6(12) Å ³	
Z	4	
Density (calculated)	1.533 mg · m ⁻³	
Absorption coefficient	1.041 mm ⁻¹	
F(000)	1522 e	
Crystal size	0.16 x 0.08 x 0.05 mm ³	
θ range for data collection	2.809 to 33.316°	
Index ranges	-32 ≤ h ≤ 24, -16 ≤ k ≤ 16, -22 ≤ l ≤ 24	
Reflections collected	31424	
Independent reflections	10918 [R _{int} = 0.0322]	
Reflections with I > 2σ(I)	8637	
Completeness to $\theta = 25.242^\circ$	91.60%	
Absorption correction	Gaussian	
Max. and min. transmission	0.96 and 0.88	
Refinement method	Full-matrix least-squares on F ²	
Data / restraints / parameters	10918 / 0 / 389	
Goodness-of-fit on F ²	1.032	
Final R indices [I > 2σ(I)]	R ₁ = 0.0468	wR ₂ = 0.1206
R indices (all data)	R ₁ = 0.0641	wR ₂ = 0.1315
Largest diff. peak and hole	1.5 and -2.0 e · Å ⁻³	

6.2.24 Crystal Data and Structure Refinement of Compound 138b



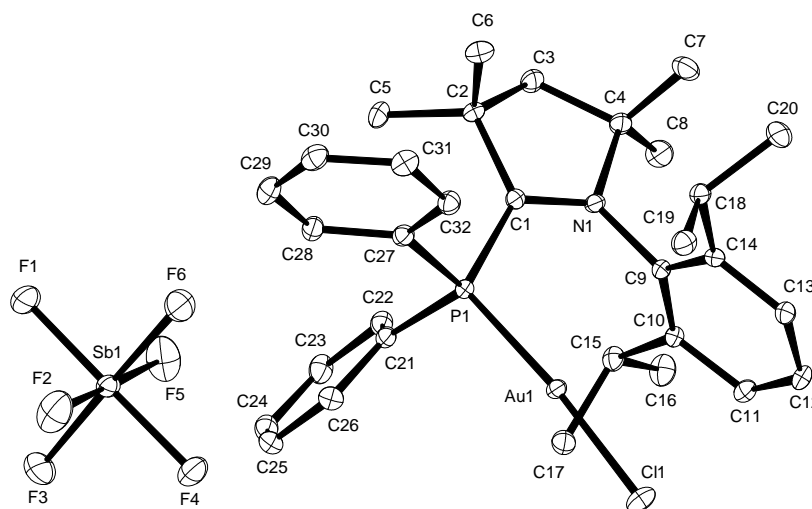
Empirical formula	$C_{32}H_{53}F_6NP Sb$	
Color	yellow	
Formula weight	718.47 g · mol ⁻¹	
Temperature	100.15 K	
Wavelength	0.71073 Å	
Crystal system	MONOCLINIC	
Space group	P2₁/c, (no. 14)	
Unit cell dimensions	a = 16.9548(10) Å b = 12.0609(8) Å c = 19.0889(13) Å	$\alpha = 90^\circ$ $\beta = 122.735(4)^\circ$ $\gamma = 90^\circ$
Volume	3283.5(4) Å ³	
Z	4	
Density (calculated)	1.453 mg · m ⁻³	
Absorption coefficient	0.945 mm ⁻¹	
F(000)	1488 e	
Crystal size	0.14 x 0.08 x 0.07 mm ³	
θ range for data collection	2.722 to 33.180°	
Index ranges	-25 ≤ h ≤ 26, -18 ≤ k ≤ 18, -29 ≤ l ≤ 27	
Reflections collected	64557	
Independent reflections	12528 [R _{int} = 0.0314]	
Reflections with I > 2σ(I)	10720	
Completeness to $\theta = 25.242^\circ$	99.70%	
Absorption correction	Gaussian	
Max. and min. transmission	0.95 and 0.88	
Refinement method	Full-matrix least-squares on F ²	
Data / restraints / parameters	12528 / 0 / 378	
Goodness-of-fit on F ²	1.054	
Final R indices [I > 2σ(I)]	R1 = 0.0256	wR2 = 0.0606
R indices (all data)	R1 = 0.0346	wR2 = 0.0655
Largest diff. peak and hole	0.728 and -1.593 e · Å ⁻³	

6.2.25 Crystal Data and Structure Refinement of Compound 138c



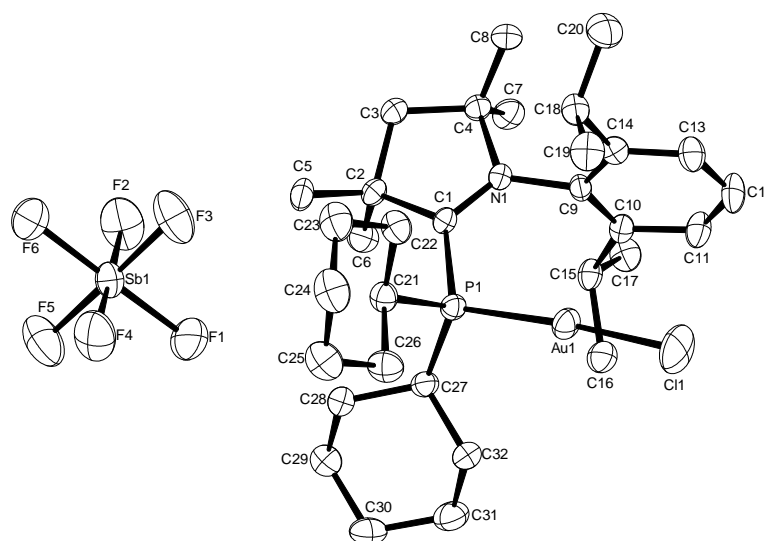
Empirical formula	$C_{34}H_{39}F_{12}NP Sb$	
Color	yellow	
Formula weight	842.38 g·mol ⁻¹	
Temperature	100 K	
Wavelength	0.71073 Å	
Crystal system	MONOCLINIC	
Space group	<i>p</i> 21, (no. 4)	
Unit cell dimensions	<i>a</i> = 10.6294(9) Å <i>b</i> = 17.9592(17) Å <i>c</i> = 18.9360(18) Å	$\alpha = 90^\circ$ $\beta = 101.285(5)^\circ$ $\gamma = 90^\circ$
Volume	3544.9(6) Å ³	
Z	4	
Density (calculated)	1.578 mg·m ⁻³	
Absorption coefficient	0.912 mm ⁻¹	
F(000)	1696 e	
Crystal size	0.30 x 0.13 x 0.12 mm ³	
θ range for data collection	3.576 to 38.006°	
Index ranges	$-18 \leq h \leq 18$, $-31 \leq k \leq 31$, $-32 \leq l \leq 32$	
Reflections collected	259850	
Independent reflections	38502 [R _{int} = 0.0336]	
Reflections with $I > 2\sigma(I)$	36933	
Completeness to $\theta = 25.242^\circ$	99.20%	
Absorption correction	Gaussian	
Max. and min. transmission	0.90987 and 0.78315	
Refinement method	Full-matrix least-squares on F ²	
Data / restraints / parameters	38502 / 1 / 895	
Goodness-of-fit on F ²	1.044	
Final R indices [$I > 2\sigma(I)$]	R1 = 0.0272	wR2 = 0.0705
R indices (all data)	R1 = 0.0295	wR2 = 0.0725
Absolute structure parameter	-0.0103(16)	
Extinction coefficient	n/a	
Largest diff. peak and hole	1.400 and -1.179 e·Å ⁻³	

6.2.26 Crystal Data and Structure Refinement of Compound 139a



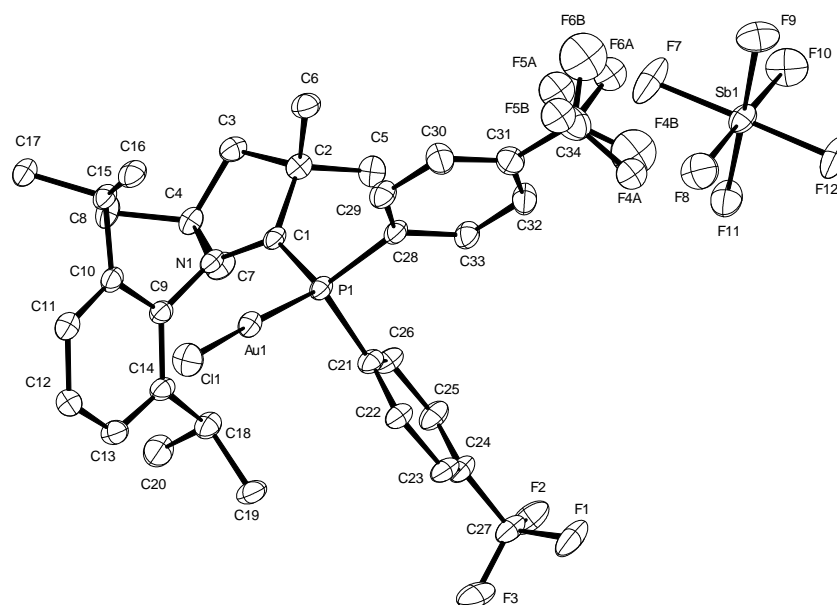
Empirical formula	$C_{32}H_{41}AuClF_6NP Sb$	
Color	yellow	
Formula weight	938.79 g · mol ⁻¹	
Temperature	100 K	
Wavelength	0.71073 Å	
Crystal system	ORTHORHOMBIC	
Space group	Pbc2₁ , (no. 29)	
Unit cell dimensions	a = 15.9504(19) Å	$\alpha = 90^\circ$
	b = 13.9759(16) Å	$\beta = 90^\circ$
	c = 14.6811(17) Å	$\gamma = 90^\circ$
Volume	3272.7(7) Å ³	
Z	4	
Density (calculated)	1.905 mg · m ⁻³	
Absorption coefficient	5.491 mm ⁻¹	
F(000)	1824 e	
Crystal size	0.28 x 0.21 x 0.18 mm ³	
θ range for data collection	2.915 to 31.355°	
Index ranges	-23 ≤ h ≤ 22, -20 ≤ k ≤ 20, -21 ≤ l ≤ 21	
Reflections collected	87398	
Independent reflections	10246 [Rint = 0.0235]	
Reflections with I > 2σ(I)	9981	
Completeness to $\theta = 25.242^\circ$	99.70%	
Absorption correction	Gaussian	
Max. and min. transmission	0.50 and 0.23	
Refinement method	Full-matrix least-squares on F ²	
Data / restraints / parameters	10246 / 1 / 396	
Goodness-of-fit on F ²	1.038	
Final R indices [I > 2σ(I)]	R1 = 0.0130	wR2 = 0.0366
R indices (all data)	R1 = 0.0136	wR2 = 0.0368
Absolute structure parameter	0.0213(14)	
Largest diff. peak and hole	1.4 and -0.6 e · Å ⁻³	

6.2.27 Crystal Data and Structure Refinement of Compound 139b



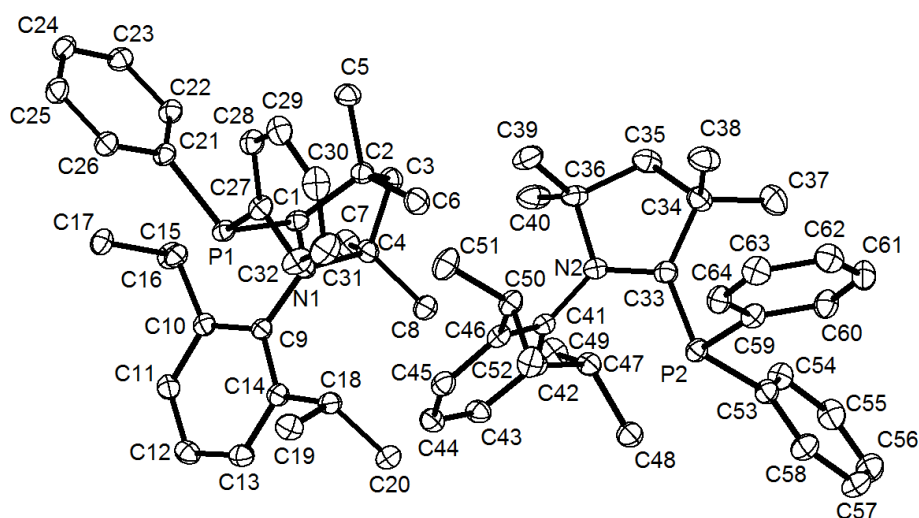
Empirical formula	$C_{32}H_{53}AuClF_6NP Sb$	
Color	colourless	
Formula weight	950.89 g·mol ⁻¹	
Temperature	200 K	
Wavelength	1.54178 Å	
Crystal system	ORTHORHOMBIC	
Space group	<i>pbc</i> a, (no. 61)	
Unit cell dimensions	<i>a</i> = 12.2072(4) Å	$\alpha = 90^\circ$
	<i>b</i> = 16.6468(6) Å	$\beta = 90^\circ$
	<i>c</i> = 34.4701(12) Å	$\gamma = 90^\circ$
Volume	7004.7(4) Å ³	
Z	8	
Density (calculated)	1.803 mg·m ⁻³	
Absorption coefficient	15.486 mm ⁻¹	
F(000)	3744 e	
Crystal size	0.33 x 0.13 x 0.09 mm ³	
θ range for data collection	2.564 to 67.932°	
Index ranges	$-14 \leq h \leq 14, -19 \leq k \leq 19, -41 \leq l \leq 41$	
Reflections collected	158214	
Independent reflections	6320 [Rint = 0.0545]	
Reflections with $I > 2\sigma(I)$	5711	
Completeness to $\theta = 67.679^\circ$	99.70%	
Absorption correction	Gaussian	
Max. and min. transmission	0.34226 and 0.06402	
Refinement method	Full-matrix least-squares on F ²	
Data / restraints / parameters	6320 / 0 / 396	
Goodness-of-fit on F ²	1.077	
Final R indices [$I > 2\sigma(I)$]	R1 = 0.0313	wR2 = 0.0750
R indices (all data)	R1 = 0.0354	wR2 = 0.0775
Extinction coefficient	n/a	
Largest diff. peak and hole	0.482 and -1.356 e·Å ⁻³	

6.2.28 Crystal Data and Structure Refinement of Compound 139c



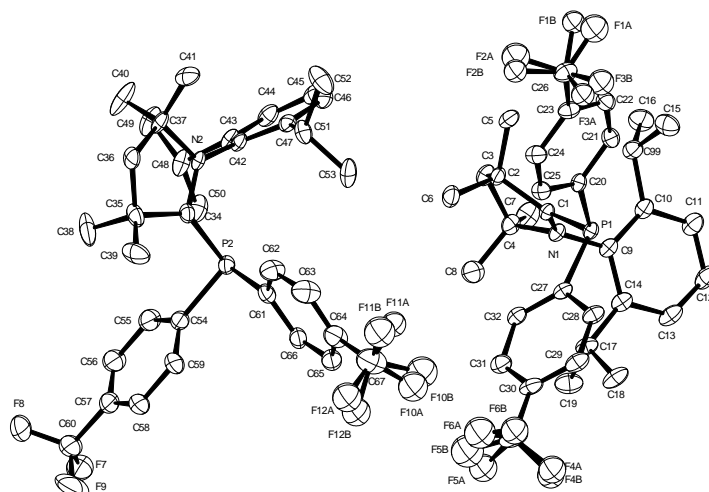
Empirical formula	$C_{34}H_{39}AuClF_{12}NP Sb$	
Color	yellow	
Formula weight	1074.80 g · mol ⁻¹	
Temperature	100 K	
Wavelength	0.71073 Å	
Crystal system	TRICLINIC	
Space group	P$\bar{1}$, (no. 2)	
Unit cell dimensions	$a = 10.5114(12)$ Å $b = 11.3443(3)$ Å $c = 18.509(3)$ Å	$\alpha = 85.859(6)^\circ$ $\beta = 73.535(10)^\circ$ $\gamma = 65.998(4)^\circ$
Volume	1931.2(4) Å ³	
Z	2	
Density (calculated)	1.848 mg · m ⁻³	
Absorption coefficient	4.687 mm ⁻¹	
F(000)	1040 e	
Crystal size	0.06 x 0.03 x 0.02 mm ³	
θ range for data collection	3.448 to 33.142°.	
Index ranges	$-16 \leq h \leq 16, -17 \leq k \leq 17, -26 \leq l \leq 28$	
Reflections collected	38171	
Independent reflections	14633 [R _{int} = 0.0818]	
Reflections with $I > 2\sigma(I)$	12487	
Completeness to $\theta = 25.242^\circ$	99.80%	
Absorption correction	Gaussian	
Max. and min. transmission	0.92 and 0.77	
Refinement method	Full-matrix least-squares on F ²	
Data / restraints / parameters	14633 / 0 / 465	
Goodness-of-fit on F ²	1.04	
Final R indices [$I > 2\sigma(I)$]	R ₁ = 0.0567	wR ₂ = 0.1447
R indices (all data)	R ₁ = 0.0668	wR ₂ = 0.1543
Largest diff. peak and hole	3.3 and -6.1 e · Å ⁻³	

6.2.29 Crystal Data and Structure Refinement of Compound 140a



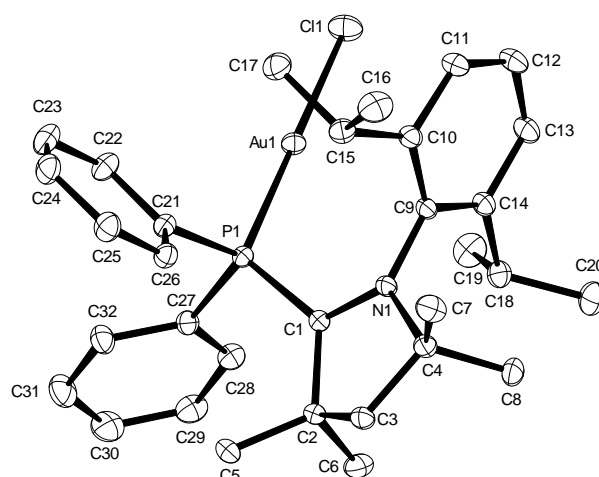
Empirical formula	$C_{32}H_{41}NP$	
Color	colourless	
Formula weight	470.63 g·mol ⁻¹	
Temperature	80(2) K	
Wavelength	0.56305 Å	
Crystal system	monoclinic	
Space group	$P 2_1/c$, (no. 14)	
Unit cell dimensions	$a = 17.015(3)$ Å $b = 10.280(2)$ Å $c = 31.520(6)$ Å	$\alpha = 90^\circ$ $\beta = 101.80(3)^\circ$ $\gamma = 90^\circ$
Volume	5397(2) Å ³	
Z	8	
Density (calculated)	1.158 mg·m ⁻³	
Absorption coefficient	0.072 mm ⁻¹	
F(000)	2040 e	
Crystal size	0.035 x 0.059 x 0.076 mm ³	
θ range for data collection	0.969 to 22.047°	
Index ranges	$-22 \leq h \leq 22$, $-13 \leq k \leq 13$, $-42 \leq l \leq 42$	
Reflections collected	175228	
Independent reflections	13398 [Rint = 0.0811]	
Reflections with $I > 2\sigma(I)$	11256	
Completeness to $\theta = 19.745^\circ$	100.00%	
Refinement method	Full-matrix least-squares on F ²	
Data / restraints / parameters	13398 / 0 / 613	
Goodness-of-fit on F ²	1.036	
Final R indices [$I > 2\sigma(I)$]	R1 = 0.0443	wR2 = 0.1140
R indices (all data)	R1 = 0.0545	wR2 = 0.1210
Extinction coefficient	0	
Largest diff. peak and hole	0.404 and -0.556 e·Å ⁻³	

6.2.30 Crystal Data and Structure Refinement of Compound 140c



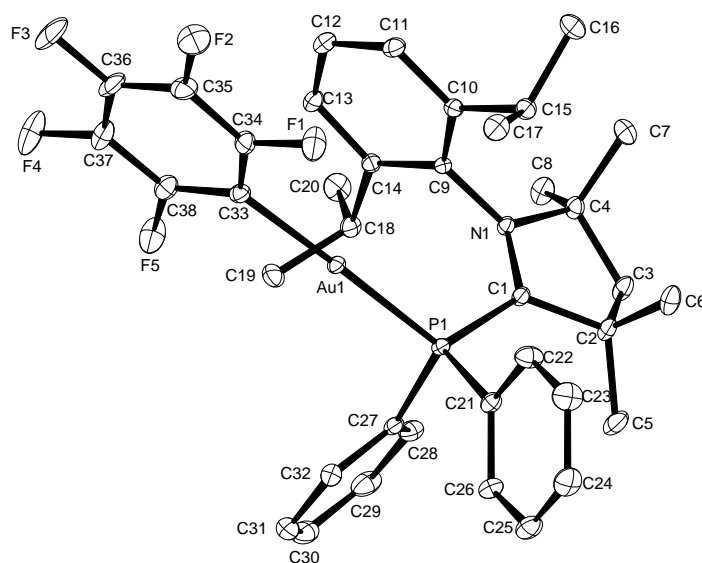
Empirical formula	$C_{34}H_{39}F_6NP$	
Color	brown_black	
Formula weight	606.63 g·mol ⁻¹	
Temperature	100 K	
Wavelength	0.71073 Å	
Crystal system	MONOCLINIC	
Space group	<i>c</i> 2/ <i>c</i> , (no. 15)	
Unit cell dimensions	<i>a</i> = 61.265(8) Å <i>b</i> = 16.892(2) Å <i>c</i> = 15.1854(19) Å	$\alpha = 90^\circ$ $\beta = 104.35^\circ$ $\gamma = 90^\circ$
Volume	15225(3) Å ³	
Z	16	
Density (calculated)	1.059 mg·m ⁻³	
Absorption coefficient	0.121 mm ⁻¹	
F(000)	5104 e	
Crystal size	0.30 x 0.15 x 0.08 mm ³	
θ range for data collection	1.253 to 31.018°.	
Index ranges	-88 ≤ <i>h</i> ≤ 88, -24 ≤ <i>k</i> ≤ 24, -21 ≤ <i>l</i> ≤ 21	
Reflections collected	174699	
Independent reflections	21294 [R _{int} = 0.1008]	
Reflections with <i>I</i> > 2σ(<i>I</i>)	12135	
Completeness to $\theta = 25.242^\circ$	79.90%	
Absorption correction	Gaussian	
Max. and min. transmission	0.99085 and 0.97202	
Refinement method	Full-matrix least-squares on F ²	
Data / restraints / parameters	21294 / 0 / 764	
Goodness-of-fit on F ²	0.996	
Final R indices [<i>I</i> > 2σ(<i>I</i>)]	R ₁ = 0.0749	wR ₂ = 0.2094
R indices (all data)	R ₁ = 0.1260	wR ₂ = 0.2387
Extinction coefficient	n/a	
Largest diff. peak and hole	1.023 and -0.719 e·Å ⁻³	
Remarks	SQUEEZE was used !!	

6.2.31 Crystal Data and Structure Refinement of Compound 141



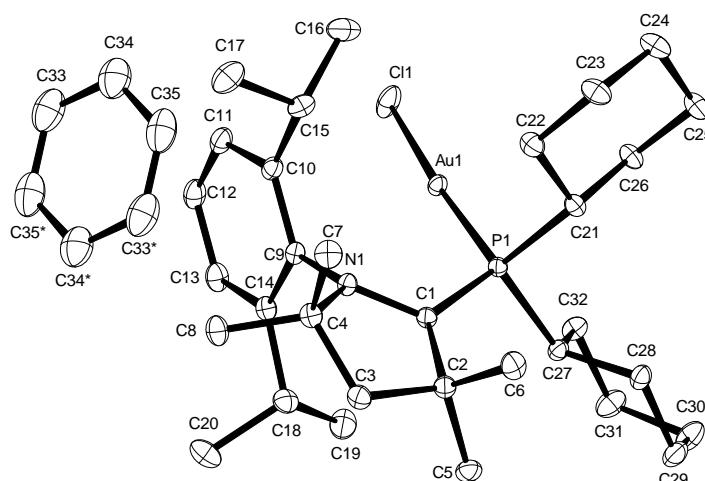
Empirical formula	$C_{32}H_{41}AuClNP$	
Color	red	
Formula weight	703.04 g·mol ⁻¹	
Temperature	100 K	
Wavelength	0.71073 Å	
Crystal system	Triclinic	
Space group	<i>P</i> 1, (no. 1)	
Unit cell dimensions	<i>a</i> = 9.5266(4) Å <i>b</i> = 10.7603(6) Å <i>c</i> = 15.1726(8) Å	$\alpha = 96.442(4)^\circ$ $\beta = 93.835(5)^\circ$ $\gamma = 107.932(4)^\circ$
Volume	1461.94(13) Å ³	
<i>Z</i>	2	
Density (calculated)	1.597 mg·m ⁻³	
Absorption coefficient	5.199 mm ⁻¹	
<i>F</i> (000)	702 e	
Crystal size	0.09 x 0.06 x 0.06 mm ³	
θ range for data collection	3.146 to 33.135°	
Index ranges	-14 ≤ <i>h</i> ≤ 14, -16 ≤ <i>k</i> ≤ 16, -23 ≤ <i>l</i> ≤ 23	
Reflections collected	41586	
Independent reflections	11061 [<i>R</i> _{int} = 0.0416]	
Reflections with <i>I</i> > 2σ(<i>I</i>)	10796	
Completeness to $\theta = 25.242^\circ$	98.30%	
Absorption correction	Gaussian	
Max. and min. transmission	0.77363 and 0.65074	
Refinement method	Full-matrix least-squares on <i>F</i> ²	
Data / restraints / parameters	11061 / 0 / 333	
Goodness-of-fit on <i>F</i> ²	1.031	
Final <i>R</i> indices [<i>I</i> > 2σ(<i>I</i>)]	<i>R</i> ₁ = 0.0186	<i>wR</i> ₂ = 0.0490
<i>R</i> indices (all data)	<i>R</i> ₁ = 0.0192	<i>wR</i> ₂ = 0.0495
Extinction coefficient	n/a	
Largest diff. peak and hole	0.906 and -2.467 e·Å ⁻³	

6.2.32 Crystal Data and Structure Refinement of Compound 142



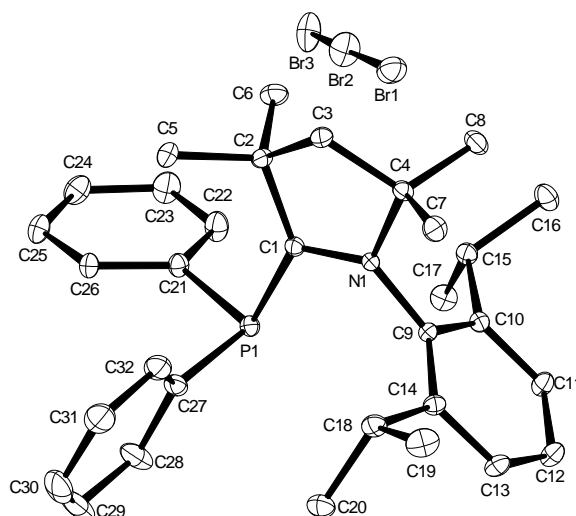
Empirical formula	$C_{38}H_{41}AuF_5NP$	
Color	red brown	
Formula weight	834.65 g·mol ⁻¹	
Temperature	100 K	
Wavelength	0.71073 Å	
Crystal system	MONOCLINIC	
Space group	p 21/c, (no. 14)	
Unit cell dimensions	a = 10.195(3) Å b = 17.089(5) Å c = 19.065(5) Å	$\alpha = 90^\circ$ $\beta = 92.858(5)^\circ$ $\gamma = 90^\circ$
Volume	3317.5(15) Å ³	
Z	4	
Density (calculated)	1.671 mg·m ⁻³	
Absorption coefficient	4.540 mm ⁻¹	
F(000)	1660 e	
Crystal size	0.21 x 0.06 x 0.04 mm ³	
θ range for data collection	1.601 to 34.434°	
Index ranges	-16 ≤ h ≤ 16, -27 ≤ k ≤ 27, -30 ≤ l ≤ 30	
Reflections collected	234997	
Independent reflections	13970 [R _{int} = 0.0478]	
Reflections with I > 2σ(I)	12179	
Completeness to $\theta = 25.242^\circ$	99.90%	
Absorption correction	Gaussian	
Max. and min. transmission	0.82889 and 0.52465	
Refinement method	Full-matrix least-squares on F ²	
Data / restraints / parameters	13970 / 0 / 423	
Goodness-of-fit on F ²	1.042	
Final R indices [I > 2σ(I)]	R ₁ = 0.0169	wR ₂ = 0.0355
R indices (all data)	R ₁ = 0.0242	wR ₂ = 0.0377
Extinction coefficient	n/a	
Largest diff. peak and hole	0.709 and -0.504 e·Å ⁻³	

6.2.33 Crystal Data and Structure Refinement of Compound 143



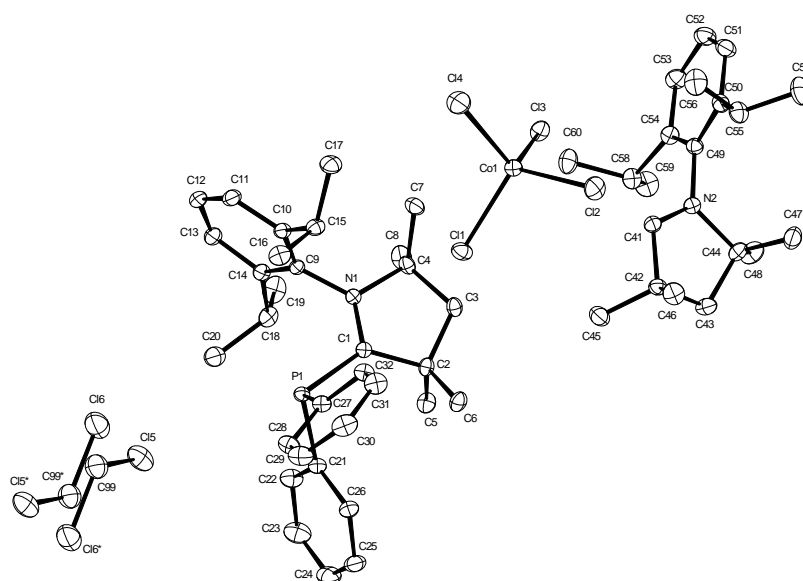
Empirical formula	$C_{35} H_{56} Au Cl N P$	
Color	yellow	
Formula weight	754.19 g·mol ⁻¹	
Temperature	100.15 K	
Wavelength	0.71073 Å	
Crystal system	MONOCLINIC	
Space group	<i>p</i> 21/n, (no. 14)	
Unit cell dimensions	<i>a</i> = 15.848(2) Å <i>b</i> = 11.1500(4) Å <i>c</i> = 19.4741(18) Å	$\alpha = 90^\circ$ $\beta = 104.562(9)^\circ$ $\gamma = 90^\circ$
Volume	3330.6(6) Å ³	
<i>Z</i>	4	
Density (calculated)	1.504 mg·m ⁻³	
Absorption coefficient	4.569 mm ⁻¹	
<i>F</i> (000)	1536 e	
Crystal size	0.12 x 0.08 x 0.07 mm ³	
θ range for data collection	3.722 to 37.981°	
Index ranges	-27 ≤ <i>h</i> ≤ 27, -19 ≤ <i>k</i> ≤ 19, -33 ≤ <i>l</i> ≤ 33	
Reflections collected	138753	
Independent reflections	18058 [R _{int} = 0.0335]	
Reflections with <i>I</i> > 2σ(<i>I</i>)	16658	
Completeness to $\theta = 25.242^\circ$	99.40%	
Absorption correction	Gaussian	
Max. and min. transmission	0.7475 and 0.6354	
Refinement method	Full-matrix least-squares on <i>F</i> ²	
Data / restraints / parameters	18058 / 0 / 360	
Goodness-of-fit on <i>F</i> ²	1.055	
Final <i>R</i> indices [<i>I</i> > 2σ(<i>I</i>)]	<i>R</i> ₁ = 0.0175	<i>wR</i> ₂ = 0.0411
<i>R</i> indices (all data)	<i>R</i> ₁ = 0.0209	<i>wR</i> ₂ = 0.0428
Extinction coefficient	n/a	
Largest diff. peak and hole	0.704 and -2.347 e·Å ⁻³	

6.2.34 Crystal Data and Structure Refinement of Compound 144



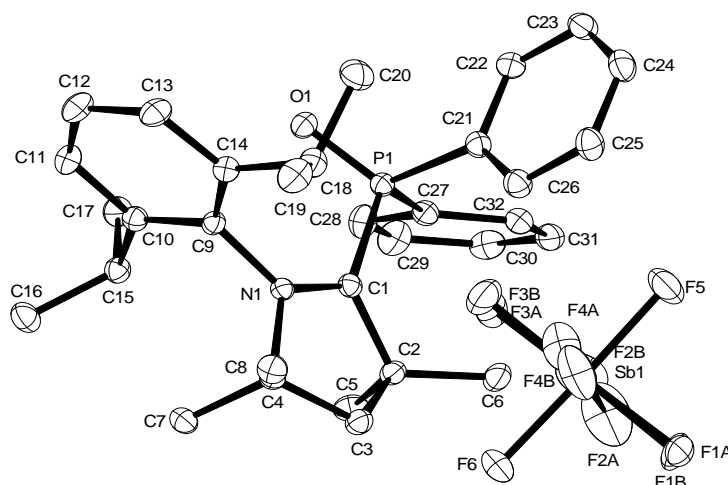
Empirical formula	$C_{32}H_{41}Br_3NP$	
Color	yellow	
Formula weight	710.36 g·mol ⁻¹	
Temperature	100 K	
Wavelength	0.71073 Å	
Crystal system	ORTHORHOMBIC	
Space group	p 21 21 21, (no. 19)	
Unit cell dimensions	a = 10.2579(8) Å	$\alpha = 90^\circ$
	b = 12.5039(12) Å	$\beta = 90^\circ$
	c = 23.888(2) Å	$\gamma = 90^\circ$
Volume	3063.9(5) Å ³	
Z	4	
Density (calculated)	1.540 mg·m ⁻³	
Absorption coefficient	4.024 mm ⁻¹	
F(000)	1440 e	
Crystal size	0.20 x 0.13 x 0.10 mm ³	
θ range for data collection	3.411 to 36.060°	
Index ranges	-16 ≤ h ≤ 16, -20 ≤ k ≤ 20, -39 ≤ l ≤ 39	
Reflections collected	147315	
Independent reflections	14503 [R _{int} = 0.0247]	
Reflections with I > 2σ(I)	13716	
Completeness to $\theta = 25.242^\circ$	98.50%	
Absorption correction	Gaussian	
Max. and min. transmission	0.85103 and 0.69602	
Refinement method	Full-matrix least-squares on F ²	
Data / restraints / parameters	14503 / 0 / 343	
Goodness-of-fit on F ²	1.105	
Final R indices [I > 2σ(I)]	R1 = 0.0332	wR2 = 0.0979
R indices (all data)	R1 = 0.0372	wR2 = 0.1025
Absolute structure parameter	0.028(6)	
Extinction coefficient	n/a	
Largest diff. peak and hole	1.307 and -2.311 e·Å ⁻³	

6.2.35 Crystal Data and Structure Refinement of Compound 145



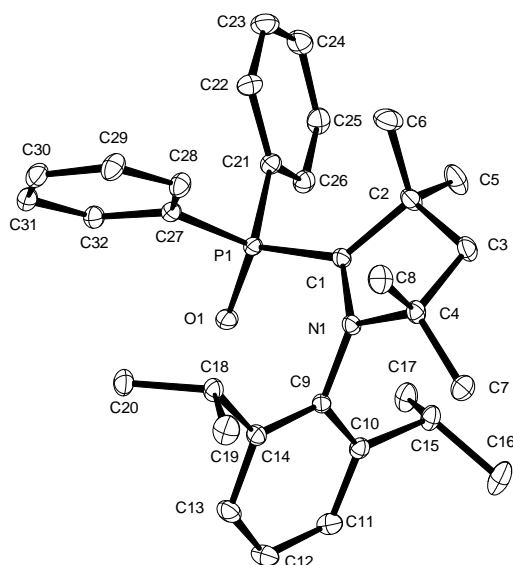
Empirical formula	$C_{52.50}H_{73}Cl_5CoN_2P$	
Color	green	
Formula weight	999.27 g · mol ⁻¹	
Temperature	1070 K	
Wavelength	0.71073 Å	
Crystal system	Triclinic	
Space group	P$\bar{1}$, (no. 2)	
Unit cell dimensions	$a = 9.6217(17)$ Å	$\alpha = 88.834(8)^\circ$.
	$b = 16.010(2)$ Å	$\beta = 74.718(13)^\circ$.
	$c = 17.5101(8)$ Å	$\gamma = 87.487(11)^\circ$.
Volume	2599.3(6) Å ³	
Z	2	
Density (calculated)	1.277 mg · m ⁻³	
Absorption coefficient	0.654 mm ⁻¹	
F(000)	1058 e	
Crystal size	0.17 x 0.16 x 0.04 mm ³	
θ range for data collection	2.600 to 34.985°.	
Index ranges	-15 ≤ h ≤ 15, -25 ≤ k ≤ 25, -28 ≤ l ≤ 27	
Reflections collected	78065	
Independent reflections	22645 [Rint = 0.0467]	
Reflections with I > 2σ(I)	19493	
Completeness to $\theta = 27.500^\circ$	99.60%	
Absorption correction	Gaussian	
Max. and min. transmission	0.97108 and 0.88551	
Refinement method	Full-matrix least-squares on F ²	
Data / restraints / parameters	22645 / 0 / 584	
Goodness-of-fit on F ²	1.108	
Final R indices [I > 2σ(I)]	R1 = 0.0407	wR2 = 0.1157
R indices (all data)	R1 = 0.0499	wR2 = 0.1278
Largest diff. peak and hole	0.7 and -1.3 e · Å ⁻³	

6.2.36 Crystal Data and Structure Refinement of Compound 146



Empirical formula	$C_{32}H_{41}F_6NO P Sb$	
Color	light_yellow	
Formula weight	722.38 g·mol ⁻¹	
Temperature	100 K	
Wavelength	0.71073 Å	
Crystal system	MONOCLINIC	
Space group	p 21/n, (no. 14)	
Unit cell dimensions	a = 10.1990(7) Å b = 29.947(2) Å c = 10.7797(12) Å	a = 90°. b = 106.681(7)°. g = 90°.
Volume	3153.8(5) Å ³	
Z	4	
Density (calculated)	1.521 mg·m ⁻³	
Absorption coefficient	0.987 mm ⁻¹	
F(000)	1472 e	
Crystal size	0.12 x 0.09 x 0.03 mm ³	
θ range for data collection	3.428 to 33.166°.	
Index ranges	-15 ≤ h ≤ 15, -46 ≤ k ≤ 46, -16 ≤ l ≤ 16	
Reflections collected	96734	
Independent reflections	12014 [R _{int} = 0.0512]	
Reflections with I > 2σ(I)	9562	
Completeness to θ = 25.242°	99.70%	
Absorption correction	Gaussian	
Max. and min. transmission	0.97109 and 0.89230	
Refinement method	Full-matrix least-squares on F ²	
Data / restraints / parameters	12014 / 0 / 423	
Goodness-of-fit on F ²	1.066	
Final R indices [I > 2σ(I)]	R ₁ = 0.0336	wR ₂ = 0.0745
R indices (all data)	R ₁ = 0.0515	wR ₂ = 0.0836
Extinction coefficient	n/a	
Largest diff. peak and hole	0.852 and -1.303 e·Å ⁻³	

6.2.37 Crystal Data and Structure Refinement of Compound 147



Empirical formula	$C_{32}H_{41}NOP$	
Color	orange	
Formula weight	486.63 g·mol ⁻¹	
Temperature	100 K	
Wavelength	0.71073 Å	
Crystal system	TRICLINIC	
Space group	<i>p</i> -1, (no. 2)	
Unit cell dimensions	<i>a</i> = 10.4546(15) Å <i>b</i> = 10.6918(15) Å <i>c</i> = 14.304(2) Å	$\alpha = 74.418(3)^\circ$ $\beta = 81.735(3)^\circ$ $\gamma = 62.736(2)^\circ$
Volume	1368.6(3) Å ³	
<i>Z</i>	2	
Density (calculated)	1.181 mg·m ⁻³	
Absorption coefficient	0.125 mm ⁻¹	
<i>F</i> (000)	526 e	
Crystal size	0.14 x 0.1 x 0.06 mm ³	
θ range for data collection	2.353 to 37.160°	
Index ranges	-17 ≤ <i>h</i> ≤ 17, -17 ≤ <i>k</i> ≤ 17, -24 ≤ <i>l</i> ≤ 23	
Reflections collected	54925	
Independent reflections	13485 [R _{int} = 0.0333]	
Reflections with <i>I</i> > 2σ(<i>I</i>)	10776	
Completeness to $\theta = 25.242^\circ$	99.80%	
Absorption correction	Gaussian	
Max. and min. transmission	0.99258 and 0.97918	
Refinement method	Full-matrix least-squares on <i>F</i> ²	
Data / restraints / parameters	13485 / 0 / 324	
Goodness-of-fit on <i>F</i> ²	1.031	
Final <i>R</i> indices [<i>I</i> > 2σ(<i>I</i>)]	<i>R</i> ₁ = 0.0378	<i>wR</i> ₂ = 0.1000
<i>R</i> indices (all data)	<i>R</i> ₁ = 0.0526	<i>wR</i> ₂ = 0.1090
Extinction coefficient	n/a	
Largest diff. peak and hole	0.596 and -0.364 e·Å ⁻³	

7 Bibliography

- [1] E. W. Abel, F. G. A. Stone, G. Wilkinson, *Comprehensive Organometallic Chemistry II, Vol. 7-9*, Pergamon, **1995**.
- [2] E. Jacobsen, A. Pfaltz, H. Yamamoto, *Comprehensive Asymmetric Catalysis, Vol. 1-3*, Springer, New York, **1999**.
- [3] J. F. Hartwig, *Organotransition metal chemistry: from bonding to catalysis*, Univ Science Books, **2010**.
- [4] D. J. Cole-Hamilton, *Science* **2003**, 299, 1702-1706.
- [5] B. Averill, J. Moulijn, R. van Santen, P. van Leeuwen, *Catalysis: An Integrated Approach: An Integrated Approach, Vol. 123*, Elsevier, **1999**.
- [6] B. Cornils, W. A. Herrmann, *Applied homogeneous catalysis with organometallic compounds, Vol. 2*, VCH Weinheim etc., **1996**.
- [7] B. Cornils, W. A. Herrmann, *Aqueous-phase organometallic catalysis: concepts and applications*, John Wiley & Sons, **2006**.
- [8] H. Olivier-Bourbigou, C. Vallee, Wiley-VCH: Weinheim, **2005**.
- [9] B. Cornils, *J. Mol. Catal. A: Chem.* **1999**, 143, 1-10.
- [10] D. M. Chisholm, J. Scott McIndoe, *Dalton Trans.* **2008**, 3933-3945.
- [11] J. Fenn, M. Mann, C. Meng, S. Wong, C. Whitehouse, *Science* **1989**, 246, 64-71.
- [12] W. Henderson, J. S. McIndoe, *Mass Spectrometry of Inorganic and Organometallic Compounds: Tools-Techniques-Tips*, John Wiley & Sons, **2005**.
- [13] M. Eberlin, *Eur. J. Mass Spectrom.* **2007**, 13, 19-28.
- [14] N. Taccardi, R. Paolillo, V. Gallo, P. Mastroilli, C. F. Nobile, M. Räisänen, T. Repo, *Eur. J. Inorg. Chem.* **2007**, 2007, 4645-4652.
- [15] A. B. Chaplin, P. J. Dyson, *Organometallics* **2007**, 26, 2447-2455.
- [16] P.-A. Enquist, P. Nilsson, P. Sjöberg, M. Larhed, *J. Org. Chem.* **2006**, 71, 8779-8786.
- [17] C. Vicent, M. Viciano, E. Mas-Marzá, M. Sanaú, E. Peris, *Organometallics* **2006**, 25, 3713-3720.
- [18] L. S. Santos, J. O. Metzger, *Angew. Chem. Int. Ed.* **2006**, 45, 977-981.
- [19] J. S. Uppal, D. E. Johnson, R. H. Staley, *J. Am. Chem. Soc.* **1981**, 103, 508-511.
- [20] P. Chen, *Angew. Chem. Int. Ed.* **2003**, 42, 2832-2847.
- [21] C. Hinderling, C. Adlhart, P. Chen, *Angew. Chem. Int. Ed.* **1998**, 37, 2685-2689.
- [22] C. Adlhart, C. Hinderling, H. Baumann, P. Chen, *J. Am. Chem. Soc.* **2000**, 122, 8204-8214.
- [23] K. Ohmatsu, M. Ito, T. Kunieda, T. Ooi, *Nat. Chem.* **2012**, 4, 473-477.
- [24] M. Alcarazo, *Chem. Eur. J.* **2014**, 20, 7868-7877.
- [25] F. W. Bennett, G. R. A. Brandt, H. J. Emeleus, R. N. Haszeldine, *Nature* **1950**, 166, 225-225.
- [26] T. Drews, D. Rusch, S. Seidel, S. Willemsen, K. Seppelt, *Chem. Eur. J.* **2008**, 14, 4280-4286.
- [27] Y. Canac, C. Maaliki, I. Abdellah, R. Chauvin, *New J. Chem.* **2012**, 36, 17-27.
- [28] U. Zoller, *Tetrahedron* **1988**, 44, 7413-7426.
- [29] N. Kuhn, J. Fahl, D. Bläser, R. Boese, *Z. Anorg. Allg. Chem.* **1999**, 625, 729-734.
- [30] C. Maaliki, C. Lepetit, Y. Canac, C. Bijani, C. Duhayon, R. Chauvin, *Chem. Eur. J.* **2012**, 18, 7705-7714.
- [31] M. Azouri, J. Andrieu, M. Picquet, P. Richard, B. Hanquet, I. Tkatchenko, *Eur. J. Inorg. Chem.* **2007**, 2007, 4877-4883.
- [32] J. J. Weigand, K.-O. Feldmann, F. D. Henne, *J. Am. Chem. Soc.* **2010**, 132, 16321-16323.

- [33] Y. Wang, Y. Xie, M. Y. Abraham, R. J. Gilliard, P. Wei, H. F. Schaefer, P. v. R. Schleyer, G. H. Robinson, *Organometallics* **2010**, *29*, 4778-4780.
- [34] B. D. Ellis, C. A. Dyker, A. Decken, C. L. B. Macdonald, *Chem. Comm.* **2005**, 1965-1967.
- [35] A. A. Tolmachev, A. A. Yurchenko, A. S. Merculov, M. G. Semenova, E. V. Zarudnitskii, V. V. Ivanov, A. M. Pinchuk, *Heteroat. Chem.* **1999**, *10*, 585-597.
- [36] N. Debono, Y. Canac, C. Duhayon, R. Chauvin, *Eur. J. Inorg. Chem.* **2008**, *2008*, 2991-2999.
- [37] I. Abdellah, N. Debono, Y. Canac, L. Vendier, R. Chauvin, *Chem. Asian J.* **2010**, *5*, 1225-1231.
- [38] Y. Canac, N. Debono, L. Vendier, R. Chauvin, *Inorg. Chem.* **2009**, *48*, 5562-5568.
- [39] I. V. Komarov, M. Yu. Kornilov, A. A. Tolmachev, A. A. Yurchenko, E. B. Rusanov, A. N. Chernega, *Tetrahedron* **1995**, *51*, 11271-11280.
- [40] V. Lavallo, Y. Canac, B. Donnadiu, W. W. Schoeller, G. Bertrand, *Science* **2006**, *312*, 722-724.
- [41] J. Petušková, H. Bruns, M. Alcarazo, *Angew. Chem. Int. Ed.* **2011**, *50*, 3799-3802.
- [42] Á. Kozma, T. Deden, J. Carreras, C. Wille, J. Petušková, J. Rust, M. Alcarazo, *Chem. Eur. J.* **2014**, *20*, 2208-2214.
- [43] H. Tinnermann, C. Wille, M. Alcarazo, *Angew. Chem. Int. Ed.* **2014**, *53*, 8732-8736.
- [44] N. Burford, T. Stanley Cameron, K. N. Robertson, A. D. Phillips, H. A. Jenkins, *Chem. Comm.* **2000**, 2087-2088.
- [45] D. Gudat, *Coord. Chem. Rev.* **1997**, *163*, 71-106.
- [46] B. D. Ellis, P. J. Ragona, C. L. B. Macdonald, *Inorg. Chem.* **2004**, *43*, 7857-7867.
- [47] N. Burford, P. J. Ragona, R. McDonald, M. J. Ferguson, *J. Am. Chem. Soc.* **2003**, *125*, 14404-14410.
- [48] N. Burford, P. Losier, A. D. Phillips, P. J. Ragona, T. S. Cameron, *Inorg. Chem.* **2003**, *42*, 1087-1091.
- [49] H. Jansen, F. B. Läng, J. C. Slootweg, A. W. Ehlers, M. Lutz, K. Lammertsma, H. Grützmacher, *Angew. Chem. Int. Ed.* **2010**, *49*, 5485-5488.
- [50] R. Weiss, S. Engel, *Synthesis* **1991**, 1077-1079.
- [51] G. Bouhadir, R. W. Reed, R. Réau, G. Bertrand, *Heteroat. Chem.* **1995**, *6*, 371-375.
- [52] J. J. Weigand, K.-O. Feldmann, A. K. C. Echterhoff, A. W. Ehlers, K. Lammertsma, *Angew. Chem. Int. Ed.* **2010**, *49*, 6178-6181.
- [53] H. Bruns, M. Patil, J. Carreras, A. Vázquez, W. Thiel, R. Goddard, M. Alcarazo, *Angew. Chem. Int. Ed.* **2010**, *49*, 3680-3683.
- [54] H. Clavier, S. P. Nolan, *Chem. Comm.* **2010**, *46*, 841-861.
- [55] T. Dröge, F. Glorius, *Angew. Chem. Int. Ed.* **2010**, *49*, 6940-6952.
- [56] D. G. Gusev, *Organometallics* **2009**, *28*, 6458-6461.
- [57] G. Kuchenbeiser, B. Donnadiu, G. Bertrand, *J. Organomet. Chem.* **2008**, *693*, 899-904.
- [58] W. W. Schoeller, G. D. Frey, G. Bertrand, *Chem. Eur. J.* **2008**, *14*, 4711-4718.
- [59] N. H. T. Huy, B. Donnadiu, G. Bertrand, F. Mathey, *Chem. Asian J.* **2009**, *4*, 1225-1228.
- [60] J. Petušková, M. Patil, S. Holle, C. W. Lehmann, W. Thiel, M. Alcarazo, *J. Am. Chem. Soc.* **2011**, *133*, 20758-20760.
- [61] F. D. Henne, A. T. Dickschat, F. Hennersdorf, K. O. Feldmann, J. J. Weigand, *Inorg. Chem.* **2015**, *54*, 6849-6861.
- [62] Y. H. So, *Macromolecules* **1992**, *25*, 516-520.
- [63] Y. Canac, C. Lepetit, M. Abdalilah, C. Duhayon, R. Chauvin, *J. Am. Chem. Soc.* **2008**, *130*, 8406-8413.
- [64] C. A. Tolman, *Chem. Rev.* **1977**, *77*, 313-348.

- [65] C. A. Tolman, *J. Am. Chem. Soc.* **1970**, *92*, 2953-2956.
- [66] O. Köhl, *Coord. Chem. Rev.* **2005**, *249*, 693-704.
- [67] O. Schuster, L. Yang, H. G. Raubenheimer, M. Albrecht, *Chem. Rev.* **2009**, *109*, 3445-3478.
- [68] M. Alcarazo, T. Stork, A. Anoop, W. Thiel, A. Fürstner, *Angew. Chem. Int. Ed.* **2010**, *49*, 2542-2546.
- [69] S. Wolf, H. Plenio, *J. Organomet. Chem.* **2009**, *694*, 1487-1492.
- [70] A. B. P. Lever, *Inorg. Chem.* **1990**, *29*, 1271-1285.
- [71] A. B. P. Lever, *Inorg. Chem.* **1991**, *30*, 1980-1985.
- [72] S. Leuthäuser, D. Schwarz, H. Plenio, *Chem. Eur. J.* **2007**, *13*, 7195-7203.
- [73] C. Palau, Y. Berchadsky, F. Chaliier, J.-P. Finet, G. Gronchi, P. Tordo, *J. Phys. Chem.* **1995**, *99*, 158-163.
- [74] J. P. Bullock, A. M. Bond, R. T. Boeré, T. M. Gietz, T. L. Roemmele, S. D. Seagrave, J. D. Masuda, M. Parvez, *J. Am. Chem. Soc.* **2013**, *135*, 11205-11215.
- [75] D. G. Gusev, *Organometallics* **2009**, *28*, 763-770.
- [76] J. Sirieix, M. Oßberger, B. Betzemeier, P. Knochel, *Synlett* **2000**, *2000*, 1613-1615.
- [77] S. Saleh, E. Fayad, M. Azouri, J.-C. Hierso, J. Andrieu, M. Picquet, *Adv. Synth. Catal.* **2009**, *351*, 1621-1628.
- [78] C. C. Brasse, U. Englert, A. Salzer, H. Waffenschmidt, P. Wasserscheid, *Organometallics* **2000**, *19*, 3818-3823.
- [79] D. J. Brauer, K. W. Kottsieper, C. Liek, O. Stelzer, H. Waffenschmidt, P. Wasserscheid, *J. Organomet. Chem.* **2001**, *630*, 177-184.
- [80] I. Alonso, B. Trillo, F. López, S. Montserrat, G. Ujaque, L. Castedo, A. Lledós, J. L. Mascareñas, *J. Am. Chem. Soc.* **2009**, *131*, 13020-13030.
- [81] P. Mauleón, R. M. Zeldin, A. Z. González, F. D. Toste, *J. Am. Chem. Soc.* **2009**, *131*, 6348-6349.
- [82] J. Carreras, M. Patil, W. Thiel, M. Alcarazo, *J. Am. Chem. Soc.* **2012**, *134*, 16753-16758.
- [83] J. Carreras, G. Gopakumar, L. Gu, A. Gimeno, P. Linowski, J. Petušková, W. Thiel, M. Alcarazo, *J. Am. Chem. Soc.* **2013**, *135*, 18815-18823.
- [84] J. W. Dube, C. L. B. Macdonald, P. J. Ragogna, *Angew. Chem. Int. Ed.* **2012**, *51*, 13026-13030.
- [85] R. J. Abernethy, A. F. Hill, M. K. Smith, A. C. Willis, *Organometallics* **2009**, *28*, 6152-6159.
- [86] R. E. Cobbley, F. W. B. Einstein, *Acta Crystallogr., Sect. B: Struct. Sci.* **1975**, *31*, 2731-2733.
- [87] Z. B. Maksic, B. Kovacevic, *J. Chem. Soc., Perkin Trans. 2* **1999**, 2623-2629.
- [88] B. Machura, R. Penczek, R. Kruszynski, J. Kłak, J. Mroziński, J. Kusz, *Polyhedron* **2007**, *26*, 4833-4840.
- [89] J. Zhou, Y. Tang, *Chem. Comm.* **2004**, 432-433.
- [90] F. Malbosc, V. Chauby, C. Serra-Le Berre, M. Etienne, J.-C. Daran, P. Kalck, *Eur. J. Inorg. Chem.* **2001**, *2001*, 2689-2697.
- [91] E. Lee, A. S. Kamlet, D. C. Powers, C. N. Neumann, G. B. Boursalian, T. Furuya, D. C. Choi, J. M. Hooker, T. Ritter, *Science* **2011**, *334*, 639-642.
- [92] P. Neves, S. Gago, S. S. Balula, A. D. Lopes, A. A. Valente, L. Cunha-Silva, F. A. A. Paz, M. Pillinger, J. Rocha, C. M. Silva, I. S. Gonçalves, *Inorg. Chem.* **2011**, *50*, 3490-3500.
- [93] S. Gaillard, J.-L. Renaud, *Dalton Trans.* **2013**, *42*, 7255-7270.
- [94] D. J. M. Snelders, G. van Koten, R. J. M. Klein Gebbink, *Chem. Eur. J.* **2011**, *17*, 42-57.

- [95] S. Bontemps, G. Bouhadir, K. Miqueu, D. Bourissou, *J. Am. Chem. Soc.* **2006**, *128*, 12056-12057.
- [96] F. Inagaki, C. Matsumoto, Y. Okada, N. Maruyama, C. Mukai, *Angew. Chem. Int. Ed.* **2015**, *54*, 818-822.
- [97] Y. Tulchinsky, M. A. Iron, M. Botoshansky, M. Gandelman, *Nat. Chem.* **2011**, *3*, 525-531.
- [98] X. Luo, H. Zhang, H. Duan, Q. Liu, L. Zhu, T. Zhang, A. Lei, *Org. Lett.* **2007**, *9*, 4571-4574.
- [99] S. Basra, J. G. de Vries, D. J. Hyett, G. Harrison, K. M. Heslop, A. G. Orpen, P. G. Pringle, K. von der Luehe, *Dalton Trans.* **2004**, 1901-1905.
- [100] K. M. Gillespie, C. J. Sanders, P. O'Shaughnessy, I. Westmoreland, C. P. Thickitt, P. Scott, *J. Org. Chem.* **2002**, *67*, 3450-3458.
- [101] A. F. Holleman, E. Wiberg, *Lehrbuch der anorganischen Chemie*, Walter de Gruyter, **1995**.
- [102] W. Levason, G. Reid, M. Webster, *Acta Crystallogr., Sect. C: Cryst. Struct. Commun.* **2006**, *62*, 438-440.
- [103] G. Mancino, A. J. Ferguson, A. Beeby, N. J. Long, T. S. Jones, *J. Am. Chem. Soc.* **2005**, *127*, 524-525.
- [104] R. Jackstell, H. Klein, M. Beller, K.-D. Wiese, D. Röttger, *Eur. J. Org. Chem.* **2001**, *2001*, 3871-3877.
- [105] S. L. Mukerjee, S. P. Nolan, C. D. Hoff, R. Lopez de la Vega, *Inorg. Chem.* **1988**, *27*, 81-85.
- [106] C. Taouss, P. G. Jones, *Z. Naturforsch., B: Chem. Sci.* **2013**, *68*, 860-870.
- [107] M. C. Nielsen, K. J. Bonney, F. Schoenebeck, *Angew. Chem. Int. Ed.* **2014**, *53*, 5903-5906.
- [108] T. Korenaga, T. Kosaki, R. Fukumura, T. Ema, T. Sakai, *Org. Lett.* **2005**, *7*, 4915-4917.
- [109] T.-a. Koizumi, A. Yamazaki, T. Yamamoto, *Dalton Trans.* **2008**, 3949-3952.
- [110] M.-N. Birkholz, Z. Freixa, P. W. N. M. van Leeuwen, *Chem. Soc. Rev.* **2009**, *38*, 1099-1118.
- [111] J. E. Marcone, K. G. Moloy, *J. Am. Chem. Soc.* **1998**, *120*, 8527-8528.
- [112] J. F. Hartwig, *Science* **2002**, *297*, 1653-1654.
- [113] X. Yao, C.-J. Li, *J. Org. Chem.* **2005**, *70*, 5752-5755.
- [114] Z. Wang, B. J. Reinius, G. Dong, *J. Am. Chem. Soc.* **2012**, *134*, 13954-13957.
- [115] F. Mo, G. Dong, *Science* **2014**, *345*, 68-72.
- [116] B. M. Trost, C. Jäkel, B. Plietker, *J. Am. Chem. Soc.* **2003**, *125*, 4438-4439.
- [117] B. M. Trost, J. Xie, J. D. Sieber, *J. Am. Chem. Soc.* **2011**, *133*, 20611-20622.
- [118] M. R. Uehling, A. M. Suess, G. Lalic, *J. Am. Chem. Soc.* **2015**, *137*, 1424-1427.
- [119] A. M. Suess, M. R. Uehling, W. Kaminsky, G. Lalic, *J. Am. Chem. Soc.* **2015**, *137*, 7747-7753.
- [120] M. J. Goldfogel, S. J. Meek, *Chem. Sci.* **2016**.
- [121] A. Fürstner, P. W. Davies, *Angew. Chem. Int. Ed.* **2007**, *46*, 3410-3449.
- [122] H.-B. Sun, B. Li, R. Hua, Y. Yin, *Eur. J. Org. Chem.* **2006**, *2006*, 4231-4236.
- [123] M. Soleilhavoup, G. Bertrand, *Acc Chem Res* **2015**, *48*, 256-266.
- [124] A. Igau, H. Grutzmacher, A. Baceiredo, G. Bertrand, *J. Am. Chem. Soc.* **1988**, *110*, 6463-6466.
- [125] M. N. Hopkinson, C. Richter, M. Schedler, F. Glorius, *Nature* **2014**, *510*, 485-496.
- [126] A. J. Arduengo, R. L. Harlow, M. Kline, *J. Am. Chem. Soc.* **1991**, *113*, 361-363.
- [127] J. Vignolle, X. Cattoën, D. Bourissou, *Chem. Rev.* **2009**, *109*, 3333-3384.
- [128] A. J. Arduengo, G. Bertrand, *Chem. Rev.* **2009**, *109*, 3209-3210.

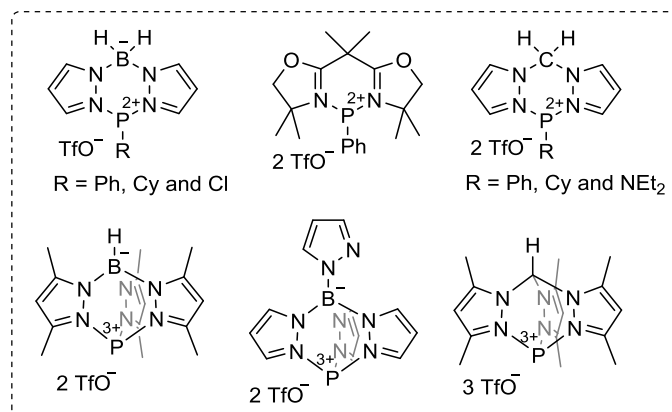
- [129] W. A. Herrmann, M. Elison, J. Fischer, C. Köcher, G. R. J. Artus, *Chem. Eur. J.* **1996**, *2*, 772-780.
- [130] V. Lavallo, Y. Canac, C. Präsang, B. Donnadiou, G. Bertrand, *Angew. Chem. Int. Ed.* **2005**, *44*, 5705-5709.
- [131] O. Back, B. Donnadiou, P. Parameswaran, G. Frenking, G. Bertrand, *Nat. Chem.* **2010**, *2*, 369-373.
- [132] R. Kretschmer, D. A. Ruiz, C. E. Moore, A. L. Rheingold, G. Bertrand, *Angew. Chem. Int. Ed.* **2014**, *53*, 8176-8179.
- [133] R. Kinjo, B. Donnadiou, M. A. Celik, G. Frenking, G. Bertrand, *Science* **2011**, *333*, 610-613.
- [134] D. A. Ruiz, G. Ung, M. Melaimi, G. Bertrand, *Angew. Chem. Int. Ed.* **2013**, *52*, 7590-7592.
- [135] P. Jerabek, H. W. Roesky, G. Bertrand, G. Frenking, *J. Am. Chem. Soc.* **2014**, *136*, 17123-17135.
- [136] D. S. Weinberger, M. Melaimi, C. E. Moore, A. L. Rheingold, G. Frenking, P. Jerabek, G. Bertrand, *Angew. Chem. Int. Ed.* **2013**, *52*, 8964-8967.
- [137] N. Arnold, H. Braunschweig, P. B. Brenner, M. A. Celik, R. D. Dewhurst, M. Haehnel, T. Kramer, I. Krummenacher, T. B. Marder, *Chem. Eur. J.* **2015**, *21*, 12357-12362.
- [138] S. Roy, K. C. Mondal, J. Meyer, B. Niepötter, C. Köhler, R. Herbst-Irmer, D. Stalke, B. Dittrich, D. M. Andrada, G. Frenking, H. W. Roesky, *Chem. Eur. J.* **2015**, *21*, 9312-9318.
- [139] D. S. Weinberger, N. Amin Sk, K. C. Mondal, M. Melaimi, G. Bertrand, A. C. Stückl, H. W. Roesky, B. Dittrich, S. Demeshko, B. Schwederski, W. Kaim, P. Jerabek, G. Frenking, *J. Am. Chem. Soc.* **2014**, *136*, 6235-6238.
- [140] G. Ung, J. Rittle, M. Soleilhavoup, G. Bertrand, J. C. Peters, *Angew. Chem. Int. Ed.* **2014**, *53*, 8427-8431.
- [141] K. C. Mondal, S. Roy, S. De, P. Parameswaran, B. Dittrich, F. Ehret, W. Kaim, H. W. Roesky, *Chem. Eur. J.* **2014**, *20*, 11646-11649.
- [142] K. C. Mondal, P. P. Samuel, Y. Li, H. W. Roesky, S. Roy, L. Ackermann, N. S. Sidhu, G. M. Sheldrick, E. Carl, S. Demeshko, S. De, P. Parameswaran, L. Ungur, L. F. Chibotaru, D. M. Andrada, *Eur. J. Inorg. Chem.* **2014**, *2014*, 818-823.
- [143] P. P. Samuel, K. C. Mondal, H. W. Roesky, M. Hermann, G. Frenking, S. Demeshko, F. Meyer, A. C. Stückl, J. H. Christian, N. S. Dalal, L. Ungur, L. F. Chibotaru, K. Pröpper, A. Meents, B. Dittrich, *Angew. Chem. Int. Ed.* **2013**, *52*, 11817-11821.
- [144] A. P. Singh, P. P. Samuel, H. W. Roesky, M. C. Schwarzer, G. Frenking, N. S. Sidhu, B. Dittrich, *J. Am. Chem. Soc.* **2013**, *135*, 7324-7329.
- [145] Y. Li, K. C. Mondal, H. W. Roesky, H. Zhu, P. Stollberg, R. Herbst-Irmer, D. Stalke, D. M. Andrada, *J. Am. Chem. Soc.* **2013**, *135*, 12422-12428.
- [146] R. Kinjo, B. Donnadiou, G. Bertrand, *Angew. Chem. Int. Ed.* **2010**, *49*, 5930-5933.
- [147] O. Back, M. A. Celik, G. Frenking, M. Melaimi, B. Donnadiou, G. Bertrand, *J. Am. Chem. Soc.* **2010**, *132*, 10262-10263.
- [148] P. Bissinger, H. Braunschweig, A. Damme, I. Krummenacher, A. K. Phukan, K. Radacki, S. Sugawara, *Angew. Chem. Int. Ed.* **2014**, *53*, 7360-7363.
- [149] K. C. Mondal, P. P. Samuel, H. W. Roesky, B. Niepötter, R. Herbst-Irmer, D. Stalke, F. Ehret, W. Kaim, B. Maity, D. Koley, *Chem. Eur. J.* **2014**, *20*, 9240-9245.
- [150] K. C. Mondal, P. P. Samuel, M. Tretiakov, A. P. Singh, H. W. Roesky, A. C. Stückl, B. Niepötter, E. Carl, H. Wolf, R. Herbst-Irmer, D. Stalke, *Inorg. Chem.* **2013**, *52*, 4736-4743.
- [151] K. C. Mondal, H. W. Roesky, M. C. Schwarzer, G. Frenking, B. Niepötter, H. Wolf, R. Herbst-Irmer, D. Stalke, *Angew. Chem. Int. Ed.* **2013**, *52*, 2963-2967.

-
- [152] C. D. Martin, M. Soleilhavoup, G. Bertrand, *Chem. Sci.* **2013**, *4*, 3020-3030.
- [153] J. K. Mahoney, D. Martin, F. Thomas, C. E. Moore, A. L. Rheingold, G. Bertrand, *J. Am. Chem. Soc.* **2015**, *137*, 7519-7525.
- [154] J. K. Mahoney, D. Martin, C. E. Moore, A. L. Rheingold, G. Bertrand, *J. Am. Chem. Soc.* **2013**, *135*, 18766-18769.
- [155] S. Styra, M. Melaimi, C. E. Moore, A. L. Rheingold, T. Augenstein, F. Breher, G. Bertrand, *Chem. Eur. J.* **2015**, *21*, 8441-8446.
- [156] S. Roy, A. C. Stuckl, S. Demeshko, B. Dittrich, J. Meyer, B. Maity, D. Koley, B. Schwederski, W. Kaim, H. W. Roesky, *J. Am. Chem. Soc.* **2015**, *137*, 4670-4673.
- [157] J. C. J. Bart, *J. Chem. Soc. B* **1969**, 350-365.
- [158] S. Styra, M. Melaimi, C. E. Moore, A. L. Rheingold, T. Augenstein, F. Breher, G. Bertrand, *Chem. Euro. J.* **2015**, *21*, 8441-8446.
- [159] L. Ackermann, A. R. Kapdi, C. Schulzke, *Org. Lett.* **2010**, *12*, 2298-2301.
- [160] D.-F. Hu, C.-M. Weng, F.-E. Hong, *Organometallics* **2011**, *30*, 1139-1147.
- [161] Y.-C. Chang, W.-C. Chang, C.-Y. Hu, F.-E. Hong, *Organometallics* **2014**, *33*, 3523-3534.
- [162] Y. Ji, R. E. Plata, C. S. Regens, M. Hay, M. Schmidt, T. Razler, Y. Qiu, P. Geng, Y. Hsiao, T. Rosner, M. D. Eastgate, D. G. Blackmond, *J. Am. Chem. Soc.* **2015**, *137*, 13272-13281.
- [163] M. Filatov, D. Cremer, *J. Chem. Phys.* **2005**, *123*, 124101.
- [164] J. A. Pople, P. M. W. Gill, N. C. Handy, *Int. J. Quantum Chem.* **1995**, *56*, 303-305.
- [165] B. J. Stokes, L. Liao, A. M. de Andrade, Q. Wang, M. S. Sigman, *Org. Lett.* **2014**, *16*, 4666-4669.
- [166] J. M. Landesberg, M. A. Slam, M. Mandel, *J. Org. Chem.* **1981**, *46*, 5025-5027.

Summary

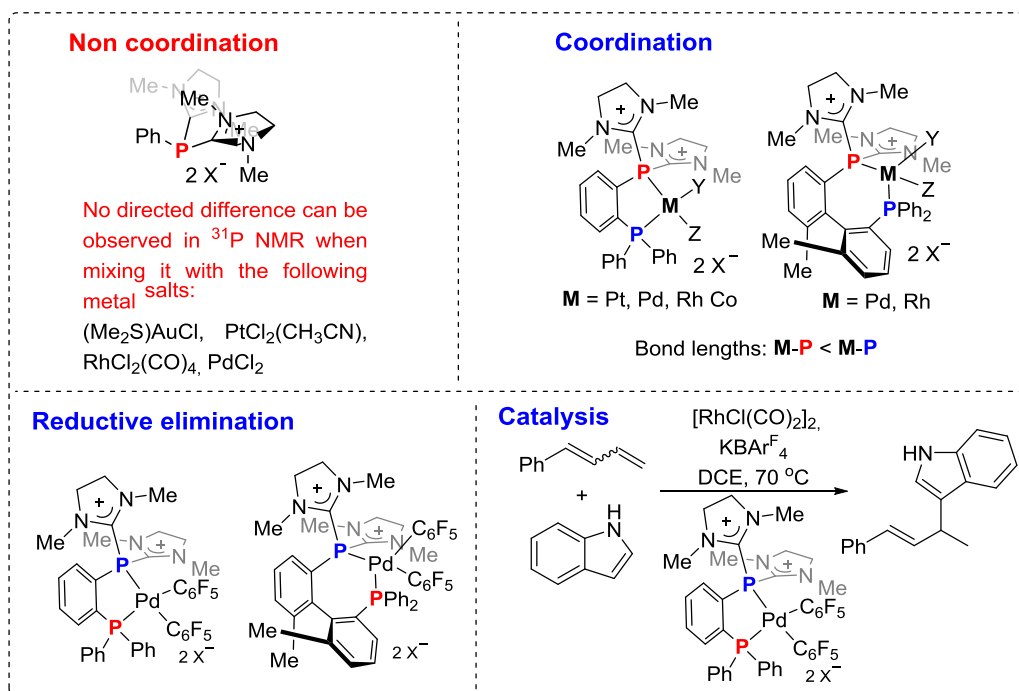
1) Bis- and Trispyrazoylborate/methane-Stabilized P(III)-Centered Cations

Making use of an -onium substituent transfer strategy, we have been able to isolate and structurally characterize several P-centered polycations stabilized by bis- and tris-(pyrazoyl)borate or methane ligands. In all of these compounds, the phosphorus center adopts a pyramidal environment, which is indicative of the presence of a lone pair mainly located on this atom. However, the high positive charge at phosphorus lowers the energy of this orbital to a level that makes it unavailable for donation. The same positive charge also stabilizes quite efficiently the $\sigma^*(\text{P-N})$ orbitals, thus conferring Lewis acid character to the phosphorus atom. This Lewis acidity is evident from the short contacts observed between the triflate anions and the phosphorus centers.



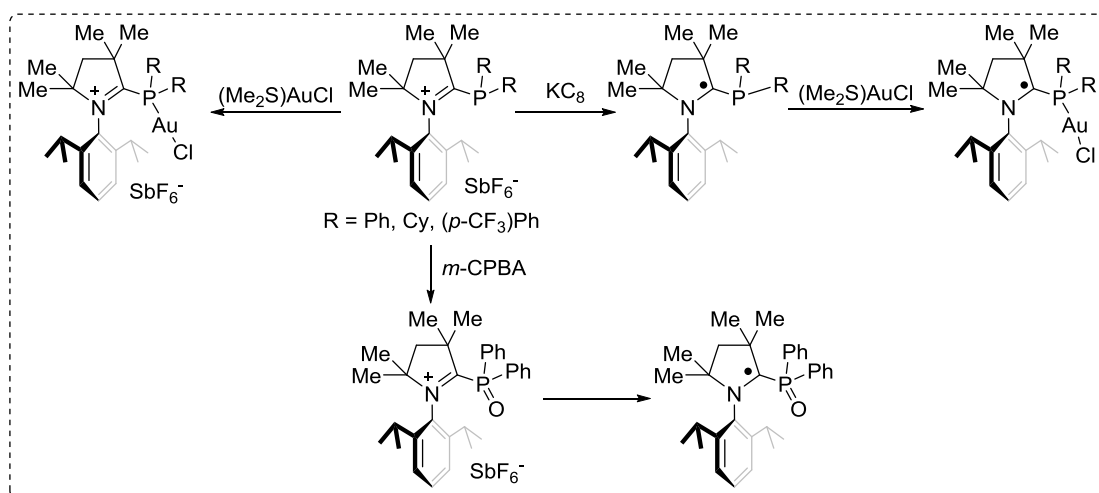
2) Dicationic Chelating Phosphines: Synthesis, Structure and Reactivity

We outlined the preparation of new bidentate dicationic phosphines and their coordination chemistry towards different metals. Moreover, we showcased for the first time the utility of cationic ligands to promote difficult reductive elimination processes under mild condition, such as the formation of polyfluorinated biaryls from Pd(II) centers. Finally, the unique properties of these ligands in catalysis has been proven in the hydrosilylation of phenyl diene with indoles and electron rich arenes.



3) Isolation and Coordination Chemistry of CAACs Substituted α -Radical Phosphines

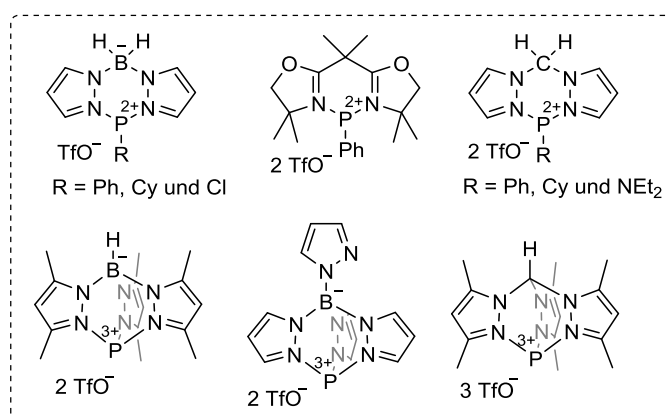
We have successfully isolated and characterized a series of CAAC (Cyclic (Alkyl)(Amino)Carbene) derived cationic phosphines. Their cyclic voltammetry showed a quasi-reversible redox potential, which indicated that stable radicals were formed after one electron reduction. As a result, a series of α -radical phosphines have been synthesized and fully characterized. More intriguingly, these radical phosphines could coordinate to Au(I) and form a range of stable gold complexes that are unprecedented. In addition, we were also able to synthesize the radical phosphorus oxide. All of the synthesized radicals have been characterized by EPR and most have been crystallized. These novel compounds could be named as α -radical phosphine ligands, which might be useful in catalysis.



Zusammenfassung

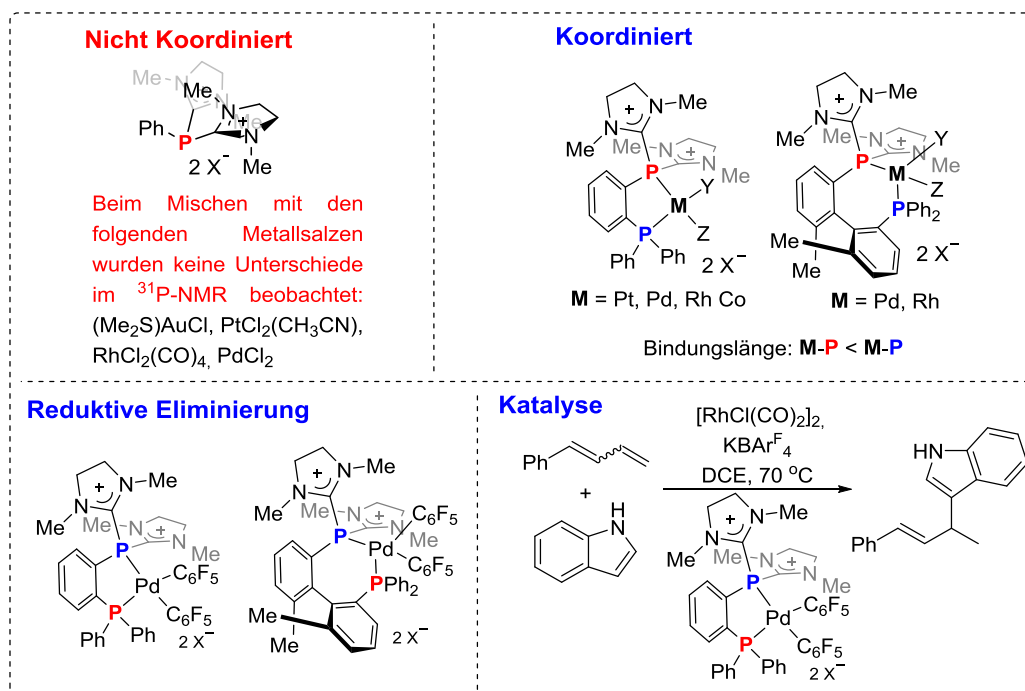
1) Bi- und Tri-Pyrazolyl(borat/methan) stabilisierte P(III)-zentrierte Kationen

Durch eine Onium-Substituenten-Transfer-Strategie ist es uns gelungen, mehrere Phosphor-zentrierte Polykationen, die durch Bi- und Tri-Pyrazolyl(borat/methan)-Liganden stabilisiert sind, zu isolieren und strukturell zu charakterisieren. Bei all diesen Verbindungen befindet sich das Phosphor-Zentrum in einer trigonal-pyramidalen Umgebung, was auf ein hauptsächlich am Phosphor lokalisiertes, freies Elektronenpaar hinweist. Die hohe positive Ladung am Phosphor senkt die Energie dieses Orbitals so weit ab, dass es als Donor nicht mehr zur Verfügung steht. Des Weiteren stabilisiert diese positive Ladung das $\sigma^*(\text{P-N})$ -Orbital und sorgt so für einen Lewis-aciden Charakter am Phosphor-Atom. Die Lewis-Acidität spiegelt sich in der geringen Bindungslänge zwischen dem Triflat-Anion und dem Phosphor-Zentrum wieder.



2) Dikationische chelatisierende Phosphine: Synthese, Struktur und Reaktivität

Im Rahmen dieser Arbeit haben wir die Darstellung und Koordinationschemie bidentater dikationischer Phosphine gegenüber verschiedenen Metallen beschrieben. Ebenso haben wir erstmalig die Anwendung kationischer Liganden auf schwierige reduktive Eliminierungen unter milden Bedingungen aufgezeigt, wie z.B. die Bildung polyfluorierter Biaryle von Pd(II)-Zentren. Darüber hinaus konnten die besonderen Eigenschaften dieser Liganden in Hydroarylierungen von Phenyl-Dienen mit Indolen und elektronenreichen Aromaten aufgezeigt werden.



3) Isolierung und Koordinationschemie von CAACs-substituierten α -radikalen Phosphenen

Wir haben erfolgreich eine Reihe von „CAAC“ (Zyklische(Alkyl)(Amino)Carbene) abgeleiteten kationischen Phosphenen isoliert und charakterisiert. Durch Cyclovoltammetrie konnte ein quasi-reversibles Redoxpotential aufgezeigt werden, was ein Indiz für die Bildung stabiler Radikale durch Ein-Elektron-Reduktion ist. Wir haben eine Reihe α -radikaler Phosphine synthetisiert und diese voll charakterisiert. Diese Radikale wurden an Au(I) koordiniert und lieferten eine Reihe stabiler Gold-Komplexe, welche bis dato unbekannt waren. Wir konnten ferner ein Phosphoroxid-Radikal darstellen. Die Radikale wurden durch EPR-Spektroskopie charakterisiert und die meisten wurden darüber hinaus durch Kristallstrukturanalysen bestätigt. Die neuen Verbindungen können als α -radikale Phosphin-Liganden bezeichnet werden mit potentiellen Anwendungsmöglichkeiten in der Katalyse.

